THEORY AND DESIGN OF AIR CUSHION CRAFT

L. YUN & A. BLIAULT

ARNOLD

Theory and Design of Air Cushion Craft

This page intentionally left blank

Theory and Design of Air Cushion Craft

Liang Yun
Deputy Chief Naval Architect of the Marine Design & Research Institute of China

Alan Bliault
Shell International Exploration and Production Hollan

A member of the Hodder Headline Group
LONDON

Copublished in North, Central and South America by
John Wiley & Sons Inc., New York · Toronto

First published in Great Britain in 2000 by
Arnold, a member of the Hodder Headline Group,
338 Euston Road, London NW1 3BH

http://www.arnoldpublishers.com

Copublished in North, Central and South America by
John Wiley & Sons Inc., 605 Third Avenue,
New York, NY 10158–0012

British Library Cataloguing in Publication Data
A catalogue record for this book is available from the British Library

Library of Congress Cataloging-in-Publication Data
A catalog record for this book is available from the Library of Congress

ISBN 0 340 67650 7
ISBN 0 470 23621 3 (Wiley)

1 2 3 4 5 6 7 8 9 10

Typeset in 10/12 pt Times by J&L Composition Ltd, Filey, North Yorkshire
Printed and bound in Great Britain by Redwood Books Ltd

This book is dedicated to advancement of Air Cushion Technology, and to the special band of researchers and engineers worldwide who have created its foundation.

This page intentionally left blank

Contents

Preface

It is 39 years since sea trials of the first hovercraft. Hovercraft are a new means of transportation, and so machinery, equipment and structural materials have had to be adapted for successful use in their special operating environment, which differs from that in aviation and for other marine vessels.

A somewhat difficult technical and economic path has been negotiated by the developers of hovercraft technology to date. Currently about 2000 craft are in operation for commercial water transportation, recreation, utility purposes and military applications around the world. They have taken a key role for a number of military missions, and provide utility transportation in a number of applications which are quite unique.

Hovercraft in China have developed from prototype tests in the 1960s, to practical use as ferries and military craft. More than 60 hovercraft types have been constructed or imported for operation in China. This book has been written to summarize the experience in air cushion technology in China and abroad to date, with the aim of improving understanding of air cushion technology.

Due to the relatively quick development of the cushion technology relative to other water transportation, the theories and design methods applied to hovercraft design and operations are continuing to develop at present. For instance various quasi-static theories of the air jet cushion were derived in the 1960s, but once the flexible skirt was developed, the hydrodynamic and aerodynamic forces acting on hovercraft changed so significantly that these earlier theories and formulae could not continue to serve in practice.

The theory of air cushion performance has therefore changed significantly since the 1960s. On one hand a lot of technical references and some technical summaries and handbooks with respect to air cushion technology are available to translate the physical phenomena but on the other, owing to different research methods, objects and means, there are many different methods which suggest how to deal with such theories. So far no finalized rules and regulations for hovercraft construction can be stated. In addition regulatory documents concerned with stability, seaworthiness and the calculation methods determining the static and dynamic deformation have not reached public literature.

The aim in writing this book has been to summarize the technical experience, both in China and abroad, to systematically describe the theory and design of hovercraft, and endeavour to connect the theories with practice in order to solve practical problems in hovercraft design.

There are three parts to this book. The first chapter gives a general introduction to hovercraft, which introduces briefly the classification of hovercraft, and the development and civil and military applications of the hovercraft in China and abroad in the last three decades. The second part, from Chapters 2 to 9, systematically describes ACV and SES theory – primarily the hydrodynamics and aerodynamics of cushion systems. The third part, from Chapters 11 to 16, describes the design methods of ACV and SES, including the design criteria and standards for craft performance, lift system design, skirt design, hull structure design, and methods for determining the principal dimensions of craft.

The principles for material presented in this book are to describe the features of air cushion technology, and give sufficient design information to allow the reader to prepare a basic project design. Engineering subjects which are similar to those for conventional ships are not covered here, being available to the student in existing naval architecture or marine engineering texts. Thus, stability here covers only the calculation method for stability of ACV and SES on cushion, and not stability of hovercraft while floating off cushion.

With respect to the design of machinery and propulsion systems of ACV and SES, for instance, air or water propeller design, water-jet propulsion installation and machinery installtion in hovercraft, which is rather different from that on conventional ships, these are covered in summary in the last chapters.

The intent is to guide the reader on how to perform machinery and systems selection within ACV or SES overall design. Detail design of these systems requires support of specialists in turbo-machinery, piping design, etc. who will normally be included in the project team. The student is referred to specialists in these fields for interface engineering advice, or to the marine or aeronautical engineering department at his college or university.

The intended audience for this book are teachers and students, both at undergraduate and postgraduate level in universities, and engineers, technicians and operators who are involved in ACV/SES research, design, construction and operation or wish to work in this field.

During the writing of this book, the authors have had the help and support from senior engineers and researchers of MARIC and used research results and theories from many sources, such as the references listed at the end of this book, and they would like to express sincere thanks to those authors for their inspiration. Meanwhile the authors also would like heartily to thank Professor J.S. Dong of the Chinese Naval Engineering Academy for his help and revision suggestions for this book.

Hovercraft and component manufacturers throughout the world have kindly supplied data and many of the photos. Our thanks for their continuing support and advice.

Alan Bliault and Liang Yun
August 1999

Acknowledgements

The authors wish to thank all organizations and individuals who have assisted in the preparation of this book by supplying key data and illustrations. These include the following: ABS Hovercraft, British Hovercraft Corporation, Dowty, Griffon Hovercraft, Hoffman Propeller, Hovermarine International, KaMeWa, KHD Deutz, Kvaerner, Marine Design and Research Institute of China (MARIC), MJP Waterjets, Mitsui Shipbuilding Corporation, MTU Motoren, Rolls Royce, the US Navy, and many persons too numerous to name individually. Thank you all sincerely.

Publications of the China Society of Naval Architects and Marine Engineers (CSNAME), the Society of Naval Architects and Marine Engineers (USA), the Royal Institution of Naval Architects (UK), and the Canadian Aeronautics and Space Institute document that core research by engineers and scientists on ACV and SES which has been an essential foundation resource for our work. We trust that this innovative material has been repressented acceptably in this book.

The tremendous assistance of colleagues at MARIC, as well as assistance and inspiration of experts, professors, and students at the Harbin Shipbuilding Engineering Institute, Wu Han Water Transportation Engineering University, Naval Engineering Academy of China, and other shipyards and users in China, is gratefully acknowledged as the driving force behind the publication of this book.

Sincere thanks goes to our two families over the long period of preparation, which has spanned most of the last decade.

Finally, the staff at Arnold have given tremendous support to see the task through. Many thanks for your unending patience!

This page intentionally left blank

1

Introduction to hovercraft

1.1 Hovercraft beginnings

Transport is driven by speed. Since the 1970s, with the price of fuel becoming an important component of operating costs, transport efficiency has become a significant factor guiding concept development. During the last century, the service speed of many transport concepts has dramatically increased, taking advantage of the rapid development of internal combustion engines. Aeroplane flying speed has increased by a factor of 10, and the automobile by a factor of three. In contrast, the highest commercial ship speeds have increased by less than a factor of two, to a service speed of about 40 knots.

Some planing craft and fast naval vessels reached this speed in the 1920s. They were able to do this because payload was not a key requirement, so that most of the carrying capacity could be devoted to power plant and fuel. Hydrodynamic resistance was the prime factor limiting their performance. A displacement ship moving at high speed through the water causes wavemaking drag in proportion to the square of its speed. This limits the maximum speed for which a ship may be designed, due to practical limitations for installed power. It is possible, however, to design ship forms using the surface planing principle to reduce wavemaking at higher speeds. Many planing boat designs have been built, though the power required for high speed has limited their size. Their application has mostly been for fast pleasure and racing craft, and for military vessels such as fast patrol boats.

Planing vessels demonstrated the potential for increased speed, but slamming caused by wave encounter in a seaway still created problems for crews, passengers and the vessels themselves, due to high vertical accelerations. Two possibilities to avoid slamming are either to isolate the hull from contact with the water surface, or submerge it as completely as possible under the water to reduce surface wave induced drag. Hydrofoils, air lubricated craft, amphibious hovercraft (ACV), surface effect ships (SES) and wing in ground effect machines (WIG and PARWIG) arose from the first idea, while the latter concept produced the small waterplane thin hull vessel (SWATH) and, more recently, thin water plane area high speed catamarans. Fig. 1.1 shows a classification of high speed marine vehicle types.

ACV and SES – the subject of this book – developed from the idea to design a craft which is supported by a pressurized air 'cushion'. By this means the hard structure is

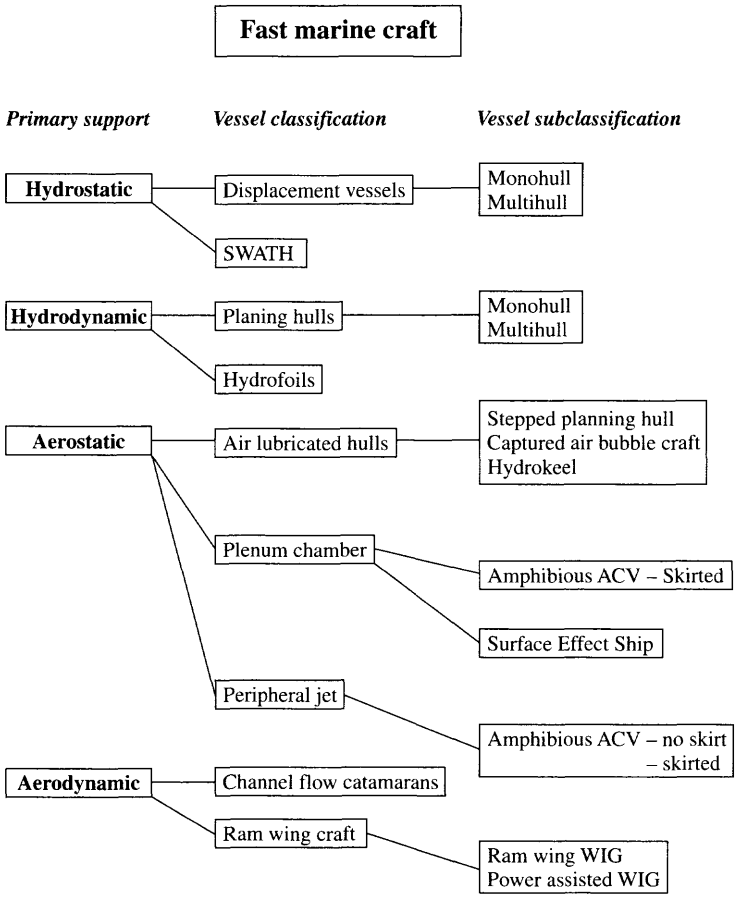

Fig. 1.1 Classification of high-performance marine vehicles.

just far enough away from the water surface to reduce the surface interference, water drag and wavemaking, while at the same time close enough to trap the pressurized air between the ground and the lifted body. Under these circumstances the pressure generated is many times greater than the increased pressure under a free aerofoil, while the drag of the lifted body is much reduced compared to a planing surface.

The idea to take advantage of an air cushion to reduce the water drag of a marine craft has actually been established for over one hundred years. [210] [211] In Great Britain, Sir John I. Thornycroft worked on the idea to create a thin layer of air over the wetted surface of a ship, and was awarded a UK patent in 1877. He developed a number of captured air bubble hull forms with cavities and steps in the bottom and model tested them as alternatives to conventional displacement torpedo boats, which his company built for the British Navy at the time. No full scale vessels were built to translate the idea into practice, though the model testing did give favourable results.

A patent for air lubrication to a more conventional hull form was awarded to Gustav de Laval, a Swedish engineer, in 1882. A ship was built based on the proposals,

but Laval's experiments were not successful. The air lubrication created a turbulent mixture of air bubbles and water around the hull, rather than a consistent layer of air to isolate the hull surface, and so drag was not reduced.

Air lubrication has been pursued at various times since these early experiments by engineers and scientists. In practice it has been found that it is very difficult to create a consistent drag reducing air film on the wetted surface of a normal displacement hull. On the contrary sometimes an additional turbulent layer is added, increasing the water friction drag. A more substantial 'captured air bubble' is needed.

In 1925, D. K. Warner used the captured air bubble principle to win a boat race in Connecticut, USA. He used a sidewall craft with planing bow and stern seals. A little later, the Finnish engineer Toivio Kaario developed and built prototypes of both the plenum chamber craft and the first ram wing craft (Fig. 1.2).

To investigate thin film air lubrication, some experiments were carried out in the towing tank of MARIC in Shanghai, China by the author and his colleagues in 1968, but the tests verified the earlier results of Laval and others. Based on these results they confirmed that a significant air gap was necessary to separate the ship hull fully from the water surface. This needed a concave or tunnel hull form.

In the mid 1950s in the UK, Christopher Cockerell developed the idea for high pressure air jet curtains to provide a much greater air gap. This invention provided sufficient potential for a prospective new vehicle technology that the British and later the US government committed large funds to develop ACV and SES. China and the USSR also supported major programmes with similar goals over the same period.

Air cushion supported vehicles could only be successfully developed using suitable light materials for the hull and engines. Initial prototypes used much experience from aircraft design and manufacture to achieve the necessary power to weight ratio. Experience from amphibious aeroplanes or flying boats was particularly valuable since normal aircraft materials are not generally designed to resist corrosion when

Fig. 1.2 Finnish ACV constructed by Toivio Kaario in 1935.

immersed in salt water – an important design parameter for marine vehicles. Additionally, it suggested a number of alternatives to the basic principle of pumping air into a cavity under a hull, using a modified wing form instead, to achieve vehicles with speeds closer to that of aircraft. Several vehicle concepts have developed from this work.

Amphibious hovercraft (or ACV)

The amphibious hovercraft (Fig. 1.3) is supported totally by its air cushion, with an air curtain (high pressure jet) or a flexible skirt system around its periphery to seal the cushion air. These craft possess a shallow draft (or a negative draft of the hull structure itself) and amphibious characteristics. They are either passive (being towed by other equipment) or active, i.e. propelled by air propellers or fans. Some 'hybrid' craft have used surface stroking, balloon wheels, outboard motors and water jets to achieve different utility requirements.

Fig. 1.3 First Chinese medium-size amphibious hovercraft model 722-1.

Sidewall hovercraft (or SES)

This concept (Figs 1.4 and 1.5) reduces the flexible skirt to a seal at the bow and stern of a marine (non-amphibious) craft, using walls or hulls like a catamaran at the sides. The walls or hulls at both sides of the craft, and the bow/stern seal installation, are designed to minimize the lift power.

Due to the lack of air leakage at the craft sides, lift power can be reduced significantly compared with an ACV. Also, it is possible to install conventional water propellers or waterjet propulsion, with rather smaller machinery space requirements compared to that for air propellers or fans used on ACVs. This more compact machinery arrangement, combined with the possibility for higher cushion pressure supporting higher specific payload, has made a transition to larger size much easier for this concept than for the ACV.

Fig. 1.4 Chinese passenger sidewall hovercraft model 719-II.

Fig. 1.5 First Chinese passenger sidewall hovercraft type, *Jin Sah River.*

Wing-in-ground effect (WIG) and power augmented ram wing (PARWIG) craft

These craft are rather different from the ACV or SES. They are more like low flying aircraft, and use ground proximity to increase lift on the specially shaped wing. The craft are supported by dynamic lift rather than a static cushion.

The WIG (Fig. 1.6) initially floats on the water and its take-off is similar to a seaplane. An aeroplane wing operated close to the ground generates lift at the pressurized surface of the wings which is increased significantly due to the surface effect. The aero-hydrodynamic characteristics of a WIG are therefore a significant optimization of the design of a seaplane to improve payload.

The PARWIG shown in Fig. 1.7 differs from a WIG by the different location of lift fans, in which the lift fans (or bow thrusters) are located at the bow and beyond the air cushion; consequently a large amount of air can be directly injected into the

cushion space under the wing and produce static lift. This gives a PARWIG the ability to hover through static cushion lift alone. Due to the distinct differences for both hydrodynamics and structural design between PAR/WIG and ACV/SES craft, the theory and design of PAR/WIG are not discussed further in this book.

Air cushion craft are part of the larger group of high performance vehicles shown in Fig. 1.1, and may be divided as shown in Fig. 1.8 with respect to their operational features, applications, flexible skirt system and means of propulsion.

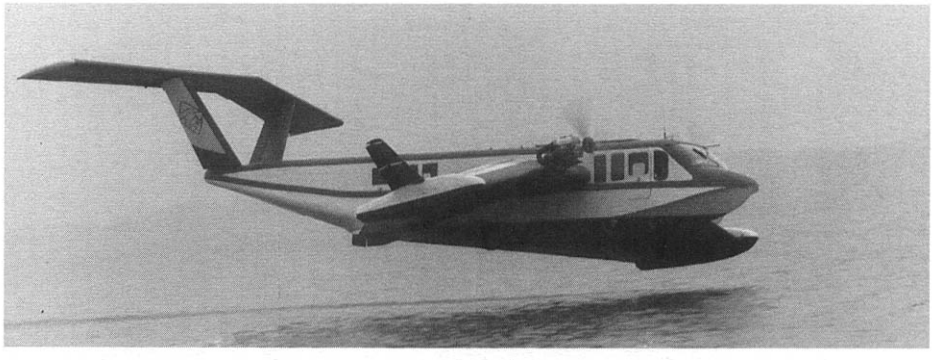

Fig. 1.6 Chinese ram wing craft model 902.

Fig. 1.7 First Chinese power augmented wing in ground effect craft model 750.

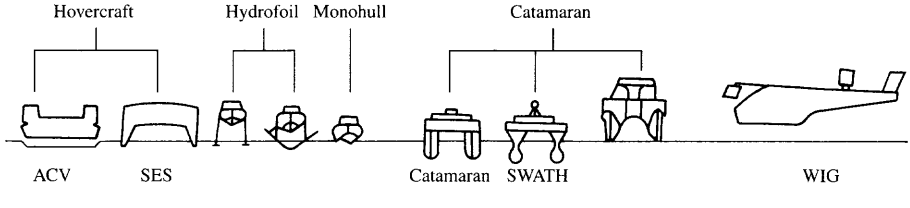

Fig. 1.8 Classification of hovercraft.

The work of Sir Christopher Cockerell resulted in the first successful full scale hovercraft to be built in Europe, the Saunders Roe SR.N1, which crossed the English Channel for the first time on July 25, 1959. China began her own hovercraft research in 1957 in Harbin Shipbuilding Engineering Institute, which successfully operated their first open sea trials with a plenum chamber cushion hovercraft on the coast of Port Lu Shun in July 1959. The principal particulars for both the Chinese and British prototype hovercraft may be seen in Table 1.1.

Table 1.1 *Principal particulars for the first Chinese and British hovercraft*

Craft Name	SR.N1 (Fig 1.9)	Craft '33' (Fig 1.10)
Nationality	England	China
Research and Manufacturing Unit	Saunders Roe, Cowes, IoW	Harbin Shipbuilding Engineering Institute, Harbin Aeroplane Manufactory
Craft Type	Peripheral Jet	Plenum Chamber
Craft Weight (tonnes)	3.4	4.0
Machinery	Aviation piston engines with a total output of 319.7 kW, 70% of which is used as lift power and 30% for propulsion	Aviation piston Engines 176.4 kW for lift and 117.6 kW for propulsion
Hull Materials	Aluminium Alloy	Aluminium Alloy
First Sea Trial	English Channel	Port Lu Shun
Distance	25 nautical miles	16 nautical miles

Fig. 1.9 SR.N1 – the first British ACV, which successfully crossed the English Channel.

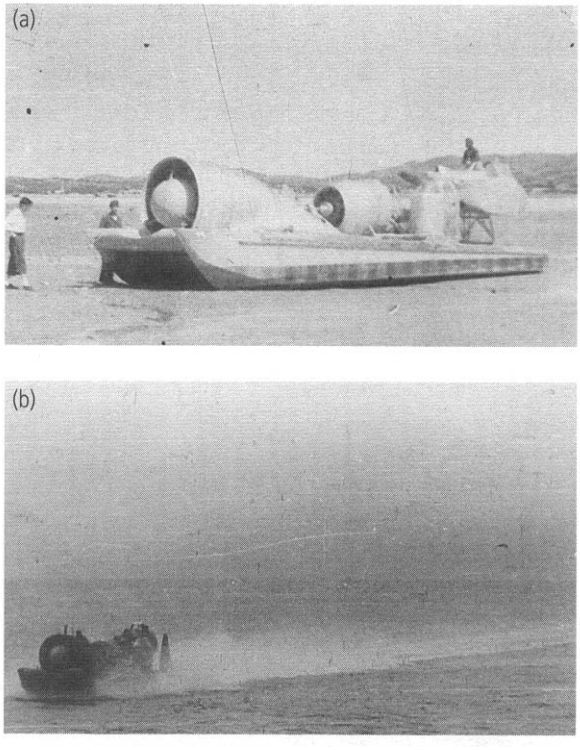

Fig. 1.10 First Chinese experimental hovercraft (with plenum chamber cushion) successfully operated in long range in the coast of Port Lu Shun in July 1959, (a) on beach; (b) operating at high speed.

Since these first sea trials for hovercraft were successfully undertaken both in China and England, the number of hovercraft designed and built for both commercial and military purposes has exceeded 2000 world-wide, including as many as 1000 Soviet hover platforms in the Arctic and oil exploration fields. Thanks to rapidly developing materials, engines, electronics and computer systems in recent years, hovercraft have developed quickly from the research stage into commercial and military applications, (see comparisons with other transport concepts in Table 1.2) reaching the high speeds aimed for in just 20 years, a rare achievement in the development of transport concepts. Examples of this are the US SES-100B, weighing a hundred tons and operated at a speed of 90.3 knots, and the BHC SR.N4 ACV which has achieved similar speeds to service across the English channel when lightly loaded.

Hovercraft have had their difficulties during development in the 60s and 70s, in the same way as most new transport concepts. The concept has now matured, and SES in particular are beginning to be developed at the size originally predicted by the early pioneers: 1000 tonnes and larger. Although different approaches have been adopted for hovercraft development in different countries, they have followed almost the same stages: initial research, concept development, market development and then the development stage again to improve economic performance to compete with craft such as fast catamarans which have developed so rapidly since 1985.

In the following sections of Chapter 1 we will summarise the development of

Table 1.2 Time interval for various military transport vehicles from invention to first application

Type of Vehicle	Time Interval from invention to first application (years)
Steam boat	41
Hydrofoil craft	35
Submarine	25
Hovercraft	**13**
Jet aircraft	12
Aircraft	8

hovercraft, focussing on the UK, former USSR, USA and China which have been leading centres of both analytical and practical craft development.

In Britain the hovercraft has been developed mainly for civil applications, while the US government has strongly supported development for military use, and only lately has commercial interest increased. In China, the main developments paralleled the UK, beginning with prototypes for full scale testing, followed by commercial craft, and some experimental military vehicles. Most ACV and SES in China are for commercial use. In the former USSR medium sized amphibious hovercraft have been developed for military use, SES for inland river transport and air cushion platforms for oil exploration, followed in the late 1970s by some very large military vechicles. Less information is available about the USSR craft, though it is clear that similar technology developed in parallel with the other three major centres described here.

While these countries have been pioneers in the design and construction of ACV and SES, many others now have significant programmes. In Norway, large SES have been developed as Coastal Mine Warfare vessels and Fast Patrol craft. In Korea significant numbers of large commercial SES and ACVs have been built, and in Japan a large development programme has been carried out through the 1990s to develop SES high speed short sea cargo vessels.

1.2 ACV and SES development in the UK

Initial research: before 1963

In 1953, Christopher Cockerell, an electronics engineer with a small commercial boat-building interest, began thinking about the age-old problem of decreasing the resistance to ships' travel through the water. First he tried introducing air films under model boats to give a kind of lubricated surface. This was not successful and the next stages towards the evolution of the hovercraft principle are best described in his own words:

> *After I had learnt from, and found out the shortcomings of 'air-lubrication' experimentally, the first idea I had was fixed sidewalls with hinged doors at the ends, with air pumped into the centre. The next idea, at about the end of 1954, was fixed sidewalls with water curtains sealing the ends. I stuck here for a bit,*

because I didn't know enough to be able to work out the probable duct and other losses and the sort of power that would be required.

Then one Saturday evening I thought I would have a look at using air curtains. A simple calculation looked all right on a power basis, and so that Sunday I made up an annular jet using two coffee tins, and found that the air did follow the 'predicted' path and that there was a 'predicted' gain in lift – very exiting.

Cockerell secured the assistance of a fellow boatbuilder in constructing a working model of the type of craft envisaged. This was used as a test model for several years and is now in the Science Museum in London. In December 1955 Cockerell applied for his first British patent covering lift by means of peripheral annular jets.

Until 1956, air cushion technology was considered to have military potential and was put on the list of projects which had public information restrictions when it was offered to the British Government for development sponsorship by Sir Christopher Cockerell. At this time, study was centred on investigation using free flying models. For the next two years he made the rounds of industry and government departments with remarkably little to show for it. The shipbuilding firms said 'It's not a ship – try the aircraft industry', and the aircraft firms said 'It's not an aircraft – try the shipbuilders'. Three engine manufacturers said 'Not for us, but if you want your invention taken up, remember to use our engines'. However, he did receive valuable encouragement from Mr R. A. Shaw of the Ministry of Supply, and eventually during 1957 the Ministry approached Saunders-Roe who accepted a contract to undertake a feasibility study and to do model tests.

The Saunders-Roe design team who undertook this initial study also formed the nucleus of British Hovercraft Corporation's technical staff later in the 1960s. Prior to involvement with hovercraft they had for many years been engaged in the design and construction of flying boats and hydrofoils. It was precisely because of this background of 'fish and fowl' expertise that the hovercraft principle was enthusiastically pursued.

Christopher Cockerell in the meantime had approached the National Research Development Corporation (N.R.D.C.) who also realised that hovercraft were likely to became a revolutionary new form of transport and through them, a subsidiary Company known as Hovercraft Development Limited (H.D.L.) was set up in January 1958 with Cockerell leading the research group as Technical Director.

The report of the Saunders-Roe feasibility study was favourable, as a result of which N.R.D.C. placed a further contract with the company for a programme of work which included the design and manufacture of a manned development craft designated SR.N1 (Fig. 1.9). This historic craft was completed on 28th May 1959. On July 25th 1959, in its original form, it crossed the English Channel from Calais to Dover with Christopher Cockerell on board to mark the 50th anniversary of the first cross-channel flight by Bleriot in an aeroplane.

Although the first cross channel operations on relatively calm water were very successful, the craft performance, manoeuvrability, seakeeping quality and propulsion efficiency were very poor. The craft had an air gap over the ground of about 100 mm whilst the lift power, at about 36.7 kW/t, was rather high. The efficiency of the air jet propulsion used was low, and manoeuvrability was so poor that the pilot was unable to handle the craft in a stable manner. The SR.N1 was built in an aviation factory, and aviation engines, equipment, structures and construction technology were used. For

this reason, the construction and operation costs were high relative to other marine vehicles. Although it was only originally intended for a six month trials programme, it eventually proved to be an excellent research tool for over four years. This small craft (weighing 4 tons) demonstrated the basic principles of riding on a cushion of air to be sound. A series of development modifications associated with alternative power plant and plan-form shapes in succeeding years increased the speed boundary from 25 knots to as high as 60 knots. More significant than the increased speed in calm conditions was the development of long flexible skirts which enabled the craft to operate successfully in 4–5 feet waves, whereas in its original form it was only capable of operating in wave heights of no more than 1.5 feet.

The invention of flexible skirts by C. H. Latimer Needham in 1958, which he sold to Saunders-Roe in 1961, and later the segmented skirt by Dennis Bliss of Hovercraft Development Limited (HDL) represented a break-through in hovercraft technology from experimental investigation to engineering practice. The cushion depth could be increased several hundred times, allowing practical operation of hovercraft on rough water and unprepared ground. In addition, skirt shifting systems, controllable pitch air propellers, jetted rudders and puff ports began to be used for improving the manoeuvrability, course stability and obstacle capability of hovercraft.

Concept development: from the early 60s to the early 70s

The results of research trials with SR.N1 indicated that a truly competitive commercial hover ferry would probably need to be 125 to 150 tons in weight and some four times the length and breadth of the SR.N1 manned model, in order to cope with 4 to 6 feet seas. A jump from 4 to 125 tons represented such a major engineering step that it was decided by Saunders-Roe to approach this in three stages over a 7 years programme.[207] The first stage was implemented with the 27 ton SR.N2, which was used to develop the swivelling pylon mounted propeller control system, and the integrated lift/propulsion concept. The second step was to stretch the SR.N2 design to become SR.N3, and obtain the largest craft capable of being operated with the 3600 horsepower of the SR.N2. The intended final stage was to use the experience gained with the developed machinery and systems to produce a 125 ton SR.N4 (Fig. 1.11). Westland Aircraft Limited, who had taken over Saunders-Roe Limited in 1959, backed this long range programme, and in 1960 the SR.N2 was jointly funded by N.R.D.C. and Westland. SR.N2, capable of carrying 70 passengers at 60 knots, was launched in January 1962 and was used on trial passenger services in the Solent and the Bristol Channel. Additionally it was taken to Canada for trials and made an historic crossing of the Lachine Rapids on the St. Lawrence river just below Montreal. The SR.N3 was originally intended as a 150 seat craft, but it was eventually ordered by the British Government for military evaluation trials. These continued for many years, culminating in explosion trials for shock resistance of air cushions against underwater mines [21, 213] (see Fig. 1.12). These trials were the start of a new application for ACV and SES, mine countermeasures, which continues in many countries today, particularly Norway and the USA.

During the 1961–3 period a number of other British companies developed research and experimental craft with a view to commercialization later on. Vickers built the VA.1 to 3 series, Denny Brothers built two sidewall craft, Britten-Norman built the

Fig. 1.11 The world's largest commercial amphibious hovercraft, the SR.N4.

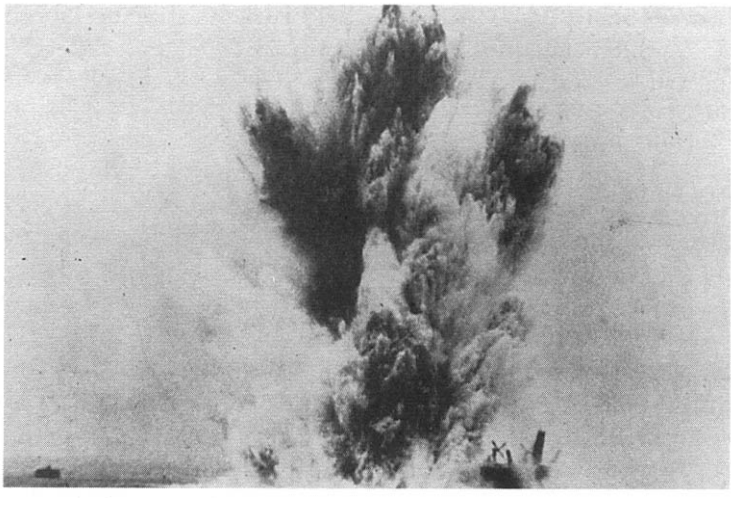

Fig. 1.12 British ACV SR.N3 on underwater explosion tests.

CC1, 2, and 5 and H.D.L. designed and built its own HD–1. The basic craft performance problems encountered during the early 60s encouraged continued development, especially in the application of flexible skirts. Nevertheless, as operating experience was gained, researchers, designers and manufacturers all faced many difficulties along the way. Various practical problems had to be solved, for instance improving skirt life from a few hours to thousands of hours, so as to meet the commercial user's requirements; designing filters to prevent accumulation of salt, which is very harmful for engines, especially gas turbines, due to the significant spray caused by hovercraft; anti erosion design for air propellers and lift fans; and internal/external noise

reduction. A number of accidents occurred to hovercraft in service at this stage due partly to the lack of handling experience and understanding of the capabilities and limitations of transverse/course stability of ACVs at high speed. ACVs operate with significant sideslip, and have very different handling characteristics to other marine craft due to unique phenomena such as 'plough-in'. Operation over land or ice has no real parallel with other vehicles, so experience had to be built from zero. Understanding the causes of these accidental events and revising craft design or handling procedures to prevent recurrence was essential to continued technical progress.

Reference 4 recorded damage from accidents which happened in the period between 1963–1978, as shown in Table 1.3. This shows that 82% of such accidents were in the time interval between 1967–1974, i.e. the concept development stage of hovercraft. The table details all accidents except those in the former Soviet Union, for which data are not available. A large number of accidents also happened to smaller (utility or recreation) hovercraft, but only a small number of these were used commercially so that the details are not accessible. A selection of the key accidents recorded in this period are illustrated in Table 1.4.

To return to developments in the 60s, BHC's experience gained with SR.N2 and SR.N3, together with the improving skirt technology developed through SR.N1, SR.N5 and SR.N6, indicated that the original proposed design of the SR.N4 needed to be revised. Project studies commenced in 1964, and the SR.N4 emerged with a new shape, structural design, engines and skirt arrangements at an all up weight of 165 tons. The SR.N4 commenced trials in February 1968, and made its first channel crossing from England to France on the 11th June, about 9 years after the historic SR.N1 crossing. SR.N4 was the first truly open-water passenger/car ACV ferry capable of all-year-round services over sea routes where wave heights of 8 to 12 feet can be encountered. It has achieved speeds in excess of 90 knots and, operated out of specially designed terminals at Dover and Calais, can normally deliver passengers and cars across the channel faster than services through the new Channel tunnel, 25 years after the craft first entered service.

The SR.N4 Mk2 (Fig. 1.11), in its basic form weighing 165 tons, can accommodate 254 seated passengers and 30 cars. SR.N4 is powered by four Rolls-Royce 'Marine Proteus' gas turbine engines of 3400 shp, each driving a variable pitch propeller mounted on a pylon (see Fig. 6.7). Interconnected with the propellers are four centrifugal fans for delivering cushion air. The craft is operated by a three man crew and is controlled by varying the propeller blade angles and by swivelling the pylons to change the direction of thrust. Some 5 years after its introduction the SR.N4 was

Table 1.3 Accidents and Incidents to Hovercraft in Western countries from 1963–1978[4]

Incident	Damaged	Sinking	Total
Overturning	41	2	43
Damage due to strong wind, rough sea, grounding	31	3	34
Collision	19	1	20
Fire and explosion	5	8	13
Damage due to technical faults	18	–	18
Ice damage	21	1	22
Other damage	5	–	5
Total	**140**	**15**	**155**

Table 1.4 Early Hovercraft accidents causing overturning and major skirt damage

Item	Model	Country	Date	Damage	Data source
1	XR-1	USA	Dec. 1964	Transverse overturning in waves	ACV 1965 Vol. 6 No 34
2	SR.N5-004	UK	Apr. 1965	Overturn in calm water due to plough-in at yaw angle (in Norway)	ACV 1965 Vol. 6 No 34
3	SR.N6-012	UK	Mar. 1972	Overturn, flooding, in very choppy seas on the Solent, 5 passengers died of drowning	Hovercraft & Hydrofoil 1972 No 1
4	SR.N5-007	UK	May 1965	Overturn in calm water due to plough-in at yaw angle (in San Francisco, USA)	ACV 1965 Vol. 6 No 35
5	SR.N5-005	UK	July 1965	Overturn in calm water due to plough-in at yaw angle (in UK waters)	ACV 1965 Vol. 6 No 39
6	SR.N4-001	UK	Sept. 1968	Skirt damage from waves, subsequently hull structure damage, while in service	Lloyds List 1968, 47951
7	SR.N4-003	UK	July 1971	Skirt damaged and hull damage while in service	Hovercraft & Hydrofoil 1971 No 7
8	SK5-015	UK	Nov. 1971	Severe damage to hull structure from waves, craft sank	ACV 1976 Vol. 11 No 7
9	N.500	France	May 1977	Craft caught fire while in workshop, almost completely destroyed	Hovercraft & Hydrofoil Vol. 16 No 7

stretched to the Mark III version, at 208 tons, so that 400 seated passengers and 55 cars and coaches could be accommodated. In itself, the SR.N4 is more than just another hovercraft, rather, it even now symbolises the hopes and aspirations of the entire industry, particularly those elements pursuing the development of the amphibious skirted hovercraft. The basic concept, modified to include the technological developments in gas turbine engines, skirts and structures is still capable of extension to around 750 tonnes, with the tremendous work capacity that this represents.

At B.H.C., [207] the follow up to SR.N4, designated the BH.7, was built first as a trials craft for the British Royal Navy, and later as a patrol craft for Iran. Smaller than the SR.N4 and grossing 45 tons it makes extensive use of components developed for SR.N4. While the trials showed that the BH.7 was a useful coastal patrol craft, its operation was too different to the units in many navies already operating traditional high speed patrol boats, so the expected market did not arise. The British military services formed a joint trials unit to test and develop ACV technology in September 1961, located at a Naval Air Station (HMS Ariel, Later HMS Daedalus) in Gosport. The unit was in operation until December 31st 1974, and during this period tested most of the major marques developed in the UK. [213] A flypast of SR.N6, BH.7, and Vosper Thornycroft VT.2 is shown in Fig. 1.13. Hovermarine Limited was founded in the UK in 1965 in order to undertake the research and development of sidewall hovercraft which offered the possibility to save lift power and be more attractive to the traditional ferry operators. The first of this kind of craft, HM–2, was launched in 1968 (Figs 1.14 to 1.17). This was developed with a modified skirt system to become HM–2 MK2, and lengthened from 16m to 18m to become HM–2 MK3 over a relatively short period, and later to 21m, to become the HM–221 (Fig. 1.18).

Fig. 1.13 British military ACVs from the 1970s, SR.N6, BH.7 and VT.2, in formation on the Solent.

About 30 HM–2 sidewall hovercraft are operated by the Hong Kong and Yaumati Ferry Company on various Hong Kong routes, while many SR.N6s, and HM–2s were operated on British mainland coastal routes for transporting passengers, such as Isle of Wight to Southampton and Portsmouth, from the early 1970s. Many of these services were short-lived, lasting only a summer season or so. The Solent services continue successfully, having progressed from SR.N6 to AP1-88 craft. Meanwhile in Japan, Mitsui, who had a technology sharing agreement with BHC, built and supplied the MV.PP5 (Fig. 1.19) and the larger MV.PP15 to passenger transport routes on the coast.

In the later 60s and early 70s ambitious development programmes were mapped out by the three main UK companies, progressing through various stages to proposals for open ocean hover freighters of up to 4000 tons with a transatlantic range. Such craft were projected to have exceptionally high work capacity and carry payloads of up to 2000 tons of containerized cargo. On such craft, air screw popullsion would be replaced by water-jets as limitations imposed by propeller development and transmission gearing occur at an all up weight of 750 to 1000 tons. The main problem occurred

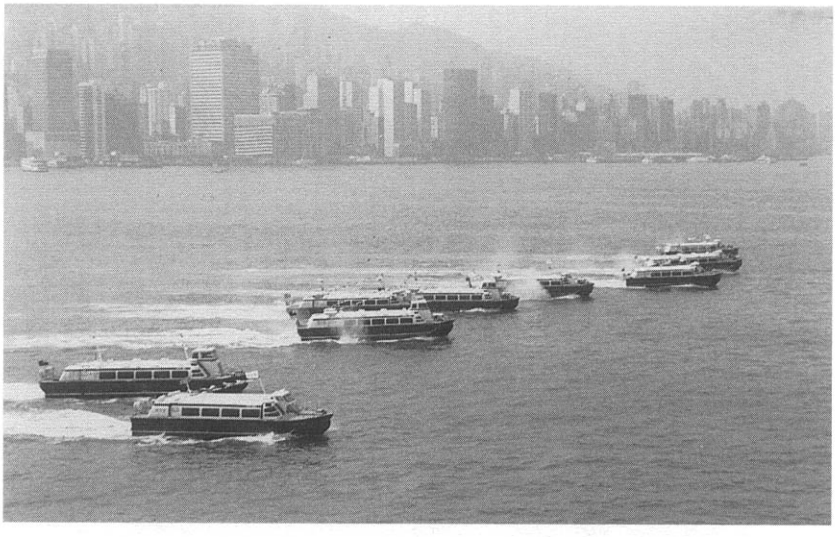

Fig. 1.14 British sidewall hovercraft HM-218 in operation in Hong Kong.

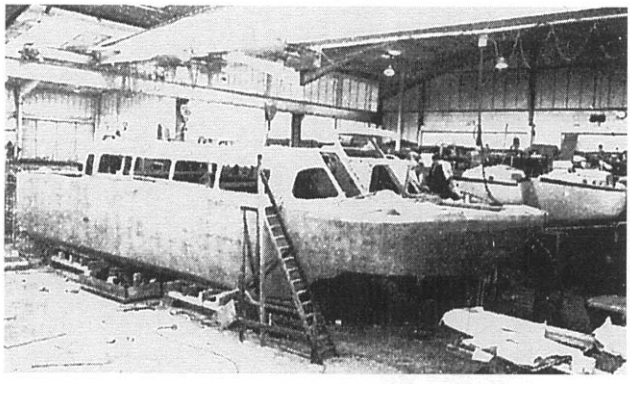

Fig. 1.15 HM-2 glass reinforced structures under construction.

shortly after these ideas were put forward: the fuel crisis of 1974. Suddenly the world changed. With fuel costs now a major consideration, these very large ACV and SES concepts became uneconomic, and thus not attractive to the prospective operators, the ferry companies. It was only in the mid 1990s when fuel costs reduced again in relative terms and became more stable, that very high speed ferries became economically attractive. The vogue of the early 1990s had been catamarans in sizes now approaching that originally projected for SES. With this market acceptance, the next step will eventually be the re-introduction of air cushion technology to further increase speeds and work capacity above the practical limits for catamarans.

After ten years' endeavour, many of the practical problems had been solved for ACV and SES in the UK, and hovercraft operated on well known routes in many areas of the world. The SR.N4 fleets of Hoverlloyd (4 craft) and Seaspeed (2 craft) operated in the English channel (Fig. 1.11) to transport almost two million passengers

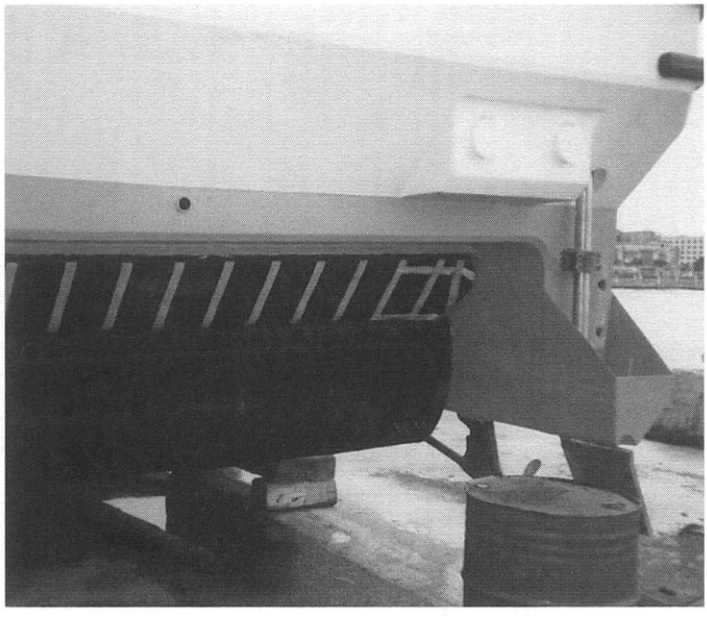

Fig. 1.16 HM-2 stern seal.

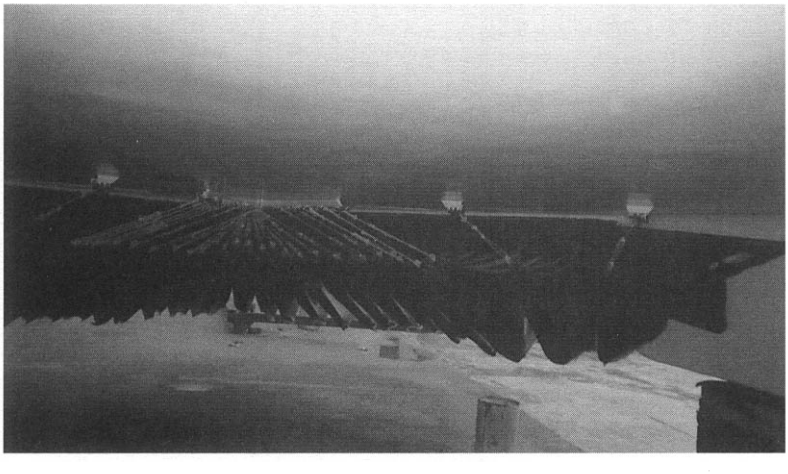

Fig. 1.17 HM-2 bow seal.

and four hundred thousand cars per year. In the 1970s and 80s on average about one third of passengers and cars on these routes were transported by hovercraft, with transport efficiency of about double that of hydrofoil craft.

Market development: from the beginning of the 80s to the present

Although air cushion technology had advanced significantly by the end of the 70s, there were still difficulties to overcome in order for hovercraft to compete fully with

Fig. 1.18 Hovermarine HM-221 SES fireboat on trials before delivery to port of Tacoma.

other transport systems such as hydrofoils, high-speed monohull passenger craft, high speed catamarans and long range buses and trains where appropriate. During the 1970s many companies had been set up in the UK and USA to develop business in constructing ACVs of all sizes from 2 seat recreation craft to large ferries. Many of these companies did not exist very long, often producing little more than design proposals. Those that were active found marketing difficult, as the public found the concept intriguing, and more of a 'solution looking for a problem'. Trial passenger services gained a reputation for unreliability, and short lived operation. Only the established services across the Solent and the Channel proved viable in the long term.

This situation did not support the planned development of larger hoverferries. On the other hand, Hovermarine developed the right 'formula' with their sidewall ferries, which demonstrated reliability and demonstrable economy at higher speeds than available displacement ferries. A tunnel was planned across the English Channel, and construction began in the mid 1980s, which lessened the need for an SR.N4 replacement. At other places, such as Hong Kong to the delta area of the Pearl river, the situation for SES transport market developed rapidly, supplied by Hovermarine Ltd.

Following the initial phase of entrepreneurs establishing companies to build hovercraft, those which survived were those who were able to supply practical vehicles to customers who were mostly in remote areas, on the other side of the world. This is a tall order for a small enterprise, though an essential one for a craft such as the ACV. The use of local representatives is one way forward, though this can also be difficult, since unless the local representative is competent – difficult with a new vehicle concept – then the client will once again become frustrated that the ACV appears not to perform as expected. Expectation by the clients matured over the 1980s, as craft themselves became more reliable, and to some extent 'under-sold' by the manufacturers. While the initially expected expansion of an ACV ferry market did not materialise, due to their limited open sea capability, the utility market for craft with payloads from 10 tonnes downwards developed steadily. This is the core application for ACVs. In the UK, Hovermarine developed a second generation of thin sidewall SES, the 250 seat

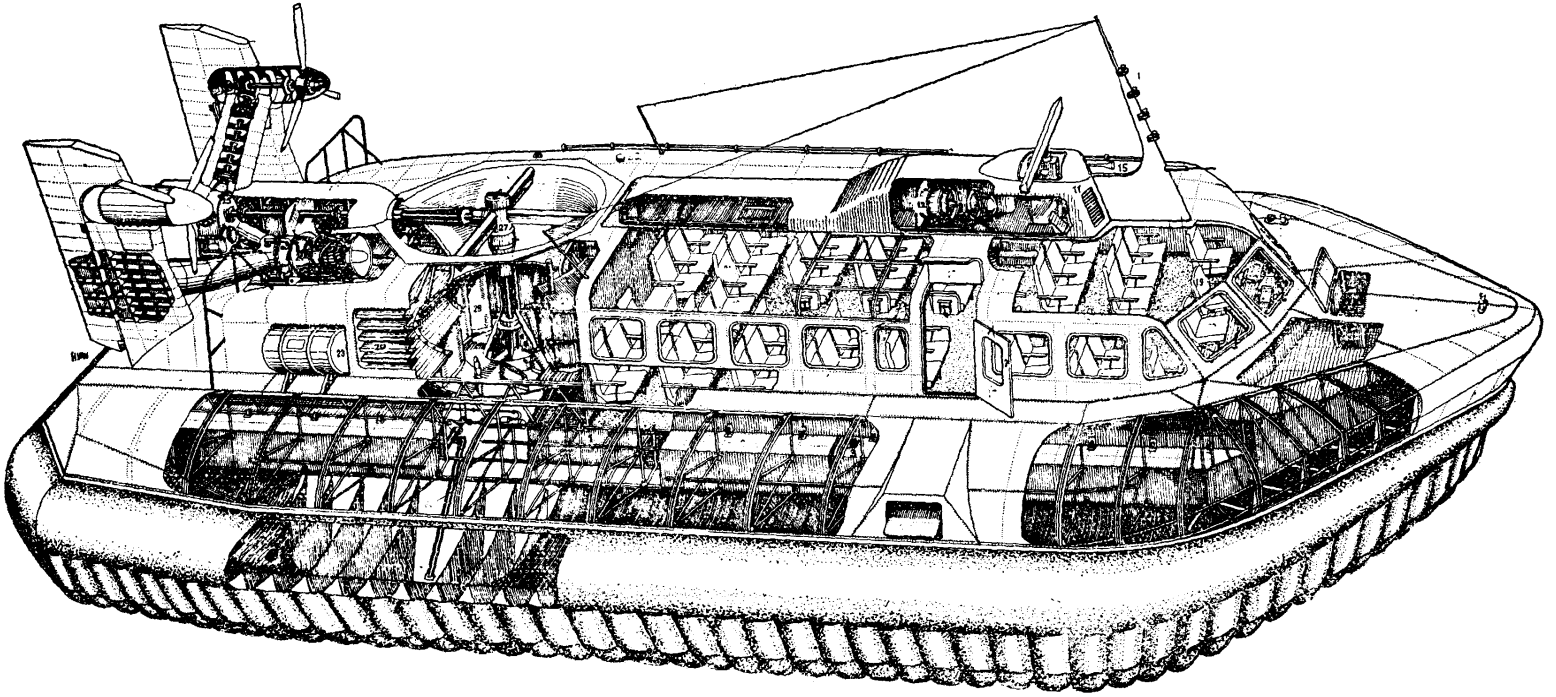

Fig. 1.19 Perspective drawing of Japanese amphibious passenger hovercraft MV.PP5.

HM–5 series, of which two craft were built for service in Hong Kong. Development beyond this point proved difficult, and it took Bell-Halter and Brodrene Aa to move the concept forward in the direction of Air Cushion catamarans in the early 1980s. Hovermarine nevertheless continued to have commercial success with variants of its HM–2. A further trend which began in this period was the transfer from designers, mainly in the UK, to licencees, in Australia and the USA. More recently the AP1.88-400 (Fig. 16.12) construction has been carried out in Canada, and the ABS M10 (Fig. 16.7(b)) has been constructed under licence in Sweden.

The main drive through the 1980s on the technical side was to improve overall service reliability, economy, seakeeping quality, habitability and maintainability. Additionally there was a drive to maintain commercial competition, as catamaran and hydrofoil manufacturers also began to target this market. In the UK some of the measures taken to improve competitive ability in the commercial market were as follows:

1. Replace aviation engines with lightweight marine diesels, and use marine hull materials and ship construction technology in place of aviation methods, so cutting down the cost of craft;
2. Improve the configuration of skirts (for instance, adopting the responsive skirt with low natural frequency) to enhance seakeeing quality and assist item 3, below;
3. Improve the lift and propulsion system to enhance economy and reduce fuel consumption;
4. Improve the internal outfit of cabins and other measures to reduce internal noise level and improve the craft habitability.

Consequently, features of second generation British ACV/SES were:

1. Procurement and operation costs reduced to less than 50% of first generation craft;
2. Maintenance costs significantly reduced;
3. Much reduced noise level, both internal and external to craft;
4. ACV/SES transport efficiency enhanced greatly, as shown in Table 1.5.

While the specific weight of a diesel engine is much higher than a gas turbine, by introducing a series of overall design measures such as responsive skirts, low bag to cushion pressure ratio, lift systems with smaller cushion flow rate etc., main engine power output could be reduced from 74 to 29–37 kW/tonne. For this reason the British ACV AP.1-88 (Fig. 1.20 (a)) was very competitive as a ferry compared to conventional ships when it entered the market. Later, utility versions such as the AP1 88-300 also proved very successful. See Fig. 1.20 (b).

Table 1.5 The reduction of power consumption per ton-knot of British ACV over time

Date of Construction	Craft	Engine	Structure	Total power/(payload, speed) kW/(tonne.knot)
1960	SR.N1	Aircraft, piston	Aluminium, riveted	2.35
1965	SR.N5	Gas turbine	,,	1.83
1970	BH.7	Gas turbine	,,	1.25
1975	SR.N4	Gas turbine	,,	0.74
1980	SR.N4 Mk3	Gas turbine	,,	0.51
1983	AP1.88	Air cooled diesel	Aluminium, welded	0.59

Fig. 1.20 (a) BHC AP188-100 Hovercraft Ferry operating over ice in Dresund between Malmö and Copenhagen. (b) Canadian Coastguard Eastern Division BHC AP1.88-300 Utility ACV Waban Aki.

In the 1960s and 70s BHC had some success in marketing their SR.N6 and BH.7 craft for military service, to Saudi Arabia, Iraq and Iran. There has been no significant fleet development to follow this. The British Navy carried out trials for many years [213] without moving forward to integration of ACV and SES technology with its fleet. This was partly due to defence policy in this period which concentrated on projection of UK power to far flung colonies – the 'blue water' Navy – rather than operations in the European coastal area. Without support from the UK government, it was difficult for British ACV/SES manufacturers to develop and market suitable products for sale abroad. UK companies were therefore limited to what was possible in a self resourced commercial environment. The utility market had requirements which could be met in this respect, and the operational support, though demanding, was not on the scale that military customers would demand.

In the SES market, the UK shipbuilding industry was already in decline from the early 1960s, and so development of larger SES vessels, which would require considerable investment, was not taken up. This opportunity was taken up first by Bell Halter, and latterly by shipyards in a number of other countries.

1.3 ACV and SES development in the former USSR

The former USSR has carried out ACV and SES research since the beginning of the 1960s. More than two hundred sidewall passenger hovercraft have been built since then, and over two hundred amphibious ACVs for military missions and passenger

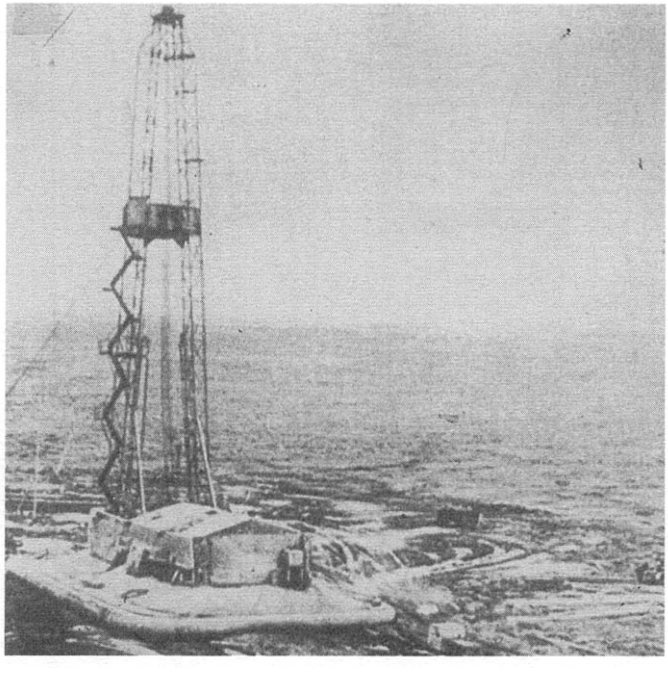

Fig. 1.21 USSR air cushion oil exploration platform model BU-75-VP.

Fig. 1.22 Sormovich *Aist* large amphibious assault ACV.

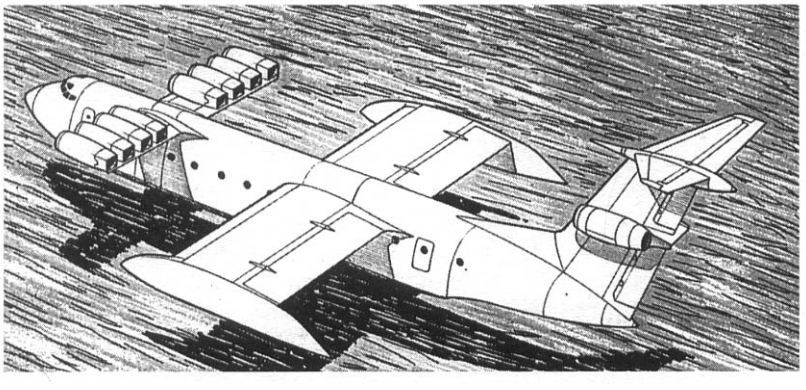

Fig. 1.23 USSR large military WIG *Caspian Sea Monster.*

transport. In addition about 1000 air cushion platforms have been constructed, mainly for oil industry support in marsh/swamp areas (Fig. 1.21). About one hundred military ACV have been constructed, including the five largest amphibious landing craft in the world, called Pormornik (550 tonnes, 57.6 m, 65 knots, payload 120t), over the period 1988–94. Twenty two amphibious landing craft code named AIST by NATO (275t, 47.3 m, 70 knots, payload 90t) were constructed in the 1970s (Fig. 1.22), and sixteen medium sized LEBED amphibious landing craft (87t, 24.4 m, 50 knots cruise, payload of 35 t) during the early 1980s. The LEBED can be operated into the stern docks of large Landing Ships such as the 'Ivan Rogof' class. The USSR has also developed the largest WIG in the world, named 'Caspian Sea Monster' (Fig. 1.23).

The principal design offices and shipyards for ACV and SES are all located in what

has become the Russian Federation. Since 1993 the Russian government has pursued a policy of conversion of its military construction facilities into commercial ventures. The main shipyard which constructed ACVs for the Russian Navy is located on the river Neva, and is now called Almaz Shipbuilding Company. Almaz built two of the total 31 Gus class amphibious hovercraft (20.6 m, 27 tonnes) which were produced for the Russian Navy between 1969 and 1979. Three Gus can operate out of the Ivan Rogov class landing ships. Almaz shipyard also built two Utenok class (70t, 27 m, 65 knots) amphibious assault craft in 1982. Recently the Dolphin Design Bureau has redeveloped this design as a passenger ferry for 98 persons, marketed by the shipyard as the Utenok-D3. A commercial version of the Pomornik has also been prepared. The Russian Navy also has in service a group of inshore minesweeping ACVs which were commissioned in 1985/86; these are 86m, 100t class vessels.

SES have been principally developed as passenger carrying craft for river traffic, at Krasnoye Sormovo, which has also been the main ACV design group since the early days. Craft were built at the Leningrad, Sosnovka, and Astrakhan shipyards. The Vostok Central Design Bureau, also in St Petersburg (Leningrad), had responsibility for military ACV designs, many of which were built at the Leningrad shipyard.

Soviet commercial developments in the 1960s were initially focused on alternatives to the passenger hydrofoils, which operated along its extensive river network. The resulting sidewall craft had high length to beam ratio, shallow cushions and simple skirt systems, for example the experimental Gorkovchanin from 1969 (Fig. 1.24). Production vessels, mainly the Zarnitsa and Luch classes for 60 to 80 passengers, have been very successful. A number of other designs for more exposed waters have been built as prototypes. Since the breakup of the USSR several design bureaux and shipyards have been developing larger SES designs in closer competition to those available from China, and Korea.

Commercial ACV development has focused on smaller utility craft in the range 6 to 30 seats, with designs such as the Barrs, Gepard, Taifun, Irbis and Puma. Current technical data for these craft may be found in reference 12a and later editions of this book. These craft paralleled the development of craft such as the AV Tiger and Griffon range of craft in the UK. Medium pressure bag and finger skirt designs are used. Nearly 100 Barrs and Gepard have been built since 1981. The 16 seat Puma has

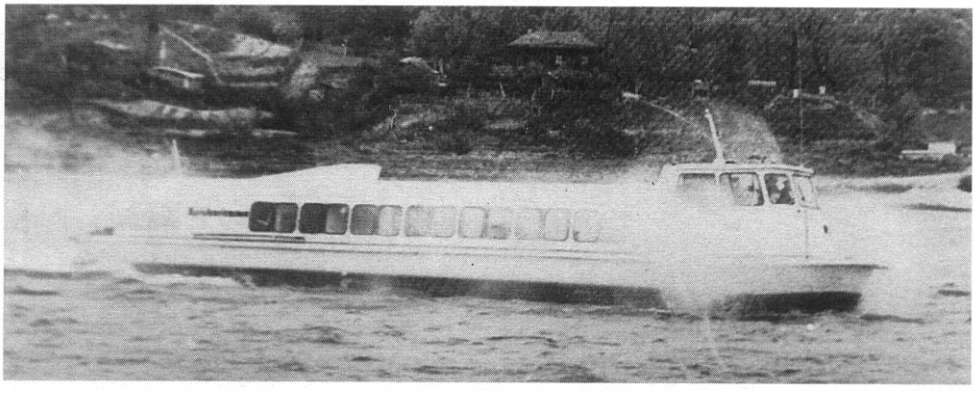

Fig. 1.24 USSR passenger sidewall hovercraft *Gorkovchanin.*

been used as an ambulance vehicle in the region between Tomsk and Kolpashevo from 1985, and in 1987 a passenger service was established with three Pumas between Tomsk and Krasny Yar, a 100 km route along the Volga river.

1.4 US hovercraft development

Amphibious craft

The US Government has supported the development of air cushion technology primarily through its military applications. Americans like to use the aeroplane and car as passenger transport both for long and short range journeys, but have paid less attention to the development of high speed marine vessels as water transport for passengers. For this reason the development of US military hovercraft represents the main development of the US hovercraft. The US Armed Forces initially aimed to apply air cushion technology to amphibious patrol vessels. In the early 1960s a number of experimental craft were built and tested, using air jet curtains, and later skirts, following the lead in the UK. Interestingly, one of the larger test craft, the SKMR-1, used twin fixed ducted propellers for propulsion, a system which is most commonly used today, due to its efficiency.

In the late 60s and early 70s versions of the British SR.N5 were built under licence from BHC by Bell Aerospace, and used in military service in Vietnam. Post Vietnam, the main objective became direct over-the-shore delivery of personnel as a new generation of amphibious landing craft. It was considered that the coast line which could be used as a landing area would increase from 17% for conventional landing craft to 70% for ACVs. For this reason the US Navy realised that the ACV should play a major role in amphibious warfare to decrease combat casualties, and would be a break-through tactic for amphibious warfare as an alternative to using helicopters for personnel transfer. The US navy decided to construct two competitive prototype air cushion craft, the Aerojet General JEFF(A) and Bell JEFF(B), as test craft for this concept of amphibious assault warfare. Each craft weighed about 160t and carried up to 60 tonnes of cargo. The costs of the craft at that time were eighteen million US dollars each. The craft could accommodate both tanks and soldiers. The craft engineering schedule was as shown in the table below.

Primary design	1970
Review and summary of engineering design	1972
Detail design and construction preparations	1971–1975
Construction in factory	1972–1976
The installation of components for subsystems	1975
Delivery to naval test base	1977
Inspection of systems	1976–1987
Craft bollard test	1978
Craft trial	1978
Crew training	1977–1978
Various warfare systems trials, which included tests in Alaska, in Arctic conditions	1977–1984

The US Navy approved the tests and decided to use the prototype craft JEFF(B) as the basis for the amphibious landing craft series LCAC (Landing Craft, Air Cushion). The Navy signed a contract with Bell Textron Aerospace Corporation for building 12

LCAC craft in December 1981, and the first one was launched in May 1984. Further, the prototype trials were successful enough that the US Navy planned to build a total number of 90–110 such LCAC craft during the 80s and 90s. The US naval planning office for amphibious warfare (PMS-377) planned to build landing ships of types LSD-1 and LHD-4, with the capability to accommodate LCACs. In addition, the US Army had built a series of 26 LACV-30 hovercraft for logistic supply, with a payload of 25–30t, power output 2058 kW, and a speed of 40 knots.

Shortly after this period, Bell Halter designed a series of smaller utility craft powered by diesel engines, following the lead of the British AP1.88, and supplied a craft for oil field logistic duties in the Louisiana swamp. However Systems Inc. made agreements with Griffon Hovercraft in the UK and supplied craft for operation at the World Exposition in Vancouver in 1986, logistic support in the Antarctic, and coastal police duties in Maryland.

Similarly to the UK, in the USA a number of smaller enterprises were set up in the 1980s to build utility craft. Their business has been slow in developing, so that entrepreneurs aiming at high growth have been disappointed. The potential nevertheless remains for significant business development in the eastern Gulf of Mexico, and Alaska in particular.

Surface effect ship development

The US Navy were also interested to develop the SES as a military combat ship. They met with several setbacks during the development of these air cushion vehicles, which can be divided into three stages, as outlined below.

In 1963, the US naval aviation development centre constructed a test craft, model XR-1A (Fig. 1.25), which was rather successful. For this reason, under the suggestion

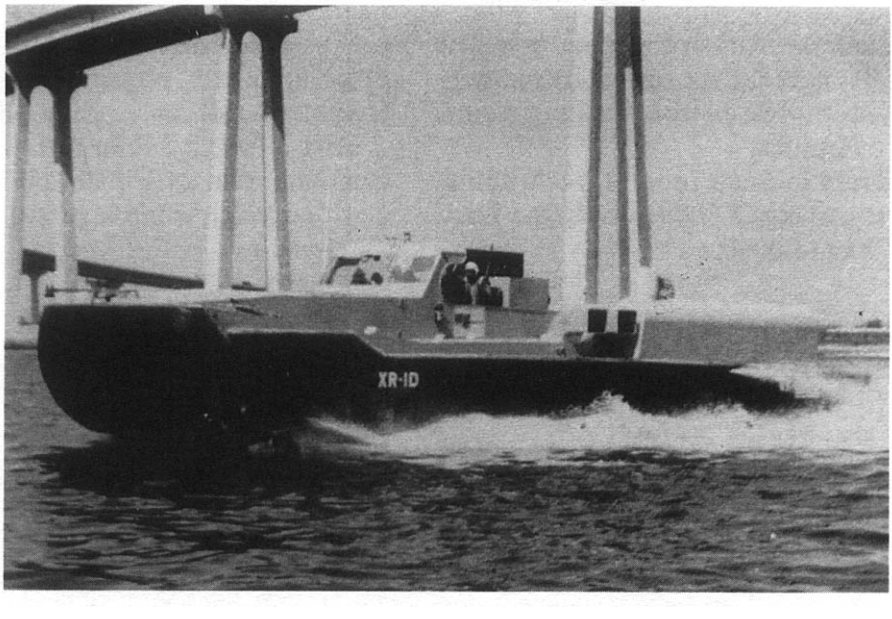

Fig. 1.25 Early US SES test craft XR-1A.

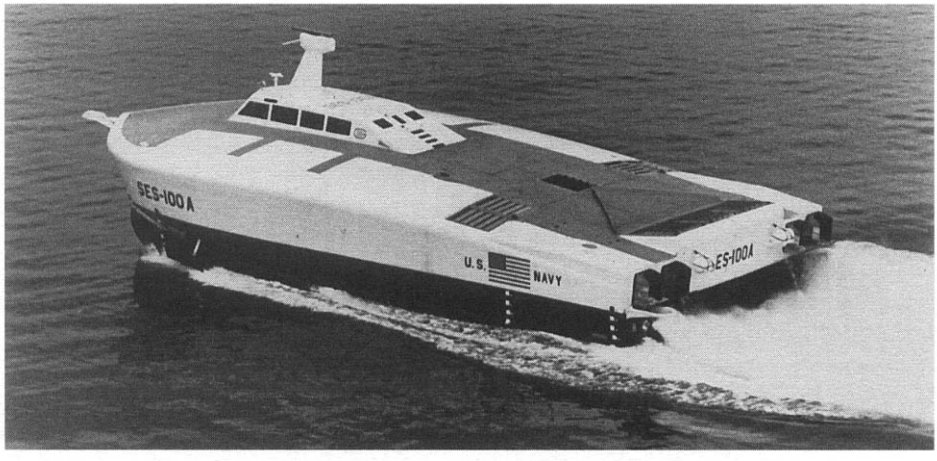

Fig. 1.26 US water-jet propelled sidewall hovercraft SES-100A.

Fig. 1.27 Successfully launched guided missile on US SES-100B at speed of 60 knots.

of former secretary of the US Navy Admiral Zumwalt proposals were developed to design high speed surface warships with a speed of more than 80 knots. This would lead to the SES becoming the main fleet resource for attack purposes. Two test SES, the Aerojet General model SES-100A (Fig. 1.26) and Bell Aerospace SES-100B (Fig.

1.27) were procured under a design competition and completed in 1971. The speeds achieved by each craft were 70 knots and 90.3 knots, respectively. A ship-to-ship guided missile was successfully launched from the SES 100B, and hit its target (Fig. 1.27), as part of the trials. Based on this success the US Navy proposed the 3K-SES in 1974. It was planned to construct an air cushion guided missile destroyer weighing 3000 tonnes and with a speed of 80 knots. Further, a mini aircraft carrier would be completed on the basis of the 3K-SES. A design competition was held between Bell Aerospace and Rohr Marine Industries, won by Rohr. In order to complete this development, new work shops, facilities for testing high speed water jet propulsion systems, lift fans, skirts etc. and new carrier borne weapon systems would be formed in Rohr Marine Industrial Corporation on the west coast of America. The plan was technically demanding, and the SES was power intensive, to reach the 80 knot goal.

In 1974, the fuel crisis hit the Western world. Policy changed overnight to one of extreme energy consciousness, so that the 100 knot Navy appeared the wrong direction to be developing. The 3K-SES programme was therefore cancelled. It was only in the mid 1990s that vehicle carrying commercial ferries began to use this technology. It was disappointing at the time that the 3K-SES plan was cancelled, though fuel consumption was not the only challenge faced by the 3K-SES. Further reasons included the following.

Technical risks

High frequency vibration could occur to a flexible skirt at the craft speed of 80 knots, and so produce very high accelerations (more than 500 G on certain skirt components). In addition, heat generation at prototype skirt tips at the time seriously affected their life, reducing it to a limited period of operation.

The high power propulsion systems on both craft were novel: SES 100A had variable geometry ducting water jets, while SES 100B had semi-submerged supercavitating propellers. Water jets for commercial applications have developed greatly since then, based partly on that experience.

There were also a series of technical problems with respect to seakeeping quality, ride control systems, high power transmission gear boxes and fire resistance of marine aluminium alloy structures, which had to be solved during the 3K-SES programme itself. The high power also led to a limited range, only just sufficient for the mission, which was not fully cleared through the Defense Department at the time.

Novel materials and systems

The material, equipment, weapon systems etc. which were in use on other ships of the fleet would have had to be abandoned for the 3K-SES, and new equipment, material and weapons with aviation type would have had to have been adopted and so lead to new construction methods. This would not have helped the Navy maintenance system. US Naval administration concluded that very high speed craft would lead to a series of problems not only on some ship materials and equipment, but also with some ship performance parameters, for instance high drag peaks, low range and large speed loss of craft in waves etc. This arose from the choice of a low cushion length/beam ratio, and thin sidewall configuration.

Model tank and small scale prototype tests at DTNSRDC had already indicated that high L/B could have advantages. For this reason, the US naval administration considered that the second generation of SES should be craft with a high cushion

Fig. 1.28 Bell Halter BH.110 SES in service with the US Coastguard in Florida.

length to beam ratio and thicker sidewalls, such as those on the US Navy test SES XR-5 and the Soviet passenger SES model Gorkovchanin. The draft of these craft in off cushion condition is such that the 'wet deck' no longer enters the water to provide buoyancy. These concepts are more like a slender hulled catamaran when floating.

The Bell Aerospace Corporation united with Halter Marine Inc. to form a new company named Bell-Halter Corporation, with the intention of developing a new type of medium speed SES with commercial marine use in mind: the BH-110 (Fig. 1.28). Bell-Halter used the following guidelines when designing the BH.110:

1. Use the sophisticated SES technical knowledge and experience of Bell Aerospace Corporation;
2. The craft was specified with medium operational speed, low fuel consumption and seakeeping quality not worse than that on an equivalent planing monohull, high speed catamaran or high speed displacement ship;
3. Use conventional marine equipment, materials and construction methods, for a simpler and more reliable craft, as well as with good maintainability and low initial cost;
4. Adopt marine diesel power, welded aluminium alloy structure and subcavitating fixed pitch water propellers;
5. Adopt thickened sidewalls. During off cushion operating mode, the twin hulls provide a large buoyancy similar to that on a catamaran, up to 100% of craft weight, and the clear distance between the wetted deck of craft and water surface was similar to that on catamaran, improving the manoeuvrability and performance of craft at low speed.

The prototype BH-110 was launched in 1978, and was later purchased and modified in 1980 by the US Navy. Subsequently the crew was increased to 14, and the range to 1000 nautical miles after increasing the fuel capacity. The craft was delivered to the US Coastguard in July 1981 for trials, and proved to be a craft with good seakeeping quality and simple hull structure.

Some time later, the US Navy extended the craft from 110 ft to 160 ft, and the all up weight increased from 127t to 205t. The payload of the craft was increased by 62%,

and it was re-named as SES-200. As a result of the modifications, the craft drag was reduced at cruising speed, and the economy and seakeeping quality of such SES with high L_c/B_c and thickened sidewalls was improved significantly. The craft speed on calm water was about 30 knots but the speed loss less than 20% in a sea state of Beaufort 4. In these conditions the craft captain would have to throttle back the governor so as to reduce the engine revolutions, or change the course, in order to avoid the extreme slamming motions and shipping of water. The BH-110 has good seakeeping: it can maintain a speed of 28 knots in calm seas, 16 knots in head seas of 8 ft and 25 knots in following seas of 12 to 14 ft, respectively.

Three production BH-110 craft in service with the US Coastguard during the 1980s have been operated for up to 181 consecutive days and nights. The Coastguard concluded that maintenance labour was equal or less than that on conventional coastal patrol vessels, and also realised that the crews had a good rest during a three day patrol operation.

Features of third generation SES craft are as follows:

1. A fair performance at low/medium speed, and low peak drag as well as increased range;
2. Good seakeeping capability in cushion borne operation due to its raised wetted deck, which was similar to a catamaran;
3. Thanks to the craft ride control system (RCS), the cushion pressure could be kept almost constant, arising from regulating both the air inlet and outlet control valves, so as to reduce the vertical motion of craft in waves. The RCS had been mounted on the XR-1D, SES 100A and SES-200, and a large number of tests had been carried out which validated the excellent effect of these systems. Vertical acceleration could be reduced by 50%, 30% and 25% at sea states of 1 to 2, 3 and 4, respectively;
4. The pitch angle of SES-100 at full speed in head seas was decreased, as shown in Table 1.6. It was found that the pitch motion of the craft was less than the required pitch motion for landing helicopters (less than 3°). It is probably safe to assume that the helicopters could be landed safely on SES-200 weighing 200t at less than sea-state 4;
5. Thanks to the medium speed of the craft, the wear rate of skirt bow segments tip improved to between 1500 and 3000 hours, whereas the life of the bow skirt might be reduced to 300–700 hours at operational speeds of 40–60 knots. In addition, the maintenance cost was reduced further due to adopting a skirt design which could be replaced while the craft was moored on water, and was found to be lower than the main engine maintenance cost which was relatively low due to the use of diesel engines.

The US Navy were encouraged by the success of tests carried out on the SES-200 craft, and later worked on the development of two applications of such craft, the Mine Countermeasures SES and the medium sized Patrol SES.

Table 1.6 The pitch motion of SES-200 at full speed and in head sea

Sea State	Pitch angle (single amplitude)
1	< 0.2 degrees
2	< 0.9
3	< 2.2
3.5	2.5

SES mine countermeasure craft (SES MCM)

The development of these craft, shown in an artist's impression in Fig 1.29, was developed as follows:

Initial design phase (December 1982–November 1984)

Since the shock vibration of hull structure due to underwater mine explosions could be reduced by 60–80% compared with that on conventional craft, it was expected that hull structure weight could be reduced considerably. Additionally the underwater hydrodynamic pressure signature and acoustic field due to the motion of these ships were expected to be decreased dramatically because of the existence of the air cushion. SES were therefore projected to be very suitable for MCM because of these advantages. Meanwhile, the craft could provide a larger deck area than that on conventional ships and a more stable platform for continuing work on mine sweeping operations in rough seas. For this reason the US Navy began to develop the MCM SES in December 1982.

Detail design and construction

The US Navy signed a contract with Bell Halter Corporation at the end of 1984 to build an SES MCM entitled the 'Cardinal' class, with a length of 57.6m, width of 11.9m and draught of 3.68m in off-cushion condition, 2.41m on-cushion. The cushion pressure was 7000 Pa and light/full displacement of craft were 359/452 t, respectively.

Fig. 1.29 Artist's impression of US Navy MCMH SES.

The craft structure was made of GRP following the methods of Karlskronavarvet AB of Sweden, while a set of mine sweeping gear, and retractable crane with lift capability of 2.7t were to be mounted on the upper deck stern. Two diesels with rated power 1600 kW for each were to be mounted as main propulsion engines, driving 5 blade fixed pitch water propellers with diameter of 1.02m, giving low noise level, via a gearbox with reduction ratio of 2:1. The wet deck of this craft was above the water when floating. A variable depth sonar (VDS) was to be mounted on the main hull, and could be extended into the water inside the cushion. In addition, a retractable swivelling thruster and two fixed pitch propellers driven by hydraulic motors were mounted on the craft to propel it during the mine sweeping operation. Since all mine sweeping operations were carried out on craft in on-cushion mode, the acoustic signature under water would be weaker. This application lends itself to SES with high cushion length beam ratio, and thick sidewalls. The total power of the air cushion catamaran would be slightly larger than that on conventional mine sweeper craft.

The craft were planned to be completed in the 90s, although a construction order was never placed. The Royal Norwegian Navy have since further developed this technology and commissioned 9 SES MCM vessels between 1994 and the summer of 1997.

Medium sized patrol SES

The medium sized SES was seen as a replacement or supplement to the hydrofoil patrol boat (PHM). The seakeeping quality of a 500t SES would be the same as that of a PHM, but the SES would possess greater range, deck area and cabin space. For this reason, some naval strategy experts considered that a combination of 1–2 SES and 6 PHM would be a good fleet to perform anti-aircraft and anti-submarine missions, because of its capacity for accommodating various electronic and other equipment as well as more fuel to support the PHM.

Some experts considered that the weapon system on the Spruance class destroyers, the DD-963 series, was suitable for providing a weapon system for SES. In this way an SES could be an ideal frigate, destroyer, even aircraft carrier. Its shallow draft, low underwater noise emission, high speed and large upper deck for carrying helicopters, guided missiles and STOL/VTOL aircraft to implement various Air-to-Air and Air-to-Surface missions would all add to the usefulness of the SES.

Enthusiasm to develop military SES/ACV has slowly improved once again in the USA since the mid 1970s, but based on a steady, step by step approach. The LCAC programme has become an important cornerstone for ACV technology application. Design displacement of SES has been extended gradually from 100t to 200t. Vessels with 500t, and 1000–2000t displacements are quite practical, but the US technology lead has been lost, now being taken over by Norway on the military application side, and China/Japan/Korea for commercial vessels.

1.5 ACV and SES development in China

The Harbin Shipbuilding Engineering Institute (HSEI) started to develop a new kind of water transport concept – the hovercraft with plenum chamber type air cushion – in 1957, and completed the first model craft in China with a length of 1.8 metres. The

model was constructed in both wood and aluminium alloy, and used an aviation type electric motor for lift power. Because of the lack of high speed towing tank facilities at that time the towing model experiments were carried out in a natural lake and were towed by hydrofoil craft to decrease the wavemaking interference.

A manned test craft, version '33' weighing 1.7t, was designed by HSEI in 1958, followed by detailed design and construction at the Wei-Jian aeroplane manufacturing plant of Harbin. The craft was launched on Soon Hua river on 1 August 1958. Static hovering tests were carried out successfully on Soon Hua river, but the craft failed to take off above 'hump speed' onto planing mode. After several modifications, it took off smoothly and successfully operated on the coast close to Port Lu Shun (Fig. 1.10). It reached a speed of 50 km/h during tests, and completed its first long range sea trial on 12 July, 1959. Seakeeping tests were also carried out.

During 1960 ACV research and development in China reached a climax. The Sheng Yang Aviation Engineering Industry School joined with the Sheng Yang Aeroplane Manufacture Plant to carry out research and development and finally completed an amphibious hovercraft in that year. The first domestic conference for air cushion technology was held in a tanker training school in the outskirts of Beijing in August 1960. About forty experts from Universities, Institutes and industrial plants with their manned or self-propelled models attended the conference. There was some demonstration of ACV carried out at the conference. Most models couldn't run straight due to their poor manoeuvrability and directional stability. The conference resolved to develop air cushion technology vigorously.

Unfortunately owing to the famine which lasted for three years in China, air cushion technology research was now interrupted. Then in 1963, under very difficult circumstances, the Marine Design & Research Institute of China (MARIC) re-commenced ACV research and development. Through theoretical study, model experimental research and development, and in spite of all sorts of difficulties encountered and failures met, eventually the first manned amphibious hovercraft version 711-I (Fig. 1.30) was completed in June 1965, and operated steadily at Jin Sah Lake at a speed of 90 km/h. The same year the craft was modified with flexible extending nozzles, and successfully completed its sea trials in this form. The flexible skirt greatly reduced the drag peak, and the time interval for taking off through hump speed was reduced from several minutes to just under twenty seconds. The craft could be operated steadily for

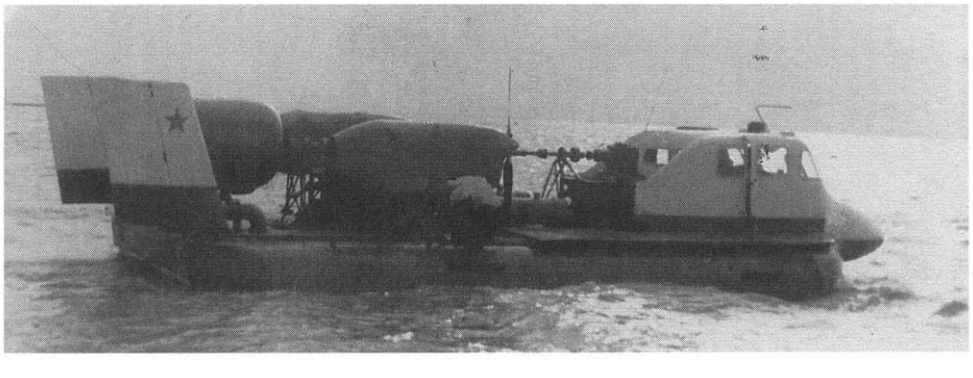

Fig. 1.30 First Chinese amphibious prototype hovercraft 711-I.

a long time, but owing to its poor course/transverse stability and due to the craft driver at the time applying too much rudder at high speed, it overturned during an emergency turn to avoid collision with a boat. This accident was similar to the casualties which happened on SR.N5. Fortunately the craft still floated flat with bottom up, and no one was injured.

Based on the tests of craft 711-I, MARIC completed another test craft version, 711-II, with improved manœuvrability. The adoption of an integrated lift and propulsion system greatly improved the handling and manœuvrability. The craft has now served as a test craft for MARIC for about 20 years, and so has provided a great deal of test data (Fig. 1.31). A test sidewall hovercraft, version 711-III weighing 1.7t, was developed successfully in 1967. The main hull was made in plywood coated with GRP. With one 190 kW petrol propulsion engine it obtained a maximum speed of 58 km/h (Fig. 1.32). Various operations of both craft on rapids, shallow water, swamp and areas not navigable by boats on the Jin-Sah and Lan Chang rivers were carried out in June–August 1967. From the test results, it was obvious that the SES would be more suitable for passenger transport on the Jin-Sah River. For this reason, the first Chinese

Fig. 1.31 Prototype ACV model 711-III in operation.

Fig. 1.32 First Chinese prototype sidewall hovercraft 711-III in 1967, fitted with bow hydrofoil to improve seaworthiness.

commercial SES type 'Jin Sah River' (Fig. 1.5) was completed in Shanghai Hu Dong Shipyard, and was delivered to Chong Cheng Shipping Company in April 1971. Three high speed Chinese manufactured diesels were installed for lift and propulsion. The craft could accommodate 70–80 passengers and operated at a speed of 57 km/h. The craft has now been operated on Jin Sah River for many years.

Since then the division which was responsible for research and development of ACV/SES/WIG, the Hovercraft Research and Design Division, was formed in MARIC. The division established the first static hovering laboratory of China in 1971–74, and completed the first Chinese water jet propelled SES, version 717 (Fig. 1.33), as well as the first Chinese amphibious test landing craft, version 722, which could accommodate about 150 passengers.[133]

During the investigation and operation of the ACV and SES mentioned above it was found that although China had commenced her ACV/SES research undertaking early, it was difficult to develop the ACV/SES from test stage to a more practical stage

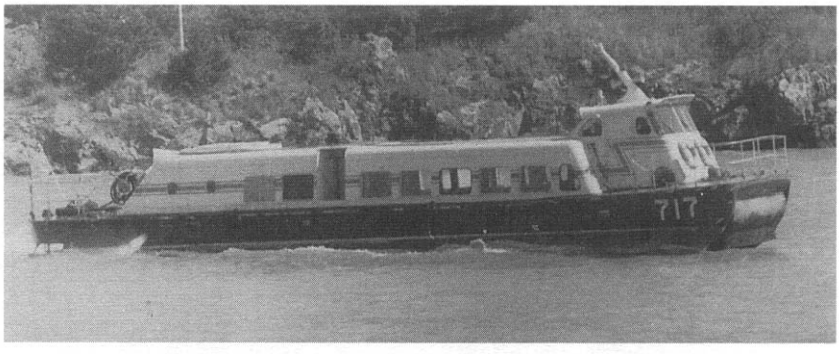

Fig. 1.33 First Chinese water-jet propelled passenger SES series 717.

Fig. 1.34 Small air-cushion vehicle design 7202.

because of the lack of some reliable and credible critical materials, engines, equipment and components, such as corrosion resistant aluminium alloys for the hull, lightweight main engines, special air propellers and flexible skirts, etc. It was evident that obtaining the key material and equipment was the most important problem faced by the researchers and designers, and that this had to be solved either by import or by improving the quality of domestic products. In this respect, it was considered that development had better be tried on smaller sized craft. For this reason MARIC completed various small hovercraft in the 70s, such as a hover-jeep, 7202 (Fig. 1.34), 7210, 7210B, etc. while at the same time some commercial passenger SES were completed, such as versions 717-II, 7203 and 719-II (Figs 1.35, 1.36 and 1.4). Owing to a lack of the corrosion resistant aluminium alloys in China, and some technology problems with respect to fabricating welded structures in aluminium alloy which still had not been solved, marine steel was selected as the hull material of those craft.

Meanwhile, MARIC rebuilt the ACV 716 and adopted Deutz marine air cooled

Fig. 1.35 717-II in operation on Yangtze River by Chong Quing city.

Fig. 1.36 Chinese SES design 7203.

Fig. 1.37 Diesel engine propulsion ACV design 716-II.

Fig. 1.38 Passenger SES design WD-901 with single water-jet propulsion unit.

diesels as the main engines for this craft. The economy of modified craft 716-II (Fig. 1.37) was improved significantly by this engine change. Meanwhile, the rigid sidewall hovercraft type WD-901 (Fig. 1.38) was designed as a water bus for shallow water, developed jointly by Shanghai Ship and Shipping Research Institute (SSSRI), the Communication Bureau of An-Hui Province, and Chao Hu Shipyard. The WD-901 craft hull was made of GRP, while one 221 kW 12V150 marine diesel was used as the integrated power system to drive a two-stage axial flow waterjet propulsion with an impeller diameter of 385 mm. The craft ran at a maximum speed of 30–35 km/h. It had the advantage of low cost operating economy, and was suitable to be the preferred

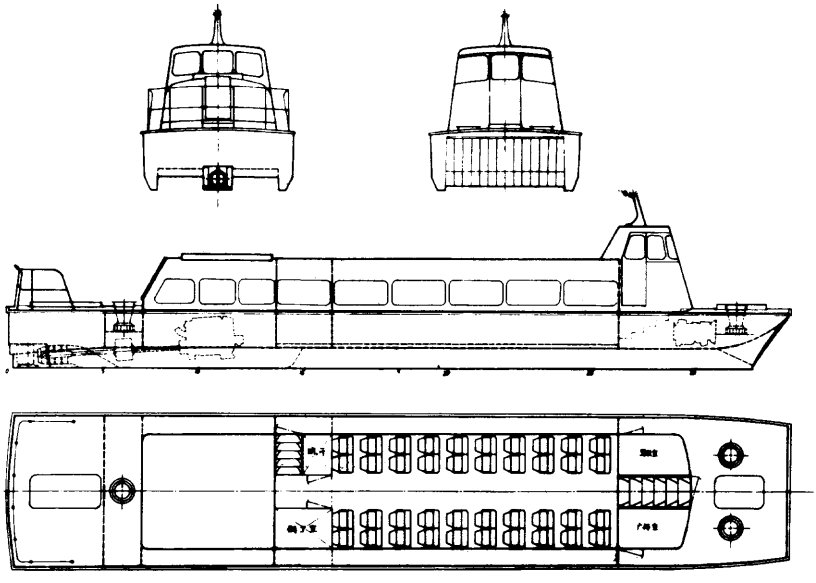

Fig. 1.39 Line drawing of passenger SES design WD-902.

Fig. 1.40 200 seat, 32 knot passenger SES built in GRP, delivered for service December 1995.

passenger craft for operating on small rivers. The WD-901 was followed by the WD-902 (Fig. 1.39) with increased passenger capacity.

In 1985 MARIC developed the largest SES in China, the 719-II (Fig. 1.4), which has been regularly operated between Shanghai municipality and Qong Ming island since that time. More recent examples of SES designs placed in service are those shown in Figs 1.40 and 1.41. The SES in Fig. 1.40 is a 200 seat passenger SES built in GRP which operates at 32 knots, and has been in service since December 1995. Fig. 1.41 shows an SES with a steel hull which carries 2 tonnes of cargo, and 70 passengers at 33 knots. This entered service in August 1995.

To date more than 100 ACV and SES, of 15 different types, have been built and operated in China, including 700t and 2000t capacity oil exploration air cushion platforms. Figure 1.42 shows an early model of an ACV load carrying platform being tested over simulated ice in a towing tank. Wax is used for this purpose. The near future holds considerable potential for ACV and

Fig. 1.41 70 seat/sleeping berth, 2 tonne cargo, steel hull, 33 knot SES, delivered for service August 1995.

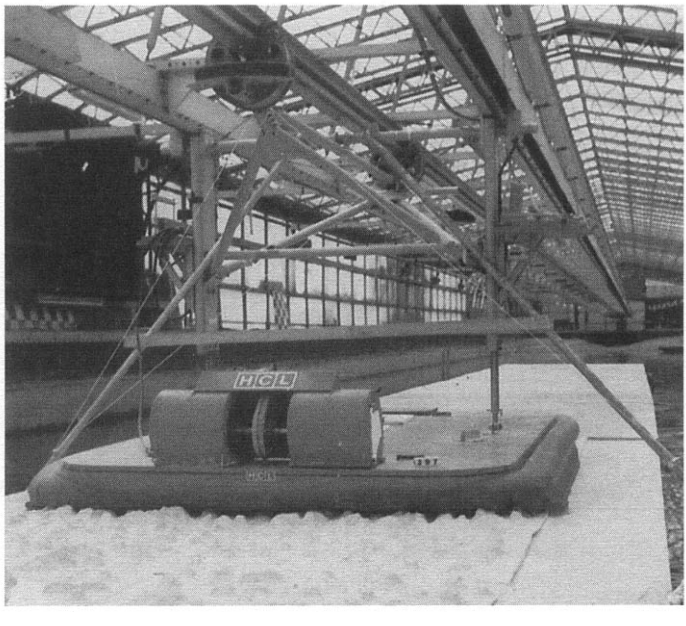

Fig. 1.42 ACV model testing on simulating ice surface.

SES to be operated on lakes, rivers, around the coast and at sea in China for water transport, tours, passenger ferries, oil exploration and other applications.

1.6 SES and ACV developments in the 1990s

In 1984/85 a shipbuilder in Norway, Brødrene Aa, teamed up with a firm of Naval Architects, Cirrus, to design a large passenger SES, after being impressed with the performance of the US Navy's test craft SES200 when it performed a series of demonstrations in Europe for NATO. Their concept was a GRP hulled development similar in concept to the BH-110, with catamaran hulls and diesel engine power. Propulsion

was by propellers. Passenger capacity was 264. This craft performed very well, reaching 42 knots in light weather, and was eventually placed in service between Harstad and Tromso. Brødrene Aa followed this success with the construction of several similar SES with higher passenger capacity, powered by water jets, which have been operated at many locations in the world on charter. Most continue in regular work today.

Other builders in Norway developed their own designs, initially for ferries, as a higher speed variant to their main product, the high speed catamaran. In 1986 the Norwegian Navy began a programme to develop an SES Mine counter measures vessel, again encouraged by the earlier US Navy Programme. After keen competition, a consortium of companies in Mandal, Southern Norway won the contract. Cirrus provided technical expertise for the cushion system. A total of nine craft were built and are in operation with the Royal Norwegian Navy. The commercial SES product development started by Brødrene Aa was taken over by Ulstein Industries, who have in turn licenced their design to a shipyard in Western Australia.

The MCMH programme is now succeeded by a similar development programme for an SES High Speed Coastal Patrol Vessel. The construction programme for this class will begin with a prototype, and continue with further vessels into the first decade of the next century. Due to the increased performance of catamarans during the 1980s, SES have not become as widespread as passenger ferries, as had been expected. The technology will need to take the next advance in size to high speed coastal cargo vessels before moving forward commercially. Japan leads this development at present.

Over this same period builders in Holland, Germany, France and Italy all studied the SES, and produced design proposals. In Germany, a prototype similar in size to the Brødrene Aa SES, the MEKAT, was built by Blohm and Voss for the Navy. In Holland Royal Schelde built a 22m prototype for test, which was put in service on the Solent for a summer. Royal Schelde have since progressed to the construction of large car-carrying catamarans. At the end of the 80s, proposals were made for larger car-carrying SEC, and in Italy, a shipyard, SEC, designed and obtained orders for 4 craft suitable for 750 passengers and 120 cars. Unfortunately this SEC, incorporating a steel hull, was not completed, as the operator who had ordered the SES went into liquidation.

Since 1990 there has been a national development programme in Japan to develop high speed short sea cargo vessels. The first SES prototype is a 70 metre vessel with a speed of 42 knots, which is itself a scale model of the planned cargo SES. Power is from industrial gas turbines, and propulsion by water jets. Trial results have so far been very encouraging.

In Korea, SES and ACVs have been built for many years. In the early 80s Korea Tacoma Marine Industries built a number of SES similar in size to the Hovermarine HM2 series and 5 series. More recently Semo Shipbuilders have developed a craft similar in size to the Brødrene Aa/Ulstein SES. Several such craft are in service. Attention is now towards larger car-carrying SES, which are under development. SES development is now also active in Western Australia where two craft of 300 passenger class have been completed for ferry services, based on Ulstein SES designs.

In the UK, a number of AP1-88 amphibious ACVs were built during the 80s, for both ferry and utility roles. The most recent craft have been a coastal passenger/cargo craft for the White Sea Coast in Russia and the development of the AP1-88 400 class for the Canadian Coastguard. There may be up to 4 of these craft in service. An open

deck utility AP1-88 constructed at NQEA in Queensland (the fifth built by NQEA) was put into service for coastal oil field supply in Angola at the end of 1995; this has subsequently been transferred to Peru for oilfield logistics operations supporting a drilling programme. Griffon Hovercraft and Slingsby Hovercraft both have capable designs for utility passenger ACVs. Griffon's range extends to 50 passengers, Slingsbys' to 22. This technology has matured over the last decade, and the potential operators appear more realistic about their expectations. While the order stream is not large, it is steady, suggesting that the market is slowly developing.

1.7 Applications for ACV/SES

What are the potential uses of a modern ACV or SES? To identify the applications which ACV or SES may fulfill more efficiently than other vehicles, we need to review the characteristics which set them apart. Some key ACV/SES performance characteristics may be identified as follows:

Amphibious capabilities

Due to the light footprint pressure, as shown in Table 1.7 below, the ACV possesses excellent amphibious capability. The footprint is about the same as a cross country skier, and so can safely traverse most flattish terrain.

The cushion as noise and shock damper

The low and uniform cushion pressure ($\leq$ 500 Pa), use of air propellers or ducted fans for ACV propulsion, and waterjet propulsion for SES make these craft insensitive to underwater mines. It is evident that both ACV and SES are suitable for applications as mine sweeper and anti-submarine vessels.

Deck area and cabin volume

The ACV and SES both give spacious deck area and cabin volume. These vessels need to be large relative to their displacement, to keep cushion pressure realistic. They are therefore suited to applications where volume is the most important parameter:

Table 1.7 The footprint pressure of various forms of transport

The configuration of transport forms	Footprint pressure (Pa)
Human footprint	60 000
Amphibious tank version 60	56 000
Light tank version 1KV91	40 000
British reconnaissance tank	35 000
Car type footprint	10 000
Skier	4000
ACV/SES	1000–5000

passenger and car ferries, fast military logistics vessels, utility vehicles and, at larger size, short sea container feeder transport.

In order to accommodate weapon systems on marine craft such as aeroplanes and helicopters, conventional displacement craft sometimes have to be enlarged to provide the required deck area and hangar space, and also follow by increasing main engine output, construction and maintenance cost. The SES solves this problem efficiently, and creates a new concept of ship design philosophy. For instance, a large conventional aircraft carrier of 30,000 tonne displacement can be replaced by a lighter SES only weighing several thousand tonnes. Helicopters can land or take off on or from the SES weighing only 200–300t, compared to a conventional ship which displaces at least a thousand tons.

A 100 ton ACV/SES can accommodate up to 300 passengers. This can also be achieved on a conventional monohull with the same displacement, unlike smaller craft. In order to accommodate twenty berths on a conventional planing hull, designers have to select a craft displacement of about 30–50t and power the craft by two sets of marine diesel 12V150 to achieve a speed of about 35 km/h. In contrast, owing to the spacious cabin, an SES weighing only 20t can satisfy the requirement of berth arrangement and can reach a speed of up to 50 km/h with the same main engines.

It is probably safe to assume that a 300t anti-submarine SES with upper deck of about $50 \times 12 = 600\text{m}^2$ could provide a suitable flying deck/platform for landing anti-submarine helicopters. This would improve anti-submarine capability significantly by comparison with conventional anti-submarine warfare displacement ships with the same displacement.

Development to larger size

For a fast boat, the 'fast' is always limited by its displacement. This means that fast craft always appear with small displacement. Using the air cushion to support most of the weight, and with the existence of rigid sidewalls, it is relatively simple to develop the SES to a large size (up to thousands of tons displacement) without difficulty, with a selection of water propulsors such as water propellers, waterjet propulsion, etc. The air cushion distributes loads evenly over the primary structure, so that while an SES hull is large, lightweight structural design can be employed effectively, minimizing capital cost.

Similar to other high performance vehicles such as planing boats and hydrofoils, ACV/SES also belong to the hydrodynamic support group of marine craft (c.f. static or buoyancy support). The difference between the ACV/SES and planing hull and hydrofoil craft are that the ACV/SES lift system operates at very low interface pressure, so that significant overload only leads to reduced craft speed, and does not seriously affect take off capability.

One can also combine SES with other high performance vehicle characteristics to create a hybrid craft obtaining higher performance. There are two modes of operation for air cushion catamarans: off cushion and on cushion modes. The SES with ordinary thin sidewalls has a large difference of speed between the two modes: the off cushion speed is low at about 10–20 knots. In the case of an air cushion catamaran with thick sidewalls, it will operate as a high speed catamaran in the case of off

cushion mode, and an SES in on cushion mode. The US BH-110 craft had thick sidewalls, and a maximum speed of 38 knots. In off cushion mode, its cruising speed was 18 knots. Such craft possess an advantage for military applications, where loitering is part of the mission.

There seems to be a misunderstanding on the seakeeping quality of SES: some commentators considered in the developmental stage of ACV/SES that seakeeping was poor, and this view seems to persist. Following a series of measures to improve seakeeping quality, SES are better than conventional displacement vessels with the same displacement. For this reason the missions which in general are undertaken by conventional vesssels could be undertaken by SES with lighter craft weight. The air cushion catamaran 719-II, being operated between Shanghai municipality and Chong-Ming Island, can be operated reliably in the same limiting sea state as for the conventional catamaran weighing a thousand tons on the same route, though the all up weight of the SES is only 220t. The seakeeping quality of SES can be improved still further by measures such as improving skirt design, adopting high cushion length beam ratio, improving sidewall configuration or adding anti-pitch hydrofoils, optimising sidewall lines and installation of cushion damping systems.

The ride quality of fine hulled catamarans has improved greatly during the last decade, partly due to the competition between the concepts of catamaran, SES and hydrofoil. The catamaran concept is currently very attractive for speeds of up to 50 knots, for vessels in the up to 120m size range. It is likely that the SES will prove attractive for applications in this size range at speeds above 50 knots, and for rather larger craft in the future.

Speed

The air cushion is a device to reduce surface friction or over water drag. ACV and SES have lower installed total power than other transport concepts for service speeds in excess of 40 knots. This creates the prospect of lower operating costs for high speed designs. These characteristics suggest that ACV and SES craft may be most effectively applied where there are special requirements which cannot be fulfilled by any other vehicle, or where there is a clear margin of efficiency which can justify a more complex craft from the operational and maintenance point of view. An overview is given below.

Military applications

The ACV can be used effectively as an amphibious assault craft, across the shore landing craft, guided missile craft, mine sweeper, mine layer or amphibious coastal patrol craft. As one example, the US Navy continues to develop its amphibious landing fleet with the LCAC, each of which can accommodate heavy or medium sized tanks and landing troops. Landing ships constructed in the future must possess the capability to accommodate the LCAC. The effectiveness of the US Navy craft, and Russia's equivalent, has resulted in Japan forming its own squadron for coastal defence duties.

During the 1990s the design of the 55 tonne capacity LCAC and it's equivalent have matured as service experience has suggested ways to cut build cost, and maintenance analysis has shown approaches to minimize the operational cost. In the meantime

there has been a gap in the payload capacity range between 10 and 50 tonnes. Developments with the BHC AP1.88 and the ABS M10 have resulted in capable utility craft which can also be applied to slightly different missions. The GRP structure M10 is particularly suited to missions requiring stealth, such as anti-piracy patrols, while the AP1.88-400 fills the gap in payload capacity.

In the smaller utility range, craft from Griffon and Slingsby deliver payload capacity between 1 and 5 tonnes suitable for amphibious coastguard patrol, which has proven effective in a number of European countries. The high speed, good seakeeping qualities and spacious deck and cabin areas suggest that SES, particularly the air cushion catamaran, could be used as patrol boats, anti-submarine vessels to join with PHM, and also as air cushion guided missile vessels. During the 1990s Norway has provided the technology leadership with the development of its fleet of MCM SES, followed by Fast Attack SES.

Following the end of the 'Cold War' in 1990, the conflict in the Arabian Gulf, and later the Bosnian conflict, many countries have experienced a significant shift in the missions which their military forces were designed to meet. Rapid deployment to a remote conflict feature significantly. Over the shore deployment, often coupled with the maintenance of a force of arms close by for an extended period, are also important requirements. This is mostly met by the delivery of aircraft carriers and amphibious assault ships. The SES may in the medium term offer an alternative, or extension to this strategy. Some marine weapons systems, such as ship-to-ship guided missiles, ship-to-air guided missiles, helicopters and antisubmarine weapons may be distributed into an integrated Sea Action Group (SAG) using a number of smaller fast vessels, rather than a single large unit such as present aircraft carriers. This could lead to a revision of the surface fleet into a larger number of smaller units.

Civil ferry and utility applications

SES can be used as passenger craft on inland rivers, estuaries, river mouths and coastal areas. SES have proven to be very successful in the payload range between 60 and about 400 passengers for inshore and coastal routes. Development of vehicle carrying craft remains a challenge, awaiting market demand for craft with service speeds above 50 knots.

ACV can be used as passenger ferries, logistics vehicles or pleasure craft, operating on shallow water, beaches, swamps and other regions which conventional ships find it difficult to have access to. Craft with payloads up to the equivalent of 100 passengers have matured in the 1990s, and have found a widening market as buildup of operating experience has encouraged new operators. Utility operations prove to some extent to be niche applications, since the requirement often cannot be fulfilled by any other vehicle, and so past experience is not available to the ACV designer. This track record is slowly being built by the different ACV operations themselves.

Oil field applications

It is most convenient to use ACV as air cushion platforms in onshore and coastal regions, particularly where the ground is swampy or sensitive tundra. ACV platforms

have been used to deliver plant and major construction modules, and as drilling rigs in these areas. On beach areas, which conventional craft have difficulty in accessing, the ACV can be used as work boat, communication vessel and exploration survey craft, and even as air cushion oil exploration platform. Hover platform payload requirements are generally in the range of 100 to 250 tonnes, although if the market were to develop in the future then 500 to 2000 tonnes would be a more useful unit for wider application.

Arctic transport

The ACV air cushion platforms can be used on ice as transport and communication vehicles. They can also be used as ice breakers at high or low speed using two different mechanisms for breaking the ice which are exclusive to these vehicles. The ACV Waban Aki operates successfully as a high speed ice breaker in Eastern Canada. This application generally demands craft with a payload in the range 5 to 30 tonnes.

Work boats and other special applications

The ACV can also be used as a utility work craft, as a multipurpose craft for the purpose of rescue, ferry, security, border defence, hunting, flood and mud survey, etc. The main market for this type of craft is in the payload range between 500 kg and 5 tonnes.

Load transporters

Air cushion technology can also be applied to carrying modules, heavy equipment and components in warehouses and workshops. To achieve this, an external source of compressed or blown air is fed to an air cushion pallet or collection of pallets linked together under the load. Such equipment can be designed to lift loads between 1 and 10 tonnes. Water cushion pallets using the same principles can be used for movement of much heavier loads.

1.8 The future

The advent of the hovercraft has led to the creation of a new branch of technology, involving the marriage of hydrodynamic and aerodynamic design and production principles. Despite the rapid pace of development, hovercraft are still in their infancy, especially for the larger vehicles, and much still has to be learned. Progress has been encouraging, particularly in the field of skirt engineering, and more recently with less expensive structures and more efficient power units.

Apart from marine hovercraft, equally exciting developments are taking place in the application of the air cushion principle in the industrial field. Already air cushion transporters are in commercial use, facilitating the carriage of extremely heavy loads (up to 200 tons) over weak bridges and road surfaces and smaller loads (up to 9 tons) over farmland and open country. With the former vehicle, the heavy cost of bridge

strengthening and road repairs is obviated, and with the latter the payment of compensatory costs to farmers is also avoided. Unfortunately the high work capacity of such systems, and the limited number of movements required, make this a niche market.

At the other end of the scale are hover pallets which operate on the air lubrication principle at relatively low pressures, such as are available from normal industrial supply air lines. Current types can carry containerised loads of up to 5 tons in weight and several are in service with shipping companies and other industrial organizations. Their high manoeuvrability and simplicity of operation have led to economics in manpower, time and a more efficient utilization of storage space. This application has a wider market than large transporters, but is more easily considered an extension of industrial mechanical handling systems than a new standalone business. The most successful ventures in this area have been just that – extensions of existing industrial handling companies.

The main subjects of this book, the ACV and SES, are both vehicles which have significant potential for further improved economy and performance. In common with most other forms of transportation, development of the vehicle is closely linked with technological developments in the power units which are used to drive them. In the case of the ACV and SES the story began with aircraft engines and gas turbines, and has now moved on to high speed diesel engines. The development of new lightweight water cooled diesels is encouraging ACV design at larger payloads, though perhaps not yet with the potential to provide a replacement for the SRN.4. Marine gas turbines with increased efficiency and lower maintenance demands, driven by the demand for powering catamarans, open the opportunity to develop larger SES which will begin to release the full potential of the technology. At speeds above 60 knots, it may be the propulsor which is the limiting factor once again rather than the power plant, until further improvements in waterjet technology are available.

ACV and SES at small to medium size have been developed by standalone businesses. Larger ACV and SES have to use the leverage of existing shipyards or marine construction companies if they are to achieve necessary economy in construction. A number of shipyards now have experience in large scale aluminium and GRP construction which may form a suitable basis.

The rate of development of the hovercraft principle has been relatively rapid. The widespread adoption of this principle may take many more years, but it has nevertheless started encouragingly. However, its future growth will depend on the continuation of research and development efforts throughout the world.

1.9 SES and ACV design

The reader should now have a fair idea of ACV and SES historical development. Before looking at the design process itself, we will now spend some time exploring the theory behind air cushions, and their interaction with the water surface over which these craft normally operate.

We begin with an explanation of the air cushion itself. The basic idea behind these vehicles is that all (ACV) or a large part (SES, 60 to 90%) of the weight is supported

directly by a small over-pressure of the air contained in the cushion. Our first aim is to understand what defines the requirements for cushion air flow and pressure.

By reducing the contact area, drag is reduced. The air cushion interacts with the water surface in a similar way to the classic potential theory developed by Lamb [208] in the 1930s. In addition, flexible skirts, and the momentum of the cushion air, introduce drag components. Once the means is available to estimate drag as well as the static forces on an air cushion, stability, trim and manoeuvrability can be investigated.

Skirts are generally considered as a separate element for analysis, though they can influence craft performance, particularly instabilities such as tuck under which may lead to 'plough-in', and skirt bounce.

SES and ACV motions are complicated by the influence of the air cushion pressure variations on the water surface, and resulting variations of dynamic trim. We present non-linear analysis methods for solving the equations of motion in this text, as this approach gives the most accurate means for estimation.

In the same way as for ships, it is often easier to carry out model tests than theoretical analyses, to determine some of the design parameters needed. SES and ACV model testing needs careful interpretation, since responses which are susceptible to different scaling laws (Froude and Reynolds) both have a significant effect on the total response. Recommendations are discussed in Chapter 9.

The Design Methodology section of this book begins with a review of the basic design requirements, including rules and regulations which have to be met. This is followed by a discussion on the estimating methods to determine principal dimensions. Once these have been estimated, the craft can be developed first by designing the lift system, the skirt, the hull structure and propulsion system. Main engines can then be formally selected, and after optimization of the main dimensions, consideration can be given to the craft systems and controls, and internal outfit.

2

Air cushion theory

2.1 Introduction

Development of air cushion theory is closely related to the development of hovercraft themselves, particularly of flexible skirts.

Early air cushion vehicles were conceived with the object of drag reduction for a marine craft. The concept used was air lubrication of the wet hull surface. From practical experience with high-speed stepped hull planing boats in the early part of this century, it was realized that air lubrication did reduce the water friction; however, it was difficult to reduce wave-making resistance. For this reason, the concept of injecting lubricating air over the wetted surface was replaced by use of a thicker air cushion.

In China, this theory was put into effect as a plenum chamber hovercraft with thin 'sidewalls' at the edge of the cushion, the hovercraft '33', built at the Harbin Shipbuilding Engineering Institute (HSEI) in 1958. The air clearance under the sidewalls was very small, so it 'skated' over the water or ground and it is difficult to say that this craft had real amphibious qualities.

Sir Christopher Cockerell invented the principle of the peripheral jet hovercraft, whereby the air cushion was fed with air and also maintained by means of air flow momentum change at a high-velocity peripheral air curtain. Air cushion efficiency (depth of air cushion and thus obstacle clearance) was enhanced several times compared with that of the plenum chamber hovercraft fed with air directly into the cushion. Even so, prototype craft barely had amphibious ability. The Saunders Roe SR.N1 weighing 3.4 t, with an air clearance of approximately 200 mm, could only operate on smooth surfaces such as concrete, level beach or smooth water. The initial principles were nevertheless proved and a test bed made available for further development.

In practical terms, the amphibious capability of the SR.N1 was almost non-existent. It required another technological leap before the concept could be used for practical purposes. Nevertheless, the various theories to explain the peripheral jetted hovercraft were enthusiastically followed up in the 1960s by the scientific community. These include thin jet theory, thick jet theory, jet equilibrium theory and the various research efforts to understand the effect of different cushion plan-forms and compartmentation.

Flexible skirts to contain and deepen the cushion were the key idea needed to step forward. This concept began its development on hovercraft such as the SR.N1 as

flexible extensions to the air jet nozzles. These skirts significantly enhanced the obstacle clearance, giving real capability in a seaway as well as over rough ground and truly demonstrated amphibious capabilities.

The necessary condition for a hovercraft with peripheral jets to take off from static hovering to planing is that the air clearance of such a craft is at least larger than 0.5–0.8 times the depression caused by the cushion pressure on the water surface. If the hover gap is less than this, the hard structure will interact with the induced waves as the craft accelerates, greatly increasing the drag. However, for a hovercraft with flexible skirts the air gap underneath the skirt itself is not a key condition for the take-off of the craft, since the skirts will deform under the action of the induced wave-form.

The flexible skirted ACV is easier to accelerate through hump speed in rough water as well as over calm water for the same reasons – the skirt deforms under the action of the water surface. Nevertheless the power needed to traverse the drag peak (or 'hump') between the displacement and the planing condition is relatively high for a jetted skirt.

Engineers looked at different concepts of cushion geometry and skirts (see Chapter 7) to reduce the drag. Jet extensions gave way to bag skirts with smaller jet extensions and eventually the jet extensions were replaced with convolutions called fingers by the end of the 1960s (see Fig. 2.3). Thus, although the actual air clearance decreased because of the lower air cushion efficiency of such skirt types, the effective cushion depth greatly increased and both drag and required power were reduced.

The bag and finger type skirt has had great vitality, its design evolving continuously from the mid 1960s to the present, with gradually improving resistance characteristics and responsiveness, improving ride quality over rough surfaces. To date specific lift power has decreased to 14.7–19.4 kW/t (20–25 shp/t) for current craft compared with 73 kW/t (100 shp/t) for early ACVs (SR.N1), i.e. a factor of five, due to decreasing air clearance requirements beneath the flexible skirt.

At the present stage of development of ACVs and SES, the problems with respect to take-off from displacement mode to planing mode are no longer a key technical issue. Rather, the flexible skirt should be designed to meet the designer's seaworthiness requirements. In this respect, the concept of wave pumping has been identified as an important issue (the physical concept will be described later in this chapter) and designers consequently pay more attention to pitch and heave damping characteristics.

It may safely be taken for granted from this that it is better for designers to determine the lift power according to non-dimensional flow rate rather than relative air gap. It is also more convenient and reasonable to calculate lift power according to non-dimensional flow rate. The air gap is not a unique criterion for deciding the air cushion performance of craft; however, by experience, one still can use the air gap as one measure for assessing the air cushion performance.

Static air cushion theories derived in the 1960s are still suitable for describing the powering performance of craft with modern flexible skirt designs and so these are summarized below. The text in this chapter will proceed with air cushion theory from early research; then the flow rate coefficient method; the wave-pumping concept and its requirements; the determination of the heaving damping coefficient and finally the heave stability derivatives of ACVs.

2.2 Early air cushion theory developments

Although the theories mentioned below may seem to be out of date, it is useful to study them in order to understand the air cushion rationale. While peripheral air jets are no longer used in practice, the basic understanding developed through these theories is still equally valid for modern ACVs.

Theory of thin peripheral jet air cushion hovering on a rigid surface

This theory was used on early ACVs with rigid jet nozzles over ground for determining the air cushion performance. It assumes that:

- The nozzles are infinitely thin, therefore the air flow is jetted uniformly perpendicular to the centre line of the jet.
- The air flow jetted from nozzles is non-viscous and incompressible.
- The air flow jetted from nozzles will not combine with media around the air jet (induced flows are not treated).
- The cushion is supported on a rigid surface.

The transverse section of such an ACV is shown in Fig. 2.1. According to the theory for flow momentum,

$$hp_c = \rho_a V_j^2 t\,(1 + \cos\theta) = \rho_a V_j^2 xh \tag{2.1}$$

where p_c is the cushion pressure (N/m^2), ρ_a the air density (Ns^2/m^4), t the width of nozzle (m), h the air clearance (m), V_j the mean velocity of jets (m/s), θ the angle between the centre-line of the nozzle and the craft baseline (°) and

$$x = (1 + \cos\theta)t/h$$

Then the total pressure of the jet can be expressed as

$$P_t = 0.5\rho_a V_j^2 + fp_c \tag{2.2}$$

where P_t is the total pressure of the jet at the nozzle (N/m^2) and f the coefficient for relative air clearance, as shown in Table 2.1.

If we neglect the problems regarding three-dimensional flow and flow from stability trunks (internal skirts to divide the air cushion), then the air flow rate from the jet nozzles of the craft could be written as

$$Q = V_j t L_j \tag{2.3}$$

Table 2.1 Coefficient f relative to h/t

h/t	f
1	0.75
2	0.65
3	0.54
≥4	0.50

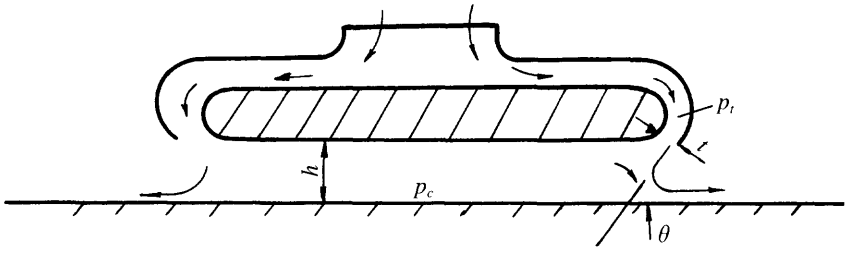

Fig. 2.1 ACV cushion cross-section.

where Q is the total flow rate jetted from the peripheral nozzle of the craft (m^3/s) and L_j the peripheral length of the nozzle (m). Then the lift power can be expressed by

$$N_{el} = QP_t/(75\eta_f\eta_d) \tag{2.4}$$

where N_{el} is the lift power of craft (kW), η_f the fan efficiency and η_d the air duct efficiency. Regarding the cushion pressure as uniformly distributed, then the weight of craft which can be lifted is

$$W = p_c S_c \tag{2.5}$$

where W is the weight of craft (N) and S_c the cushion area (m^2).

In order to develop a relation for N_{el} relative to W, we need to determine V_j. To do this we need to look at the various air jet theories.

Exponential theory for air cushion performance on a rigid surface

Thin nozzle theory was based on the assumption of infinite thinness, namely the jet velocity along the direction of nozzle thickness distributes uniformly. As a matter of fact, the jet velocity does not distribute uniformly because the back pressure of jet flow along this direction is rather different.

Mr Stanton-Jones of the British Hovercraft Corporation developed a relation based on the assumptions that the back pressure at the edge of nozzle, namely the side close to the atmosphere, was equal to the pressure of the atmosphere, and the back pressure at the inner edge of the nozzle was equal to p_c. The flow rate and total pressure of the lift fan can then be derived as

$$p_c/p_t = 1 - e^{-2x} \tag{2.6}$$

where

$$x = (1 + \cos\theta)t/h \quad \text{(as in equation 2.1)}$$

$$Q = [2/\rho_a].\ \{l_j h p_t^{0.5}[1 - (1 - p_c/p_t)^{0.5}]/(1 + \cos\theta)\} \tag{2.7}$$

These equations gave results which correlated with practical experience.

Theory for plenum chamber on a rigid surface [9]

Similar to thin peripheral jet theory, we assume that air flow is incompressible and non-viscous, but the flow streamline for the air escaping from the cushion periphery

is rather different from hovercraft with peripheral jets, because of its different duct configuration.

A typical transverse section for this type is shown in Fig. 2.2, similar to the craft '33' constructed by HSEI. The cushion flow is pumped from air ducts directly into the cushion rather than from peripheral nozzles as for a peripheral jet hovercraft.

Flow diffuses in the plenum chamber and forms the air cushion. For this reason, the relation may be derived simply because the pressure in the plenum chamber can be considered as a uniform distribution. In fact, this was validated by testing of manned craft, with the exception of hovercraft operating at high speed and with high-frequency heaving and pitching. Thus the unit flow rate around the craft periphery can be written as follows:

$$Q = \int [2p_c/\rho_a]\, \Phi l_j \mu(j) h(j) \mathrm{d}j \tag{2.8}$$

where $\mu(j)$ is the discharge coefficient for the peripheral seals, in general 0.5–1.0, and $h(j)$ the air gap along the periphery of craft. Generally we take $\mu(j)$ and $h(j)$ as constants, so that the integration of the above expression can be written as

$$Q = [2p_c/\rho_a]\mu h l_j \tag{2.9}$$

The A. A. West single wall theory [10]

Flexible skirt configurations evolved from the peripheral jets, via the jetted bag skirt to bag and finger type skirts. Transverse sections showing these skirts are shown in Fig. 2.3.

The physical phenomenon with respect to bag–finger skirts now widely used in ACV/SES, is not suitable for explanation by the theories mentioned above, such as thin jet theory and exponential theory.

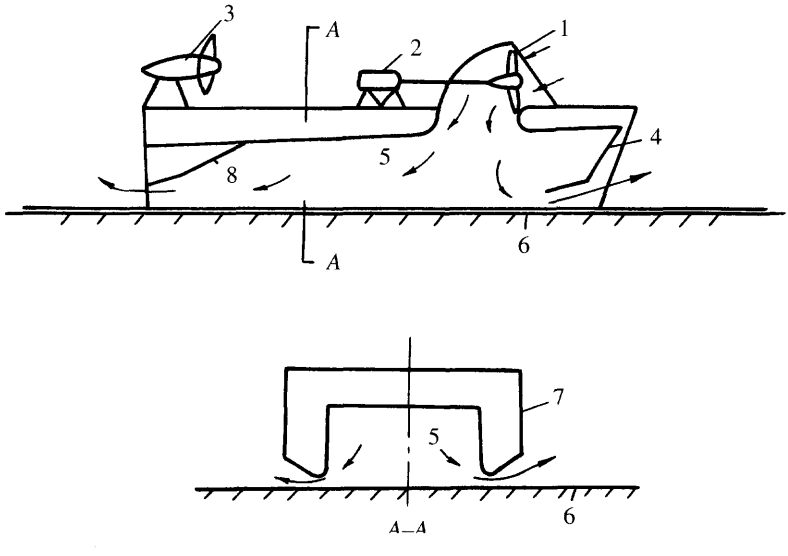

Fig. 2.2 Cross-section of SES with plenum chamber cushion. 1: lift fan, 2: lift engine, 3: propulsion engine and propeller, 4: bow seal, 5: air cushion plenum chamber, 6: rigid surface, 7: sidewall, 8: stern seal.

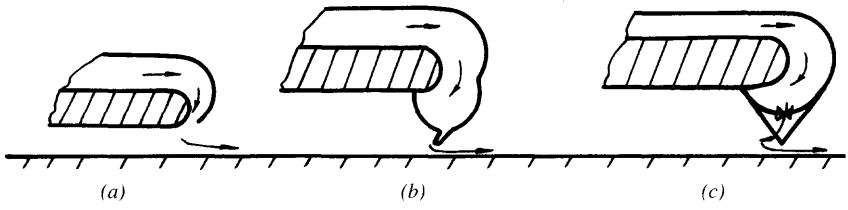

Fig. 2.3 Skirt configurations: (a) rigid peripheral jet; (b) inflated bag with short nozzles; (c) bag and finger type skirt.

A. A. West assumed that the flow completely stuck to the inner surface of the skirts as soon as it jetted from the nozzles in the bag, in the manner as shown in Fig. 2.4. He also assumed that:

- The total pressures along the section of jet were constant.
- At section e, part of the flow blows to the atmosphere and another part blows into the air cushion. Point B′ is its separation point.
- The static pressure along the nozzle (section j) is also constant.

Thus the flow momentum for the air jetted into the cushion, per unit length of nozzle, may be written as follows (cf. equations 2.1–2.4)

$$M_j = \rho_a V_j^2 t \tag{2.10}$$

According to the Bernoulli equation, the total pressure of the jet at the nozzle, the sum of the static pressure head and dynamic (kinematic) pressure, can be written as

$$p_t = p_c + 0.5\rho_a V_j^2$$

thus

$$M_j = 2(p_t - p_c)t \tag{2.11}$$

where V_j is the jet velocity at nozzle, t the nozzle thickness, p_c the cushion pressure and p_t the total pressure of the jet at the nozzle.

Meanwhile, it is assumed that the flow momentum per unit length of air curtain along the streamlines AA′ and BB′ to the atmosphere was M and remains constant at the locations e and o. On this basis there is no loss of flow momentum along the streamline AA′. This assumption was not precise, but it was proved realistic by the experimental results presented in the references of A. A. West's paper [10].

According to Newton's formula, the equation which describes the controlling section shown in Fig. 2.4 may be written as follows:

$$M_j \cos\theta + M_e = p_c h_b - p_0 h_s - \int_0^l p \sin\theta \, dl \tag{2.12}$$

where h_b is the vertical distance between the rigid bottom of the craft and the rigid surface, h_s the vertical distance between the lower tip of the single wall skirt and the rigid surface, p the static pressure of cushion air on the inner wall of the skirt, p_0 the atmospheric pressure, and l the length of the angled skirt wall.

The static pressure locally along the inner wall of a skirt is variable, hence the integral in the last term of equation (2.12). The closer it approaches the lower tip of the

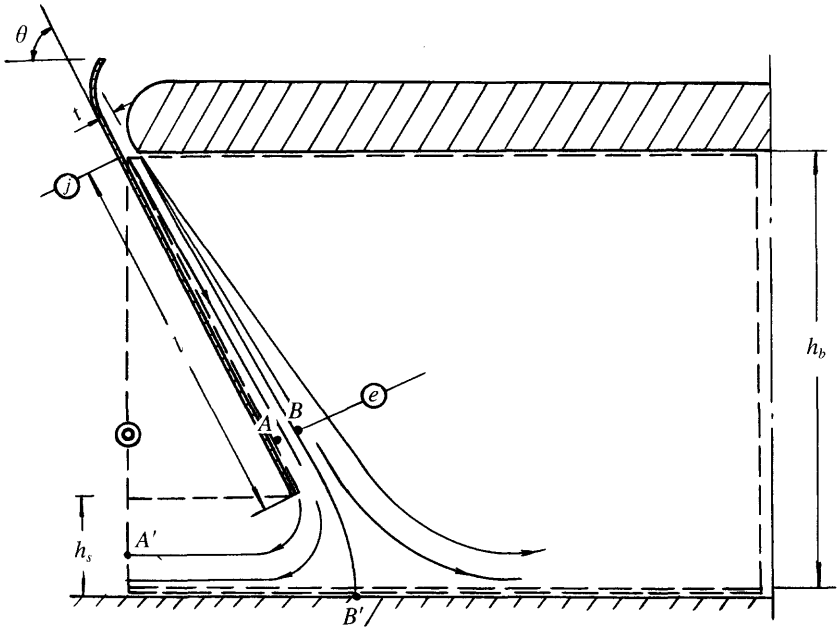

Fig. 2.4 Hypothesis for air jet streamlines based on A. A.West's single wall theory.

skirt, the lower the pressure and nearer to atmospheric pressure. However, globally it is reasonable to assume that the static pressure mentioned above is constant, namely cushion pressure p_c and then the above formula may be written as

$$M_j (\cos\theta + M_e/M_j) = (p_c - p_0)h_s \tag{2.13}$$

Based on the Mayer velocity distribution and boundary layer thickness for a two-dimensional jet with enclosing wall and turbulent flow, the ratio of flow momentum at section e to that at section j has been derived by A. A. West as follows:

$$M_e/M_j = 2.75\,(l/t)^{-0.45} = 2.75\,((h_b - h_s)/(t\sin\theta))^{-0.45} \tag{2.14}$$

where h_s is the air clearance of the nozzle.

Upon the substitution of equations (2.11) and (2.14) in equation (2.13), we have

$$\frac{p_c - p_0}{p_t - p_0} = \frac{1}{1 + \{h_s/[2t\cos\theta + 2.75\,((h_b - h_s)/(t\sin\theta))^{-0.45}]\}}$$

Thus, the flow rate per unit air curtain length can be written as

$$m = \rho_a[2(p_t - p_c)/\rho_a]^{0.5}\, t/h_s$$

or

$$\frac{m}{[\rho_a(p_c - p_0)]^{0.5}} = \left| \frac{1}{h_s[\cos\theta + 2.75\,((h_b - h_s)/t\sin\theta)^{-0.45}]} \right|^{0.5} \tag{2.15}$$

The lift power per unit air curtain area can be written as

$$N[\rho_a/(p_c - p_0)^3]^{0.5} = (2^{0.5}t/h_s)[1 + \{h_s/[2t\cos\theta + 2.75((h_b - h_s)/t\sin\theta)^{-0.45}]\}]^{0.5}$$

$$\times \{h_s/[2t\cos\theta + 2.75((h_b - h_s)/t\sin\theta)^{-0.45}]\}^{0.5} \quad (2.16)$$

where m is the flow rate per unit air curtain length and N the lift power per unit air curtain area.

While A. A. West's theory could be applied to real craft with a bag and finger skirt, the disadvantages of this approach would be as follows:

- The assumption made by West that the bag and finger type skirt may be simplified as a simple single wall skirt and the air curtain jetted from a nozzle stuck to the skirt finger does not agree with practice.
- The theory does not consider the effect of viscosity of air as a real fluid. Real flow conditions can be illustrated as in Fig. 2.5. Thanks to the viscosity of flow a lot of air will be ingested from the atmosphere into the air curtain to form a combined flow, namely the curtain jet flow m_c which will separate into two curtains, one to the atmosphere and another into the cushion.
- The theory does not consider the flow energy losses from nozzles in the bag. Clearly this is not reasonable for bag and finger skirts, though it is acceptable for open loop designs.
- It is not reasonable to assume zero energy loss between the flow streamlines AA′ and BB′, i.e. losses in a two-dimensional jet in a real fluid as against an infinitely thin jet.

2.3 Practical formulae for predicting air cushion performance

The various theories described above to predict the static air cushion performance of craft over ground, have disadvantages as follows :

- The theory based on a thin nozzle correlated with experimental results in the early research stage of hovercraft has precision at large hover heights (clear air gap), but is not realistic for small hovering heights, as is the case of craft with bag and finger skirts. This is because the air curtain jetted from under segments or fingers will be distorted by the proximity of the ground and the complex geometry of the finger itself.

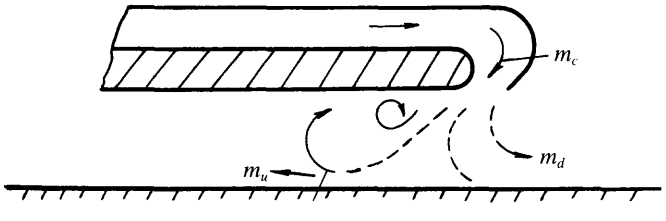

Fig. 2.5 Actual air streamlines including air viscosity.

- In order to simplify the formulae, the viscosity of air is not considered in the theory. This was because it was too difficult analytically to predict the air cushion characteristics including the viscosity (turbulence) of air flow. For air jet cushions, some approximations may be made, but for a segmented skirt, this becomes too complex for analytical treatment.
- The hydrodynamic performance of the bag and finger type flexible skirt will change dramatically from the above formulae, therefore some experts, such as Professor P. Kaplan [11], considered that the simple theory for craft with a plenum chamber is better applied to such skirts even though this approach is somewhat conservative.

The plenum chamber theory does not include the enclosing wall effect of the flow and for this reason experimentally derived methods for predicting static air cushion performance may be used to reduce the inherent conservatism. MARIC commenced the experimental investigation on static air cushion performance for two-dimensional flexible skirts on rigid surfaces in 1974. Since then the theories for three-dimensional skirts and also performance over a water surface have been investigated regarding the influence of the seal effect. This will now be outlined.

Experimental method and equipment

MARIC used two skirt test rigs as the main experimental method; a small rig (Fig. 2.6) was used for qualitative analysis and a larger one for quantitative analysis (Figs 2.7–2.9) to obtain a higher Reynolds number at its jet nozzles. The principal dimensions of the two rigs are listed in Table 2.2.

The full-scale skirt of a 50–80 t ACV can be simulated in the big test rig and the air flow rate can be measured by means of conversion from static pressure measurements

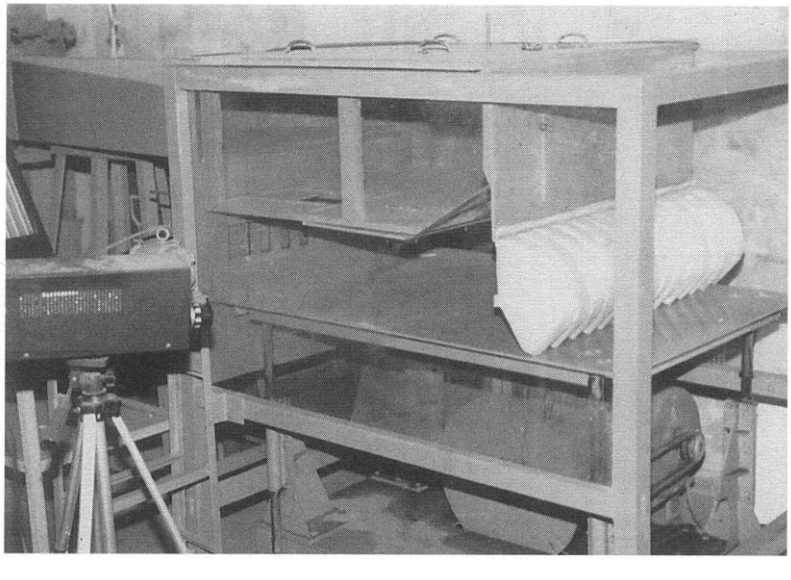

Fig. 2.6 MARIC's small skirt test rig.

Table 2.2 The principal dimensions for large and small sized MARIC skirt test rigs

	Small box	Big box
Box length (mm)	1050	4400
Box width (mm)	700	2230
Box height (mm)	1000	3350
Permitted max. height for test skirt (mm)	350	1500
Permitted max. width for test skirt (mm)	700	2200
Reynold's number, Re, for jet flow	$2 \times 10^3 \sim 4 \times 10^4$	$5 \times 10^4 \sim 2 \times 10^5$

at the air inlet of the centrifugal fan. In addition, air gap, cushion pressure and bag pressure can all be measured. The calculation error is small because of its relatively large size and the *Re* for flow in the jet can be above the minimum *Re* required for turbulent flow.

Test data obtained are more precise and stable from the large box. The box length is about 4 m, which was found to be the minimum length to give stable cushion pressure within the box (early experiments with skirt boxes had problems with unstable flow). This has been verified by experiments carried out.

We use the following main dimensional ratios of skirts for investigation (see Fig. 2.9):

$$H_1/H_2 \qquad S/B_b \qquad x/B \qquad \theta$$

where H_1 is the height of skirt bag, H_2 the height of fingers, S the area of the air feeding hole in each finger space, B_b the finger width, x the location of holes, relative to finger attachment and θ the angle of segment or finger outer face to the ground.

Tests for three sets of skirts were carried out in the small test rig, giving test sample data as shown in Table 2.3. It was found that influence of H_1/H_2 on static air cushion performance of a two-dimensional skirt was small. For this reason, for simplicity, we neglected the parameter H_1/H_2 to save on test time and expense on a large skirt box. Owing to the lower accuracy both for manufacture of the skirt and regulation of hovering height, as well as the irregular shape for small size of skirts, the errors for test

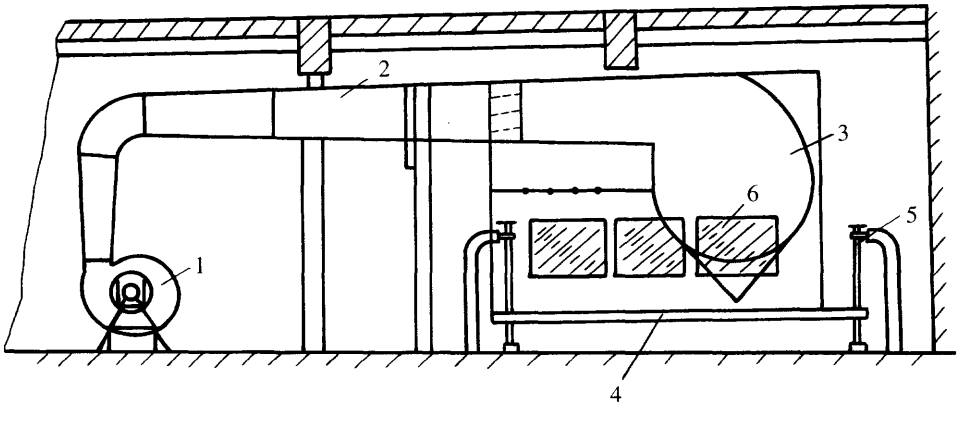

Fig. 2.7 Sketch of MARIC's large skirt test rig. 1: air supply fan, 2: air ducting system to skirt section, 3: skirt section, 4: movable ground plate, 5: ground plate oscillation system, 6: observation windows.

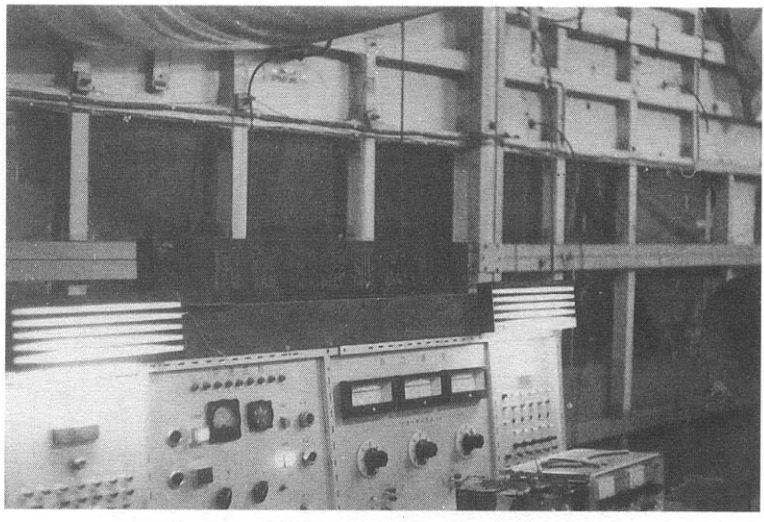

(a)

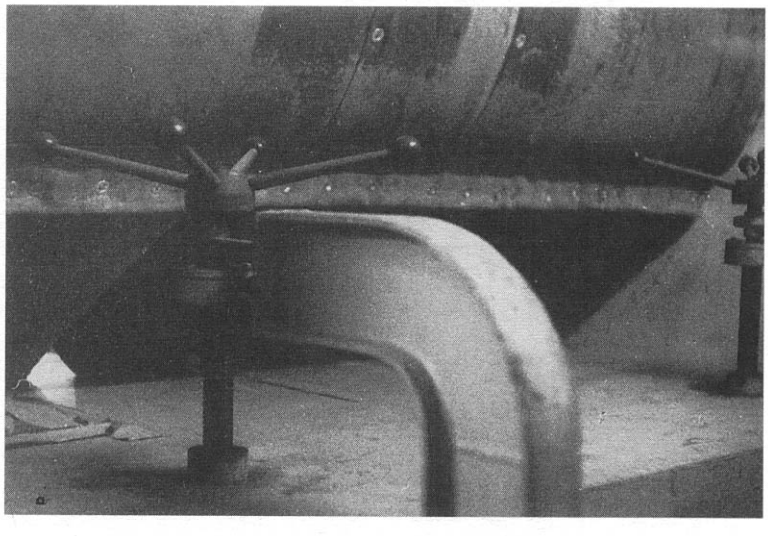

(b)

Fig. 2.8 Test section of the large skirt test rig: (a) side view; (b) skirt and movable bottom.

Table 2.3 Test sample data for small skirt test rig

$S/B_b = 0.0289$ $x/B = 0.512$	H_1/H_2
Project 1	0.715
Project 2	1.0
Project 3	1.285

results would be increased, thus the test data would be unstable and scattered. Nevertheless it could be used as a qualitative investigation for selecting the skirt configuration for test in the larger rig. The test sample data for the big skirt test rig are shown in Table 2.4.

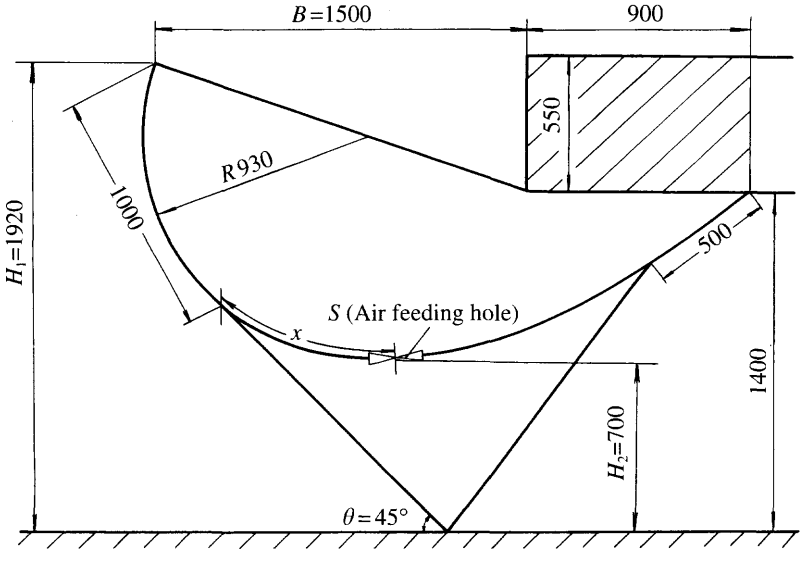

Fig. 2.9 Dimensions of typical bag and finger type skirt on the large skirt test rig.

Table 2.4 Test sample data for big skirt test rig

Items	x/B	S/B_b
1	0.512	0.0203
2	0.512	0.0289
3	0.512	0.0424
4	0.512	0.0610
5	0.512	0.0289
6	0.333	0.0289
7	0.700	0.0289

Analysis methods

The cushion pressure can be expressed by the following relations:

$$p_c = f\{h, H_1, H_2, b, t, v_j, Re_j, \ldots\} \tag{2.17}$$

where the geometrical parameters are as shown in Fig. 2.9 and h is the hover height, t the average nozzle thickness, $t = S/b$, v_j the jet velocity, Re_j the Reynold's number for the jet nozzle, $Re_j = v_j t/\upsilon$, and υ the kinematic viscosity coefficient. According to the theory of dimensionless analysis, this equation can be written as

$$\bar{p}_c = p_c/q_j = f_1\,(h/t,\ H_1/H_2,\ S/B_b,\ x/B,\ Re_j) \tag{2.18}$$

Bag pressure can also be written as follows:

$$\bar{p}_t = p_c/p_t = f_2\,(h/t,\ H_1/H_2,\ S/B_b,\ x/B,\ Re_j) \tag{2.19}$$

where p_t is the skirt bag pressure and $q_j = 0.5\rho_a v_j^2$.

Considering that the jet nozzle *Re* on the big skirt test rig is in the turbulent region and the effect of H_1/H_2 to p_c can be neglected, then the relative cushion pressure can be written as follows:

$$\bar{p}_c = f_1\,(h/t,\ S/B_b,\ x/B) \tag{2.20}$$

In order to save time for test and analysis and also considering that the foregoing formula should be processed by three-dimensional regression analysis, the test projects can be arranged as shown in Table 2.4 and also taking the $\bar{p}$ as the function of relative hovering height, namely $\bar{p}_c = f(h/t)$. Then the correction with respect to S/B_b and x/B can also be considered. The same method can be used with the other characteristics of hovercraft such as cushion flow rate coefficient, cushion power coefficient and skirt bag pressure coefficient to derive these as well. These coefficients can be written as follows:

$$\begin{aligned}
\bar{p}_c &= f_{pc}(h/t) \\
\bar{p}_t &= p_c/p_t &&= f_{pt}(h/t) \\
\bar{m} &= m/(\rho_a p_c)^{0.5} &&= f_m(h/t) \\
\bar{n} &= (N\rho_a^{0.5})/p_c^{1.5} &&= f_p(h/t)
\end{aligned} \tag{2.21}$$

where $\bar{p}_c$ is the cushion pressure coefficient, namely the relative cushion pressure, $\bar{p}_t$ the bag to cushion pressure ratio coefficient, $\bar{m}$ the cushion flow rate coefficient, $\bar{n}$ the cushion power consumption coefficient, $\bar{m}$ the mass flow rate per unit area of air curtain, $m = Q\rho_a/l_j h$, l_j the peripheral length (m), ρ_a the air density (Ns^2/m^4), Q the cushion volumetric flow rate (m^3/s) and N the power consumption of hovercraft per unit area of air curtain (Nm/s per m^2). All of the coefficients mentioned above are dimensionless.

Analysis of streamlines from tests

Due to the large size of the skirt test rig, the streamlines may be plotted (Figs 2.10 and 2.11) for two hovering conditions, one for large hovering height ($h/t < 1$) and one for small hovering height ($h/t \cong 0.15$).

The length and thickness of the enclosing wall for the jet (the total pressure of flow will drop dramatically outside such thickness so Pitot and total pressure measurements can be used to survey it), the total pressure and the separation point B can be measured. The streamline chart for large/small hovering height was obtained as shown in Figs 2.10 and 2.11 respectively. It is found that the following physical phenomena are observed:

- The length and effect of enclosure for a jet with definite angle can be found by testing, although in the case of the bag and finger skirt, in which the flow will diffuse suddenly at the location of holes, it will also be related to the location of the holes and hovering height.
- Owing to the effect of the enclosing wall on the jet, the air flow at the segment tip possesses the function of sealing the air cushion, especially in the case of large air clearance (Fig. 2.10) and the separation point *B* appears very close to the ground. Its position inside or outside the skirt tip line is dependent on the cushion pressure

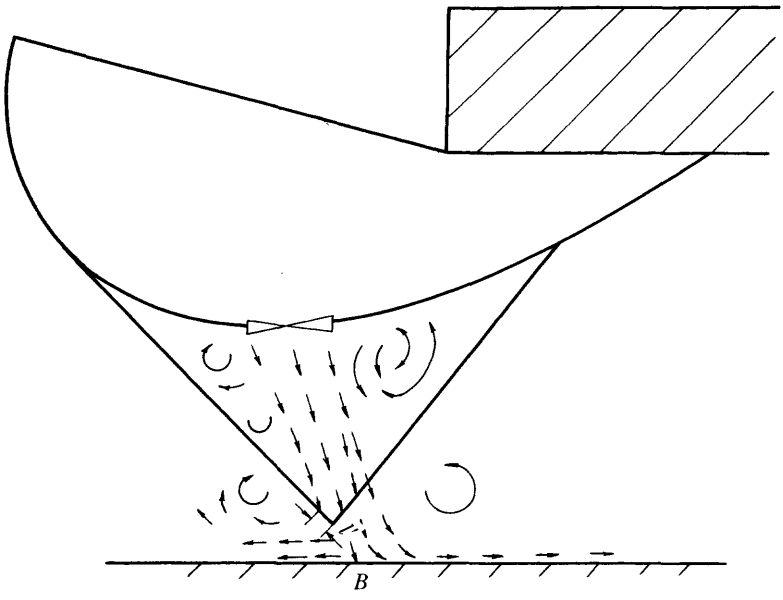

Fig. 2.10 Air streamline diagram at higher air clearance.

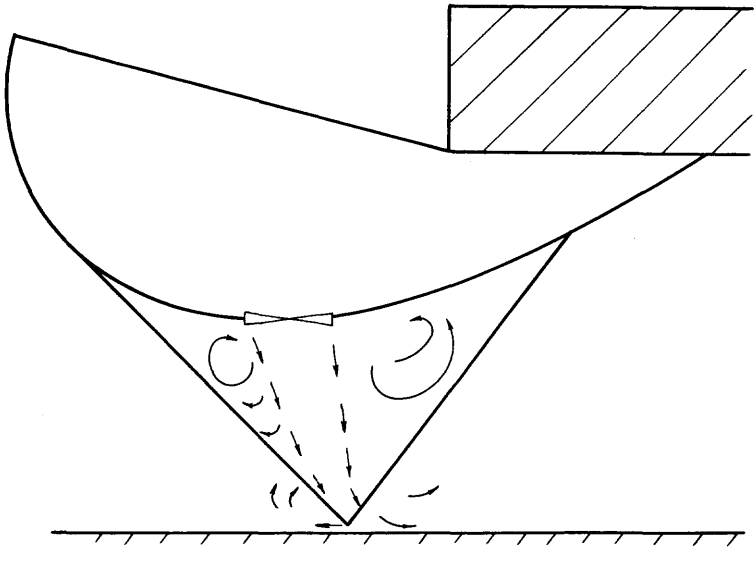

Fig. 2.11 Air streamline diagram at lower air clearance.

and the segment geometry. These factors can affect the dynamic response of the skirt in operation.

- A series of vortices is formed around the nozzle which causes some flow energy losses, but these do not affect cushion pressure very much because of its weak

vorticity, even though the range of vortices is rather large. Simultaneously, the test cushion pressure distributes uniformly.

- According to analysis of the streamline charts, it is found that the location of the feed holes in the bag will affect the jet flow enclosing length and consequently the air cushion performance.

  For this reason, an optimum hole location x/B and relative area of hole S/B_b may be found. The best location is generally close to the segment upper attachment, though some experimentation is necessary for optimization, once the overall skirt section has been designed. This is always a worthwhile exercise.
- Owing to the enclosing effect of the jet flow assisting sealing of the air cushion, this is equivalent to a reduced flow coefficient during leakage of air from a small hole to the atmosphere, consequently the approach will be to concentrate on defining the relative flow coefficient $\bar{m}$ and cushion pressure coefficient $\bar{p}_c$ at different ground clearances (air gap under skirt tip).

Experimental results and analysis

The loss of air (leakage) between the skirt and box wall has to be considered, which leads to the equivalent air clearance of the skirt h, and can be written as

$$h = h_0 + h'$$

where h_0 is the actual air clearance of the skirt, namely, the vertical distance between the lower edge of the skirt finger and the ground, and h' the equivalent air clearance of skirt considering the air leakage loss between the skirt and box wall as well as the gap between the fingers. The air leakage therefore has to be corrected in the case of fitting a regression line for cushion flow derived from the test results. The following observations were made at MARIC:

1. It was found that the test results are concentrated, having a small standard deviation, which was also verified by test results gathered for another series which was carried out one year later. The test data were considered stable and the selected parameters to be reasonable.
2. For a conventional bag and finger type skirt, with parameters such as $H_1/H_2 = 1$; $x/B = 0.512$; $S/B_b = 0.0289$; the cushion pressure coefficient $\bar{p}_c$, cushion flow rate coefficient $\bar{m}$, bag and cushion pressure ratio $\bar{p}_t$ and cushion lift power coefficient $\bar{N}$ can be regressed to the following expressions (see Figs 2.12, 1.14 and 1.26):

$$\bar{p}_c = p_c/q_j = 0.602\,(h/t)^{-0.403} \tag{2.22}$$

$$\bar{p}_t = p_c/p_t = 0.638\,(h/t)^{-0.49} \tag{2.23}$$

while

$$h/t < 1.05 \quad \bar{m} = m/(\rho_a p_c)^{0.5} = 0.625\,(h/t) - 0.415 \tag{2.24a}$$

$$h/t > 1.05 \quad \bar{m} = m/(\rho_a p_c)^{0.5} = 0.848 - 0.147\,(h/t) \tag{2.24b}$$

$$h/t = 1.05 \quad \bar{m} = m/(\rho_a p_c)^{0.5} = \text{average of (equations 2.24a and b)}$$

These expressions are suitable for h/t between 0.4 and 2.5; alternatively, the following may be used:

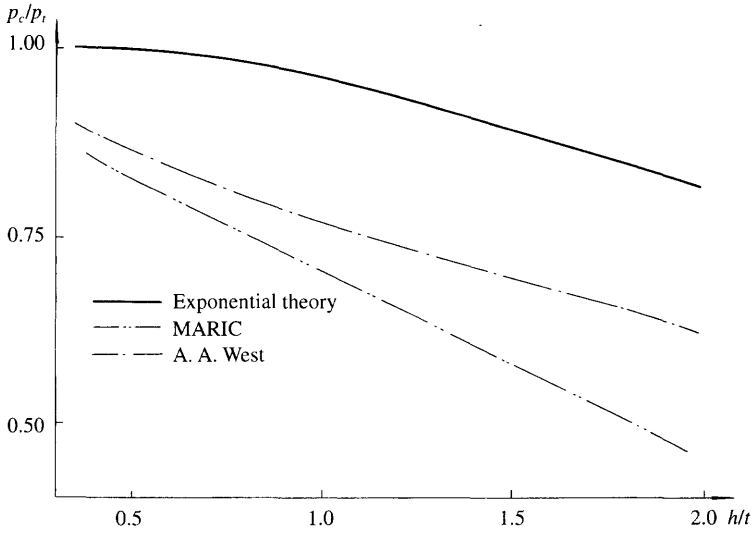

Fig. 2.12 Comparison of bag / cushion pressure ratio versus h/t between various theories.

$$\bar{m} = \mathrm{m}/(\rho_a p_c)^{0.5} = 0.632\,(h/t)^{-0.336} \tag{2.25}$$

$$\bar{N} = (N\rho_a^{0.5})/p_c^{1.5} = 1.05\,(h/t)^{-0.067} \tag{2.26}$$

This equation can be corrected with regard to various x/B and S/B_b, as described in [12].

3. The optimum location of x/B can be derived as $(x/B)_{opt} = 0.48$–0.54. It seems that this is not in relation to h/t, i.e. the air curtain can be sealed as long as the flow jetted from the nozzle can attach to the skirt wall, even though only a little way up the segment. The effect will reduce in the case of $x/B > 0.54$ and the effect of the jet enclosing wall will be enhanced in the case of small x/B, but at a penalty of increasing internal flow losses.
4. The loss across the nozzle jet increases as the area of the nozzle decreases, i.e. p decreases inversely with p_t.
5. The calculated results from exponential theory, the theory of A. A. West, plenum theory and MARIC theory may be compared and discharge coefficient μ applied to plenum chamber theory. The results can be written as [9]

$$\mu \approx 0.5 + 0.05\,(\pi/2 - \theta')^2$$

or

$$\mu = 0.5 + 0.4 \times 10^{-3}\,\theta' + 0.109 \times 10^{-4}\,\theta'^2 - 0.494 \times 10^{-7}\,\theta'^3 + 0.345 \times 10^{-9}\,\theta'^4$$

where θ' is the inclination angle of the skirt finger. We take $\mu \cong 0.53$ where $\theta = 45°$

It is found that the value of $\bar{m}$ from test results is smaller than that given by the formula from plenum chamber theory, in the case of $h/t > 0.6$, because the jet flow

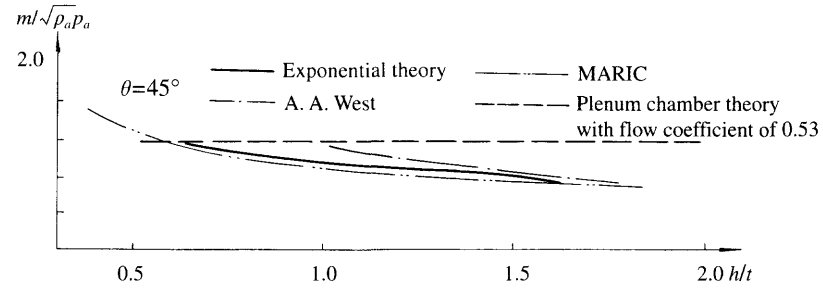

Fig. 2.13 Comparison of air flow coefficient between various theories: exponential theory; A. A. West theory; MARIC theory; plenum chamber theory with air flow rate coefficient of 0.53.

follows the angle of the wall of the finger, consequently contracting the cushion outflow jet so as to reduce the cushion flow rate.

From the figure the greatest difference in $\bar{p}_t$ is found between the test results and the results calculated by the exponential formula and the West formula in the case of large h/t values. However, all of them will be closer in the case of smaller h/t. The test result for the cushion lift coefficient (Fig. 2.14) is higher than that calculated from the exponential and A. A. West's theories, because the experiments accurately simulate the losses through the feed holes of bag–finger skirts and the weak effects of the jet enclosing the walls.

6. The effect of the skirt material on the static air cushion performance. Reference 13 listed eight test samples with different materials which are shown in Table 2.5. The test results showed the effect of specific weight of skirt material on the static shape of skirts.

   It is found that skirt material characteristics do not greatly affect the static air cushion performance in the case of any given configuration and hovering height of the skirts. The effect of skirt material characteristics on the hovering height can therefore normally be neglected and the hovering height can be measured directly during tests. The effect of specific weight of skirts on the geometric shape will be described in Chapter 7. From such tests it is also found that the effect of elasticity of skirt material on the shape of the skirt is weak.

Table 2.5 Experimental samples of skirt for various skirt materials [14]

Model	Scale ratio λ	Width of air duct/ width of bag	Equivalent nozzle width/0.095	Skirt material	Test equipment
1	1	0.625	1	9514 Rubber core	Large rig
2	1	1	1	9514 Rubber core	Large rig
3	1/2	1	1	6408 Rubber core	Large rig
4	1/2	1	1/2	6408 Rubber core	Large rig
5	1/2	1	1/2	1533 Rubber single surface coating	Large rig
6	1/2	1	1	1533 Rubber single surface coating	Large rig
7	1/8.9	1	1/8.9	Plastic diaphragm	Small rig
8	1/8.9	1	1/8.9	9514 Rubber core	Small rig

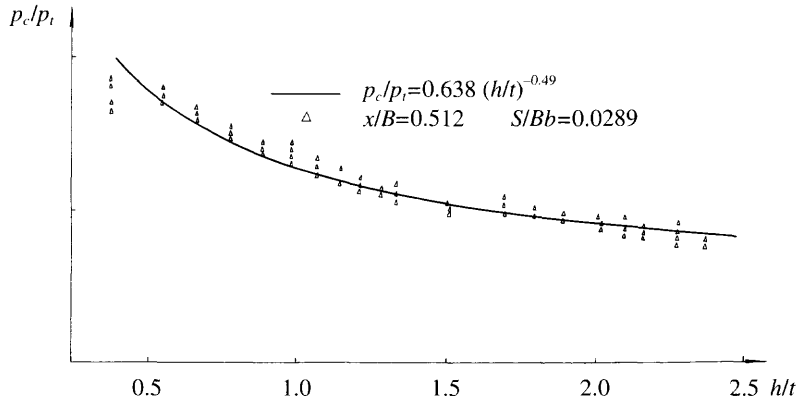

Fig. 2.14 Relation between bag/cushion pressure ratio p_c/p_t and relative air gap h/t.

7. Scale effect. From the tests described above, it was found that the Re_j greatly affects static hovering performance of skirts. In general the turbulent flow region can be established as $Re_j > 8 \times 10^4$.

   In the experiments themselves the data points do not scatter, as long as $Re > 10^5$. Because the Re on the small skirt test box is smaller than that on the large box, in general $Re_j = 1.1\text{–}2.4 \times 10^4$ for the small box, this leads to greater scatter and to errors in evaluated $\bar{p}_c$, $\bar{m}$ and $\bar{p}_t$. It demonstrates that the air clearance of model craft is less than that of full-scale craft even though the fans, air ducts and the geometric configurations for both are similar, because the model Re is less than the critical Re, i.e. $< 10^5$.

   For this reason, model simulation experimental results gain an error not only from static hovering tests in a skirt test box, but also calm water resistance tests and seaworthiness tests because of their low Re and thus lower air clearance of models. Sometimes, in order to eliminate such errors, one increases the revolution of model fans deliberately, to increase the air gap, since one would rather be similar on air clearance than the dynamic simulation on model fans.

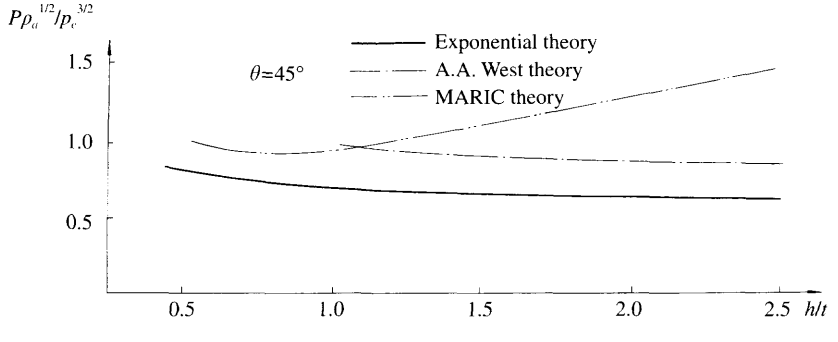

Fig. 2.15 Comparison of lift power output coefficient between various static air cushion theories.

2.4 Static air cushion characteristics on a water surface

Static hovering performance of SES on water

The various shapes of mid-sections of sidewalls are shown in Fig. 2.16; a typical one is figure (a), namely sidewalls with perpendicular inner and outer walls near the water surface. The craft total weight is supported by a combination of cushion lift and buoyancy of the sidewall, which can be expressed as

$$W = p_c S_c + 2V_0 \gamma_w \tag{2.27}$$

where W is the craft weight (N), p_c the cushion pressure (N/m^2), S_c the cushion area (m^2), V_0 the volumetric displacement provided by each sidewall (m^3) and γ_w the specific weight of water (N/m^3).

According to Archimedes' principle, the relationship between cushion beam, inner and outer drafts and width of sidewalls with different shape can be determined by the following expressions and those in Fig. 2.16:

$$S_c = B_c l_c \tag{2.28}$$

$$t_o - t_i = p_c/\gamma_w \tag{2.29}$$

where t_o is the outer draft of sidewalls (m), t_i the inner draft of sidewalls (m), l_c the cushion length (m), B_c the cushion beam (m) and w the calculating width of sidewalls (m). The inner sidewall draft gradually reduces as lift power is increased and cushion air will leak from under both sidewalls once the cushion pressure exceeds the inner sidewall draft (Fig. 2.17), as well as under the bow and stern seals, and form the plenum type of craft, similar to the craft model '33' of HSEI and the US Navy SES–100B. The drag of this type of craft decreases dramatically as lift power is increased.

The outer draft of sidewalls, t_o, is dependent upon the lift fan(s) flow rate and the inner draft, t_i, is dependent upon the cushion pressure p_c. The air leakage from the

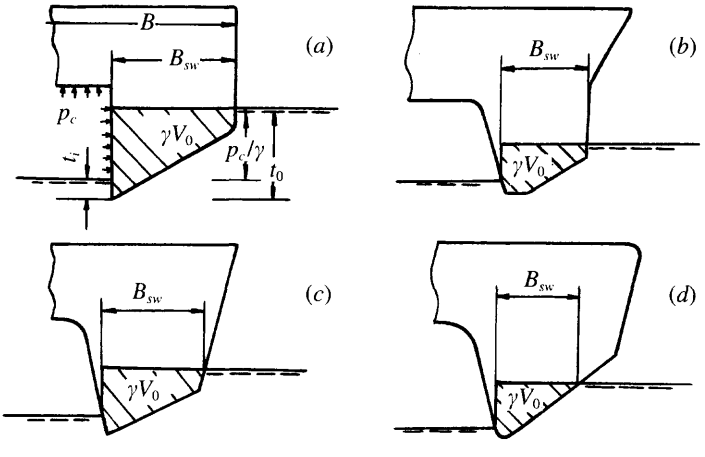

Fig. 2.16 Sidewall thickness on various sidewall configurations.

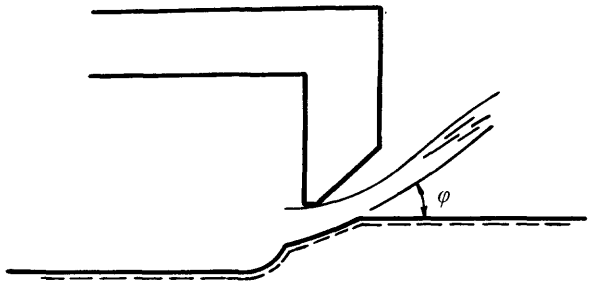

Fig. 2.17 Air leakage under SES sidewall with large air flow rate, hovering static over water.

cushion at the bow (also at the stern), can be illustrated as in Fig. 2.18. The flow rate of an SES hovering statically on a water surface is normally calculated using the following assumptions:

- The air flow is non-viscous and incompressible.
- For simplicity, the outlet flow streamline chart can be considered as Fig. 2.18 and takes the actual air clearance as $\phi(z_b - t_i)$ because of considering the contraction of leaking air flow, where z_b is expressed as the bow seal clearance, namely the vertical distance between the craft baseline and the bow seal lower tip. ϕ is the flow contraction coefficient at the bow seal.
- The distribution of static pressure for leaking air flow is a linear function. As shown in Fig. 2.18, the static pressure of leaking air flow is $p_\eta = p_c$ for $\eta = 0$, but while $\eta = (z_b - t_i)\,\phi$, $p_\eta = 0$, where represents the ordinate with the original point B and upward positive.

Thus the static pressure of leaking air flow at any point can be represented by

$$p_\eta = p_c[1 - \eta/(\phi(z_b - t_i))] \tag{2.30}$$

According to the Bernoulli theory, the horizontal flow velocity at any point between AB can be represented by following expression:

$$0.5\rho_a U_\eta^2 = p_c - p_c[1 - \eta/(\phi(z_b - t_i))\,] = p_c\eta/(\phi(z_b - t_i)) \tag{2.31}$$

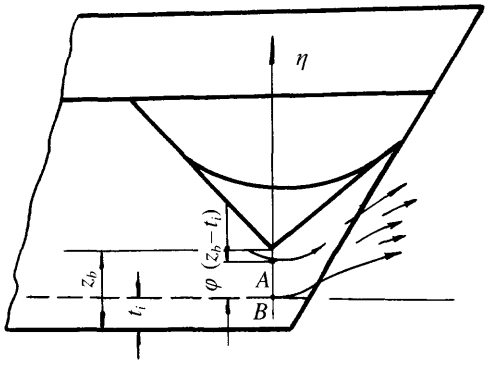

Fig. 2.18 Air leakage under SES bow seal hovering static over water.

where $U\eta$ is the leaking air flow speed in the horizontal direction. It is clear that the flow rate leaking under the bow skirt can be represented by

$$U_\eta = (2p_c\eta)/(\rho_a\phi(z_b - t_i))$$

then

$$Q_b = B_c \int_0^{\varphi(z_b - t_i)} U_\eta d\eta = 2/3\, B_c\phi(z_b - t_i)[2p_c/\rho_a]^{0.5} \tag{2.32}$$

As a consequence, the air cushion flow for craft statically hovering on a water surface is equal to 2/3 of that on a rigid surface, because of the action of back pressure of leaking air.

This estimate is approximate, but realistic and is generally applied as a method of estimation of the flow rate of an SES, because of its simplicity and the difficulty in measuring the steady flow in an SES on a water surface. By the same logic, the flow leaking from the stern seal can be obtained by this method; consequently, the total flow for craft hovering statically on the water surface can be obtained.

It is useful to note that the same reduction in air leakage rate also applies to an ACV hovering over water rather than land.

The static air cushion performance of ACVs on a water surface

The difference between the ACV and SES for static air cushion performance is that the sidewalls provide buoyancy. The typical static hovering attitude of an amphibious ACV can be seen in Fig. 2.19. If one neglects the reaction of the perpendicular components of jets flowing from peripheral and stability nozzles (the value of which is small in the case of small skirt clearance with a bag–finger type), then the cushion lift can be written as

$$\left.\begin{aligned} W &= p_c S_c \\ S_c &= l_c B_c \end{aligned}\right\} \tag{2.33}$$

where l_c and B_c are the cushion length and beam, which can be measured from the line on the plan of the water surface, which the lower tip of skirt is projecting on.

From Fig. 2.19, it is found that the craft weight is equal to the weight of water displaced from the depression; for this reason, the actual skirt clearance is equal to the

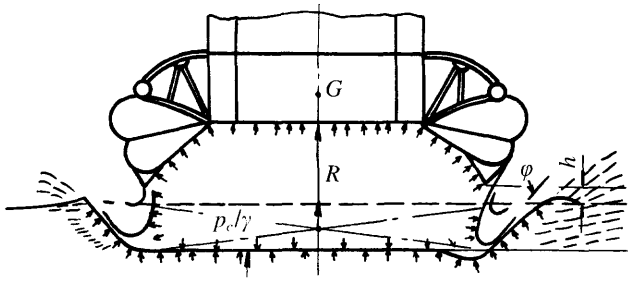

Fig. 2.19 ACV hovering static on water.

vertical distance between the lower tip of the skirt and an undisturbed water surface. Owing to the application of bag and finger skirts and the improvement in performance through development, skirt clearance on a water surface has decreased year by year.

One can observe that the skirt clearance on a water surface is very small on modern ACVs and sometimes the value may be negative for larger craft with responsive skirts. Therefore, it is suggested that cushion air flow can be calculated by plenum chamber theory or the foregoing methods applied to SESs. The peripheral jet requires much higher air flow to seal the air cushion in the case where the craft hovers with a significant gap to the calm water surface.

It is noted that the hovering process for an ACV with flexible skirt is more complicated, and is shown in Fig. 2.20, in which the numbers are explained as follows:

1. This represents that the craft floats off cushion statically on a water surface, the draft of craft is T_0.
2. Lift fan starts to operate, but owing to the low revolutions, fan pressure is low, therefore $T < T_0$. Though the craft is partially supported by air pressure, the draft of the buoyancy tank is still larger than zero to provide partial support of the craft.
3. Fans speed is continuously increasing. In the case of $T = 0$, namely zero draft of the buoyancy tank, then the weight of the craft will be completely supported by cushion lift.
4. The fan speed is increasing further, pressure remains almost constant while flow rate is increased, thus the skirts begin to inflate. A positive hull clearance h' begins to be gained, but smaller than design hull clearance.
5. The hull clearance is equal to design value h_s', a large amount of cushion air is now leaking under the peripheral skirt, the volume being dependent on the fan characteristic and lift power.

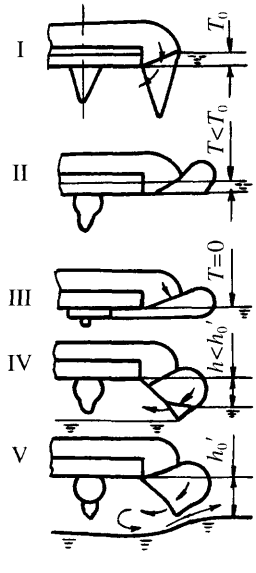

Fig. 2.20 Various static hovering positions of an ACV.

The air cushion characteristic curves for both ACV/SES are shown by Fig. 2.21 (the calculation in detail can be found in Chapter 11, Lift system design), where

- H_j–Q represents the characteristic curve of lift fans, p_t–Q represents the characteristic of the air ducting, i.e. the characteristic curve of a fan at any given revolution minus the pressure loss of flow in air duct, p_t represents the bag pressure of skirts and p_t–Q also represents the characteristic of the bag.
- p–Q represents the characteristic for static air cushion performance, namely the relation between flow and bag pressure at various hovering heights, which can be obtained by the foregoing formula. For this reason, the curve p–Q represents the relation between the bag pressure and flow rate and p_t–Q denotes the total pressure of air duct (or bag) at various hovering heights and fan revolutions.

The intersection point of both curves represents the hovering height of the craft at a given craft weight (a given cushion pressure) and any given fan speed. Hence, the air cushion characteristic curve for an ACV can be described as follows (also similar for an SES):

1. The minimum fan speed for inflating the skirt of an ACV (similar to the hovering attitude 4 in Fig. 2.20), will be that at which the total pressure of the lift fan equals the cushion pressure at the zero flow rate. At this point the craft weight is supported by cushion lift perfectly, but without having risen from the static condition. In the case of zero flow rate the total pressure of the fan is equal to the total pressure of the duct bag and thus to the cushion pressure.
2. The factors necessary for hovering the craft, i.e. from attitude 1 transient to attitude 3, is that the bottom of the buoyancy tank has to leave the water surface in order to exert the cushion pressure to the bottom and lift the craft. At MARIC

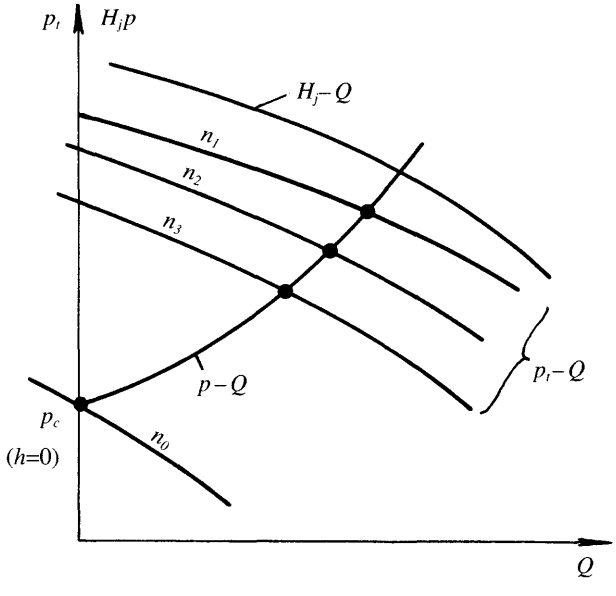

Fig. 2.21 Air duct and air cushion characteristics curves of ACV/SES.

there is experience that a hole for take-off has had to be installed in the craft bottom or skirt near the water surface (Fig. 2.22) in order to blow off the water in the cushion in order to exert cushion pressure on the bottom, because the height of a skirt of a jetted bag type (say, $H > 1$ m for medium-sized ACV) is always higher than the cushion pressure measured by the water head (namely $p_c < 0.3$ m H_2O).

3. The minimum fan speed of an SES for static hovering can also be defined, namely the condition of zero flow is equivalent to the situation that the inner draft of sidewalls t, has to equal the bow/stern clearance and also satisfy the following equation:

$$W = P_{c0}S_c + V_{io}\gamma$$

where P_{c0} is the cushion pressure, namely, the fan total pressure at given speed and zero air flow rate, S_c the cushion area, at the sidewall draft for zero flow from bow and stern seals, V_{i0} the displacement (volumetric) of the sidewalls at W the weight of craft. This is the same draft, the necessary condition for an SES hovering in such a mode, namely the cushion air just blows off under the bow/stern skirt (not under the sidewalls).

It should be noted here that it is important for sidewall craft to have a positive value of t_i (Fig. 2.16) so that air is not leaked under the sidewalls. Experience suggests that t_i should be 15–20% of t_o. Below 15% air will start to be lost under the keels in relatively small sea states, restricting performance. SES may also need deeper draft and t_i at the stern to prevent propeller cavitation or water jet ingestion of cushion air. Sometimes a fence, or keel extension may be installed to help solve this problem.

2.5 Flow rate coefficient method

The relation between the cushion air flow rate and pressure for craft hovering on a rigid surface and calm water has been derived. However, the bag and finger type skirt with a small number of large holes for feeding the air into the air cushion from the

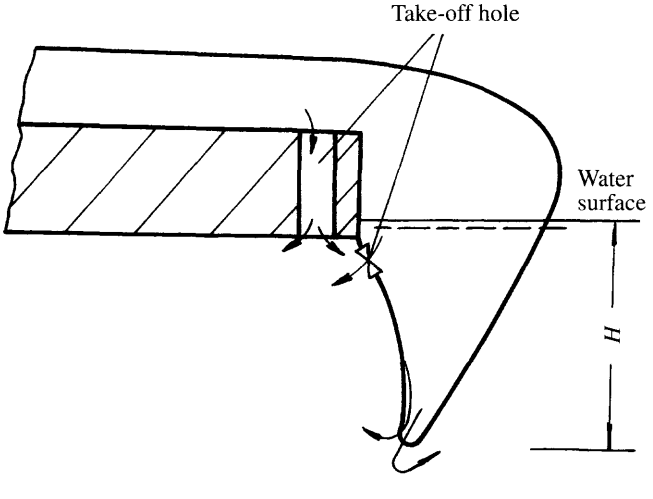

Fig. 2.22 Take-off holes on an ACV.

higher pressure bag is improved by the arrangement of a larger number of small feeding holes. This design improves the strength of skirt bags by reducing stress concentrations and thus the tendency to tear after fatigue due to operation.

The air cushion characteristics of such skirts are closer to those represented by plenum chamber theory. Moreover, the take-off performance and obstacle clearance ability is improved, therefore the flow for the take-off to the planing condition over water is not such an important parameter as concerned designers in the early stage of ACV/SES development. For this reason, rather than spend time on deriving the mathematical expressions for predicting the static air cushion performance, we take the flow rate coefficient $\bar{Q}$ as the factor to represent the static air cushion performance of craft. The relation for $\bar{Q}$ can be written as

$$Q = \bar{Q} S_c \sqrt{(2p_c/\rho_a)} \tag{2.34}$$

In general, we take the values of $\bar{Q}$ to be [15]:

$$\bar{Q} = 0.015 - 0.050 \quad \text{for ACV}$$

$$\bar{Q} = 0.005 - 0.010 \quad \text{for SES}$$

The required value of $\bar{Q}$ is related to the following performance factors:

1. craft drag at full or cruising speed on calm water;
2. take-off ability;
3. seaworthiness;
4. longitudinal/transverse stability of craft;
5. resistance to plough-in, etc.

Acceptable craft performance can normally be obtained if the cushion air system is designed with $\bar{Q}$ in the range above. The quoted range is rather large when designing a large SES or ACV and so it is normally best to start with the lower value (suitable for calm water operation, medium-speed craft) and then assess the additional flow required for items 2 to 5. These factors will be discussed further in following chapters.

As an alternative, particularly for amphibious ACVs, one often takes the skirt clearance of the craft hovering on a rigid surface as the factor to characterize its hovering ability and so to design the lift system. This is a common approach of designers because it is easy to measure the skirt clearance of an ACV both in model and full-scale craft. Although it is not accurate for the reasons outlined in the discussion of the various air jet theories above, it is easier to compare with other craft (or models).

Typically, for smaller amphibious craft the following relation is used:

$$Q = V_c D_c h L (\text{m}^3/\text{s})$$

where

$V_c = \sqrt{(2p_c/\rho_a)}$, the cushion air escape velocity (m/s),

$\rho_a = 1.2257 \text{ kg/m}^3/9.8062 = 0.12499 \text{ (kg m/s}^2\text{)}$

$= (0.07656 \text{ lb/ft}^3/32.17 = 0.00238 \text{ slug/ft}^3 \text{ in imperial units})$

D_c = nozzle discharge coefficient (2.3.4 item 5), $D_c \cong 0.53$ for 45° segment, L = peripheral length of cushion at the ground line (m) and h = effective gap height, typically 0.125 × segment width, or if it may be assumed that segment width is approximately $h_c/2.5$ then $h = 0.05\, h_c$. Thus

$$Q \cong 2.12hL\sqrt{p_c} \tag{2.34a}$$

This relates the required flow to the escape area and should result in a small free air gap under the inflated segment tips of a loop and segment skirted craft over concrete.

2.6 The 'wave pumping' concept

The flow rate, calculated by equation (2.34), may only meet the requirements of skirt clearance for a craft hovering on calm water. As a matter of fact, craft often operate in rough seas, in which the craft pitches and heaves. Therefore designers have to calculate the vertical motion of craft in waves so as to determine the average required flow; this will be demonstrated in detail in Chapter 8.

Here we introduce a concept [16], namely wave pumping, which deals with the extreme hovering attitude of craft in waves. We assume that the cushion inflow rate of craft operating in waves will stay constant, namely the same as that in the static hovering condition. Thus the cushion flow changes as the volume occupied by the wave which is passing through the craft changes, as shown in Fig. 2.23.

Consequent to this, the cushion pressure will fluctuate because of the fluctuation of cushion outflow while constant inflow rate and the incompressibility of cushion air are assumed. Thus, the motion caused by fluctuating cushion pressure is called 'wave pumping' motion. To simplify the calculation, we assume as follows:

- Cushion air is incompressible.
- Waves are simple sinusoidal waves.
- Skirt clearances at bow/stern seals are constant, while the craft operates in head waves.
- The wave peak will never contact the wet deck of craft.
- The lowest edge of the cushion (i.e. the base line of sidewalls) coincides with the horizontal line of trough, namely no air leakage under the sidewalls.

Two typical situations for wave pumping motion of craft operating in waves are shown in Table 2.6. In fact we may assume that the SES can operate in one of three following modes.

First operation mode – platforming

In this mode of operation, the ACV or SES cannot respond to the waves, normally short steep chop, and so as wave peaks pass through cushion pressure is raised, and

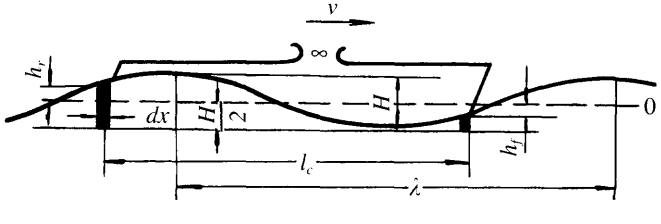

Fig. 2.23 Platforming of SES in waves.

Table 2.6 Craft operational modes with respect to the wave pumping motion

Operation mode due to wave pumping	Running attitude	Cushion over wave crest	Cushion over wave trough
Mode 1	Platforming	Air blown off from cushion	Air feed to cushion to fill cavity
Mode 2	Cushion volume constant	Craft lifted up	Craft drops down

as a trough passes, the air gap under the skirts increases and volume flow increases. The result is a rapid oscillation in the fan characteristic and vibration felt by operators. If lift power is not increased, skirt drag increases and speed reduces, often with a bow-down trim induced and in very short chop possibly a plough-in tendency. In very small sea states, small vibrations can be induced, which feel rather like driving a car over cobbles, hence the effect is called 'cobblestoning'. Normally this only occurs in craft which have a cushion with high volume flow rate.

Second operation mode – constant cushion volume

If the flow rate and cushion volume are held constant, keeping the lift power output at a minimum, then a definite vertical acceleration will exert on the craft because of wave pumping motion. Thus the maximum vertical acceleration can be derived under the action of pumping as follows:

$$(d_z^2/d_t^2)_{max} = [\pi v^2]/[\,10 \times l_c\,] \tag{2.35}$$

This calculation is approximate, because a lot of assumptions have been made. In particular, the heave and pitch motion of the craft in waves and air leakage around the sides of cushion have not been considered, therefore the calculation is very simple and does not demonstrate the seaworthiness quality of the craft.

It does, however, indicate the acceleration which will occur if the craft follows the wave surface profile, where no reserve lift power or inflow rate is available. To reduce this, it is necessary to allow the skirt to respond to the waves, which will then allow air to be pumped out of the cushion. An example calculation for this is given below. The aim of this calculation is to help designers to consider the reserve of lift power which is needed to be available to counteract the extreme motion of craft operating in rough seas.

Third operation mode – combination of first and second modes

The cushion pressure, cushion volume and the height of wet deck relative to the water surface are changed together, namely trading-off both the foregoing motions. In practice this is the mode which practical ACVs operate in.

Platforming analysis

The first mode is platforming, i.e. the cushion pressure and the vertical position of the wet deck remain constant, then the vertical acceleration will also be constant. This is the ideal operating attitude of craft and what the designer requires. However, one has

to regulate the lift power and lift inflow rate to keep the cushion pressure constant. This condition is also the one which will absorb the greatest volume of air; therefore we will make an analysis of this case.

When the craft moves along the x-axis for a distance of dx, then the change of water volume in the cushion can be expressed by the change of water volume at the bow/stern of the craft as shown in Fig. 2.23, then

$$dV = B_c[(H/2 + h_f)dx - (H/2 + h_r)dx] \tag{2.36}$$

where H is the wave height, h_f the bow heave amplitude relative to the centre line of the waves, h_r the stern heave amplitude relative to the centre line of the waves and B_c the cushion beam. Thus

$$\frac{dV}{dt} = b_c[(H/2 + h_f) - (H/2 + h_r)]\frac{dx}{dt}$$

because $dx/dt = 0$,

$$dV/dt = B_c\,(h_f - h_r)\,v$$

where v is the craft velocity relative to the waves.

The wave profile can be expressed by

$$h = (H/2)\sin a$$

where $a = 2\pi x/\lambda$, thus

$$a_f = a_r + 2\pi l_c/\lambda$$

where h is the wave amplitude, l_c the cushion length and λ the wave length. Therefore

$$\begin{aligned}\frac{dV}{dt} &= \frac{B_c H}{2}(\sin a_f - \sin a_r)\,v \\ &= \frac{B_c H}{2}\left[\sin\left(a_r + \frac{2\pi l_c}{\lambda}\right) - \sin a_r\right]v \\ &= \frac{B_c H v}{2}\left[\left(\cos\frac{2\pi l_c}{\lambda} - 1\right)\sin a_r - \sin\frac{2\pi l_c}{\lambda}\cos a_r\right]\end{aligned} \tag{2.37}$$

In order to determine the maximum instantaneous wave pumping rate, we take the first derivative of function dV/dt with respect to a equal to zero, then

$$\frac{d}{da}\frac{dV}{dt} = \frac{B_c H v}{2}\left[\left(\cos\frac{2\pi l_c}{\lambda} - 1\right)\cos a_r - \sin\frac{2\pi l_c}{\lambda}\sin a_r\right] = 0$$

This expression can be written as

$$\tan a_r = (\cos(2\pi l_c/\lambda) - 1)/\sin(2\pi l_c/\lambda) \tag{2.38}$$

Substituting expression (2.38) into (2.37), the maximum instantaneous wave pumping rate can be written as

$$\left(\frac{dV}{dt}\right)_{max} = \frac{B_c H v}{2}\left[\left(\cos\frac{2\pi l_c}{\lambda} - 1\right)\sin a_r - \left[\left(\sin^2\frac{2\pi l_c}{\lambda}\right)\Big/\left(\cos\frac{2\pi l_c}{\lambda} - 1\right)\right]\sin a_r\right]$$

so, using the relation $\sin^2 = 1 - \cos^2$

$$\left(\frac{dV}{dt}\right)_{max} = -B_c H v \sin a_r = -B_c H v \sin a_r \tag{2.39}$$

where $(dv/dt)_{max}$ is the maximum instantaneous wave pumping rate written as

$$a_r = -\pi l_c/\lambda$$

For instance, for the UK's SR.N5 hovercraft, in the case of $\lambda/2 = l_c = 9$ m, $H = 0.8$ m, $v = 35$ m/s then $(dV/dt)_{max} \cong 150$ m^3/s, i.e. the maximum power due to the wave pumping is 172.7 kW. The total lift and propulsion power is 735 kW, of which about 30% or 221 kW is used to power the lift fan. It can be seen, therefore, that the lift system of SR.N5 can compensate the cushion flow rate consumed by the wave pumping motion at this speed.

2.7 Calculation of cushion stability derivatives and damping coefficients

In this section we will discuss the air cushion stability and hovering damping which are very important parameters concerning the longitudinal and vertical motion of ACVs hovering on a rigid surface. These parameters will greatly affect the natural heaving frequency, seaworthiness and comfort of craft, but are only relative to the static air cushion characteristics of ACVs. For this reason, these parameters are discussed in this chapter.

With respect to the SES, the air cushion stability and damping are also influenced by the buoyancy and damping force of sidewalls, because they are immersed in the water. The effect of sidewalls will be discussed at greater length in Chapter 9, though of course it is not difficult to derive them by means of the methods demonstrated in this chapter.

We take the ACV running over ground as an example and based on this the heaving motion can be illustrated in Fig. 2.24. $\dot{z}_c$ and $\dot{z}_e$ are heaving displacement and velocity respectively and z_e, $\dot{z}_e$, denote the motion amplitude and velocity of the ground plane, similar to the amplitude for waves.

The ACV can be described as an elastic system with a spring and damper connected parallel to each other. Strictly speaking, the spring and damping coefficients are nonlinear and asymmetric, i.e. they are rather different for upward and downward motion. As a first approximation, assuming vibration movement with minute displacement, the motion can be considered as approximately linear.

Thus an ACV running on a rough ground surface may be considered equivalent to

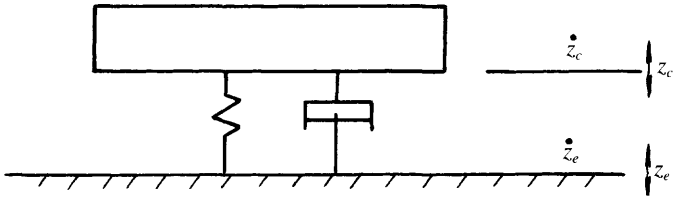

Fig. 2.24 Heave motion of a hovercraft model on rigid surfaces.

a vibration system with one degree of freedom (only the heaving motion is considered here) and the frequency response can be shown in Fig. 2.25, in which ω_e/ω_n denotes the tuning factor, ω_e represents the encounter frequency, namely the exciting frequency of ground relative to craft, ω_n is the natural vibration frequency, i.e. the heaving natural frequency of craft, and M represents magnification factor, i.e. the ratio of heave displacement to ground amplitude.

In Fig. 2.25, it can be seen that the higher the damping coefficient, the lower the magnification factor in the case where the tuning factor is close to 1. In the case of lower tuning factor, then higher damping coefficients give higher magnification factor. This means that the vertical motion of craft with a large damping coefficient will be violent in the case where the craft run in short waves or on a rough ground surface. Therefore the damping coefficient is very important for decreasing the vertical vibration of craft.

Before discussing these problems, we prefer to introduce three typical flow modes for craft in heaving motion as shown in Fig. 2.26: (a) shows equilibrium flow, i.e. static hovering mode of craft; (b) shows the flow underfed, i.e. the instantaneous skirt clearance will be smaller than the equilibrium skirt clearance as the craft drops down, consequently the jet flow cannot seal the cushion air causing some air leakage from the cushion; (c) shows the flow overfed, i.e. the instantaneous skirt clearance will be larger than the equilibrium skirt clearance as the craft lifts up, consequently more air flow will get into the cushion to fill up the air cavity. These three modes appear alternately as the craft heaves.

Calculation method for heaving stability derivatives and damping coefficients

First of all, the profile of the skirt is assumed unchangeable in the case of deriving the air cushion stability derivatives and damping coefficient. This assumption is

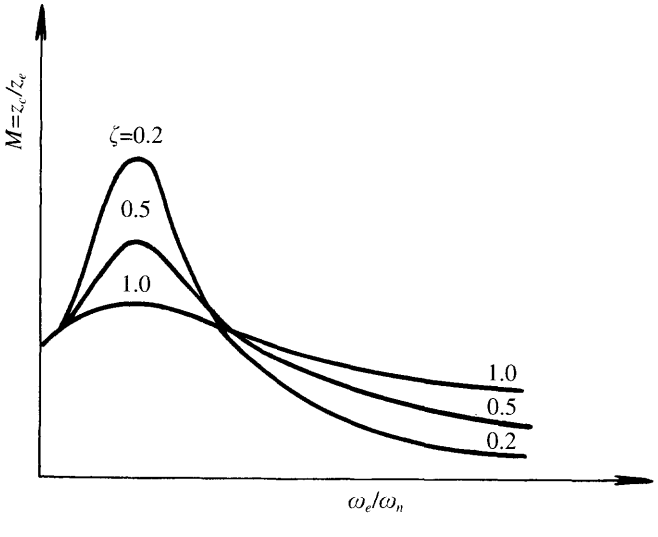

Fig. 2.25 Frequency response for heave motion with one degree of freedom.

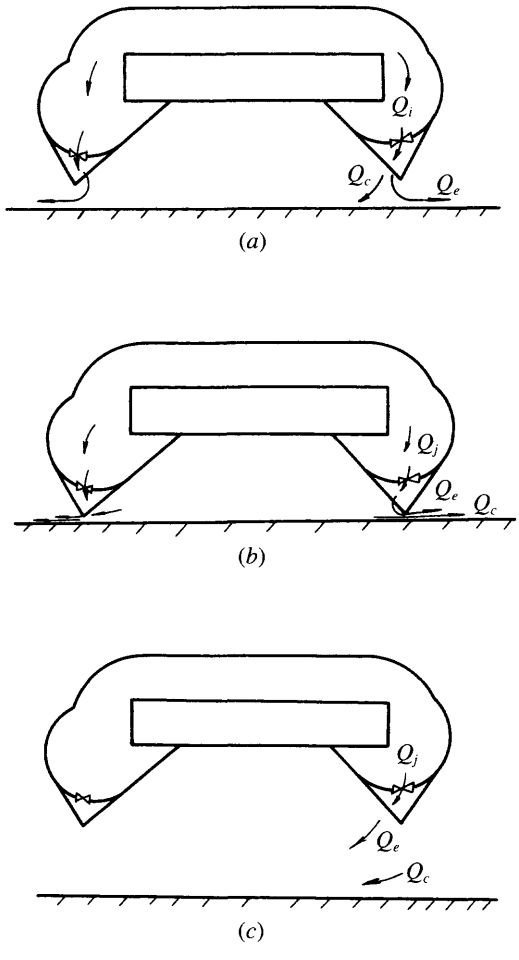

Fig. 2.26 Three conditions for heave motion of ACV: (a) equilibrium; (b) underfed; (c) overfed.

reasonable for a conventional medium pressure bag and finger type skirt for small perturbations. A responsive skirt with high deformability may have lower effective damping.

Regarding the effect of hovering performance and fan and air duct characteristics on the heaving stability and damping, we assume as follows:

1. The hovering performance of the skirt complies with the plenum chamber formula.
2. The flow air in the cushion is incompressible.
3. In order to compare the calculation value with experimental results, the rigid ground surface is considered to heave vertically, and we keep the craft hard structure unmovable.

Then, according to the flow continuity equation, we have

$$\frac{\mathrm{d}m}{\mathrm{d}t} = \rho_{\mathrm{a}}(Q_{\mathrm{i}} - Q_{\mathrm{o}}) = \frac{\mathrm{d}}{\mathrm{d}t}(\rho_{\mathrm{a}} V) = \rho_{\mathrm{a}} \frac{\mathrm{d}V}{\mathrm{d}t} + \frac{\mathrm{d}\rho_{\mathrm{a}}}{\mathrm{d}t} \tag{2.41}$$

where Q_o is the outflow rate from the cushion (m^3/s), Q_i the inflow rate into the cushion (m^3/s), V the cushion volume (m^3), m the mass of air in the cushion (Ns^2/m) and ρ_a the air density (Ns^2/m^4).

Considering the cushion as incompressible, thus $d\rho_a/dt = 0$. Then

$$Q_o = \psi A_t (2p_c/\rho_a)^{0.5}$$

where A_t is the area of air leakage (m). Now Q_i can be written as

$$Q_i = Q_{i0} + (\partial Q/\partial p_c)\, \Delta p_c$$

where $\Delta p_c = p_c - p_{c0}$, p_{c0} is the cushion pressure at equilibrium feed mode and p_c is the instantaneous cushion pressure.

If we assume that z, the displacement of the ground, is upward positive and there is no rotation of ground motion, then

$$dV/dt = -S_c \dot{z}$$

and

$$S_c = A_{i0} + (dA_i/dz)\, z = A_{i0} - lz$$

where S_c is the cushion area (m^2), A_{i0} the area of air leakage at equilibrium flow mode (m^2) and l the peripheral length for air leakage (m). Then substitute the foregoing equation into (2.41), which gives

$$-S_c \dot{z} = [Q_{i0} + (\partial Q/\partial p_c)\, \Delta p_c] - \psi (A_{i0} - z_1) \cdot (2p_c/\rho_a)^{0.5}$$

or

$$-S_c \dot{z} = Q_{i0} + (\partial Q/\partial p_c)\, \Delta p_c - \psi A_{i0} (2p_c/\rho_a)^{0.5} + \psi l_2 (2p_c/\rho_a)^{0.5}$$

Extend the $(2p_c/\rho_a)^{0.5}$ term into a Taylor series and neglect the nonlinear terms, and then these expressions can be written as

$$-S_c \dot{z} = Q_{i0} + \frac{\partial Q}{\partial p_c} \Delta p_c - \psi A_{i0} \left[\left(\frac{2p_{c0}}{\rho_a} \right)^{0.5} + \left(\frac{2}{\rho_a} \right)^{0.5} 0.5 \frac{\Delta p_c}{(p_{c0})^{0.5}} \right] + \psi l \left(\frac{2p_c}{\rho_a} \right)^{0.5} z$$

then

$$-S_c \dot{z} = Q_{i0} + \frac{\partial Q}{\partial p_c} \Delta p_c - Q_{i0} - \frac{Q_{i0}}{2p_{c0}} \Delta p_c + \psi l \left(\frac{2p_c}{\rho_a} \right)^{0.5} z \tag{2.42}$$

$$= \frac{\partial Q}{\partial p_c} \Delta p_c - \frac{Q_0}{2p_{c0}} \Delta p_c + \frac{Q_0}{h_0} z \tag{2.43}$$

where h_o is the skirt clearance at equilibrium flow mode (m), Q_{i0} the inflow rate at equilibrium flow mode (m^3/s) and p_{c0} the cushion pressure at equilibrium mode (N/m^2).

Equation (2.43) can be written as

$$K_1 \Delta p_c = -K_2 \dot{z} - K_3 z$$

or

$$\Delta p_c = \frac{-K_2}{K_1} \dot{z} - \frac{K_3}{K_1} z \tag{2.44}$$

where

$$K_1 = \frac{\partial Q}{\partial p_c} - \frac{Q_0}{2p_{c0}}$$

$$K_2 = S_c$$

$$K_3 = \psi l(2p_c/\rho_a)^{0.5} = Q_0/h_0 \tag{2.45}$$

Assume the cushion pressure is a linear function of heaving amplitude and velocity, then

$$\Delta p_c = \frac{\partial p_c}{\partial z}\dot{z} + \frac{\partial p_c}{\partial z}z \tag{2.46}$$

Using the equivalent terms of (2.46 and 2.44), we have

$$\frac{\partial p_c}{\partial \dot{z}} = -S_c\left[\frac{\partial Q}{\partial p_c} - \frac{Q_0}{2p_{c0}}\right] \tag{2.47}$$

$$\frac{\partial p_c}{\partial \dot{z}} = -(Q_0/h_0)\left[\frac{\partial Q}{\partial p_c} - \frac{Q_0}{2p_{c0}}\right] \tag{2.48}$$

where $\partial p_c/\partial \dot{z}$ is the velocity derivative of p_c with respect to z, i.e. the cushion damping coefficient, $\partial p_c/\partial z$ the derivative of p with respect to z, i.e. heaving stability derivatives and $\partial Q/\partial p_c$ the derivative of Q due to the characteristic curves of cushion air duct–fan systems with respect to p_c. Then

$$\frac{\partial Q}{\partial p_c} = \frac{\partial Q}{\partial H_j}\cdot\frac{\partial H_j}{\partial p_c}\cdot\frac{\partial p_t}{\partial p_c}$$

where $\partial Q/\partial H_j$ is the slope of the fan characteristic, if $H_j = A + BQ + CQ^2$, i.e.

$$\partial Q/\partial H_j = 1/(B + 2CQ)$$

$\partial H_j/\partial p_c$ is the slope of the air duct characteristic and $\partial p_t/\partial p_c$ the derivative of bag pressure with respect to cushion pressure, which can be calculated according to expression (2.3).

It is then not difficult to calculate the natural heave frequency without damping and heave damping rate:

$$\omega_z = \left[\frac{\partial p_c}{\partial z}\cdot\frac{S_c}{M}\right]^{0.5}$$

$$\zeta_z = \left[\frac{\partial p_c}{\partial \dot{z}}\cdot\frac{S_c}{2M\omega_z}\right] \tag{2.49}$$

where ω_z is the natural heave frequency without damping (s^{-1}), ζ_z the heaving damping rate and M the mass of the craft (kg).

Experimental methods for heave stability derivatives and damping coefficient

The foregoing formulae can be proved by experimental methods, in particular tests using ground excitation (a hinged base plate) in test skirt box equipment, then measuring the time history of cushion pressure, vertical displacement of the ground plate, total pressure of fans and flow rate, $z(t)$, $p_c(t)$, $H_j(t)$, $Q(t)$, as shown in Fig. 2.27.

Typical test equipment is shown in Fig. 2.6. This uses a 400 W electric motor via eccentric wheel to drive the ground plate in heaving motion. The heave amplitude $z(t)$ can be changed by changing the position of the eccentric wheel and a sliding linear resistance and potentiometer used to measure the time history of displacement of the ground plate.

The ground plate will move in simple harmonic motion, i.e. the eccentric wheel moves in circular motion with constant angular velocity. For this reason the variables $p_c(t)$, $H_j(t)$, $Q(t)$, are also in simple harmonic motion. $H_j(t)$ and $p_c(t)$ can be measured by capacitance type pressure sensors.

The following physical phenomena can be observed during such tests:

- The fluctuation of fan total pressure is small.
- As shown in Fig. 2.27, the cushion flow forms underfed mode as the ground platform is moved upward, i.e. the points B, C denote underfed and points D, A denote overfed flow mode with p dropping down.
- As shown in Fig. 2.27, the $p_c(t)$ precedes the $z(t)$ and the phase lead is ε. Heave velocity equals zero at points A and C and the heaving velocity reaches maximum heave displacement equal to zero at points B and D.

Then the stability coefficient and damping coefficient can be written as

$$-\partial p_c/\partial h = \partial p_c/\partial z = -\Delta p_{cA}/z_m = \Delta p_{cC}/z_m \tag{2.50}$$

$$-\partial p_c/\partial h = \Delta p_{cB}/\omega z_m = -\Delta p_{cD}/\omega z_m \tag{2.51}$$

B and D denote the maximum heaving velocity, while A and C are the maximum heaving displacement z. In addition because of simple harmonic motion in heave, z can be written as

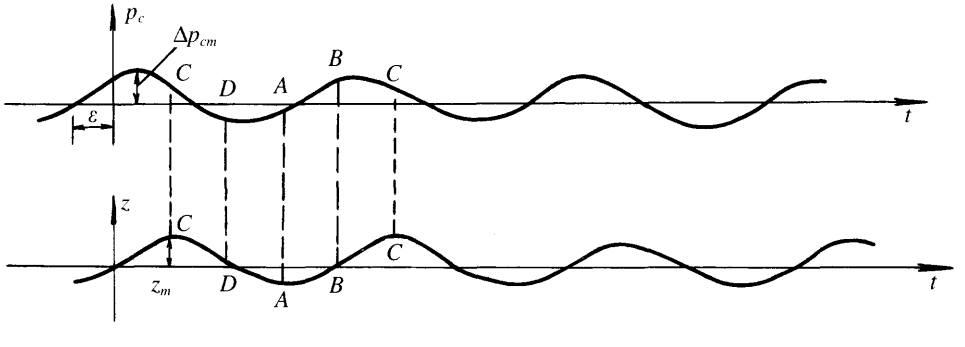

Fig. 2.27 Time history of cushion pressure and heave amplitude.

$$
\begin{aligned}
z &= z_m \sin \omega_t \\
\Delta p_c &= \Delta p_{cm} \sin(\omega t + \varepsilon) \\
&= \Delta p_{cm} \sin \omega t \cos \varepsilon + \Delta p_{cm} \cos \omega t \sin \varepsilon
\end{aligned} \tag{2.52}
$$

and

$$
\begin{aligned}
\Delta p_c &= \frac{\partial p_c}{\partial z} \cdot z + \frac{\partial p}{\partial \dot{z}} \cdot \dot{z} \\
&= \frac{\partial p_c}{\partial z} \cdot z_m \sin \omega t + \frac{\partial p}{\partial \dot{z}} \cdot z_m \omega \cos \omega t
\end{aligned} \tag{2.53}
$$

then

$$
\begin{aligned}
\frac{\partial p}{\partial \dot{z}} &= \frac{\Delta p_{cm} \sin \varepsilon}{z_m \omega} \\
\frac{\partial p}{\partial z} &= \frac{\Delta p_{cm} \cos \varepsilon}{z_m}
\end{aligned} \tag{2.54}
$$

The stability and damping coefficient can then be obtained using equations (2.50), (2.51) and (2.54) from measurements taken on the rig using known values.

Comparison of calculations with test results

1. A comparison of calculations with test results is shown in Figs 2.28 and 2.29 and it is found that the calculated values are in good agreement. The latter are higher than the former, because of the air leakage from the connecting parts of the flexible skirts (the results are uncorrected). The flow in test is consequently larger than the actual value, and the calculation values are smaller than the test results.
2. From equation (2.47), it is found that because $\partial Q/\partial p_c < 0$ and both $Q_0 > 0$ and $p_c > 0$, this means that the steeper the fan characteristic curve (H_j–Q), the smaller $\partial Q/\partial H_j$ and the larger the damping coefficient.
3. From the formulae, one can see that the heave stability is proportional to flow rate and inversely proportional to skirt clearance; and that the relation between the heave stability and the characteristic curve of fan/air ducting is similar to the relation between the damping coefficient and the characteristic of fan/air ducting, namely that mentioned in (2) above.

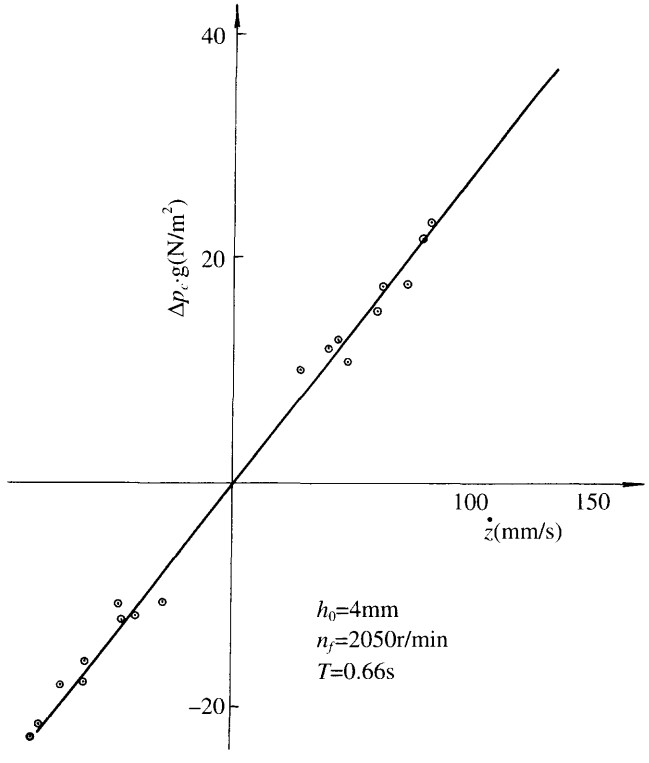

Fig. 2.28 Comparison of p_c between the calculated and experimental result as a function of heaving velocity.

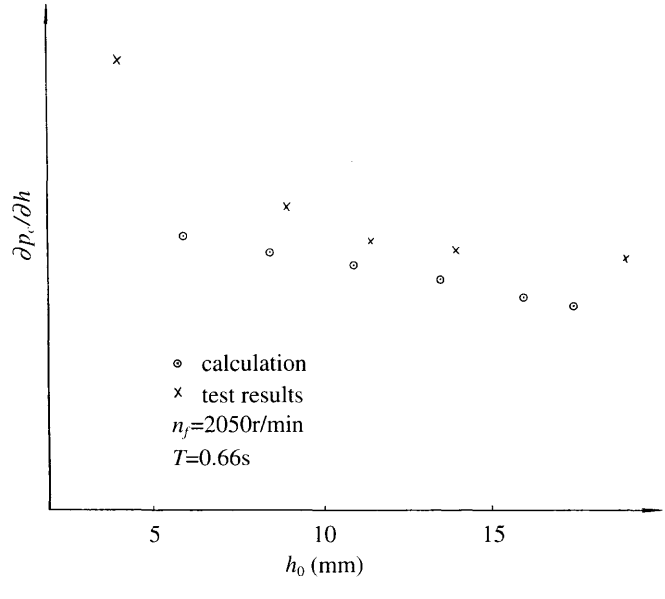

Fig. 2.29 Comparison of heave position derivative between calculations and measurements as a function of air gap.

3

Steady drag forces

3.1 Introduction

ACVs and SESs create drag forces as they move over the water surface. The most important drag components are those due to friction with immersed components such as sidewalls, skirt, propellers, rudders and other appendages; and wave-making drag from the moving cushion pressure field and sidewalls. In addition, momentum drag due to acceleration of the air used for the supporting air cushion, and aerodynamic profile drag of the ACV or SES become important components at higher speeds.

In this chapter we will outline the theory behind these drag components and describe methods for their estimation.

3.2 Classification of drag components

The method of calculating drag forces on an ACV or SES is similar to that for predicting the drag of a planing hull or a sea plane before take-off. ACVs and SES also generate spray drag, skirt friction drag and skirt inertia drag in addition to the water drag components associated with a normal ship. For this reason drag calculations are more complicated than for other marine craft.

Based upon calculation methods for predicting the drag of a planing hull, the principal author and colleagues at MARIC have developed a methodology for predicting the drag for ACV/SES which may be summarized as follows:

- First of all we obtain the total drag from model tests in a towing tank and some other main components of drag by means of reliable and practical methods, e.g. according to the Reynolds analogue theory to obtain the test results in wind tunnels for predicting air profile drag.
- Then the residual drag of models can be determined by deducting the main components of drag which can be calculated individually, from the total drag of the model measurements.

According to Froude's analogue theory we can define the residual drag of full-scale ships from that of models; consequently the total drag for a full-scale ship can be

obtained by adding the residual drag of the ship to the main components of ship drag which can be determined by calculations.

In general, the total drag of craft can be written as follows:

$$R_{acv} = R_w + R_a + R_m + R_{sk} + R_{a''}$$

or

$$R_{ses} = R_w + R_a + R_m + R_{sk} + R_{swf} + R_{ap} + R_{mw} + R_{a''}$$

where R_{acv} is the ACV total drag; R_{ses} the SES total drag; R_w the wave-making drag due to the air cushion; R_a the aerodynamic profile drag; R_m the aerodynamic momentum drag; R_{sk} the skirt drag for ACVs and bow/stern seal drag for SESs; R_{swf} the friction drag of sidewalls; R_{ap} the underwater appendage drag (e.g. rudders, air ingestion fences, propeller brackets); R_{mw} the hydrodynamic momentum drag due to the cooling water of engines and $R_{a''}$ the drag due to the differential air momentum leakage from bow and stern skirts.

Fig. 3.1 shows the various components of drag of the SES-100A built in the USA. The principal dimensions and parameters of the SES-100A are $L/B = 2.16$, $p_c/L_c = 19.5$ kgf/m, $v_{max} = 76$ knots.

The following sections of this chapter outline the methodology for determination of each drag component listed above.

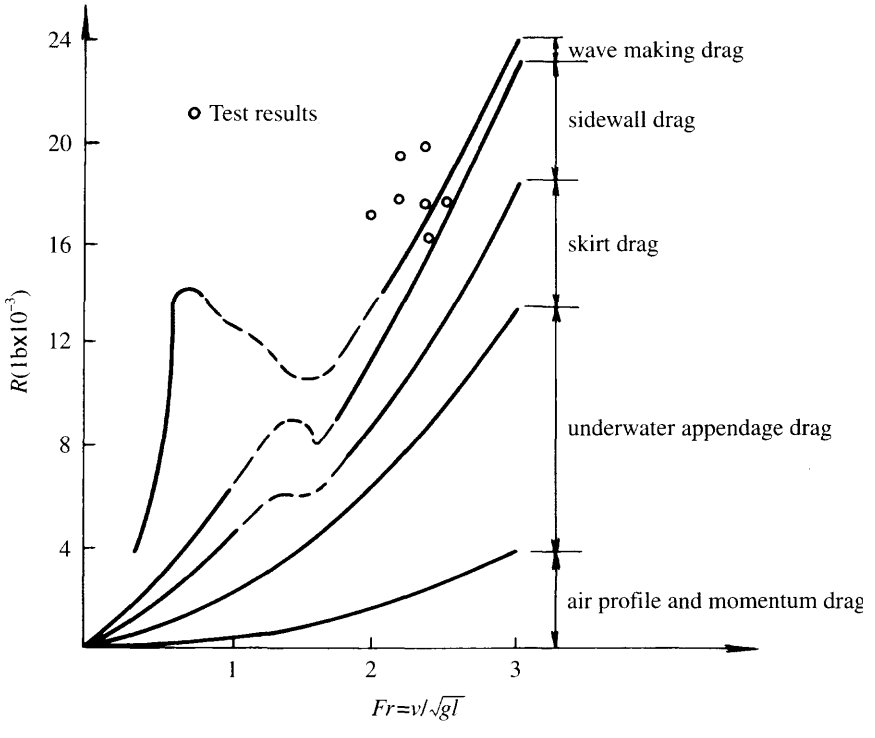

Fig. 3.1 SES-100A drag as a function of Froude number.

3.3 Air cushion wave-making drag (R_w)

Wave-making drag generated by a pressure distribution is a classical theme of hydrodynamics, since a ship's hull is generally represented by a surface consisting of a varying potential function which applies positive pressure in the forebody and suction pressure around the stern [8,17].

The equivalent problem for a hovercraft was addressed by Newman and Poole [18], who derived a calculation method for predicting the wave-making drag. They simplified the air cushion to an equivalent rectangular surface with a uniform pressure distribution and calculated the wave-making drag as

$$R_w = C_w \left[\frac{p_c^2 \cdot B_c}{(\rho_w \cdot g)} \right] \tag{3.1}$$

where

$$C_w = f\,(F_{r_i} \text{ and } l_c/B_c\,)$$

and R_w is the wave-making drag due to air cushion, (N), p_c the cushion pressure (N/m^2), B_c the cushion beam, (m), l_c the cushion length (m), ρ_w the water mass density (0.10177 − 0.1045) ($N\ s^2/m^4$), g the gravitational acceleration (9.8066)(m/s^2) and C_w the wave-making drag coefficient due to the air cushion travelling on a waterway with infinite depth, as shown in Fig. 3.2.

Figure 3.2 shows that as cushion length is increased, so the primary hump at F_r approx. 0.56 reduces. Craft with l_c/B_c in the range 2–4 have a significantly higher drag peak at F_r approx. 0.33, so thrust margin at this speed should also be checked during design. Figure 3.3 shows the variation of C_w against l_c/B_c for various F_r, interpreted from Fig. 3.2. It can be seen that below l_c/B_c of about 6, the primary drag hump at F_r 0.56 begins to build up. Figure 3.4 shows plots of C_w vs F_r for selected l_c/B_c, taken from Fig. 3.3.

It is important to note here that wave-making drag is proportional to p_c^2 and the cushion width. Craft drag can therefore be significantly reduced by increasing craft length. This was used successfully by BHC in stretching the SR.N6 craft in the UK, and the US Navy SES-100 to SES-200.

In fact, the wave-making drag can be defined as

$$\frac{R_w}{p_c\, S_c} = \frac{R_w}{W} = \sin \alpha' \tag{3.2}$$

where $\alpha - \alpha'$ is the average slope of the wave generated by a moving air cushion. This is most suitable for a cushion moving at high F_r, generating a wave, rather longer than cushion length.

Meanwhile, equation (3.1) can also be written as

$$\frac{R_w}{W} = C_w \left[\frac{p_c^2\, B_c}{\rho_w\, g\, W} \right]$$

$$= C_w \cdot \frac{1}{\rho_w\, g} \cdot \frac{p_c}{l_c} \tag{3.3}$$

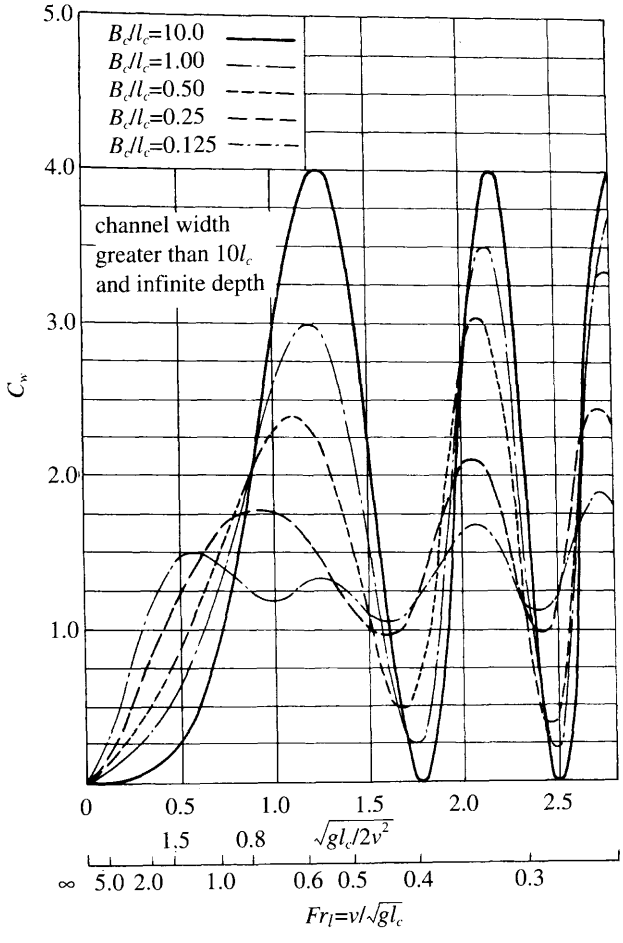

Fig. 3.2 C_w plotted against F_{rl} for constant L_c/B_c.

or

$$\frac{R_w}{W} = f\,(F_{r_l},\, l_c/B_{c_l},\, p_c/l_c)$$

where p_c/l_c is the pressure/length ratio of hovercraft.

As mentioned above, the wave-making drag is a function of cushion length to beam ratio, pressure to length ratio and Froude number. The cushion length/beam ratio therefore plays a significant role in the craft performance.

Reference 19 also offered another similar formula for estimating the wave-making drag:

$$R_w = C_w(4\,p_c\,W)/(\rho_w\,g\,l_c) \tag{3.4}$$

where l_c is the equivalent cushion length, i.e. $l_c = S_c/B_c$, S_c the cushion area, B_c the cushion beam and C_w the wave-making drag coefficient as shown in Fig. 3.4.

It should be noted that it is best to use the formula above together with formulae

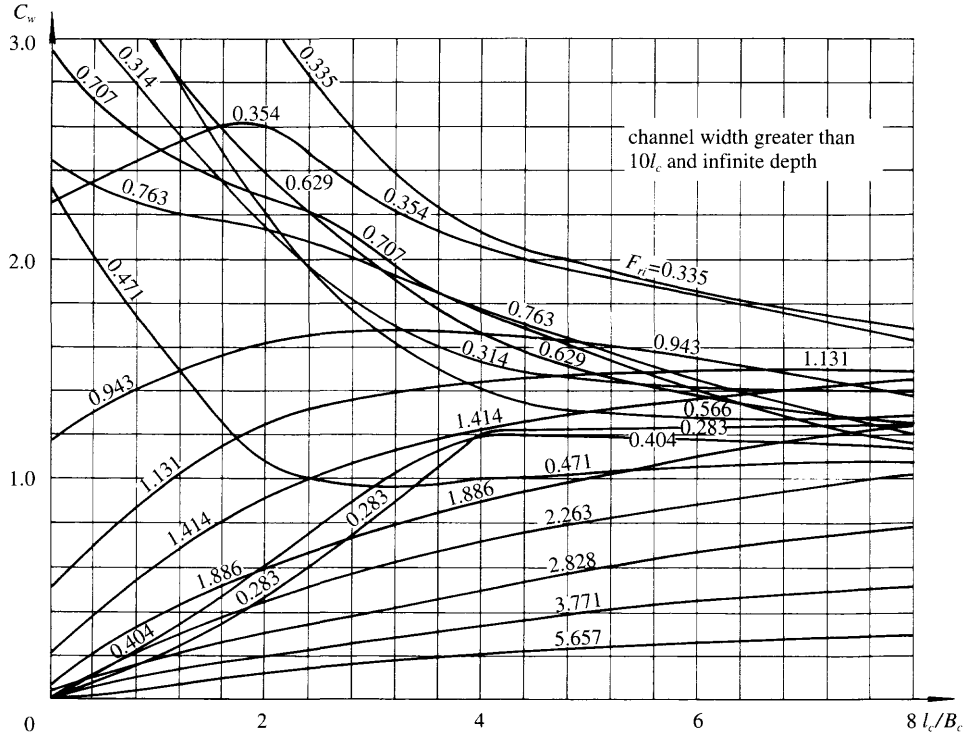

Fig. 3.3 Cushion wave-making drag coefficient for a rectangular air cushion over calm water against L_c/B_c.

predicting the other components of drag also developed by the same authors, e.g. when one uses the equation (3.4) for estimating the wave-making drag, it is better to use this together with the other formulae offered by ref. 19 for estimating the seal drag, sidewall water friction and the residual drag of sidewalls, otherwise the user may find inconsistencies in calculation of the total resistance of the ACV.

Owing to the easy application and accuracy of Newman's method, MARIC often uses Newman and Poole's data for estimating the wave-making resistance of craft. It is evident from this work that the bow wave strongly interacts with the stern wave. The lower the cushion beam ratio, the stronger the disturbance between the two components. This causes a series of peaks and troughs on the resistance curve. With respect to water with infinite depth, the last peak appears at $Fr = 1/\sqrt{\pi} \cong 0.56$.

The theory mentioned above was validated by the experimental results carried out by Everest and Hogben [20]. The theoretical prediction agreed quite well with experimental results except at low speed. In this latter case, only two pairs of troughs and peaks appeared in the test results rather than that in the calculation results. This can be interpreted as follows:

- Hogben proposed that the wave steepness (h/λ) at lower Fr predicted by linear theoretical calculation exceeded the theoretical limit value of 1/7 between the troughs and peaks, so that the surface geometry would be unstable, similar to a

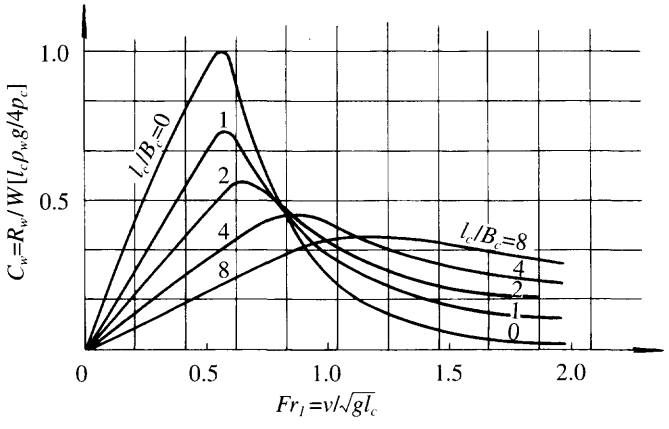

Fig. 3.4 C_w plotted against F_{rl} for constant L_c/B_c.

breaking wave. The linear assumptions in wave-making theory have to be replaced by nonlinear wave-making theory at these *Fr*.

- Doctors [21] considered the predicted sharp peaks and troughs at low *Fr* are caused by assuming a uniform pressure distribution, which implies a step pressure change at the bow and stern, which clearly is not reflected in reality. The sharp peaks and troughs will disappear and the theoretical prediction will agree quite well with test results, when one assumes the uniform distribution of pressure inside the cushion is combined with a smooth pressure transient at the bow and stern (or the whole periphery for an ACV) with hyperbolic decay to ambient.

Since then, Bolshakov has calculated the wave-making drag of an air cushion with uniform distribution of cushion pressure with a round bow and square stern in horizontal plane (similar to an SR.N5 or SR.N6). Tatinclaux [22] has extended these data by calculating the velocity potential and wave-making of air cushions with uniform cushion pressure distribution and various plan shapes such as rectangle, circle and semicircles. Because the velocity potential used is linear, the potential due to the combined plan shapes of an air cushion can be obtained by the superposition of velocity potentials due to the separate area components, so as to obtain the corresponding total wave-making drag.

Comparing the coefficients for wave-making drag of air cushions of various plan shapes, a rectangular air cushion is found to have the minimum coefficient, particularly near hump speed. The rectangular air cushion will gain more advantage if the drag–lift ratio R_w/W is also considered. This can be demonstrated as follows; first, define a shape factor for the cushion, which is the envelope rectangle, divided by the actual area, by which we have

$$\varphi_s = (l_c B_c/S_c)^2$$

also define the non-dimensional cushion pressure/length ratio:

$$\bar{p}_c = \{W/(l_c B_c)\}/(\rho_w g l_c)$$

then

$$R_w/W = C_w \varphi_s \bar{p}_c' \tag{3.5}$$

where R_w/W is the wave-making drag–lift ratio, W the weight of craft and C_w the wave-making drag coefficient.

From this equation we can see that for constant cushion length l_c, cushion beam B_c and craft weight W, the non-dimensional cushion pressure–length ratio $\bar{p}_c$, will stay constant, but φ_s will change with respect to different shape of cushion plan.

For a rectangular air cushion, $\varphi_s = 1$ and will be the minimum, meanwhile C_w will be minimum when the cushion plan is rectangular; therefore an air cushion with rectangular shape will gain more advantage not only on the ratio between wave-making drag and craft weight but also on take-off ability through hump speed.

Selection of the plan shape for an ACV should consider take-off ability, together with seaworthiness and general arrangement of craft, as well as the configuration and fabrication of skirts, etc., not just for minimum drag.

The study mentioned above was based upon the assumption of uniform distribution of air pressure within the cushion and with a discontinuous sudden change of pressure at the cushion edges. The sudden change of pressure distribution can only appear at the sidewalls of an SES, and cannot exist on an ACV with flexible skirts. Therefore this method will make a calculation error for an ACV.

Doctors [21] and Tatinclaux [22] each made studies of the pressure distribution with various rules to overcome this problem. Doctors assumed that the pressure distribution formed a hyperbolic tangent, while Tatinclaux assumed a linear distribution. The calculation results demonstrated that both methods agreed quite well with the calculation results by Newman's method at post-hump speed and did not produce the sharp peaks and troughs in the resistance curve at pre-hump speed (Fig. 3.5).

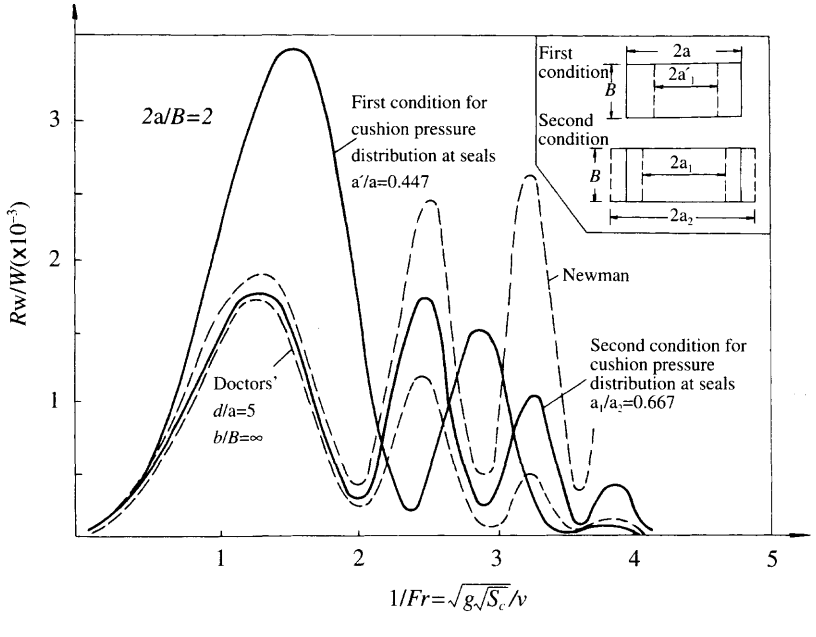

Fig. 3.5 Comparison of wave-making drag between the test results and calculation by various formulae.

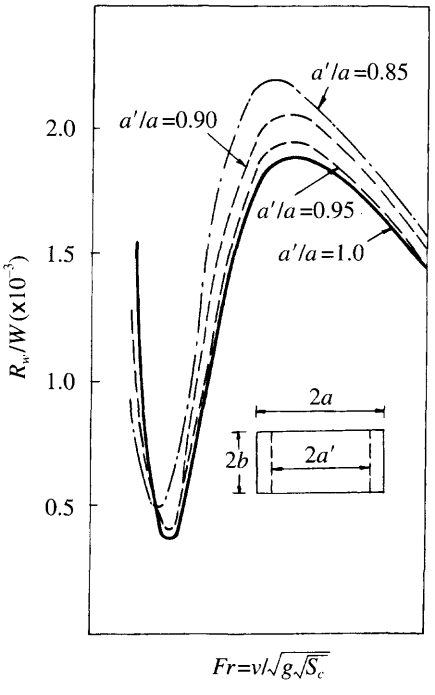

Fig. 3.6 Cushion wave-making drag ratio as a function of equivalent Froude Number. [22]

In addition, Tatinclaux calculated two further pressure distribution combinations, i.e. linear distribution at bow/stern and sudden change at two sides (similar to an SES), as well as distribution at two sides and sudden change at bow/stern (Figs 3.6 and 3.7). It is shown that the first condition influenced the wave-making drag dramatically, but the latter did not. For this reason it is clear that wave-making is mainly generated from the bow and stern (this is similar in principle to the bow and stern wave patterns generated by a normal ship's hull).

With respect to shallow water drag, theoretical calculation demonstrated that wave-making drag in shallow water would be larger than that in water with infinite depth, particularly at hump speed. As water depth reduces, so the drag increases so as to increase the drag hump. When the effect of the water depth on the practical limit for the height of generated waves is taken into account, this limits the maximum wave drag, which is the reason operators can use shallow water to go through hump speed on a marginal craft.

If the progression through craft hump speed was not steady, but accelerating, Tatinclaux showed that the wave-making drag peaks caused by an air cushion with the hyperbolic tangent pressure distribution at the bow/stern running over both deep and shallow water at constant accelerated motion were flattened by the acceleration.

This effect will be strengthened while craft are travelling over shallow water rather than deep water (Figs 3.8 and 3.9). These figures show that the craft peak resistance will decrease in shallow water by accelerated motion, in a similar manner to that on deep water at approximately $Fr = 0.5$. This is another reason why an ACV or SES, particularly with flexible skirts, can pass through the hump speed over shallow water

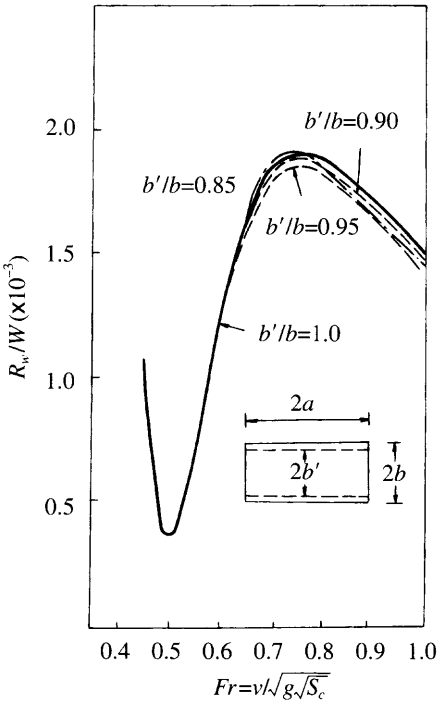

Fig. 3.7 Cushion wave-making drag ratio as a function of equivalent Froude Number. [22]

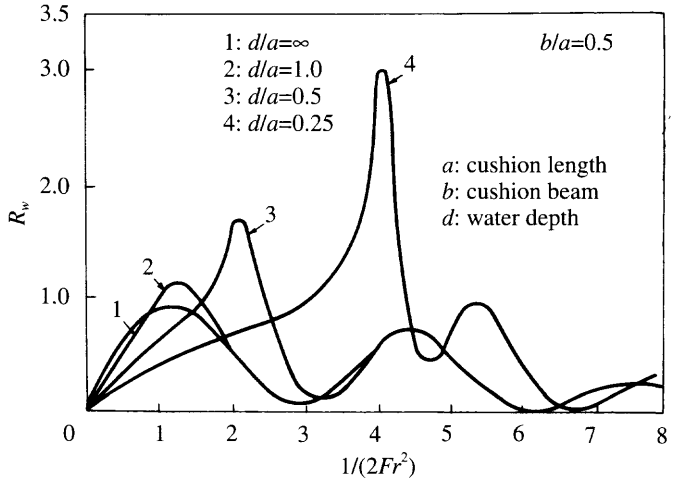

Fig. 3.8 Influence of water depth on cushion wave-making drag.

without special difficulty. Figure 3.10 shows the trial results of a full-scale craft SES–100B. It was found that the drag decreased as the craft accelerated. The drag over both shallow and deep water is presented in Fig. 3.11.

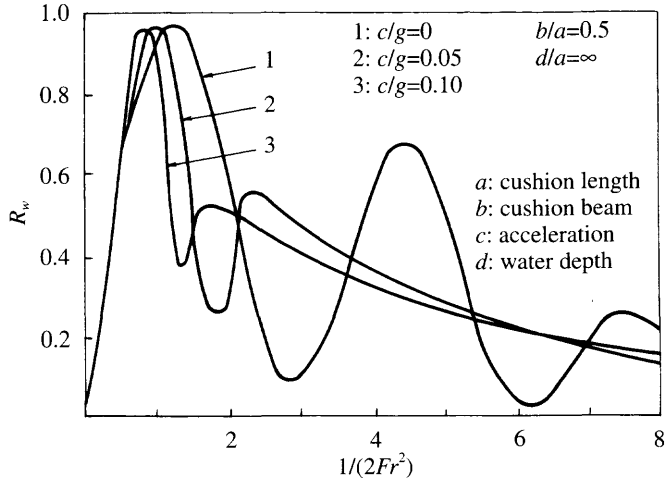

Fig. 3.9 Variation of cushion wave-making drag on accelerating craft. [21]

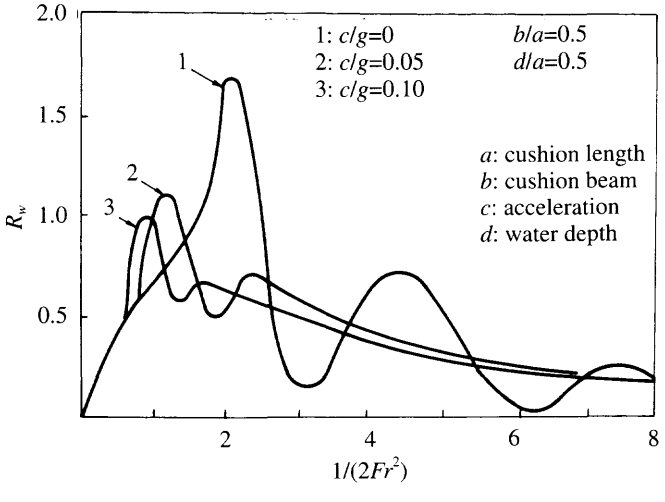

Fig. 3.10 Variation of cushion wave making drag on accelerating craft. [21]

The principal research work into wave-making drag due to an air cushion travelling in yaw was carried out by Tatinclaux, who showed that peak drag of a craft in yaw increased dramatically. MARIC also has practical experience that a craft travelling in yaw on water is very difficult to pass through hump speed, particularly for an amphibious ACV. An ACV travelling in yaw in a beam wind condition will probably have difficulty in passing through the hump speed as well as increasing handling difficulties.

Pilots with such problems in open water will usually make a track across or down wind to accelerate through the hump and then return to the intended course. In more restricted conditions, a downwind track to a more sheltered area where the craft can be turned around over the hump may be needed.

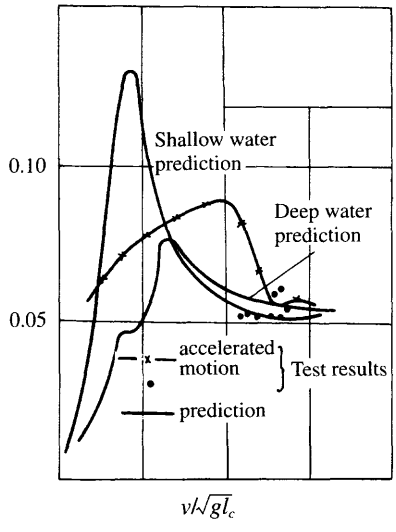

Fig. 3.11 Variation of craft drag/weight ratio on accelerating craft over shallow water.

Figure 3.12 shows the wave-making drag at various F_r, yawing angle, and cushion length–beam ratios. It may be noted that the wave-making drag when yawed is

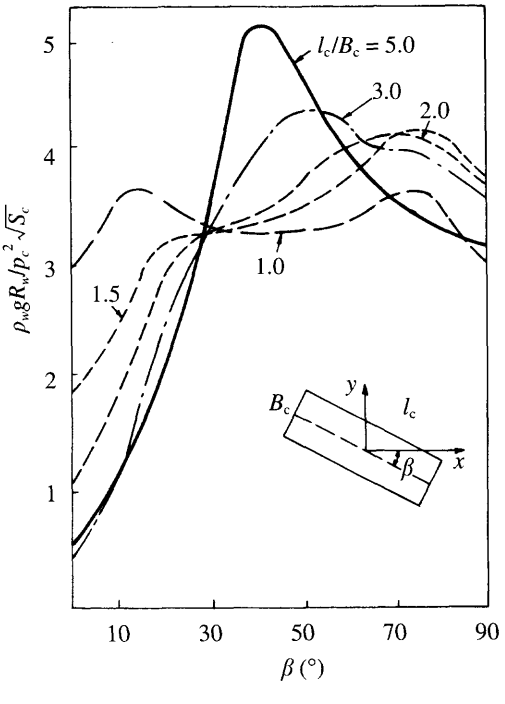

Fig. 3.12(a) Wave-making drag coefficient for yawed craft, $F_r = 0.6$.

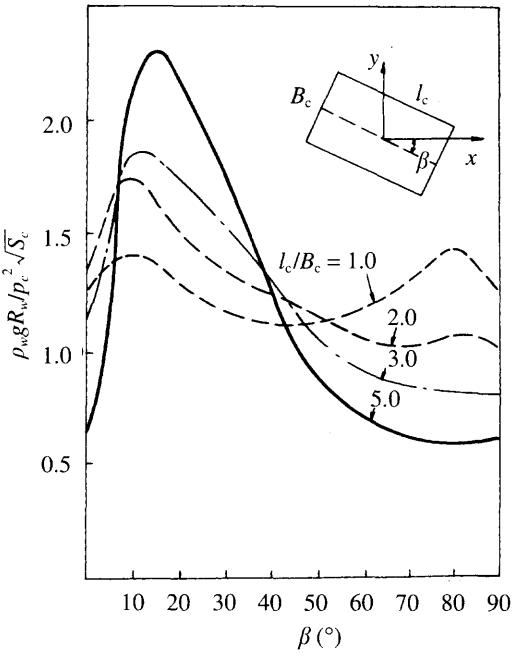

Fig. 3.12(b) Wave-making drag coefficient for yawed craft, $F_r = 1.0$.

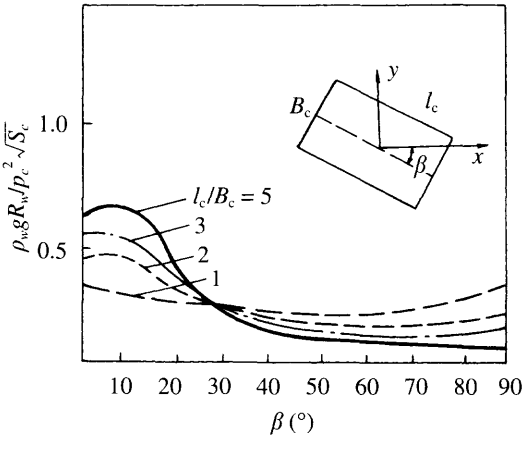

Fig. 3.12(c) Wave-making drag coefficient of yawed craft, $F_r = 2.0$.

several times greater than that on a straight course (if one takes the skirt drag due to the scooping water of the craft in yaw into account, the added drag will increase further).

3.4 Aerodynamic profile drag

The aerodynamic profile drag can be written as

$$R_a = C_a \frac{\rho_a}{2} \cdot S_a v^2 \tag{3.6}$$

where R_a is the aerodynamic profile drag (N), C_a the coefficient for the aerodynamic profile drag and S_a the frontal projecting area of the hull above the water (m^2). C_a is highly sensitive to the aerodynamic profile of the craft's hull, inclusive of the inflated skirt. Its value is generally obtained from wind tunnel tests for detailed design. Table 3.1 gives a selection of C_a data for various models and craft based on wind tunnel data. It can be seen that C_a for an ACV (particularly for passenger craft) is in general small. C_a can be estimated based on the geometry of a new craft, using data such as presented by Hoerner [23] and comparison with known data such as that in Table 3.1.

ACV aerodynamic drag is generally a significant proportion of total drag because of high design craft speed and the low water drag. For example, the aerodynamic drag of ACV 711-A built in China is 30% of the total drag of this craft at a speed at 85 km/h. Therefore it is very important to design an ACV craft superstructure with care.

In general, the C_a can be taken as 0.4–0.6 for an ACV, with extreme values of 0.3 for fine lines and 0.75 for poor lines. For example, C_a for US *Voyageur* and JEFF(B) is 0.75 due to their open well deck for accommodating tanks or large loads. C_a is typically 0.5–0.7 for SES. In the final analysis, it is best to use test results from a wind tunnel if possible, to determine this fraction of the total drag force accurately.

Table 3.1 The aerodynamic profile drag coefficient Ca for various craft (models)

Item	Craft name	Craft type	C_a	Source of data
1	SR.N2	ACV	0.25	ADAO 22583
2	SR.N4	ACV	0.30	ADAO 22583
3	SR.N5	ACV	0.38	ADAO 22583
4	SKMR.1	ACV	0.398	AIAA 73–318
5	SK–5	ACV	0.28	AIAA 73–318
6	JEFF(B)	ACV	0.495	AIAA 73–318
7	*Voyageur*	ACV	0.75	AIAA 73–318
8	N500	ACV	0.30	AIAA 73–318
9	SES-100B	SES	0.32	ADAO 22583
10	Model 719	SES	0.63	Maric Report

3.5 Aerodynamic momentum drag

Pressurized air has to be blown into the air cushion to replace air leakage out from the cushion under the skirt or seals in order to maintain the ACV/SES travelling on cushion. Thus, this mass of pressurized air contained in the cushion will be accelerated to the speed of the craft. The drag due to the momentum change of this air mass is called the aerodynamic momentum drag and can be calculated as

$$R_m = Q\rho_a v \tag{3.7}$$

where R_m is the aerodynamic momentum drag (N), Q the air inflow rate (m^3/s), ρ_a the air mass density (Ns^2/m^4) and v the craft speed (m/s). Q is generally calculated by including the cushion air inflow rate together with the air inflow rate for gas turbine intake systems and engine cooling systems.

3.6 Differential air momentum drag from leakage under bow/stern seals

According to momentum theory this drag can be written as

$$R_{a''} = \rho_a (\phi h_1 B_c P - \phi h_2 B_c P)P \approx W a'' \tag{3.8}$$

where $R_{a''}$ is the air momentum drag from differential leakage under bow/stern skirts, ϕ the discharge coefficient of air leakage (in general we take $\phi = 0.5$–0.6), h_1 the bow air leakage clearance, i.e. the vertical distance between the lower tip of bow skirt/seal and the corresponding inner water-line, (m), h_2 the stern air leakage clearance (m), a'' the declined angle between the inner water line and the line linking the lower tips of the bow/stern seals, while the craft is travelling on the cushion (°), p_c the cushion pressure, (N/m^2) and $P = \sqrt{(2p_c/\rho_a)}$. From Fig. 5.12, $R_{a''}$ can be written as

$$R_{a''} = W/l_c\,[(z_b - t_{bi}) - (z_s - t_{si})] \tag{3.9}$$

where z_b, z_s are the vertical distances of the lower tip of bow/stern skirts over the craft base-line (m) and t_{bi}, t_{si} the vertical distance between the inner water line and the craft base-line (m). Because the z_b, z_s are given for the given craft and t_{bi}, t_{si} can be obtained by the equation listing in Chapter 5, $R_{a''}$ can be obtained using equation (3.9).

$R_{a''}$ relates to cushion length–beam ratio, Fr, and cushion pressure–length ratio (these parameters influence the profile of the inner wave surface), and the location of the centre of gravity (CG), (which influences the trim angle and inner/outer water line of the craft), as well as to z_b and z_s.

In order to reduce $R_{a''}$, or to increase the jet thrust from a stern seal to increase craft speed, drivers can sometimes increase the stern seal clearance to make $R_{a''}$ less than zero. In fact it is very difficult to predict this drag. According to the general custom of ACV designers and also for reasons of conservatism, we often take $a'' = 0.25$–$0.5°$ for ACVs, and neglect this drag term for SES. This may be validated by prototype tests, in which a lot of spray will be seen behind the stern seal.

With the aid of Fig. 3.13, we can demonstrate this concept. In this figure, we have AB as the line linking the lower tip of the bow/stern seal (skirts), and ψ' the angle between sea level SL and AB. ψ' does not denote the trim angle of the craft, except if the line AB is parallel to the base-line of the craft. a' is the slope angle of the inner wave surface, and R_w the wave-making drag. From Fig. 3.13, we derive the following:

- When $\psi' > 0$, i.e. the craft operates with bow up, then

$$R_{a''} = W \tan \psi' - R_w \tag{3.10}$$

If line AB is parallel to the base-line of the craft, then the drag due to the

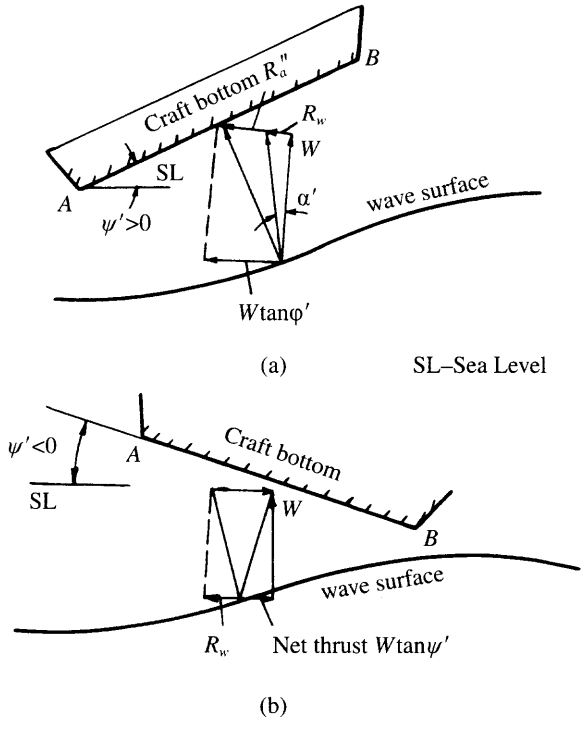

Fig. 3.13 Cushion wave-making drag and drag due to the difference of air momentum leaking from bow and stern of cushion.

differential air momentum leaking from the bow/stern skirts $R_{a''}$ is equal to the trim drag minus the wave-making drag.

- When $\psi' < 0$, i.e. the craft operates with bow down, then

$$R_{a''} = -W \tan \psi' - R_w < 0$$

which means $R_{a''}$ becomes a thrust and makes a net thrust of $W \tan \psi'$.

3.7 Skirt drag

The composition of skirt drag can be written as

$$R_{sk} = R_{sf} + R_{sp} + R_{ss} + R_{si}$$

where R_{sk} is the total skirt drag (N), R_{sf} the skirt water friction (N), R_{sp} the skirt pressure drag (N), R_{ss} the skirt spray drag (N) and R_{si} the skirt inertia drag (N).

R_{si} is the wave-making drag induced by the high frequency vibration of the skirt. For this reason, this drag is relative to the mass of the skirt, therefore this drag is also called inertia drag.

R_{sp} is the result of the cushion pressure and internal loads on the deformed part of the skirt above the water level locally balancing the water pressure acting on the part

of the skirt immersed in the water. The overall equilibrium between these forces within the whole skirt and R_{sp}, is the component along the x-direction L_s called skirt pressure drag.

Skirt drag not only relates to the immersion depth of skirts and spray making, but also the density of the skirt material. Therefore, it is very difficult to predict this drag by theoretical calculation; it can only be estimated with accuracy by full scale experimental methods or scaling from model test results.

Total skirt drag, R_{sk}

With respect to an ACV, skirt friction with the water surface is a large component of total drag, owing to the high density of water, 800 times larger than that of air.

Most of the skirt makes only slight contact with the water, while at the stern and the two stern corners of a skirt, segmented or fingered skirts may cause a large amount of scooping drag at lower speeds (particularly below hump speed, or $Fr < 0.75$). This can cause a particular problem for transiting hump speed if the skirt geometry is unfavourable. In addition the craft trim can strongly affect scooping. Above hump speed the skirt in the rear third of the craft is the most important for determining skirt drag in a steady condition. Normally the rear skirt lower tip is raised to minimize skirt drag.

Sometimes skirt drag will increase severely because of poor running trim, when either the bow skirt contacts the water surface (LCG too far forward) or the corners of the stern skirt scoop water (LCG too far back).

The skirt drag of a model tested in a towing tank will generally be less than that experienced at full scale, around 35% of total drag, as the running attitude of the craft can be regulated to be optimal. In contrast, the skirt drag for full scale craft will increase to about 55% or more of the total drag in the case of unfavourable craft trim. This drag level is generally not reproducible in the towing tank, so powering estimates for craft need to account for this difference.

A short description of each component is now given below.

Skirt friction drag, R_{sf}

We take the bag–finger type bow skirt or open loop type as an example to analyse the force exerted on the skirts and assume that the skirt fabric is perfectly flexible. That means the skirt fabric will be flattened and in close proximity to the water surface as the skirts make contact with the water surface as shown in Fig. 3.14; the deformation and applied force on the skirts can be expressed as in [24].

$$L_1 + L_2 = [d + R(1 - \cos\theta]/\sin\theta \tag{3.11}$$

where L_1 is the arc length of the part of the skirt in contact with the water surface (m), L_2 the flattening part of the skirt in close proximity to the water surface (m), R the radius of curvature due to the bending part of the skirt (m), d the immersion depth of the skirt (m) and θ the declination angle of the skirts, (°).

Meanwhile the water friction of the skirt balances with the tensions in the fabric, which can be written as

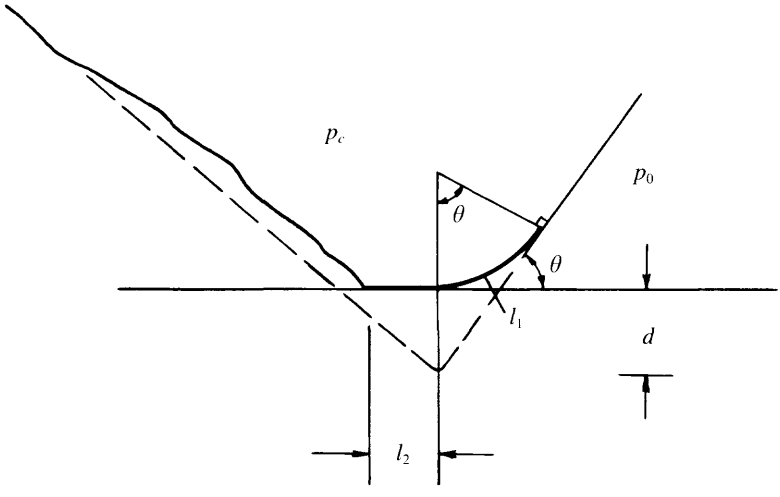

Fig. 3.14 Deflection of flexible skirts contacting water surface.

$$D = (p_c - p_0)R = p_c R = R_{sf}$$

where D is the tension of skirt fabric per unit width (N/m), p_c the cushion pressure (N/m^2), p_0 the atmospheric pressure and which equals zero and R_{sf} the water friction of the skirt per unit width (N/m).

Since the Reynolds number, Re is large for the skirt, the skirt fabric can be considered as a rough surface for friction, then

$$R_{sf} = 0.032\,(k/p_z)^{0.2} p_z\, q_w \tag{3.12}$$

in which k is the coefficient due to equivalent roughness and q_w the hydrodynamic pressure (N/m^2), $= 0.5\,\rho_w\, v^2$. Thus equation (3.11) can be written as

$$l_2 = \frac{d}{\sin\theta} + \frac{R_{sf}}{p_c}\left[\frac{1-\cos\theta}{\sin\theta} + \frac{\theta}{57.29}\right] \tag{3.13}$$

The values of R_{sf} and l_2 can be defined from equations (3.12) and (3.13), i.e. the two-dimensional equations. It is usual to assume that $d = l_2$ when calculating the wet surface of the skirt. In fact, this creates some errors due to neglecting the definite radius of curvature R, which is not equal to zero, but relative to the water friction and skirt fabric tension this is a small error. In the case of calculating the friction of stern skirts, the determination of the friction coefficient is in fact very complicated because the immersion depth of the stern skirt of a craft running over water is so small and it also makes a large amount of spray due to the pressure of the air cushion. Therefore, the problem becomes the drag concerned with the dynamics of two-phase flow – thus R_{sk} can be written as

$$R_{sk} = f\,(Re_j, \bar{Q}, d/p_c, W_e, F_{rl} \ldots) \tag{3.14}$$

where Re_j is the Reynolds number for jet air, $\bar{Q}$ the flow rate coefficient, which affects the spray, W_e the Weber number $= \rho_w\, v_j^2\, t/\sigma_t$ which also affects the initiation of spray,

V_j the jet velocity from the stern cushion, t the thickness of the jet from the stern cushion and σ_t the surface tension of water.

The water friction of the stern skirt will decrease due to two-phase flow through the gap under the segment tips or bag lower point, since the turbulent air flow creates dense spray.

Skirt pressure drag, R_{sp}

This may be written as

$$R_{sp} = (p_c - p_0)\mathrm{d} = p_c\mathrm{d} \tag{3.15}$$

As mentioned above, the various components of skirt drag, such as friction drag in two-phase flow, the inertia drag of the skirt due to the flutter of the skirt fabric and spray drag of skirts at both sides of the craft, are difficult to calculate. For this reason, the total skirt drag is best estimated by experience-based formulae [25, 26], as follows:

$$R_{sk} = R_{sk1} + R_{sk2} \tag{3.16}$$

$$R_{sk1} = C_{sk1} \times 10^{-6} (h/l_j)^{-0.34} l_j S_c^{0.5} q_w \tag{3.17}$$

$$R_{sk2} = C_{sk2} R_w \tag{3.18}$$

$$C_{sk2} = \{[2.8167 (p_c/l_c)^{-0.259}] - 1\}$$

where R_{sk} is the skirt total drag, R_{sk1} the wet drag of the skirt, R_{sk2} the wave-making drag due to the skirt, h the average clearance for air leakage where $h = S_j/l_j$ in static hovering mode, where S_j denotes the area of air leakage under the skirts, l_j the total peripheral length of the skirts, including the delta area for air leakage at the tip of finger in the case of using bag and finger type skirts, R_w the wave-making drag due to the air cushion, S_c the cushion area, q_w the hydrodynamic head due to craft speed $= 0.5 \rho_w v^2$, C_{sk1} the coefficient for hydrodynamic drag, $C_{sk} = 2.5$–3.5 or $[1.35 + 0.112 p_c/l_c]$, and C_{sk2} the coefficient due to wave-making drag of the skirt, obtained by equation (3.16) or Fig. 3.15.

These equations were obtained from model experimental data. In fact equation (3.17) can be written as

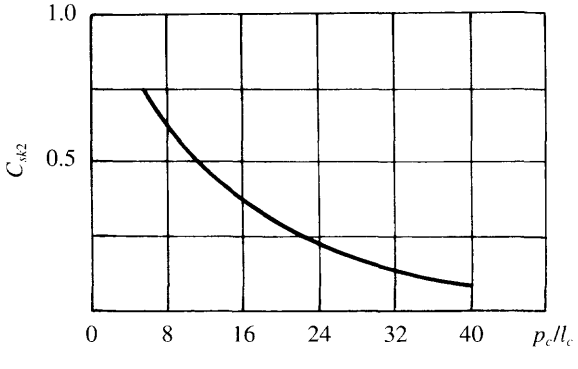

Fig. 3.15 Variation of skirt wave-making drag coefficient C_{sk2} with cushion length/beam ratio P_c/L_c.

$$R_{skl}/W = C_{skl} \times 10^{-6} (h/l_j)^{-0.34} l_j/p_c \, q_w/S_c^{0.5} \tag{3.18a}$$

where W is the weight of the craft (N).

Drag of bow/stern seals of an SES, R_{sb}, R_{ss}

This is also estimated based on test data. Two methods for predicting this drag are as follows.

MARIC method [27]

Based upon a series of model tests, a statistical analysis was carried out at MARIC. Putting the skirt (bow/stern) drag, the drag due to the differential momentum from the bow/stern seals, the wave-making drag of sidewalls, and the interference drag due to sidewalls, all into a single term 'residual drag' and then processing this by regression analysis, the following equation is obtained:

$$R_r = C_r' \, B_c \, h_c \, q_w \tag{3.19}$$

where R_r is the residual drag of an SES (N), C_r' the residual drag coefficient and h_c the water surface depression induced by air cushion pressure.

C_r' may be obtained from Fig. 3.16. An intermediate value might be chosen. The lower value relates to the better performing seals (making the flow of air leakage under the stern seal significantly larger than that under the bow seal), and the better running attitude of the craft. In contrast, the larger value relates to a skirt with no designed rear gap at level trim, or the craft trim being more bow up, for example due to a service requirement for open sea conditions rather than coastal or protected waters.

This experimental expression is based upon the following conditions:

$$l_c/B_c = 3.5\text{–}4.0 \qquad p_c/l_c = 15\text{–}18.5 \text{ kgf/m}^3 \qquad 0.7 < Fr_l < 1.2$$

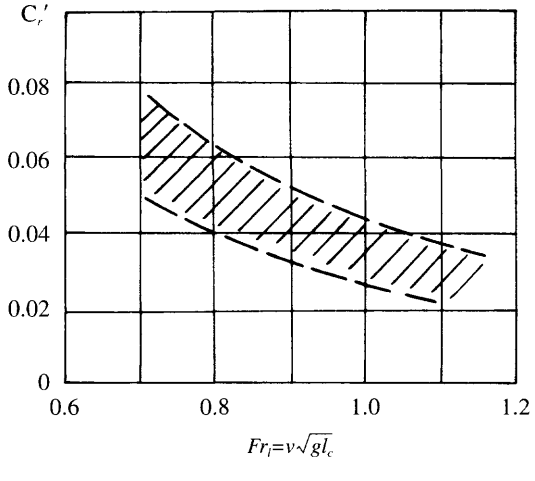

Fig. 3.16 Variation of seal drag coefficient C_r' with Froude Number.

Rin-Ichi Marao method [28]

Model experiments were carried out on an SES with thin plates as sidewalls and with $l_c/B_c = 2$ approximately, by Rin-Ichi and Marao. The air profile drag was then deducted and the aerodynamic momentum drag and wave-making drag obtained from analysis of the measured wave profile. These components were then deducted from the total drag of models to obtain the residual drag. The form drag of sidewalls can be neglected due to the thin plate sidewalls used, so that the residual drag can be approximated directly to the seal drag and written as

$$R_{sk} = C_{sk}\ B_c\ h_c\ q_w \tag{3.20}$$

where R_{sk} is the seal drag of an SES, C_{sk} the coefficient for skirt (seal) drag, as shown in Fig. 3.17 and q_w the hydrodynamic head of the craft at speed.

B. A. Kolezaev method

From reference 19, expressions for skirt drag can be written as

$$R_{sk} = (a + b\ Fr_d)\ B_c\ p_c\ v \tag{3.21}$$

where Fr_d is the Froude number due to the volumetric displacement,

$$Fr_d = v/(g\ D^{0.33})^{0.5}$$

and D is the volumetric displacement of the craft (m^3), a the experimental coefficient, $0.00225 \leqslant a \leqslant 0.021$, b the experimental or experience coefficient, $0.0015 \leqslant b \leqslant 0.0087$ and v the velocity (m/s). Coefficients a and b are dependent upon the material configuration and aerodynamic performance of the seals.

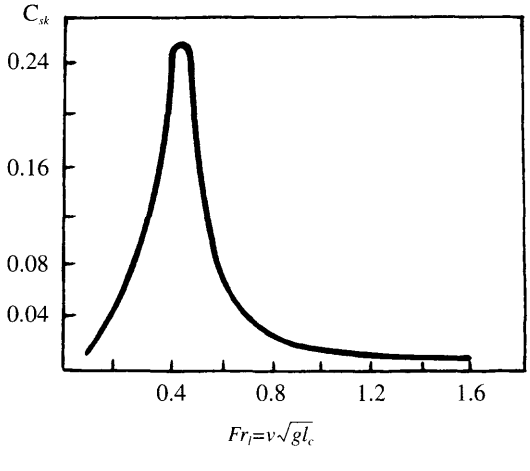

Fig. 3.17 Seal drag coefficient vs Froude Number at optimum trim angle.

3.8 Sidewall water friction drag

Friction drag is a large proportion (up to 30–40% for high speed craft) of total craft drag, as shown in Fig. 3.1. For this reason, calculation has to be made carefully. The main difficulty is to determine the wetted surface accurately.

In general, two methods are used: one is the theoretical method as described in Chapter 5 and the other is a model experimental method similar to that used in planing hull design, i.e. the wetted area can be obtained by photographs. We will introduce four different practical methods for predicting the wetted surface by experimental and statistical analysis methods.

With respect to the sidewall water friction drag, the following equation can be used:

$$R_{swf} = (C_f + \Delta C_f)\, S_f\, q_w \tag{3.22}$$

where R_{swf} is the water friction drag of sidewalls (N), C_f the coefficient for the friction of the plate, obtained by $0.455/[l_s\, Re]^{2.58}$ (3.23), ΔC_f the coefficient due to added roughness of the sidewalls, between 0.3 and 0.4×10^{-3}, Re the Reynolds number $= l_s v_s/\upsilon$, l_s the wetted length of sidewalls (m), v_s the craft speed, (m/s^2), υ the kinematic viscosity coefficient (m^2/s) and S_f the wetted surface of the craft running on the cushion (m^2).

MARIC method [29]

The sidewall wetted surface is dependent upon craft trim. It is subsequently a function of wave-making generated by the air cushion, the sidewalls and their interference with each other, lift system characteristics, as well as the seal clearance over the base line of the craft, etc. The theoretical method for prediction is therefore complicated. For this reason, the simplest way to predict the wetted surface area may be by means of measurement from photographs.

Figure 3.18(a) shows the outer surface of an SES model running at below hump speed (Fr = 0.239), Fig. 3.18(b) shows that above hump speed (Fr = 2.15) and Fig. 3.19 shows the added wave-making due to the bow seal pushing water (described in detail in the following paragraphs of this chapter). Thus, the curve showing the relation between the wetted surface of inner/outer sidewalls and the Fr can be obtained by the photographic method from model experiments.

Then the wetted surface of sidewalls of craft running on cushion can be written as

$$S_f = K_i\, S_{i0} + K_{out}\, S_{out0} \tag{3.24}$$

where K_i, K_{out} are correction coefficients for the inner/outer wetted surface of sidewalls, which can also be written as

$$K_i = S_i/S_{i0}$$

$$K_{out} = S_{out}/S_{out0}$$

These coefficients can be determined by photographs or experimental results from similar craft models. Also S_{io}, S_{out0} are the wetted inner/outer surface breadth of sidewall of craft hovering static (Fig. 3.20) (m) and S_i, S_{out} the wetted inner/outer surface area of sidewall of craft running on the cushion.

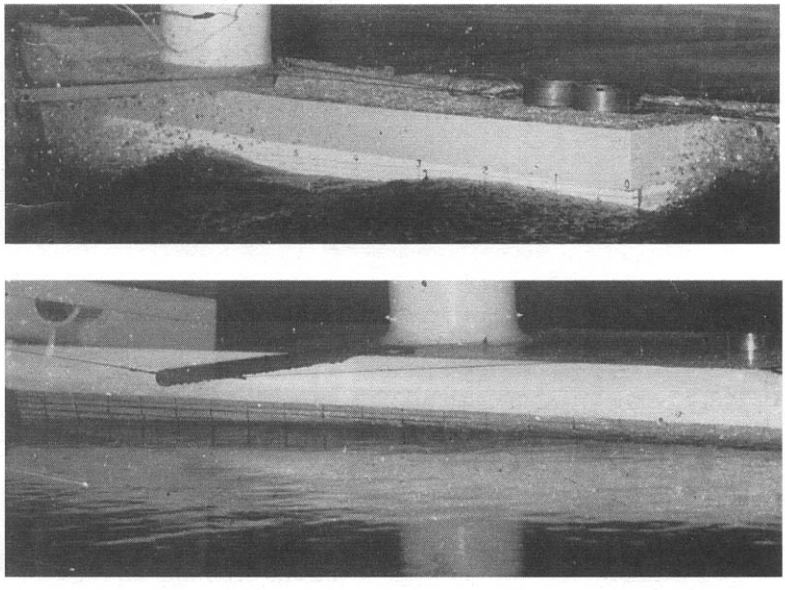

Fig. 3.18 Running attitude of SES model on cushion: (a) $F_r = 0.239$ (during take-off); (b) $F_r = 2.15$ (post take-off).

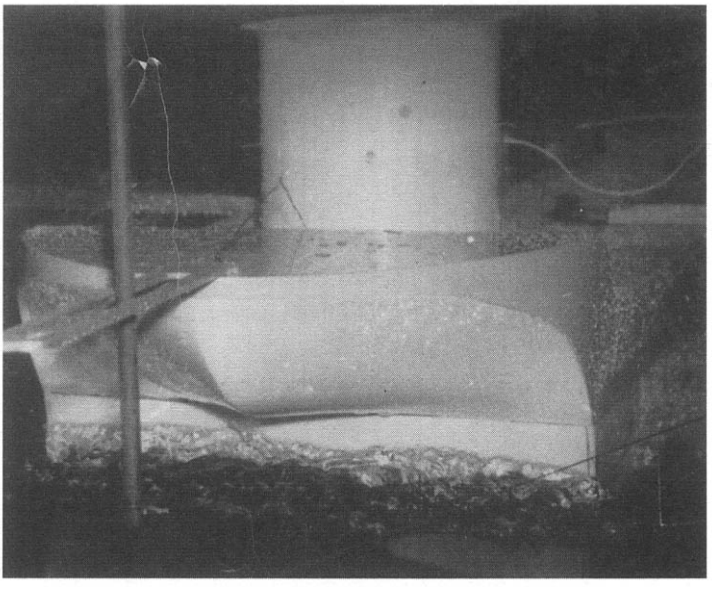

Fig. 3.19 Water contact phenomenon of bow seal during take-off.

Owing to the smaller inner wetted surface area by comparison with the outer one and also the difficulty in photographing the inner wetted surface, the total area of wetted surface is estimated as

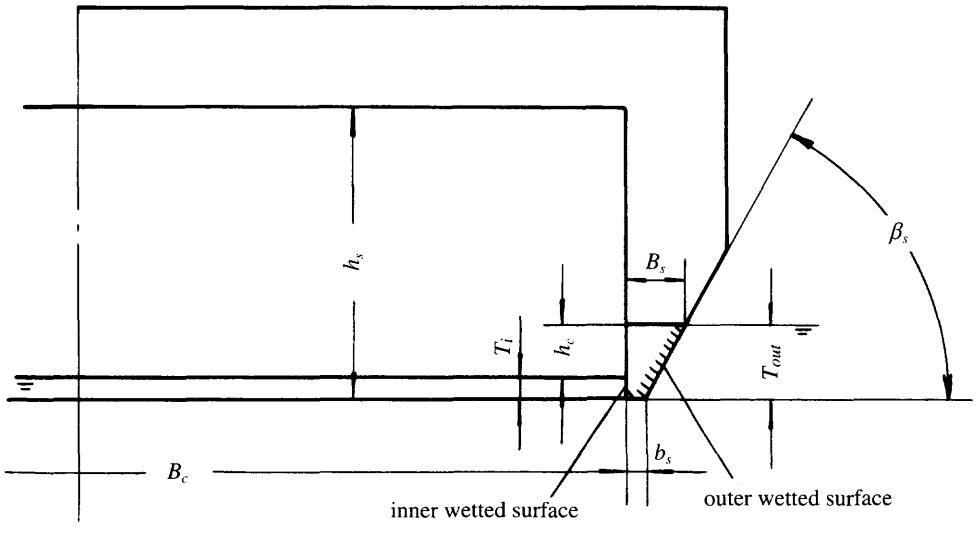

Fig. 3.20 Sketch of wetted surface of SES.

$$S_f = S_{i0} + S_{out0} K_{out} \tag{3.25}$$

where K_{out} can be obtained from Fig. 3.21, which has been obtained by statistical analysis of photographs on model no. 4 by MARIC. It is found that there are two hollows on the curve of the outer wetted surface area, the first is due to the hump speed, which leads to a large amount of air leakage amidships, and the second is caused by small trim angle at higher craft speed.

Method used in Japan [28]

Reference 28 introduces the measurement of the inner/outer wetted surface area of a plate-like sidewall of an SES with cushion length beam ratio (l_c/B_c) of about 2 on the cushion and represented as follows (Fig. 3.22):

$$S_f = S_{f\infty} + (S_{f0} - S_{f\infty})\, e^{-Fr} + 4h_c\, l_s f_s \tag{3.26}$$

where S_f is the area of the wetted surface of sidewalls (m^2), $S_{f\infty}$ the area of the wetted surface of sidewalls at high speed (m^2) and f_s the correction coefficient for the area of the wetted surface, which can be related to Fr_l, as shown in Fig. 3.23 and which is obtained by model test results.

In the case of craft at very high speed (higher than twice hump speed), the water surface is almost flat at the inner/outer wave surface and also equal to each other. With respect to the rectangular transverse section of the sidewalls, the wetted area can be written as

$$S_{f\infty} = [4(h_2 - h_{eq}) + 2\, B_s]\, l_s \tag{3.27}$$

S_{f0} is the wetted surface area of the sidewalls of craft hovering statically (m^2),

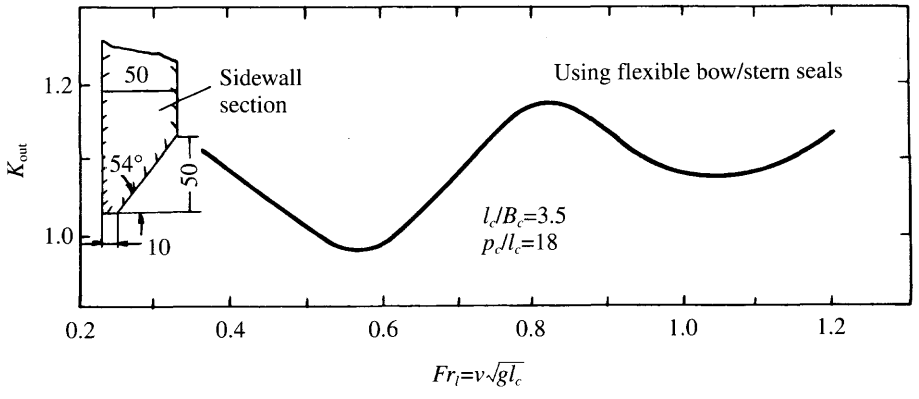

Fig. 3.21 Correction coefficient of outer wetted surface area of SES with flexible bow/stern seals.

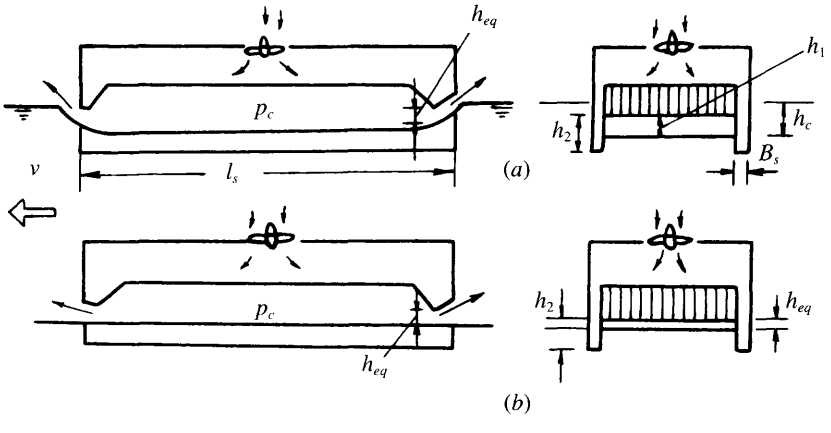

Fig. 3.22 Sketch of SES running attitude at F_r = 0(a) and F_r = 00(b).

$$S_{f0} = [4(h_2 - h_1) + 2\,h_c + 2\,B_s]\,l_s$$
$$= 4\,[T_i + 2\,h_c + 2\,B_s]\,l_s \qquad (3.28)$$

where B_s is the width of the sidewalls with rectangular transverse section (m), l_s the length of sidewalls (m), h_c the depth of cushion air water depression, hovering static (m), h_1 the vertical distance between the lower tip of skirts and inner water surface, i.e. $h_1 = h_2 - T_i$, as shown in Fig. 3.24, hovering static (m), h_2 the vertical distance between the lower skirt tip and craft baseline (i.e. z_b, z_s, in Chapter 5) (m), T_i the inner sidewall draft, hovering static, and h_{eq} the equivalent air gap,

$$h_{eq} = Q/(l_j\,(2p_c/\rho_a)^{0.5})$$

where Q is the cushion flow rate (m^3/s), p_2 the cushion pressure (N/m), ρ_a the air density (Ns^2/m^4), l_j the total length of air leakage at the bow/stern seal (m) and B_c the cushion beam (m).

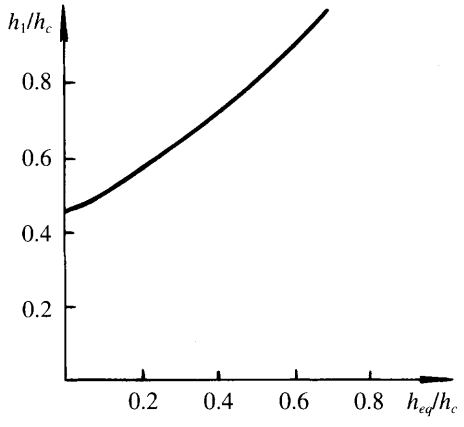

Fig. 3.23 Equivalent leakage h_{eq} compared to the distance from seal lower edge to the cushion inner water surface.

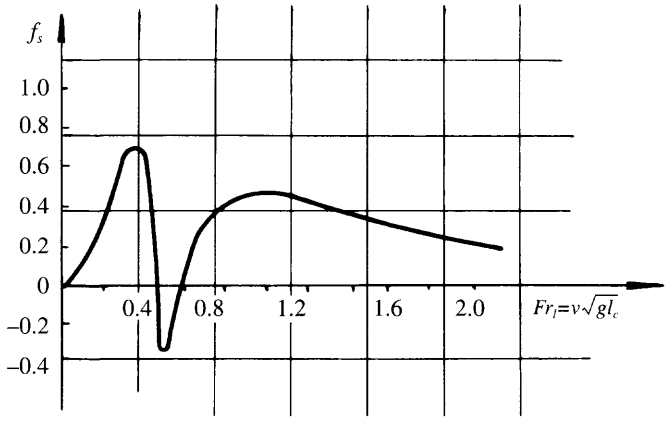

Fig. 3.24 Correction coefficient for sidewall wetted surface area.

From equations (3.27) and (3.28) the area of wetted surface at any given Fr_1, can be interpolated from

$$\text{at } Fr_1 = 0, \qquad S_f = S_{f0} \text{ (max. area of wetted surface)}$$

$$\text{at } Fr_1 = \infty \qquad S_f = S_{f\infty} \text{ (min. area of wetted surface)}$$

and

$$S_{f\infty} < S_f < S_{f0}$$

NPL method (The UK National Physical Laboratory) [15]

Based on model tests in their towing tank, the following method was obtained by NPL:

$$S_f = (S_{f0} + \Delta S_f)\,(1 + 5\,B_{smax}/l_s) \tag{3.29}$$

where B_{smax} is the max. width of sidewalls at design water line (m), ΔS_f the area correction to the wetted surface due to the speed change (m^2) and S_{f0} the area of wetted surface of sidewalls during static hovering (m^2).

This expression is suitable for the following conditions:

$$8 < p_c/l_c < 16 \quad \text{and} \quad Fr_l \geq 1.2$$

Figure 3.25 shows a plot enabling ΔS_f to be determined within these conditions.

B. A. Kolezaev method (USSR) [19]

B. A. Kolezaev derived the following expression for sidewall drag:

$$S_f = K_f\,S_{f0}$$

where S_f is the area of wetted surface, hovering static (Fig. 3.26), K_f the correction coefficient for the wetted surface, related to Fr (Fig. 3.27). S_{f0} can also be written as below (see Fig. 3.26):

$$S_{f0} \approx 2l_s\left[T_i + T_o + b_s + (B_s - b_s)\left(1 - \frac{\sin\beta}{\cos\beta}\right)\right] \tag{3.30}$$

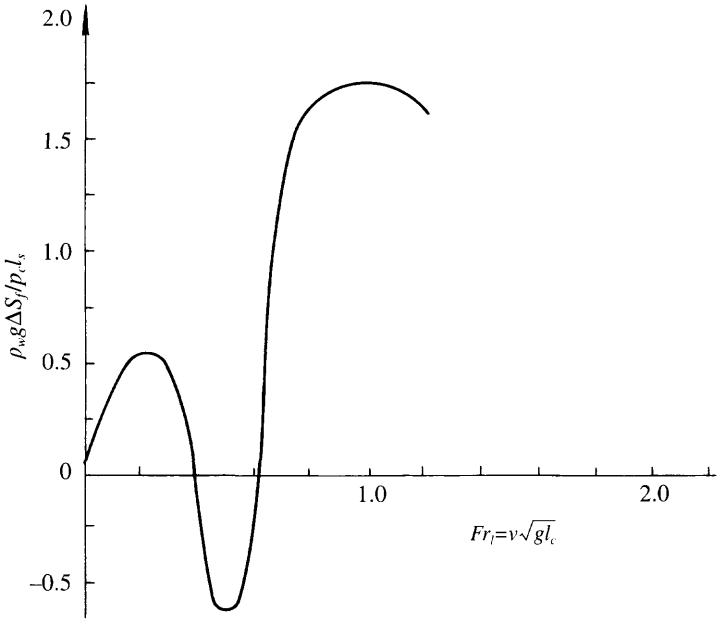

Fig. 3.25 Correction coefficient of wetted surface area of sidewall vs Froude Number. [15]

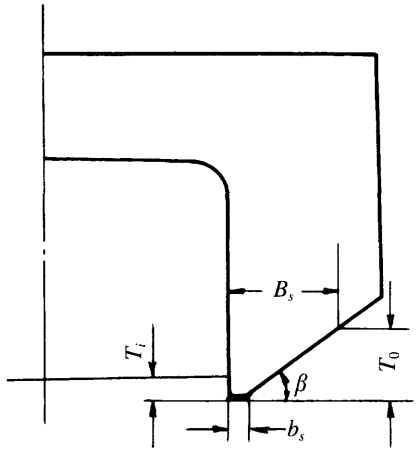

Fig. 3.26 Typical dimensions for wetted surface of sidewalls.

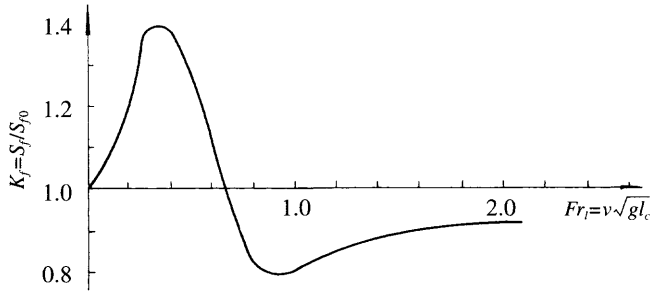

Fig. 3.27 Correction coefficient of wetted surface area of sidewalls vs Froude Number.

where T_i, T_o are the inner/outer drafts, hovering static (m), b_s the width of the base plate of the sidewalls (m), B_s the width of sidewalls at designed outer draft (m) and β the deadrise angle of sidewalls (°).

A number of methods used for predicting the area of the wetted surface have been illustrated in this section. It is important to note that one has to use these expressions consistently with expressions by the same authors to predict the other drag components, such as skirt drag, residual drag, etc., otherwise errors may result.

As a general rule, the methods derived from model tests and particularly photo records from the actual design or a very similar one will be the most accurate. The different expressions may also be used to give an idea of the likely spread of values for the various drag components during the early design stage.

3.9 Sidewall wave-making drag

Equivalent cushion beam method

SES with thin sidewalls create very little wave-making drag, owing to their high length/beam ratio, which may be up to 30–40. To simplify calculations this drag may be included in the wave-making drag due to the air cushion and calculated altogether, i.e. take a equivalent cushion beam $\bar{B}_c$ to replace the cushion beam B_c for calculating the total wave drag. Thus equation (3.1) may be rewritten as

$$R_w = \bar{C}_w p_c^2 \bar{B}_c/(\rho_w g) \tag{3.31}$$

where R_w is the sum of wave-making drag due to the cushion and sidewalls, $\bar{C}_w$ the coefficient of wave-making drag, $C_w = f(Fr_l, l_c/\bar{B}_c)$ and $\bar{B}_c$ the equivalent beam of air cushion including the wave-making due to the sidewalls.

The concept of equivalent cushion beam can be explained as the buoyancy of sidewalls made equivalent to the lift by an added cushion area with an added cushion beam. The cushion pressure can be written as

$$p_c = (W - W_s)/(l_c B_c)$$

where W_s is the buoyancy provided by sidewalls and W the craft weight. Then the equivalent cushion beam can be written as

$$\bar{B}_c = \frac{W}{p_c l_c} = \frac{W}{[(W - W_s)/(l_c B_c)]\, l_c} = \frac{B_c}{1 - W_s/W} \tag{3.32}$$

The method mentioned above has been applied widely in China by MARIC to design SES with thinner sidewalls and high craft speed and has proven accurate. Following the trend to wider sidewalls, some discrepancies were obtained between the calculation and experimental results. For this reason, [29] gave some discussion of alternative approaches.

Equation (3.31) can be rewritten by substitution of (3.32) into (3.31), as

$$R_w = \left[\frac{C_w p_c^2 B_c}{\rho_w g}\right] \cdot \left[\frac{\bar{C}_w}{C_w}\right] \cdot \left[\frac{\bar{B}_c}{B_c}\right]$$

$$= \frac{\bar{C}_w}{C_w} \cdot \frac{R_{wc}}{1 - W_s/W} \tag{3.33}$$

Where R_{wc} is the wave-making drag caused by the air cushion with a beam of B_c and without the consideration of wave-making drag caused by sidewalls, $\bar{C}_w$ the coefficient due to the wave-making drag with respect to Fr, $l_c/\bar{B}_c$

$$\bar{C}_w = f\,(Fr_l, l_c/\bar{B}_c)$$

and C_w the coefficient due to the wave-making drag with respect to Fr, l_c/B_c

$$C_w = f\,(Fr_l, l_c/B_c)$$

The total wave-making drag of SESs can now be written as

$$R_w = R_{wc} + R_{sww} + R_{wi} \tag{3.34}$$

where R_{wc} is the wave-making drag caused by the air cushion, R_{sww} the wave-making drag caused by the sidewalls and R_{wi} the interference drag caused by the air cushion and sidewalls. Therefore

$$R_{sww} + R_{wi} = R_w - R_{wc} \tag{3.35}$$

as

$$R_{wc} = C_w \, p_c^2 \, B_c/(\rho_w \, g) \tag{3.36}$$

and

$$p_c = W - W_s/(l_c \, B_c)$$

Therefore

$$R_{wc} = [C_w \, B_c/(\rho_w \, g)] \; [W - W_s/(l_c \, B_c)]^2 \tag{3.37}$$

If we substitute equations (3.36) and (3.33) into (3.35), we obtain

$$R_{sww} + R_{wi} = \frac{\bar{C}_w}{C_w} \; \frac{R_{wc}}{1 - W_s/W} - R_{wc}$$

$$= R_{wc} \left[\frac{\bar{C}_w}{C_w} \; \frac{1}{1 - W_s/W} \right] - 1 \tag{3.38}$$

If R denotes the buoyancy of sidewalls and equals zero, then the whole weight of the craft will be supported by the air cushion with an area of S_c ($S_c = l_c \, B_c$) and the wave-making drag could then be written as

$$R_{wc0} = [C_w \, B_c/(\rho_w \, g)] \; [W/(l_c \, B_c)]^2 \tag{3.39}$$

From equations (3.37) and (3.39) we have

$$R_{wc}/R_{wc0} = (1 - W_s/W)^2 \tag{3.40}$$

Upon substitition of equation (3.40) in (3.38) and using equation (3.39), then equation (3.38) can be written as

$$R_{sw} + R_{wi} = R_{wc0} \, [(\bar{C}_w/C_w) \, (1 - W_s/W) - (1 - W_s/W)^2] \tag{3.41}$$

The calculation results are shown in Fig. 3.28. It can be seen that the less the W_s/W, the less the wave-making drag of the sidewalls ($R_{sww} + R_w$), which is reasonable. The greater the W_s/W, the more the wave-making drag of the sidewalls.

Figure 3.28 also shows that wave-making drag decreases as the W_s/W exceeds 0.5. This seems unreasonable. The calculation results of [30] and [31] showed that wave-making drag will increase significantly as W_s/W increases. Reference 32 also showed that the wave-making drag of sidewalls could be neglected in the case of $W_s/W <$ 15%.

The equivalent cushion beam method is therefore only suitable to apply to SES with thinner sidewalls. It is unreasonable to use this method for SES with thick sidewalls or for air cushion catamarans (e.g. $W_s/W \approx 0.3$–0.4) and for these craft the wave-making drag of sidewalls has then to be considered separately.

Yim [30] calculated the wave-making drag due to sidewalls by means of an even simpler method. He considered that the total wave-making of an SES would be equal to that of an ACV with the same cushion length and beam, i.e. it was considered that the sidewalls did not provide any buoyancy, and the total craft weight would be supported only by an air cushion as to lead the same wave-making due to this equivalent air cushion. The effective wave-making drag coefficient of the sidewalls calculated by this method is similar to that for $W_s/W > 0.5$ above (see Fig. 3.28).

Hiroomi Ozawa method [31]

The theoretical calculation and test results of the wave-making drag of air cushion catamarans have been carried out by Hiroomi Ozawa [31]. Based on rewriting his equations found in [29], the final equation for predicting total wave-making drag may be written as (when $Fr = 0.8$)

$$R_w = R_{ws} + R_{sww} + R_{wi} \tag{3.42}$$

$$R_w = [1 - 0.96\, W_s/W + 0.48\, (W_s/W)^2]\, [C_w\, B_c/(\rho_w\, g)]\, [W/(l_c\, B_c)]^2$$

A comparison between the equivalent cushion beam method, the Ozawa method and the Yim method is shown in Fig. 3.28. It can be seen that satisfactory accuracy can be

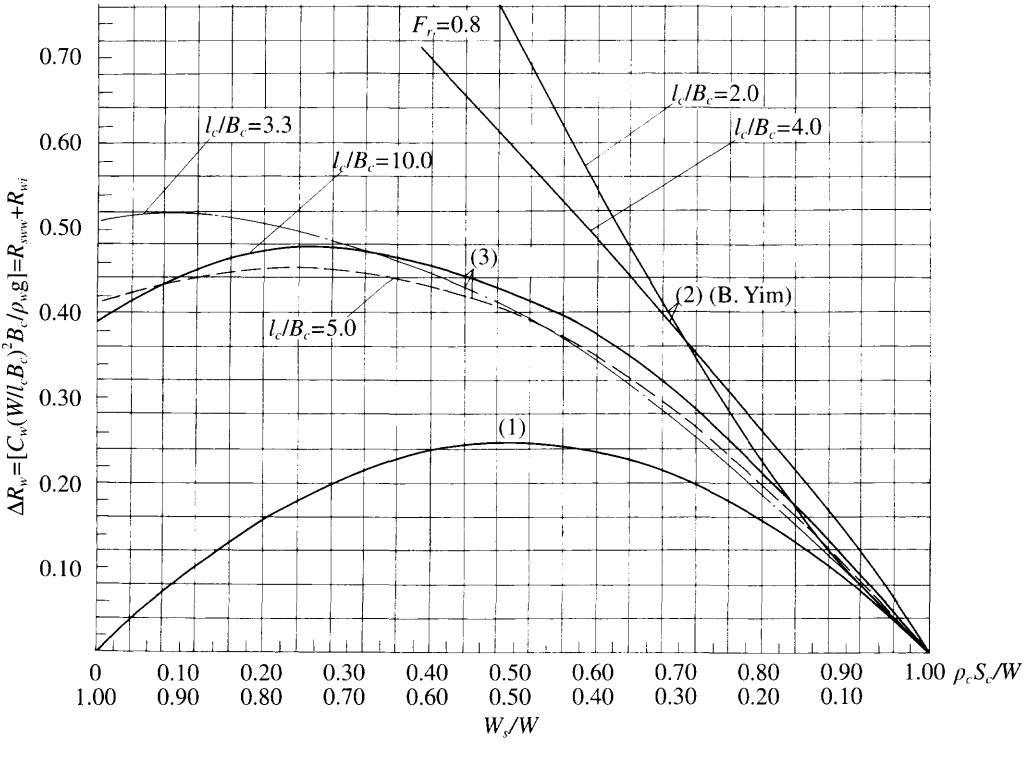

Fig. 3.28 Comparison of calculations for sidewall wave-making drag by means of various methods.

obtained by the equivalent method in the case of $W_s/W < 0.2$, but the wave-making drag of sidewalls and its interference drag with the air cushion have to be taken into account as W_s/W increases.

In conclusion, the methods for estimating sidewall drag introduced here are suitable for SES with sidewall displacement up to about 30% of craft total weight. Where a larger proportion of craft weight is borne by the sidewalls, the sidehull wave-making should be considered directly, rather than as a 'correction' to the cushion wave-making. Below 70% contribution to support from the air cushion, the beneficial effect of the cushion itself rapidly dies away, and so it is more likely that optimizing catamaran hulls will achieve the designer's requirements in the speed range to 40 knots. Above this speed, an air cushion supporting most of the craft weight is most likely to give the optimum design with minimum powering.

Calculation method for parabola-shaped sidewalls [33]

In the case where the sidewall water lines are slender and close to parabolic shape, then the wave-making drag of sidewalls can be written as

$$R_{sww} = C_{sww} (8 \rho_w g/\pi) (B_s^2 T_o^2/l_s) \tag{3.43}$$

where R_{sww} is the wave-making drag of the sidewall (N), C_{sww} the wave-making drag coefficient (Fig. 3.29), ρ_w the density of water (Ns^2/m^4), B_s the max. width of sidewalls (m) and T_o the outer draft of sidewalls (m).

B. A. Kolezaev method [19]

Kolezaev defined the residual drag of sidewalls as a function of craft weight:

$$R_{sww} = K_{fr} W$$

where R_{sww} is the residual drag of sidewalls (N), K_{fr} the coefficient of sidewall residual drag, obtained from Fig. 3.30, and W the craft weight (N).

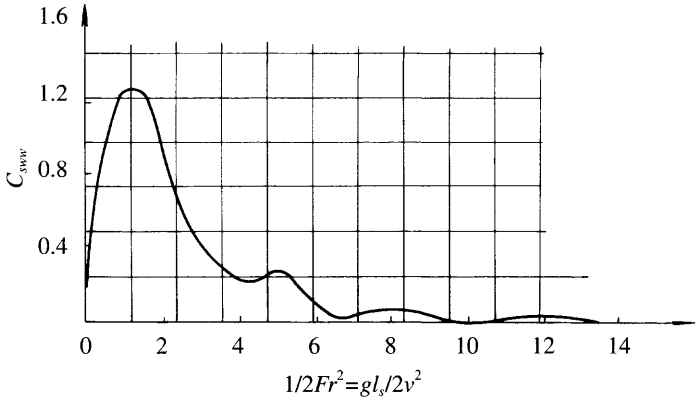

Fig. 3.29 Wave-making drag coefficient of slender sidewalls with the parabolic water planes. [39]

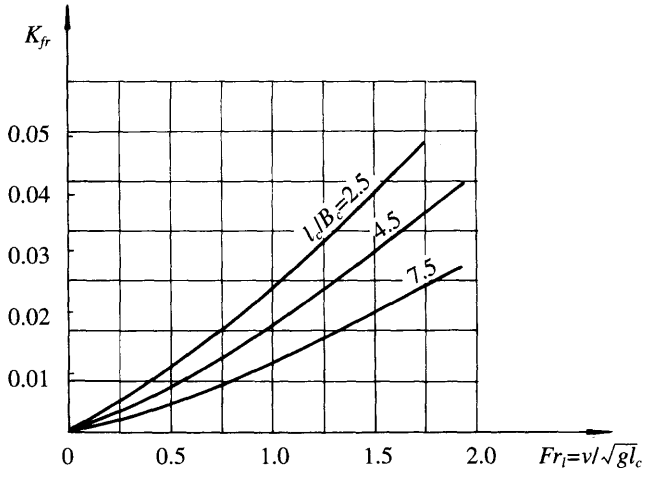

Fig. 3.30 Residual drag coefficient of sidewall as a function of L_c/B_c and Froude number.

3.10 Hydrodynamic momentum drag due to engine cooling water

In general, the main engines mounted on SES have to be cooled by sea water which is ingested from Kingston valves or sea water scoops mounted at propeller brackets, via the cooling water system, then pumped out from sidewalls in a transverse direction. The hydrodynamic momentum drag due to the cooling water can be written as

$$R_{mw} = \rho_w V_j Q_w \tag{3.44}$$

where R_{mw} is the hydrodynamic momentum drag due to the cooling water for engines (N), V_j the speed of inlet water, in general it can be taken as craft speed (m/s), and Q_w the flow rate of cooling water (m/s).

3.11 Underwater appendage drag

Drag due to rudders, etc.

Drag due to rudders and other foil-shaped appendages, such as plates preventing air ingestion, propeller and shafts brackets, etc. can be written as [34]:

$$R_r = C_{fr}(1 + \delta v/v)^2 (1 + r) S_r q_w \tag{3.45}$$

where R_r is the drag due to the rudder and foil-shaped propeller and shaft brackets (N), C_{fr} the friction coefficient, which is a function of Re and the roughness coefficient of the rudder surface. In this case $Re = (vc/v)$ where c is the chord length of rudders or other foil-like appendages (m), $\delta v/v$ is the factor considering the influence of propeller wake:

$\delta v/v = 0.1$ in general, or

$\delta v/v = 0$ if no effect of propeller wake on this drag;

v is craft speed (m/s), r the empirical factor considering the effect of shape, $r = 5\ t/c$, where t is foil thickness, S_r the area of wetted surface of rudders or foil-like appendages (m^2) and q_w the hydrodynamic head due to craft speed.

This equation is suitable for rudders or other foil-shaped appendages totally immersed in the water.

Drag of shafts (or quill shafts) and propeller boss [35]

This drag can be written as :

$$R_{sh} = C_{sh}\,(d_1\,l_1 + d_2\,l_2)\,q_w \tag{3.46}$$

where R_{sh} is the drag of the shaft (or quill shaft) and boss (N), d_1 the diameter of the shaft (or quill shaft) (m), d_2 the diameter of the boss (m), l_1 the wetted length of shafts (quill shaft) (m), l_2 the wetted length of the boss (m) and C_{sh} the drag coefficient of the shaft (quill shaft) and boss. For a perfectly immersed shaft (quill shaft) and boss and $5.5 \times 10^5 > R_{e_m} > 10^3$, then it can be written:

$$C_{sh} = 1.1 \sin^3\beta_{sh} + \pi\, Cf_{sh} \tag{3.47}$$

where β_{sh} is the angle between the shaft (quill shaft), boss and entry flow (for stern buttocks), Cf_{sh} the friction coefficient, which is a function of R_{e_m}, where

$$R_{e_m} = v\,(l_1 + l_2)/\upsilon$$

and also includes the roughness factor; for example, if $\beta_{sh} = 10°–12°$, with the shafts (quill shafts) immersed perfectly in water, then we take $Cf_{sh} = 0.02$.

Drag of strut palms

According to ref. 34, the drag of strut palms can be written as

$$R_{pa} = 0.75 C_{pa}\,(h_p/\delta)^{0.33}\,y\,h_p\,(\rho_w/2)\,v^2 \tag{3.48}$$

where R_{pa} is the drag of strut palms (N), y the width of strut palms (m) and δ the thickness of the boundary layer at the strut palms:

$$\delta = 0.016 x_p\ (\text{m})$$

where x_p is the distance between the stagnation point of water line and strut palms (m), h_p the thickness of strut palms (m) and C_{pa} the drag coefficient of strut palms, $C_{pa} \cong 0.65$.

Drag of non-flush sea-water strainers

According to ref. 34, the drag of non-flush sea-water strainers can be written as

$$R_0 = S_0\,C_0\,(\rho_w/2)\,v^2 \tag{3.49}$$

where R_0 is the drag due to non-flush sea-water strainers (N), S_0 the frontal projected

area of the sea-water inlet (m), C_0 the drag coefficient due to sea-water strainers, and v the craft speed (m/s).

There are a number of methods for predicting the appendage drag. In this respect, there is no difference between the appendages of SES and planing hulls, or displacement ships: the data from these can therefore be used for reference.

3.12 Total ACV and SES drag over water

Different methodologies to calculate the total drag of ACV/SES have been compiled and compared at MARIC [27]. Three methods for ACVs and five methods for SES may be recommended, as summarized below.

ACV

The calculation methods are shown in Table 3.2. Notes and commentary are as follows:

- It is suggested that method 1 can be used at design estimate or initial design stage. Since many factors cannot be taken into account at this stage, the method is approximate, taking a wide range of coefficients for residual drag. Method 3 is still approximate, although more accurate than method 1. For this reason it can be applied at preliminary design stage. With respect to method 2, it is suggested using this at detail design or the final period in preliminary design, because the dimensions in detail and the design of subsystems as well as the experimental results in the towing tank and wind tunnel should have been obtained.
- The drag for above-water appendages (air rudders, vertical and horizontal fins,

Table 3.2 Methods for calculating ACV over water drag

Drag components	Method 1 Estimation	Method 2 Conversion from model tests	Method 3 Interpretative
Aerodynamic profile drag		$R_a = 0.5\rho_a C_a S_a v^2$	
Aerodynamic momentum drag		$R_m = \rho_a Q v$	
Momentum drag due to differential leakage from bow and stern skirts		$R_w = C_w p_c^2 B_c/(\rho_w g)$	C_w can be obtained from Figs 3.2 and 3.3
Wave-making drag	$R_{\alpha''} = W\alpha''$	$R_{\alpha''}$ is included in R_r	$R_{\alpha''} = W\alpha''$
Skirt drag or residual drag	$R_s = (0.5 \sim 0.7)(R_a + R_m + R_w + R_{\alpha''})$	$R_r = (R_{tm} - R_{am} - R_{mm} - R_{wm})(W/W_m)$	$R_{sk} = C_{sk1} \times 10^{-6} (h/l_j)^{-0.34} l_j q_w S_c^{0.5} + \{[2.8167 (p_c/l_c)^{-0.259}] - 1\} R_w$ $C_{sk1} = 1.35 + 0.112 P_c/l_c$
Total drag	$R_T = K_T(R_a + R_m + R_w + R_{\alpha''})$ where $K_T = 1.5 \sim 1.7$	$R_T = R_a + R_m + R_w + R_r$	$R_T = K'_T (R_a + R_m + R_w + R_{\alpha''} + R'_{sk})$
Remarks	See Note 1	See Note 1	See Note 2

Note 1: In methods 1 and 3 α'' denotes the angle between the inner water surface and the line linking the lower tips of bow and stern skirts.

Note 2: In method 3, normally $K'_T = 1.15$–1.25, but where a large amount of references and experimental data are available, then K'_T may be reduced to 1.0–1.1.

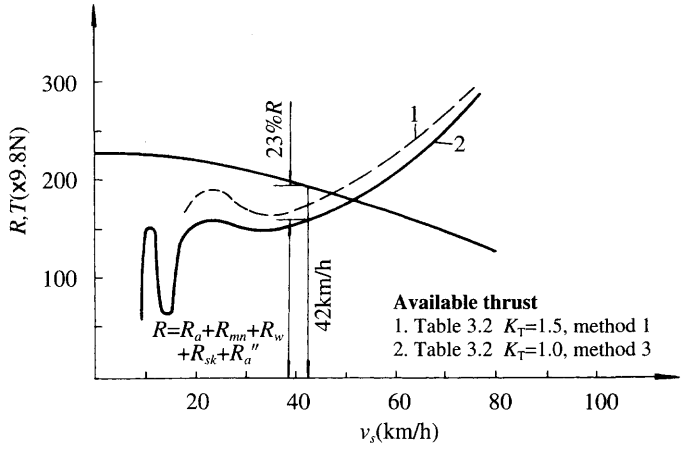

Fig. 3.31 Comparison of total drag of ACV model 7202 between calculations and measurements. $w = 2.775$t, $l_i/B_c = 2.14$, $p_c/l_c = 11.96$, $C_a = 0.6$, $\alpha'' = 0.5°$

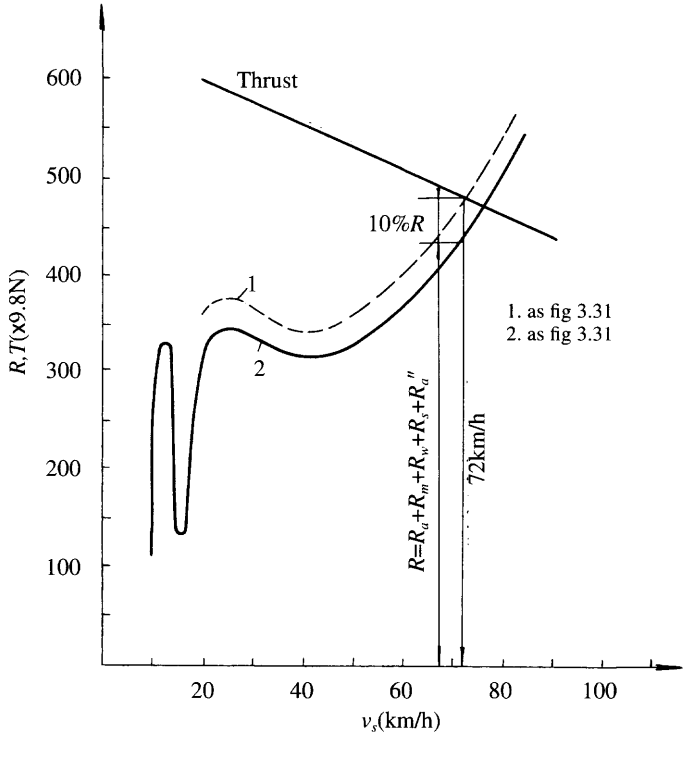

Fig. 3.32 Comparison of total drag of ACV model 711-IIA between calculations and measurements. $w = 6.4$t, $l_i/B_c = 2.15$, $p_c/l_c = 12{,}54$, $C_a = 0.4$, $\alpha'' = 0.25°$

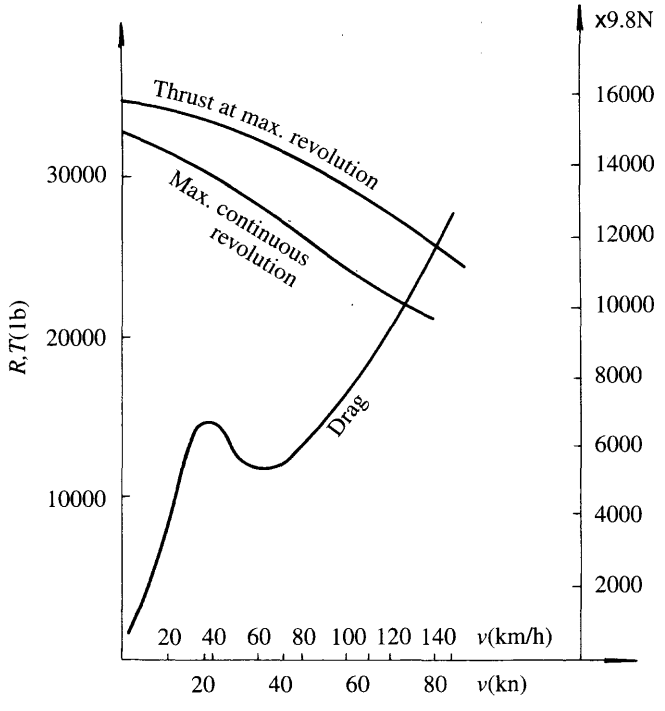

Fig. 3.33 The drag and thrust curves of SR.N4.

etc.) is included in the air profile drag, because in general the air profile drag coefficient C_a, which can be obtained either by model experimental data or by the data from prototype craft or statistical data, implicitly includes appendage drag in the coefficient.

- Similarly to conventional ships, model drag can be converted to drag of full scale craft according to the Froude scaling laws (see Chapter 9).
- Taking the Chinese ACV model 7202 and 711-IIA as examples, we calculate the drag components for these craft as shown in Figs 3.31 and 3.32. The propeller thrust in the figure was calculated according to the standard method for predicting the air propeller performance published by the British Royal Aeronautical Society. If K_T is assumed equal to 1.23 and 1.1 for craft 7202 and 711-IIA respectively and method 3 is used, then the calculated results agree well with the trial result.

  When MARIC used method No. 1, taking K_T as 1.65 for craft 7202 and 1.5 for craft 711-IIA, then the calculations agreed with test results. It can be seen that method 1 is approximate, because of the large K_T value.
- A typical resistance curve for the British SR.N4 can be seen in Fig. 3.33.

SES

There are many methods for calculating the drag components of an SES as are mentioned above, though one has to use these methods carefully and not mix them with

Table 3.3 Methods for calculating the drag of SES over calm water

Method	Method 1 Estimation	Method 2 Conversion from model tests	Method 3 NPL Method	Method 4	Method 5 Kolezaev Method
Drag items					
Aerodynamic profile drag			$R_a = 0.5\rho\, C_a\, S_a\, v^2$		
Wave-making drag due to air cushion			$R_m = \rho_a\, Q\, v$		
Friction drag of the sidewalls		$R_w = C_w\, p_c^2\, B_c/(\rho_w\, g)$ C_w can be obtained from Fig. 3.2 and 3.3			$R_w = C_w\,(4\ p_c\ W)/(\rho_w\ g\ l_c)$ C_w from Fig. 3.4
Wetted surface area of sidewalls			$R_{swf} = (C_f + \Delta C_f)\, S_f\, q_w$	$C_f = 0.455 / [l\ g\ Re]^{2.58}$	$\Delta C_f = 0.0004$ approx
Residual drag of sidewalls	$R_w = 0.05\, C_w\, (p_c^2\, B_c)/(\rho_w\, g)$ where C_w is from Figs 3.2 and 3.3	R_{sww} is included in R_r		$R_{sww} = 0.05\, C_w$ $(p_c^2\, B_c)/(\rho_w\, g)$ where C_w is from Figs 3.2 and 3.3	$R_{sww} = Kf_r\, W$ Kf_r from Fig. 3.30
Appendage drag		R_{ap} can be obtained by the same methods as for high-speed boats			Residual drag for sidewalls is included in appendage drag
Skirt drag or residual drag	$R_{sk} = k_s\,(R_w + R_a + R_m + R_{swf} + R_{sww} + R_{ap})$ or according to Fig. 3.19	$R_r = R_{tm} - (R_{wm} + R_{am} + R_{mm} + R_{swfm} + R_{apm})$ W/W_m		$R_{sk} = C_{sk}\, B_c\, h_c\, q_w$ C_{sk} from Fig. 3.17	$R_{sk} = (a + b\, Fr_d)\, B_c\, p_c\, v$ where $0.00225 \leqslant a \leqslant 0.021$, and $0.0015 \leqslant b \leqslant 0.0087$
Total drag	$R_T = R_w + R_a + R_m + R_{swf} + R_{sk} + R_{sww} + R_{ap} + R_{mw}$	$R_T = R_w + R_a + R_m + R_{swf} + R_{ap} + R_r$		$R_T = R_w + R_a + R_m + R_{swf} + R_{sk} + R_{ap} + R_{sww}$	$R_T = R_w + R_a + R_m + R_{swf} + R_{sk} + R_{sww}$
Remarks				If the craft is at optimum trim angle then use C_{sk} as shown in Fig. 3.17, otherwise increment.	

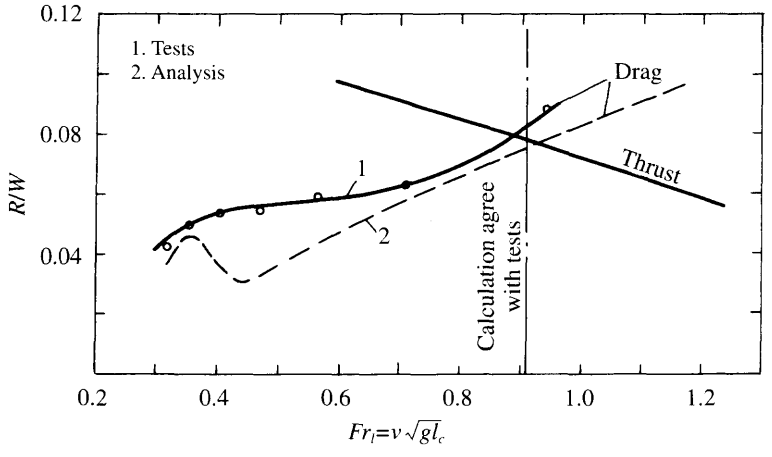

Fig. 3.34 The drag and thrust curves of 717C.

each other, otherwise errors may be made. We introduce five methods for SES total drag reference, outlined in Table 3.3 and add some commentary as follows:

1. It is suggested that method 1 can be used at the preliminary design stage and by comparison with methods 3, 4 and 5. With respect to method 2, this can be used at the final period of preliminary design or the detailed design stage.
2. The key problems for predicting the friction resistance of sidewalls are to determine accurately the wetted surface area. Of course it can be obtained by model tests in a towing tank. However, it can also be estimated by Figs 3.24, 3.25 and 3.27.
3. The sidewall residual drag (or sidewall wave-making drag) can be calculated according to Table 3.3, i.e. one can use the Newman method to calculate the wave-making drag (use Fig. 3.2 and 3.3) due to the air cushion, then take 5% of this as the sidewall residual drag. In the case of small buoyancy provided by the sidewalls ($W_s/W < 0.2$) the total wave-making drag can be calculated by the equivalent cushion method. The sidewall resistance can also be estimated by equation (3.43) or the Kolezaev method.
4. Seal drag R_{sk} can be calculated by the statistical method (MARIC method) or by taking 25–40% of total resistance (except R_{sk} itself) as the seal drag.
5. Taking Chinese SES model 717 as an example measurements and calculations are as shown in Fig. 3.34. It is found that the calculation results agree quite well with the test results, The typical SES resistance curve can be seen in Fig. 3.1.

3.13 ACV skirt/terrain interaction drag

For an ACV which operates mainly over land, such as self-propelled air cushion platforms, it is important to accurately determine the skirt/terrain interaction drag, as it

is a high percentage of the total drag. The total overland drag of ACV can be written as follows:

$$R_{gacv} = R_a + R_m + R_{sp} + R_{si} + R_{sk} \tag{3.50}$$

where R_{gacv} is the total overland drag of ACV (N), R_a the aerodynamic profile drag (N), R_m the aerodynamic momentum drag (N), R_{sp} the spray (debris) momentum drag (N), R_{si} the slope drag (N) and R_{sk} the skirt/terrain interaction drag (N).

R_a, R_m can be calculated by the methods outlined above. R_{sp} can usually be neglected due to the craft's low speed. The slope drag can be calculated according to the geography of the terrain. The skirt/terrain interaction drag is very strongly sensitive to lift air flow and is a function of craft speed and terrain condition. It is difficult to determine analytically and is usually determined from experimental data.

The overland drag curve of an ACV can be divided in three modes controlled by cushion flow rate as shown in Fig. 3.35:

1. Mode A, ACV profiles the terrain perfectly (i.e. a clear air gap between ACV and terrain);
2. Mode B, ACV experiences strong skirt/terrain interaction effects;
3. Mode C, ACV operates in 'ski' mode.

In mode A, at high flow rates, drag is relatively low. Normally in this flow region there is an air gap under most of the skirt periphery. In mode B, segment tips drag on the surface, but the delta regions between skirt tips still exist. In mode C, segment tips are pressed against the surface and the air flow acts more as a lubricant.

Figure 3.35 shows that the skirt/terrain interaction drag is closely related to skirt tip air gap. According to Chapter 2, the lift air flow Q can be written as

$$Q = l_j\, h\, \phi\, [2p_c/\rho_a]^{0.5} \tag{3.51}$$

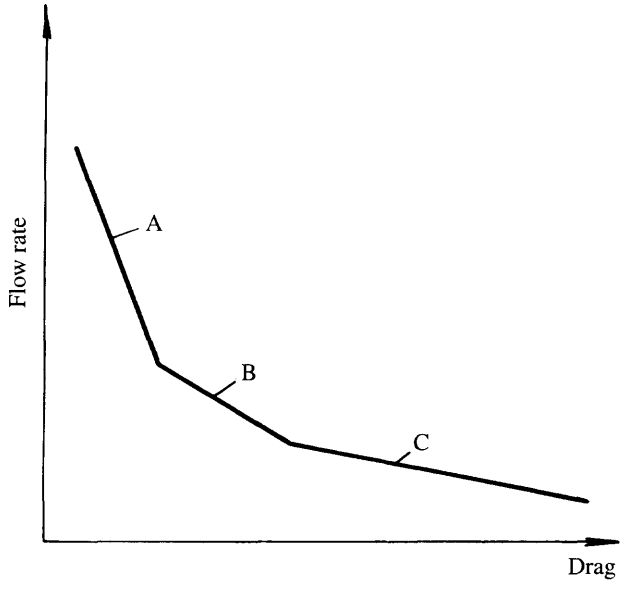

Fig. 3.35 Three operation modes of an ACV over ground terrain.

where Q is the lift air flow (m^3), l_j the peripheral length of the skirts (m), h the skirt clearance, including the equivalent clearance regarding the air leakage from the delta area of fingers, ϕ the air flow discharge coefficient and p_c the cushion pressure (N/m^2).

Different terrain conditions can radically change the effective discharge coefficient, (see Table 3.5). Grass or rock have the greatest effect. It is inappropriate therefore to characterize the air gap by h alone, since rough terrain and stiff grasses or reeds will reduce the skirt clearance significantly at the same air flow.

Fowler [36] defined $h_f K$ as the gap height instead of using h alone (i.e. $h_f K = h$), where K is referred directly to the terrain condition. This gap height for various craft is shown in Table 3.4. Then it can be seen that a high gap height $h_f K$ is normal for a high-speed ACV and low $h_f K$ for hover platforms.

Test results demonstrating the relation between skirt/terrain interaction drag and $h_f K$ as well as the terrain conditions are shown in Fig. 3.36 [36]. It is clear that the skirt/terrain interaction drag is very strongly sensitive to lift air flow.

Skirt/terrain interaction drag will increase at a higher rate as the skirt air gap is reduced below a critical value. For this reason, an optimum skirt air gap has to be selected as shown in Table 3.5 [37], recommended by Fowler.

Figure 3.37 shows the relation between the skirt/terrain interaction drag and craft speed. Figure 3.38 shows the drag for craft running on an ice surface in relation to the Froude number. These test results are provided for reference.

Table 3.4 Gap height $h_f K$ of various ACV

Item	Craft	Type	$h_f K$
1	SR.N5	ACV	0.08
2	SR.N6	ACV	0.07
3	SR.N4	ACV	0.084
4	SR.N4 Mk2	ACV	0.073
5	*Voyageur*	ACV	0.08
6	*Viking*	ACV	0.068
7	LACV-30	ACV	0.062
8	ACT 100	ACP	0.019
9	*Sea Pearl*	ACP	0.018
10	*Yukon Princess*	ACP	0.012
11	Hex-55	ACP	0.018
12	Hex-1B	ACP	0.015

Table 3.5 The suggested gap height $h_f K$ for various ACV terrain conditions [36]

Ground terrain	$h_f K$	K	Drag coefficient %
Smooth concrete, slow speed	0.0035	1.0	2
Firm snow	0.0055	1.5	2.5
Short grass	0.02	6	2
Moderate grass	0.02	6	2
Long reedy grass (1st pass)	0.022	6	40
Long reedy grass (10th pass)	0.022	6	5
Crushed rock	0.02	6	15–30
Mudflats	0.016	5	2–5
Concrete, high speed	0.013	4	2

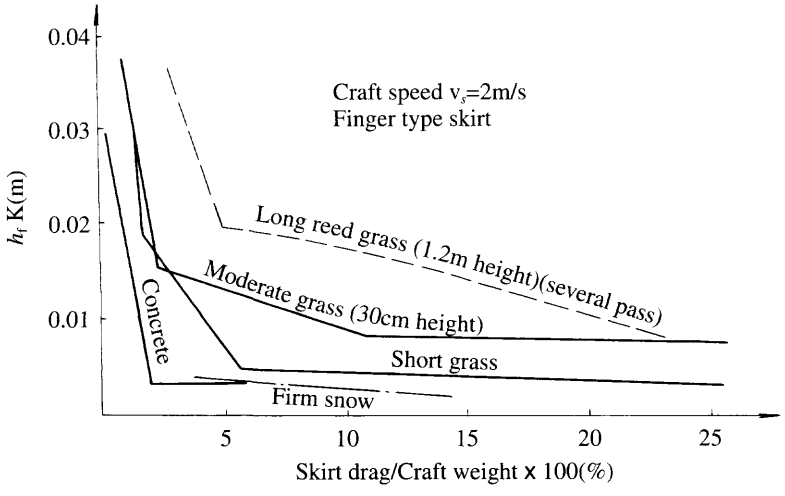

Fig. 3.36 Skirt ground interference drag as a function of surface condition and ACV equivalent air gap h_f K. [37]

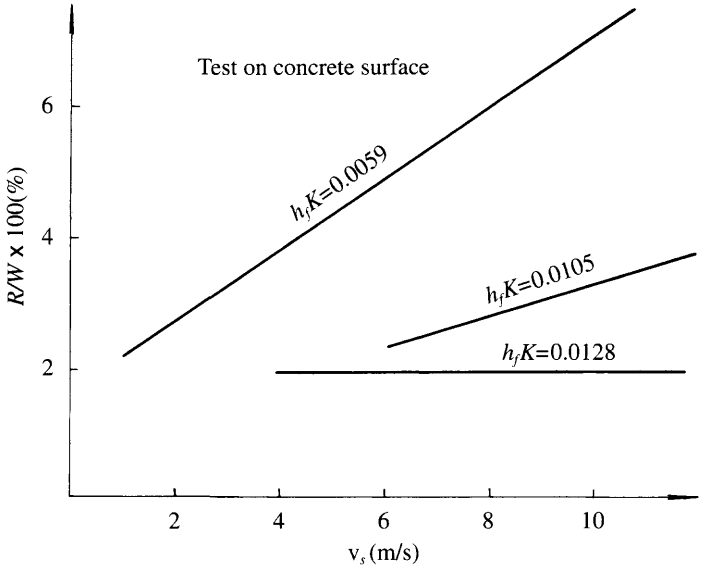

Fig. 3.37 Skirt ground interference drag as a function of h_fK and craft speed.

3.14 Problems concerning ACV/SES take-off

The acceleration capability of ACV/SES through hump speed is a very important design feature. Designers and users are therefore often concerned about the 'take-off' capabilities of ACV/SES running over water, because the hump speed is only one-

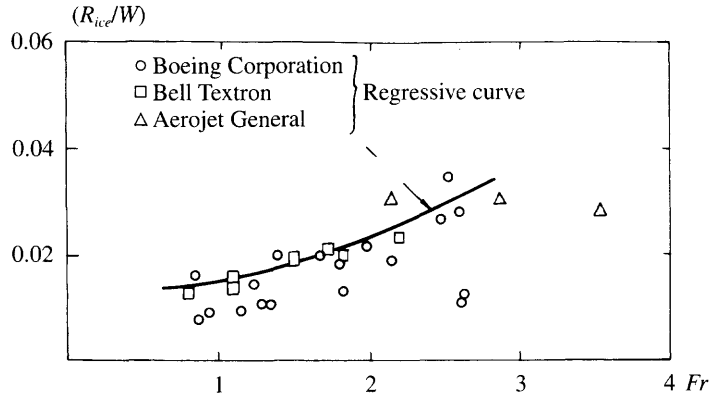

Fig. 3.38 Skirt drag of ACV running on ice as a function of *Fr*.

third to one-fifth of normal design speed. The physical phenomenon of take-off is therefore considered here and some comments on craft optimization presented.

When craft speed increases, at *Fr* of about 0.38 the craft begins to ride between two wave peaks located at the bow and stern respectively. The midship portion of the craft is then located at a wave hollow and a large outflow of cushion air blowing up water spray is clearly observed in this region, as shown in Figs 3.18(c) and 3.39. This in turn reduces the air gap below the bow and stern, which in the present case with wave peaks located at the bow and stern seals, would result in contact of water with the planing surface of the seals and present a new source of drag acting on the craft.

This condition was investigated by MARIC by towing tank model experiments. The surface profile was obtained with aid of a periscope and photography [28].

Seal drag consists of two parts. One part is the induced wave drag of the seals and the other is frictional drag acting on the planing surfaces. A large amount of induced wave drag can be built up when the seals are deeply immersed in water and the planing surfaces contact at large angles of attack.

The skirt-induced wave is also superimposed on the wave system induced by internal cushion pressure and constitutes secondary drag. In the case of poorly designed seals or skirts, the peak drag at $Fr = 0.38$ may be larger than that at $Fr = 0.56$ (main resistance hump speed). Meanwhile, transverse stability will most probably also decrease.

A craft will tend to pitch bow down when the craft has a rigid stern seal (such as fixed planing plate with a large angle of attack or a balanced rigid stern seal) and a relatively flexible bow seal. The craft will most probably be running at a large yawing angle as well, due to poor course stability. The operator of the ACV or SES will be obliged to use the rudder more frequently.

The forces arising from these situations are complicated and quite large in magnitude. Meanwhile the ship may be difficult to control, the propulsion engines are overloaded and a lot of water spray is blown off from the air cushion and flies around the craft, interfering with the driver's vision, making handling of the craft even more difficult. Operation would probably become very complicated if the sea were rough rather than the calm conditions considered in this chapter. Such phenomena are the features of a craft failing to accelerate successfully through secondary hump speed.

Meanwhile, if the thrust of the propellers is larger than the resistance of the craft,

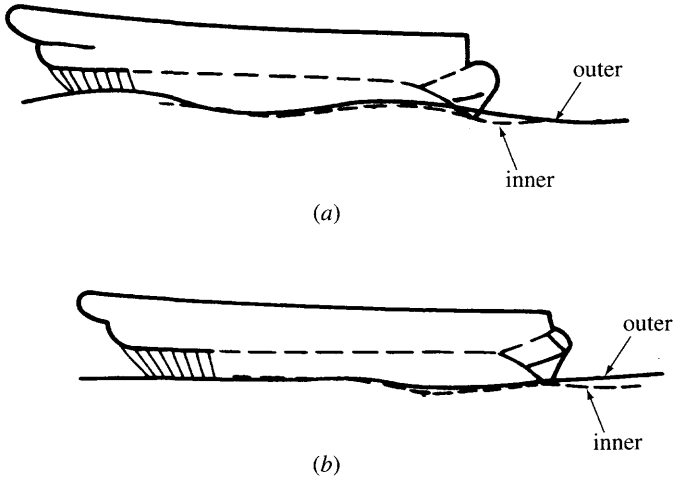

Fig. 3.39 Inner/outer water lines of an SES model at $Fr_l = 0.38$(a), $Fr_l = 0.51$(b).

then the craft speed will increase so as to move to the wave trough position. The main resistance hump occurs at $Fr = 0.56$. In this case the craft is located on the wave with the wave peak at the bow and the trough at the stern (wavelength is twice craft length) and the craft has maximum trim angle. The craft drag will generally drop down once the speed of the craft is over the secondary hump speed (i.e. $Fr = 0.38$) and the craft will accelerate to run over the main hump speed ($Fr = 0.56$) because the drag of the craft will be reduced due to the accelerating motion of the craft.

On an SES, the main propulsion engines normally cannot provide full thrust, due to the lower speed of advance at the secondary hump ($Fr = 0.38$). Smooth transition through hump speed then depends on the margin of thrust included by the designer at secondary hump speed, which will be the source of accelerating thrust. If this is too low, then transition will be very slow, as was the case with early SESs.

When the craft accelerates continuously, the wave trough will then move to the stern and the craft will be accelerated, so long as the skirt elements do not scoop; meanwhile the craft should travel with good course stability, transverse stability, little spray and beautiful running attitude to give the crew or passengers an excellent feeling (Fig. 3.18(b)). For this reason, the running attitude is rather different for the pre- and post-hump speed. Whether or not the craft can pass though the hump speed depends on such factors as the characteristics of the seals/skirts, the cushion pressure length ratio, the transverse stability of the craft and the correct handling of the craft.

In the early days of hovercraft research, people used to worry about whether the hovercraft could ever ride over the hump speed. It seemed merely to be a stroke of luck, because of poorly designed seal/skirt configurations or using rigid bow/stern seals which lead to a large additional wave-making drag.

From the point of view of craft drag (other factors will be discussed later), the factors influencing take-off can be summarized as follows:

- magnitude of resistance peak, especially at secondary hump speed ($Fr = 0.38$);

- the added wave-making drag due to seal/skirt at secondary hump speed and the flexibility of skirts to yield to waves without scooping;
- the ability of the craft to keep straight course stability and good transverse stability during take-off through hump speed.

It is not difficult to improve the ability to accelerate through hump speed if the factors mentioned above are taken into account. According to research experience at MARIC, we give some examples to illustrate these factors for the reader's reference.

1. The ACV model 711, the first Chinese amphibious test hovercraft, was found to suffer difficulties on passing through hump speed in 1965. The craft, weighing 4 t, was powered by propulsion engines rated 191 kW and obtained a thrust of 5000 N during take-off. This meant that the thrust/lift ratio of the craft was about 1/8. It was difficult to get the craft to take off, owing to large water-scooping drag of the peripheral jetted nozzle and shorter extended flexible nozzle, especially at the stern position. After a time, MARIC used the controlling valve of the air duct to adjust the running attitude of the craft in order to decrease the water contact drag of the skirt and the craft successfully passed though the hump speed.
2. After a time, craft model 711 had been chosen to mount a flexible skirt. The take-off ability of the craft was improved significantly due to the enlarged air cushion area, which reduced the cushion pressure and cushion pressure–length ratio, and also the flexible skirts' ability to yield to the wave hump. The wave-making drag at secondary hump speed was reduced by the same modifications.
3. The modified craft model 711 with flexible skirts was occasionally found to suffer difficulties in passing though the hump speed. The flexible jetted bag stern skirt with relatively larger area forward (Fig. 3.40) induced large skirt drag during take-off because the stern skirt took a form allowing scooping. It was observed that sometimes the original craft could still struggle to cross over the hump speed after a long running time. A breakthough occurred (literally!) after the diaphragms of the jetted skirt were accidentally broken and the stern skirt had changed from A to B as shown in Fig. 3.40.
4. The probability of successful take-off for the first Chinese experimental SES, the 711 in 1967, was about 60–70%, and it could be improved by retracting the stern seal during the course of passing though the hump speed (Fig. 3.41) and reached 100% take-off probability. This was a successful method for the following reasons:

   (a) Drag due to water scooping was reduced by decreasing the water scooping area of the stern seal as the stern seal is raised.
   (b) Angle of attack of the stern seal was reduced with consequential reduction in drag.
   (c) The running attitude was changed to a trimmed condition with bow up; as a result the bow seal drag was reduced and the course stability was also enhanced.

   It was noted that similar methods have been developed in other countries. For instance, there was a retractable stern seal mounted on the Soviet passenger craft *Gorkovchanin* and similar equipment was also mounted on the US test craft XR-3 to improve the dynamic stability during take-off, as shown in Fig. 3.42. Figure 3.42 shows that hump drag can be reduced considerably by retracting the stern seal.
5. When the Jin-Sah river passenger SES with the balanced rigid seal performed

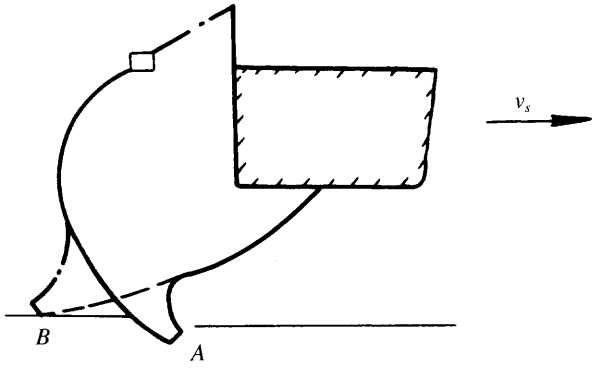

Fig. 3.40 Sketch of skirts with bag and jetted extensions.

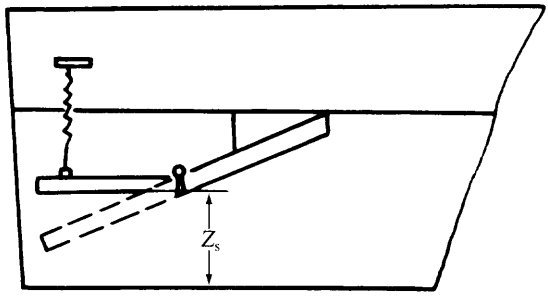

Fig. 3.41 Rigid stern seal with the function of controlling the air gap.

trials on water in 1970, it was found that a large amount of drag also acted on the stern, and as a result it was difficult for the craft to pass through hump speed. This may be traced to the following reasons:

(a) Suppose the stern seal was balanced hydrodynamically so that the lift moment (about point B in Fig. 3.43) due to the rear part of the seal would be greater than that due to the fore part of the seal. The stern seal plate would assume a negative angle of attack with the flexible nylon cloth taking the form of a concave bucket as shown by line 2 in Fig. 3.43. This would lead to a large amount of stern seal drag and it would be difficult for the craft to take off.

(b) On the other hand, if the hinge of the stern seal were moved to the rear with a longer nylon cloth, then it would take up the form of line 2 in Fig. 3.43. Here although the lift moment of the fore part would be greater than that of the rear part, forming a positive angle of attack, the planing surface is discontinuous, which would lead to a large amount of drag. In such a case the drag of the stern seal would be so large that it would be impossible to take off. The normal form of the stern seal is as shown in line 1 of Fig. 3.43 with proper length of nylon cloth to combine with the proper position of the hinge. In this case it is easy for the craft to take off.

6. The SES version 719 with bag and finger type skirt for bow seal and twin bag for

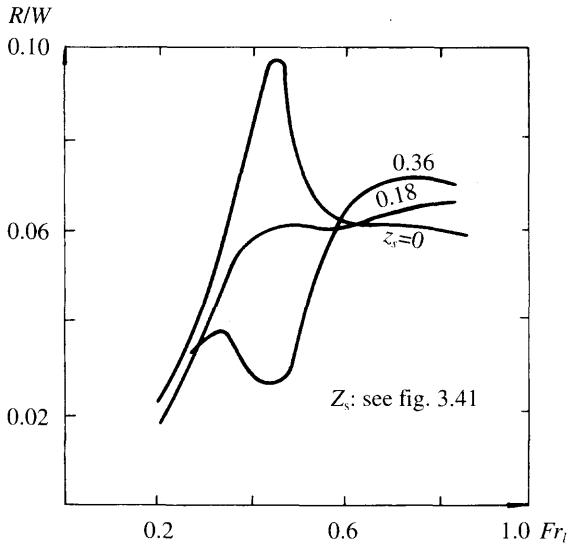

Fig. 3.42 Influence of the vertical distance between the base-line and lower tip of stern seal Z_s on drag ratio *R/W*.

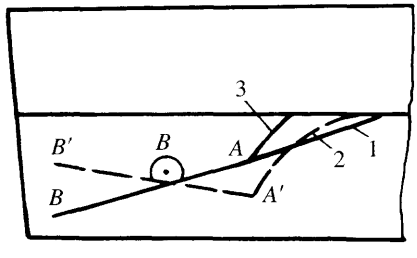

Fig. 3.43 Various locations of balanced type stern seal. 1, 2, 3: flexible connection seal; AB, A'B': two modes for solid seal.

stern seal took off very easily because of good yielding features of the skirts in waves. After a time, the craft was extended by 6 m and L_c/B_c stretched from 4 to 5.05 and reduced cushion pressure–length ratio from 17.6 to 14.6 kgf/m. For this reason, the peak wave-making drag was reduced drastically and moved the hump speed to larger *Fr*. Therefore, the engines could supply more power because of the large magnitude of the hump speed. Take-off performance improved greatly, with shortened time for take-off and less spray.

3.15 Effect of various factors on drag

The themes to be discussed here are the problems related to the drag of craft running over calm water. The performance on rough sea will be discussed in Chapter 8. Since the hovercraft, especially ACVs, travels close to the water surface at high speed, the drag will increase dramatically as soon as the skirts come into contact with the water surface occasionally making the drag unstable in magnitude. The effect of various factors on the craft performance are as follows.

The effect of position of LCG

The effect of LCG on craft drag, mainly skirt drag, is deterministic. A slight change of LCG will lead directly to varying craft drag due to its effect on bow and stern skirt friction, especially in the case of poorly designed bow/stern skirts.

With respect to SES, especially SES with thin sidewalls, the change of LCG will also lead to a draft change at bow/stern seals, increasing seal drag, in the case of no transverse cushion compartmentation on an SES. Figure 3.44 shows the effect of LCG on drag of an SES based on model testing data. It can be seen that when the centre of gravity of the model is moved just 3% of L_c, a drag increase of about 70% may result. Figure 3.45 [30] shows the relation between lift–drag ratio and trim angle of the US SES-100B. It is clear that the deviation of trim angle from an optimum of about 2° leads to an increase in drag about twice at a speed of 40 knots.

Figure 3.46 shows the influence of LCG on the speed of SES model 717C during trials. For this reason, it is necessary to determine the LCG carefully. Based on

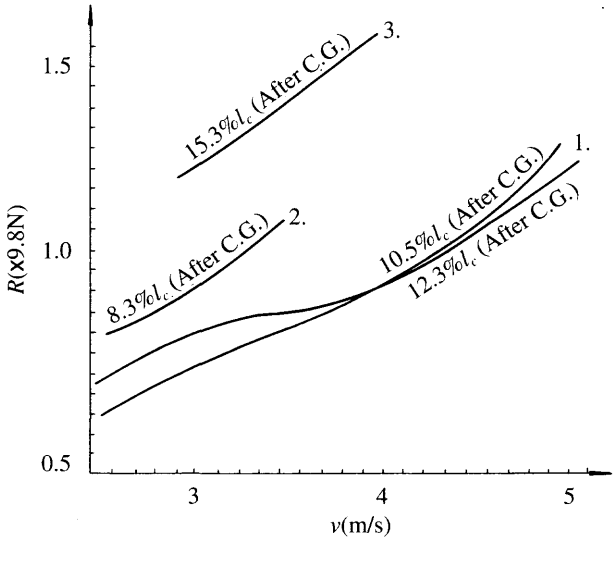

Fig. 3.44 Influence of longitudinal centre of gravity on total drag of SES model. 1: $P_c/l_c = 15.4$, 2: $P_c/l_c = 17.3$, 3: $P_c/l_c = 19.4$.

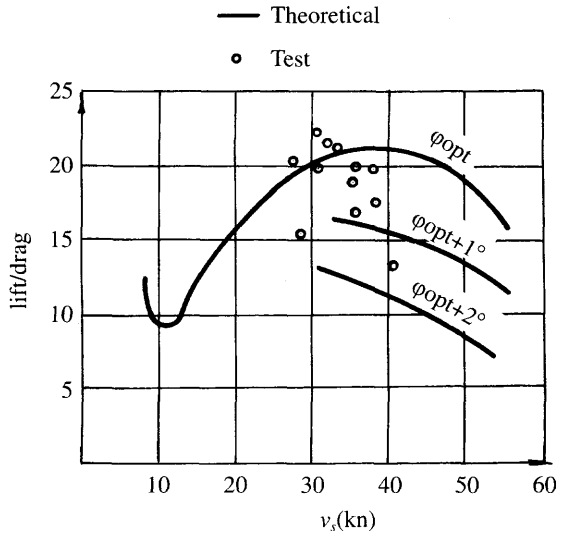

Fig. 3.45 Lift-weight ratio of SES-100B vs trim angles and craft speed.

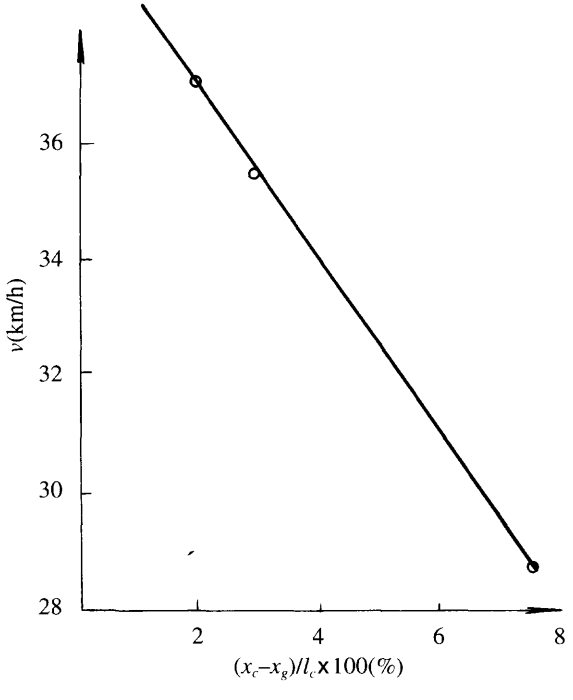

Fig. 3.46 Influence of longitudinal centre of gravity on speed of craft model 717C.

MARIC experience and ref. 39, it is suggested that the LCG of an SES (also an ACV) should normally be in the range

$$(X_g - X_c)/L_c \approx -(0 \sim 0.5)\% \text{ [aft of CG.]}$$

where X_g is the LCG, measured from the stern, X_c the longitudinal centre of buoyancy, measured from the stern and L_c the cushion length.

Effect of cushion pressure–length ratio

Wave-making drag increases in proportion to the square of cushion pressure. Cushion pressure also affects the craft outer draft, therefore the cushion pressure seriously affects the craft drag. The effect of cushion pressure on hump drag will be further increased in the case of poorly designed skirt/seals. Figure 3.47 shows the effect of cushion pressure of an SES model on drag, while Fig. 3.48 shows the effect of various cushion pressure / length ratios on the drag of craft tested in a towing tank at different times.

Effect of inner draft (t_i)

Hump drag will decrease in the case of increasing the inner draft of an SES during take-off, because air leakage from the cushion is decreased amidships, decreasing the cushion pushing/scooping drag of the bow/stern seals. The drag of SES will also increase at the post hump speed in the case of increasing the inner draft, because this will lead to an enlarged wetted surface of the sidewalls. Figure 3.49 shows the effect of inner draft change on drag of an SES model running on calm water.

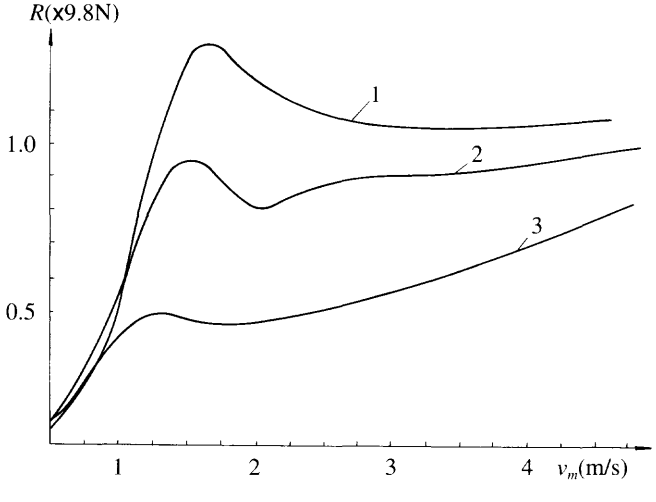

Fig. 3.47 Influence of cushion length/beam ratio and p_c/l_c on total drag of craft models. 1, 2, 3: see Fig. 3.44.

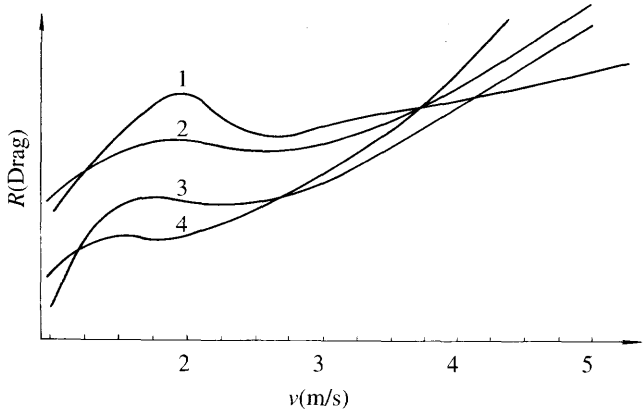

Fig. 3.48 Influence of cushion length/beam ratio on total drag of craft models in different test tanks. 1: tests in MARIC $p_c/l_c = 20$; 2: same model, thicker skirt, different tank; 3: as 2, $p_c/l_c = 15.7$; 4: as 3, but in MARIC tank.

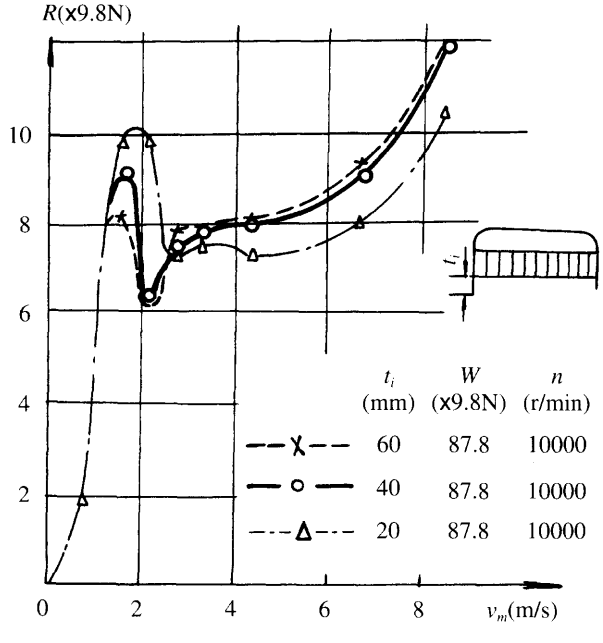

Fig. 3.49 Influence of inner draft of sidewalls t_i on total drag of SES model on still water.

Effect of air flow rate

It is probable that the air flow coefficient $\bar{Q}$ magnitude will not affect the take-off performance of hovercraft (except too small values of $\bar{Q}$) when the skirt has been carefully designed, because of the good wave-yielding performance for flexible skirts. However, craft drag at post-hump speeds will be closely related to $\bar{Q}$. Therefore, the

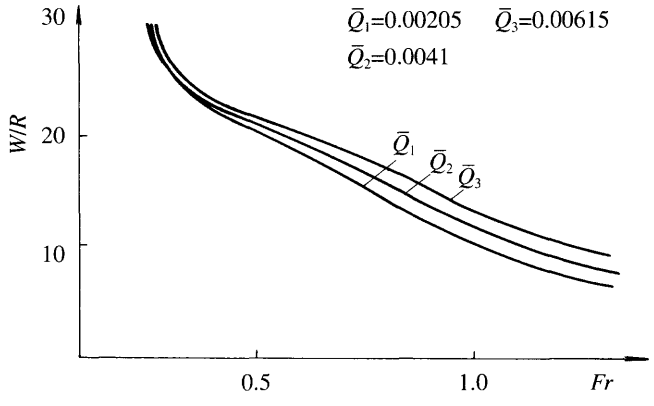

Fig. 3.50 Influence of cushion air flow rate on Lift/drag ratio of SES on calm water.

importance of air flow rate of a modern ACV/SES is rather more significant than early ACV/SES craft, which were generally designed with high cushion flow rates. In the latter case, a large gap height was pursued in order to reduce the contact drag of the bow/stern skirt, but in the former, it seems unnecessary to design a large gap height due to the beneficial properties of the flexible skirt.

The air flow still affects spray drag and water friction drag at post-hump speeds, because a large air flow rate will increase the air component of the two-phase flow blown from the air cushion, producing air lubrication effects on the stern skirt/seal. This can be clearly seen in Fig. 3.50.

In the case where the $\bar{Q}$ is so small as to cause significant immersion of skirts, the take-off performance will deteriorate. For example, a Chinese ACV with too small air flow could run over the hump speed on calm water, but could not take off even in small head winds and waves. Take-off performance was improved by increasing the lift power by 15%.

Effect of skirt configuration

The configurations of skirts are strongly sensitive to the craft drag. Figure 3.51 shows the effect of both rigid and flexible seals on drag of an SES. It can be clearly seen that the drag of craft with a flexible skirt is less than that with a rigid seal by a significant margin. Table 3.6 demonstrates that the drag coefficient for skirts of French ACVs improved significantly over eight years.

Table 3.6 The improvement of skirt drag coefficient of French ACVs over several years

Time interval	Craft model	Skirt drag coefficient
June 1968–June 1969	N102	0.36–0.42
Sept. 1967–March 1969	N300-02A	0.16–0.22
March 1969–June 1970	N102C	0.26–0.32
July 1970–June 1971	N102L	0.26–0.32
June 1973–Feb 1975	N300–02B	0.05–0.12
1973–1976	N500 (model)	0.05–0.07

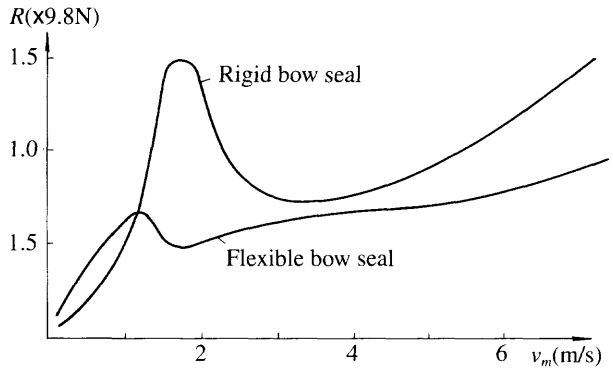

Fig. 3.51 Influence of seal types on total drag of SES: (a) with rigid bow seal; (b) with flexible bow seal.

Summary

Many factors affect craft drag. Due to the drag peak between displacement and planing mode of operation, this has been one of the challenges for designers, manufacturers and operators to try to minimize.

Efficient skirt systems can greatly improve drag and therefore attention has to be paid to optimizing this system if an ACV or SES is to be a successful design. Skirts are discussed in detail in Chapters 7 (theory) and 13 (design). As an example, by adopting the fixed planing stern seal for SES model 717, this obtained a stable cruising speed of 43 km/h, while adopting the balanced planing stern seal, the drag of the craft was very unstable and at full power the craft speed fluctuated between 57 and 50 km/h. From our point of view a craft with a stable speed of 55 km/h is better than one with an unstable speed sometimes at 60 km/h and sometimes at 50 km/h!

4

Stability

4.1 Introduction

Hovercraft are rather different from conventional ships in that they operate in various modes:

- Floating on their hull like a boat;
- on cushion as a displacement craft below 'hump' speed;
- planing on the water surface above hump speed;
- running on various solid terrain conditions including ground, ice, snow, swamp, etc.

Additionally, the transition between modes 2 and 3 creates significant trim and may exert dynamic loads on the skirt system which make the craft less stable. Safe operation in waves while in mode 3 also requires attention to the influence of skirts on craft stability, particularly while the craft is travelling sideways or down-wave (or both at once!) at speed. Some of these manœuvres are unique to the ACV. Hovercraft stability changes in each of the different operating modes.

In chapter 1, we illustrated the limited stability of early craft, which led to a number of hovercraft overturning. Three British ACV overturned in April, May and July 1965 in Norway, the USA and England respectively. An American prototype SES, the XR.1 test craft, also overturned during trials and the Chinese air cushion craft 711 also overturned in Din Sah lake close to Shanghai during trials. An even more serious event happened to the Hovertravel passenger hovercraft, SR.N6–012, operating on the Solent between Portsmouth and Ryde in the Isle of Wight in March 1972. This overturned as a result of the combined action of both wind and waves in a sudden storm, with the deaths of five passengers (see section 4.7).

These accidents showed that the problems of dynamic instability are very complex and may result not only from unsatisfactory transient stability, but also poor course stability and the combined action of both wind and waves.

In this chapter we will investigate many problems which might lead to the capsizing of hovercraft due to dynamic instability and review the following analyses which form part of a typical ACV design:

- Stability of an SES hovering statically or travelling on a cushion;
- stability of an ACV hovering statically or travelling on a cushion;

- course stability and plough-in of ACVs running at high speed on calm water;
- longitudinal stability of an SES running at high speed in following waves – the broaching problem.

Owing to possible serious damage to structures, skirt, equipment and injury to passengers, or even capsizing of craft due to plough-in, the dynamic stability of an ACV and SES has been an important research topic for a number of years. Evaluation of the transient stability of an ACV/SES during take-off through hump speed and of the transverse stability of the craft in wind and waves has not yet been solved analytically due to the complicated nature of the response. Some work has been done and theoretical papers published, but at present the primary tools available to the designer are full scale trials of craft and their interpolation to new designs.

The criteria, standards, and rules of stability of an ACV/SES will be studied in Chapter 10, as they form a natural part of the design process. Most of these standards have been developed from the research, both analysis and testing, which is described in this chapter.

What is acceptable stability?

A hovercraft or SES requires a minimum positive stability moment arm in roll and pitch while floating or hovering statically and while moving. While moving, there should also be stability in yaw and sufficient moment to stabilize unsteady dynamic forces. Some simple rules may be given for guidance:

Static stability
Pitch: $h/L_c > 0.05p_c$ (metres)
Roll: $h/B_c > 0.08p_c$

Dynamic stability
Pitch: $h/L_c > 0.05p_c$
Roll: $h/B_c > 0.08p_c$
Yaw: $h/L_c > 0.02p_c$

Note: p_c is measured in metres of water head. Dynamic stability is measured at craft designed speed.

4.2 Static transverse stability of SES on cushion

Calculation of static transverse stability of an SES off cushion is similar to that for a conventional catamaran, so we can solve the problem for an SES by extending the calculation method for catamarans. As shown in Fig. 4.1, the air cushion force ($p_c.S_c$) will make a heeling moment with craft weight W, and the buoyancy of both sidewalls (γv_1, γv_2) will create a restoring moment.

This can be seen more clearly in the case of large heeling angle as shown in Fig. 4.2. While the heeling angle is zero, the cushion pressure is p_{c0} and when the heeling angle is θ, the cushion pressure becomes $p_{c\theta}$, which produce together with the craft weight a heeling moment, and the buoyancy caused by immersed section of the sidewalls produce a restoring moment.

The air leaks from under the left sidewall to cause a drifting motion. For this reason, the stability of an SES cushion is related not only to the thickness and

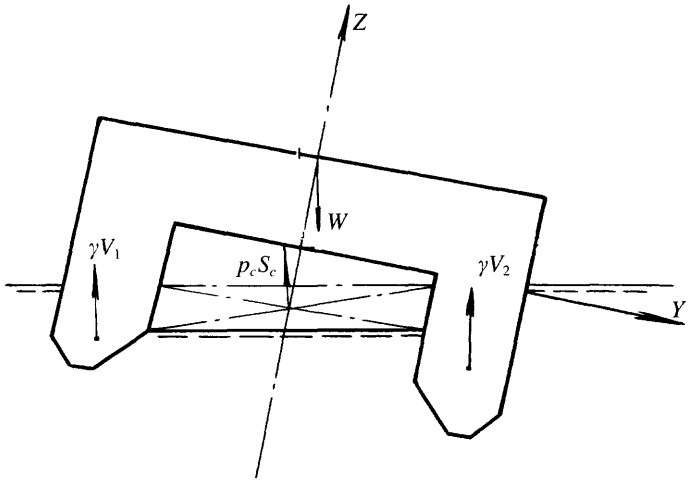

Fig. 4.1 Forces acting on SES due to heeling (sidewall emergence has not occurred).

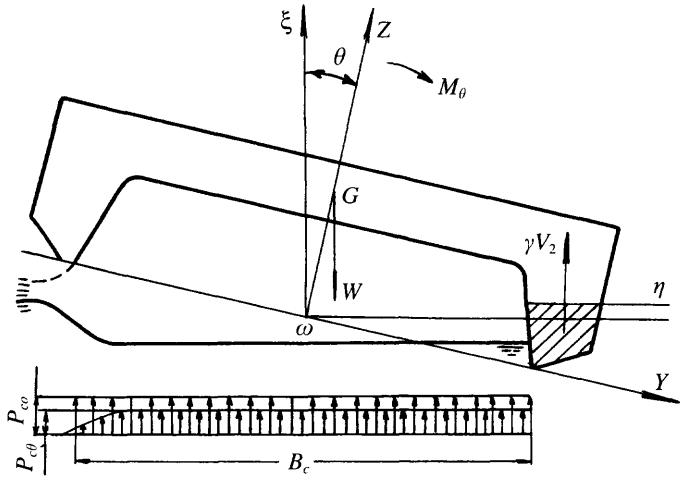

Fig. 4.2 Forces acting on SES due to heeling (one of the sidewalls has emerged).

displaced volume of the sidewalls, but also to the cushion pressure, air flow, gap height, vertical CG and bow/stern seal clearance.

Transverse stability on the US SES XR-1 decreased so severely during trials that it overturned while turning at high speed. This was caused by a combination of adoption of thin sidewalls to decrease water friction drag and the relative positions of the craft's longitudinal and vertical CGs.

In China, there has also been such experience. Poor transverse stability was experienced on the SES model 711–3 with thin sidewalls, the craft weight was increased from 1.825 to 2.2 t and the cushion pressure–length ratio from 19 to 24 kgf/m^3. The transverse stability decreased to an unacceptable degree so that

the ship rolled violently and periodically at low frequency, causing problems of control for the crews during sea trials.

It became clear that bow and stern skirt clearance needed to be altered to improve the transverse stability. However, over a long period of time, designers in China did not dare to remove the longitudinal stability keel (LSK), which was mounted in order to compartmentalize the cushion to improve the transverse stability, even though this gave a penalty of added drag and weight. Designers for a long time lacked the analytical and calculation methods to accurately predict transverse stability on cushion and so took the safe option, installing the LSK.

In order to estimate the transverse stability of an SES at the preliminary design phase, the graph in Fig. 4.3, showing the relation between transverse stability of craft on cushion and key craft geometrical parameters, may be used to ensure satisfactory stability. The figure shows that a satisfactory ratio of transverse metacentric height to cushion beam h/B_c can be obtained as soon as the relative thickness of sidewalls meets the relations shown in Fig. 4.3 for the cushion length/beam ratio (l_c/B_c) and pressure coefficient $p_c/(\sqrt[3]{D})$ (where D denotes the volumetric displacement of the craft and p_c cushion pressure) [40]. Figure 4.4 shows that the relation between the relative thickness of sidewall and cushion length/beam ratio. The shaded zone, represents the craft parameters with satisfactory transverse stability [19]. The figure was plotted by Kolezaev from statistical data obtained from practical ships. The figures are given for designer's reference as a starting point.

These two figures were made for reference at preliminary design. But since design norms have led to the change of some parameters, some craft have satisfactory transverse stability even though they do not comply with the requirements suggested by the two figures. Because these craft have other different parameters, such as different geometric

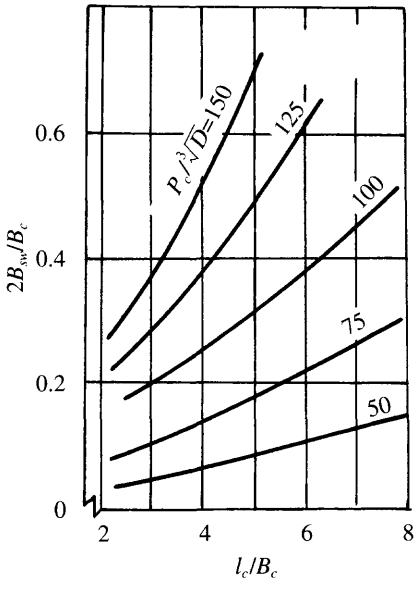

Fig. 4.3 Relation between relative sidewall thickness $2B_{sw}/B_c$ and L_c/B_c as well as equivalent cushion pressure length ratio $P_c/D^{0.33}$ (where D is the volumetric displacement of the craft).

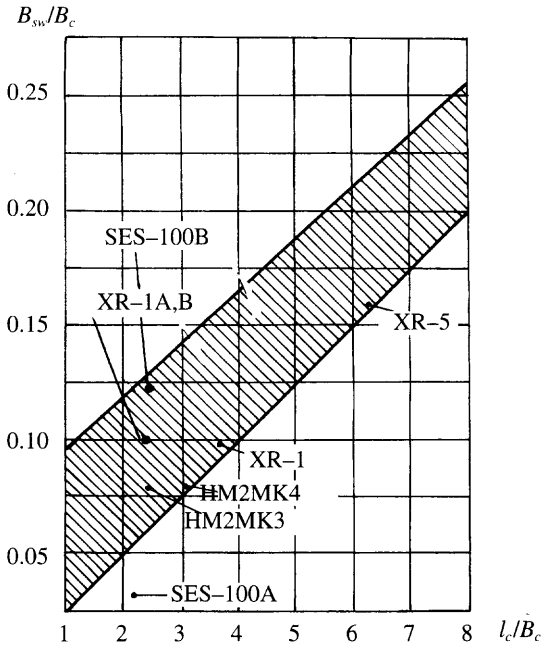

Fig. 4.4 Craft statistics of relative sidewall thickness and cushion length/beam ratio.

configuration of sidewalls, characteristic parameters of lift fans, and bow/stern seal clearance, one has to keep in mind that the various craft design parameters have to be similar to that adopted in the foregoing literature and the data cannot be used blindly.

For this reason, a number of complementary methods of calculating the transverse stability of an SES on cushion may be used to analyse the stability of the craft and understand the effect of various parameters on transverse stability.

Calculation method for predicting SES static transverse stability on cushion [41]

We introduce here a calculation method for predicting the static transverse stability of SES without LSK on cushion. The method for the SES with longitudinal keel can also be obtained by similar deduction, but it is not necessary to introduce the latter because no LSKs are mounted on modern SES.

The general assumptions for the calculation method are as follows:

1. The cushion pressure is distributed uniformly in the plenum chamber of the craft in the case of either upright condition or heeling.
2. One may presume that the drifting force caused by the difference of the leakage air momentum under both sidewalls of a heeling craft is equal to the lateral hydrodynamic force acting on them and the heeling moment caused by this induced couple may be neglected.
3. The fan outlet is perpendicular to the wet deck of the craft and the total fan flow blows directly into the plenum chamber.

4. The gaps between the lower edge of both bow and stern seals and the base-line are equal.

Calculation of static transverse stability for an SES without LSK

The typical midship transverse section of an SES and the forces acting on it are shown in Fig. 4.5. First of all, we can determine the equilibrium water line of the craft in the case of heeling, which is very similar to the method for predicting the running attitude of craft introduced in Chapter 5. The method is based on the equations of weight, flow continuity, fan characteristic and energy. Then the resulting moment at the given heeling angle can be obtained according to the equilibrium water-line.

1. Energy equation:

$$H_j = P_c + 0.5\rho_a\xi\,(Q/S_o)^2 \tag{4.1}$$

where H_j is the total pressure of the fan (N/m^2), P_c the cushion pressure (N/m^2), ξ the coefficient due to the pressure loss, Q the flow rate (m^3/s) and S_o the area of outlet of the air duct (m^2).

2. Flow continuity equation:

$$Q = Q_{sb} + Q_{sw} \tag{4.2}$$

$$Q_{sb} = Q_s + Q_b \tag{4.3}$$

$$Q = Q_s + Q_b + Q_{sw} \tag{4.4}$$

where Q_s is the air leakage from under the stern seal (m^3/s), Q_b the air leakage due to bow trim (m^3/s), and Q_{sw} is the air leakage under the sidewalls.

3. Flow rate equation:
Air leakage flow under the bow/stern seals can be written as

$$Q_s = Q_b = K\phi A_{j1}\sqrt{2p_c/\rho_a} \tag{4.5}$$

where K is the correction coefficient due to the effect of water surface, ϕ the flow coefficient and A_{j1} air leakage area under the bow and stern seals (m^2) (they are a function of inner draft t and craft trim angle).

The flow under the sidewalls can be written as

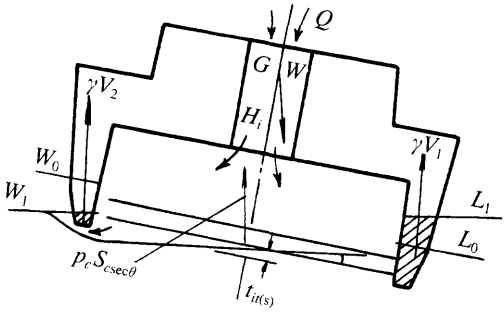

Fig. 4.5 Typical forces acting on skirt heeling craft.

$$Q_{sw} = K\phi A_{j2}\sqrt{2p_c/\rho_a} \tag{4.6}$$

where A_{j2} is the leakage area under sidewalls (m^2) (they are a function of inner draft t_i and heeling angle θ).

4. Fan characteristic equation:

$$H_j = A + BQ + CQ^2 \tag{4.7}$$

where A, B, C are fan characteristic coefficients which can be obtained according to the type, speed, etc.

5. Weight equilibrium equation:

$$W = p_c S_c \cos\theta + \gamma (V_1 + V_2) \tag{4.8}$$

where S_c is the cushion area (m^2), γ the specific weight (N/m^3), V_1 the volumetric displacement of the immersed sidewalls (m^3), V_2 the volumetric displacement of the emerged sidewalls (m^3) and W the craft weight (N).

Substitute equations (4.1)–(4.6) into equation (4.7), then we have

$$[1 + (2A_{j1} + A_{j2})^2 k^2\phi^2/S_0^2 - 2C/\rho_a(2A_{j1} + A_{j2})^2 k^2\phi^2]p_c - B(A_{j1} + A_{j2})k\phi(2p_c/\rho_a) - A = 0 \tag{4.9}$$

Equation (4.9) only includes p_c and air leakage area A_{j1}, A_{j2} which are only related to inner draft t_i and heeling angle θ. Therefore by combining the two equations (4.8) and (4.9), the p_c and t_{i0} at different θ can be solved by iteration with the aid of a computer.

This method is similar to that used on conventional ships, i.e. determining the equilibrium water line at the heeling condition, then the buoyancy of the sidewalls and cushion pressure can be easily obtained; the difference is that the weight of the craft must equal the sum of cushion lift and buoyancy provided by the sidewalls and the cushion pressure has to satisfy the fan characteristic equation, flow equation and energy equation.

Based on the equilibrium water line, the righting moment can be obtained as follows:

$$M_\theta = (l_{m1}V_1 - l_{m2}V_2)\gamma - (\overline{KG} - t_{im})W\sin\theta \tag{4.10}$$

where M_θ is the righting moment of the craft at the heeling angle (Nm), l_{m1} the transverse distance between the centre of buoyancy of γV_1 and CG of the craft (m), l_{m2} the transverse distance between the centre of buoyancy of γV_2 and CG of the craft (m) at any given heeling angle and $\overline{KG}$ the height of the centre of gravity above the keel.

6. A block diagram for the calculation can be seen in Fig. 4.6.

Model and full-scale tests for static transverse stability of an SES on cushion

Measurements of hovercraft static trim and heel can be made directly from a scale model, or a full-scale craft. The trim or heel can be related to known shifts of weight and therefore turning moment. Such data may be plotted against theoretical calculations such as that described in 4.2 to verify the analysis, or allow empirical adjustment to it. An example is described below, from MARIC experience.

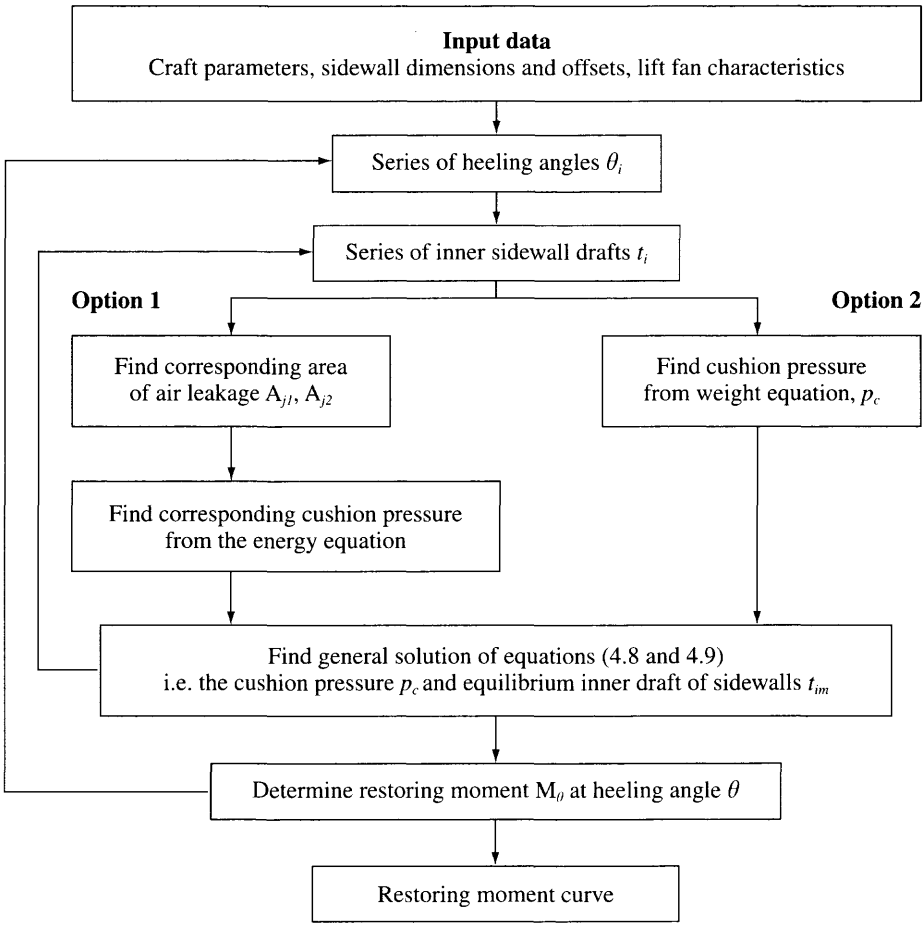

Fig. 4.6 Block diagram for calculating the static transverse stability of SES on cushion.

Model and test facility

The static transverse stability for two SES models on cushion were determined by direct measurements at MARIC and dynamic transverse stability tests were also carried out for one of these models.

The leading particulars for both models are shown in Table 4.1 and a typical section of the sidewall is shown in Fig. 4.7. During the tests, solid ballast was moved to cause model heeling, then the heeling angle measured by a clinometer.

Experimental results

During heeling of an SES on cushion, the restoring moment of the craft will be due mainly to the difference in buoyancy of the sidewalls unless the sidewalls are very thin. Experiments normally include the following:

1. Determining the effect of the fan speed on the static transverse stability.

Table 4.1 The leading particulars of two craft models

Name	Units	Nomenclature	Model No. 1	Model No. 2
Cushion length	m	l	1.61	2
Cushion beam	m	B_c	0.35	0.492
Height of sidewalls	m	h_s	0.056	0.167
Height of hard chine	m	h_k	0.042	0.067
Width of sidewalls	m	B_{sw}	0.05	0.067
Width of sidewall keel	m	B_1	0.015	0.025
Sidewall deadrise angle	deg	α	65	75
Flare angle of sidewall above hard chine	deg	β	89	90
All-up weight	N	W	156	406
Cushion pressure	N/m^2	p_c	290 approx.	370 approx.

2. Determining the effect of the longitudinal stability keel on the static transverse stability if this is fitted. This can be achieved by blocking the delivery duct to the stability keel on the model or full-scale craft to stop it inflating.

The effect of fan speed of the models on transverse stability is shown in Figs 4.8 and 4.9.

Similar experiments may be carried out for trim (longitudinal stability). In this case, the sidewall buoyancy has greater effect trimming bow up than bow down, due to the finer bow form.

Effect of various parameters on transverse stability

It is not practical to study the effect of all the various parameters by testing because of the amount of work involved. Therefore the research method at MARIC has been to gather sufficient data to verify the foregoing calculation method with aid of model experiments. We can discuss the effect of some of the remaining parameters on the transverse stability by using the calculation methods.

Effect of sidewall geometric configuration on the static transverse stability

Taking the SES model 717 as an example, we calculate the static transverse stability of the craft with a specific fan speed, duct configuration and form of the seals, and

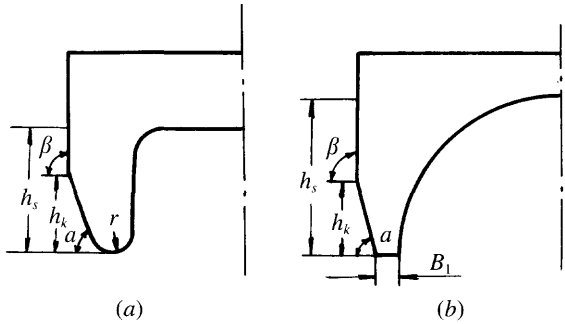

Fig. 4.7 Typical transverse section of two craft models with different inner sidewall geometries. (a) Model 1, (b) model 2.

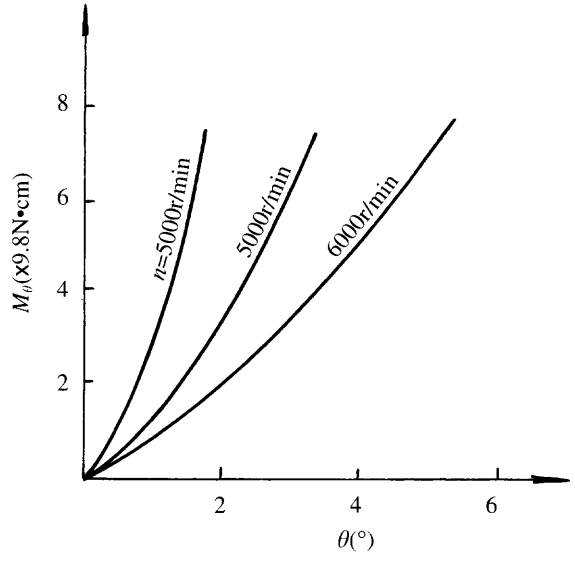

Fig. 4.8 Heeling restoring moment of model craft No. 1 with different fan speeds and heeling angles.

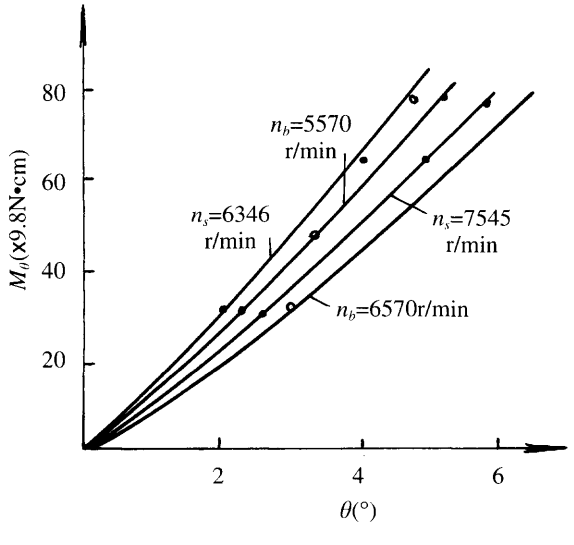

Fig. 4.9 Heeling restoring moment of model craft No. 2 with different fan speeds and heeling angles.

vary the geometric configurations of the sidewall amidships, in order to evaluate the effect of the geometric configuration of sidewalls on transverse stability.

The effect of the lines of a bow sidewall is smaller than that of midship lines. If we assume that the lines of the bow sidewall will be fixed and the line of hard chine is above the loaded water line, then the main parameters of the sidewall can be defined as follows:

1. width of keel plate of sidewall, B_1;
2. deadrise angle of midships section of sidewalls, a;
3. height of hard chine line amidships, h_k;
4. width of sidewall, B_{sw};
5. flare angle of sidewall above hard chine, β;
6. external draft of the sidewall, t_0.

From Fig. 4.10, we have

$$B_{sw} = B_1 + t_0 \cot a \tag{4.11}$$

$$B_{sw}/B_c = (B_1 + t_0 \cot a)/B_c \tag{4.12}$$

In general, B_1 can be kept as a constant, t_0 can be determined by the cushion pressure p_c, so we can take the parameters a, β and B_{sw} as variables, the variable range of which is shown in Table 4.2.

The calculation results are shown in Fig. 4.11. In order to investigate the effect of B_1 on stability, we obtain the second set of variables shown in Table 4.3. The basic parameters were kept the same as for craft type 717, such as principal dimensions, cushion pressure/length ratio, flow rate coefficient, flare angle of sidewall section above the hard chine, the gap between the lower edge of the bow/stern seals and the base-line, fan characteristic, etc., except the parameters a and β. Then the static transverse stability could be calculated. The results are as shown in Fig. 4.12.

From the figures, it is found that:

1. The static transverse stability of craft at large heeling angles is strongly affected, but not at small angles.

Table 4.2 The variable range of a, β, B_{sw}

a (°)	40	45	50	55	60
β (m)	55, 60, 65	50, 60, 65	60, 65, 70	60, 65, 70	65, 70
B_{sw}	0.62	0.54	0.472	0.414	0.362
B_{sw}/B_c	0.177	0.154	0.135	0.118	0.104

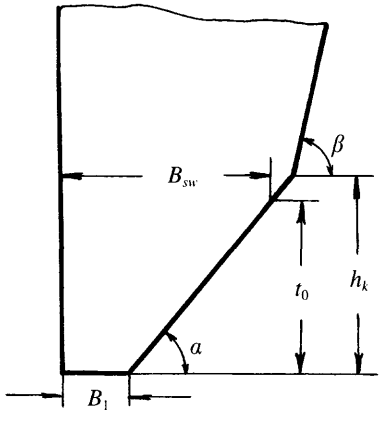

Fig. 4.10 Geometrical parameters for sidewalls.

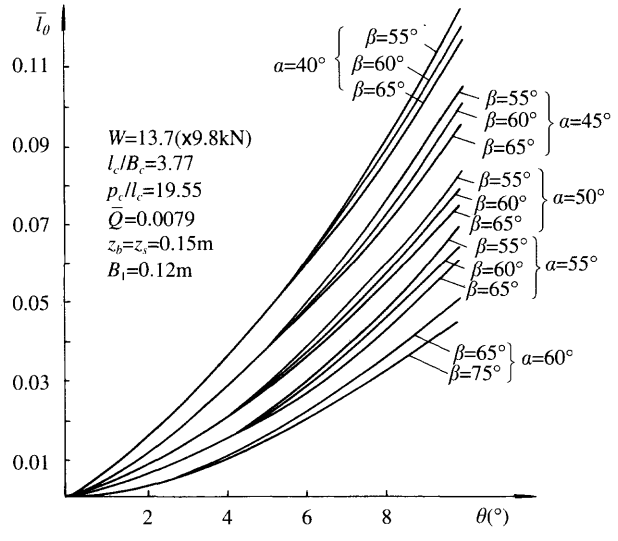

Fig. 4.11 Influence of parameters α, β on relative heeling righting arm.

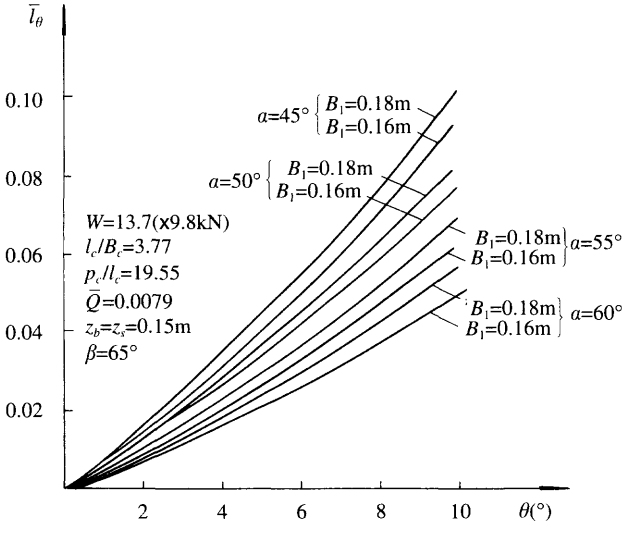

Fig. 4.12 Influence of parameters α, β on relative heeling righting arm.

2. Linearity in the relation of the righting arm with respect to the heeling angle only exists at small heeling angles to about 3–4°, therefore it is convenient to take the relative metacentric height $\bar{h} = h/B_c$, where h is the metacentric height and B_c is the cushion beam, as one of the stability criteria of the craft.
3. The width of the keel plate on the sidewall does not strongly affect the stability either at small heeling angles or at large angles.
4. α strongly affects the stability at both small or large heeling angles.

Table 4.3 The variable range of a, B

a (°)	45	45	50	50	55	55	60	60	60
B (m)	0.16	0.18	0.16	0.18	0.16	0.18	0.16	0.18	0.20
B_{sw}/B_c	0.166	0.171	0.146	0.152	0.13	0.135	0.115	0.121	0.126

5. According to the two sets of variables mentioned above, we can obtain the relation of the relative metacentric height $\bar{h}$ with respect to the relative thickness of the sidewall, B_{sw}/B_c (Fig. 4.13). It is found that this relation is stable whatever set of variables are used to obtain the values of B_{sw}/B_c. Therefore, it is convenient to take the relative thickness of the sidewall B_{sw}/B_c as a main parameter assumed to control transverse stability, at the preliminary design stage.

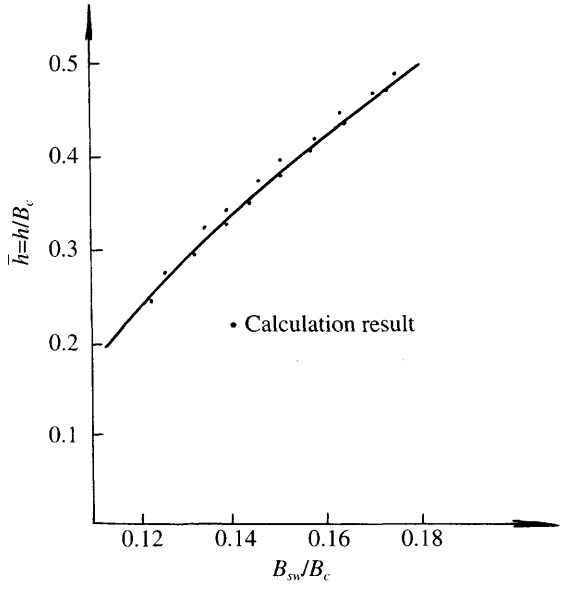

Fig. 4.13 Relative sidewall thickness B_{sw}/B_c and relative initial static transverse metacentric height.

Effect of the lift power (or the fan speed) on the transverse stability

In the calculation equations we can see that the fan flow rate strongly affects the stability. In general the static transverse stability deteriorates as the fan flow rate increases. It seems that the stability of a craft on cushion is worse than that off cushion, because the cushion pressure causes a negative transverse stability.

Figure 4.14 shows the effect of the relative flow coefficient $\bar{Q}$ on the relative metacentric height $\bar{h}$. For example, $\bar{h}$ decreases from 0.163 to 0.135 when $\bar{Q}$ increases from 0.006 15 to 0.008 92 (i.e. fan speed increases from 1300 to 1600 rpm).

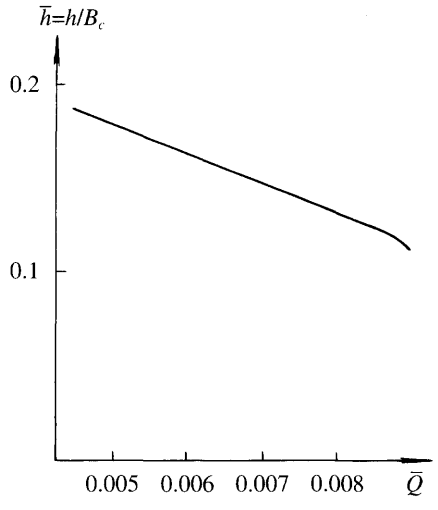

Fig. 4.14 Variation of relative initial static transverse metacentric height with air flow rate coefficient $\bar{Q}$.

Effect of the cushion pressure length ratio (p_c/l_c) on the transverse stability

The calculated results of stability with various cushion pressure/length ratios are shown in Fig. 4.15. It is found that the relative metacentric height $\bar{h}$ decreases from 0.133 to 0.123 when the cushion pressure/length ratio increases from 21.47 to 23.06 kgf/m^2.

Effect of the gap between the lower edge of bow/stern seals and the base-line

To make a simple calculation of the transverse stability, at MARIC we assumed the gaps between the base-line and the lower edge of bow/stern seals to be the same, to calculate the transverse stability of craft type 711–3 with various inner drafts of the sidewalls, $z_{b,s}$, by running the fan at different speeds.

The calculated results are shown in Fig. 4.16. Transverse stability increases with the inner draft of the sidewalls, though the benefit is not greater than that obtained by increasing the thickness of the sidewalls. This means that adjustment of the draft of the sidewall is a good way to control transverse stability of a craft in operation.

This phenomenon can be traced back to the trials of craft type 717-III in 1969. At the beginning, the craft operated quite well with satisfactory speed and transverse stability. After some modifications, the all-up weight of the craft increased from 1.8 to 2.2 t, and the cushion pressure/length ratio increased from 19 to 24 kgf/m^3 and it was discovered that the transverse stability of the craft had deteriorated. The craft used to roll slowly with a rolling angle up to 12° even in ripples. After increasing the inner draft of the sidewall at the stern from 0.24 to 0.28 m the unstable rolling disappeared.

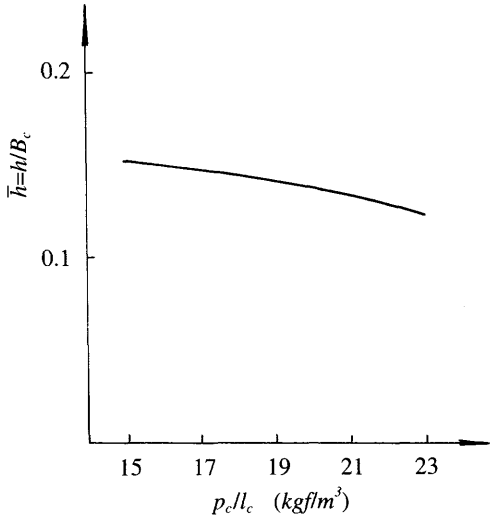

Fig. 4.15 Relative transverse righting arm l_θ variation with cushion length beam ratio P_c/L_c.

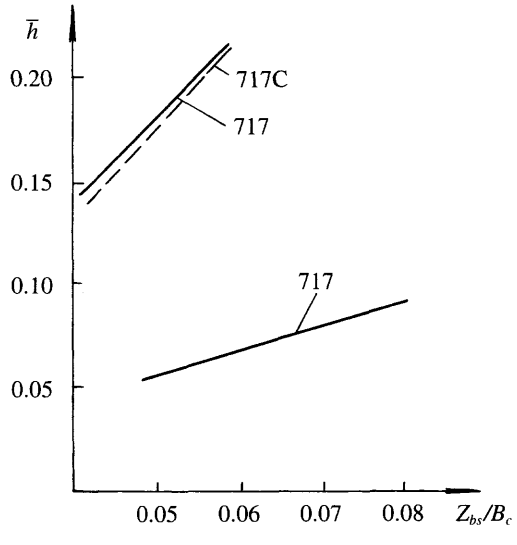

Fig. 4.16 Influence of bow/stern seal relative gap $Z_{b,s}/B_c$ on relative initial static transverse metacentric height.

Effect of the cushion length beam ratio on the transverse stability

The calculated transverse stability of craft type 717 with different cushion length/beam ratios is shown in Fig. 4.17.

From Table 4.4, it is found that the initial transverse stability at large heeling angles will not change significantly, for several variations of SES type 717, as long as the cushion pressure is kept constant, even though with different cushion length/beam ratio, weight and cushion pressure/length ratio for different types of craft. It is not

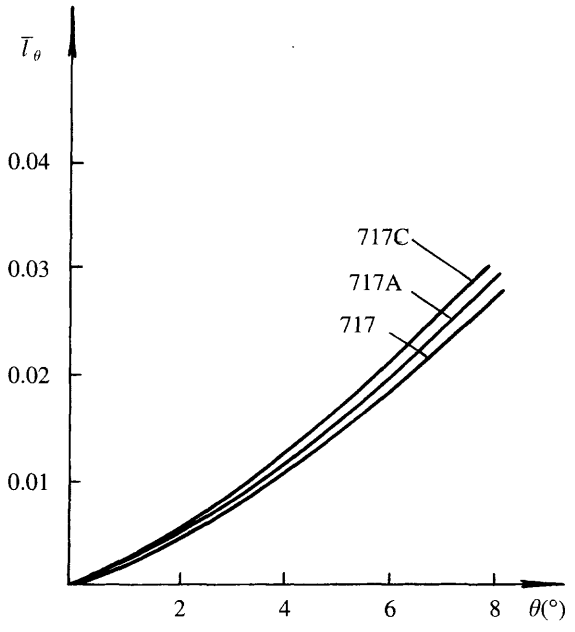

Fig. 4.17 Static transverse stability for three craft of series 717.

Table 4.4 The leading particulars for three SES type 717

Item	Symbols	Dimensions	717	717A	717C
Craft weight	W	t	13.7	15.95	18.20
Cushion length	l_c	m	13.2	15.2	17.3
Cushion beam	B_c	m	3.5	3.5	3.5
Cushion *l*/*b* ratio	l_c/B_c		3.77	4.34	4.94
Cushion pressure length ratio	p_c/l_c	kgf/m^3	19.93	17.31	15.38
Cushion pressure	p_c	N/m^2	2630	2630	2660
Flow coefficient	Q		0.00757	0.00658	0.00570
VCG	KG	m	1.27	1.27	1.27
Bow and stern seals clearance	$z_{b,s}$	m	0.15	0.15	0.15
Sidewall midship deadrise angle	α	deg	60	60	60
Sidewall flare above hard chine	β	deg	89	89	89
Sidewall keel plate width	B_1	m	0.12	0.12	0.12

correct, therefore, to say that the transverse stability will definitely deteriorate with increasing cushion length/beam ratio; one has to analyse the particular craft design to identify its sensitivity to this possible problem.

Summary

1. The calculated results of the static transverse stability of craft by means of this method agree well with the experimental results, therefore it can be recommended to use this method to check and analyse the static transverse stability of the designed or constructed SES.

2. The relative thickness of the sidewall might be considered as a main parameter that will strongly affect the transverse stability of craft.
3. The transverse stability of constructed craft can be improved by decreasing the flow rate coefficient ($\bar{Q}$), cushion pressure/length ratio (p_c/l_c) and by increasing the sidewall draft under the bow/stern seals ($z_{b,s}$).
4. Increasing cushion length/beam ratio might occasionally result in a deterioration of the transverse stability, but it might not be the only result since so many factors are involved. It is best to carry out a parametric sensitivity analysis of stability to make a first assessment and if possible follow up with model tests, if the geometry is significantly changed from the base case.

Approximate calculation of SES static transverse stability on cushion

At the preliminary design stage, computer methods (apart from spreadsheet calculations) cannot be adopted because the offsets and some main parameters of the craft are lacking. Therefore the following relationship deduced from experimental results from Hovermarine SES craft [42] can help:

$$h = \gamma A_s (B_c + A_s/L_s)^2 / 2W - \gamma S_c p_c / W + [0.5 L_s \tan \tau + p_c] - \overline{KG} \qquad (4.13)$$

where h is the initial transverse metacentric height of craft (alternately GM) (m), γ the mass density of water (N/m^3), A_s the water-plane area of one sidewall at hovering water-line excluding internal bulges (m^3), B_c the cushion beam of craft at water-line (m), L_s the sidewall length (m), τ the static trim angle (°), p_c the cushion pressure head (m H_2O), S_c the cushion area (m^2), KG the height of centre of gravity (m) and W the mass of craft (N).

This expression assumes a small angle of heel with no loss of cushion pressure. In practice it is suitable for estimation up to an angle of $\tan^{-1}(p_c/B)$, i.e. typically 3–5° heel. It is also significantly affected by craft trim and cushion air flow. Blyth [42] has carried out a substantial model test programme to investigate the dynamic stability of SES of differing geometries in a seaway; this has been the basis for stability criteria adopted by the IMO. The recommendations are presented following the description of similar investigations carried out by MARIC below.

4.3 SES transverse dynamic stability

SES often run at high speed, so the forces acting on an SES during heeling are rather different from the static situation. It is therefore very important to investigate the transverse stability of an SES on cushion in order to develop appropriate calculation methods by which the effect of speed and various geometrical parameters can be determined.

We will introduce a method for calculating the dynamic transverse stability of craft in this section. First of all we have to determine the craft trim at speed, then define the righting moment of the craft in motion during the heeling situation.

Calculation of craft trim

According to the method in Chapter 5, we can determine the craft trim at various speeds based on four relationships from equation (5.12) and the other two equations (5.13, 5.14) due to the deformation of the water surface caused by wave-making of the craft. This method is rather complicated, especially for the calculation of deformation of the water surface. We recommend the use of a simplified method for estimating craft trim and for calculating the forces acting on the craft as follows:

1. In the case of a craft with bag and finger type skirt, the lift of skirt can be calculated as

$$\left.\begin{array}{ll} \text{when } (z_b - t_{bi}) \geqslant 0 & L_{bs} = 0 \\ \text{when } (z_b - t_{bi}) < 0 & L_{bs} = P_c S_c |(z_b - t_{bi})| \cos(\alpha_b) \end{array}\right\} \quad (4.14)$$

   where L_{bs} is the lift due to the bow skirt with bag and finger type, z_b the gap between lower tip of bow finger and sidewall base-line (m), t_{bi} the inner draft of sidewalls at bow (m), and α_b the declination angle of bow fingers with horizontal plane, as shown in Fig. 4.18 (°).
2. In the case of using a planing plate as the stern seal, the planing plate can be calculated by the theory of Chekhof [43], i.e. as a two-dimensional planing plate running in gravitational flow, and estimate the lift as follows:

$$\left.\begin{array}{ll} \text{when } (z_s - t_{si}) \geqslant 0 & L_{ss} = 0 \\ \text{when } (z_s - t_{si}) < 0 & L_{ss} = 0.5\pi\rho_w v^2 l B_c \alpha_s [l - Fr_l^{-2}(\pi^2 + 4)/2\pi] \end{array}\right\} \quad (4.15)$$

   where z_s is the gap between the lower tip of the stern seal and base-line (m), t_{si} the inner draft of sidewall at stern (m), v the craft speed (m/s), L_{ss} the lift acting on planing plate (N), l the length of wetted plate (m), α_s the angle of attack (°) (here we assume the trim angle is zero, therefore the angle of attack is equal to the angle between the plate and flow direction).

   Since the wetted length is small and Fr is large, the calculation can also be simplified to a two-dimensional plate in non-gravitational flow as follows:

$$L_{ss} = 0.5\pi\rho_w v^2 l B_c \alpha_s \quad (4.16)$$

3. In the case of stern seals of the double bag type (Fig. 4.19(b)), the lift acting on the skirt can be calculated as

$$\left.\begin{array}{ll} \text{when } (z_s - t_{si}) \geqslant 0 & L_{ss} = 0 \\ \text{when } (z_s - t_{si}) < 0 & L_{ss} = p_c B_c |t_{si} - z_s| \operatorname{cosec} \alpha_s \end{array}\right\} \quad (4.17)$$

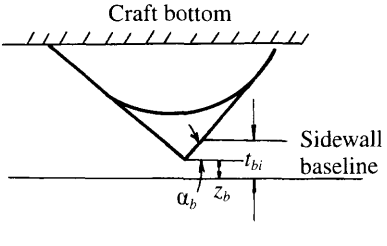

Fig. 4.18 Configuration of bag and finger type bow skirt.

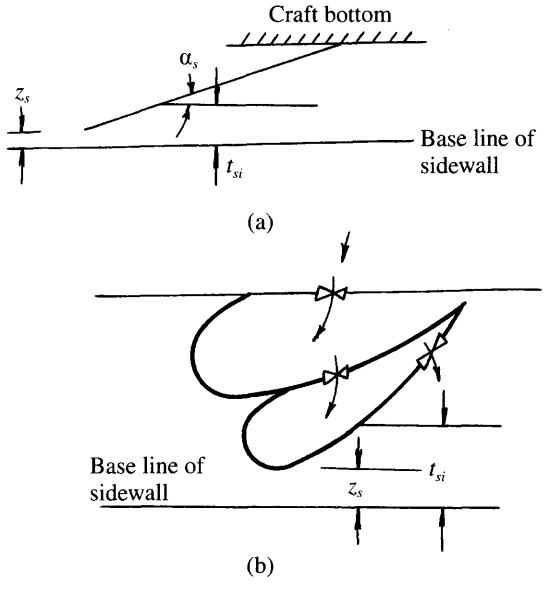

Fig. 4.19 Geometry of stern seals: (a) planing stern seal; (b) twin bag skirt.

where L_{ss} is the lift acting on the stern skirt (N) and α_s the declination angle between the lower base-line of stern seal and sidewalls (°). The calculation is also similar for triple-bag SES stern skirts.

4. Two simplified added equations can be adopted from equation (3.12),

$$t_{bi} \approx t_{bo}$$
$$R_w \cong W(t_{os} - t_{is})/l_c \tag{3.12}$$

The wave-making drag R_w can be calculated by the methods described in Chapter 3, and then the running attitude of the craft may be obtained using the foregoing equations.

SES transverse stability on cushion in motion

It is not difficult to define the transverse stability moment and lever arm after determining the SES trim. Two conditions of the craft can be analysed as follows.

Calculation of transverse stability for the SES with flexible bow/stern seals

In the case of an SES with flexible bow/stern seal, it can be assumed that the restoring moment acting on the craft running on cushion and heeling is equal to the sum of the heeling moment caused by the air cushion and the restoring moment due to sidewalls and both bow/stern seals. Considering that the length/beam ratio of the sidewalls is very large, normally 34–50 in fact, the dynamic lift due to the sidewalls is very small and can be neglected, thus the restoring moment can be calculated as follows. When $(z_b - t_{bi}) > 0$

$$\Delta M = \int_{(z_b - t_{bi})\cot\theta}^{Bc/2} p_c[y\tan\theta - (z_b - t_{bi})]c_{sc}a_b y\mathrm{d}y$$
$$= 1/3\, p_c c_{sc} a_b \tan\theta\,[B_c^3/8 - (z_b - t_{bi})^3\cot^3\theta]$$
$$- 0.5\, p_c c_{sc} a_b (z_b - t_{bi})[B_c^2/4 - (z_b - t_{bi})^2\cot^2\theta] \quad (4.18)$$

where ΔM is the transverse restoring moment due to bow/stern skirts (N m) and y the abscissa of the craft (m) (Fig. 4.20).

The block diagram for predicting the craft trim in motion is as shown in Fig. 4.21.

Calculation of the transverse stability of SES with rigid stern seal

The foregoing calculation procedure cannot be used in the case of the rigid stern seal, because the lift acting on the planing plate is so much larger than that on the flexible skirts at same heeling angles, and leads to a trim moment to change the running attitude, cushion pressure and other parameters, etc. The changing running attitude may be obtained by means of an iteration method, from which the stern plate lift and restoring moment on the craft can then be determined.

Since the end of the planing plate is close to the craft sidewall when heeling it can be considered as a two-dimensional planing plate and the other end of the plate can be considered as a three-dimensional planing plate. The lift of whole plate can also be considered as the arithmetic mean of both two- and three-dimensional planing plates. The transverse restoring moment due to the stern plate can be written as

$$\Delta M = \int_{(z_s - t_{si})\cot\theta}^{B_c/2} (0.5\,\rho_w v^2 \pi a_s)[y\tan\theta - (z_s - t_{si})]c_{sc}a_s y\mathrm{d}y$$
$$= 1/3\,(0.5\,\rho_w v^2\pi a_s)c_{sc}a_s\tan\theta\,[B_c^3/8 - (z_b - t_{bi})^3\cot^3\theta]$$
$$- 0.5\,(0.5\,\rho_w v^2\pi a_s)c_{sc}a_b(z_s - t_{si})[B_c^2/4 - (z_s - t_{si})^2\cot^2\theta] \quad (4.19)$$

where ΔM is the restoring moment due to the stern plate of the craft at heeling (N m) and θ the heeling angle (°).

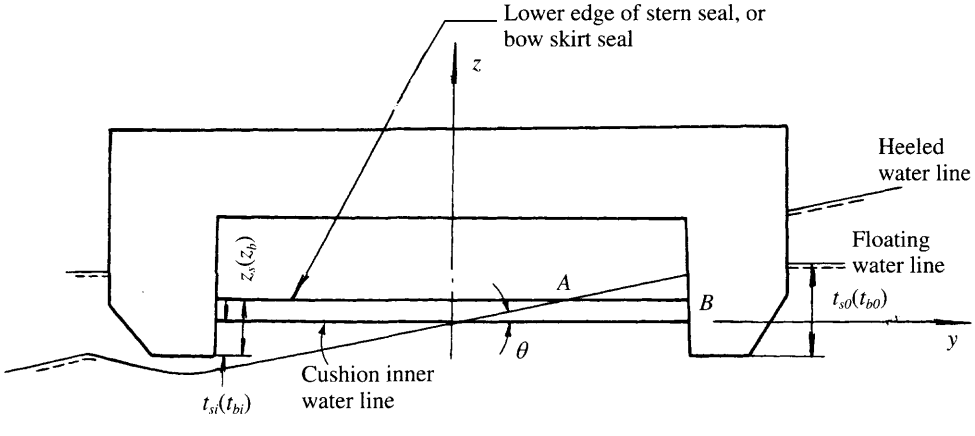

Fig. 4.20 Calculation for righting moment of bow/stern seal during heeling of craft.

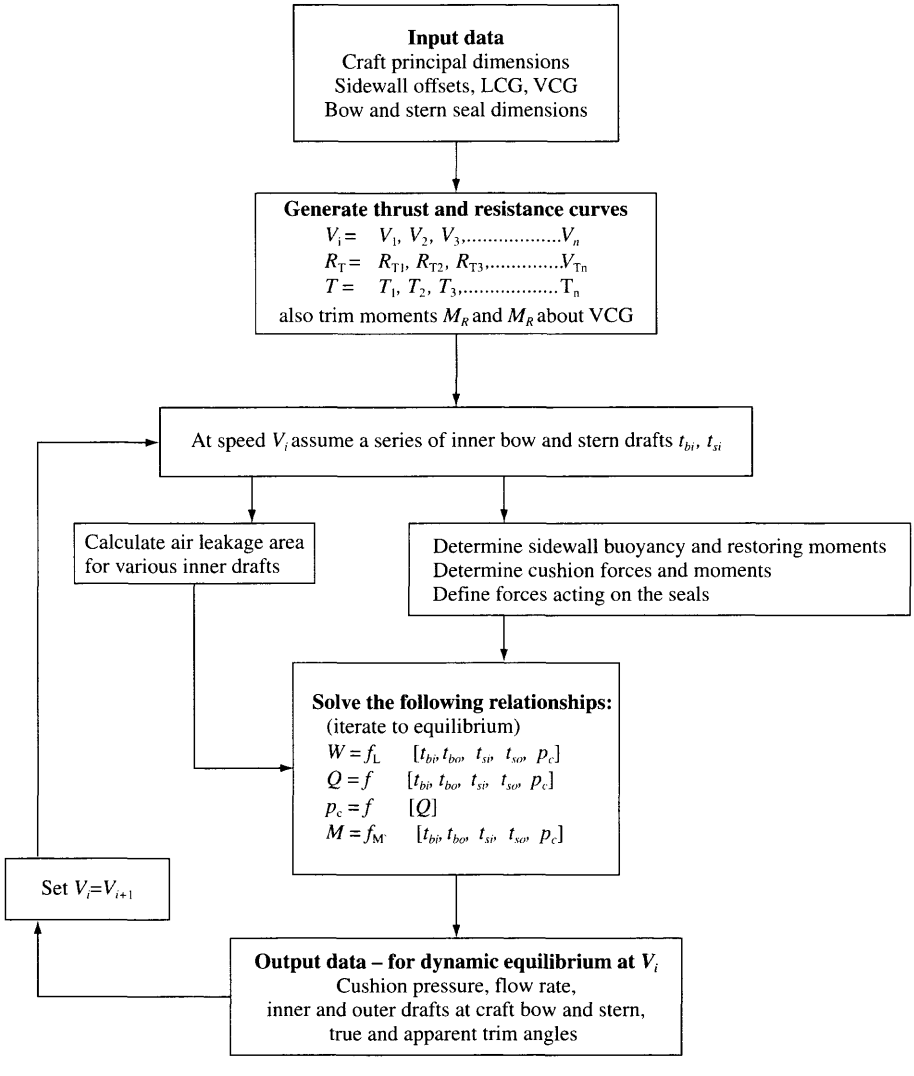

Fig. 4.21 Block diagram for calculating craft dynamic trim.

The block diagram for predicting the transverse stability of the craft at speed is shown in Fig. 4.22.

Calculation results for two actual craft

The calculation results for the SES types 717A and 717C using the foregoing method and computer analysis can be described as follows.

Calculation of running attitude of the craft (simplified method)

1. For SES type 717A (Table 4.5):

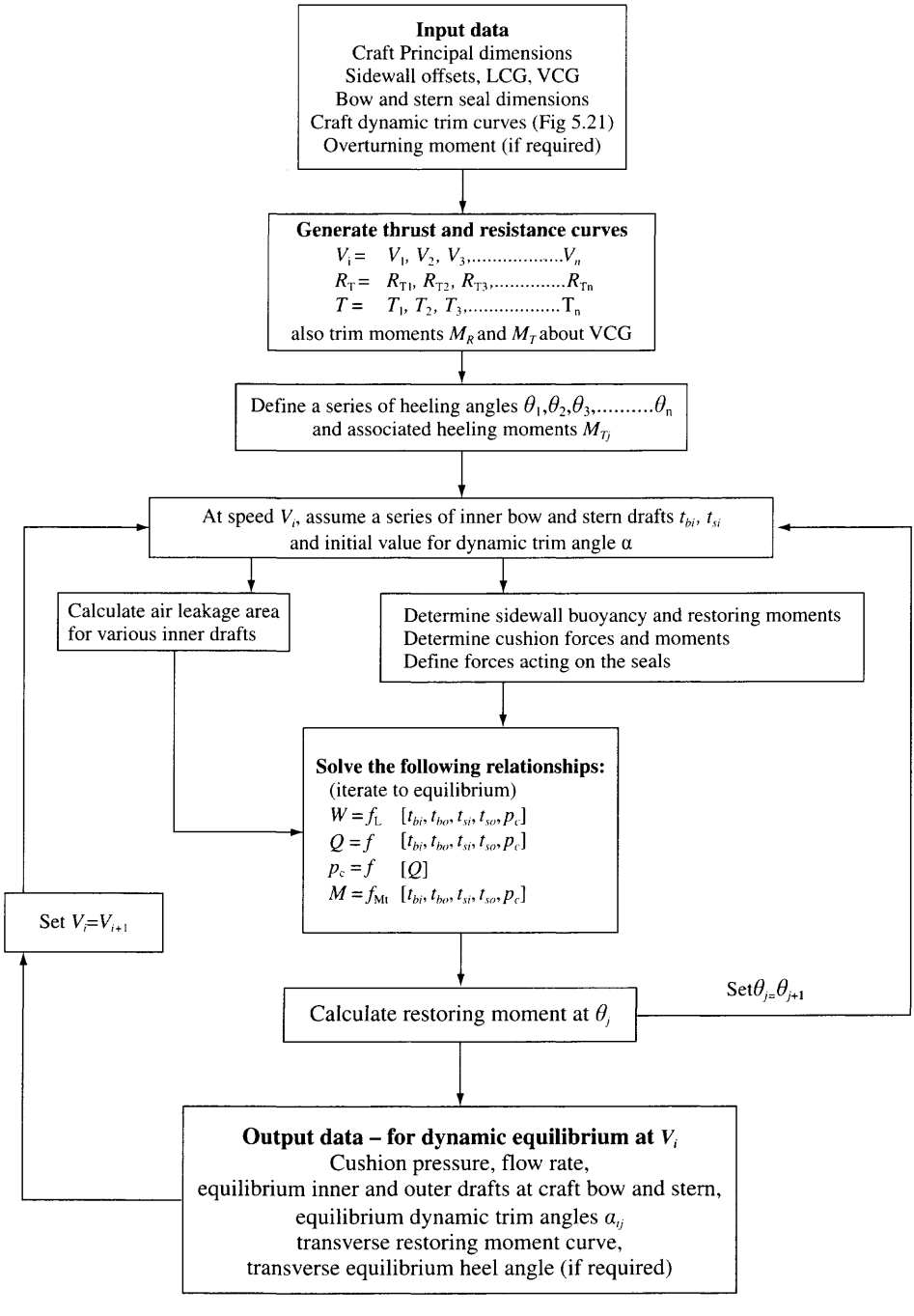

Fig. 4.22 Block diagram for calculating dynamic transverse stability.

Craft weight: $W = 156$ kN
Fan characteristics: $A = 631$
$B = -1.80$
$C = -0.187$
$S_i = 0.24\ m^2$

Principal dimensions and parameters of the craft:

$B_c = 3.5$ m
$B_{sw} = 0.13$ m
$B_{swb} = 0.06$ m (width of the sidewall at bow)
$H_{sw} = 0.43$ m (height of the sidewall)
$a_b = 70°$ (deadrise of sidewall at bow)
$a = 60°$ (deadrise of the sidewall amidships)
$S_a = 14\ m^2$ (frontal area of the superstructure)
$a_s = 9.23°$ (inclination between the stern plate and base-line)
$x_g = -0.20$ m (aft amidships)
$\overline{KG} = 1.22$ m
$H_s = 0.50$ m (height of thrust for water jet propulsion over base-line)

2. SES type 717C (Table 4.6):

Craft weight: $W = 156$ kN
Fan characteristics: $A = 631$
$B = -1.80$
$C = -0.187$
$S_i = 0.24\ m^2$

Table 4.5 The calculation of running attitude of the SES type 717A at various speeds

Item	Symbol	Units			
Craft speed	V	km/h	30.67	42.90	51.08
Cushion pressure	p_c	N/m^2	2690	2716	2763
Flow rate	Q	m^3/s	23.65	23.55	23.38
Outer draft at stern	T_{so}	m	0.402	0.386	0.356
Inner draft at stern	T_{si}	m	0.0389	0.0399	0.0517
Outer draft at bow	T_{bo}	m	0.1535	0.1385	0.111
Inner draft at bow	T_{bi}	m	0.1535	0.1385	0.111

Table 4.6 The calculation results of running attitude of SES 717C at various speeds

Item	Symbol	Units				
Craft speed	V	km/h	26.5	33.1	44.2	55.2
Cushion pressure	p_c	N/m^2	2813	2789	2776	2787
Flow rate	Q	m^3/s	5.115	5.115	5.165	5.15
Outer draft at stern	T_{so}	m	0.5254	0.5823	0.5952	0.5599
Inner draft at stern	T_{si}	m	0.2066	0.2008	0.1986	0.2006
Outer draft at bow	T_{bo}	m	0.086	0.0858	0.0868	0.089
Inner draft at bow	T_{bi}	m	0.086	0.0866	0.0868	0.089

Principal dimensions and parameters of the craft:

B_c = 3.5 m
B_{sw} = 0.13 m
B_{swb} = 0.06 m (width of the sidewall at bow)
H_{sw} = 0.42 m (height of the sidewall)
a_b = 70° (deadrise of sidewall at bow)
a = 60° (deadrise of the sidewall amidships)
S_a = 14 m^2 (frontal area of the superstructure)
a_s = 9.23° (inclination between the stern plate and base-line)
x_g = −0.47 m (aft amidships)
$\overline{KG}$ = 1.22 m
H_s = 0.50 m (height of thrust for water jet propulsion over base-line)

Dynamic transverse righting moment of the SES

Figure 4.23 shows the transverse righting moment M_θ of SES type 717C hovering statically and in motion. Figure 4.24 shows the components of dynamic righting moments M_θ of the SES type 717C running on cushion. It is found that the relative metacentric height h/B_c of the craft in motion is larger than that hovering statically by 20–30%. This added righting moment is mostly provided by the stern planing plate seal and it indicates that the craft type 717C is more stable when moving than when static. This has been validated in practice.

Further investigation

Transverse stability of craft during take-off

As mentioned above, the transverse stability of an SES at post-hump speed can be improved significantly with the hydrodynamic force on the stern seals of the planing plate type. It will deteriorate in the case of craft at low speed, particularly at hump

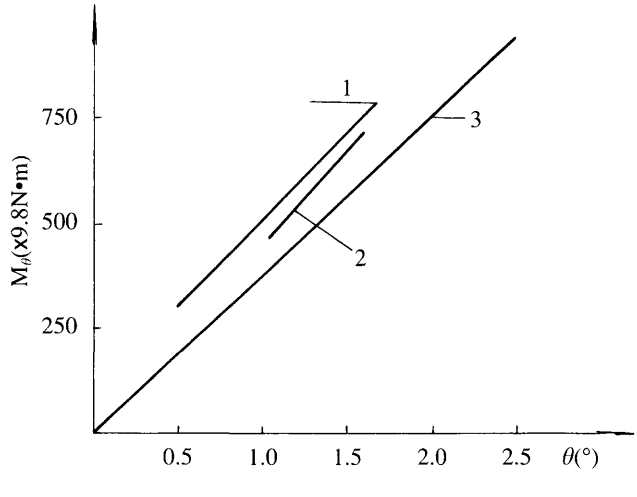

Fig. 4.23 Transverse righting moment of SES model 717C at different forward speeds. 1: v = 26.5 kph, h/bc = 0.439; 2: v = 33.1 kph, h/bc = 0.369; 3: v = 0, h/bc = 0.311.

speed. This was found both on model test and full-scale ship trials. This occurred to the SES type 717C with thinner sidewalls, which rolled violently at hump speed and even led to unstable yawing and plough-in. For this reason, it is very important to analyze the stability of craft during take-off.

Figure 4.25 shows experimental results of transverse stability of an SES model running at different speeds over water obtained by Soviet engineer A.Y. Bogdanov [44]. He presents the relative stability moment $M_\theta^v = M_\theta^v / M_\theta^0$, in which M_θ^v denotes the restoring moment of model at speed of v, M_θ^0 denotes the restoring moment of model at zero speed and Fr_D denotes the Froude number based on volumetric displacement of the craft.

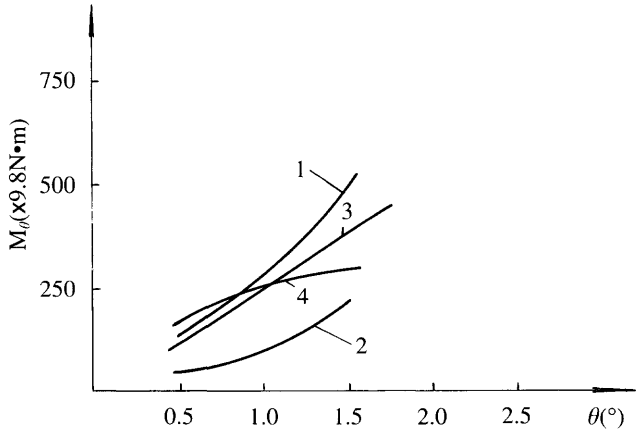

Fig. 4.24 Composition of transverse righting moment of SES model 717C. 1: Sidewall moment, $v = 44.2$ kph; 2: Stern planing seal moment, $v = 44.2$ kph; 3: Sidewall moment, $v = 26.5$ kph; 4: Stern planing seal moment, $v = 26.5$ kph.

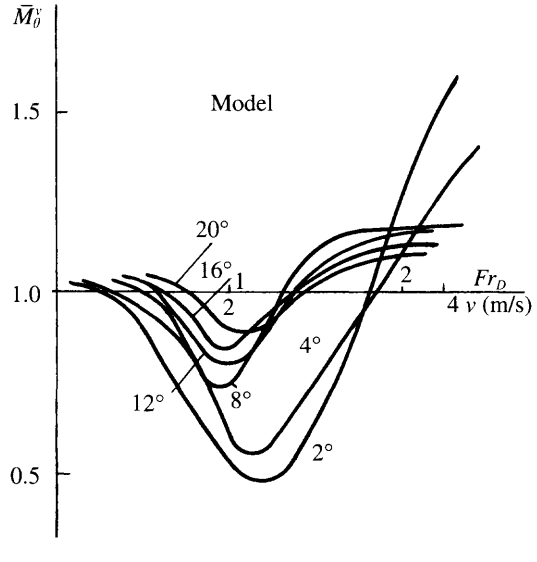

Fig. 4.25 Transverse stability moment of heeled SES at speed.

It can be seen that the transverse stability of the models reduces significantly during take-off, particularly in the case of small heeling angle $\theta = 2°$. The transverse stability even reduces to half of that at zero speed, though it increases rapidly above hump speed.

Bogdanov showed that the craft bow was situated at the wave peak and the stern at the trough when travelling at hump speed. The immersed sidewalls therefore cause added wave-making at this speed. When a craft is heeling this will cause a deeper trough at the stern for the immersed sidewall and in contrast, the trough would be reduced at the stern of the emerged sidewall. The restoring moment is therefore reduced due to such asymmetric drafts at both sidewalls and seals.

In the case where the craft speed is over the hump speed, the wave trough caused by the sidewalls and air cushion system will be far behind the craft stern and the immersed sidewall and seals will provide a large hydrodynamic force and righting moment. The transverse righting moment therefore increases rapidly at speeds above hump.

Transverse stability in waves

The transverse stability of hovercraft in waves needs to be considered together with craft motions, particularly with respect to the roll characteristics of SES in waves. This will be described further in Chapter 8.

Criteria and standards for the stability of SES

Criteria and standards for stability are a very important input to the design and construction of SES. The standards derived from various national bodies are described in Chapter 10. These vary somewhat. An approach to setting criteria is described below, based on Andrew Blyth's work for the UK CAA reported in [42].

Designs should always be evaluated at several loading conditions within the designed operating range, since this can often affect the results significantly. In order to address the differing needs of different stages of the design process, as well as the different levels of sophistication of analysis appropriate to craft ranging in size between tens and thousands of tonnes in displacement, compliance with each criterion may be demonstrated by a range of methods, ranging from simplistic formulae, through more complex mathematical methods, to model tests or full-scale trials (if appropriate).

Naturally, the more simplistic the method, the more important it is that the results can be expected to be conservative. So the use of more sophisticated and hence expensive techniques will often enable higher VCGs to be used with confidence. Failure to pass the simple methods does not necessarily imply total unacceptability.

Static stability

The initial, lateral roll stiffness averaged over the range 0–5° of heel should not be less than a transverse metacentric height (GMt) of 10% of the craft maximum beam, when measured or calculated for a static longitudinal trim angle within about half a degree of level keel. This is equivalent to a percentage CG shift per degree of 0.175. Calculation, model test or full-scale experiment are considered appropriate for evaluation.

Stability in waves

The SES should just be capable of surviving regular steepness limited waves (crest to trough height – 0.14 × wavelength) with breaking (as opposed to plunging) crests, of any individual height up to the limiting wave height, encountered beam-on while using full available lift power and combined with:

1. A TCG equal to twice the maximum normal TCG.
2. A beam wind as specified in the design environmental conditions. Special consideration of the safety margins would be required where this wind speed exceeds a velocity (knots, at 10 m high) equal to

$$15 \times B_c^{0.5} \text{ (in metres)}$$

The limiting wave height shall be taken as 1.9 times the significant wave height specified in the design environmental conditions.

An analysis of static on-cushion righting lever characteristics was conducted by Blyth to provide a relatively simple calculation method [42], although it was found that the minimum required properties of the curve vary substantially with hull configuration, due to the dominant effects of forcing and damping characteristics. Other acceptable methods of demonstrating compliance include mathematical simulations and model tests.

Stability in turns

Since the behaviour of an SES in high-speed turns is very dependent on both speed (which declines rapidly in tight turns) and the rate of turn achievable, the following criteria should be met when the vessel is at approximately 45° change of heading, in the test achievable turn, at a range of approach speeds within the operational range, for each weight condition to be considered. Note that behaviour is not always most critical at maximum speed.

1. The minimum net roll stiffness (expressed as minimum effective GMt) in the tightest attainable turn should always be greater than 5% of craft overall beam (Bc). This is equivalent to a percentage CG shift per degree of 0.087. This requirement need not be met if the total roll restoring moment in the upright condition is equivalent to an inward TCG greater than 2.5 times the maximum normal TCG, since this is considered to provide a good reserve beyond the maximum roll moments realizable in practice.
2. The net roll stiffness in a turn should not permit a greater outward heel angle than $(3 - Fn_c)^2$ degrees when the maximum normal TCG is applied in an outward direction where Fn_c = cushion Froude number = $V/(L_c \times g)^{0.5}$.
3. In order to avoid undesirable roll/pitch/yaw coupling effects, the hull form should be such that when a roll moment is applied at speed, any bow-down trim angle change should not exceed one-fifth of the heel angle.

Relatively simple calculation methods have been derived for assessment, but model tests are also acceptable and in many cases desirable. Some full-scale trials will always be required to demonstrate that the expected maximum rate of turn cannot be exceeded.

Commentary

It has been shown by Blyth's test programme that the on-cushion stability of an SES should be principally assessed in relation to rolling behaviour in synchronous beam seas and in relation to the hydrodynamic forces developed in high-speed turns.

In a seaway, capsizing of an SES is most probable in steepness-limited beam seas with a period close to resonance. An alteration in course and/or a reduction in lift power both substantially reduce the probability of capsize occurring. It has been shown that for each design, there is a VCG below which capsizing becomes improbable.

In high-speed turns, the hitherto unidentified possibility of large amplitude roll/yaw oscillations occurring has been detected and examined. It seems probable that this behaviour is associated with a zone of negative roll stiffness in turns, created by the manner in which hydrodynamic forces vary with roll attitude.

4.4 Calculation of ACV transverse stability

Introduction

An ACV has no natural restoring moment from the cushion (plenum chamber) itself while heeling on cushion. Air jet craft derived stability moments from the increased force of the jet on the downgoing side and reduced force on the upgoing side, though these were small and so such craft were very sensitive to movements of craft payload.

As an ACV heels, due perhaps to the movement to one side of a person on board creating an overturning moment, a negative restoring moment will act on the ACV if no other stability moments are created by deformation of the peripheral skirts, as shown in Fig. 4.26. This is because the cushion pressure will be the same across the craft width in the case of no cushion compartmentation.

The skirt geometry and in the case of skirts with pressurized loops or bags, p_l/p_c has a strong influence on the righting moment which is generated for an ACV. When travelling over water, the skirt stiffness will then affect the water displaced on the downgoing side, in a similar way to the action of SES sidewalls, below hump speed. Above hump speed, the skirt surface presented to the water acts as a planing surface, though the force that can be generated is limited to that which can be transmitted around the fabric membrane back to the craft's hard structure.

Cushion compartmentation

In the case where an ACV compartmented longitudinally hovers statically on a rigid surface, cushion pressure on the side heeling down increases due to reduced air flow and the cushion pressure decreases for the other side because of increased escape area and therefore flow rate. Thus the different cushion pressures give a direct restoring moment, moving the effective centre of pressure to the downward side of the craft, as shown in Fig. 4.27.

Meanwhile, the transverse component of $P_{c\theta}\sin\theta$ of the cushion pressure resultant $P_{c\theta}$ will also lead to a drifting motion. For this reason, drifting in general always

occurs with heeling. This phenomenon also happens on an ACV hovering on a water surface as shown in Fig. 4.28. In the case where the ACV heels on the water surface as shown in Fig. 4.28, the cushion pressures for left/right cushion compartments are rather different, thus it causes a different water surface deformation for each of the compartments. The water hollow under the left cushion compartment is deeper than that in the right compartment and the water displaced by the hollow is equal to the lift caused by the cushion pressure on each side. Thus it can be seen that the restoring moment and the drifting force are caused by the different cushion pressure in the left and right cushion compartments.

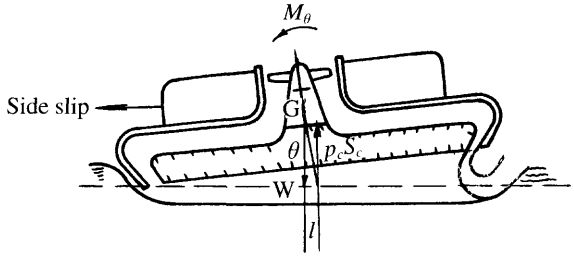

Fig. 4.26 Heeling of an ACV without air cushion compartmentation on water.

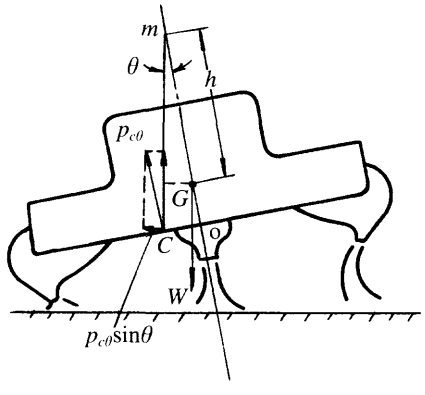

Fig. 4.27 Heeling of an ACV with air cushion compartmentation on rigid surface.

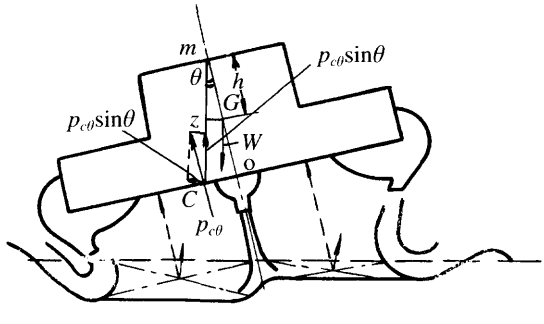

Fig. 4.28 Heeling of an ACV with air cushion compartmentation on water.

Separated bag or cell

Figure 4.29 shows the skirt configuration of the US ACV type JEFF(A). Since the air supply for left- and right-hand cells is separated, the pressure for the side heeling down will be increased in the case where the craft is heeling, and the pressure at the other side will be decreased, consequently causing a restoring moment. The French multi-cell skirt system (called the 'jupe' skirt) possesses the same effect as the JEFF(A) skirt system except that each jupe creates a moment independently.

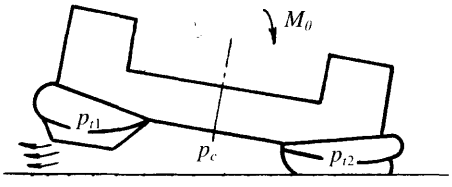

Fig. 4.29 Influence of pericell type skirt on craft stability.

Skirt lifting or shifting systems

The skirt shifting system and its principle of action was developed by Hovercraft Development Limited of the UK. The skirts might be shifted in the transverse direction to change the centre of pressure subsequently, to cause righting or heeling moments as shown in Fig. 4.30. Such systems have been mainly applied to move skirts side to side, particularly to allow a craft to bank into a turn. The system is convenient to install on a loop and segment skirt with the same pressure in the loop as the cushion, or with slight overpressure, 5–10%.

The British Hovercraft Corporation developed a simpler system for their bag and finger skirts whereby the segment is lifted, heeling a craft opposite to the external overturning moment. The geometry of a bag and finger skirt was found easier to deform by lifting and the effect was similar to that of the loop and segment skirt transverse shift system.

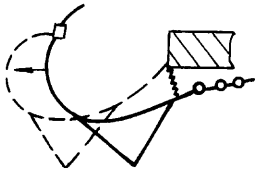

Fig. 4.30 Skirt with transverse shifting system for improving the transverse stability.

The transverse shift of centre of cushion area

The centre of cushion area may be shifted in order to produce a restoring moment, as shown in Fig. 4.31. When an ACV is heeling, the centre of cushion area will shift to the side which is heeling down (from C to C′ in Fig. 4.31) to offer a restoring moment.

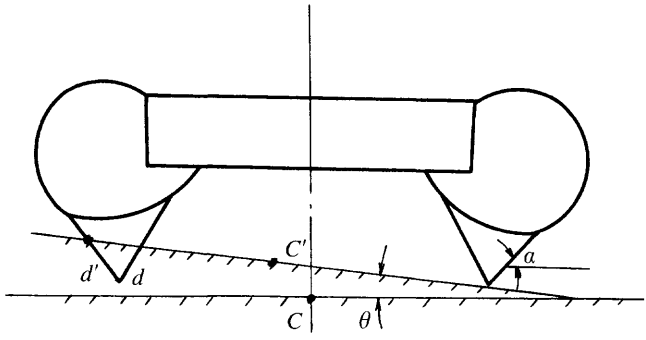

Fig. 4.31 Transverse movement of centre of cushion area of ACV with bag and finger type skirt on heeling. *c*, *c'*, centre of area; *d*, skirt contact with ground level; *d'*, skirt contact heeled.

Statically this may be estimated in two dimensions by determining the static equilibrium of the downgoing skirt as the ground point is raised from d to d'. In general this will result in just a small increase compared with the cruder assumption that the skirt does not move at all. The exception to this is if segments are replaced by pericells.

Larger ACVs (above around 5 t displacement) commonly use longitudinal and transverse stability skirts to improve craft stability; we will present analysis of stability including cushion compartmentation, with some additional guidance regarding the choice available to a designer to avoid such complexity.

Calculation of transverse stability for an ACV

It is very complicated to calculate the transverse stability of an ACV hovering over water because of the deformation of the water surface. The suggested analysis procedure is therefore to investigate the transverse stability of an ACV hovering on a rigid surface, followed by the corrections necessary due to the water surface deformation, obtained with the aid of model experiments.

The coordinate system and the basic assumptions can be written as follows:

1. Since the ACV is supported on a rigid surface, we neglect the effect of hydrodynamic force acting on the skirt and the deformation of skirts (i.e. we assume that the skirts are not deformable or at least have small deformations which can be neglected).
2. We simplify the cushion plane as rectangular and adopt a longitudinal stability skirt to compartmentalize the air cushion, assuming that the cushion pressure distributes uniformly both in left/right cushion compartments.
3. We consider the GXYZ system as the body coordinate system and the $0\xi\eta\zeta$ system as the fixed coordinate system as shown in Fig. 4.32.

The calculation method for predicting the static transverse stability of an ACV on cushion is very similar to that for an SES, i.e. in the case where the ACV is heeling, the lift due to the cushion pressure has to be equal to the weight of craft and the heeling moment equivalent to the restoring moment about the CG caused by the cushion pressure which satisfies the fan duct characteristic equation. The flow of the fan has

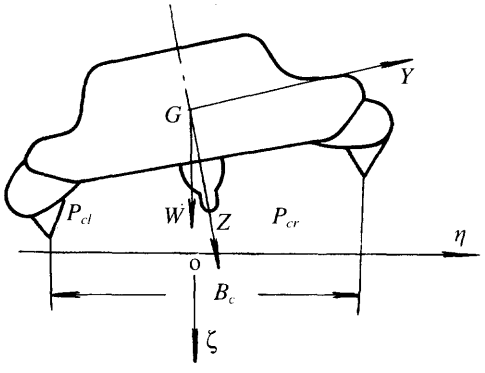

Fig. 4.32 Coordinate system of craft for stability.

to satisfy the flow rate continuity equation. Thus the equations of weight and moments can be expressed in matrix form as follows:

$$[A_n]\begin{bmatrix} P_{cl} \\ P_{cr} \end{bmatrix} = \begin{bmatrix} W \\ M \end{bmatrix} \tag{4.20}$$

where $[A_n]$ is the parametric matrix for cushion geometry of the craft and can be written as

$$[A_n] = \begin{bmatrix} A_{cl} & A_{cr} \\ A_{cl}Y_{pl} & A_{cr}Y_{pr} \end{bmatrix} \tag{4.21}$$

where W is the craft weight, M the heeling moment, $M = M_c + M_g$, M_c the righting moment due to the cushion pressure at the heeling angle of θ, M_g the heeling moment due to the height of CG at the heeling angle of θ, i.e. the moment of W about the intersection point of line GZ with the line linking to the lower tip of skirts, A_{cl} the area of left cushion, suffix l denotes left cushion, A_{cr} the area of right cushion, suffix r denotes right cushion, Y_{pl} the vertical distance between the CG and centre of left cushion area and Y_{pr} the vertical distance between the CG and centre of right cushion area.

The total pressure–flow rate characteristic of the fan and duct can also be expressed by

$$P_t = A + BQ + CQ^2 \tag{4.22}$$

where P_t is the bag pressure, Q the flow rate of the fan and A, B, C the parameters for fan characteristics.

Expression (4.22) defines the relation between bag pressure and flow rate. As a matter of fact, we have to put the total pressure of fan H_j into the foregoing equation instead of bag pressure P_t. Here we neglect the pressure of the air duct from the outlet of the fan to skirt bag. The bag pressure will be different in the case of different duct configurations. One has to consider this matter in practical calculations according to the specific geometry of the craft cushion air distribution system.

To simplify the calculation, we assume that one fan supplies the flow rate to both left and right cushions instantaneously and the pressure in both left and right cushions is equal. Thus the characteristics of cushion pressure and air leakage from bag holes can be expressed as

$$\begin{aligned} P_{cl} &= P_t - E_l Q_l^2 \\ P_{cr} &= P_t - E_r Q_r^2 \end{aligned} \tag{4.23}$$

where Q_l, Q_r, are the flow rates from left/right cushion, E_l, E_r the loss coefficient of bag holes in left/right cushion and P_{cl}, P_{cr} the pressure in left/right cushion.

From the flow rate continuity equation, we have

$$\begin{aligned} Q &= Q_l + Q_r \\ Q_l &= Q_{el} + Q_{lr} \\ Q_r &= Q_{er} - Q_{lr} \end{aligned} \tag{4.24}$$

where Q_{el}, Q_{er} are the flow rates leaking from left/right cushion and Q_{lr}, the cross-flow from left cushion to right cushion, can be written as

$$Q_{lr} = \phi\sqrt{(2/\rho_a)|p_{cl} - p_{cr}|}\,\mathrm{sgn}\,(p_{cl} - p_{cr})A_{eg} \tag{4.25}$$

where ϕ is the flow rate coefficient and A_{eg} the leakage area of cross-flow. A_{eg}, Q_{el} and Q_{er} in the above equations are related to the air leakage gap; they are a function of heeling angle θ.

In the case where one side contacts the ground, the cushion area of this side kneeling down may be determined as follows. Figure 4.31 shows the contacting point of the skirt with the ground, d, in the case of a craft where the skirt touches but is not deformed. This will be shifted to d′ in the case of heeling craft due to the skirt kneeling down, the cushion area at this side (skirt kneeling down) will increase in order to provide the restoring moment.

The contacting point is related to the outer surface inclination angle of the skirts, a. The righting moment is inversely proportional to a. These effects have been considered in equation (4.21). The equation group in this section is called the coupled stability equation for heeling and heaving of ACVs, which is very similar to that for SESs.

In the case where the heeling moment (force), principal dimensions of the craft and the leading particulars for fans, skirts and cushion are given, then the parameters such as P_{cr}, P_t, Q, Q_{ei}, Q_{er}, Q_{lr} can be solved with aid of a computer and the expressions (4.20)–(4.25). The heeling angle θ as well as the vertical position of CG (ξ_g) can also be obtained.

Figure 4.33 shows a typical curve of static transverse stability of an ACV hovering on a rigid surface. It can be seen that the curve is nonlinear at larger heel angles, due to the nonlinear factors of fan characteristics and ground contact and deformation of skirts.

4.5 Factors affecting ACV transverse stability

Based on the equations mentioned above, one can discuss the effect of the various parameters on the static transverse stability of an ACV. However, the errors of calculation are rather large since no account is taken of the deformation of skirts caused by the

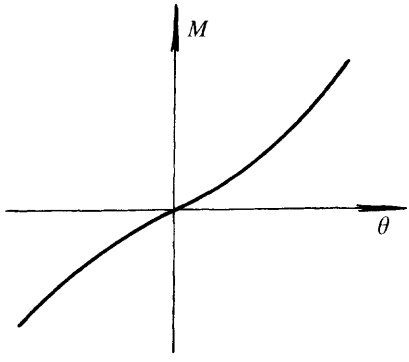

Fig. 4.33 Typical static transverse stability curve for ACV.

change of cushion pressure of the craft in heeling and the effectiveness of the air cushion blown from the nozzle of stability skirts on the stability of craft.

Therefore these problems have to be solved by experiments. References 45 and 46 offered some commentary on experimental results from model tests as discussed below.

Effect of supporting surface

Figure 4.34 shows that the static transverse stability for an ACV model with + type of cushion compartment hovering on a water surface is worse than that on rigid surface due to the deformation of the water surface. In general the static transverse stability on the water surface is about 70–80% of that on rigid surface whatever type of cushion compartment was adopted.

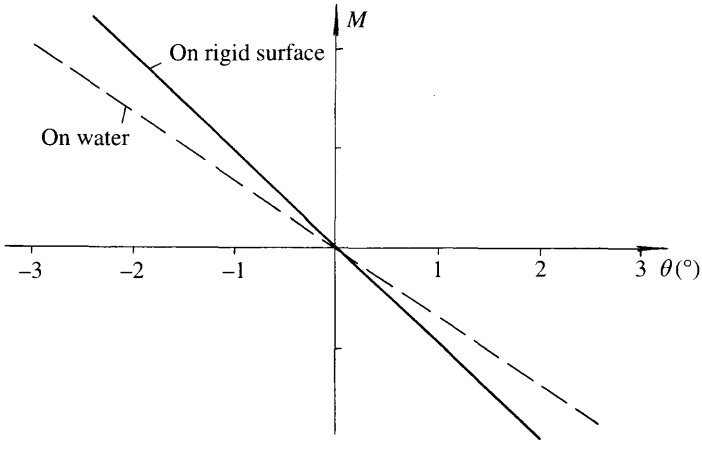

Fig. 4.34 Static transverse stability of ACV models with + type of air cushion compartmentation.

Transverse stability of an ACV without the cushion compartmentation

An ACV without the cushion compartmentation can also provide a positive restoring moment during heeling of the craft. This is due to the skirt finger with so small an inclination angle as to change the centre of cushion area and provide a positive restoring moment, as the skirt contacts the supporting surface during heeling of craft. Figure 4.35 shows a typical static transverse stability curve of an ACV without compartmentation.

With respect to ordinary ACVs, the restoring moment is due to the following factors:

1. The restoring moment is due to the cushion compartmentation inducing different pressure in different cushions. This is called compartment stability.
2. The restoring moment is due to the change of cushion area, either arising from the inclination angle of skirt fingers, or from the deformation of the skirt in the horizontal direction. This is called area stability or stability due to ground contact of the type of cushion compartment on static transverse stability of an ACV.

Figure 4.36 shows the effect of three types of cushion compartment on static transverse stability, in which l_g denotes the length of longitudinal stability skirt (measured from stern); therefore, $l_g/l_c = 0$ denotes that without cushion compartment; $l_g/l_c = 0.6$ denotes compartmentation of T type, and $l_g/l_c = 1.0$ denotes + type compartmentation.

The criterion for transverse stability can be written as

$$\bar{S}_R = [\Delta M/\Delta\theta] / [WB_c] \tag{4.26}$$

where $\bar{S}_R$ is the relative shifting distance of centre of pressure per unit heeling angle. This criterion is equivalent to the relative height of initial stability:

$$\bar{h} = h/B_c = [\Delta M/\Delta\theta \times 57.29] / [WB_c] = \bar{S}_R \times 57.29 \tag{4.27}$$

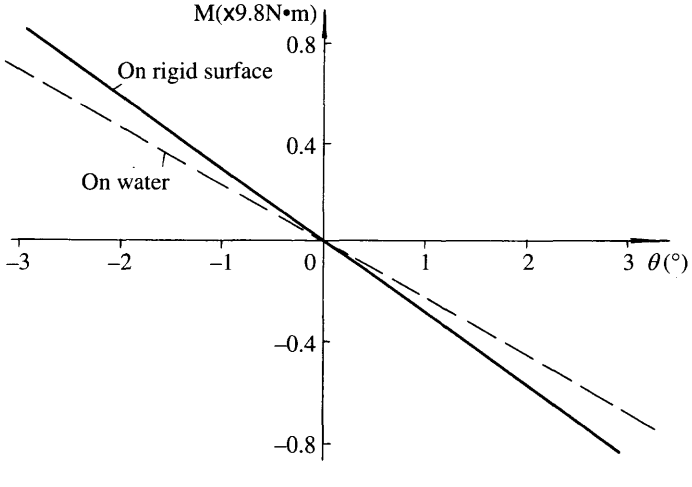

Fig. 4.35 Static transverse stability of ACV models with no air cushion compartmentation.

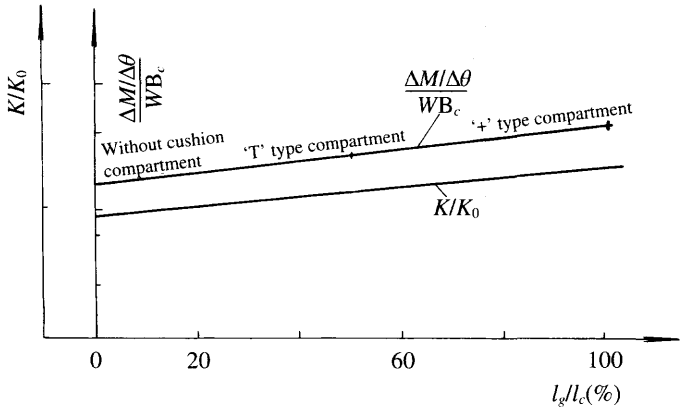

Fig. 4.36 Influence of air cushion compartmentation on static stability.

where $\Delta\theta$ is the heeling angle (for a small value) (°), ΔM the restoring moment (N m), h the initial transverse metacentric height (m), W the craft weight (N) and B_c the cushion beam (m).

K/K_0 (in Fig. 4.36) shows the effect of the depth of the stability skirt on transverse stability. It can be seen that the stability of an ACV without cushion compartmentation will be reduced to about 60% of that with the + type of cushion compartment. Reference 47 demonstrated experimental results such that the transverse stability would be decreased to 59% in the case of removing the longitudinal stability skirt and the longitudinal stability would be decreased to 68% in the case of removing the transverse stability skirt.

It is clear that this investigation is very important and plays a key role in analysing the stability of an ACV. Since transverse and longitudinal stability skirts are normally situated inside the cushion and are very difficult to repair and maintain, it is more convenient to remove stability skirts if at all possible. While this is now practical, it has take some years for skirt design technology to advance to the point where satisfactory stability can be provided (see Chapter 7).

Figure 4.36 also shows that the transverse stability for the craft with T type compartment will be decreased to 85% of that with + type compartment.

Effect of stability skirt clearance h_{ej} on the transverse stability

Stability skirt clearance has a direct effect on the effectiveness of cushion compartment and transverse stability. Figure 4.37 shows that the role of the cushion compartment will decrease as the stability skirt clearance h_{eg} increases to larger than 30% of cushion depth at CG. In general, h_{eg} is equal to 10–20% cushion depth at CG, but stability skirts of + type are more sensitive than those of T type.

Effect of VCG on transverse stability

VCG has a clear effect on transverse stability of craft. Figure 4.38 shows that VCG is directly related to height of skirts, therefore one has to make a comprehensive

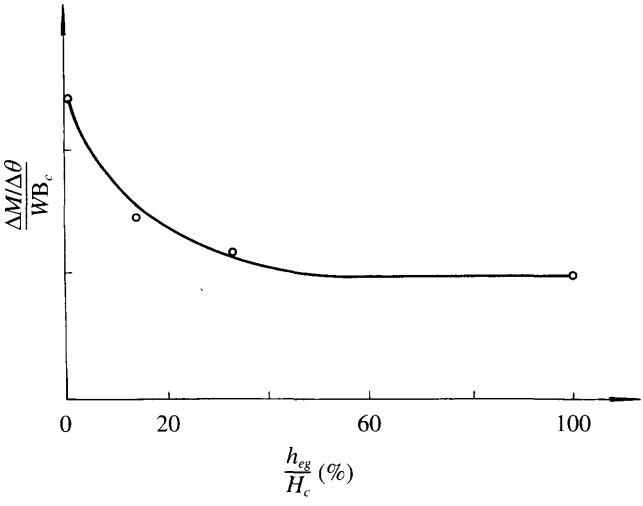

Fig. 4.37 Influence of gap between the lower tip of transverse stability skirt and ground on static transverse stability of model craft.

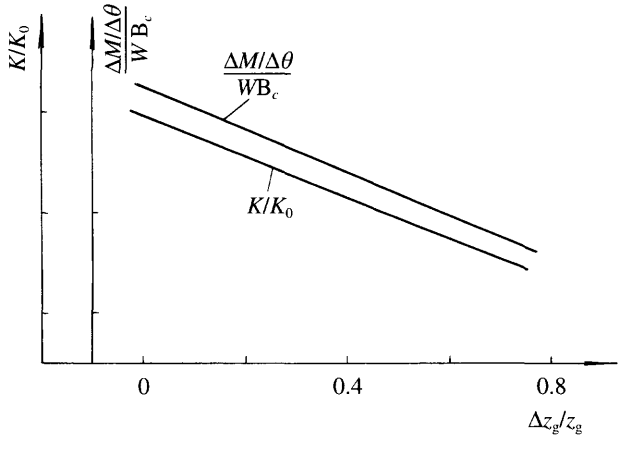

Fig. 4.38 Influence of vertical position of centre of gravity on static transverse stability.

analysis of transverse stability during the design of skirt height. If one uses higher skirts due to the requirements of obstacle-clearing capability and seaworthiness, then effective measures for stability have to be adopted during the design stage.

Effect of fan flow rate on transverse stability

Figure 4.39 shows that transverse stability of an ACV is directly proportional to the flow rate of fans, the relation of which is opposite to that for SES. Probably the rationale of this phenomenon is that the slope of total head with respect to the flow rate on a characteristic curve increases as the flow rate of the fan increases, which leads to enhanced transverse stability.

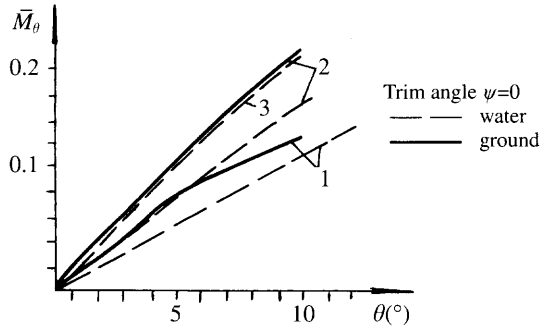

Fig. 4.39 Influence of air flow rate on static transverse stability. 1: lift for speed $n = 3000$ rpm; 2: $n = 4500$ rpm; 3: $n = 5000$ rpm.

4.6 Dynamic stability, plough-in and overturning of hovercraft

Introduction

We will now introduce the dynamic stability of ACVs travelling over water. During the early development of ACVs (see Chapter 1) hovercraft had very limited stability. The concept being developed was to use air jets to allow these machines to 'fly' close to the ground. This approach had to be revised once flexible skirts were introduced.

When operating over water, particularly at speed, the forces induced from wetting of the lower part of the skirts could produce significant changes of trim. The early design of skirts was such that these changes of trim did not create additional righting moments, but instead they were reduced. Unless the hovercraft pilot took action to maintain level trim, the craft would eventually plough-in and either come to a stop, or overturn.

There were a number of overturning accidents in those early days. As an example the Chinese experimental ACV type 711 overturned during a trial in May 1966. The craft was travelling at the speed of 50 km/h and had to make a sudden turn in order to avoid collision with a small boat. When the craft made the turn, yawing and heeling to a large angle occurred, and the craft capsized.

Some British ACVs also overturned at a high speed on calm water. The process of capsizing was as follows: bow pitching down, drifting, yawing and combined heeling, high-speed plough-in and then overturning. Figure 4.40 shows plough-in of the British ACV SR.N6 and Fig. 4.41 shows the plough-in that induced the capsizing of a radio-controlled ACV model recorded by cine camera.

The sequence of plough-in events was stated in the driver instructions of SR.N5 as follows:

> Contact of the flexible skirts with water surface leads to a bow pitching down moment and bow pitch down, which will be magnified as the water resistance increases at increased speed. The features of the plough-in phenomenon are

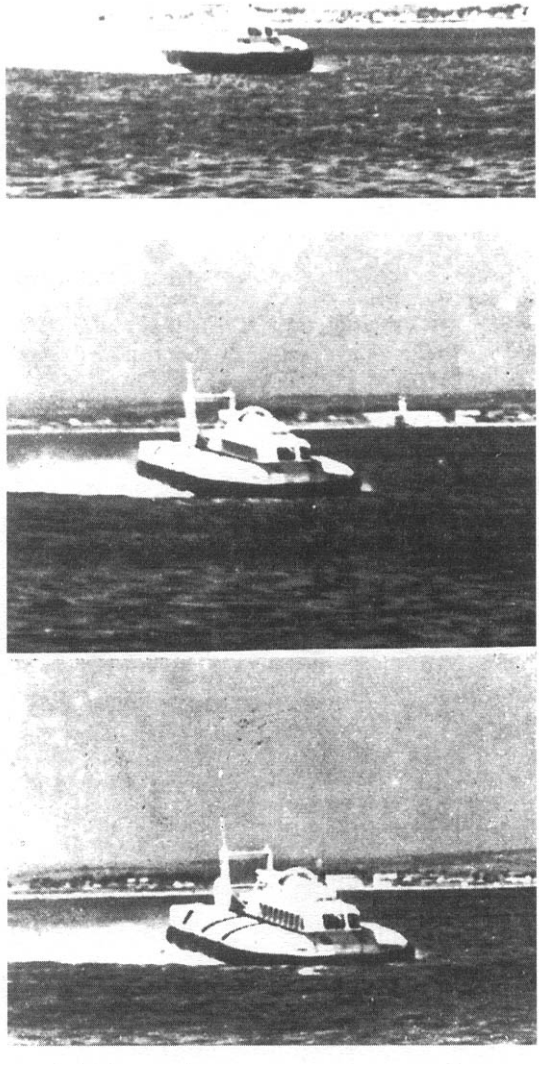

Fig. 4.40 The plough-in phenomenon of British SR.N6 in tests.

that the speed decreases, followed by large pitching down and heeling angle, as well as stern pitching up tendency so as to enlarge the drifting angle.

The principal author has had a number of such experiences; for example, the 5 t ACV model 711–II would plough-in on calm water (or in a breeze) at a speed of 70–80 km/h. In the case where the craft was travelling downwind, then the probability of plough-in would be over 90%. Violent slamming would occur to the craft and lead to speed degradation from high speed (about 80 km/h) to off cushion speed (about 5 km/h) in 2–3 seconds. Such high deceleration accompanied by the

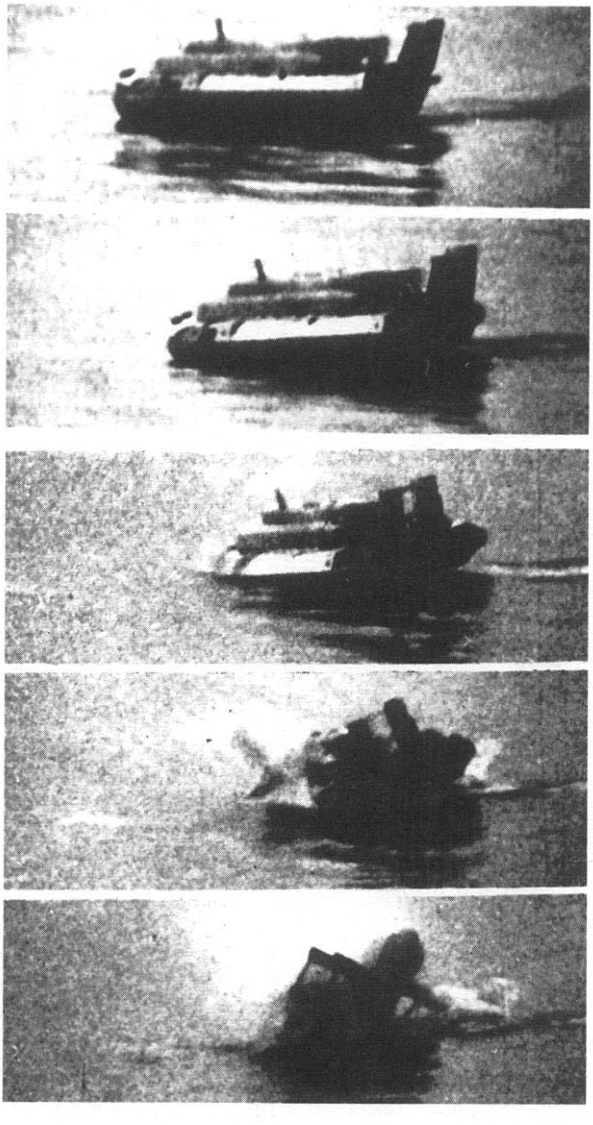

Fig. 4.41 The overturning of a hovercraft model recorded by cine camera.

slamming would lead to the skirt being damaged, engine mountings destroyed and people injured. This same phenomenon has occurred on a number of other Western and Chinese domestic ACVs in the mid 1960s to 1970s.

Similar phenomena have also occurred to SES at very high speeds, for example the US Navy SES–100A at a speed of over 70 knots. But in general it is seldom experienced. The plough-in of an SES downwave will be described in Chapter 8.

On smaller craft, with which the second author has considerable experience, the trimming moments generated by payload movement (i.e. passenger movement) can

significantly affect trim. As a result it is possible to experiment with a craft in suitable conditions, to test the stability of a bow or side skirt at different speeds. Beyond a small bow-down trim (1–2°) most skirts begin to wet (i.e. air flow is partly blocked and some of the segment surface is not lubricated by the air flow), leading to a sharp rise in drag. The beginning of this process can be seen on skirts without a swept-back bow, as the segments or bag appear to 'nibble' which can be seen directly or via movement of the loop. Beyond a further small trim-down, the rate of increase of drag causes rapid deceleration of the craft and in the case where the skirt system is not stable, either plough-in or overturning.

Sideways drift can cause a similar effect on the side skirts. Payload (CG) shift away from the drift to bank the craft can be very helpful. In this respect, provision of elevators or skirt shift mechanisms on utility size craft can be very important in maintaining dynamic stability. The CG shifts required are too great and required too quickly for larger craft, which have to rely on cushion compartmentation to keep the skirt stability envelope outside the normal operating conditions.

The increasing hydrodynamic force (and moment) due to contact of the flexible skirt with the water surface is the main reason leading to plough-in.

Before development of special skirt geometries, plough-in could be avoided only with aid of driver operating rules formulated by users, or research and design bureaux. Thus it can be seen that it is very important to study the rationale of plough-in and the overturning phenomenon.

Some ACV plough-in and overturning incidents will be examined below and a rationale developed. We will not present a theoretical analysis of this field due to its complicated hydromechanics. Readers may find [48] useful as background material, developed by the UK Department of Transport after the SR.N6 accident in 1973.

ACV overturning at low speed

In a similar way to an SES, the trough is so deformed on the water surface underneath an ACV during take-off as to reduce the stability skirt effectiveness. Figure 4.42 shows the inner water surface of a two dimensional ACV model at various Fr; it can be seen that the trough is deep at $Fr = 0.5$–0.7, which causes the detrimental influence on the transverse (or longitudinal) stability of the craft.

Figure 4.43 shows results of an investigation by W.A. Crago. He found that the transverse stability deteriorated dramatically at $Fr_1 = 0.33$–0.56. Figure 4.44 shows that the heeling moment and heeling angle increased at $Fr_1 = 0.4$ and the craft would capsize at overturning moments exceeding $M_\theta/(WB_c) = 0.022$.

For this reason, as far as the drivers are concerned, great attention is required during take-off, particularly in the case of long time duration for take-off due to shortage of lift and propulsion power, or if for other reasons the craft stability is low, due for example to a large amount of free surface liquid existing on the craft.

As far as designers are concerned, attention has to be paid to design skirts with a stable geometry for the hydrodynamic forces expected at hump speed and a realistic range of overturning moments and resultant craft trim.

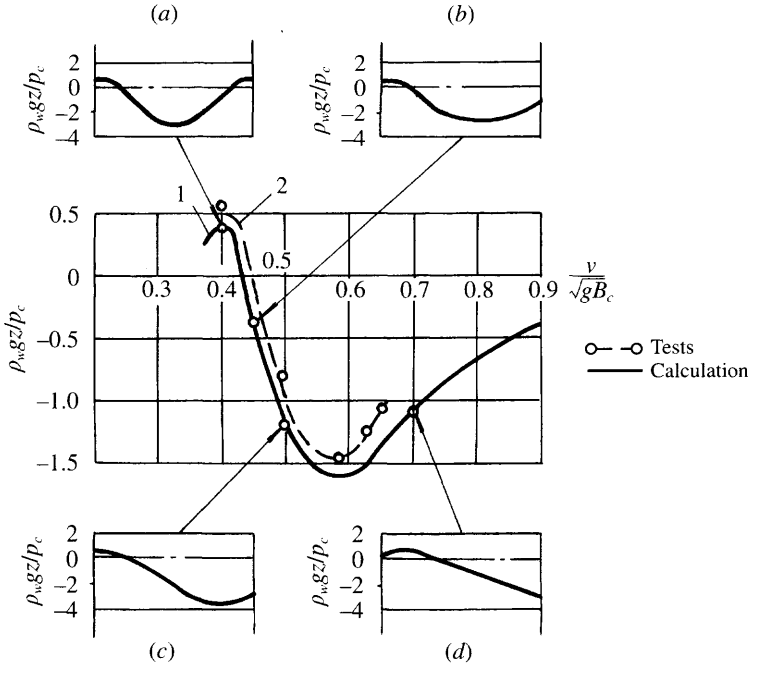

Fig. 4.42 Internal wave profiles of two dimensional ACV at different Froude Numbers. (a) $Fr_B = 0.4$, (b) $Fr_B = 0.44$, $Fr_B = 0.5$, (d) $Fr_B = 0.7$.

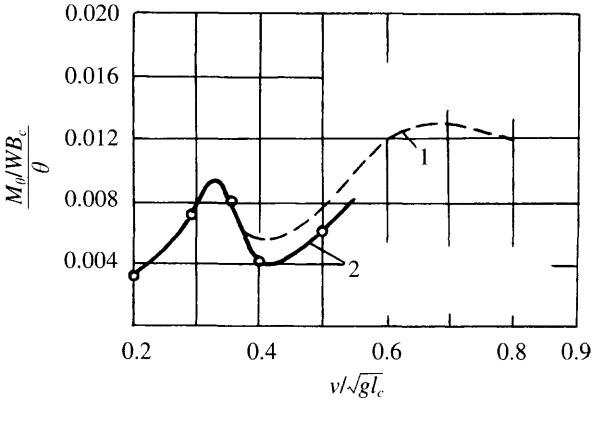

Fig. 4.43 Variation of transverse stability of ACV model as a function of Froude Number. 1: calculated from craft trim, 2: calculated from 2D cushion pressure distribution.

Plough-in and overturning of craft running at high speed

ACVs can normally be led into instability while travelling at high speed as shown in Figs 4.40 and 4.41. It is primarily due to bow down trim, or for some craft level trim, due to the aerodynamics of their body shape.

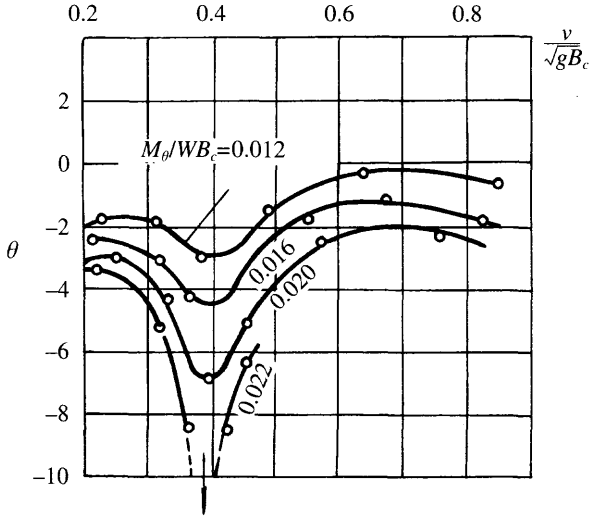

Fig. 4.44 Experimental results of rolling angle of hovercraft models as a function of craft speed.

Bow pitching down and plough-in are common terms used by the hovercraft designer often without clear distinction between them. The former means the craft bow pitching down at the bow skirt but still in a condition where the skirt segments are air lubricated and 'plough-in' means the craft is pitching bow down with so large a negative angle as to lead the skirt undergoing significant wetting giving large local drag forces and accompanied by the tuck-under of the bow skirt. Here we will investigate this problem in three phases, i.e. the progression, the reasons and the measures for improvement.

The progression during plough-in

The typical progression at plough-in can be described as follows (Fig. 4.45):

- Fig. 4.45(a): An ACV normally travels with a definite positive trim angle (bow up), and spray blown out under the fingers of bow skirt can be observed.
- Fig. 4.45(b): As the craft speeds up, the positive trim angle decreases as the thrust of the air propulsor increases. In the case where the craft is travelling downwind and a gust occurs, this causes the thrust to increase suddenly and lead to contact of the bow skirt fingers with the water surface. Meanwhile the spray blown from the delta zone between the tips of the skirt fingers can also be observed. The craft is still running with positive stability.
- Fig. 4.45(c): Hydrodynamic resistance increases as the wetted surface of skirts increases, thus the dynamic pressure of oncoming flow on stagnation will be so balanced by the cushion pressure, as to lead to the deformation of skirt fingers and cause the skirt to plane without spray. Eventually this can produce a suction acting on the skirt fingers, which leads to the fingers actually touching the water surface.

  The hydrodynamic drag increases further, light tuck-under occurs on the fingers, leading to the bow cushion being pulled back and the cushion area decreased. Subsequently the total force from the cushion drops while the cushion pressure rises

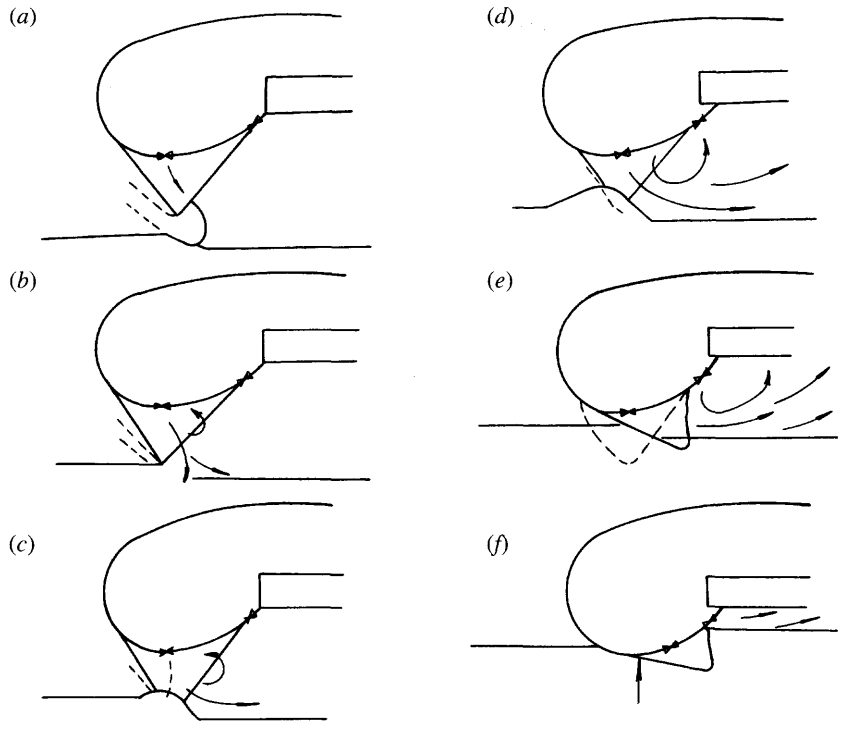

Fig. 4.45 A typical overturning process for an ACV.

and the skirts are immersed further in the water, building up drag on the bow skirt. Longitudinal stability deteriorates.

- Fig. 4.45(d): Following the situation in Fig. 4.45(c), the bow skirt tuck-under increases and craft trims further bow down. While there is still dynamic equilibrium at this point, the longitudinal stability deterioration is self perpetuating and this is the sign for plough-in.

  The plough-in phenomenon can be avoided if the driver takes measures at this point to reduce bow down trimming moments; for instance, throttle down on propulsion engines to bring the bow up; open to full throttle on lift engines; operate the horizontal rudder or air duct valve to raise the bow trim.
- Fig. 4.45(e): The wetted area of the bow fingers increases so as to increase the skirt drag violently, meanwhile the underfeed at the bow increases so seriously and strength of the flow vortex increases due to a large speed of cross-flow out to the side of the skirts, and decrease of cushion pressure at the bow and a large moment for pitching bow down, consequently the slamming of craft due to the plough-in occurs in a short period of time.
- Fig. 4.45(f): During plough-in and slamming of the craft, the bow skirt contacts the water surface producing a large hydrodynamic lift. Although a large negative acceleration occurs to the craft, the craft is still moving forward due to the inertia force, which strengthens the suction of the bow skirt and increases the bow cushion negative pressure to maximum absolute value. In the case where the plough-in and

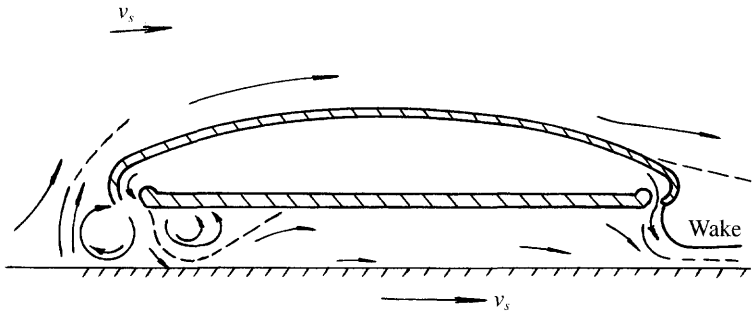

Fig. 4.46 Internal and external air stream lines of a high speed hovercraft model.

slamming occur together with drifting and slipping, then the craft may capsize, if the driver does not take any measures to prevent it.

Principal reasons for plough-in and overturning

Table 4.7 shows the main test data recorded during plough-in of a test craft.

1. The air stream ram pressure increases as craft speed increases, which leads to the sealing action of the cushion outflow (Fig. 4.46) [49]. Thus jet underfeed and cross-flow occur in the cushion, which will be accelerated due to the effect of the boundary layer under the cushion. Thus it can be seen in Fig. 4.47 that the bow cushion pressure decreases and stern cushion pressure increases as the craft speeds up, which lead to the centre of pressure being shifted to the stern. This is probably the internal reason for the plough-in.
2. Since the air propulsors of an ACV are mounted on the upper deck or superstructure, the thrust line is generally high over the supporting surface, therefore the thrust overturning moment increases as the speed increases, and will be magnified in the case of travel downwind. Thus a bowpitching down moment acts on the craft, which we consider to be the external reason for the plough-in. Figure 4.48 shows the experimental results of models running without drifting motion carried out by Crago [50], in which T/W_n denoted thrust/lift ratio. Clearly the region of plough-in increases as thrust/lift ratio increases.
3. Owing to the internal and external reasons mentioned above, the bow skirt contacts the water surface, leading to tuck-under of the skirt as the craft speeds up and during

Table 4.7 The main test data in the course of plough-in of a test ACV

Time (s)	Trim angle	Bow cushion pressure	Stern cushion pressure	Situation
1 – start	1.78	1160	1130	Normal travel
2	1.08	1200	1100	Finger contacts water surface
2.5	0.90	1180	1100	Light tuck-under
3	0.62	1150	1100	Moderate tuck-under
3.5	0.03	1050	1040	Serious tuck-under
4	−0.05	900	950	Tuck-under unstable
4.5	−1.16	250	630	Plough-in begins
5	−3.94	−1200	350	Bow structure touches
5.5	−1.14	−1000	600	Recovery of skirt
9 – end	+1.60	1200	1130	Normal trim

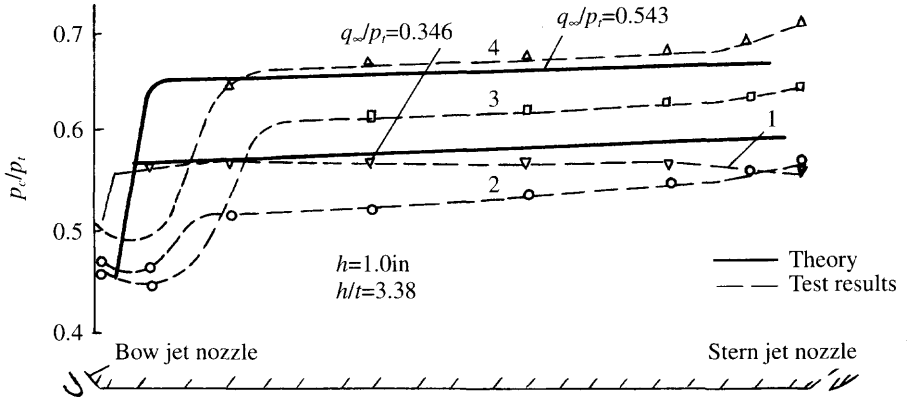

Fig. 4.47 Cushion pressure distribution vs ship speed. 1: $q_\infty/p_t = 0$, 2: $q_\infty/p_t = 0.346$, 3: $q_\infty/p_t = 0.543$, 4: $q_\infty/p_t = 0.743$.

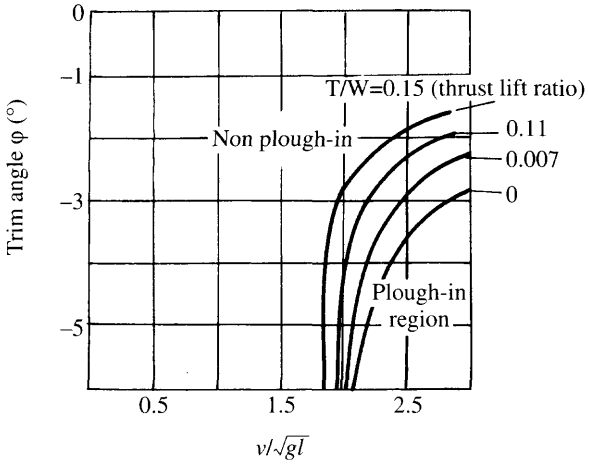

Fig. 4.48 Relation between the ACV plough-in boundary and trim angle, Froude numbers, thrust/lift ratio.

travel downwind, the area of the bow cushion decreases; meanwhile, the hydrodynamic drag on the bow and side skirts increases rapidly, which leads to increased bow pitching down moments, consequently the vicious circle concerned with drag and pitching bow down moments occurs, finally leading to capsizing of the craft.

Figure 4.49 shows the hydrodynamic lift moment increasing with the angle of the bow pitching down, which gives a restoring moment and the increased bow skirt drag (which causes the bow pitching down moment), as well as the cushion pressure reduction.

To sum up, the total bow pitching down moment increases with the angle of the bow pitching down, which may be seen in Fig. 4.49. Therefore the tuck-under of the bow skirt caused by the bow pitching down moment will normally be the direct reason causing the plough-in.

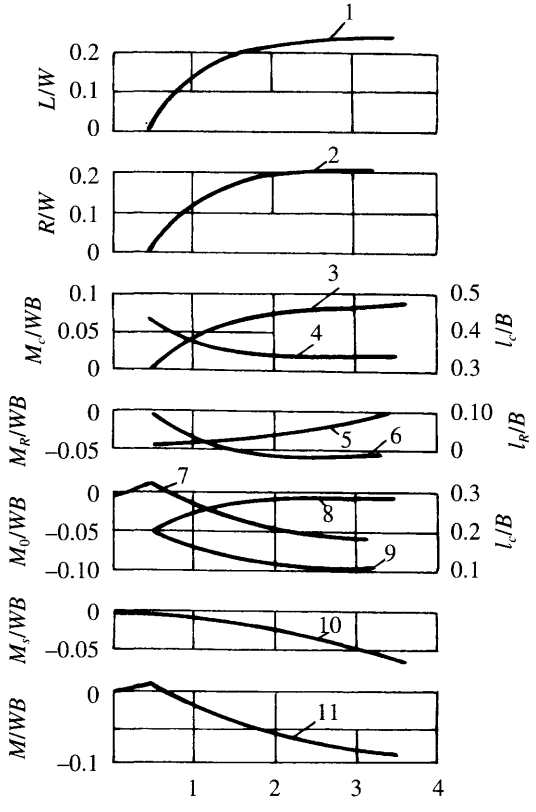

Fig. 4.49 Relation between various recorded forces on craft and trim angles. 1: Bow skirt, 2–6: bow skirt, 7: moment ratio due to *pc*, 8: moment ratio, rear cushion, 9: moment ratio fore cushion, 10: moment ratio, spray drag, 11: overall moment ratio.

4. In the case where the plough-in occurs with drifting motion, the resultant of such action might lead to capsizing of the craft. A large heeling angle and subsequent capsizing of the craft will be even more likely as a result of a high-speed plough-in while the craft is also drifting. Table 4.8 shows the speed range which might cause plough-in and capsizing [50]. It may be seen that the plough-in might occur in the case of $Fr < 0.7$, and it might lead to overturning if the drift angle was larger than 50°.

   This represents the experimental results from work carried out by Crago at the end of the 1960s. Owing to designers' efforts in recent years, the speed range where

Table 4.8 The speed range of ACV and *Fn* in which the plough-in and capsizing of craft may occur [48]

Items	High speed	Moderate speed	Low speed
Froude number Fn_B	1.7 or more	0.5–1.7	0.4 or less
Plough-in start	Probable	Impossible*	Impossible
Overturning	Probable in the case of drifting angle larger than 50°	Low probability	Probable according to motion records

* It is very difficult to overturn the ACV, but plough-in might be initiated in this speed range in the case of plough-in of craft at high speed and dropping down to this speed range.

positive stability is practical has been greatly extended, and sensitivity to plough-in and capsizing has been significantly reduced.

Figure 4.50 shows the relation between craft capsizing and drifting angle, in which the solid line denotes the position of the craft during turning using air rudders at the beginning of turning and then keeping the rudder in a central position. It can be seen that the drift angle remains stable. The dashed line denotes the position of the craft during turning using the rudder at a constant angle from the beginning to the end of turning. Here it can be seen that the ACV overturned at the drifting angle of approximately 70°.

Measures for improving resistance to plough-in and overturning

(A) Cushion and skirt air supply system

1. Keep a definite reserve on fan inflow rate and so increase the speed of fan, air gap, especially, the air supply flow rate at bow. If necessary, to increase the bow air gap and restore the running attitude to normal (in time), in the case where the craft develops a bow pitching down trim. It is very effective to provide a special air duct to supply pressured air to the cushion at the bow in order to improve the plough-in resistance. This has been validated by model experiments and modifications to many ACVs in the UK as well as China.
2. Use a separated duct system (or separate fan(s)) for supplying the pressured air to fore and rear cushion and skirt bags or loops.
3. Improve the cushion compartmentation for fore and rear cushion.

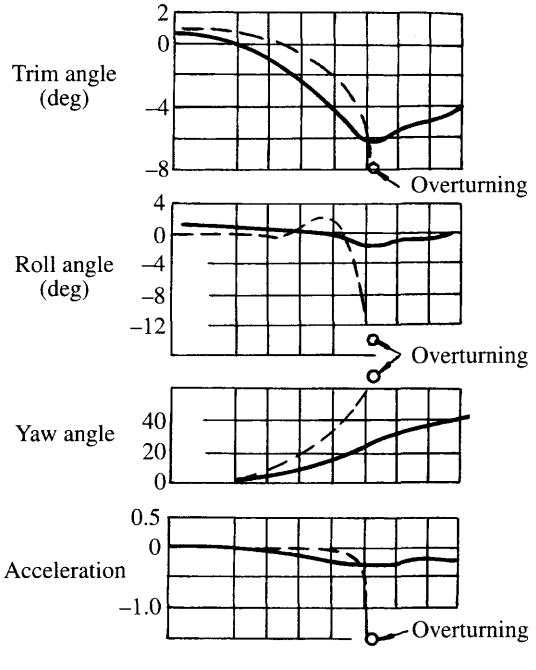

Fig. 4.50 Influence of yawing angles on the overturning of craft.

4. Increase the bag–cushion pressure ratio of skirt bags and the bow skirt separately if the bag is divided, to increase the stiffness of the bag of the bow skirt.

(B) Skirt systems

1. Install diaphragms in a D-type skirt bag at the bow to enhance the ability to prevent tuck-under. Figure 4.51 demonstrates the experimental results of a skirt carried out on a water circulating tank, which predicts in quality the effect of the tightness of a D-type bag and its diaphragms on the plough-in resistance of the craft. This is one of the general measures for plough-in resistance which is currently widely adopted in China.
2. Decrease the drag due to the contact of the skirt fingers with the water surface to prevent tuck-under of the bow skirt fingers.

   A large number of small air lubrication holes were fitted at the lower hem of the bow bag of the British SR.N6, so that air leaking from the cushion through the holes and along the outside of fingers at the water surface lubricated the contacting surface of the finger with the water surface and reduced the drag dramatically at a negative pitching angle, reducing the tuck-under of the fingers as shown in Fig. 4.52.

   This idea has not been developed further, as BHC redesigned the bow bag of later skirts, moving the fingers forward and increasing the bow bag radius (the bulbous bow bag). This skirt geometry creates increasing stability moments as the bow is trimmed down and so has 'safe' plough-in characteristics – see Chapter 7.
3. Careful manufacture of the skirt, to give an even bag or loop hem line and even segment or finger tip line (tidy the skirt geometry) decreases the dynamic drag, especially at the rear corners and reduces uneven loads within the skirt, which can contribute to ACV instability.
4. Adopt skirt-lifting equipment to control the height of the stern skirt, and so the trim angle of the craft.

(C) LCG Include ballast tanks, horizontal fins and duct valves, etc. to control the trim angle of the craft, especially in the case of travelling downwind, to increase the ability to trim bow up dynamically.

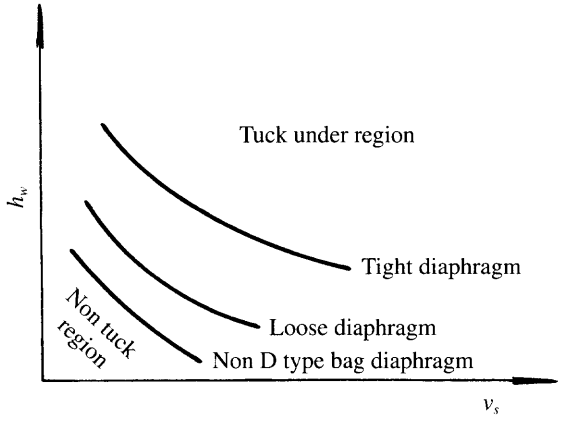

Fig. 4.51 Influence of craft speed, immersion height of skirt fingers h_w and the tightness of diaphragm of D-type skirt bags on plough-in of craft.

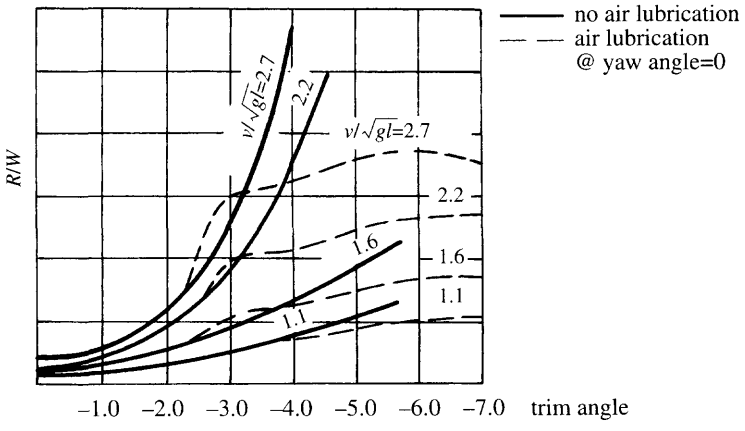

Fig. 4.52 Relation between the lift-drag ratio and trim angle of ACV.

(D) Driver technique Improve the drivers' technique for preventing the plough-in of craft and understanding the operational boundary curve for avoiding plough-in. Figure 4.53 shows the operational boundary for preventing plough-in on British ACV model SR.N6. Drivers have to take care during operation to avoid large drifting angles for overturning.

(E) Hull design It is not possible to completely avoid the possibility of plough-in on an ACV or SES. The designer should therefore investigate the attitute of the lower hull in the case of a bow-on or side-on collapse of the leading skirt. The hull lower plating, or the configuration of the deflated skirt drawn back over the hull structure, should form a planing surface with between 5 and 10° trim to the water surface. The moment arm of the resulting drag and lift forces from the planing surface should provide a righting moment sufficient to stabilize the craft at the roll or pitch angle from the plough-in.

4.7 Overturning in waves

Accidents of this type have occurred to ACVs as shown in Table 1.4. SR.N6–012, running on a passenger route between Portsmouth and Ryde, Isle of Wight, in England, overturned in March 1972, a result of the combined action of wind and waves. The craft flooded, which led to capsizing due to the waves and the deaths of five passengers.

This is the biggest tragedy in ACV/SES transport history to date. Figure 4.54 [51] describes the situation of the ACV at that time. Owing to the large winds and waves, the driver decided to navigate the craft along the beach. However, the surf close to the beach was very steep and acted with the wind and tide on the craft which had to run in beam seas and this caused the craft to roll severely, the side skirt to tuck under at the trough of a wave and then the craft capsized.

At that time the wind speed was about 60 knots, wave height 4.6 m, the speed of

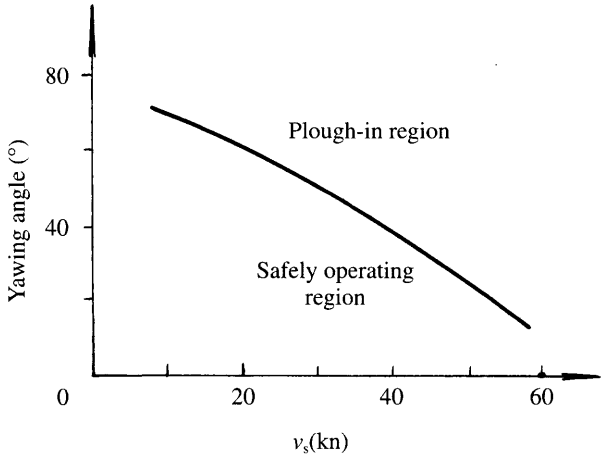

Fig. 4.53 The plough-in boundary of SR.N6.

circular motion of water particles 11 knots and speed of tide flow was about 4 knots. It is clear that part of the fault was due to incorrect craft navigation, but at least it teaches us a lesson that while it may seem safe to navigate a craft along the beach, as a matter of fact it is not safe due to the high surf which could act on the craft to capsize it in heavy weather.

Following this accident, the UK government set up an investigation, which included a major study of hovercraft stability including parametric model tests of several current large craft designs to identify possible improvements, particularly to the skirt systems [48]. This study produced much useful information and led to the development of the bulbous bow skirt, the tapered skirt and revised cushion feed designs. Some of these items have been introduced above, the remainder will be described in Chapter 7.

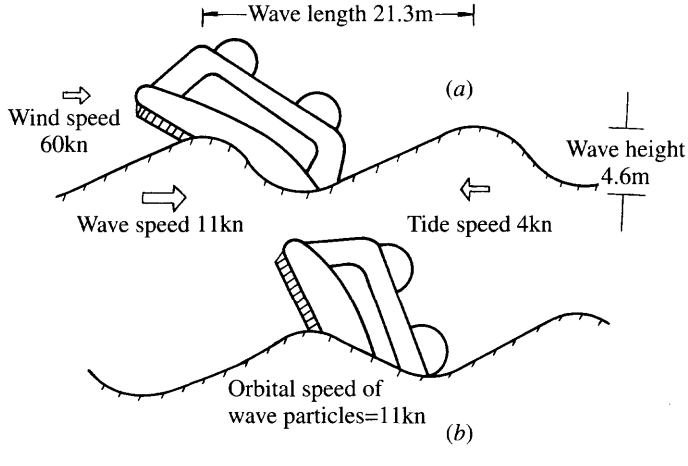

Fig. 4.54 The overturning of SR.N6 in very steep beam waves.

5

Trim and water surface deformation under the cushion

5.1 Introduction

Dynamic trim is determined by equilibrium of the steady forces acting on the ACV or SES at speed. The trim will affect drag forces acting on the craft and therefore its ability to accelerate through hump speed to the operational cruising speed. The main purpose of this chapter's investigation is therefore to enable estimation of craft trim at various speeds and identify the optimum values.

The starting point for determination of equilibrium is the centre of pressure of the cushion for an ACV and in addition the force vector which results from the hydrodynamic force acting on the hulls of an SES or through the skirt. This may be compared with the forces acting on the hull of a planing boat or catamaran.

An important difference from conventional ships regarding determination of the hydrodynamic force and moment is caused by the inner water surface under the pressurized cushion. Conventional ships have only an outer draft, while the ACV and SES have both inner and outer drafts. The inner water surface profile is very difficult to observe, though a number of model experiments have been carried out to verify analytical models developed using classical hydrodynamic theory in the 1960s and these have largely confirmed analysis.

The SES has water propellers or water jets and other underwater appendages which will affect its dynamic trim in a similar way to a fast planing craft. The amphibious ACV on the other hand normally has air propellers or fans which induce pitching moments and fins and elevators or elevons to control dynamic trim. The ACV and SES are also both affected by the trimming moments from aerodynamic drag and lift of the hull and superstructure above the water profile.

Considering first the dynamic equilibrium of the cushion itself, the craft dynamic trim, including inner and outer drafts and trim angle, is influenced by a number of design and performance parameters of the craft as follows.

Trim

Trim is influenced by many cushion characteristic parameters, for example:

- position of cushion LCP;
- bow/stern skirt clearance (air gap) over the base line;
- cushion pressure ratio of air supply from lift fans and thus skirt stiffness;
- position of LCG based on distribution of craft mass, payload and ballast;
- position of the thrust line and thus dynamic trimming moments.

Bow and stern seal interaction

The inner water surface at bow and stern seals will influence skirt drag and trimming moment, particularly in the case of craft take-off through hump speed.

Wetted surfaces

The geometry of inner/outer water surfaces will directly influence wetted surface and friction drag of sidewalls (SES) and side skirts (ACV).

Location of SES inlets and appendages

The design and location of water-jet propulsion inlets, cooling water inlets, propellers, rudders and stabilizer fins, are all influenced by the shape of the inner/outer water surface. At the same time all of these items introduce thrust or drag forces affecting the craft's dynamic trim.

Some early SES projects at MARIC suffered a lot from imperfect selection of water-jet inlet locations. The water-jet propulsion inlet of SES model 717 and water-cooling pump of SES model 713 were not ideally positioned when first built. Due to lack of knowledge about the inner/outer water surface shape, MARIC located the inlet of the water-cooling pump of SES 713 inside the air cushion and the inlet of water-jet propulsion of SES 717 at the outer wall of the sidewalls. Air was ingested into the inlet of both these systems in the course of take-off through hump speed.

On SES model 713, the air ingesting into the cooling water pump led to air blockage of the system and interrupted the circulation of the cooling water. Thus the temperature of cooling water rose rapidly, sometimes up to 95°C, which was very dangerous for the engines. As for SES model 717 with water-jet propulsion, the craft sometimes did not pass though hump speed due to air ingestion into the water-jet pump, decreasing thrust. Both these problems almost became stumbling blocks for SES development in their early phase of research in China, arising from lack of knowledge concerning the dynamic trim of ACV/SES.

Figure 5.1 shows a picture of the inner and outer draft of model sidewalls taken from a towing tank model. Figure 5.2 shows the deformed water surface inside the craft cushion, obtained by the theoretical calculation. It may be noticed that a large hollow in the water surface at the rear and centre parts of the cushion occurs at Froude numbers close to 'hump speed', the transition between displacement mode and planing mode of operation. It is this that caused the air ingestion which happened

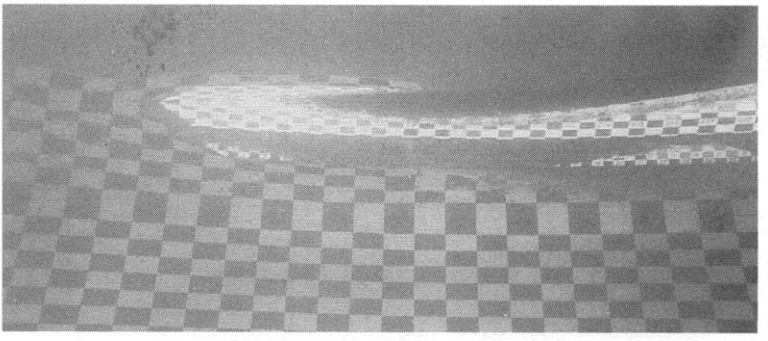

Fig. 5.1 Picture showing water surface deformation in/off cushion during model tests in towing tank.

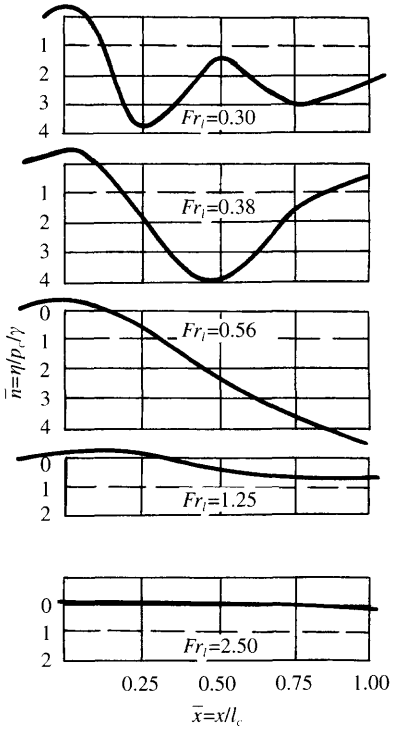

Fig. 5.2 Wave profile inside a cushion at various Froude numbers.

on early SES in China, for example, the air ingestion into the water cooling pump in SES model 713 and into the water propulsion system for model 717 and WD-901.

The depth of the wave hollow inside the cushion is equal to four times the cushion pressure depression, i.e. $\bar{n} = \eta\ [p_c/\gamma] \cong -4$ where η denotes wave hollow depth inside the cushion, p_c, the cushion pressure (N/m^2) and γ the weight density of water (N/m^3,$\gamma = \rho_w\, g$, where ρ_w is normally taken as 998.4 kg/m^3 at 20°C and g as 9.81 m/s^2). Once the overall craft trim has been estimated at primary hump speed, it may therefore be

necessary to adjust the sidewall lines over the stern half of the vessel to ensure intakes and propellers stay fully immersed.

Internal stability skirts

The design of longitudinal and/or transverse stability skirts inside the cushion of an ACV strongly affects dynamic trim. The deeper these skirts, the larger the water drag, due to skirt wetting in the complex internal cushion wave pattern. The shallower these skirts are, the less effective they are. Determination of the optimum for a particular craft is only practical through parametric model tests in a towing tank, or trial and error with a prototype, which is likely to be rather more expensive.

Basic concepts for design

Misunderstanding of some basic concepts may lead to incorrect choices being made for craft design, trials and analysis. For example:

- Does the trim characterized by outer drafts of the craft at bow and stern represent the apparent or real trim angle of the craft?
- What is the relation between the trim angle formed by the outer water surface and the trim angle formed by the inner water-line?
- Is the craft's trim drag defined by the trim angle at the outer or inner water-line?
- What is the relation between the trim drag and wave slope induced by moving cushion pressure?

These problems are not immediately obvious without some practical experience of ACV behaviour and in some cases have been inaccurately described in the technical literature.

It can be seen that determination of ACV dynamic trim at different speeds is somewhat complicated and should be carefully dealt with during the design process. Based on a clear understanding of the basic concepts, one can solve the design problem by the method of initial predictions using theoretical analysis, later correlated with experimental testing.

In order to understand the interaction of craft dynamic trim with the cushion inner water surface, the water surface inside the cushion can be observed either by periscope in a model test [52], or by direct observation via a transparent window on a craft sidewall. This has been carried out in SES model 713. The outer water surface can be determined by photos as shown in Fig. 5.1.

5.2 Water surface deformation in/beyond ACV air cushion over calm water

ACV moving over deep water

When an ACV hovers statically on water, a depression will be formed between the inner and outer water surface, the depth of which will be

$$\eta = -p_c/\gamma$$

where η is the depth of depression, upward positive.

In the case of a craft moving over a water surface, the dynamic deformation of the water surface caused by the ACV has to be determined. According to linear water wave theory, when an air cushion with the length of L, beam of b and pressure distribution of $p(x,y)$ running on the free surface of calm water with the depth of H at constant speed of c, the disturbance velocity potential can be written by [53]

$$\phi = \frac{-\mathrm{i}}{4\pi c\rho_w} \int_{-\pi}^{\pi} \sec\theta \int_0^{\infty} AB \, \mathrm{d}k \int_{-\infty}^{\infty} \int_{-\infty}^{\infty} C \, \mathrm{d}m \, \mathrm{d}n \tag{5.1}$$

where

$$A = \frac{\mathrm{e}^{\mathrm{i}k(x\cos\theta + y\sin\theta)}}{k - [g/c^2]\tanh kH(\sec\theta)^2 + \mathrm{i}\mu/c\sec\theta}$$

$$B = \frac{\cosh k(H+z)}{\cosh kH}$$

$$\mathrm{C} = p(m,n)\,\mathrm{e}^{\mathrm{i}k(\mathrm{m}\cos\theta + n\sin\theta)}$$

and c is the moving velocity of the cushion (m/s), H the water depth (m), m,n any given variate, g the acceleration of gravity (9.81 m/s^2), ρ_w the water density (kg/m^3), (sea water 1021 at 20°C, fresh water 998.2 at 20°C), r the aspect ratio of the air cushion, $r = b_c/l_c$ and μ the dynamic viscosity coefficient (Ns/m^2) (1.3 at 10°C, 1.009 at 20°C, 0.8 at 30°C).

Assuming the pressure of the rectangular air cushion to be uniformly distributed, then the exciting disturbance potential can be written as

$$\phi = \frac{\mathrm{i}p_c}{\pi^2 c\rho_w} \int_{-\pi}^{\pi} \sec\theta \, \mathrm{d}\theta \int_0^{\infty} DBEF\,k \, \mathrm{d}k \tag{5.2}$$

where

$$D = \frac{\mathrm{e}^{-\mathrm{i}k(x\cos\theta + y\sin\theta)}}{k - [g/c^2](\sec\theta)^2\tanh kH + \mathrm{i}\mu/c\sec\theta}$$

$$E = \frac{\sin(kl\cos\theta)}{k^2\cos\theta\sin\theta}$$

$$F = \frac{\sin(krl\cos\theta)}{k^2\cos\theta\sin\theta}$$

Thus, the water surface deformation should meet the relation

$$\eta = \frac{l}{c}\left[\frac{\partial\theta}{\partial x}\right]_{x=0} - \frac{p_c}{\gamma} \tag{5.3}$$

where x, y, z form the perpendicular coordinates, x denotes the direction of air cushion movement and forward positive z denotes the vertical coordinate, upward positive.

The water surface deformation caused as the air cushion with uniformly distributed pressure moves forward may be defined by equations (5.2) and (5.3).

To determine the actual water surface profile, one has to take into account both the depression of the water surface induced by the air cushion hovering statically over the water and the water surface deformation caused by the air cushion moving on the water, i.e. the ratio between the x direction component of disturbing velocity on the free surface and its forward velocity.

Calculated results are shown in Fig. 5.3, where it can be seen that the water surface deformations will be rather different between in and beyond the cushion, and are a function of Froude number. Figs 5.4–5.6 show calculation results selected from ref. 54. They can be compared as follows:

1. From Fig. 5.4, it is found that the bow wave amplitude in the cushion is equal to that beyond the cushion. At high values of Fr_1 the bow water surface deformation both in the cushion and also beyond the cushion decreases so as to keep the same value. This agrees with test results.

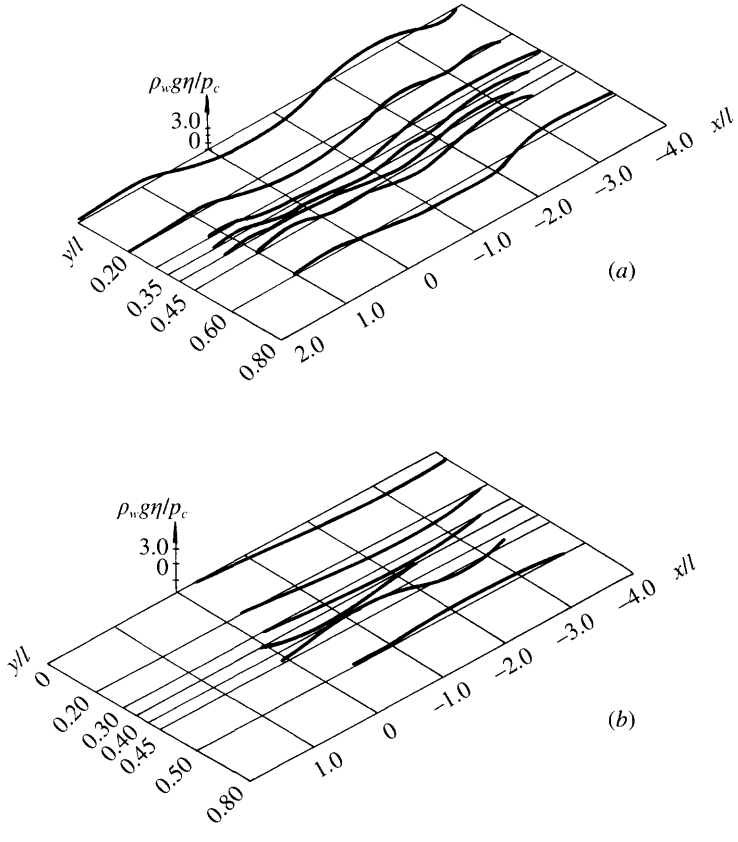

Fig. 5.3 Water surface deformation due to a moving air cushion pressure distribution $b/l = r = 0.4$: (a) vertical displacement of free water surface at $Fr = 0.9$, (b) vertical displacement of free water surface at $Fr = 3.0$.

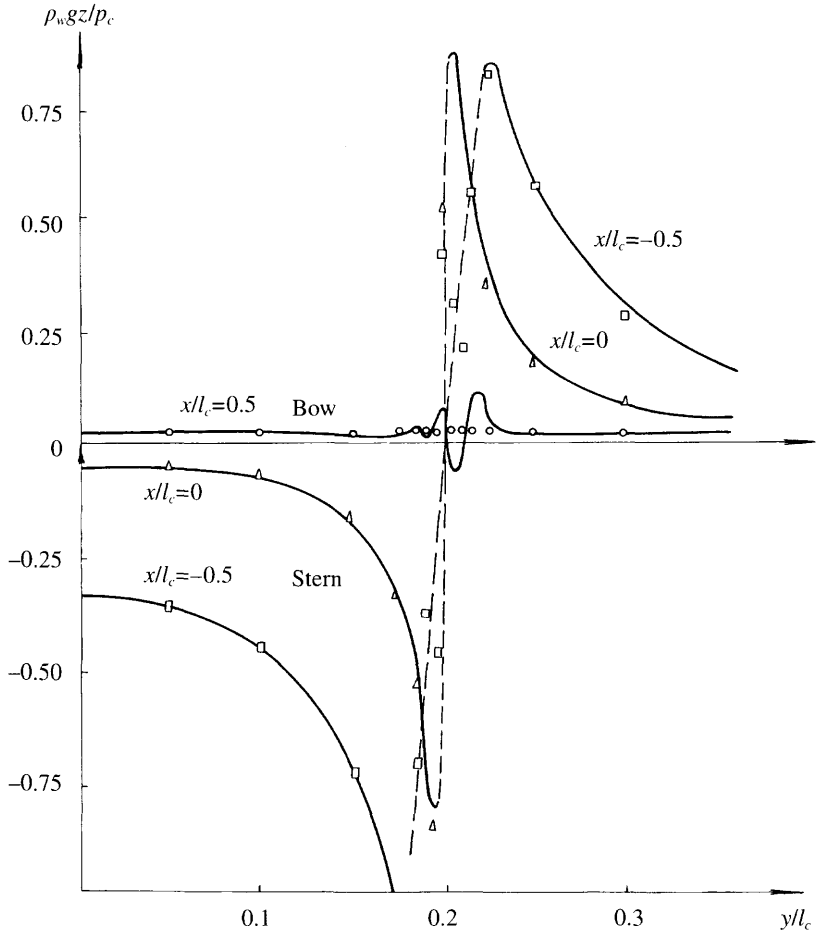

Fig. 5.4 Wave profile in/off cushion due to a moving rectangular air cushion at zero yawing angle and Fr = 2.12, r = 0.4, where the origin point of co-ordinates is at amidships, bow positives.

2. Behind amidships, particularly at the cushion stern, the water surface descends dramatically at hump speed (Fn = 0.56), the depth of depression can reach up to 3–4p_c/γ (see also Figs 5.5 and 5.2).
3. The height of the water surface changes suddenly from inside the cushion to beyond the cushion (see Figs 5.1 and 5.6). The water surface deformation is also different in the transverse (y) direction.
4. The actual depth of the water surface depression in the cushion is greater than found by calculation (see Fig. 5.6) [54]. This may be due to neglecting viscosity effects of the water as a real fluid and its surface tension, as well as the assumption of linear equations for potential flow in calculation.

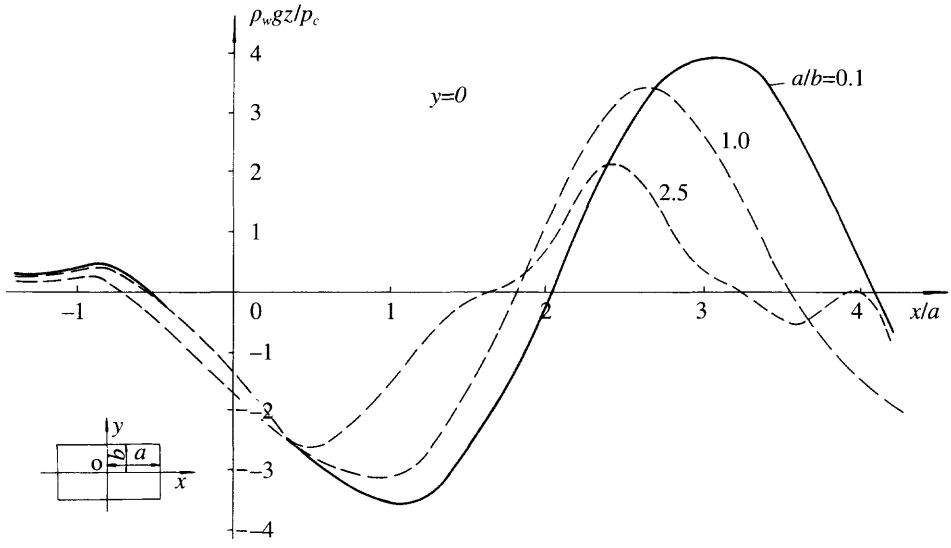

Fig. 5.5 Deformation of water surface of ACV at $Fr = 0.57$ on centreline for different a/b.

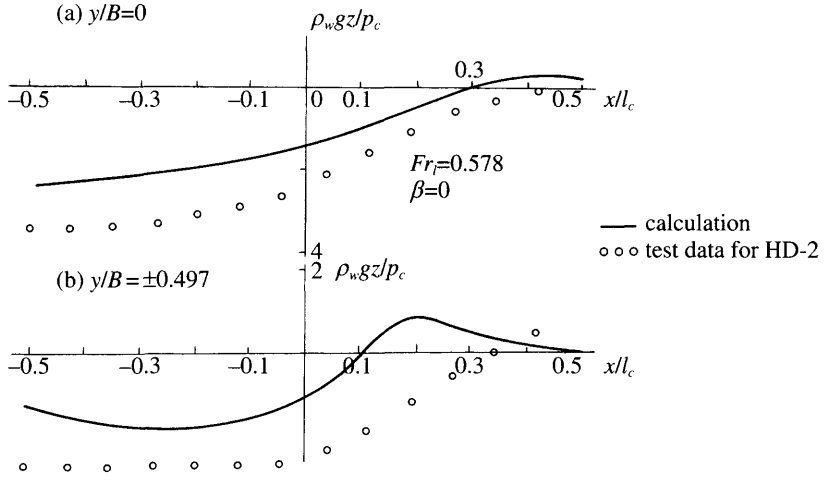

Fig. 5.6 Comparison of water surface deformation of craft HD-2 between calculation and test results. (a) at centreline; (b) in cushion but in close proximity to cushion peripheral boundary.

ACV over shallow water

In shallow water, tanh kH [53] can be considered as a small value, i.e. tanh $kH \cong kH$ and cosh $kH \cong 0$. Then, when $l/H > 10$, the analytical expressions (5.2) can be simplified as

$$\phi = \frac{\mathrm{i}p_c}{\pi^2 \rho_w g} \int_{-\infty}^{\infty} \sin \beta \, rl \, \mathrm{e}^{-\mathrm{i}\beta y} \frac{\mathrm{d}\beta}{\beta} \int_{-\infty}^{\infty} G \, \mathrm{d}\alpha \tag{5.4}$$

where

$$G = \frac{\text{sind. } l e^{i\alpha x}}{H(\alpha^2 + \beta^2) - Fn_H^2 \alpha^2 H - \text{ic}\mu a/g}$$

$$Fn_H = \text{c}/(gH)^{0.5}$$
$$\tan\theta = \beta/\alpha$$
$$\gamma = b/l$$

This equation can be developed into an algebraic equation for practical use:

1. When $Fn_{\text{H}} > 0$, let

$$\mathbf{a} = (x - l)/[l\,(Fn_H^2 - 1)^{0.5}]$$

$$\mathbf{b} = (x + l)/[l\,(Fn_H^2 - 1)^{0.5}]$$

$$\mathbf{c} = [\text{sgn}(-\mathbf{a} + r - y/l) + \text{sgn}(\mathbf{a} + r - y/l) + \text{sgn}(-\mathbf{a} + r + y/l) + \text{sgn}(\mathbf{a} + r + y/l)]$$

$$\mathbf{d} = [\text{sgn}(-\mathbf{b} + r - y/l) + \text{sgn}(\mathbf{b} + r - y/l) + \text{sgn}(-\mathbf{b} + r + y/l) + \text{sgn}(\mathbf{b} + r + y/l)]$$

$$(\rho \text{w}\, g\, \eta)/p_{\text{c}} = [Fn_H^2/(4(Fn_H^2 - 1)]\mathbf{c}H(1 - \text{x/l}) - \mathbf{d}\,H(-1 - x/l) - 0.25[\text{sgn}((y/l) + r) - \text{sgn}((y/l) - \text{r})]\,[\text{sgn}((x/l) + 1) - \text{sgn}((x/l) - 1)] \quad (5.5)$$

2. When $Fn_H < 1$, let

$$\mathbf{e} = \arctan\,[rl|\text{x} - \text{l}|\,(1 - Fn_H^2)^{0.5}]/[\,(x - l)^2 + (y^2 - r^2 l^2)\,(1 - Fn_H^2)]$$

$$\mathbf{f} = \arctan\,[rl|\text{x} + \text{l}|\,(1 - Fn_H^2)^{0.5}]/[\,(x + l)^2 + (y^2 - r^2 l^2)\,(1 - Fn_H^2)]$$

$$(\rho \text{w}\, g\, \eta)/p_{\text{c}} = [Fn_H^2/(2\pi(1 - Fn_H^2)]\,\mathbf{e}\,\text{sgn}((x/\text{l}) - 1) - \mathbf{f}\,\text{sgn}((x/l) + 1) - 0.25\,[\text{sgn}((y/l) + \text{r}) - \text{sgn}((y/l) - r)]\,[\text{sgn}((x/l) + 1) - \text{sgn}((x/l) - 1] \quad (5.5a)$$

where

$$\text{sgn}\,(x) \begin{cases} 1 & \text{when} \quad x > 0 \\ 0 & \quad\quad\; x = 0 \\ -1 & \quad\quad\; x < 0 \end{cases}$$

and $H(x)$ is the unit step function.

The wave-making of an ACV running over shallow water can be calculated according to equations (5.5) and (5.5a) in the case where $Fn_H = (v/(gH)^{0.5}) > 1$. The maximum height of the wave can be simplified [55] as

$$\begin{aligned} a_0 &= 1/(Fn_H^2 - 1) \\ a_1 &= Fn_H^2\, a_0/2 \\ \alpha &= \arctan\left[1/\left(Fn_H^2 - 1\right)^{0.5}\right] \end{aligned} \tag{5.6}$$

where Fn_H is the Froude number at the particular water depth, v the craft speed (m/s) and H the water depth (m), see Fig. 5.8 below.

The wave-making in/beyond an air cushion running over shallow water can be estimated approximately by means of Fig. 5.7 and equation (5.6). This method is rough, but it is very practical. Figure 5.7 shows the calculation and test results. It may be noticed that theoretical prediction and test results compare well. Figure 5.7 is suitable for conditions where $Fn > 1.38$ and $l/H < 10$, where l denotes the length of air cushion.

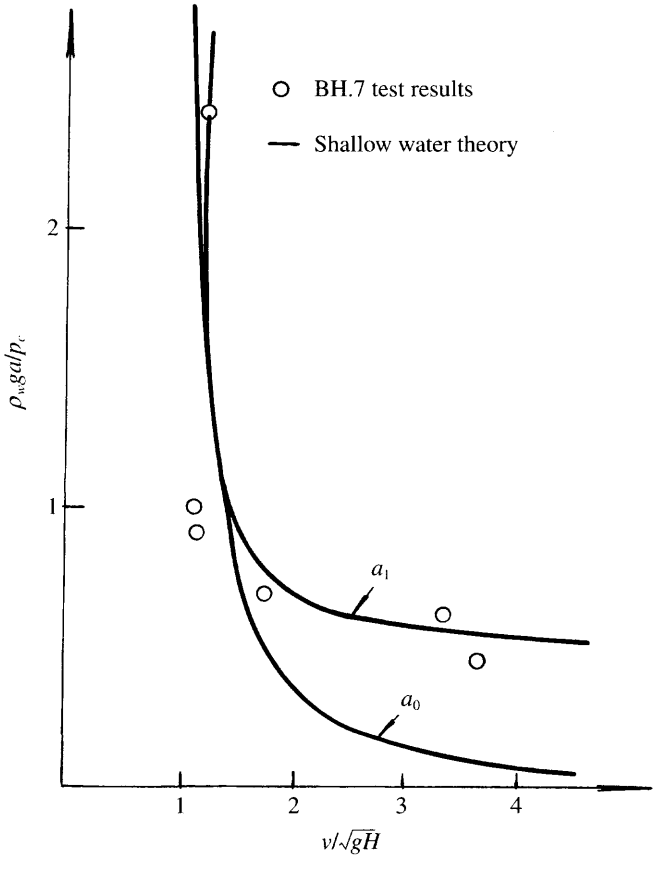

Fig. 5.7 Comparison of non dimensional wave amplitude between the calculation by shallow water wave theory and test results on BH.7.

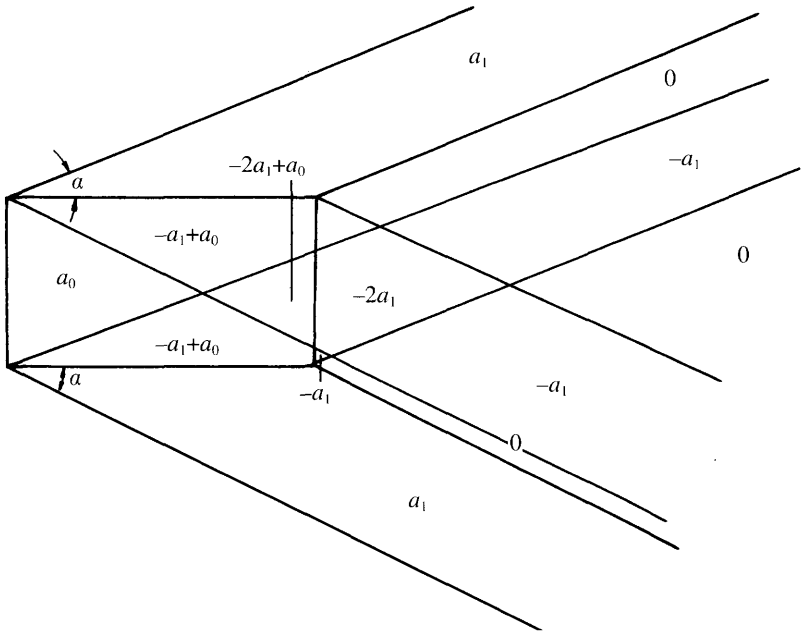

Fig. 5.8 Wave amplitude due to an ACV on shallow water in/off air cushion.

5.3 Water surface deformation in/beyond SES air cushion on calm water

The wave-making of an SES moving on water is different from that of an ACV, resulting from immersion of the two sidehulls in the water. Thus in addition to wave-making induced by the air cushion, the interference of wavemaking between two sidewalls and sidewalls with the air cushion has to be considered.

Based on Standing's formula [54], senior research engineer H. Z. Rong of MARIC developed the wave profile calculation of an ACV into that for an SES [32]. He assumed that the flow around the craft was uniformly distributed, incompressible, non-viscous, with no vortex flow and that the wave height was small with respect to the wave length.

On this basis he established a mathematical model for an SES running at constant speed over water with infinite depth, namely distributed Kelvin sources on the surface of calm water (i.e. the pressure surface at $z = 0$) and on the centre longitudinal plane of both sidewalls (i.e. $r = b$) and also distributed a Kelvin doublet (source/sink) on the surface extending as far as infinity. The coordinate system is as shown in Fig. 5.9.

Using linear water wave theory [56], the equation which defines the disturbing velocity potential and its boundary condition can be obtained and the ϕ broken down into

$$\phi = \phi^{P} + \phi^{R} + \phi^{L} + \phi^{M} \tag{5.7}$$

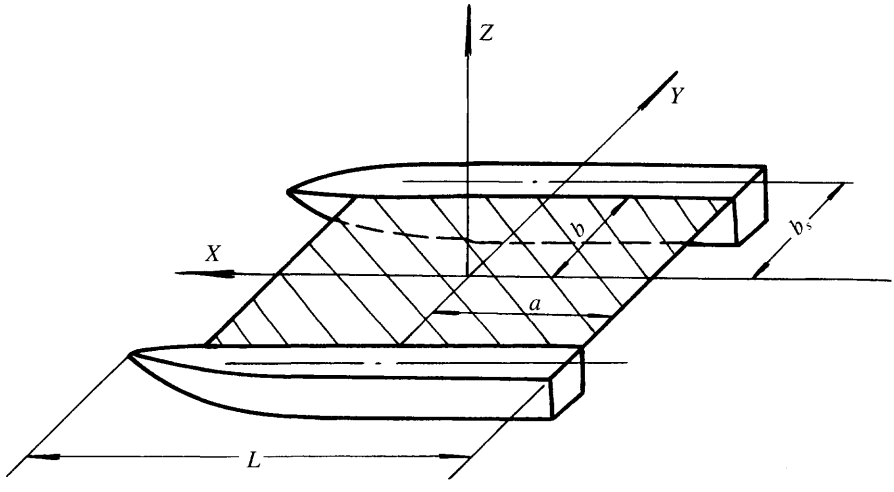

Fig. 5.9 Co-ordinate system and principal dimensions of SES for calculating the inboard/outboard wave profile of SES running on calm water.

where the ϕ^P denotes the distribution of pressure sources on the cushion surface, ϕ^R, ϕ^L the source distribution on the centre longitudinal sidewalls, and doublet ϕ^M the action of interference caused by various factors, each of them meeting the given equations and their boundary conditions. Meanwhile, the amplitude of water surface deformation can also be broken down as follows:

$$\eta = \eta^P + \eta^R + \eta^L + \eta^M \tag{5.8}$$

The terms on the right-hand side in equation (5.8) denote the deformation of the water surface induced by each equivalent source. Figures 5.10 and 5.11 show a comparison of wave profile between calculations and experimental results on the inside ($y = b$) and outside ($y = 1.2b$), of the sidewalls. Experiments were carried out in a towing tank and the results were obtained by analysing photographs. From comparison of the results, MARIC have concluded as follows:

1. The calculated results show that the wave amplitude induced by cushion air pressure is the main component of the total wave height. The wave amplitude induced by interference of both sidewalls and cushion pressure is small relative to the former.

   It may be noted that the volume displacement of sidewalls of this craft only occupy 10% of craft displacement. For an air cushion catamaran with wider sidewalls and larger sidewall displacement, the interference effect will increase somewhat. The cushion pressure induced wave components are nevertheless dominant.

   The theoretical results generally agree with the tests, which means that the influence of thin sidewalls on the deformation of the water surface induced by cushion air is small.
2. The fluctuations of calculated wave profile (η) shown in Fig. 5.11 may be a reflection of the linear equation used as a mathematical model. In practice the fluctuation can be smoothed by nonlinearity of real water waves and viscosity effects.

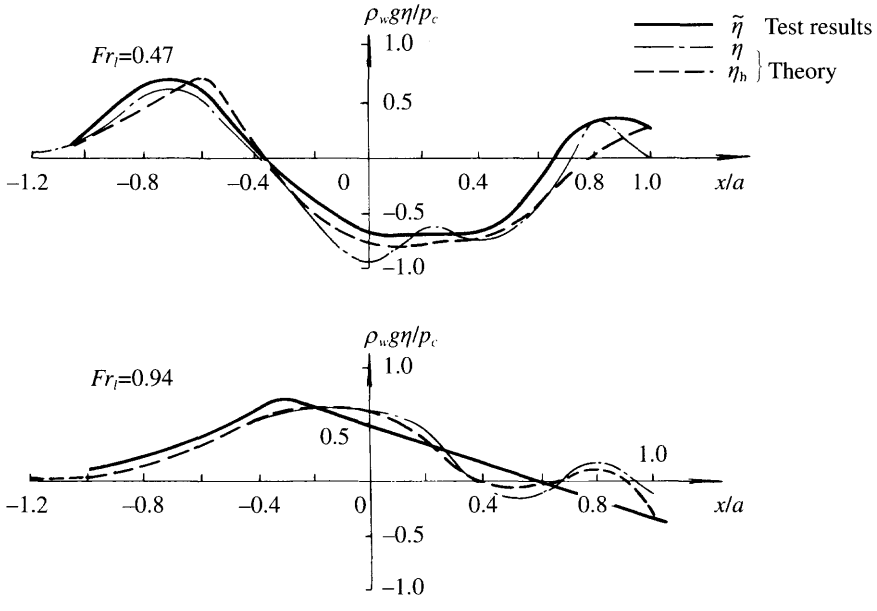

Fig. 5.10 Calculation and experimental results of wave profile at outside of sidewall on model 7205.

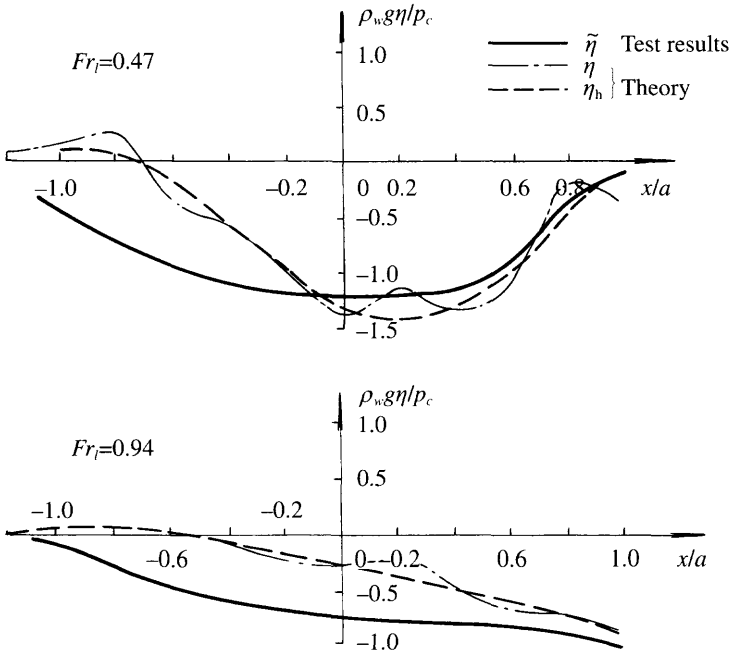

Fig. 5.11 Calculation and experimental results of wave profile at inside of sidewall ($y = b$) on model 7205.

3. In the same way as that in Fig. 5.6 [54], the actual depression in the deformed water surface is deeper than that obtained from calculations.

5.4 Dynamic trim of ACV/SES on cushion over calm water

A theoretical method for predicting ACV/SES dynamic trim over calm water

We take the SES as an example to calculate the dynamic trim. The calculation method predicting the dynamic trim of an ACV on cushion is similar to that of an SES.

Factors determining the dynamic trim of an SES on cushion are numerous, e.g. craft speed (*Fn*), LCG, configuration of sidewalls, lift fan flow rate and total pressure, cushion length/beam ratio, cushion pressure/length ratio and skirt clearance over the water surface.

The determination of dynamic trim of a craft on cushion has to meet the following conditions:

1. The craft weight must be equal to the sum of buoyancy components and exerting forces, such as lift of air cushion, the static buoyancy and dynamic lift force of sidewalls, the static and dynamic lift force of the bow/ stern seals.
2. The moments of these forces about the CG of the craft must be equal to zero.
3. The inflow and total air pressure of fans must satisfy the air duct characteristic curve and the hovering characteristics of the craft.
4. The water surface elevation (both inboard and outboard of the sidewalls) must follow the wave profiles generated by a uniform distribution of cushion pressure travelling over the calm water at constant speed.

We also make the following assumptions:

1. Owing to the absence of longitudinal and transverse stability keels in the air cushion, the air pressure of the cushion is assumed to be spatially constant, while the craft speed is not very high. This was validated approximately by trials of the craft model 717.
2. Sidewall wave-making effect on dynamic trim and water surface elevation may be neglected.
3. The air cushion is assumed to be incompressible, i.e. the air density in the cushion is constant.

The typical dynamic trim of SES running over calm water on cushion is shown in Fig. 5.12, where we define that:

t_{bo} = outer draft of the sidewall at bow
t_{bi} = inner draft of the sidewall at bow
t_{so} = outer draft of the sidewall at stern
t_{si} = inner draft of the sidewall at stern
z_b = vertical distance between the lower end of bow seal and baseline
z_s = vertical distance between lower end of stern seal and base line
SL = sea level
WL_o = outer water-line
WL_i = inner water-line

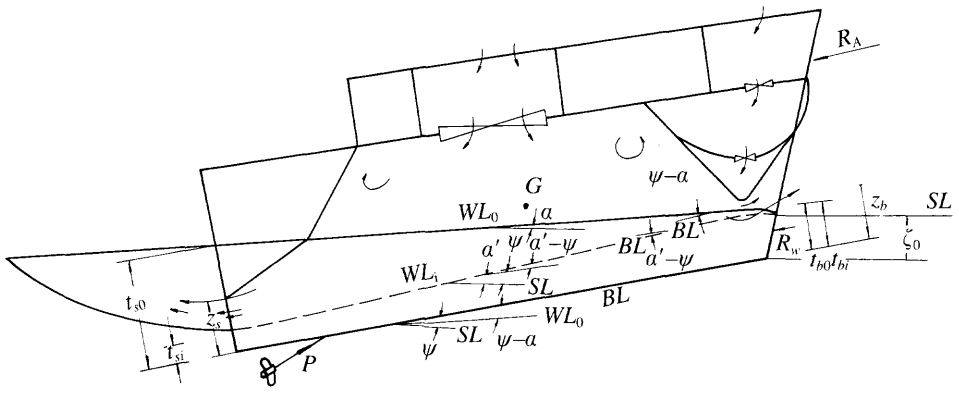

Fig. 5.12 Sketch of running attitude of SES running on calm water.

α	=	the slope angle of the outer wave surface to the horizontal plane
α'	=	the slope angle of the inner wave surface to the horizontal plane
ψ	=	trim angle of craft to the horizontal plane
ψ-α	=	apparent trim angle, which can be calculated by the outer water-line
ζ_0	=	vertical distance between the base-line of craft at bow and sea level
z_{bi}	=	wave elevation at bow inside cushion
z_{bo}	=	wave elevation at bow outer cushion
z_{si}	=	wave elevation at stern inside cushion
z_{so}	=	wave elevation at stern outer cushion

Then the wave steepness for both inner and outer water-lines can be written as

$$\begin{aligned} t_{bi} &= \zeta_0 + z_{bi} \\ t_{bo} &= \zeta_0 + z_{bo} \\ t_{so} &= \zeta_0 + z_{b0} + l_c \tan(\psi - \alpha) \\ t_{si} &= \zeta_0 + z_{bi} - l_c \tan(\psi - \alpha') \end{aligned} \tag{5.9}$$

where l_c is the cushion length.

Owing to the small values of ψ, α which are smaller than 5°, the effect on the value mentioned above can be neglected, and the wave steepness for both inner and outer water line can be written as

$$\begin{aligned} \tan\alpha &= (z_{so} - z_{bo})/l_c \\ \tan\alpha' &= (z_{bi} - z_{si})/l_c \end{aligned} \tag{5.10}$$

where $\tan\alpha$ is the steepness of the outer wave surface and $\tan\alpha'$ the steepness of the inner wave surface.

Because the elevation of both the inner/outer wave surface can be obtained by the calculation method above the inner/outer draft at bow/stern can be written as

$$t = f(Fn_i, L_c/B_c, p_c/l_c, \psi, \zeta_0) \tag{5.11}$$

where l_c/B_c is the cushion length beam ratio and p_c/l_c the cushion pressure length ratio.

Parameters t_{bi}, t_{bo}, t_{so}, t_{si}, can be written as a function of Fn_i, L_c/B_c, P_c/L_c, ψ and ζ_0, so that the inner/outer sidewall draft of the craft with given principal dimensions and

speed can be obtained as a function of the trim angle and vertical location of bow over sea level.

In order to find ψ and ζ_0, the other equations to be satisfied are as follows:

$$\begin{aligned} \Sigma L_i &= W \\ \Sigma M_i &= 0 \\ H_j &= A + BQ + CQ^2 \\ &= p_c + 0.5\rho_a \sum_{i=1}^{n} (Q/S_i)^2 \xi_i \\ Q &= (2p_c/\rho_a)^{0.5} \phi A_{es} + (2(p_c - p_v)/\rho_a))^{0.5} \phi A_{eb} \end{aligned} \tag{5.12}$$

in which ΣL_i is the sum of various lift and buoyancy components

$$\Sigma L_i = L_c' + L_{sw} + L_{ss} + L_{bs} + L_a$$

where L_c' are the lift forces due to the air cushion pressure $L_c' = p_c s_c$, L_{sw} the buoyancy of sidewalls, L_{ss} the lift forces of the stern seal, L_{bs} the lift force of the bow seal and L_a the aerodynamic lift of the superstructure. ΣM_i is the sum of various moments with respect to the CG of the craft

$$\Sigma M_i = M_c + M_{sw} + M_{ss} + M_{bs} + M_a + M_w + M_p$$

where M_w is the moment of water drag R_w about the CG of the craft, M_a the moment of air drag R_a about the CG of the craft, M_c, M_{sw}, M_{ss}, M_{bs} the moments of L_c', L_{sw}, L_{ss}, L_{bs} about the CG of the craft and M_p the moment of the propeller thrust about the CG of the craft.

In addition, W is the all-up weight of the craft, H_j the total air pressure of the fans, A ,B, C are coefficients of the fan characteristic curve, which are a function of type, dimensions and revolution of fans, ξ_i the air pressure loss coefficients for various air ducts, S_i the area of equivalent air ducts; the calculation for pressure loss of various air ducts in equation (5.12) is hypothetical and one can calculate according to the specific condition. ϕ is the discharge coefficient of air leakage, A_{es} the cross-sectional area of cushion air leakage at the stern, $A_{es} = (z_s - t_{si})\, B_c$, A_{eb} the cross-sectional area of cushion air leakage at the bow, $A_{eb} = (z_b - t_{bi})\, B_c$ and P_v the ram pressure at bow due to the craft speed v.

Substituting these expressions into equation (5.12), then the four variables ψ, ζ_0, Q and p_c can be obtained by solving the four equations by iteration. Substitute ψ, ζ_0 into equation (5.11), then the dynamic trim characterized by t_{bo}, t_{bi}, t_{so}, t_{si}, can be obtained.

The method for determining the various forces and moments will be described in following chapters. Solution of these equations is very complicated because this is an iterative process and the forces and moments involved in the equations are a function of inside/outside air cushion conditions and the craft dynamic trim.

The inner/outer drafts are also a function of various forces (moments) and factors of lift systems, e.g. p_c, H_f, Q, but can be easily solved by computer.

This method can also be extended to other parameters for solving the differential equations with respect to stability, heaving, rolling and pitching motions, etc., which will be described in following chapters.

Some important concepts presented in the first section of this chapter, which are often neglected by researchers and designers, may be clarified as follows:

1. The angle calculated by the outer draft of sidewalls at bow and stern is actually the apparent trim angle of the craft (i.e. $\tan(\psi - \alpha) = (t_{so} - t_{bo})/l_c$) and not the true craft trim angle, which often seems misunderstood by some operators. An exception is in the case of high craft speed, when the slope angle of outer wave surface approaches zero, then the apparent trim angle equals the actual trim angle.
2. The trim angle measured by trigonometry (ψ) is the actual trim of the craft.
3. The wave slope of inner water surface α' is related to the cushion wave-making drag and can be written as

$$R_{wc} = W \tan \alpha'$$

This formula is similar to that used for predicting the wave-making drag of a planing hull

$$R_w = W \tan \alpha$$

where R_w is the wave-making drag, W the craft weight and α the wave surface slope (or trim measured by drafts, for a boat).

For an SES the sidehull wavemaking and cushion wavemaking each relate to the proportion of weight supported by displacement and cushion pressure.

4. Trim drag, which is due to the difference of momentum of air leakage from bow and stern skirts, is a function of the slope of the inner water-line and the bow/stern skirt clearance over the base-plane and is directly related to the apparent trim angle ($\psi - \alpha$) and true trim angle ψ.

Therefore it is not correct to estimate the trim drag by this method. The estimation method for trim drag and wave-making drag will be defined in following chapters; however, the concept and method of predicting the dynamic trim of craft, which has been discussed above, is very important to clarify the fundamental relations of the hydrodynamic performance of hovercraft, although the physically correct method is rather more complicated.

Simplified method for predicting hovercraft trim above hump speed on calm water

We assume as follows:

1. The inner/outer water-line may be considered as a straight line because of high craft speed.
2. According to calculation and practical observations, it is found that the inner draft is equal to the outer draft.
3. Owing to the small slope angle of the outer wave surface, we can assume $\alpha \cong 0$ so that $t_{bi} = t_{bo}$ can be added into equation (5.12).

Then because $\alpha \cong 0$ and $t_{bi} = t_{bo}$

$$\begin{aligned} R_w &= W \tan \alpha' \\ &= W \tan [\psi + (\alpha' - \psi)] \end{aligned}$$

$$\begin{aligned} &\cong W\tan\psi + W\tan(\alpha' - \psi) \\ &\cong W\tan(\psi - \alpha) + W\tan(\alpha' - \psi) \\ &\cong W(t_{so} - t_{bo})/l_c + W(t_{bi} - t_{si})/l_c \\ &\cong W(t_{so} - t_{si})/l_c \end{aligned} \tag{5.13}$$

From Chapter 4, we have

$$R_w/W = f(Fn_l, l_c/B_c, p_c/l_c) \tag{5.14}$$

Thus equations (5.13) can be used to determine dynamic trim, since the wave-making drag R_w of the given ACV/SES can be estimated and then t_{so}, t_{bo}, t_{si}, t_{bi}, Q, P_{co}, i.e. the dynamic trim of the craft, can be obtained using equations (5.11)–(5.13). The method is so simple that the inner/outer wave profile can be obtained without complicated calculation, as demonstrated in refs 54 and 32.

6

Manœuvrability

6.1 Key ACV and SES manœuvrability factors

Basic concepts to be introduced in this chapter are vehicle directional stability on a straight course, including when wind and waves are not from the bow, the ability of a craft to turn in a controlled manner and the ability of craft to manœuvre at slow speed.

The various control surfaces and sources of turning moment available to the SES and ACV designer will be discussed, followed by the means to estimate the control forces and responses.

Features of ACV/SES

The manœuvrability of an SES and a high-speed catamaran or high-speed monohull are all similar, because there is no air leakage under the main part of SES sidewalls. Drifting does not occur during turning, except in the case of an SES with thin sidewalls and at a very high speed. We will therefore introduce the manœuvrability of this type of SES as a separate subject.

The manœuvrability of amphibious ACVs has some characteristics of each of conventional ships, wheeled vehicles and aeroplanes, as follows:

1. During turning (or holding a straight course in beam winds), the craft needs to maintain a yawed attitude, pointing into the centre of the turning circle or into the wind in order to maintain the intended track. This is because an ACV has very little contact with the water surface and so the drifting drag of the ACV is very small. The low righting moments at small angles of an ACV hovering over water result in heeling, pitching, yawing, drifting and surging motions all being significant.
2. The manœuvrability of an ACV is different from that of wheeled vehicles. During turning of wheeled vehicles, there is large sideways friction of wheels against the ground and large centripetal force acting on CG in the case of banked ground surface at the turn. These forces stop wheeled vehicles slipping sideways. In the case of an ACV turning, the craft will slip considerably unless special measures are taken by the driver. The desired craft trim is a bank into the turn. Some SES have canted rudders which create a rolling moment to achieve this effect. Amphibious ACVs

may be fitted with skirt lift or skirt shifting systems which move the cushion centre of pressure relative to the CG to roll the craft. Smaller craft may have elevators installed to achieve a similar effect.

3. ACV manœuvrability is also different from aeroplanes. When in flight, pilots can use the air rudder and wing elevators in co-ordination to make an inward banked turn and create a centripetal force in order to reduce the turning diameter and slipping distance. In addition, the aeroplane has less space restriction on its manœuvring should significant side-slip occur. An ACV on the other hand may be required to travel on narrow rivers, canals, under bridge spans, or to land in enclosed docks of landing ships, all of which represent limiting space for manœuvres.

Thus it can be seen that the manœuvrability of an ACV is rather different from conventional ships, vehicles and aeroplanes and so needs special features to provide adequate manœuvring power. The essentials are: the ACV is bound to flat surface; little drag in all horizontal directions; direct generation of control forces needed to provide centripetal forces to manœuvre the craft around corners. Meanwhile, the SES is very similar in behaviour to a slender hull catamaran.

Background to ACV manœuvrability

Manœuvrability has had a considerable impact on ACV development. Many ACV models and experimental manned craft exhibited at the first Conference on Air Cushion Technology in Beijing in August 1960 performed with unstable turns and manœvering capability.

At that time, in the era of peripheral jets and no flexible skirts, most craft had a considerable air gap above the ground. They had a tendency to make continuous small movements in all directions and the pilots found them very difficult to hold on a steady course due to lack of contact with the ground and the small propulsion units installed at that time. As the craft could not travel on a straight course, potential operators considered the ACV impractical to put into service at that time.

Considerable development efforts were consequently made by the pioneering designers, experimenting with all possible control surfaces which could be applied to the ACV, to improve its characteristics. This led to successful improvements in the manœuvrability of ACVs and assisted their development throughout the world at the end of the 1960s. The different means of control developed are reviewed through this chapter.

Following the widening of the range of ACV applications in the 1960s, military ACVs for amphibious assault were required to land in the stern well deck of a landing ship's dock (Fig. 6.1). These craft have been developed through the 1970s and 1980s. This requires very good manœuvrability at low craft speed in order to get onto the landing ship ramp in rough seas.

ACV or air cushion platforms have also been developed to manœuvre on the surface of swamps, marshy fields, rapids and narrow waterways. For these applications new challenges for manœuvrability and course stability have presented themselves to the designer.

Fig. 6.1 US LCAC-001 entering into the landing ship *Pensacola*.

Subjects covered in this chapter

Attention will be concentrated on the following:

1. The effectiveness of various control surfaces on ACV (or air cushion platform) manœuvrability in individual use or integrated application.
2. Experimental investigation of manœuvrability of ACVs at low speed with aid of radio controlled free-flying models.
3. Experimental investigation of manœuvrability of ACVs at high speed.
4. Theoretical study of ACV manœuvrability at low/high speed, including calculation and measurements of various hydrodynamic position derivatives and rotational derivatives, formation and solution of manœuvrability equations, etc. Electronic computers are applied widely in the solution of these equations, because designers can choose various control surfaces to assist the manœuvrability of craft according to the computer results in order to save a large amount of labour and expense to carry out model and full scale ship tests.

6.2 Introduction to ACV control surfaces

There are a lot of possible control surfaces that can be mounted on an ACV. They can be divided into three groups, i.e. rudder equipment, air propulsion systems and the control surfaces affecting the cushion force, as shown in Table 6.1.

Table 6.1 The equipment for controlling the course of ACV

Equipment for controlling the course of an ACV	Rudder Equipment	Vertical air rudders Swivelling air stabilizers Retractable water rudders Jetted rudders Horizontal air rudder Guided wheels on terrain
	Cushion air forces	Flexible skirt-lifting system Flexible skirt-shifting system Valves in air ducts Separately variable fan rpm or blade pitch from several fans Weight shifting using water ballast or shifting of crew to adjust trim or heel
	Air propellers	Separately variable propeller rpm or blade pitch from several units Swivelling pylons Controllable pitch of air or ducted propellers Swivelling jetted thrusters Puff ports

Rudders

Vertical rudder

A vertical rudder is shown in Figs 6.2–6.4. Due to the high position of a vertical air rudder over the CG, its action not only creates turning moments but also a drifting force and rolling moment, which leads to the craft performing an outward banked turn. Thus when the ACV is turning over water by means of an air rudder, in addition to turning, yawing, heeling and drifting will occur simultaneously and even lead to 'tiptoe' turn in the case of applying unsuitable control actions to the craft, such as excessive rudder angle or too long action of the rudder, especially for craft operating on ice and over ground.

Vertical fins for course stability (Fig. 6.2)

Vertical fins are used for improving course stability and efficiency of an air rudder. Their primary use is at high speed.

Jetted air rudder

This was a system developed at BHC in the 1960s to improve the manœuvrability of ACVs with a single air propeller. The jet was led from the air cusion into proximity to the rudder surface, so increasing the effectiveness of the rudders especially at lower craft speeds. After limited application on the SR.N6 craft, such equipment has not been applied to later designs, as other control systems with greater turning force for craft manœuvring have appeared.

Horizontal air rudders, or elevons

These are shown in Fig. 6.4. They are designed and installed on ACVs to regulate dynamic trim. Elevators are very effective and fast acting. Meanwhile, the craft

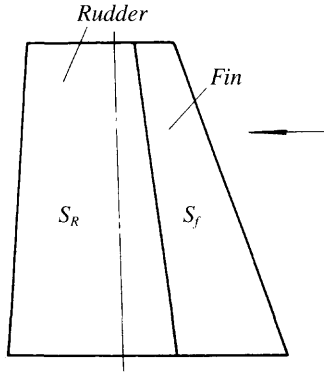

Fig. 6.2 Air rudder and fixed vertical stabilizer fin.

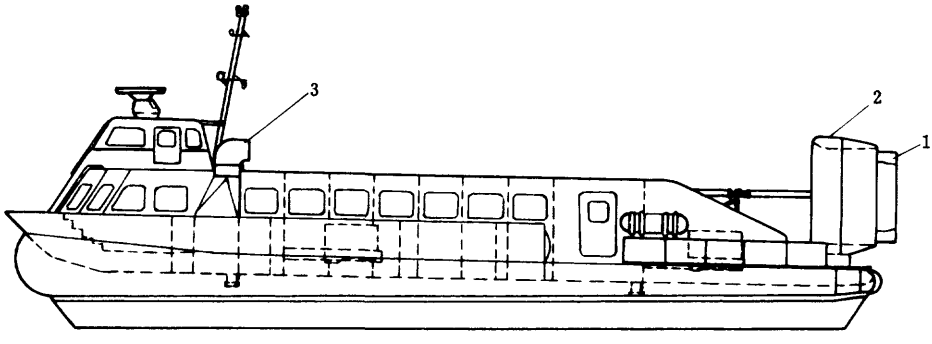

Fig. 6.3 The control surfaces of British ACV model AP.1-88. 1: vertical rudder; 2: propeller duct; 3: bow thruster.

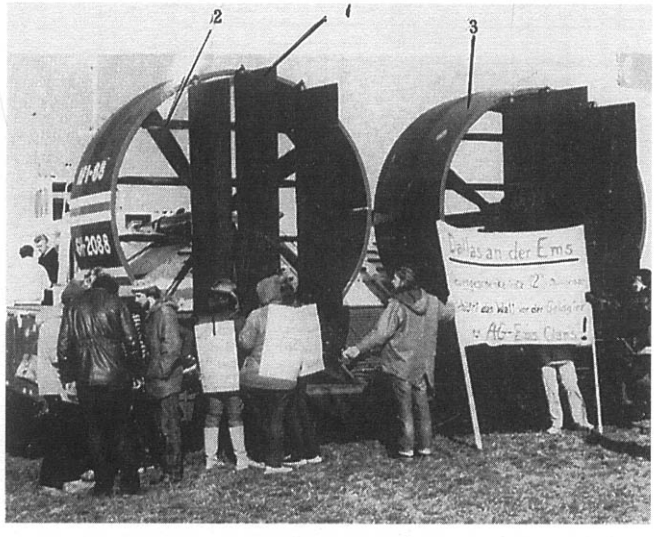

Fig. 6.4 The ducted air propellers and rudder of AP.1-88. 1: rudders; 2: elevators; 3: propeller duct.

loading condition and operational environment will also affect the steady trim of an ACV, so it is very convenient to mount elevators for fast adjustment of craft trim in various conditions. Elevons are a variation on the basic elevator design. The control wires or rods are arranged in such a way that forward movement of a control stick causes pitch movement, while sideways movement causes the elevons to move differentially, causing a roll moment.

Retractable water rudder [57]

This device is shown in Fig. 6.5, which is suitable for handling the ACV at high speed. These control surfaces can be designed with smaller size due to the higher density of water than that of air. Moreover, this control surface may be mounted under the VCG of the craft and one of a pair can be put down during turning. This equipment will prevent drifting and outward banking motion during the turn, but it is less effective in the case of low speed on ACVs; in addition the equipment is more complicated.

Such rudders can cause severe rolling if deployed from a craft which is travelling with some drift, or even cause overturning. For this reason, the equipment was only installed on experimental ACVs in the early development period.

Guide wheels on land

In the case where an ACV operates over land with various conditions such as grassland, swamp, marsh, sand beaches and ice surfaces, etc. resistance for preventing drifting is very small, so it can be very difficult to handle an ACV precisely, preventing drifting and turning about the CG of the craft. Moreover, the speed of craft will be low in the case where an ACV travels over ground, leading to low effectiveness

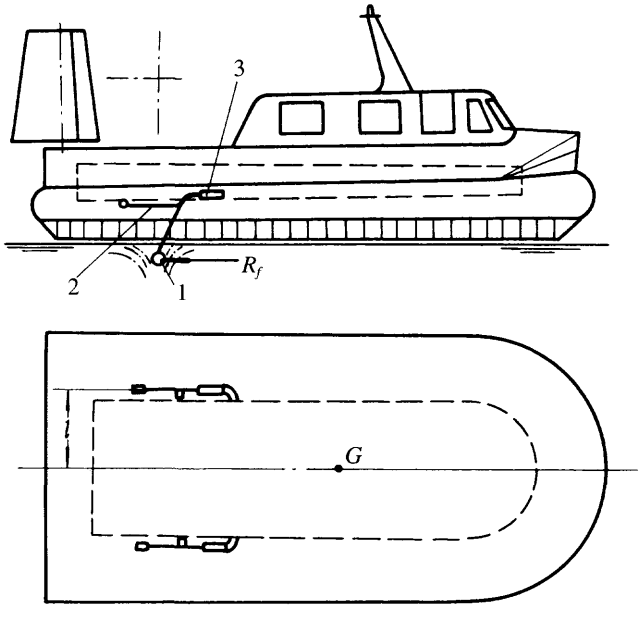

Fig. 6.5 Retractable water rudder. 1: retractable water rudder; 2: control bar; 3: actuator; *Rf* = addition drag due to rudder.

of rudders; so guide wheels can improve manœuvrability and course stability of ACVs and air cushion platforms considerably. Figure 6.6 shows guide wheels in operation on an ACV.

Air propulsors used for manœuvring

Steering by differential thrust from air propellers

The difference of rpm of two or more than two air propellers on both sides can be applied to ACVs to present a turning moment to make the ACV turn about the CG of the craft. This method is especially suitable for ACVs at low speed. Figures 6.3 and 6.4 show two sets of ducted air propellers at the stern. Owing to the high efficiency of ducted propellers, the effectiveness of this method for improving the manœuvrability of ACVs at low speed is very satisfactory.

Swivelling pylons

Figure 6.7 shows a sectional view of swivelling pylons with an integrated lift fan and air propeller system. It can be seen that the swivelling pylon can be rotated by means of a pair of hydraulic actuators. This apparatus can provide side forces as well as a turning moment, therefore various handling modes can be exploited with the aid of several swivelling pylons and their various force couples (moment). Figure 6.8 shows two modes of handling on British ACV model SR.N4: (a) shows the yoke handling, i.e. the thrust line of the propeller rotating in synchronism whereby the system can provide transverse force to prevent ACV drift, if the rotating angle of four swivelling pylons are same and the rudders are kept in neutral position; (b) shows the rudder bar control, i.e. the pilot moves not only the yoke but also the rudder bar and makes the fore and aft pair of pylons swivel with the same angle but inverse direction. Here the thrust of swivelling pylons will act as an additional rotation moment about the CG of the craft to accelerate the yawing angular velocity and reduce the turning diameter of the craft.

Controllable pitch air propellers (or ducted propellers)

Variable forward and reverse thrust and rotating moment (in the case of two or four air propellers) can be provided by means of controllable pitch air propellers. The available manœuvring forces from differential thrust are high, therefore pilots like it

Fig. 6.6 Ground wheels for the guidance of air cushion platform.

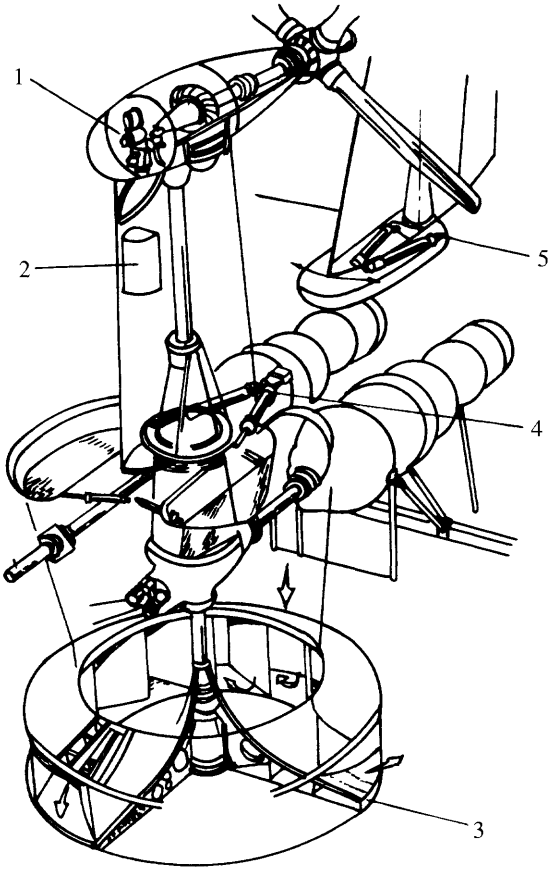

Fig. 6.7 Sectional view of SR.N4 swivelling air propeller pylon. 1: propeller; 2: pylon; 3: lift fan; 4: actuator for pylon; 5: actuator for rudder.

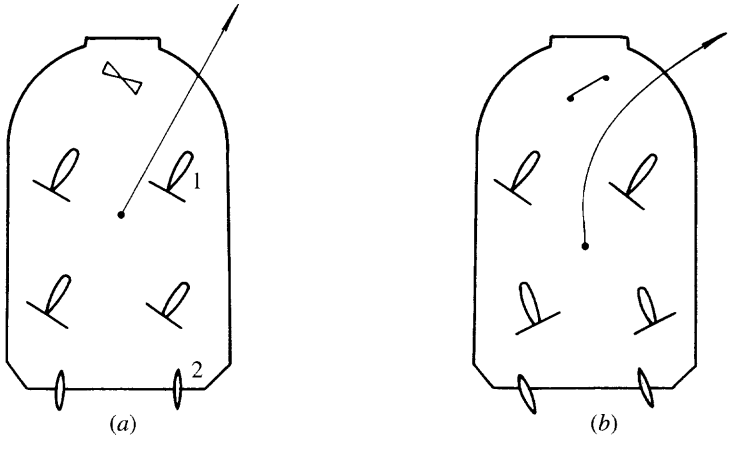

Fig. 6.8 Two control modes of SR.N4: (a) yoke control – pylons swivel together; (b) rudder bar control – pylons swivel in opposition. 1: pylons; 2: rudders.

very much. These pieces of equipment are complicated and expensive, and therefore are usually only installed on medium and large ACVs.

Rotating ducted thrusters

These are also called rotating jet nozzles, as applied to the British ACV model AP.1–88 shown in Fig. 6.3. A diagrammatic sketch of this apparatus is shown in Fig. 6.9. Using the pressurized air from centrifugal fans and ejected from a rotating nozzle, the ACV can obtain the jetted thrust. Fine manœuvrability of an ACV at low and high speed as well as in beam wind conditions can be obtained by means of co-ordinated operation of bow thrusters and stern rudders as well as stern air propeller pitch. The thrust efficiency of jet nozzles is low, but this is usually not important, since the power requirement is not high and may be less expensive than installing variable pitch propellers or fans for example.

Puff ports (Fig. 6.10) [57]

The working principle of this installation is the same as that of rotating thrusters, except that thrust is simply directed to port or starboard of the bow, so it is normally only used for increased rate of turn at low speed. The merit of puff ports is simplicity of structure and low cost. There are no separate fans for this installation. The lift fans have to be upgraded to account for the additional air flow.

The disadvantage of this installation is that a part of the cushion air will be consumed for this system, leading to a reduction of the cushion pressure at the side of the cushion on which the puff ports are in action. Thus the craft heels to one side and causes the air leakage at the other, consequently a drifting force is created in the inverse direction, which compensates for the jetted thrust provided by the puff port and reduces its effectiveness.

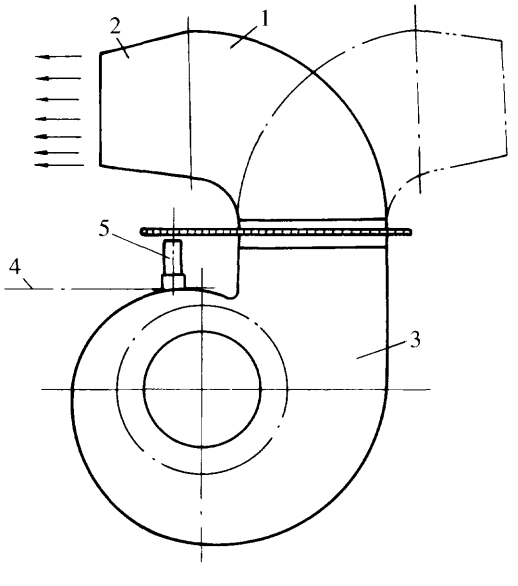

Fig. 6.9 Sketch of the arrangement of air thrusters. 1: rotating duct; 2: jet nozzle; 3: fan and duct; 4: ACV deck level; 5: rotation mechanism.

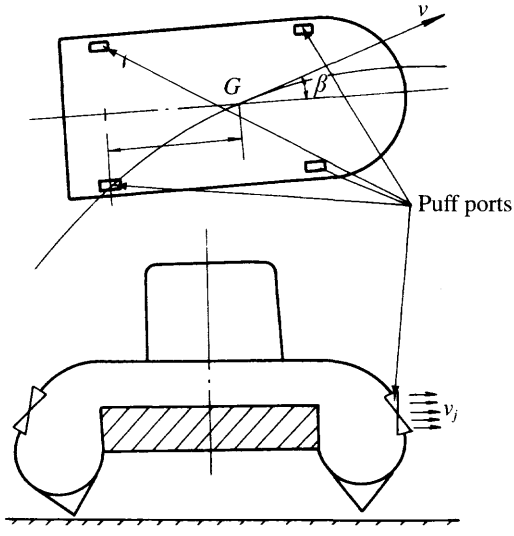

Fig. 6.10 Typical puff port installation.

This installation was mounted on SR.N6 in the 1960s and 1970s, but has not been developed since then. Such an installation was also tried on the Chinese ACV 711-II, but was not developed because of its low efficiency.

Cushion forces

Since the cushion force is equal to craft weight, it is very effective to use this force to control the craft for static (trim) adjustments. There are several methods in use.

Skirt lift apparatus

Figure 6.11 shows a diagrammatic sketch of a skirt lift apparatus: (a) shows the action of this apparatus to lift skirt bags, and (b) shows the action of this apparatus lifting the skirt fingers. The action of both causes lift to the skirt at one side of the craft, thus making this side heel down and presents not only a heeling moment but also a transverse force, which is useful in a turning manœuvre.

The effectiveness of lifting skirt fingers will be better than lifting skirt bags, because it may cause the change of jet direction and increase the transverse momentum of cross-flow. Nevertheless, in practice, type (a) will be more practical than type (b).

Owing to the inward heeling moment and centripetal force supplied by skirt lift, which can compensate for the centrifugal force of the craft during craft turning, the turning diameter will be reduced and also safety will be enhanced; so this apparatus has been applied widely in the industry.

The disadvantage of skirt lift is its complexity, since an extensive pulling system of wires and pulleys has to be installed and a set of hydraulic or mechanical operating systems has to be installed on the ACV. In addition, the large lift may shorten the life of the skirt; for this reason, it is not suitable to equip large ACVs with skirt lift.

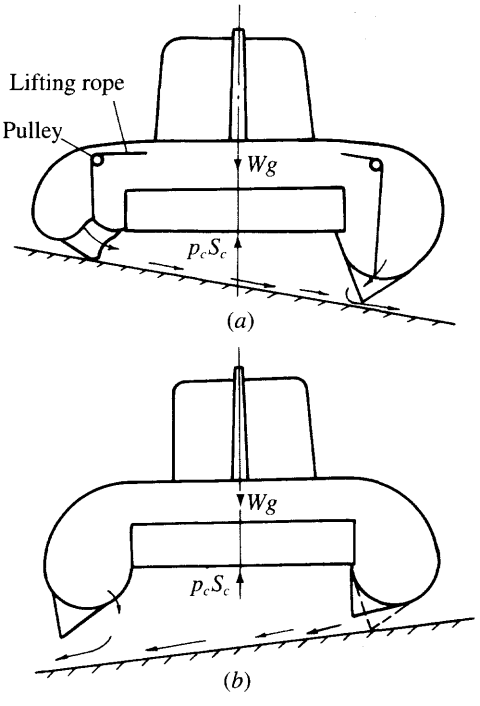

Fig. 6.11 Skirt lifting installation: (a) action of lifting bag; (b) action of lifting fingers.

Skirt-shifting installation

This apparatus is shown in Fig. 4.30, which can provide transverse force and heeling moment. It has been used on relatively few craft (HD.2, VT.1) mainly because it suits the open loop and segment skirt rather than the bag and skirt. On larger craft (VT.1) it was found that the system was not really needed for satisfactory manœuvring and it was simply ignored. The possible large shifts of craft CP could actually be dangerous in a high-speed turn for a craft of the size of VT.1 and so on the later amphibious VT.2 the skirt shift system was decommissioned. Utility craft such as the Griffon series are well suited to this installation.

Using the weight of persons and water (oil) ballast to regulate the trim and heel

On small ACVs, the weight of people can be used for regulating the running attitude and obtain an excellent effect just as riding a bicycle. But it is impractical for large commercial ACVs. However, the water (oil) ballast can replace the weight of people as the mass for regulating the trim or heel, but it cannot be regulated dynamically in regard to the operational environment, such as the action of beam wind, the shift of CG, etc., because the shift of ballast water (oil) needs enough time. For this reason this method cannot be used as handling apparatus, just for static trim.

Air duct valves

The centre of pressure of an air cushion can be changed with the aid of air duct valves to produce the heel/trim forces (moment). This is not used except in experimental conditions, as it is not efficient in use of cushion air.

Using the difference of rate of revolution or regulation of fan blades

The principle of this is the same as air duct valves. It is used experimentally.

The state of the art and control surface features on Chinese and European ACVs

This is shown in Table 6.2, and the application of air rudders and fins are shown in Table 6.3. The features of control surfaces on various ACVs can be seen as follows:

1. Because of the many control surfaces mounted on the ACV 711-IID, its manœuvrability is most satisfactory, however the installation is too complicated.
2. The control surfaces mounted on ACV version 7210 are simple and cheap, with the penalty of poor handling performance, particularly if the craft is running with a single propeller.
3. The manœuvrability of craft version 722-I is satisfactory because of relatively large control surface areas, even if the craft is of medium size.
4. Owing to the single non-swivelling propulsor and fan of SR.N6, the manœuvrabil-

Table 6.2 A selection of control surfaces mounted on Chinese and Western ACVs

Craft identification	711-IID	7210	716-II	722-I	SR.N6	SR.N4	AP.1-88
Nationality	China	China	China	China	UK	UK	UK
Craft type	ACV	ACV	ACV	ACV	ACV	ACV	ACV
Rudder installation							
Vertical	✓	✓	✓	✓	✓	✓	✓
Jetted					✓		
Vertical fin(s)	✓			✓	✓		
Retractable water rudder							
Horizontal air rudder	✓			✓	✓		✓
Guide wheels on terrain							
Air propulsor							
Air propeller	2	1 Ducted	2 Ducted	4	1	4	2 Ducted
Swivelling pylon(s)	–	–	–	2	–	4	–
Propeller + thrusters	✓			✓	✓	✓	
Swivelling jet nozzle							✓
Puff ports					✓		
Cushion Air Controls							
Skirt lifting	✓			✓	✓		
Skirt shifting							
Air duct valves				✓			
Ballast water or oil tanks					✓	✓	✓
Differential fan speed				✓		✓	✓

Table 6.3 Application of air rudders and fins on Chinese and European ACV

Craft identification	SR.N5	SR.N6	N.300	SR.N4	711-IID
Nationality	UK	UK	France	UK	China
No. of vertical fins + rudders	2 + 2	2 + 2	–	2 + 2	2 + 2
No. of inclined fins + rudders	–	–	2 + 0	–	–
No. of horizontal fins + rudders	0 + 2	0 + 2	–	–	1
Total area of vertical fins and rudders (m^2)	2.2	2.2	?	14.8	3.96
Total area of horizontal fins and rudders (m^2)	0.1	0.1	–	–	2
Total fin area/craft side area (%)	6	4.5	?	5	7.3
Total rudder area/craft side area (%)	23.2	18	?	?	18
Fin/rudder inclination from horizontal (°)	90	90	87	90	90
Distance fin to propeller disc/prop. dia. (m)	0.5	0.5	?	0.5	2.3

ity had to be improved by installing many additional devices such as jetted air rudder, lifting skirt and puff port.

5. Two sets of bow-swivelling thrusters together with two set of propulsors make the manœuvrability of ACV AP.1–88 most satisfactory, even though the adjustable pitch air propeller is replaced by a fixed pitch propeller.

6.3 Differential equations of motion for ACV manœuvrability

To identify the necessary forces which a control surface may have to apply, we need to solve the equations of motion for a given ACV design, the relevant manœuvre and environmental condition.

The manœuvrability of an ACV is different from that of conventional ships in that the cushion air blows from the side skirt to provide the transverse force during manœuvring. Therefore from the point of view of hydrodynamics, we should not investigate the manœuvrability by means of forming differential equations of motion with three degrees of freedom as usually used on conventional ships, such as yawing, swaying and surging.

One or two additional degrees of freedom have to be considered such as rolling, caused by transverse forces and its coupled motion, pitching. In the strict sense, the last degree of freedom, heaving, also should not be neglected.

Because of the longitudinal asymmetry of the cushion, pitch will couple with the rolling motion, and consequently the differential equation of motion with six degrees of freedom has to be investigated, which will cause a lot of difficulty for solving the differential equations. Furthermore, the solution of the position derivatives and rotation derivatives will be hard and complicated work, expending a great deal of labour and money, However, designers often pay great attention to this, particularly where an ACV will probably operate on land and ice.

The differential equations of motion are the basis for studying the manœuvrability of ACVs; once obtained, designers will find it simple to analyse the manœuvrability, course stability and handling characteristics of ACVs operating on ice, land and other complicated support surfaces with the aid of a computer. References 55 and 58 have described some methods in this respect.

These methods can also be applied to analyse the effect of principal dimensions, parameters and control surfaces on the manœuvrability of ACVs, in order to choose reasonable design criteria and save a great deal of time and labour on radio-controlled free-flying models and full-scale ship tests.

Basic assumptions and nomenclature

1. The ACV is running on calm water or flat land and we neglect the effect of spray and its added mass on the manœuvrability of craft.
2. The differential equations of motion for manœuvrability of an ACV are based on four degrees of freedom, i.e. the motions of craft in a horizontal plane (sea surface or ground surface) and the drifting motion of ACVs on this plane as well as the roll motion during turning of craft.

   In a strict sense, there are some problems with this basis which affects the accuracy of the solution of the differential equations, because the turning of an ACV will also lead to a heeling motion of the ACV and air leakage of cushion air from the side skirts, as well as drifting motion due to the strong coupling of heeling with heaving motion. However, for reasons of simplification, we neglect the heaving and pitching motions. It may be useful to consider the heeling motion as a separate consequence of a turn, to assess the effect on stability.
3. The body coordinate system on ACVs is $GXYZ$ and the fixed coordinate system is shown in Figs 6.12 and 6.13. Here

V = linear velocity of craft on CG
β = yawing angle of track of CG of craft (i.e. the angle between the X axis and velocity vector of craft motion)
ω = yawing angular velocity of craft at CG
φ = angle between the 0ξ axis and velocity vector of the craft at CG

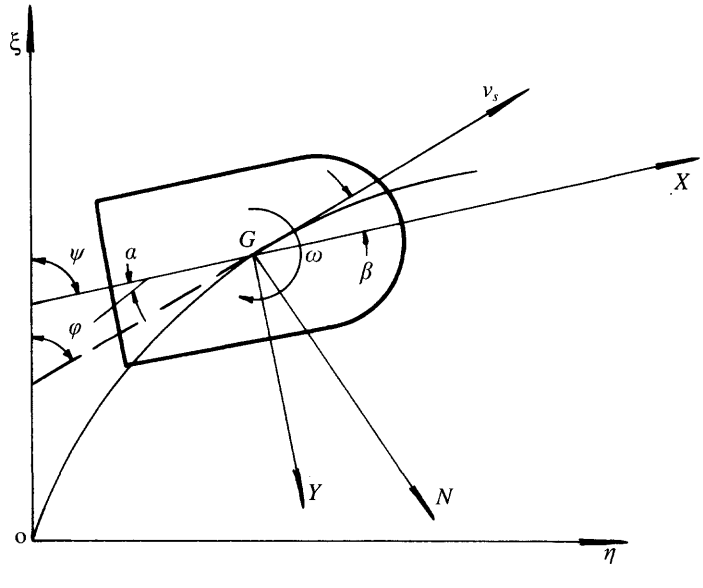

Fig. 6.12 Operation track nomenclature for ACV in turning manœuvres.

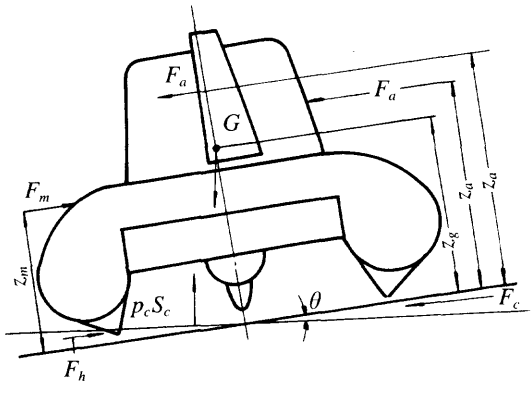

Fig. 6.13 Forces acting on an ACV when turning.

ψ = course direction of the craft
α = rudder angle
R = turning radius
m = craft mass
W = craft weight
θ = heeling angle of craft
F_a = force acting on rudder
z_g = VCG
z_a = arm of force exerting on rudder (distance from ground to the centre of force acting on rudder)
F_s = resistance due to air cushion and skirt
F_c = jetted thrust due to air leakage from cushion during turning manœuvre
F_m = air momentum force
z_m = distance from ground to the centre of air momentum force
F_a = aerodynamic profile drag
x_a = distance from ground to the centre of aerodynamic profile drag

Formation of the equations of motion

The differential equations of motion concerning the manœuvrability with four degrees of freedom can be written as

$$\begin{aligned} \text{Surging:}\quad & F_x = m(\dot{x} - \dot{\beta}\dot{y}) \\ \text{Yawing:}\quad & F_y = m(\dot{y} - \dot{\beta}\dot{x}) \\ \text{Swaying:}\quad & M_z = I_z\ddot{\beta} \\ \text{Rolling:}\quad & M_x = I_x\ddot{\theta} \end{aligned}$$

where F_x, F_y, M_z, M_x are the forces and moments acting on the craft with respect to the x and y axes, I_z the moment of inertia of the craft about the z axis, I_x the moment of inertia of the craft about the x axis.

Since the air gap of a modern ACV is very small, in the case where craft are manœuvring over water, the craft will be in yawing and heeling motion, to be exerted by various forces, such as external aerodynamic force, hydrodynamic force, cushion force, air momentum force and propeller thrust and the moments due to these forces. Meanwhile the ACV is basically hovering over the water surface, and so the added water mass can be neglected.

If the forces (moments) (i.e. corresponding static force derivatives and rotary moment derivatives) can be obtained, then the differential equations of motion can be solved with the aid of computers, and the track of motion such as $x(t)$, $y(t)$, $\beta(t)$ [or $\psi(t)$], $\theta(t)$, can also be obtained.

The yawing angle β but not course angle ψ is applied to equation (6.1) and the time history of the track can be obtained by computer as shown in Fig. 6.20. The results of one point can be used as the initial data of the next point; the time interval for two points should be less 10 seconds and the calculation results can then be obtained as the time history of the motion track.

Determination of position and rotation derivatives

There is a very large volume of work on this subject. M. Murao, W. Zeifuss Jr, and E. J. Brook Jr investigated the formation and solution of differential equations of motion on the feasibility of navigation of ACVs on ice surfaces in Arctic regions.

The various forces and moments acting on ACVs such as F_x, F_y, M_x, M_z can be written as:

$$\begin{aligned} F_x &= F_{xa} + F_{xh} + F_{xc} + F_{xm} + F_{xp} \\ F_y &= F_{ya} + F_{yh} + F_{yc} + F_{ym} + F_{yp} \\ M_z &= M_{za} + M_{zh} + M_{zc} + M_{zm} + M_{zp} \\ M_x &= M_{xa} + M_{xh} + M_{xc} + M_{xm} + M_{xp} + M_{x\theta} \end{aligned} \tag{6.2}$$

in which the suffix a is the aerodynamic force, h the hydrodynamic force, c the cushion force, m the air momentum force and p the thrust.

The manœuvrability of an ACV in wind with various directions and force can be included in the equations above, as long as the wind vector can be included in these equations. However, this can be neglected temporarily in order to simplify the equations, thus we in general assume:

$F_{yp} = 0$ (no swivelling pylon taken into account on the ACV)
$M_{zp} = 0$ (no difference on rpm of propellers to be taken into account)
$F_{xc} = 0$ (no trim, thus no longitudinal cushion force)
$M_{xp} = 0$

and $M_{x\theta}$ is the moment of the craft during the heeling angle of θ and M_{xc} the heeling moment from the force of the jet blown under the side skirts during heeling angle of θ.

Thus the equations (6.2) can be written as

$$\begin{aligned} F_x &= F_{xa} + F_{xh} + F_{xm} + F_{xp} \\ F_y &= F_{ya} + F_{yh} + F_{ym} + F_{yc} \\ M_z &= M_{za} + M_{zh} + M_{zc} + M_{zm} \\ M_x &= M_{xa} + M_{xh} + M_{xc} + M_{xm} + M_{x\theta} \end{aligned} \tag{6.3}$$

The forces and moments can be obtained respectively as follows.

Aerodynamic force and moment

Taking the hull, superstructure, rudder, fin, duct, etc. as a single body, which can also then be related to functions of rudder angle a, yaw angle β and yawing velocity $\dot{\beta}$, then the aerodynamic forces and moments can be written as

$$\begin{aligned} F_{xa} &= 0.5\rho_a V_s^2 C_{xa} S_a \\ F_{ya} &= 0.5\rho_a V_s^2 C_{ya} S_a \\ M_{za} &= 0.5\rho_a V_s^2 C_{mza} S_a l_a \\ M_{xa} &= F_{ya} z_a \end{aligned} \tag{6.4}$$

where S_a is the lateral area of hull, superstructure, fins rudders and air ducts, l_a the average height of the craft, z_a the vertical distance of the centre of lateral area over the lower tip of skirts; since the air gap is very small, the vertical distance of the centre of lateral area over the ground can be taken as $l_a/2$. *Cxa*, *Cya*, *Cmza* are the coefficients of aerodynamic force and moment. Thus they can be written as

$$\begin{aligned} C_{xa} &= C_{xa0} + C_{xa1}\alpha + C_{xa2}\beta + C_{xa3}\dot{\beta} \\ C_{ya} &= C_{ya0} + C_{ya1}\alpha + C_{ya2}\beta + C_{ya3}\dot{\beta} \\ C_{mza} &= C_{mza0} + C_{mza1}\alpha + C_{mza2}\beta + C_{mza3}\dot{\beta} \end{aligned} \tag{6.5}$$

where

$$\begin{aligned} C_{xa1} &= (\partial C_{xa}/\partial\alpha)\alpha = \beta = \dot{\beta} = 0 \\ C_{ya1} &= (\partial C_{ya}/\partial\alpha)\alpha = \beta = \dot{\beta} = 0 \\ C_{mza1} &= (\partial C_{mza}/\partial\alpha)\alpha = \beta = \dot{\beta} = 0 \end{aligned} \tag{6.6}$$

$$\begin{aligned} C_{xa2} &= (\partial C_{xa}/\partial\beta)\alpha = \beta = \dot{\beta} = 0 \\ C_{ya2} &= (\partial C_{ya}/\partial\beta)\alpha = \beta = \dot{\beta} = 0 \\ C_{mza2} &= (\partial C_{mza}/\partial\beta)\alpha = \beta = \dot{\beta} = 0 \end{aligned} \tag{6.7}$$

$$\begin{aligned} C_{xa3} &= (\partial C_{xa}/\dot{\beta})\alpha = \beta = \dot{\beta} = 0 \\ C_{ya3} &= (\partial C_{ya}/\partial\dot{\beta})\alpha = \beta = \dot{\beta} = 0 \\ C_{mza3} &= (\partial C_{mza}/\partial\dot{\beta})\alpha = \beta = \dot{\beta} = 0 \end{aligned} \tag{6.8}$$

The expressions in equations (6.6) and (6.7) are the position derivatives, which can be obtained by wind tunnel experiments. Equation (6.8) gives the rotation derivatives, which can be obtained by tests on rotating arm facilities or a planar motion mechanism in a wind tunnel.

Hydrodynamic forces and moments

These are due to the slipping and heeling motion of craft. The hydrodynamic forces and moments are a function of β, θ and F_{xb}, F_{yb}, M_{zh}, M_{xh} and thus the equations can be written as

$$
\begin{aligned}
F_{xh} &= 0.5\rho_w V_s^2 C_{xh} S(\theta,\beta) \\
F_{yh} &= 0.5\rho_w V_s^2 C_{yh} S(\theta,\beta) \\
M_{xh} &= F_{yh} z_g \\
M_{zh} &= 0.5\rho_a V_s^2 C_{mzh} S(\theta,\beta) l_c
\end{aligned} \tag{6.9}
$$

where C_{xh}, C_{yh} are the hydrodynamic coefficients of the cushion and skirt, which can be written as

$$
\begin{aligned}
C_{xh} &= C_{xh0} + C_{xh1}\theta + C_{xh2}\beta \\
C_{yh} &= C_{yh0} + C_{yh1}\theta + C_{yh2}\beta
\end{aligned} \tag{6.10}
$$

$S(\theta,\beta)$ is the lateral area of skirts in contact with the water surface in the case of heeling angle θ and yawing angle β of the craft.

C_{xh1}, C_{xh2}, C_{yh1}, C_{yh2} are the position derivatives of skirt and cushion; these can be written as

$$
\begin{aligned}
C_{xh1} &= (\partial C_{xh}/\partial\theta)\theta = \beta = 0 \\
C_{xh2} &= (\partial C_{xh}/\partial\beta)\theta = \beta = 0 \\
C_{yh1} &= (\partial C_{yh}/\partial\theta)\theta = \beta = 0 \\
C_{yh2} &= (\partial C_{yh}/\partial\beta)\theta = \beta = 0
\end{aligned} \tag{6.11}
$$

C_{xh1}, C_{xh2}, C_{yh1}, C_{yh2} can all be measured in model tests in a towing tank or circulating water tunnel.

M_{xh} = hydrodynamic moments of cushion and skirts about the x axis
M_{zh} = hydrodynamic moment of cushion and skirt about the z axis
l_c = cushion length
C_{mzh} = corresponding hydrodynamic coefficient

$$
C_{mzh} = C_{mzh1}\theta + C_{mzh2}\beta \tag{6.12}
$$

where

$$
\begin{aligned}
C_{mzh1} &= (\partial C_{mzh}/\partial\theta)\theta = \beta = 0 \\
C_{mzh2} &= (\partial C_{mzh}/\partial\beta)\theta = \beta = 0
\end{aligned}
$$

Cushion force and moment

Cushion force and moment F_{yc}, M_{zc}, M_{xc} can be written as

$$
F_{yc} = \rho_a Q_c V_j = \rho_a Q_c (2p_c/\rho_a)^{0.5} \tag{6.13}
$$

where V_j is the jet velocity under the side skirt, p_c the cushion pressure, Q_c the jetted flow rate under the side skirt

$$
Q_c = l_c h_c V_j \phi
$$

where ϕ is the flow coefficient, h_c the craft hover height at heeling-up side

$$
h_c = h_0 + 0.5B_c \tan\theta
$$

h_0 the initial hover height and B_c the cushion beam.

Thus equation (6.13) can also be written as

$$F_{yc} = \rho_a l_c (h_0 + 0.5B_c \tan\theta)(2p_c/\rho_a)\phi$$
$$= 2l_c \phi p_c (h_0 + 0.5B_c \tan\theta) \quad (6.14)$$

$$M_{zc} = F_{yc} l_{Gc} \quad (6.15)$$

$$M_{xc} = F_{yc} z_g \quad (6.16)$$

where l_{Gc} is the longitudinal distance between the LCG and midship, z_g the height of the VCG.

Aerodynamic force and moment

Aerodynamic forces and moments F_{xm}, F_{ym}, M_{zm}, M_{ym} can be written as

$$F_{xm} = \rho_a V_s Q \cos\beta$$
$$F_{ym} = \rho_a V_s Q \sin\beta$$
$$M_{zm} = F_{ym} z_m = \rho_a V_s Q \sin\beta (z_m - z_g)$$
$$M_{xm} = F_{ym} z_m = \rho_a V_s Q \sin\beta (l_{Gm}) \quad (6.17)$$

where Q is the fan flow rate (m^3/s), l_{Gm} the distance between the LCG and centre-line of the fan air inlet (m) and z_c the height of centre-line of the fan air inlet over ground (m).

Restoring moment ($M_{x\theta}$) during heeling (rolling) of craft

$$M_{x\theta} = Wh \tan\theta \quad (6.18)$$

where h is the metacentric height of the craft on cushion (m) and W the craft weight (N).

The differential equations of motion

Substituting equations (6.2)–(6.18) into equation (6.1), the coupled differential equations in four degrees of freedom (surge, sway, yaw and roll) can be obtained as

$$F_x = m\ddot{x} - \beta\dot{y} = -0.5\rho_a V_s^2 S_a (C_{xa0} + C_{xa\alpha}\alpha + C_{xa\beta}\beta + C_{xa\dot{\beta}}\dot{\beta})$$
$$- 0.5\rho_w V_s^2 S(\theta, \beta)(C_{xh\theta}\theta + C_{xh\beta}\beta)$$
$$- \rho_a V_s Q \sin\beta + F_{xp}$$

$$F_y = m\ddot{y} - \beta\dot{x} = -0.5\rho_a V_s^2 S_a (C_{ya0} + C_{ya\alpha}\alpha + C_{ya\beta}\beta + C_{ya\dot{\beta}}\dot{\beta})$$
$$- 0.5\rho_w V_s^2 S(\theta, \beta)(C_{yh\theta}\theta + C_{yh\beta}\beta)$$
$$- \rho_a V_s Q \sin\beta - 2l_c p_c \phi (0.5B_c \tan\theta + h_0)$$

$$M_z = I_z\ddot{\beta} = -0.5\rho_a V_s^2 S_a l_a (C_{mza0} + C_{mza\alpha}\alpha + C_{mza\beta}\beta + C_{mza\dot{\beta}}\dot{\beta})$$
$$- 0.5\rho_w V_s^2 S(\theta, \beta)(C_{mzh\theta}\theta + C_{mzh\beta}\beta) l_c$$
$$- \rho_a V_s Q \cos\beta\, l_{Gm} - 0.5 l_c p_c \phi (0.5p_c \tan\theta + h_0) l_{Gc}$$

$$
\begin{aligned}
M_x = I_z\ddot{\theta} \quad &= -0.5\rho_a V_s^2 S_a(C_{ya0} + C_{ya\alpha}\alpha + C_{ya\beta}\alpha + C_{ya\dot{\beta}}\dot{\beta})z_a \\
&\quad - 0.5\rho_w V_s^2 S(\theta, \beta)(C_{yh\theta}\theta + C_{yh\beta}\beta)z_g \\
&\quad - \rho_a V_s Q \sin\beta(z_m - z_g) \\
&\quad - 2l_c p_c \phi(0.5p_c \tan\theta + h_0)z_g - Wh\tan\theta
\end{aligned} \tag{6.19}
$$

These nonlinear differential equations of motion in four degrees of freedom (6.19) can be solved as a type of time history-response solution by the Runge–Kutta method, in which we neglect the damping moment due to rolling motion because of the small value of rolling velocity $\dot{\theta}$.

Some assumptions have been made in these equations and it is difficult to determine the various derivatives analytically, so they are normally solved by iteration using a computer.

6.4 Course stability

Amphibious ACVs generally have only a small hydrodynamic component of drag over water. When operating over relatively smooth ground, or ice, such craft are totally dependent on their aerodynamic control forces to maintain track, or make manœuvres. The ability to maintain a desired track (course stability) therefore requires effective aerodynamic control forces to be available.

Effective yawing control forces via the rudder(s) and stable aerodynamic directional stability via adequate vertical fins are important. If a craft has low rotational stability, the pilot will be obliged to turn rudders frequently to correct course and large yawing angles will be required for most turning manœuvres. High yawing angle and associated sideslip is particularly unfavourable in a seaway, as it leads to rolling motions which are uncomfortable for passengers. For this reason, course stability is a very important design criterion.

The course stability of an ACV can be divided into two, i.e. static and dynamic course stability. The static course stability can be understood as the ability of a craft to keep a given course at a yawing angle of β, and the dynamic course stability is the ability of a craft to keep a given course at a yawing angle β, heeling angle θ and yawing angular velocity ω_z.

The yawing angular velocity mentioned above does not represent the drifting angular velocity $\dot{\beta}$, but $\omega_z = \dot{\psi}_0$ which not only includes the self-rotation of the ACV, but also the revolution of ACV.

Static course stability

The condition for static course stability of an ACV can be written as

$$C_z^{\beta} < 0$$

where C_z^{β} is the coefficient of static course stability. From equation (6.19), we have

$$m_z^{\beta} = 0.5\rho_a V_s^2 S_a l_a C_{mz}^{\beta}\beta + 0.5\rho_w V_s^2 S(\beta) l_a C_{mz}^{\beta}\beta + \rho_a V_s Q \sin\beta l_{Gm}$$

where m_z^{β} is the rotating moment of an ACV about the z axis caused by the yawing angle β. The rotation moment m_z^{β} as defined above does not consider the effect of other parameters, such as heeling angle θ, on the rotating moment, therefore the coefficient of rotating moment of an ACV at the yawing angle of β about the z axis can be written as

$$\begin{aligned} C_z^{\beta} &= 1/[0.5\rho_a V_s^2 S_a l_a](\partial m_z/\partial\beta)\beta = 0 \\ &= C_{mza}^{\beta} + (\rho_w l_c/\rho_a l_a)C_{mzh}^{\beta} + Ql_{Gm}\cos\ \beta/[0.5\rho_a V_s^2 S_a l_a] \end{aligned} \tag{6.20}$$

in which we assume that $S(\beta) = S_a$ = constant and we can also neglect the item of momentum force, considering the moment due to this momentum force as a small value and the items of hydrodynamic force (moment) in the case of small yawing angle. Thus the foregoing expressions can be simplified to

$$C_z^{\beta} = C_{mza}^{\beta} < 0 \tag{6.21}$$

In order to maintain high course stability for an ACV, the yawing moment has to be negative to present a restoring moment. In other words, the centre of lateral area of the craft hull, the centre of forces acting on the air inlets and skirts have to be located to the stern of the craft LCG. Typically the lateral centre of area should be approximately 5% behind the LCG (see Table 6.3).

Dynamic course stability

The criterion for predicting the dynamic course stability can be written as

$$C_{mz}^{\beta}/C_y^{\beta} - C_{mz}^{\omega z}/C_y^{\omega z} > 0 \tag{6.22}$$

where C_{mz}^{β} is the derivative of rotating moment about the z axis with respect to yawing angle, C_y^{β} the derivative of transverse force coefficient with respect to yawing angle, $C_{mz}^{\omega z}$ the derivative of yaw moment coefficient with respect to non dimensional yawing angular velocity and $C_y^{\omega z}$ the derivative of transverse force coefficient with respect to non-dimensional yawing angular velocity. These derivatives can be obtained from equation (6.19).

The criteria for the course stability of Soviet ACV from [52] can be written as follows:

$$\begin{aligned} C_z^{\beta} &< -0.5 \quad (\textit{see}\ \text{equation (6.21)}) \\ C_{mz}^{\beta}/C_y^{\beta} - C_{mz}^{\omega z}/C_y^{\omega z} &> +1.7 \quad (\textit{see}\ \text{equation (6.22)}) \end{aligned} \tag{6.23}$$

Analysis of the course stability of some ACV models

Figure 6.14 shows experimental results of a BHC ACV with single propeller and lift fan in a wind tunnel by R. L.Wheeler [59]. In the figure, C_N can be considered as C_{mza}^{β} in equation (6.19), because of the effect of cushion force and aerodynamic momentum on course stability was not considered in [59].

Figure 6.14(a) shows yaw stability where only the lateral area of the hull/skirt, superstructure and fins had been taken into account. Thus it is seen that the ACV is not positively stable on courses with yawing angle $\beta > 18°$. The craft will be stable on

courses with worse yawing angles when the effect of not only the hull, but also the air propellers and fins affect the course stability, which can be seen in Fig. 6.14(b).

Based on using the differential equations of motion for manœuvrability (6.19) as the mathematic model, computer analysis can be carried out to analyse the course stability of an ACV with control surfaces and lateral profile as well as various operational environments, particularly when the ACV is operating on an ice surface.

Professor Murao has taken advantage of the differential equations of motion to investigate the feasibility of handling the Japanese ACV model MV PP05A on an ice surface. Figure 6.15 shows the calculation results for this ACV at three different

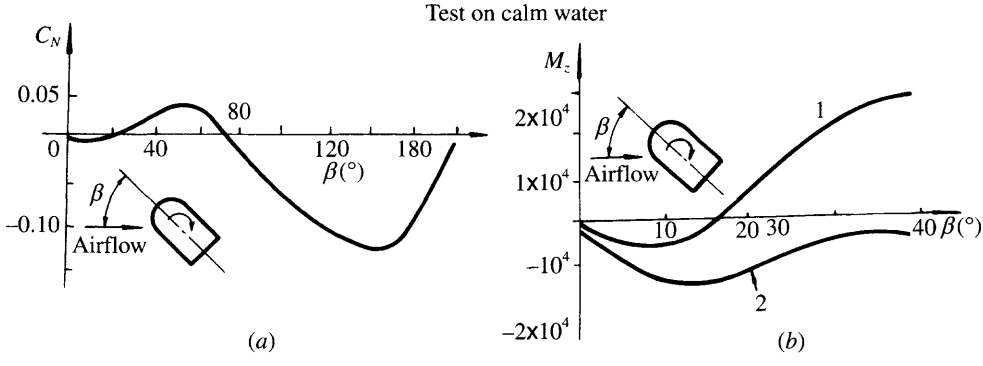

Fig. 6.14 Aerodynamic yawing moment acting on BH.7 at 50 knots: (a) hull, superstructure and stabilizers only; (b) hull, superstructure, stabilizers and air propellers. 1: yawing moment, hull only; 2: yawing moment, hull, props, fins.

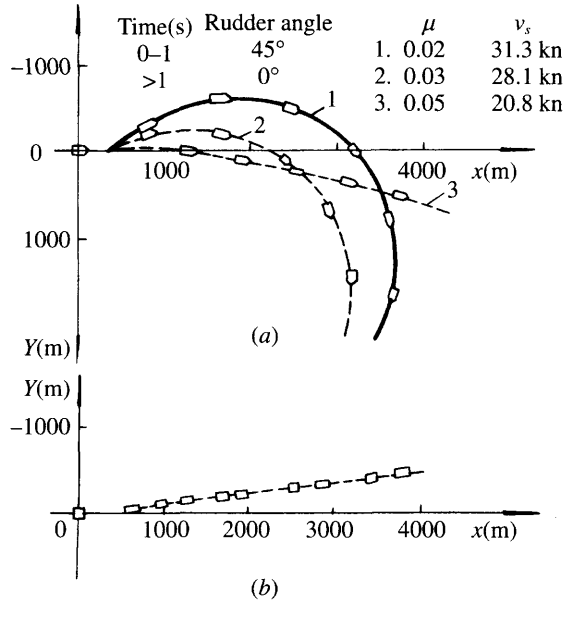

Fig. 6.15 Simulation of Japanese ACV model MV.PP5 turning manœuvre: (a) no rudder control; (b) rudder control.

speeds, 31.3, 28.1 and 20.8 knots, running on an ice surface. Three friction coefficients such as $\mu = 0.02, 0.03, 0.05$ were taken into account. Figure 6.15(a) shows the turning track of the craft with no rudder control, which means that the pilot took a step of rudder with an angle of 45° in a time interval of 0–1 s, then kept the rudders in neutral condition (rudder angle $\alpha = 0°$).

Calculation results show that the craft would not keep a straight course in the case of high craft speed and small frictional coefficient ($v = 31.3$, 28.1 knots; $\mu = 0.02$–0.05). Too high speed and too small friction coefficient would allow the rudder action to lead to continued turning of craft when the rudder is returned to zero. In the case of small craft speed ($v = 20.8$ knots) and large frictional coefficient ($\mu = 0.05$) continued turning would not occur and the ACV course would deviate, which would be the normal intent of a short application of the rudder. It is clear, therefore, that craft to be operated at high speeds in conditions of low surface interface drag need higher aerodynamic stability.

Figure 6.15(b) shows that the ACV running on an ice surface could be kept on the required course and straight course line at various craft speeds and frictional coefficients with the aid of automatic handling equipment of rudders.

6.5 ACV turning performance

The turning track of an ACV can be obtained by means of solving the differential equations of motion. The position derivatives as well as the rotation derivatives, can be obtained in water tunnel, wind tunnel and towing tank tests. Some parameters can be considered based on the computer analysis in [60], [55] and [58]:

1. Figure 6.16 presents the effect of wind directions with a wind speed of 10 knots on the turning track of an amphibious hovercraft model landing craft LCAC weighing 150 t, at an initial craft speed of 45 knots. Owing to its rotatable ducted air propellers, the ACV could be in steady turning even operating in wind.

   The longitudinal turning distance (on the x axis) would be maximum in quartering winds (angle of wind direction $\theta = 135°$) and the turning diameter would be maximum in the case of beam wind ($\theta = 90°$) and minimum in the case of head wind ($\theta = 0°$). This agrees well with experience in practice. It demonstrates that the craft can be turned quickly in a head wind because of large yawing angular velocity.
2. Figure 6.17 also shows the effect of wind directions with the wind speed of 25 knots on the turning track of the 150 t LCAC at the initial speed of 45 knots. It can be seen that the craft could be turned in the case of a head wind, while it could not be turned in the case of a tail wind ($\theta = 180°$).

   Based on practical experience ACVs travelling at high speed downwind can be very difficult to turn. The normal approach to this problem is to slow down and possibly increase skirt friction by reducing cushion power, to reduce side-slip and then begin the manœuvre.

   Rotating the craft into 'reverse' is an option for high powered craft, either military or small craft, but would be disconcerting for a passenger ferry. Based upon such computer analyses it is possible to evaluate the optimum profile of the craft

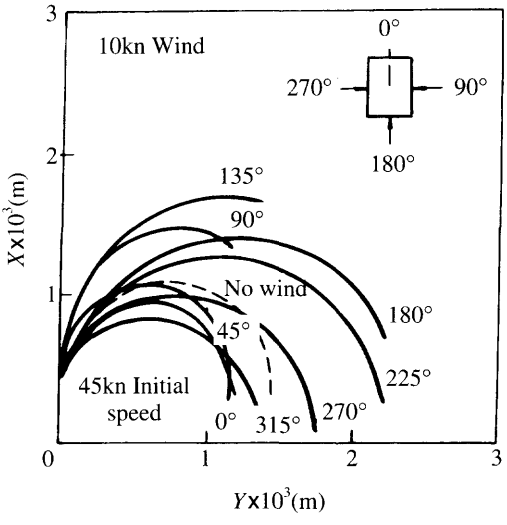

Fig. 6.16 Influence of wind direction with speed of 10 knots on the turning track of US ACV weighing 150 t at the initial speed of 45 knots.

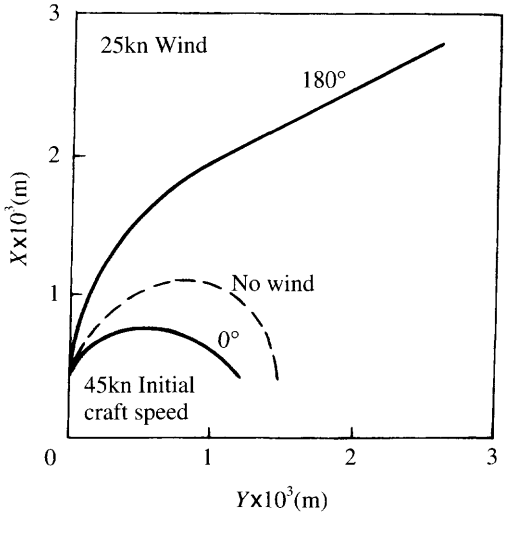

Fig. 6.17 Influence of wind direction with speed of 25 knots on the turning track of US ACV weighing 150 t at the initial speed of 45 knots.

to maximize the control capability and improve the downwind turning performance of an ACV design.

3. Figure 6.18 [55] shows comparisons of the turning track of a 150 t ACV running at initial craft speed of 45 knots in zero wind velocity with three different propulsor layouts:
   (a) First project: single air propeller located on central longitudinal plane and at 12 m aft of LCG;

(b) Second project: two propellers located on both port/starboard at 6 m from central longitudinal plane, and 12 m aft of LCG;
(c) Third project: two propellers located the same as the second project and another two propellers located on both sides of the craft at a distance of 6 m from central longitudinal plane and 12 m forward of the craft LCG.

Owing to the arrangement of two bow rotatable ducted air propeller, the third craft could be operated at large yawing angle and it had a fine turning performance at high speed.

4. Figure 6.19 shows the effect of inward banked turning of 12° on the track of the craft; calculation shows that the turning diameter would be reduced by 23% in the case of inward banked turning of 12 m, because the air leakage under the skirt of the outer side provides a centripetal force and in addition, contact of inner skirts with the water surface led to an increase of water drag of the skirt which increased the positive turning moment. All of this is known by experienced hovercraft pilots.
5. Figure 6.20, from [58], shows a typical turning track calculated by computer. Thus, Fig. 6.20(a) shows the turning track and the change of yawing angle at different locations of the craft, where v_w is the wind velocity, v the craft speed and μ the frictional coefficient of the skirt on the terrain. Figure 6.20(b) shows the time history of rudder angles. Calculation shows that the pilot had to give a positive rudder angle, then a negative rudder angle in order to avoid continuous building up of the turn. After a while the pilot gave a small positive rudder angle again to correct and stabilize the yawing angle and maintain the final angular velocity in yaw of 0.0667 rad/s, thus forming the steady turn. These calculated results of the history of the rudder angle are very similar to the practical operation of pilots.
6. The computer analysis on experimental model MV PP05 (the scaled model of MV-PP5 and MV-PP15) was also carried out in [58]. It was shown that the turning performance of the craft model with puff ports and rudders would be better than that

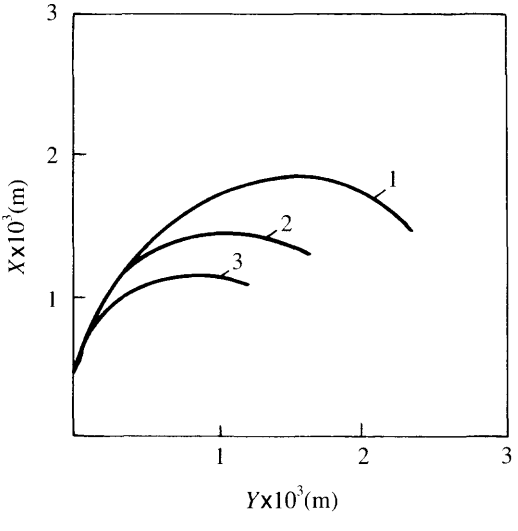

Fig. 6.18 Comparison of turning tracks between various propulsion devices on the US projects' ACV weighing 150 t at zero wind speed condition. 1: single central propulsor, 12m aft CG; 2: two propulsors offset 6m, 12m aft CG; 3: two propulsors offset 6m, 12m fwd CG.

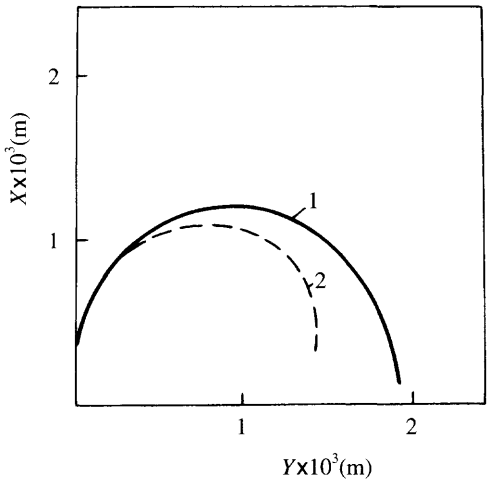

Fig. 6.19 Comparison of turning tracks between bank and non bank turn on the US ACV weighing 150 t with initial craft speed of 45 knots at zero wind speed condition. 1: turn without banking; 2: banked turn with inward heel of 12°.

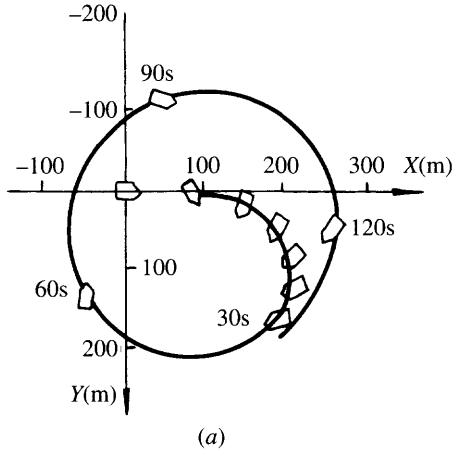

(*a*)

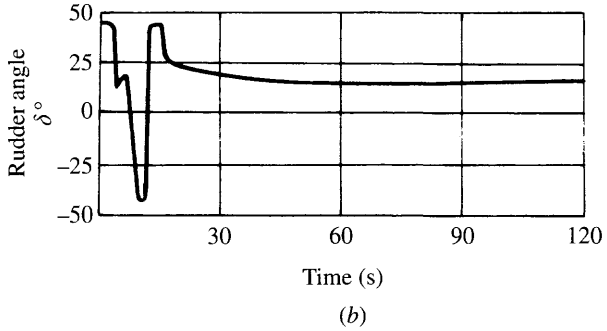

(*b*)

Fig. 6.20 A typical calculated turning track. Wind speed V_w = 60 m/s; craft speed V_s = 31 knots; μ = 0.02.

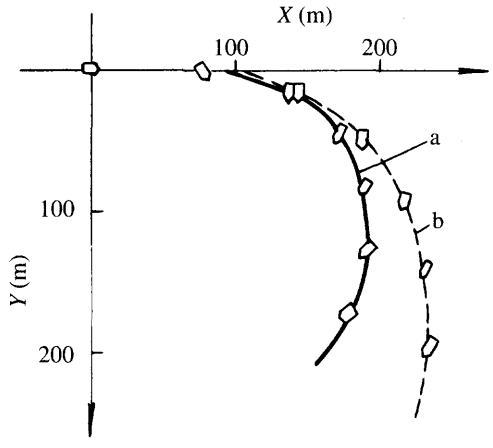

Fig. 6.21 Influence of puff ports on turning track of an ACV: (a) air rudder plus puff port; (b) air rudder control only. $V_w = 0$ m/s, $V_s = 31.3$ Kn, $\mu = 0.02$.

with only single rudder (Fig. 6.21) due to the large positive angle to get the craft quickly into steady turning. The pilots used the puff port only at the initial phase of turning to build up the required yawing angle quickly, then they shut off the puff ports and used the air rudder only to reach steady turning.

Using computer analysis for predicting the manœuvrability of craft, the time and cost of model and full-scale ship tests on manœuvrability may be reduced significantly. In addition, a large number of control surface arrangements can also be investigated. It can be seen that computer simulation provides a time history of turning track and rudder angle which is close to the practical operation of pilots; therefore, the calculation results also coincide with the practical use of control surfaces by pilots.

Owing to the practical difficulties of obtaining the various derivatives and many assumptions for deriving the differential equations of motion, solution of the differential equations is not accurate. Thus computer analysis is a tool which can be used by designers to analyse the sensitivity of changes to control surfaces on manœuvrability at the initial design phase of craft. In addition, tests of radio controlled free-flying models can be carried out to improve the predictions from analytical solutions.

7

Design and analysis of ACV and SES skirts

7.1 Introduction

Early in the development of ACVs, before the flexible skirt had been thought necessary, powerful lift engines were used to obtain a hovering gap of 50–150 mm under the hull hard structure. High-pressure peripheral air jets were used at that time to provide this vertical obstacle clearance over land and water.

These craft had sufficient amphibious capability and vertical obstacle clearance to prove the air cushion concept, but they often encountered terrain with variation in surface elevation larger than 100 mm (for example hollows in the ground, rocks and stones, tall grass). The craft hard structure then collided with the ground. For this reason, they could only operate on fairly smooth or prepared terrain, or smooth water.

These early air jet craft looked most impressive, reminiscent of a flying saucer – they literally appeared to 'hover'. The cushion demanded high power levels to achieve this clearance and they were very 'sensitive' to control. The logical way to increase the clearance height of the hull, while also reducing the height of the air jet to increase stability, was to design a flexible membrane which extended the jets. This was indeed the approach taken initially at Saunders Roe (later BHC), in the UK.

In 1958 C. H. Latimer Needham invented the flexible skirt concept and interested Saunders Roe in the idea for SR.N1. In 1960 flexible extensions to the peripheral jets of the SR.N1 were installed and this enabled a large rigid hull clearance and gave the ACV real amphibious and obstacle clearance capability. A little later this concept was extended by adding an inflated bag around the craft to act as an efficient air distribution duct, from which the flexible jets were extended (Fig. 7.1).

The advantages of flexible skirts can be outlined as follows:

1. significant reduction of lift power;
2. practical obstacle clearance;
3. true amphibious capabilities;
4. decreased calm water resistance, particularly at hump speed;
5. improved manœuvrability by use of skirt lifting and shifting;

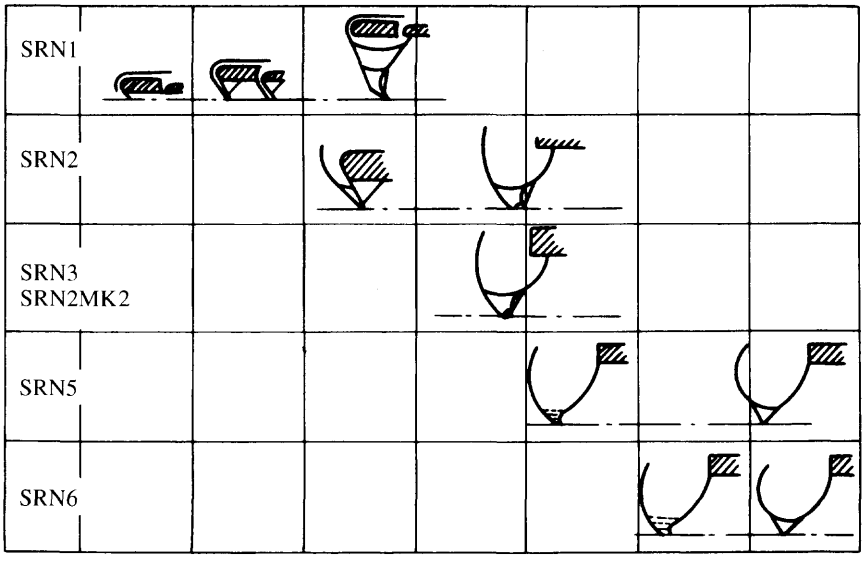

Fig. 7.1 Evolution of BHC skirt section designs from peripheral jet to segment and bag.

6. improved seaworthiness through wave-following capability of third-generation designs such as low bag pressure responsive skirts;
7. improved maintainability of ACVs and SES, since flexible skirts can be easily detached/ attached and replaced.

The appearance of flexible skirts accelerated hovercraft development at the beginning of the 1960s. The function of skirts for hovercraft has proved to be as important to the ACV as that of pneumatic tyres for an automobile.

Skirt configuration greatly affects the performance of an ACV or SES. With respect to air cushion performance, stability and seaworthiness, designers in the 1960s initially concentrated on investigation of internal air flow, the velocity distribution of jet flows from the cushion peripheral jets and the relation between air jet pressure and air gap of the craft. Investigation focused on optimization of the peripheral jet flow models by various theories, such as thin or thick nozzle theory, exponential theory etc., as discussed in Chapter 2.

The flexible skirt developments gradually improved the obstacle clearance and amphibious capabilities of hovercraft. A large air gap under the skirts was no longer necessary because their static and dynamic deformation over rough surfaces or obstacles maintained a sufficient air gap to minimize drag as the hovercraft travelled over it and so attention began to turn away from the air jet theories.

In 1962 Dennis Bliss of Hovercraft Development Ltd led by Sir Christopher Cockerell, invented the convoluted or segmented skirt (see Figs 7.13 (d) and (e)). This concept significantly reduced drag forces by the segments' ability to individually deform to an irregular surface. This allowed the air gap under the skirt to be reduced and save lift power. It was no longer necessary to use peripheral air jets to maintain a visible air gap under the cushion and so high pressures were not required in the bag-like upper skirt.

It should be noted here that two names are used for these convoluted skirt components. The segment generally refers to a geometry where the outer and inner 'faces' of the segment are at 90°. This is stable as an inflated structure. BHC and some others have used a variation where this tip angle is less than 90° and there is reinforcement of the cloth used in the 'unstable' lower area (see Figs 7.1 and 7.9) or alternatively where the base is trimmed horizontally to reduce air leakage through the delta area between the fingers. These variations can prove useful to fit fingers to the underside geometry of a medium to high-pressure bag skirt.

Over a number of years, designers experimented with lower and lower overpressures in the bag compared with the main cushion, to further save installed lift power. Below a p_b/p_c ratio of about 1.2 it was found that the upper part of the skirt also responded better to surface undulations as the craft travelled forward, giving a softer ride. This was the beginning of 'responsive skirt' technology, which has since been continuously developed in China, as well as in the UK. As skirts evolved, the bag/finger type, particularly the responsive skirt, led to a great change in air cushion efficiency, stability, seaworthiness and ride quality.

Skirts have evolved with steady improvements to the ability to deform, while still maintaining overall vehicle stability. Early skirts had a tendency to buckle beyond a certain deformation limit, causing plough-in or overturning due to sudden build-up of drag. The evolution of flexible skirts led designers to be more interested in the investigation of skirt shaping and quasi static analysis of forces acting on the skirt membrane components. This affects craft static stability and the dynamic response, which in turn affects seaworthiness and obstacle clearance.

The design issues concerned with materials, attachment, joints, damage, lifting mechanism design and internal force analysis of skirts will be discussed in Chapter 13. In this chapter we plan to introduce the geometry and theory of skirts, while in Chapter 13 component selection and design aspects will be discussed, based on these fundamentals.

We will discuss three main issues:

1. the main skirt configurations and their development, leading to the current state of the art for hovercraft and SES;
2. the static forces acting on skirts from the terrain and analysis of forces acting on different skirts, leading to determination of skirt section geometry;
3. forces leading to skirt section instability, for example skirt tuck-under over a water surface and skirt bounce, as these phenomena particularly affect the design of bow skirts and bag geometry/pressure ratio.

The study sequence, including static hovering performance, longitudinal and transverse stability, vertical stability and also seaworthiness qualities is as follows:

1. Static hovering theories, including the various jet nozzle theories, in which the relation between the total pressure of the peripheral jet, the air gap and cushion pressure, as well as flow rate, are discussed.
2. Analysis of the jet nozzle, air duct and fan characteristic as an integrated system. This means the characteristics of the air duct and fan have to be studied as well as the jet flow of nozzles.
3. Considering the jet nozzle, air ducts, fan and skirts, as an integrated system and then studying the hovering performance of such systems. This means, based upon

(2) above, that the forces acting on skirts and the deformation characteristics of skirts should be included as part of the system analysis.

7.2 Development and state of the art skirt configuration

Amphibious ACV skirt configurations

We will start with the evolution of Chinese and British skirt configurations, because most of the skirt types applied world-wide to ACVs or SES to date are similar to these (see Figs 7.1 and 7.2).

Initially the flexible skirt appeared as a type of extension jet nozzle. The skirt of SR.N1 is shown in Fig. 7.1 and its plan configuration in Fig. 7.2. Designers attempted to gain the benefit of the peripheral jet air curtain to seal the air cushion and enhance the hovering efficiency, while improving the amphibious and obstacle clearance capabilities through skirt flexibility and drag reduction.

The drag hump was found unsatisfactory with early extended jet skirts, and the inflated geometry was not completely stable. At this time the flexible components were considered as fabric ducts, rather than as 'inflated' structures. This type of skirt was also applied to the Chinese ACV 711-I in 1965.

Figure 7.4 shows the original jetted bag type skirt, which was developed from the foundation of the extended jet nozzle and had increased pressure in the diffusion bag compared to the cushion pressure, to form a stable geometry. This type of skirt was applied successfully to various types of British ACVs; the SR.N2, SR.N5, SR.N3,

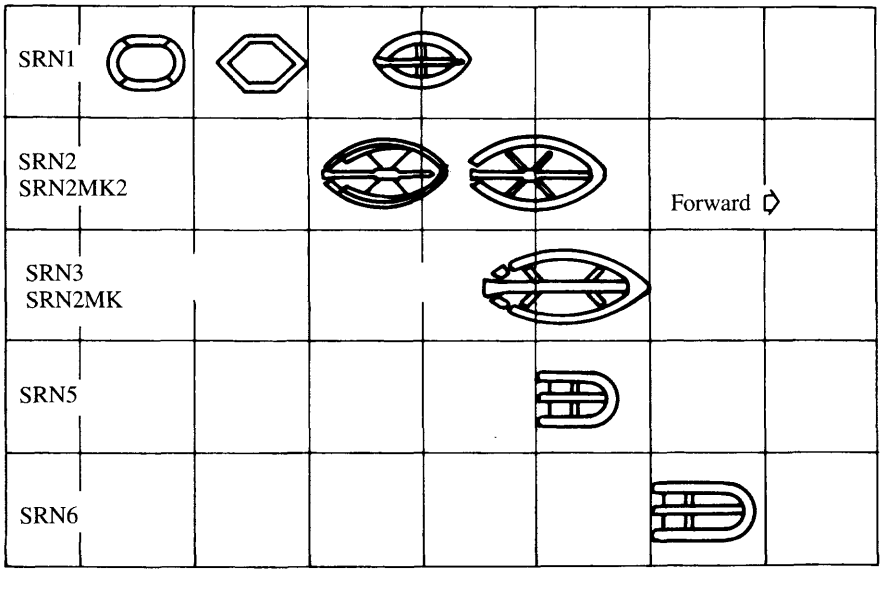

Fig. 7.2 Evolution of BHC skirt plan configuration, including stanility trunks.

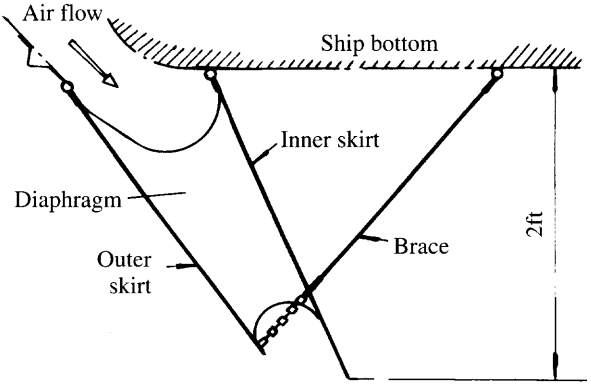

Fig. 7.3 Skirt with extended flexible nozzle.

SR.N6, etc. and was used over a long period of time. This type of skirt was also mounted on the first Chinese ACV, the model 711-I, for trials. The advantages of this type of skirt are that its geometry is stable and prevents wrinkles and crimping of the skirt cloth and can be designed to form an air jet at its base to seal the cushion air for enhancing the hovering efficiency. The disadvantages are that the jet nozzles are easily abraded and are difficult to repair and replace, as well as giving poor drag performance.

In order to form the jet nozzles, designers initially used chains to join the outer and inner skirt cloths (Fig. 7.5), but due to the force concentration on the joints and abrasion due to constant fluttering of the skirt in this area, the joint strength of the cloth/chain connection was unsatisfactory. As a consequence the skirt cloth was always damaged in trials, and operators were obliged to use a large amount of labour to repair the cloth, almost having to repair the skirt cloth with nylon stitching after every operation – poor operational efficiency.

The overhaul life of this skirt was as low as 3 hours, especially at the stern corner, as has been described in Chapter 3. After a time, cloth diaphragms were used instead

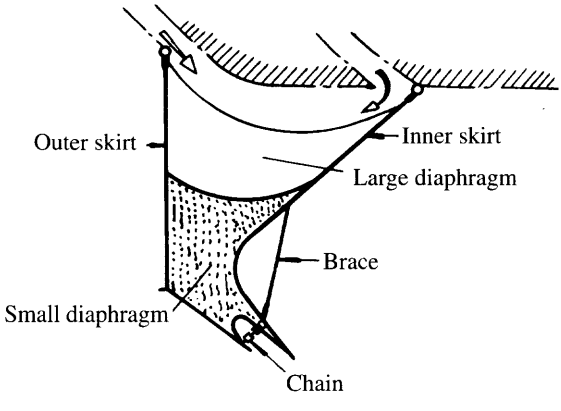

Fig. 7.4 The original geometry of jetted nozzle skirts.

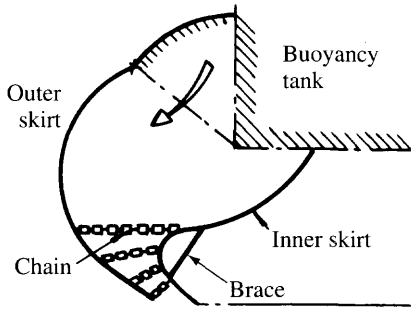

Fig. 7.5 Chain connection for bag and nozzle skirts.

of chains to join the inner and outer skirt cloths, as shown in Fig. 7.6. These were much more successful.

Figure 7.7 shows a sketch section of a bag–finger type skirt, which has been applied world wide to ACVs as a development from the earlier designs. Without the jetted nozzles at the base of this skirt type, the hover gap is similar to that of a simple plenum chamber, with slightly increased efficiency, as the angled segment wall increases the flow constriction somewhat. However, a series of other benefits are obtained, as follows:

- simple structures, easy manufacture and low cost;
- easy to repair and mount, especially for the craft which is intensively operated on a route, such as SR.N6, N4, etc., and which were required to have a long time between overhauls and short repair period for the skirts;
- fine obstacle clearance and wave-following capability (see Fig. 7.8).

There is a loss of dynamic pressure in the air flow past the bag holes. This creates the static pressure in the bag. The fewer/smaller the holes, the higher the bag pressure. High bag pressures, as used early in the design development, lead to high lift system

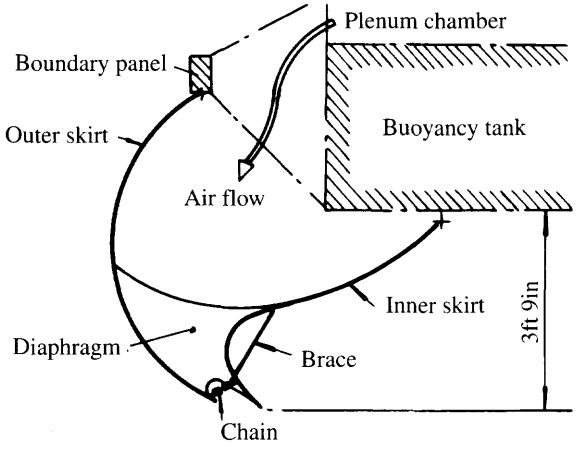

Fig. 7.6 Flexible diaphragm connection for bag and nozzle skirts.

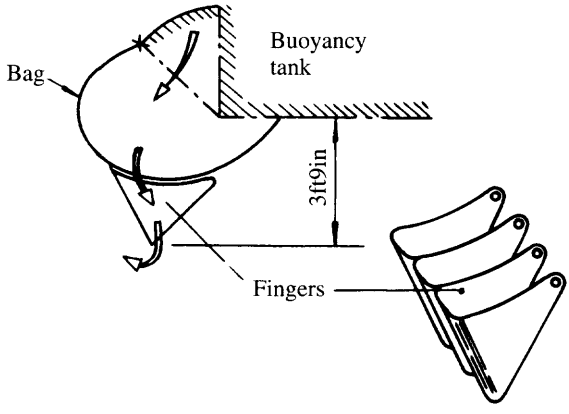

Fig. 7.7 Sketch for bag and finger skirts.

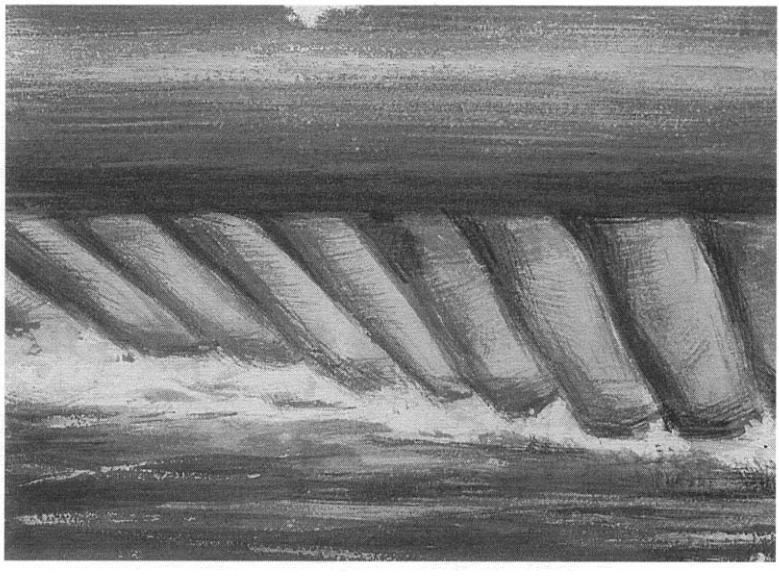

Fig. 7.8 Observation of skirts under the water by means of submersible periscope.

power. Nevertheless, the bag/segment skirt gave a much reduced water drag compared with jetted skirts, also leading to increased service life before replacement. Due to the opportunities for optimization of the bag and finger skirts, or open loop and segment design for smaller craft, these designs have had the largest number of applications world-wide.

The development of skirts based on a craft plan view at BHC is illustrated in Fig. 7.2. It can be seen that the evolution of plan shape has been essentially rectangular with rounded corners. This has been due to its simplicity for skirt geometry, ease of installation and repair, practical structural arrangement and satisfactory speed performance as well as seaworthiness. There are two basic types of stability skirts, the T type and the

+ type. The effect of these on longitudinal and transverse stability has been described in Chapter 5.

Figure 7.9 shows the skirt arrangements and configuration of the British ACV SR.N4. Transverse diaphragms were mounted in the bow skirt bag to form a D-type bag to prevent plough-in of the craft and control of skirt bounce motion. The rationale and analysis of bounce will be described in section 7.6.

Aprons were fitted at the position of the skirt fingers on the SR.N4 bag for easy detachment/attachment of the fingers and the aprons could also be elongated as an anti-spray skirt for preventing spray being blown up to the superstructure and obstructing pilot vision.

Figure 7.10 shows the skirt arrangement and its configuration of the British military ACV model BH.7. It can be seen that the bag–finger type skirt was arranged at the bow and side position and conical cells as the stability and stern skirts. The most difficult positions for this inverted U-skirt plan which have to be designed are the interception area of the stern with the rear side skirt, which is a 90° corner, i.e. the rear corner skirt. This is because scooping often occurs in this area of skirt when operating in displacement mode at low speed and while accelerating through hump speed.

The planing stern skirt with double or triple bags has generally been used in China, which improves water scooping, but it still does not solve the interface problem at the corner of the stern skirt. If the air gap under the corner skirt is high, then a large air leakage will occur from this area, but if this skirt section has no gap, then serious water scooping will occur.

In order to solve this problem, the two-dimensional stern skirt may be employed, namely, the two-dimensional side/stern skirts have to extend as far as the corner of the stern up to the intersection line with each other and some small conical cells mounted here for transition between the side/stern skirt as shown in Fig. 7.11. Figure 7.12 shows the deformation of an ordinary bag–finger skirt and responsive skirt operating in waves. The dotted line denotes the original shape of the skirt, while the solid line denotes the deformation of the skirt in waves. With respect to the ordinary bag/finger skirt, craft plough-in may happen due to the tuck-under of the skirt under the action of the waves.

An alternative is to use rounded corners at the stern as well as at the bow. Such plan-forms are used by most modern amphibious craft of all sizes. Removing the discontinuity introduced by the abrupt change at the right-angled stern corner essentially removes any tendency for scooping and dramatically improves the service life of segments in this area.

Tuck-under resistance of the responsive skirt is provided by a geometry of the bow bag such that the skirt will be deformed upward to yield to waves rather than being pulled backwards; consequently, the tuck-under phenomenon is avoided and the responsive skirt acts as a wave filter to reduce vertical acceleration and water drag in waves. The rationale for this will be introduced later.

In France, an alternative skirt type was developed, called the jupe, invented by Jean Bertin. An individual jupe is a fabric cone with a wall angle of 5–10° to the vertical. When inflated with air from inside it provides a relatively stiff cushion up to the point where the bottom edge begins to crumple or fold up; beyond this, restoring force reduces quickly. The Sedam series of craft had cushions with a series of jupes.

The highly compartmented cushion provided great heave, pitch and roll stability.

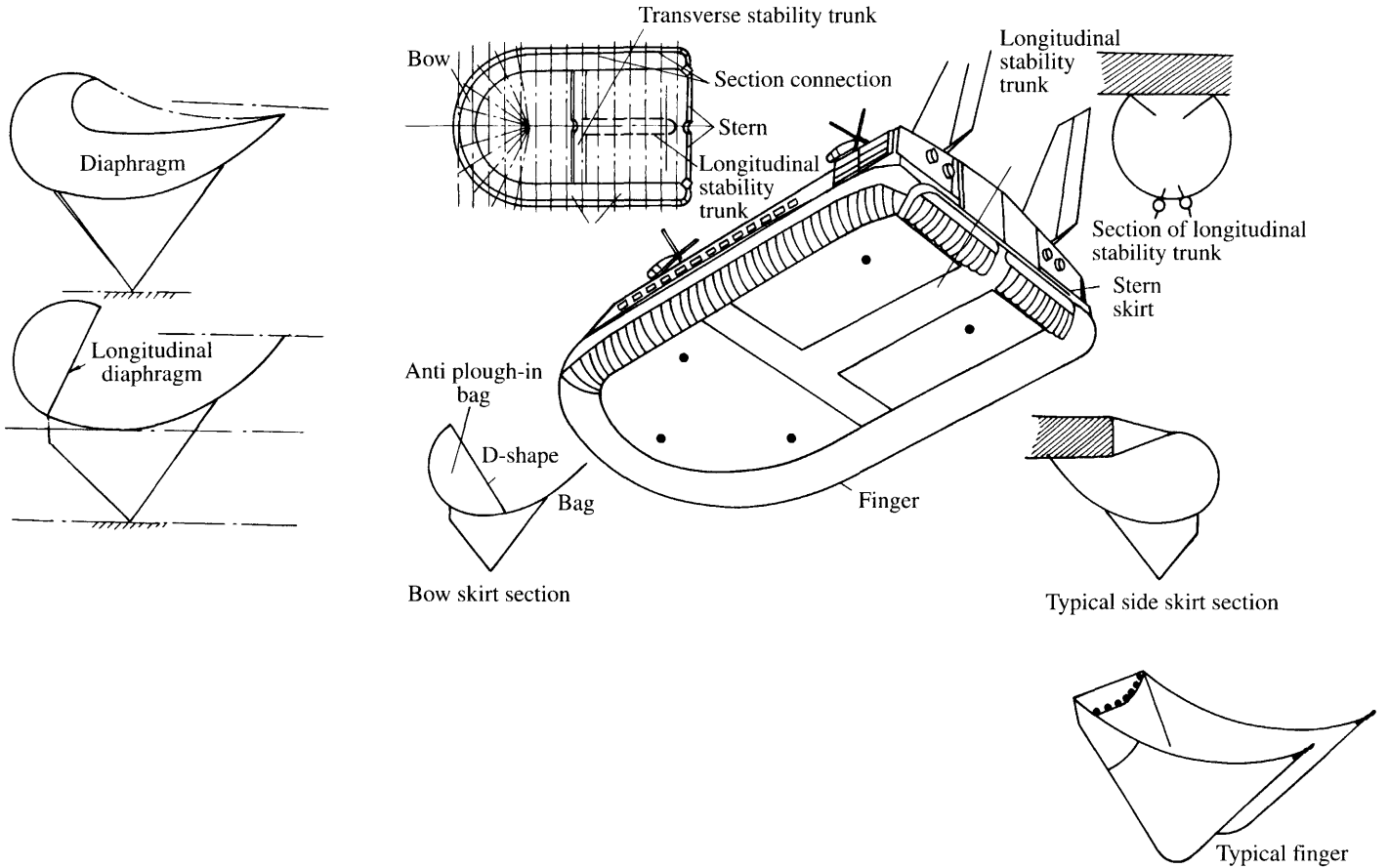

Fig. 7.9 SR.N4 skirt configuration.

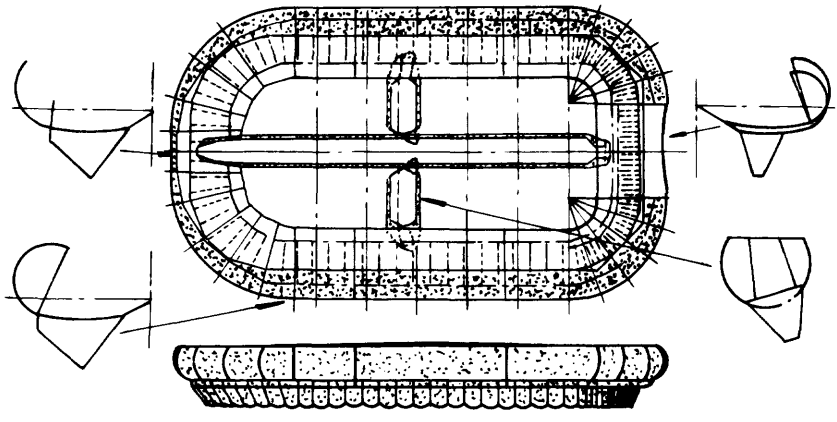

Fig. 7.10 Configuration of skirts on British military ACV BH.7.

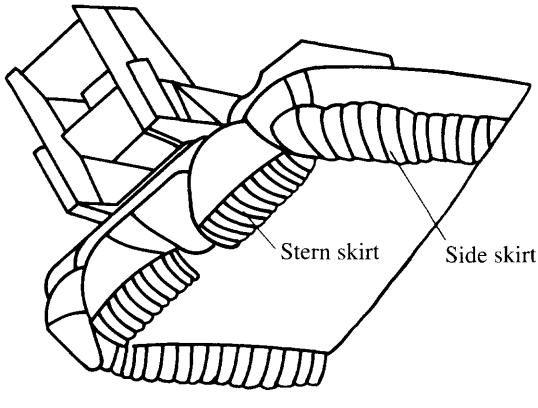

Fig. 7.11 Skirt configuration around the stern corner of SR.N6.

Jupes are not as responsive to waves as a bag/segment skirt and so give rather higher drag, resulting in higher installed power. Significant water scooping drag in the rear area of the stern jupes also reduced the acceleration margin at hump speed. As a result, the design has been superseded by the bag/segment in the industry. This could be minimized by adjustment of flow to the cells, but nevertheless still caused significant wear in this area – larger than for a bag/segment skirt.

The peripheral cell jupes skirt, a mixture of the jupe as applied to the French ACV and the bag and segment skirt, has been applied to one of the prototype LCAC craft, the JEFF-A. Excellent longitudinal and transverse stability was obtained. Maintainability and reliability were improved over a bag and segment skirt with internal stability skirts, since the greater stiffness of the pericells allowed the inner stability skirts to be deleted even though the LCAC is a high-density craft. When the craft operates in the field, it is not necessary to raise the craft in order to remove or reinstall skirt components, which are all at the external periphery of the craft.

In Japan, the finger skirt, an evolution of the jetted bag skirt with short fingers, was

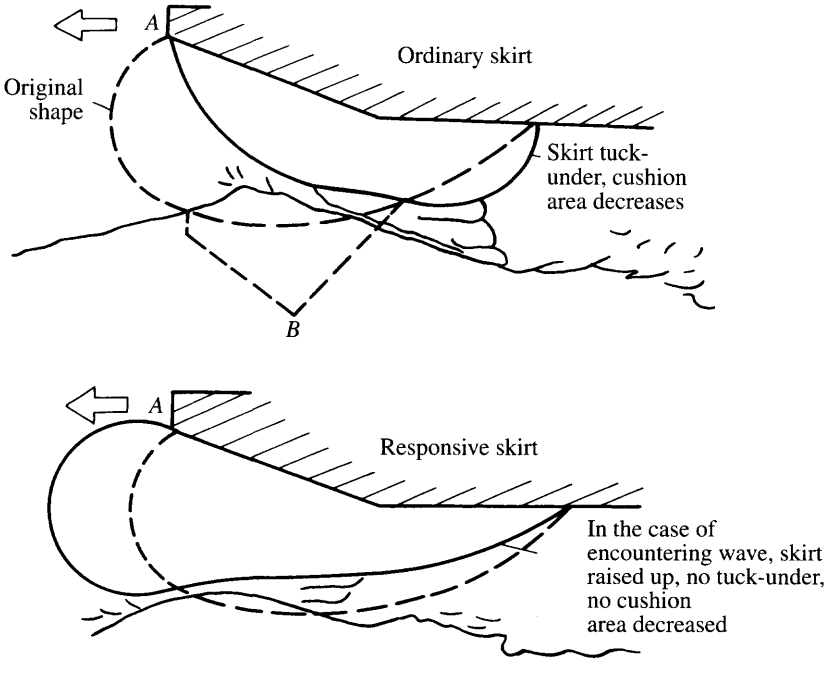

Fig. 7.12 Comparison of deformation between the ordinary and responsive skirts.

used in the 1960s and 1970s, in a similar manner to developments in the UK. More recently they use the low-pressure bag and finger skirt.

In China, the bag–finger type (or large response bag–finger skirts) is used at the side and bow and the double bag planing skirt at the stern in order to reduce the drag at hump speed and above. A D-shape bag was mounted at the bow in order to prevent plough-in and a two-dimensional skirt at the stern and corner to reduce the drag at post-hump speed. Sometimes longitudinal diaphragms are to be mounted in side skirts to improve the skirt's natural frequency bounce motion.

Small amphibious utility ACVs generally use open loop and segment skirts, low-pressure bag and segment skirts, or extended segment skirt designs.

The geometry of all of these skirt designs is determined by static equilibrium of forces, considering the skirt as a two-dimensional section of an inflated membrane. Some of the initial geometrical parameters have been determined by trial and error, through experience with model testing, or operation of actual craft. Where appropriate, these guidelines are included below.

Comparisons between the various ACV skirt configurations

We have followed the development of skirt configurations up to date. The question now is whether there is a single optimum for all ACVs, or whether the designer should select different characteristics for different craft missions.

The segmented skirt offers the best combination of drag coefficient and adaptation to irregular surfaces. With the exception of SES stern skirts the segment has now been

universally adopted as the base skirt component. Combining the segment with an inflated bag, or for smaller craft an open loop, allows a skirt to be designed to respond to undulations such as waves and swell, improving ride quality.

The designer's problem is how to select a suitable bag overpressure to obtain the right balance of static stability and dynamic response. This, combined with the overall geometry (straight or tapered), is the main variable to be investigated by a designer of an ACV for commercial or military use.

Simple segmented skirts are used successfully where cushion flow is not so important, for example on small recreational craft, or where compliance is less important than stability, as with a large load-carrying platform.

The following overview of the current skirt types may be helpful.

Bag and finger (segment) (Fig. 7.7)

This is the main skirt type in use for commercial ACVs today. The segment or finger depth is normally between 50 and 80% of the cushion height to the underside of the hull, depending on the bag pressure. In order to allow low bag pressures to be used ($1.05–1.2p_c$), larger craft generally need at least an amidships transverse stability skirt for pitch stiffness. Side skirt finger lower tips are usually placed 10–25% of the finger height inside the gunwale of the craft hull. Finger width is normally between 40 and 50% of its depth.

Responsive skirts use deep rather than shallow bag geometries. At the bow, rather than using a swept back geometry that brings the segments right under the bow, BHC has pioneered the bulbous bow skirt. The geometry is such that during pitch down movement, as the segment crushes, the bag rotates upwards maintaining stiffness and preventing the cushion centre of pressure moving backwards.

BHC also uses a tapered geometry, such that the stern hull clearance is less than at the bow, giving a hull static trim of about 2°. It has been found by experience that amphibious craft seem to have the best balance of dynamic stability and control when the trim is between 1 and 2°. Shaping the skirt allows this optimum to be maintained while minimizing cushion air flow. The optimum trim is directly related to the aerodynamics of the hull and superstructure; it is probably best to start design with 0.75–1° taper, if this approach is used by a designer.

Bag and pericell (Fig. 7.13(c))

This skirt form is where the segments are modified into a similar geometry to a jupe. It can provide similar stiffness to the equivalent bag and finger skirt with stability skirts, for high-density craft. The bag pressure required is high, $1.4–1.8p_c$, so this skirt is less suitable for craft in passenger operation.

Open loop and segment (Fig. 7.13(d))

This skirt is used on smaller craft, generally below 5 t. The loop is at p_c and so this is the most efficient skirt form. The geometry of the loop can be varied to give the right combination of responsiveness for a seaway and skirt shift mechanisms can be used to enhance manœuvring. Tapered geometry is possible, though not normally used.

A swept-back bow skirt is necessary, as it is not practical to design a stable bulbous bow geometry as for a responsive bag and finger skirt. This is not a problem for medium-speed utility craft, for which the skirt is most popular. Around the bow the

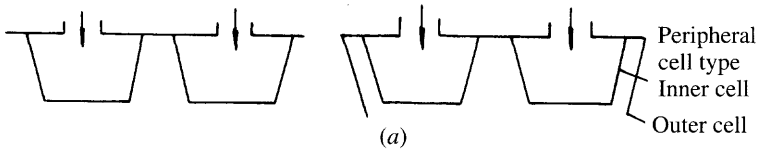
Peripheral
cell type
Inner cell
Outer cell

(*a*)

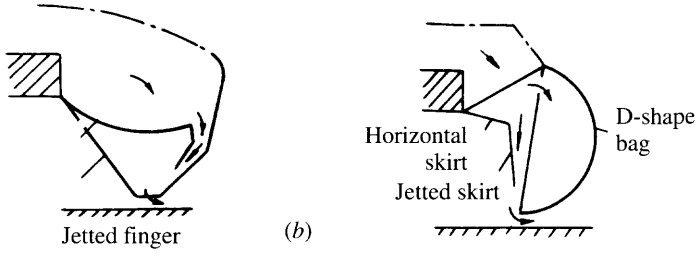
Jetted finger
Horizontal
skirt
Jetted skirt
D-shape
bag

(*b*)

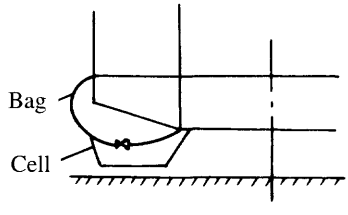
Bag
Cell

(*c*)

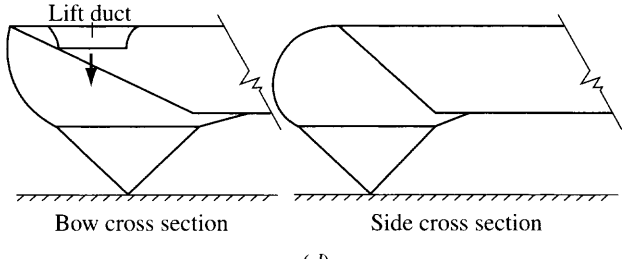
Lift duct
Bow cross section
Side cross section

(*d*)

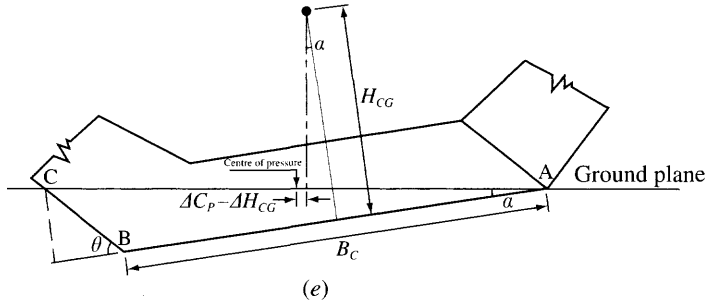
a
H_{CG}
Centre of pressure
C
A
Ground plane
$\Delta C_P - \Delta H_{CG}$
α
θ
B
B_C

(*e*)

hull gunwale is brought forward of the outer segment line by 20–40% of segment height.

The stern segments for this skirt are normally 'chip-bags', with the inner segment surface closed as well as the outer. Inner attachments to the hull are via a fabric sheet rather than skirt ties. Both of these items are for prevention of scooping while traversing hump speed.

Extended segment (Fig. 7.13(e)

This a relatively stiff skirt system for small utility and recreational craft in the size range 200–2000 kg. It does not respond greatly to waves and obstacles, except by deflection of individual segments. Segment width follows the same rule as for those attached to a loop, except that the height is now to the attachment at the craft gunwale, width being 20–25% of this total depth. Since the segments are 80–90% hull structure depth, they are generally quite wide and the air escape area is large in the segment delta region. Relatively high cushion flow is therefore required. This is not a problem for recreational craft, which do not have to meet the efficiency requirements of a commercial ACV.

Figure 7.14 illustrates a number of possible skirt plan-forms. Sketch (a) is the single-cell cushion, while (b)–(d) are variations on the skirt with inner keels, the longest keel being lengthwise in (b) and transverse in (d). Sketches (e)–(h) show variations on the jupe or pericell. Sketch (e) combines the bag and pericell with inner keels, while (f)–(h) dispense with the bag to provide a stiffer cushion. Current practice is to use as low as possible p_l/p_c, favouring designs (a) or (d) for optimum drag and seaworthiness.

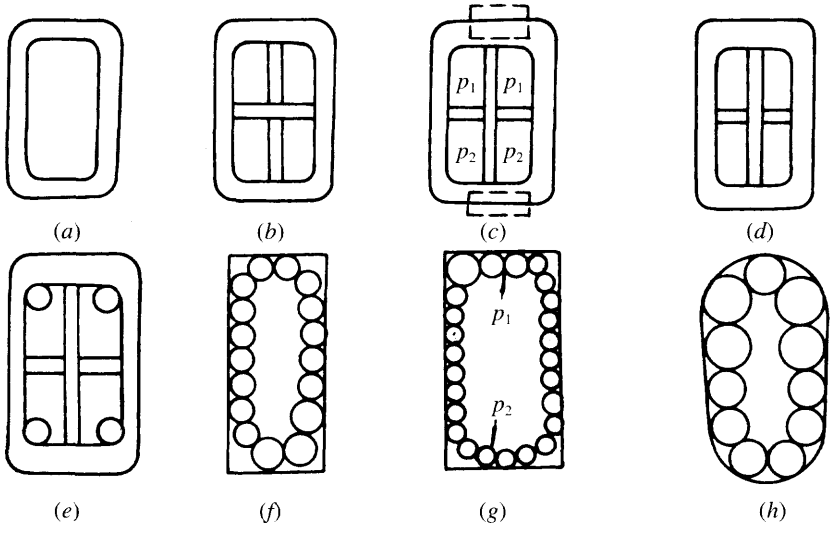

Fig. 7.14 Eight types of skirt considered as options for selection during the design of landing ACV by Bell-Textron Corporation of USA.

Fig. 7.13 (opposite) Configurations of typical skirts of France, Japan, USA and UK: (a) France – jupe; (b) Japan – jetted finger skirt, and jetted D-shaped bag; (c) USA – the bag and jupe; (d) UK – open loop and segment skirt; (e) UK – extended segment skirt.

SES bow and stern seals

SES generally use simple segments, or inflated bag and segment at the bow and multiple lobe bags at the stern. Earlier craft such as the Hovermarine series had ship-shaped bows. A shaped bag and segment bow skirt responded to waves minimizing cushion air loss in a seaway. More recently, SESs have been designed with similar planform to catamarans and almost two-dimensional segmented bow seals have been used on craft from the USA, Norway, Sweden, Germany and Japan.

The design requirements for these SES seals can be summarized as follows:

- A flexible response to the heaving motions of the SES, to minimize cushion pressure variations.
- A suitable damping rate for pitch motion of craft to give small wave resistance in rough seas.
- A suitable depth of cushion layer between the waves surface and the wet deck structure of the SES to attenuate wave slamming.
- The seals scoop less in the water in the case where craft run in waves at post-hump speed.
- The seals may be designed to 'plane' on the water surface at post-hump speeds, so that the seal will be raised up during contact with an oncoming wave and shutting as waves pass. Thus the air leakage rate might be reduced to a minimum and reduce lift power. This is similar to the captured air bubble principle which was put forward as a design many years ago, but which had little success because without flexible seals at the bow and stern, drag was very high in any sea state.

We will now briefly introduce the evolution and development of the seals on the SES.

Early developments

During the early SES development stage most researchers concentrated on the theoretical advantages of the captured air bubble principle, and thus the lift power, in order to be more suitable for development of larger-sized craft. At the end of the 1960s MARIC began to design a balanced seal (Fig. 7.15) mounted on the first

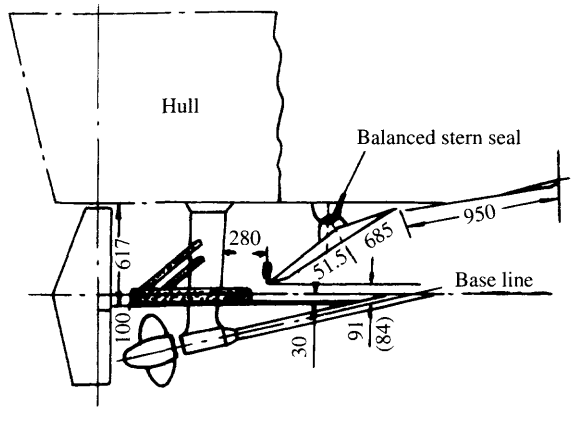

Fig. 7.15 The balanced rigid stern seal on Chinese passenger SES 713.

Chinese passenger SES model 713. The principle is the same as that of the balanced rudder, where the components due to the cushion pressure about the pivot of the stern seal were approximately equal to zero; therefore the stern seal can move up and down with the waves to reduce cushion flow rate and drag.

This type of stern seal has been successfully used on the craft model 713 but could not be developed on later ships due to the difficulty of adjustment of the balance coefficient of the stern seal, and a large amount of sand and mud piled up on the stern seal, which caused a reduction of the post-hump speed and poorer take-off performance of the craft.

Stern seal with air bag

This type, i.e. the inflatable bag, as shown in Fig. 7.16, has been mounted on both Chinese and US craft [61]. Unfortunately, most of these seals, as shown in Fig. 7.16, have not been developed due to their poor practicability and complicated structure.

Three-dimensional bag–finger bow seal and two-dimensional double bag type stern seal

As shown in Figs 1.14, 1.16, 1.17, 7.17 and 7.18, these are widely used on British SES, even though complicated technology is used for manufacture.

Pure finger bow skirt in combination with stern double planing bag

These are shown in Figs 7.16(b) and 7.17, and are widely used on the Soviet SES. With small waves on inland rivers, the bow pure finger skirts satisfy the requirements of seaworthiness for rivers, moreover the manufacturing technology and cost for this type of skirt are simpler and cheaper.

Bow skirts of bag–finger type and multi-bag stern skirt

These types are the general skirt types for the US SES. However, considering the poor abrasion characteristics of flexible skirts, they have studied the new bow seal of the piano keyboard type and composed of GRP in order to improve the operational life of the seal. The seal can be divided into several piano keyboard-like sections, which can be moved freely, and avoiding the coming waves in order to get good seaworthiness, low drag and high life of the seals (Fig. 7.20). This type of bow seal has been developed by the Americans and Dutch.

Two-dimensional bag and finger type bow skirt and stern planing rigid seal

As shown in Fig. 1.35, these are typical seals mounted on the Chinese inland river SES, which have characteristics of fine take-off capability, stable drag and low sensitivity to LCG shifting, but poor seaworthiness due to the larger heaving stiffness of the stern-fixed planing surface than that of the bow bag/finger type of skirts to stop plough-in in following waves.

Thanks to the small waves of inland rivers, these types of seals have been developed; but they are not really suitable to be used on craft operating on the coast or at river mouths. In such cases the seals will be replaced by the two-dimensional

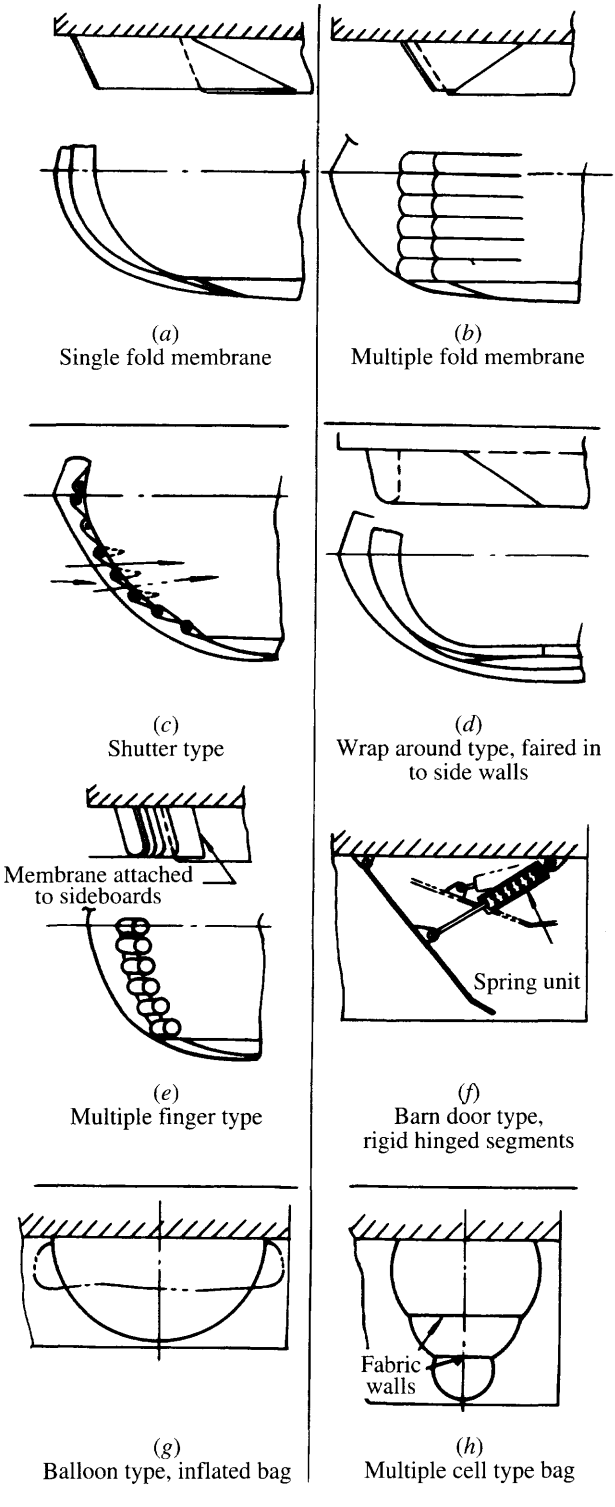

Fig. 7.16 Various experimental seals on US SES craft.

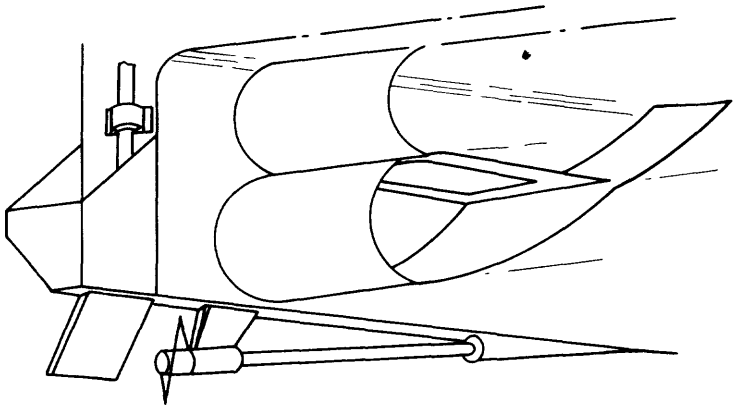

Fig. 7.17 Stern seal (double bag type) on British SES Hovermarine HM-2.

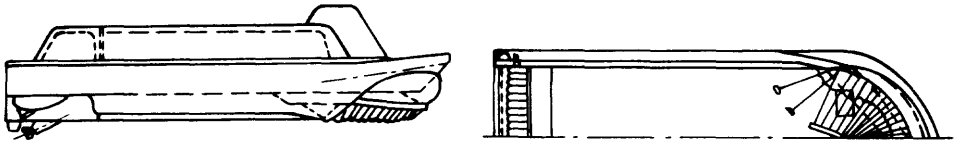

Fig. 7.18 Bow and stern seal of HM-2 Mk 3.

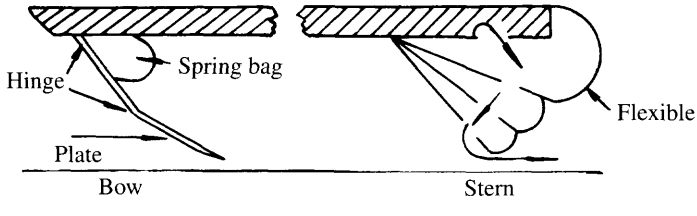

Fig. 7.19 Skirt system on US test SES.

bag–finger type bow skirt and two-dimensional double bag planing stern seals, which are similar to the skirts used on British SES.

Detachable bow/stern seals

Due to the non-amphibious capability of SES, the replacement of seals can be very difficult to carry out and the SES have to be got into floating dock or dock to repair or replace the skirts. For this reason skirt life is always an important parameter and has been investigated by researchers and manufacturers. No doubt detachable bow/stern seals will improve this situation significantly. Such seals have been applied to US and former Soviet SES.

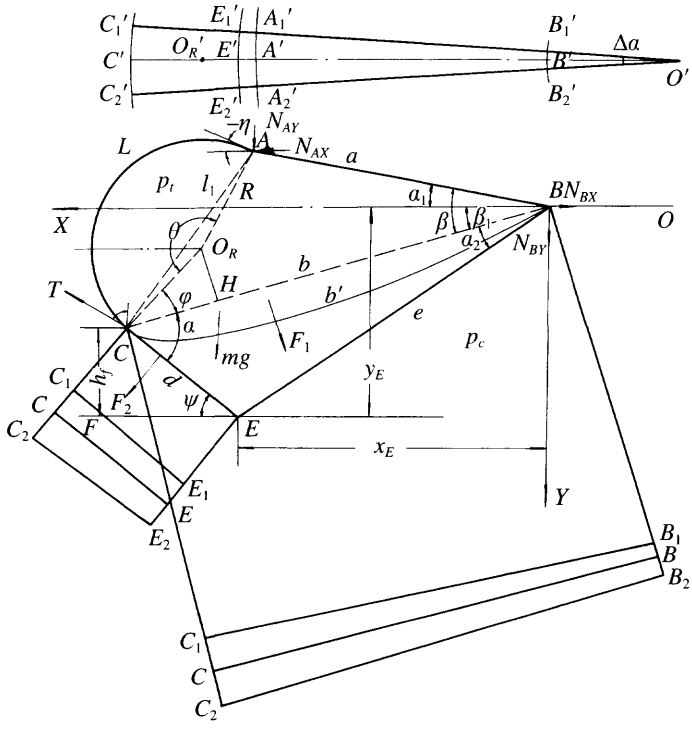

Fig. 7.20 Sketch identifying the principal parameters of bag and finger type skirts.

7.3 Static geometry and analysis of forces acting on skirts

Bag and finger type skirts are the most widely used in both modern ACVs and SES, so this type of skirt is the main object of study in this chapter. We will now review the basis for determining the static and dynamic equilibrium geometry for this type of skirt.

Static geometry of the bag and finger type skirt [62; 63]

Tests of skirts mounted on the craft 711-II and 722 have been carried out at model scale in the skirt test facilities of MARIC. During these tests some related parameters such as bag–cushion pressure ratio were varied and the variation of locations such as the joint point of the bag and finger C and the lower tip of the fingers E (as shown in Fig. 7.19) were also measured for analysis and recalculation.

Results from model tests

The following conclusions were drawn from the tests carried out:

1. *Elastic deformation and hysteresis effect on skirt geometry.* Tension deformation of the skirt fabric does not dramatically affect the shaping of the skirt, therefore it can

be concluded that the elastic modulus and the hysteresis effect of skirt cloth does not seriously affect the static deformation of the skirt, and can be neglected.

2. *Effect of bag to cushion pressure ratio.* Tests demonstrated that the skirt geometry was closely related to the bag–cushion pressure ratio p_t/p_c (p_t – bag pressure, p_c – cushion pressure).
3. *Bag chord length b.* It is found that chord length in the bag b varies only a little with variation of p_t/p_c, thus it can be considered that the lower part of skirt, triangle (Δ) BCE does not vary with the parameters, but that ΔBCE rotates about B in the X–Y plane as shown in Fig. 7.19.

   Meanwhile $b/b' \cong 0.96$–0.97 at $p_c/p_t \cong 0.85$ and b/b' will increase with p_c/p_t and vice versa, where b is the chord length of B′C′and b' the arc length between joints B and C.
4. *Distances A–B.* At a given size of air ducting of the craft, i.e. the linear distance between points A and B as shown in Fig. 7.19, it is found that the geometric parameters which greatly affect the static deformation of the bag–finger skirt are the length of the outer cloth of skirt bag b and its inner length b'. In general the vertical deformation of the skirt increases with b and the finger tip rises, but horizontal deformation increases with L and the finger tip drops down.

   It can be seen from this that skirt shaping and its deformation can be changed with L and b and it is found that the wave-yielding capability is fine when the vertical deformation of the skirt is large (Fig. 7.12). In addition, static stability can be improved when the horizontal deformation of the skirt is large. Nevertheless skirt tuck-under will occur in the large responsive skirt under the action of hydrodynamics, if no preventative measures are taken. For this reason it is not suitable for anti-plough-in of craft unless restraint diaphragms are installed in the bag.
5. *Diaphragms.* Experiments show that the D-shape bag will not affect the shaping and deformation of the skirt, if the diaphragms are loose in the static hovering condition. In the case of tight diaphragms, the joints of bag and finger C will be under the control of diaphragms to reduce the vertical deformation of skirt and enhance the anti-tuck-under stability of the skirt. But experiments demonstrate that the diaphragms of D-shape bag have less effect on the location and variation of the finger lower tip.

Mathematical models and their expressions can be formed, based on the physical models which are the basis of the experiments; thus comparison of the solution of equations with experimental results can be used to find the correction coefficients. This method can be developed from the two-dimensional skirt to the three-dimensional one.

Equations for static geometry and force analysis of skirts

The outer and inner geometry lines of the skirt form concentric circles (i.e. the arc, $B_1'B_2'$ and $A_1'A_2'$ are part of concentric circles), as shown in Fig. 7.19. If we take small element Δa as the investigated object, then the arc section $OC_1'C_2'$ is the projection of this element on the X–Z plane. The quadrilateral $C_1C_2B_1B_2$ is the section plan of the bag arc in this element, which is perpendicular to the line $\bar{B}\bar{C}$. The quadrilateral $C_1C_2E_1E_2$ is the section plan of the finger element perpendicular to the line C′E′.

MARIC experiments have demonstrated that both the joint point of the bag finger

and the lower tip of finger E rotate about the axis through the point B. The length of finger d can be considered as invariable (i.e. line C′E′ does not wrinkle under the action of the cushion pressure) and the chord line of inner bag b is assumed to be approximately constant. Thus we take the ΔBCE as a free body for calculation.

For a thin inflexible ring as shown in Fig. 7.21(a), the following relation holds:

$$\pi r_1^2 \, p = 2 \pi r_1 \, t_1 \tag{7.1}$$

where p is the cushion pressure (N/m^2), r_1 the radius of the inflatable ring (m) and t_1 the tension of the membrane (N/m). For any given membrane width and unit length, the membrane tension can be obtained through the following equation (Fig. 7.21(b)):

$$2 t_1 \sin(\theta/2) = 2pr_2 \sin(\theta/2) \tag{7.2}$$

thus

$$t_1 = pr_2 \tag{7.2a}$$

where θ is the angle as shown in Fig. 7.21(b)(°).

It can be shown from equation (7.2a) that the radius of the inner part of the bag R_1 is

$$R_1 = Rp_c/(p_b - p_c) \tag{7.2b}$$

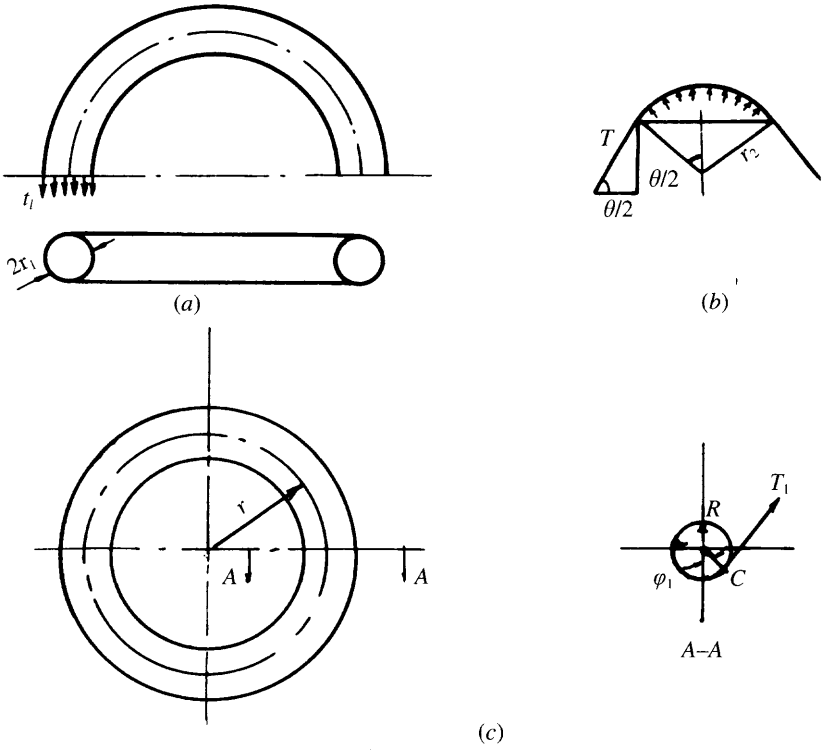

Fig. 7.21 Tension calculation for various inflatable diaphragms: (a) tension acting on inflatable loop; (b) tension on inflatable diaphragm; (c) tension acting on any point of diaphragm on inflatable circular life belt.

If the fingers are attached to the bag itself, as in a BHC skirt, the pressure force F_2 will deform this inner bag curve slightly. Readers are referred to section 7.6 for appropriate equations.

The tension of membrane T, at any given point on the inflatable circular torus, can be derived by the following expression as shown in Fig. 7.21(c):

$$T_1 \cos \phi_1 \, 2\pi \, (r + R \cos \phi_1) = \pi[(r + R \cos \phi_1)^2 - r^2] \, p_t$$

thus

$$T_1 = p_t \, R \, K_r \tag{7.3}$$

where T is the tension of the membrane (N/m), p_t the pressure in the inflatable circular life belt (N/m^2), r the radius of the large circle at that point (m), H the radius of the small circle at that point (m) ϕ_1 the angle between the tension direction and abscissa and K_r the correction coefficient due to the three-dimensional effect; according to the equilibrium condition mentioned above, which can be written as

$$K_r = (2 + R/r \cos \phi_1) / (2 \, (1 + R/r \cos \phi_1) \tag{7.4}$$

The tangential tension at any given point of the section is related to R/r and ϕ_1 and it is equivalent to that in two dimensions. If r equals infinity, where $K_r = 1$, $T_1 = p_t \, R$, it becomes the same as equation (7.2). Knowing the tension acting on the membranes due to the action of any given air pressure, the method can be developed to calculate the tension acting on the skirt bag.

There are four forces acting on ΔBCE:

- the tension of skirts at point C;
- the difference of pressure between the bag and cushion acting on the curves of inner bag BC;
- weight due to weight of the skirt fabric;
- the force due to the cushion pressure acting on the finger CE.

These forces can be calculated and substituted into the equilibrium equations. Thus the coordinates of C, E at different cushion and bag pressures can be obtained.

For curved sections, a piece with the spreading angle of Δa, like a segment of an orange, can be taken as the free body for calculation, and the equilibrium equation of forces can then be expressed as follows:

1. Tension T acting on the curve C_1C_2,

$$T = K_r \, p_t R r_c \, \Delta a \tag{7.5}$$

where R is the radius of the curve at the outer bag (m), $r_c = O'C'$ (m), p_t is the cushion pressure (N/m^2), T the tension acting on the curve C_1C_2 (N) and K_r the correction coefficient due to the three-dimensional effect, obtained according to equation (7.4)

$$K_r = \frac{(2r_o + R \cos \phi_1)}{[2(r_o + R \cos \phi_1)]}$$

$r_o = O'O'_R$ (m), when $r_o \Rightarrow \infty$, the tension is similar to the tension on the inflatable membranes per unit length at two-dimensional condition, i.e. $T = p_t R$. It is the same as in equation (7.2).

2. The force acting on the curve of inner bag $B_1B_2C_1C_2$ due to the difference of pressure between the bag and cushion is thus

$$F_1 = b/2\,(r_B + r_c)\,(1 - p_{ct})\,p_t\ \Delta a \tag{7.6}$$

where r_B = O′B′ (m), $p_{ct} = p_c/p_t$ and F_1 is the force acting on the curve at inner bag $B_1B_2C_1C_2$ (N).

3. Force acting on the skirt finger, F_2, is

$$F_2 = d/2\,(r_E + r_c)\,p_{ct}\,p_t\,\Delta a \tag{7.7}$$

where r_E is the outer radius O′E′ (m) and d the length of the skirt finger (m).

4. Weight of skirt fabric at X, with the spreading angle of Δa

$$mg = W_c\,r_c\,\Delta a\,K \tag{7.8}$$

where mg is the skirt cloth weight (N), W_c the weight of the two-dimensional section of skirt ΔBCE per unit length (N/m) and K the correction coefficient due to the three-dimensional effect, i.e. the ratio of skirt cloth weight per unit length of the curve with the radius of r_c, to W. Generally we take $K = 0.8$.

5. The formation of the skirt and some parameters such as the location of joints, can be obtained by the following equations. Taking the moment about the BZ axis with the foregoing four forces and according to the equilibrium condition, putting the sum of moments equal to zero, then

$$\begin{aligned} K_r\,P_t\,R\,r_c\,\Delta a - b\cos\phi = {} & b/2\,(r_c + r_b)\,\Delta a\,(1 - p_{ct})P_t\,(b/3\,[r_b + 2r_c]/[r_b + r_c]) \\ & + d/2\,(r_c + r_E)\,\Delta a\,p_{ct}\,P_t\,(b\cos a\,d/3\,[r_c + 2r_e]/[r_c + r_e]) \\ & + Wc\,r_c\,\Delta a\,K\,K_m\,b\cos(\beta - a_1) \end{aligned} \tag{7.9}$$

where K_m is the coefficient due to the CG of the skirt cloth, i.e. the ratio of vertical distance between the BZ axis and the action line of skirt weight to the base-line and ϕ, a, β are geometrical parameters of the skirt as shown in Fig. 7.19. Thus equation (7.9) can be rewritten as

$$\begin{aligned} \overline{CH} &= R\cos\phi \\ &= [K_1\,b/2\,(1 - p_{ct}) + d\,p_{ct}\,(K_2\cos a - K_3 d/2b \\ &\quad + K_4\,K_m\,W_c/p_t\cos(\beta - a_1)]\,1/K_r \end{aligned} \tag{7.10}$$

where K_1, K_2, K_3, K_4 and K_r, are correction coefficients for the three-dimensional effect. The skirt will become two-dimensional, i.e. both the inner and outer mounting lines will be linear, if r_b, r_c, r_E and r_o tend to infinity.

In the case where the skirt is located at the bow or stern corners of the ACV, the inner and outer mounting lines are curved (where B is the inner mounting point and A is the outer mounting point) and r_o is not larger than R, and the skirt can be considered as three-dimensional, then the four coefficients can be shown as

$$K_r = \begin{cases} \dfrac{(2r_o + R\cos\phi_1)}{[2(r_o + R\cos\phi_1)]} & \text{Three-dimensional} \\ 1 & \text{Two-dimensional} \end{cases}$$

$$K_1 = \begin{cases} 2/3 + 1/3\, r_b/r_c & \text{Three-dimensional} \\ 1 & \text{Two-dimensional} \end{cases}$$

$$K_2 = \begin{cases} 1/2 + 1/2\, r_E/r_c & \text{Three-dimensional} \\ 1 & \text{Two-dimensional} \end{cases}$$

$$K_3 = \begin{cases} 1/3 + 2/3\, r_E/r_c & \text{Three-dimensional} \\ 1 & \text{Two-dimensional} \end{cases}$$

$$K_4 = \begin{cases} \mathrm{K} & \text{Three-dimensional} \\ 1 & \text{Two-dimensional} \end{cases} \tag{7.11}$$

In addition some complementary relations concerned with the dimension ACB can be written as follows:

$$a^2 = b^2 + (2R \sin \theta/2)^2 - 2b\,(2R \sin \theta/2) \cos(\pi/2 - \theta/2 + \phi) \tag{7.12}$$

$$a^2 = (2R \sin \theta/2)^2 - b^2 + 2ab \cos \beta \tag{7.13}$$

$$R = L/\theta \tag{7.14}$$

where a and L are the geometrical parameters of the skirts and air ducts.

During calculation of the location of points C and E and the shaping of skirts and in the case where the parameters of the skirt and location of inner/outer mounting positions are given, then the values of L, b, a, d, W_c, K_m and K in the foregoing equation (in general, when $p_c/p_t = 0.8$–0.95, then $b' \approx 1.02b$–$1.05b$) are given, then ϕ, θ, β can be obtained according to equations (7.10) and (7.12)–(7.14).

This equation can be solved with aid of a computer by progressive approximation methods. Thus the shaping of the skirt, i.e. the coordinates of points C and E, can be obtained as

$$x_c = b \cos \beta_1$$

$$y_c = b \sin \beta_1 \tag{7.15}$$

$$x_E = e \cos(\beta_1 + a_2)$$

$$y_E = e \sin(\beta_1 + a_2) \tag{7.16}$$

where

$$\beta_1 = (\beta - a_1)$$

$$e = (b^2 + d^2 - 2bd \cos a)^{0.5}$$

Thus the x_c, y_c, x_E, y_E corresponding to the changing p_{ct} can be obtained, namely, the static deformation of the skirt caused by the change of p_{ct}.

If the finger tip location (x_E, y_E) of the skirt, the inclination angle of the skirt, finger depth d and the size of air duct are given, then L, b, b' and the other skirt parameters, which satisfy the design bag–cushion pressure ratio, can be obtained, and the problem concerned with laying-off the skirt can be solved.

Comparison between the experimental results and calculation

Reference 62 introduces experimental data obtained by MARIC and comparison with theoretical calculations, as follows:

1. Calculated and experimental results of the location of bow skirt point E for ACV model 711-II and 722-I are shown in Figs 7.22–7.24. It can be seen that the theoretical calculations agree with experimental results very well. The method above has therefore been used further for design, analysis and laying-off of ACV and SES skirts in China with good results.
2. From these calculations, it can be seen that in the case where the mounting point and configuration parameters have been given, then the location of points C and E will vary with bag/cushion pressure ratio p_t/p_c. As a general rule, with higher bag pressures, the skirt base-line will drop down as the bag/cushion pressure ratio increases.

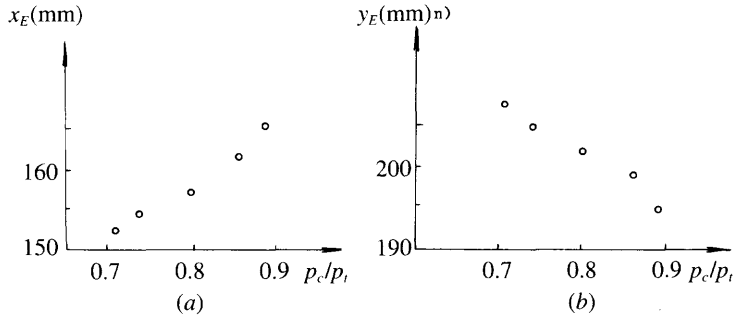

Fig. 7.22 The variation of locations for side skirts finger tip on model 711-II with changes in p_c/p_t: (a) variation of horizontal location X_e; (b) variation of vertical location Y_e.

Calculation of supporting forces acting on the joints of bag/finger skirts

The supporting forces acting on the joints (such as points A, B) are not difficult to calculate. First of all, the components of the four forces T, F_1, F_2 and mg on the x and y axes can be written as

$$\begin{aligned}
T_x &= p_t R \sin(\phi + \beta - \alpha_1) \\
F_{1x} &= -p_t b (1-p_{ct}) \sin(\beta - \alpha_1) \\
F_{2x} &= p_t d p_{ct} \sin(\alpha - \beta + \alpha_1) \\
mg &= 0 \\
T_y &= -R p_t \cos(\phi + \beta - \alpha_1) \\
F_{1y} &= p_t b (1-p_{ct}) \cos(\beta - \alpha_1) \\
F_{2y} &= p_t d p_{ct} \cos(\alpha - \beta + \alpha_1) \\
mg_y &= mg
\end{aligned} \tag{7.17}$$

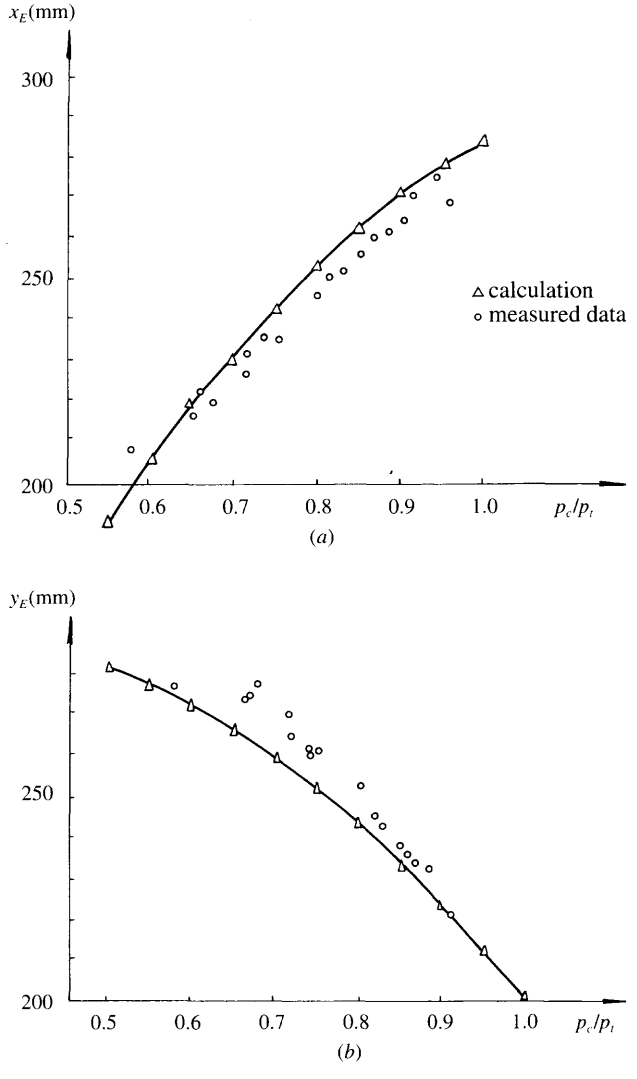

Fig. 7.23 The variation of location for finger tip of modified skirt on craft type 711-II with high responsiveness.

Then the supporting forces acting on joints A, B can be calculated:

$$\begin{aligned} NA_x &= -p_t R \cos \eta \\ NA_y &= -p_t R \sin \eta \\ NB_x &= -(T_x + F_{1x} + F_{2x} + mg_x) \\ NB_y &= -(T_y + F_{1x} + F_{2x} + mg_y) \end{aligned} \tag{7.18}$$

where η denotes the angle between tangent of curve AC at point A and the x axis as in Fig. 7.19.

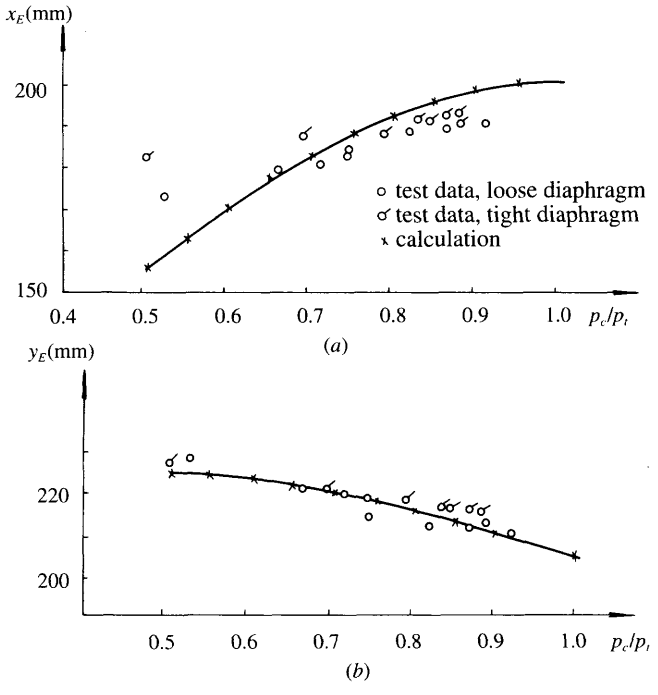

Fig. 7.24 The variation of locations x_E and y_E for bow skirt finger tip.

7.4 Geometry and analysis of forces in double or triple bag stern skirts

The geometry for bag skirts is initially designed using static balance of forces, using a two-dimensional unit slice of the skirt. Drag and other dynamic forces are initially ignored. These are considered later when analysing the craft response to waves.

For both ACVs and SES, most stern skirts on Chinese craft are double or triple planing bags, the advantages of which are:

1. In contrast to bow skirts, bag–finger type stern skirts add to water scooping drag because the direction of cushion pressure acting on the fingers is the same as that of oncoming flow. On the other hand, the double or triple loop planing skirt can plane on the water surface to reduce drag and improve response to the water surface.
2. The hole area S_{d1}, S_{d2}, S_{d3} can be varied to adjust the bag geometry by adjusting the pressure ratio between loop segments p_{t1}/p_{t2}, p_{t2}/p_{t3}, p_{t3}/p_c, etc. as shown in Fig. 7.25.

   Adjusting the response of the skirt bag to waves will improve the seaworthiness of the craft. Its natural period can be changed by changing pressure ratio p_t/p_c, or its damping response by changing volume and inter-bag feed-hole areas. It is difficult to specify a general optimum, so it is recommended that designers experiment with this parameter until the relation between pitch stiffness and skirt drag gives a

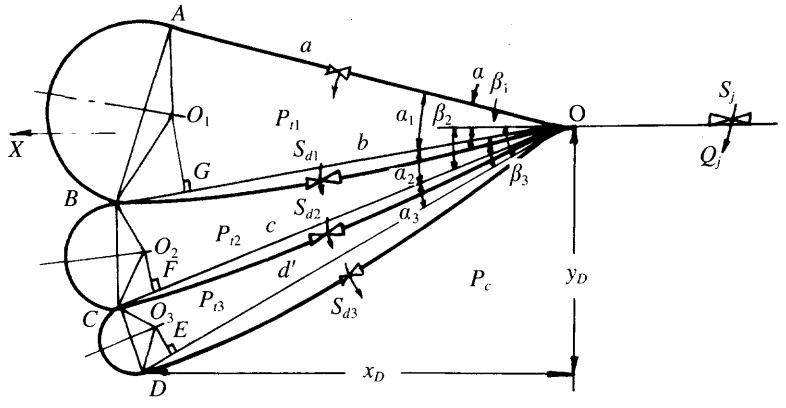

Fig. 7.25 The principal geometric parameters of triple bag skirts at stern.

satisfactory balance between craft motion response and drag forces which control the acceleration of a craft through hump speed.

3. The mounting angles β_1, β_2, β_3, etc. of the skirt bags can be adjusted to obtain the optimum angle of attack of the lowest bag. This will also affect the drag forces generated by the stern skirt. Having too flat an angle can lead to local flutter and skirt bounce on smooth surfaces.

The bag volumes and bag holes total area (S_{di}) can both be adjusted in order to provide a desired capacitance–resistance match and good wave response. At MARIC we often use the bag–finger skirt for the bow skirt and multiple bags at the stern skirt, both for ACVs and SES.

From the theoretical point of view, the calculation method for multi-bag skirts is similar to that for the bag–finger skirt as shown in Fig. 7.25 [64] :

1. The geometrical location of lowest skirt tip, X_d, Y_d, can be determined first, based on the requirements of the craft cushion area. Normally this is slightly inboard of the outer attachment point (A).
2. The bag pressure P_{t1}, P_{t2}, P_{t3}, areas of bag holes S_{d1}, S_{d2}, S_{d3} of various layers of bags, and flow rate into stern bag Q_d, flow rate into cushion Q_j and area of air inlet into cushion S_j, etc. can all be determined. A starting point is to use $P_{t1}/P_{t2}/P_{t3} = 1.2p_c$ and feed-hole area 5%.
3. The bags' volumes and their geometrical parameters such as β_1, β_2, β_3, (or α_1, α_2, α_3) etc., and the chord length of inner bag area a, b, c, d, etc. can be determined. These may be varied to achieve the balance of requirements between seaworthiness response and stiffness for stability of the craft.
4. The equilibrium condition for forces such as
   (a) tensions T acting on skirt cloths at points D, C and B;
   (b) force F due to difference of pressure between the different bags acting on OD, OC and OB;
   (c) force F_2 due to bag pressure and acting on the curve of the outer bag CD, BC, AB;
   (d) weight of skirt bag W_b

may be determined in a similar way to the calculation method for bag and finger skirts mentioned above.

According to the equilibrium of moments, namely the sum of moments about the OZ axis of these four forces (T, F, F_2 and W_b) equalling zero, the radius of curvature (i.e. R_1, R_2, R_3 and the coordinates of O1, O2, O3) and the length of curve on various outer bags AB, BC, CD can be obtained. The calculation can be started from the lowest bag, then extended to every bag.

By the same reasoning, if the skirt bags' geometry, such as the sizes of the inner/outer bag of skirt, can be given, then the coordinates of points B, C and D can also be obtained by this method.

However, the assumption implicit in the calculation above, that the cushion pressure acting on the stern skirt is uniformly distributed, may not be accurate, particularly in the case where craft are running on a water surface. Cushion air is blown from the air cushion just like a venturi tube as shown in Fig. 7.26.

According to [65], the pressure acting on the base of the skirt bag is not uniformly distributed, sometimes even some suction pressure is exerted on the stern bag as shown in Fig. 7.26. This method can therefore only be used for initial geometry and the detail shaping of stern skirts is generally determined by experiment in a skirt test facility which includes a water surface.

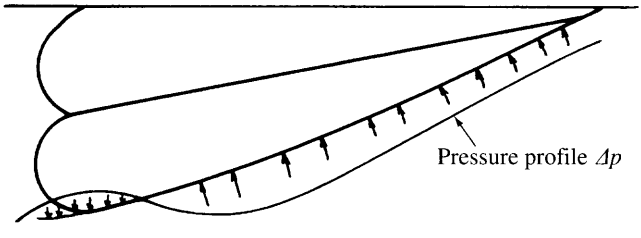

Fig. 7.26 Pressure distribution acting on the inner surface of a stern skirt.

7.5 Geometry and forces for other ACV skirts

Extended segments (Fig. 7.13(e))

The geometry for an extended segment is basically the same as an open loop and segment. The lower tip should be placed 10–20% of segment height inwards from the gunwale. It is normal to use an outer face angle between 40° and 45° (lower angle gives higher stability). Segment width is 40–50% of skirt depth. Above the main segment, the fabric sides are continued. An outer panel is sewn on to the segment forming a loop. The 'loop' radius is smaller than an open loop geometry.

The segment may be attached directly to the hull, or a short tie may be incorporated. The tie can allow some rotation of the segment, giving some responsiveness to this skirt.

Bag and pericell (Fig. 7.13(c))

This type may be considered a further variation on the bag and segment. Consider first a segment with an inner face. The force on this inner membrane will tend to distort the inner bag downwards; on the other hand, since the sealed segment will now have a higher pressure than p_c, the bag geometry will be flatter.

Now consider opening the segment rotating the walls more vertically, say to 35°. The air flowing through the segment cell will now be released at its base and the pressure in the cell will be close to p_c. If the toe line of the cell is horizontal, small vertical movements will seal the cell against the ground and the internal pressure will rise to p_b. If the movement is fast, the pressure transient in the cell will be rather higher than p_b as flow is reversed into the bag.

To soften this response, the toe line can be angled upwards 10–20°. The first part of the heaving motion will then cause a response similar to a bag and segment, then in higher roll or heave the ground plane will seal the cell and cause the stiffer response.

Open loop and segments (Fig. 7.13(d))

The open loop and segment is similar to a bag and segment, where there is no bag overpressure, thus the relations in section 7.3 all apply for detail calculation. The inner bag line becomes a straight line. Fig. 7.13(d) shows typical geometries for a side, bow and stern skirt of this type. The relations between loop radii and segment geometry are indicated graphically. Best results are obtained with this type of skirt when the hull depth is 70–100% of the cushion depth. It is advisable to keep the side loop intersection angle with the segment top less than 15° to minimize the tendency to bounce. Bounce is also a problem if the segment tip is outside the gunwale line.

At the stern, segments are sometimes raised from the base-line, leaving a clear air gap of 5–15% of cushion depth to reduce scooping at hump speed. This can lead to increased wear rate on the stern corner segments and so is only recommended if a prototype skirt gives problems.

Stability skirts

A number of different stability skirt configurations are shown in Figs 7.2, 7.9, 7.10 and 7.14. They are generally a series of almost circular trunks inflated to p_b, extended to between 60 and 80% of cushion depth. For deep cushion craft, inflated cones (similar to chip-bag segments) may be mounted on the circular trunk. The forces applied by these trunks may be determined from the membrane tension force, equation (7.2).

7.6 Analysis of forces causing the tuck-under of skirts

In the previous two sections, we have introduced the static shaping and force analysis for two- and three-dimensional bag–finger skirts. These are the basic theories for predicting the skirt shaping. In general the static shaping of bag and finger bow or side skirts, both running on water or over land, can be accurately predicted by this method, so it has become the basic method for skirt design.

That is fine statically. Unfortunately there is another problem This relates to the dynamic response of bow skirts which might cause the plough-in of an ACV through skirt tuck-under.

The responsive skirt with low natural frequency is widely applied to modern ACVs and also SESs. Due to the application of this type of skirt, the location of bag and finger interface joints (X_c, Y_c) and lower tip of fingers (X_E, Y_E) will vary considerably with the bag–cushion pressure ratio.

This gives the advantages and features of the responsive skirt. It may also lead to a reduction of the tuck-under resistance of skirts. For this reason, it is necessary to study the hydrodynamic characteristics of skirts, the rationale of skirt tuck-under and the measures for improving the tuck-under resistance. The hydrodynamic characteristics of skirts and the skirt tuck-under resistance are introduced as follows.

Basic assumptions

1. We take the two-dimensional bag–finger type skirt as an example and assume that the fingers are connected with bag at the fore and rear parts of the skirts, but not at other parts as shown in Fig. 7.27.
2. The wetted depth of the skirt will not be as deep as up to the skirt bag, namely the draft of the skirt is less than the height of the fingers. The finger will stick to the water surface flat in the case where the tiny finger is pushing the water surface, thus the lift of the skirt in this area will be compensated by cushion pressure. The water friction of skirts has to be taken into account.
3. The air pressure is uniformly distributed in inflatable skirts.

Analysis of forces acting on the skirt

1. Tension acting on curved sections of the skirt bag (see Fig. 7.28) under the action of uniform pressure, the forces acting on AC, CD, DB are

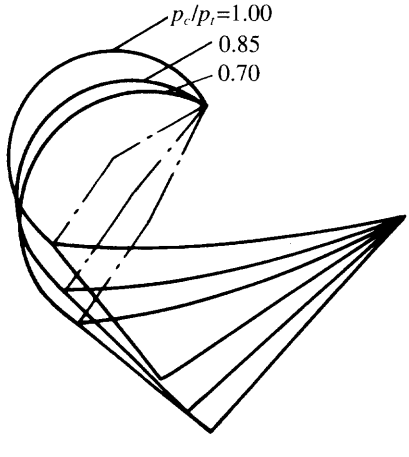

Fig. 7.27 Influence of bag cushion pressure ratio p_c/p_t on skirt shapes (test results).

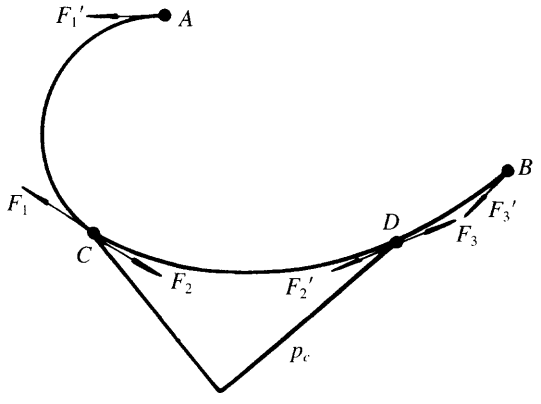

Fig. 7.28 Forces acting on bag and finger side skirt.

$$F_1 = p_t R_1$$
$$F_2 = (p_t - p_c) R_2$$
$$F_3 = (p_t - p_c) R_3 \tag{7.19}$$

where R_1, R_2, R_3 are the radius of curvature of AC, CD, DB (m) and F_1, F_2, F_3 the skirt cloth tension at A, C, D per unit length of skirt (N/m).

2. Hydrodynamic force acting on the skirt fingers. In the same way as the skirt drag analysed in Chapter 3, the finger sticks partly to the water surface and the part not touching the water surface has local bending deformation as shown in Fig. 7.29. Thus the friction drag due to water can be written as

$$F_5 = K_w p_c l_2 \tag{7.20}$$

where F_5 is the drag of skirt finger per unit length (N/m) and K_w the hydrodynamic coefficient of skirts, which can be written as

$$K_w = \zeta\, 0.5\, \rho_w\, V_w^2 / p_c$$

where ζ is the water friction coefficient of skirts, V_w the flow speed (i.e. craft speed) (m/s), l_2 the wetted length of the skirt, which can be written as follows, from equations (3.12) and (3.13):

$$l_2 = \frac{d_w}{\sin\theta} \cdot \frac{1}{a}$$

$$a = (1 - K_w [(1 - \cos\theta)/(\sin\theta) - \theta/57.3]) \tag{7.21}$$

d_w is the submerged depth of fingers (m) and θ the inclination angle of the finger (Fig. 7.29)(°).

Meanwhile, the water friction drag of the finger is balanced by the tensions of the finger fabric, thus it can be written as

$$F_s = R_w p_c$$
$$\therefore R_w = K_w l_2 \tag{7.22}$$

where R_w is the radius of curvature at the bending area of the finger (m).

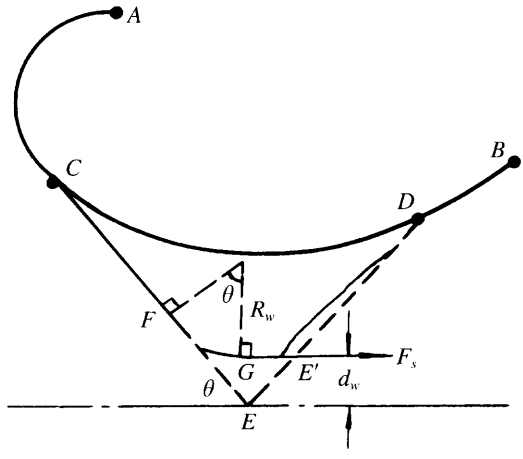

Fig. 7.29 Force acting on skirt components once finger contacts water surface.

Analysis of forces acting on fingers under the action of cushion pressure

Reference is made to Fig. 7.30. Forces acting on fingers under the action of cushion pressure F_4 can be written as

$$F_4 = (d - R_w\,\theta - l_2)\,p_c \tag{7.23}$$

where d is the finger length (m), F_4 forces acting on two joints C and D of the bag and finger via the diaphragm, and according to the theory of force analysis for a flexible rope the force can be written as

$$F_{4c} = F_4\,(d - d_h/2)\,d$$

$$F_{4D} = (F_4\,d_h)/2d \tag{7.24}$$

where $d_h = d - R_w\,\theta - l_2$, F_{4c} is the tension of the skirt fabric at point C, the direction of which is along CE (Fig. 7.30), and F_{4D} the tension of the skirt fabric at point D, as shown in Fig. 7.30.

Since the finger is in contact with the water surface, which may cause bending of the finger fabric, the diaphragms will be wrinkled, so that the direction of force F_{4D} is tangential to the direction of the curve at the point D′. The point of action is at D.

Force acting on the diaphragms of D-shape bags

Two conditions may be taken into account:

1. The pressure in a D-shape bag is the same as the bag pressure. In this case, no force acts on the diaphragms. If the diaphragm is tightly mounted, then the direction of force acting on the diaphragm will be in the direction of the diaphragm, which can be represented as

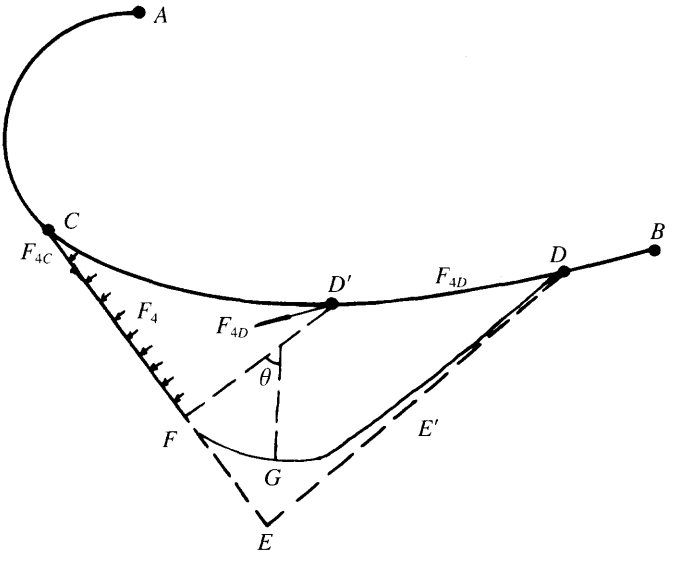

Fig. 7.30 Hydrodynamic forces acting on skirts running on water.

$F_{1w} = 0$ (where the diaphragm is loose)
$F_{1w} = F_{1w}$ (where the diaphragm is tightly mounted, the value of which can be obtained from the equilibrium equation by iteration)

2. In the case where the pressure in a D-shape bag differs from the bag pressure, then

$$F_{1w} = (p_t - p_D)\, R_{1w} \tag{7.25}$$

where F_{1w} is the tension of fabric on a D-shape bag per unit length (N/m), p_D the pressure in a D-shape bag (N/m^2) and R_{1w} the radius of curvature of the diaphragm in a D-shape bag (m).

Skirt weight

In comparison with hydrodynamic forces, the effect of skirt weight mg is small and now we assume that it is acting on points C and D. We use the unit weight of a two-dimensional slice of the skirt section, i.e. weight per meter, to evaluate the skirt loading.

Equilibrium equation of forces and its solution

Summing the forces mentioned above, the forces acting on point C are $F_1 F_{1w}$, F_{4c} F_s and the forces acting on point D are F_{2d}, F_{4d}, F_3 as shown in Fig. 7.31 respectively.

Because the skirts are in equilibrium, then summation of the components acting on points C and D on the x, y axes will be equal to zero, then

$$\Sigma F_{Cx} = \Sigma F_{Cy} = \Sigma F_{Dx} = \Sigma F_{Dy} = 0 \tag{7.26}$$

This equation can be rewritten as

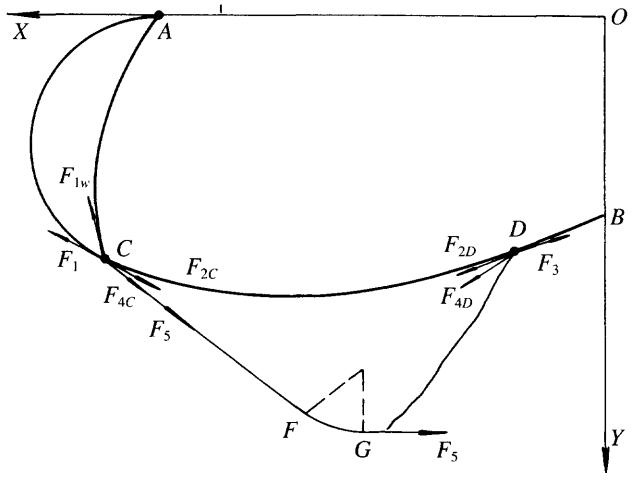

Fig. 7.31 Forces analysis for deformed fingers.

$$
\begin{aligned}
&F_{1x} + F_{1wx} + F_{2cx} + F_{4Cx} + F_{5x} = 0\\
&F_y + F_{1wy} + F_{2Cy} + F_{4Cy} + F_{5y} + K_{cmg} = 0\\
&F_{2Dx} + F_{4Dx} + F_{3x} = 0\\
&F_{2Dy} + F_{4Dy} + F_{3y} + (1 - K_c)mg = 0
\end{aligned}
\tag{7.27}
$$

where mg is the weight of the skirt on ΔCDG per unit length (kg/m) and K_c the coefficient of effective skirt weight.

The value of K_c is very difficult to estimate due to the fact that a part of the weight is supported by the water surface. In general, thanks to the small effect of skirt weight on geometry and part of the skirt weight supported on the water surface is far less, this component of the skirt weight can be neglected and does not cause large errors. Coefficient K_c can be determined by the relation between the location of points C, D and the CG of the skirt.

Now the cushion parameters p_c, p_t, the geometrical parameters of skirts d and length of curves AC, CD, DB, AC (diaphragm of D-shape bag), the location of points A, B, the parameters due to the emerged location of the skirt such as K_w, d_w, etc. are given, then the four variables R_1, R_2, R_3, β_2 (the angle between BD and the y axis) can be solved by the four equations (7.27).

In the same way as the methods for static shaping of skirts, the locations of points C, D and the angle between the F_5 and the y axis may be determined and the tuck-under sensitivity of the skirt can then be estimated. The calculation mentioned above is rather complicated, but it can be solved with the aid of a computer.

Comparison between the theoretical calculations and experimental results

Experiments at MARIC are normally carried out in a circular water tunnel. The experiments for tuck-under of skirts with various configurations, emerged depth of the finger, and friction coefficients of the skirt are all carried out in this facility.

Comparing between the theoretical calculations and experimental results obtained, MARIC has derived the following conclusions:

1. It can be seen from data plotted in Fig. 7.32 that theoretical analysis agrees well with experimental results.
2. Larger K_w (namely the larger skirt finger friction drag coefficient) gives deeper emerged length of finger d_w, so that the fingers tuck under more easily.
3. Based on calculated results for the various skirt parameters, bow skirts are less resistant to tuck-under, so one has to take care to design a large deformable responsive skirt for this location.
4. The diaphragms of a D-shape bag with the tension of F gave the capability to control skirt tuck-under, particularly in the case where the diaphragms were tightly mounted (rather than loose in the static hovering condition).
5. The calculation method mentioned above can be used in the design of bow skirts. In the case of selecting or designing the configuration of a bow skirt, the ability to prevent tuck-under had to be checked according to the K_w and permitted emerged depth d.

7.7 Skirt bounce analysis

Bounce is a low frequency vibration of the skirts, which occasionally occurs in an ACV hovering static over a smooth surface or at low speed, both on Chinese ACVs such as models 711-IIA, 716A and 7161I, and various ACVs from the UK and USA. During bounce, the skirts vibrate with a large amplitude, which will be several times

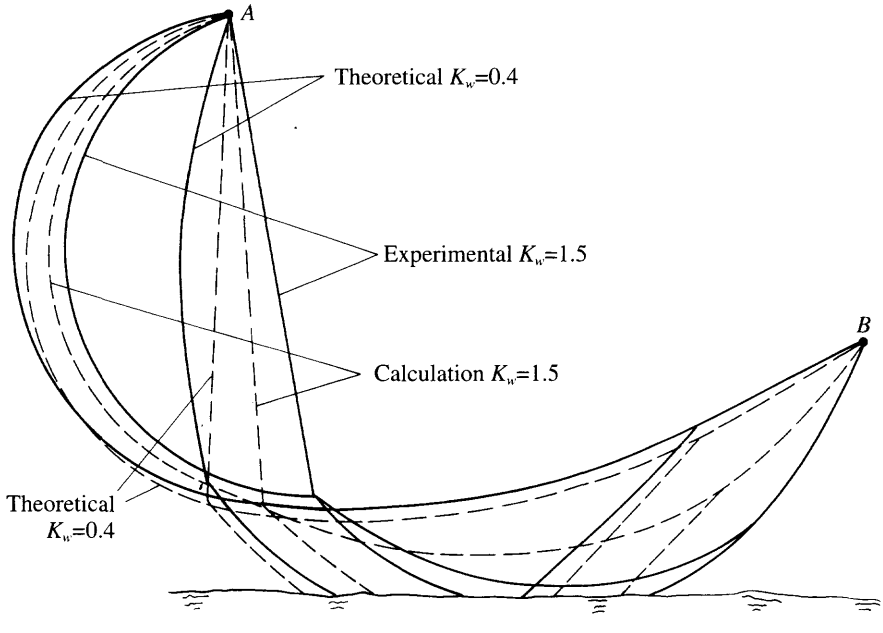

Fig. 7.32 Comparison of tuck-under between analysis and experiment.

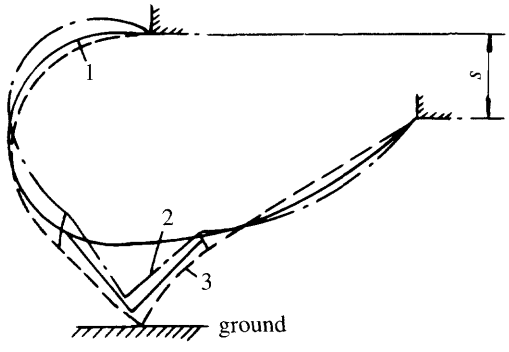

Fig. 7.33 Profile variation of skirt during bounce. 1: neutral position; 2: bounce up, air spilled; 3: bounce down, ground reaction.

the static air gap under segments or fingers (see Fig. 7.33), thus causing a heavy vibration of the hard structure in heave, which is harmful to equipment, engines and instruments and uncomfortable for the crew.

In recent years, due to the appearance of low bag pressure responsive skirts, particularly the large deformation skirt, the probability of bounce motion, similarly to skirt tuck-under, has increased.

Investigation of the causes of bounce and development of methods for preventing

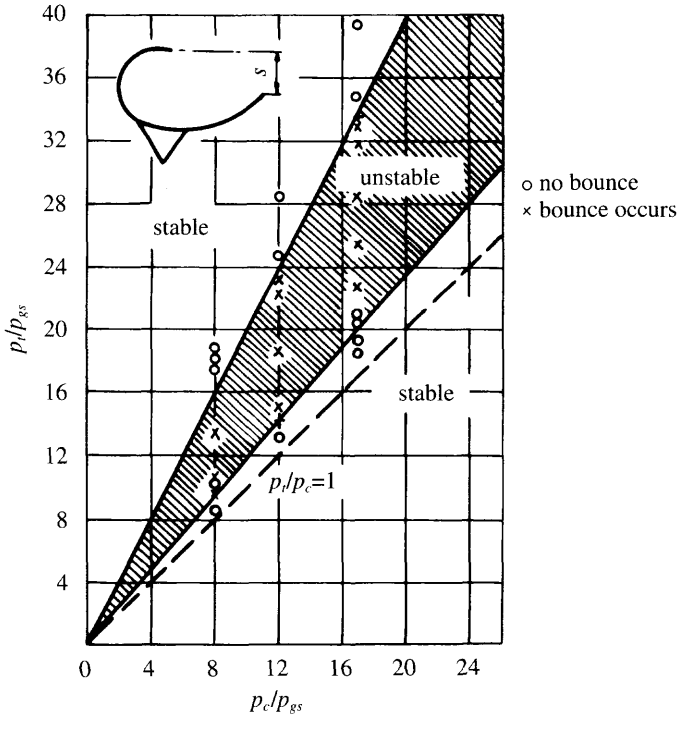

Fig. 7.34 Bounce boundary.

it are an important requirement for the designer. Refs 50 and 66 introduced some experimental investigations on this subject and obtained encouraging results. Figures 7.34 and 7.35 show the vibration range for bag/finger skirts and indicate almost the same results, but show different experimental results for bounce motion of open loop skirts. In this case, ref. 50 noted that no bounce motion occurred, but it has occurred with this skirt during tests in a Chinese skirt test rig [66].

Strictly speaking, the theory for bounce has not been completely verified, but a simple explanation for bounce can be described as shown in Fig. 7.36 [4].

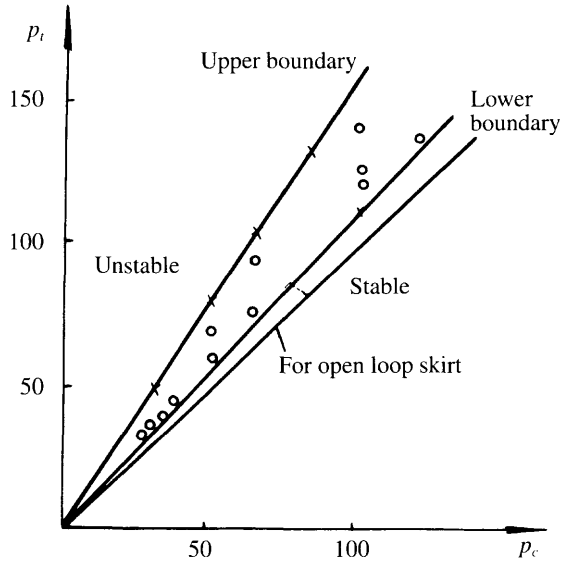

Fig. 7.35 Bounce boundary.

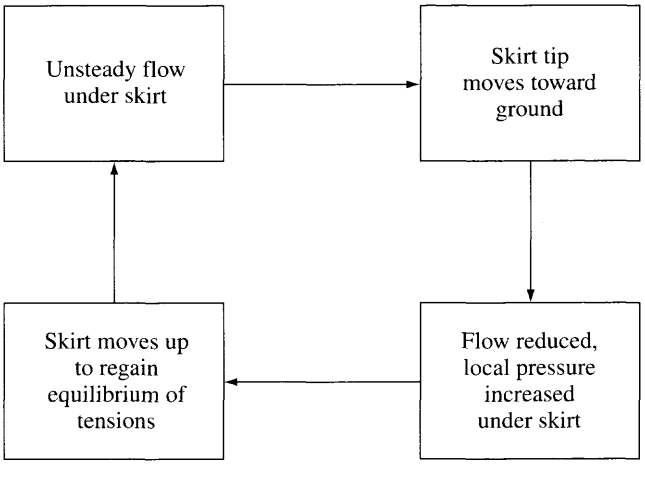

Fig. 7.36 Brief rationale for bounce.

A large radius loop or bag membrane has very little damping, particularly for small movements of a segment, as the radius changes very little. Where a significant length of the skirt is over a flat surface and this section can move as a unit, a small disturbance of the cushion air flow can begin a motion, normally downwards, sealing the cushion. Local static pressure rises, causing the skirt geometry to change, lifting it. The static pressure reduces as air is again released under the skirt and the cycle starts again. The period of oscillation is the natural period in rotation for the total skirt section.

The methods available for preventing bounce are:

1. Introduce anti-bounce diaphragms in the bag or loop to increase the damping for vibration, the shape of which is similar to the D-shape bag (Fig. 7.37). This method has given good results for solving the bounce problems which have arisen on Chinese ACV models 716-II and 711-IId.
2. Change the length of the inner bag and the outer bag of the skirt in order to change the static deformation of the skirt and adjust the natural frequency of the skirt vertical vibration.
3. Strap weights (small sandbags or similar) to the skirt at the bag/segment outer attachment. These are generally only needed in the centre section of side skirts. The mass required is relatively small, since the lever arm about the skirt rotation point is large. This is normally optimized during craft trials.

7.8 Spray suppression skirts

The high-velocity air escaping from an ACV or SES cushion will entrain water with it. This forms droplets which form a spray curtain. The higher the cushion pressure,

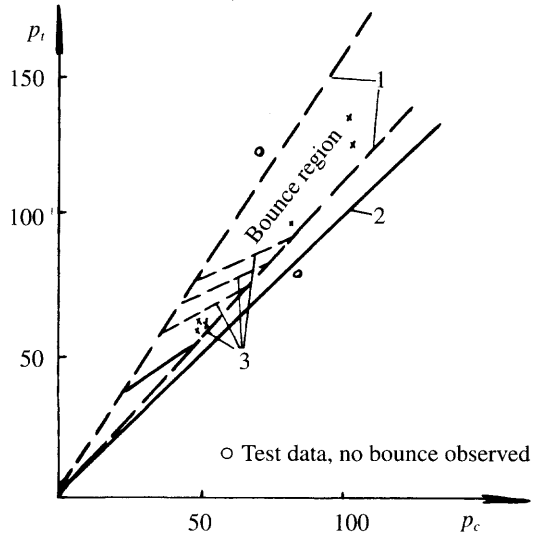

Fig. 7.37 Protection function of D bag skirts against bounce. 1: bounce boundary; 2: open loop skirt; 3: test data, bounce restrained by diaphragm.

the greater the quantity of water spray. Over land, the cushion air creates a dust or sand curtain over dry terrain.

This spray curtain will normally be thrown back on to the structure of an ACV or SES and may then enter engine intakes if they are not protected by filters. In cold climates, water spray will become an ice rime on the structure after a while, adding to the effective mass of the craft. This ice can also be dangerous since vibration, either from the cushion or the engines, can break pieces off which are then drawn through air propulsors or possibly the lift fans, causing damage or failure. In both cases, a spray suppression apron around the bow and front part of the side skirt in the case of an ACV is found to be very effective in reducing spray to an acceptable level.

There are several types of spray suppression apron. The simplest comprises a shaped piece of material which simply drapes over the bag or loop, reaching approximately halfway down the height of the segments or fingers (see Fig. 7.38(a)). A neater design, but rather more complex, comprises segment-like inflated teeth in the top half of each segment (Fig. 7.38(b)). Air pressure for inflation is provided from the cushion.

Aprons

These will flap, and they need to have an open top to avoid inflating. Flapping will be restrained by installing some weights (similar to domestic curtain hem weights) or heavier material for the lower section. Use tapes to restrain an apron and do not restrain at the segment top, just lay over the bag. Do not allow operation of a craft with a badly torn apron as this will affect performance and abrade the bag.

Teeth

These are shaped like double segments. Use cushion pressure (i.e. bleed from top of segment) to inflate. Use geometry shown in Fig. 7.38(b) approx. Attach to top of segment. Use lightweight material.

7.9 Skirt dynamic response

A skirt will respond by adjustment of geometry to two basic inputs, changes in pressure within the cushion and deformation against a solid boundary such as a wave. The deformation will change the volume of the cushion and the air distribution system and by doing so alter the balance of dynamic and static pressure within the system.

A responsive skirt is one where the segments or fingers are able to follow an undulating surface by adjustments in the skirt section geometry without inducing large changes in the pressure field in the cushion. By definition such a skirt will be less stiff than a 'non-responsive' skirt. The optimum for a given craft is therefore likely to be a skirt with just sufficient responsiveness for its mission requirements and no more.

In the next chapter we discuss ACV and SES motions in a seaway. To simplify an already complex analytical problem, skirt response is considered only as the cushion stiffness. The designer will therefore need first to assess the minimum stiffness required

for static stability from the skirt system (see Chapter 5) and once this is known, the stiffness characteristic giving most favourable motions in the design environment can be determined and the skirt geometry adjusted, so long as the dynamic requirements are greater than those from static analysis.

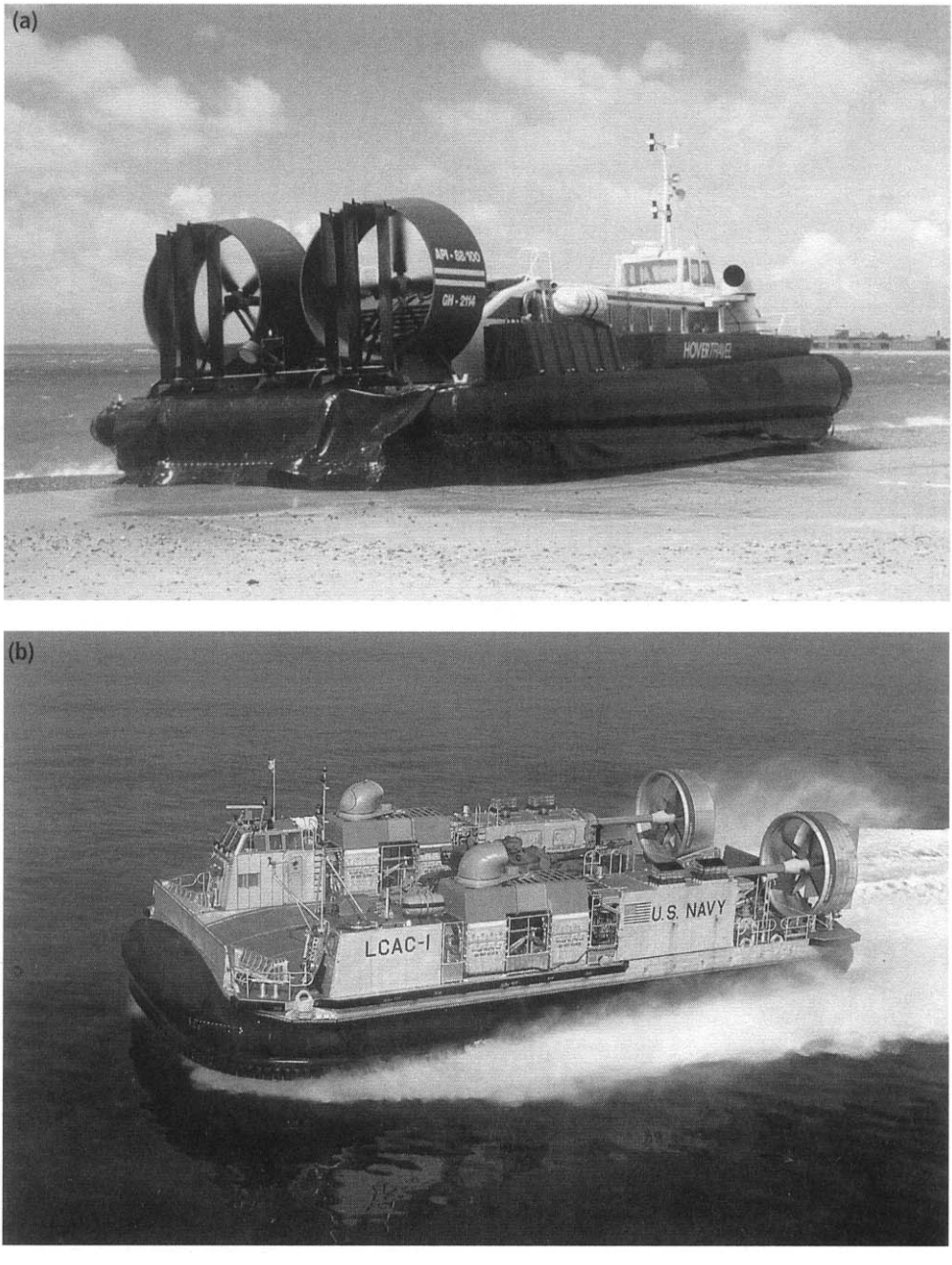

Fig. 7.38 Spray suppression skirt types: (a) spray suppression apron; (b) spray suppression 'teeth'.

8

Motions in waves

8.1 Introduction

The purpose of this chapter is to introduce the reader to ACV and SES vehicle dynamics. In a seaway (or over rough terrain for amphibious ACVs), the craft will respond to the undulating surface by pitching, heaving and rolling as it moves forward along its track. Dynamic sway and yaw motions may also be significant for ACVs over undulating terrain. These motions are generally considered together with design of the craft control systems, rather than as analysis of the motions themselves, (see Chapter 7). We will concentrate in this chapter on the heave, roll and pitch, which govern ride quality and speed loss in a seaway.

The cushion system responds as a damped spring system, while movement of the skirt and SES sidehulls into and out of the water induce varying lift and drag forces. The forces do not vary linearly. Initial models for ACV and SES motion attempted to linearize the response, to make prediction simpler. More recently, nonlinear solutions have been proposed and are now being further developed. We present these theories later in this chapter, after reviewing the main parameters which affect ACV and SES motions.

The objectives in carrying out such analyses are to identify the motion characteristics themselves as an input into defining:

- instability boundaries, e.g. plough-in, heave bounce and cobblestoning;
- criteria for dynamic stability, to compare with static stability requirements from Chapter 2;
- passenger and operating personnel motion response and so assessment of ride quality;
- assessment of externally excited vibration.

Hovercraft seaworthiness

An ACV is able to display the special characteristics for which it is best known while running at high speed over shallow water, rapids, ice and swamp – places no other craft can go. While these 'special abilities' interest many military and civil users with particular mission requirements, such environments do not include the wind-driven waves found in an open seaway. Generally, a craft's capabilities in an open seaway will

control its transit capabilities between locations where a special mission may be required.

Meanwhile, the SES can best demonstrate its own high speed and work capacity relative to displacement vessels in light weather conditions in a seaway. Where the environmental conditions are favourable, the SES is capable of demonstrating significantly higher transport efficiency than other vehicles.

In conditions typical of an open seaway, the seaworthiness of current ACV/SES still leaves a lot to be desired, especially in comparison with deep submerged hydrofoil craft, or larger high speed catamaran ferries. Part of the problem is that an ACV or SES has a higher work capacity than the competing craft, so that the comparison is almost always with a larger vessel. In a seaway, once vessel length is significantly less than L_s, the mean length of waves of height H_s, it will follow the wave surface profile, with much increased motions. A smaller ACV or SES travelling at higher speed than a more conventional vessel therefore needs a cushion system which can reduce motions by being 'responsive'.

Other key points distinguishing ACV and SES response from conventional vessels are as follows:

1. Amphibious hovercraft hydrodynamic drag is very small in calm conditions. In the case where the craft runs in waves, there will be a rapid build-up of skirt drag and speed degradation, unless the skirt and cushion system is very responsive to the waves. Such skirt systems are only now reaching the point where safe craft can be designed for high-speed operation.
2. While there is a small area in contact with the water surface on an ACV, it has a large frontal area (mostly the skirt area actually), leading to a large air profile drag when running into head winds, in a similar way to the build-up of hydrodynamic resistance of a conventional ship running in head seas. Moreover, the air propeller thrust will be reduced, leading to additional speed degradation. Further, the manœuvrability also deteriorates as described in Chapter 6.

   Ducted propulsors can be designed to have lower thrust degradation, while remaining as quiet as a large open propeller and so minimize these problems. SES powered by water jets or high speed propellers have the same design problem as any high-speed ship (see Chapter 15).
3. Wave pumping, motion pumping and the rapid changes of skirt air leakage area of hovercraft running in waves all lead to significant vertical acceleration. This can affect the operation of machinery, engines, equipment and crews etc. Use of a responsive skirt system and/or a cushion air damping system ('ride control system') can improve this enormously. This technology has been developed during the 1980s and needs further work to give really smooth ride quality at high speed.

Developments over the last decade have improved responses through the low-pressure amphibious ACV skirt and SES cushion venting systems. The design basis is now available; it is a matter of extending application to larger vessels.

Historical review

While the performance of early ACVs on calm water was very impressive, this was not the case in rough seas. Hovercraft dynamic motions were uncomfortable due to high

vertical accelerations. Speed loss and reduced manœuvrability in a seaway of some early craft were significant, resulting in a marginal ability to stay above hump speed.

Much research effort has therefore been applied to find ways to improve the seaworthiness of ACV/SES, with the aim to reduce craft motions and accelerations and allow higher speeds in a given sea state, in order to improve transport efficiency.

Initial work was concentrated on improving stability. Once ACV designers had found ways to provide acceptable dynamic stability with low-pressure ratio skirts, their attention turned to improving ride quality by improving its responsiveness to waves. SES designers initially experimented with sidewall displacement ratio and geometry, also in the search for optimum balance between dynamic stability and drag, before turning to ride quality, in this case by use of cushion air venting systems.

In the 1960s Sir Christopher Cockerell in the UK together with the research staff at Hovercraft Development Ltd studied the motion of hovercraft in waves, considering the wave effects on the cushion as a piston moving in a cylinder as an adiabatic process. This showed hovercraft motions to generate high vertical acceleration. Benya [9] considered hovercraft as a rigid body, similar to conventional ships and derived differential equations of motion with multiple degrees of freedom from an analytical basis. Unfortunately, he did not make clear how to determine the various derivatives (static force and rotary moment derivatives) in his differential equations, and their physical meaning.

In the late 1960s Beardsley [16] began introducing the wave pumping concept for hovercraft running in waves and predicted that the wave pumping motion would strongly affect the seaworthiness and vertical acceleration of hovercraft. He maintained that a hovercraft had to be designed with enough reserve lift power to reduce the vertical acceleration of hovercraft in the case where craft were travelling in waves. At that time, most researchers were interested in the static hovering theory of hovercraft and so they did not realize the significance of Beardsley's work.

In 1972 Reynolds of the UK [67] first derived the linear equations of motion for hovercraft based on the condition that skirts do not physically come into contact with the water surface. The Froude–Krilov hypothesis was assumed to be valid and he did not consider the response of an air duct–fan–skirt system to waves. Reynolds then derived the coupled heaving equations of motion for an ACV and obtained a mathematical solution of the equations.

In the 1970s, Doctors [68], and Zhou, Yun and Hua [69, 70], developed nonlinear equations of motion for hovercraft and obtained a numerical solution by iteration. Although the equations and their numerical solution were more complicated, solution by time-step iteration for several wave frequencies of a hovercraft in regular waves could be obtained with the aid of a computer. The solution gave the researchers insight into the full process of craft motions in waves. In the equations, not only the nonlinear system of fan–air duct–skirt, but also the compressibility of cushion pressure of hovercraft moving in waves was introduced.

Lavis of the USA first pointed out the effect of compressibility of cushion air on the seaworthiness of hovercraft moving in waves and predicted that great distortion would occur to the prediction of seaworthiness quality of craft from model experiments in a towing tank [71], caused by air cushion compressibility not being able to be scaled correctly. However, researchers and designers were still interested in experimental investigations using scale model tests and real ship trials to determine

seaworthiness of ACV/SES. References 72–76 give details of such work for example. Such tests demonstrated that the scale model test results could be considered as valuable data as long as the model (ship) speed was not too high and the encounter frequency causing pitching/rolling of the craft was not too large.

Moran [73] considered that the cushion pressure of an SES with high L_c/B_c at high speed was not uniformly distributed, but had a spatially non-uniform distribution. He expected the motion equations of seaworthiness mentioned above would therefore be altered.

Even though the experts have different points of view on the theoretical investigation of hovercraft motion in waves, in general they have considered that if the scale ratio of a model is not too great and the craft speed as well as the encounter frequency of craft (model) are not too high, then the predictions based either on experimental results of scale models or solution of nonlinear differential equations of motion can give accurate results. This theory is based upon the following assumptions:

- Froude–Krilov hypothesis applies (similar to conventional ships).
- Cushion pressure is uniformly distributed.
- The flexible skirt is considered as the rigid body, namely the skirt fingers will be deformed when the skirt encounters waves, but considering the skirt as a body, the skirt bag is not responsive to the waves.

This theory only considers the fan/air duct/air cushion/hull integrated motion system and does not consider the motion response of a skirt with one or two degrees of freedom. Such assumptions may be reasonable in the case of a skirt with small response, but will lead to significant errors in the case of a modern responsive flexible skirt. In this chapter we will introduce calculation methods for ACV and SES motions in waves, as follows:

- transverse motions of an SES in beam seas (coupled roll and heave motion);
- longitudinal motion of an SES in head seas (coupled pitch and heave motion);
- longitudinal motion of an ACV in waves using the linear equations of motion.

All of these are considered as coupled motions with three degrees of freedom (i.e. roll, pitch and heave together with cushion pressure).

Linear equations of motion and the solution methods using the nonlinear equations of motion are both discussed in this chapter during the investigation of longitudinal motions of ACV/SES.

After considering the basic equations of motion, we will also review some key design issues for ACV/SES running in short-crested waves:

- the 'cobblestone' effect
- SES plough-in motion in following waves
- ACV speed degradation in head winds

and discuss the effect of various factors on seaworthiness of ACV/SES.

Characteristic features of ACV and SES motions in waves

Since hovercraft are supported by an air cushion, a number of motion features are characteristic to ACV/SES running in waves. The Froude–Krilov hypothesis, coupled

vibration of skirt/air duct/fan, nonlinear effects of fans and skirts, effect of cushion air compression, spatial distribution of cushion pressure, determination of cushion damping and added mass all constitute a series of challenges in the investigation of ACV and SES seaworthiness in waves. The questions raised by each of these issues may be summarized as follows.

Rigid body dynamics

The ACV is a rigid body, just the same as a conventional ship, so coupled motions with six degrees of freedom occur to ACV/SES running in waves. Meanwhile the craft are supported by an air cushion, so motions within the six degrees of freedom are strongly influenced by cushion pressure variations, hydrodynamic forces acting on skirts and aerodynamic characteristics of fans, air ducts and the cushion chamber. The hovercraft can thus be considered as a more complicated vibration system with multiple degrees of freedom, i.e. fan/air ducts/skirt/air cushion/hull, as additional parameters to the motions.

Froude–Krilov hypothesis

The Froude–Krilov hypothesis that the passing wave shape is not affected by the hull of the vessel is an important hypothesis to be considered in studying ship motions in waves. By this assumption, any reflected or radiated wave energy is ignored. But does an air cushion affect the shape of waves while the same wave is passing through a hovercraft cushion?

Since there is a difference in density of 800 to 1 between the water in the waves and the pressurized air cushion, such an effect may be considered small. The skirt of an amphibious ACV is more likely to act as a damper rather than as a source of radiated wave energy. The hulls of an SES will be subject to the same inaccuracy as for a displacement ship, with the additional complication of the interaction of catamaran hulls.

Model tests of hovercraft have not so far provided clear data to identify deviations from the Froude–Krilov hypothesis. At present then, the Froude–Krilov hypothesis is used without any special correction factors, to determine the basic motion response of a hovercraft to waves.

Cushion pressure fluctuations

Cushion pressure will fluctuate rapidly while hovercraft are running in waves, which leads to the lift fan(s) operating off the design point and possibly causing nonlinear effects of the fan characteristics. In addition, the high-frequency fluctuation of cushion pressure causes a dynamic response with a hysteresis effect of the fans. These factors lead to considerable complications in the study of hovercraft seaworthiness.

Skirt contact drag

While hovercraft are running in waves, sometimes the skirts' contact with the water surface will cause skirt response and hydrodynamic effects on the skirts. Sometimes the skirt will leave the water surface causing an additional area of air leakage. For this reason, the nonlinear effects of skirts on craft motion will be strong. In general, because the air gap under the skirts is very small, the craft skirt will come into contact with the water surface when rolling or pitching. In addition, the skirt contact will

lead to the hydrodynamic interaction which will induce skirt fluctuation and affect the pressure of the air cushion and craft motion.

Wave pumping

Forward motion of the air cushion in waves will create wave pumping as described in Chapter 2 and will also cause compression of the air cushion similar to the motion of an engine piston in its cylinder (in the case where the peripheral skirts are sealed). Thus, on what basis does it progress in the cushion? An adiabatic process (constant temperature), or some other process? At present the process is assumed adiabatic.

Spatial distribution of cushion pressure

In the case where ACV/SES are rolling in waves at high speed and high frequency, is it possible to assume that the cushion pressure is uniformly distributed, or specially distributed non-uniformly? If the latter, what effect would this have on craft response? So far there are no analytical methods to predict this response.

Determination of damping coefficient and coefficient of added mass

While hovercraft are pitching, rolling and heaving in waves, sometimes craft are suspended in the air, sometimes they are in the water, thus added mass and damping coefficients clearly vary with time. Accurate determination of the damping coefficient due to wave-making is therefore difficult and simplifying assumptions have to be made.

Key craft parameters

Before we develop equations of motion for SES and ACVs it is useful to identify some of the key parameters which may be used to evaluate a design. In Chapter 4, SES and ACV stability was analysed. From this analysis we should be able to derive the following parameters.

- heave stiffness
- heave natural period
- cushion resonance frequencies
- pitch stiffness
- pitch natural period
- roll stiffness
- roll natural period
- damping in heave, pitch and roll

With these data, considering each motion in turn and the SES or ACV as a simple spring and dashpot system it is possible using the natural period and damping coefficient to assess the response to any wave frequency.

If the natural period in pitch or roll is close to the period of maximum energy for the sea spectrum T_p and so is likely to give high responses in the operational sea state, then it will be worth while altering the cushion system to change the natural period.

It is useful to keep in mind the craft characteristics when reviewing the results of motions analysis as presented below.

8.2 Transverse motions of SES in beam seas (coupled roll and heave) [77]

In this section, we will discuss the transverse motion of an SES in beam seas. The transverse motion of an ACV can be dealt with by similar methods.

In Chapter 4 we introduced the calculation for transverse stability of an SES hovering statically, running in calm water. The transverse stability of an SES operating on inland waterways can be estimated using these methods as the surface will be relatively calm.

In the case where an SES travels in a river estuary, coastal area or open seaway, the combined action of winds and waves on the transverse stability and safety of the SES also has to be included. This is to establish appropriate stability criteria to determine the safety margin against overturning of a seagoing SES.

When an SES travels hull-borne (floating rather than hovering), the calculation of SES roll motion can be dealt with in the same way as the calculation of that for conventional displacement for planing craft such as catamarans [78, 79]. In the case where SESs are cushion borne in waves, the rolling motions of an SES will be rather different from that in the off-cushion condition.

As an example, the Chinese SES model 717C had a satisfactory operating speed, but on cushion, particularly in the planing condition above hump speed under the action of beam waves, it rolled slowly with a large amplitude. Due to the wide craft beam, the cushion air would leak under one sidewall in the case of slight roll angle, which enlarged the roll angle and caused a sense of instability to passengers, making them uneasy.

It is important therefore to study the transverse motion of SES in beam seas, particularly in the case of high cushion length-beam ratio. In order to easily compare the calculation with the experimental results, we temporarily do not consider the effect of craft speed and swaying motion and only investigate the coupled roll and heave motion of SES in beam seas.

Basic assumptions

1. We neglect the effect of sidewall and skirt immersion on the local wave profile, but the effect of cushion pressure on waves is taken into account, i.e. the Froude–Krilov hypothesis is used.
2. Uniform distribution of cushion pressure is assumed and the cushion plane is simplified as a rectangle.
3. The change of air density and pressure inside the air cushion are considered adiabatic, but the air flow of cushion air into the atmosphere is considered incompressible.
4. Fan revolutions are kept constant and the effect of fan dynamic response is neglected.
5. Added mass and damping force of a single sidewall can be estimated from test results for conventional craft and the cross-section of a sidewall is taken as a trapezoid to simplify the calculation.
6. The wave-damping force caused by the air cushion is neglected.

Coordinate system and nomenclature

Two right-hand coordinate systems are used in the equations. The coordinate system $GXYZ$ is the body coordinate system, with its origin point taken to go through the craft CG. In the global fixed coordinate system $0\xi\eta\zeta$, the undisturbed water surface is taken to be the base plane and the origin point is taken as point 0. We also assume that the GZ axis goes through the point 0 (as shown in Fig. 8.1) during the motion of the craft. The following parameters are defined:

Z_{sw}	Vertical distance from the CG to the base-line of the sidewalls (m)
H_b	" " wet deck (m)
Z_s	" " lower edge of the bow/stern seals (m)
Z_H	Average distance between the base-line and outer hard chine of sidewalls (m)
B_s	Max. thickness of the sidewalls (m)
B_B	Width of keel plate at various stations (m)
β_{1i}	Outer deadrise angle of the sidewall at various stations, (°)
β_{2i}	Inner deadrise angle of the sidewall at various stations (°)
p_c	Cushion pressure (N/m^2)
ζ_A	Wave amplitude (m)
L_w	Wavelength (m)
ω	Circular frequency of waves (Hz)
ζ_w	Vertical position of wave surface with respect to sea level (m)
L_c	Cushion length (m)
B_c	Cushion width at base plane of craft (m)
Q_i	Total flow rate of fans (m^3/s)
Q_e	Total air leakage flow rate under bow/stern seal (m^3/s)
Q_v	Flow rate due to the cushion compressibility (m^3/s)
Q_w	Flow rate due to the volume change rate of air cushion in wave (m^3/s)
$V_{is,B}$	Leakage velocity of cushion air under the seals and sidewall (m/s)
$\rho_{w,a}$	Density of the water and air (Ns^2/m^4)
$\gamma_{w,a}$	Specific weight of water and air (N/m^3)
$N_{R,L(i)}$	Heaving damping coefficient per unit length of the right/left sidewalls at various stations
$\lambda_{R,L(i)}$	Added mass coefficient per unit length of the right/left sidewalls at various stations
I_θ	Roll moment inertia of craft (Ns^2/m^2)
W	Weight of craft (N)

Suffixes R and L represent right and left.

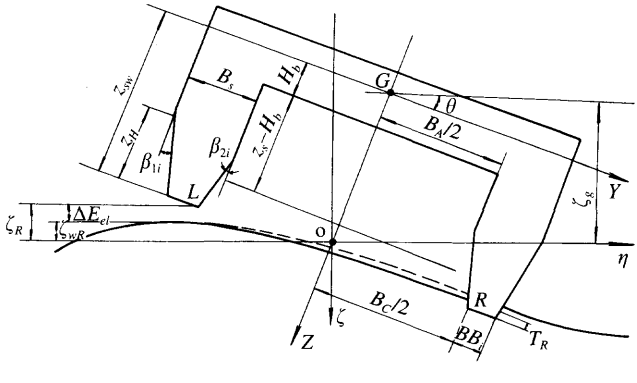

Fig. 8.1 Principal parameters of SES when rolling.

The nonlinear differential equations of motion

Calculation of draft and air leakage under sidewalls (Fig. 8.1)

The top width of air cushion chamber can be written as

$$B_A = 2Z_H \tan \beta_0 + 2BB_0 + B_c - 2B_s$$

where Z_H is the average vertical distance between the base-line and outer chine of the sidewall, β_0 the deadrise angle of sidewalls at mid-section of craft, BB_0 the width of keel plate at mid-section of craft, B_c the cushion beam at base plane of craft and B_s the thickness of the sidewalls.

If we assume the craft roll angle in waves is θ (starboard down positive), then the coordinates of points R and L located at sidewall base plane in the $0\xi\eta\zeta$ co-ordinate system are as in Fig. 8.1.

$$\eta_R = \eta_g + 0.5B_c \cos\theta - Z_{sw} \sin\theta \tag{8.1}$$

$$\zeta_R = \zeta_g + 0.5B_c \sin\theta + Z_{sw} \cos\theta$$

$$\eta_L = \eta_g - 0.5B_c \cos\theta - Z_{sw} \sin\theta \tag{8.2}$$

$$\zeta_L = \zeta_g - 0.5B_c \sin\theta + Z_{sw} \cos\theta$$

where Z_{sw} is the vertical distance between the CG of the craft and base-line of sidewalls (m).

The characteristic equation of beam waves in absolute coordinates is

$$\zeta_w = \zeta_A \cos(2\pi/L_w\, \eta - \omega t) \tag{8.3}$$

where ζ_A is the wave amplitude (m), ω the circular frequency of the wave (Hz), t the time (s) and L_w the wavelength (m).

In the GXYZ coordinate system, one takes $\eta = y \cos\theta$, then

$$\zeta_w = \zeta_A \cos[(2\pi/L_w)\, y \cos\theta - \omega t] \tag{8.4}$$

The wave elevations at points R and L are then

$$\zeta_{wR,L} = \zeta_A \cos(\pi\, B_c/L_w \cos\theta -/+ \omega t) \tag{8.5}$$

The air leakage gaps at each sidewall are

$$\Delta Z_{eR,L} = \zeta_{wR,L} + p_c/\gamma_w - \zeta_{R,L} \tag{8.6}$$

The air leaks from the air cushion under the sidewalls when $\Delta Z_{eR,L} > 0$. When $\Delta Z_{eR,L} < 0$, the sidewall immerses in the water and the draft of sidewalls is

$$\begin{aligned} T_{R,L} &= -\Delta Z_{eR,L} \\ &= -\zeta_A \cos(\pi B_c/L_w \cos\theta -/+ \omega t) - p_c/\gamma_w + \zeta_g \pm 0.5B_c \sin\theta + Z_{sw} \cos\theta \end{aligned} \tag{8.7}$$

where ζ_g is the height of the CG of the craft in the $0\xi\eta\zeta$ coordinate system.

The vertical velocity and acceleration of $T_{R,L}$ can be expressed by

$$\begin{aligned} \dot{T}_{R,L} = {} & -/+ \zeta_A \sin\theta\, (\pi B_c/l_c \cos -/+ \omega t) - \dot{p}c/\gamma_w \\ & + \dot{\zeta}_g \pm 0.5B_c \cos\theta\, \dot{\theta} - Z_{sw} \sin\theta\, \dot{\theta} \end{aligned} \tag{8.8}$$

$$\ddot{T}_{R,L} = \zeta_A \omega^2 \cos(\pi B_c / l_c \cos\theta - /+ \omega t) - \ddot{p}_c/\gamma_w + \ddot{\zeta}_g \pm 0.5 B_c \cos\theta\, \ddot{\theta} - Z_{sw} \cos\theta\, \ddot{\theta} \tag{8.9}$$

where the second-order terms are neglected.

With regard to the difference in draft of sidewalls, p_c/γ_w, between outer and inner sides, the sidewall draft for buoyancy calculation can be expressed as follows, to simplify the calculation:

$$T_{R,L1} = T_{R,L} + p_c/\gamma_w \tag{8.10}$$

However, when one calculates the added mass and heave damping force of a sidewall, the sidewall draft can be written as

$$T_{R,L1} = T_{R,L} + p_c/(2\gamma_w) \tag{8.11}$$

Air cushion and lift fan system

1. Continuity equation of flow

$$Qi = Q_e + Q_w + Q_v \tag{8.12}$$

$$Q_e = Q_{esw} + Q_{es} = Q_{eswR} + Q_{eswL} + Q_{es} \tag{8.13}$$

where Q_i is the total flow rate of the fan (m/s), Q_e the total air leakage flow rate under the bow/stern seals and sidewalls (m/s), Q_w the flow rate due to the volume change rate of air cushion in waves (m/s), Q_v the flow rate due to the cushion compressibility (m^3/s), Q_{esw} the flow rate under the sidewalls (m^3/s), and Q_{es} the flow rate under the bow/stern seals (m^3/s).

Assume the air leakage rate under the sidewall is A_{esw}, then the area of air leakage under the sidewalls is

$$A_{esw} = A_{eswR} + A_{eswL}$$

$$A_{eswR,L} = 0.5\, L_c\, (\Delta Z_{eR,L} + |\, \Delta Z_{eR,L}\,|) \tag{8.14}$$

Then the flow under the sidewalls can be written as

$$Q_{ewsR,L} = V_{ib} A_{eswR,L}\, \phi$$

where V_{ib} is the velocity of air leakage, which can be written as

$$V_{ib} = (2p_c/\rho_a)^{0.5} \operatorname{sgn}(p_c) \approx 4\,.\,(|p_c|)^{0.5} \operatorname{sgn}(p_c) \tag{8.15}$$

and ϕ is the flow rate coefficient, normally $\phi = 0.6$–0.7.

Considering the craft trim angle to be very small, the air leakage gap under the bow/stern seals can be written as follows (see Fig. 8.1)

$$\Delta Z_{es} = (p_c/\gamma_w)\sec\theta + \zeta_A \cos[(2\pi/L_w)\, y \cos\theta - \omega t] \sec\theta - \zeta_g \sec\theta - y \tan\theta - z_s \tag{8.16}$$

where z_s is the distance between the vertical CG and lower tip of bow/stern seals (m), and y the abscissa of the section at which the gaps of air leakage under the bow/stern seal are calculated. Thus the air leakage area A_{es} can be written as

$$A_{es} = \int_{-Bc/2}^{B_c/2} (\Delta Z_{es} + |\Delta Z_{es}|)\, dy \tag{8.17}$$

The velocity of air leakage under the bow and stern seals can be written

$$V_{is} = 4(|p_c|)^{0.5} \operatorname{sgn}(p_c)$$

Therefore

$$Q_{es} = A_{es} V_{is} \phi \tag{8.18}$$

We assume the change of air density in the cushion depends upon the law of adiabatic change, and the air density in the cushion at the static hovering condition is equal to that in the atmosphere, i.e.

$$p/(\rho_a v) = \text{constant}$$

where p is the total pressure in the air cushion, $p = p_c + p_a$, p_a the atmospheric pressure and v the adiabatic coefficient. In general $v = 1.4$. Thus the expression can be written as

$$\dot{\rho}_a/\rho_a = \dot{p}_a/(v(p_c + p_a))$$

Therefore

$$Q_w + Q_v = \frac{1}{\rho_a}\frac{d}{dt}(\rho_a V_c) = \dot{V}_c + V_c \frac{\dot{p}_c}{(1.4\,(p_a + p_c))} \tag{8.19}$$

where V_c is the volume of air cushion (m^3).

Assume $Z_v(y)$ represents the distance between the wave surface and the wet deck of the craft, then

$$Z_v(y) = \zeta_w \sec\theta + p_c/\gamma_w \sec\theta - \zeta_g \sec\theta - y \tan\theta - H_b$$

$$\begin{aligned} V_c &= K_v l_c \int_{-Bc/2}^{B_c/2} Z_v(y)\, dy \\ &= K_v S_c [p_c/\gamma_w \sec\theta - H_b - \zeta_g \sec\theta \\ &\quad + [\zeta_A/(\pi B_c/L_w)] \sec^2\theta \sin[(\pi B_c/L_w)\cos\theta] \cos\omega t] \end{aligned} \tag{8.20}$$

where S_c is the cushion area (m^2), $S_c = l_c B_c$ and K_v the correction coefficient for simplified sidewall configuration which leads to a calculation error on cushion volume. In general, we take $K_v = 0.90$–1.1. Therefore

$$\begin{aligned} \dot{V}_c &= K_v S_c [\dot{p}_c/\gamma_w \sec\theta - H_b - \dot{\zeta}_g \sec\theta \\ &\quad - [\zeta_A \omega L_w/(\pi B_c)] \sec^2\theta \sin[(\pi B_c/L_w)\cos\theta] \sin\omega t] \end{aligned} \tag{8.21}$$

2. Pressure head equation

$$H_j = p_c + 0.5\rho_a \xi (q_i/S_i)^2 \tag{8.22}$$

where H_j is the fan total pressure head (N/m^2), S_i the hole area for air inflow into the air cushion (m^2) and ξ the air duct head loss coefficient due to air blown from the fan outlet directly into the cushion (actually the calculation will be carried out using the head loss coefficient of the air ducts).

3. Fan characteristic equation

We will assume that there are two fans located on the craft, thus the inflow rate for each fan is equal to $Q_i/2$, so the equation for fan characteristics can be written as

$$H_j = A + BQ_i/2 - CQ_i^2/4 \tag{8.23}$$

where A, B and C are the dimensional coefficients of the fan characteristic and can be written as

$$A = A_{f0}\rho_a \cdot \pi^2 D_f^2 \eta_f^2/3600$$

$$B = B_{f0}\rho_a \eta_f/(15D_f)$$

$$C = C_{f0}\, 16\rho_a/(\pi^4 D_f^4)$$

where A_{f0}, B_{f0}, C_{f0} are the non-dimensional coefficients of fan characteristics, D_f the fan diameter (m) and η_f the revolution of the fan (r/min).

Cushion force (moment)

1. Cushion force F_c

Assume a_w, which represents the wave steepness across the craft width, can be defined as follows:

$$a_w = (\zeta_{wR} - \zeta_{wL})/B_c$$

The cushion force F_c' perpendicular to the average wave surface can be written as

$$F_c' = p_c S_c \sec(\theta - a_w)$$

Thus F_c, the projection of F_c' on the ζ axis, can be expressed by

$$F_c = -F_c' \cos a_w \tag{8.24}$$

2. Cushion moment M_c

Assume that cushion force F_c' acts on the origin point 0 of the coordinate system $0\xi\eta\zeta$, then M_c represents the cushion moment about the CG of the craft and can be written by

$$M_c = -F_c' \, LF_c' = -p_c S_c \zeta_g \tan(\theta - a_w) \tag{8.25}$$

Force (moment) acting on skirts F_s

The force (moment) acting on the skirts can be expressed by

$$F_s = -p_c/2\,(\cot a_1 + \cot a_2) \int_{-B_c/2}^{Bc/2} (-\Delta Z_{es} + |\Delta Z_{es}|)\, dy \tag{8.26a}$$

$$M_s = -p_c/2\,(\cot a_1 + \cot a_2) \int_{-B_c/2}^{Bc/2} (-\Delta Z_{es} + |\Delta Z_{es}|)\, y\, dy \tag{8.26b}$$

where F_s is the hydrodynamic force on the skirts (N), M_s the hydrodynamic moments on skirts (Nm) and a_1, a_2 the inclination angle of bow/stern seals with respect to axis GX(°).

Forces and moments acting on sidewalls (Fig. 8.2)

If $S_{R,L(i)}$ represents the immersion cross-section area of sidewalls at station i, then it can be written as

$$S_{R,L(i)} = 1/8\ (\tan \beta_{1i} + \tan \beta_{2i})(T_{R,L1} + |\ T_{R,L1}\ |)^2 + 0.5BB_i\ (T_{R,L1} + |\ T_{R,L1}\ |) \quad (8.27)$$

where β_{1i}, β_{2i} are the outer and inner deadrise angles of the sidewall at station i (°) and BB_i the width of the base-line at station i (m).

There are three cases to be considered with respect to the hydrodynamic forces acting on the craft during craft motion according to the different draft of port and starboard sidewalls; they are described as follows.

Case 1: Cushion air leaks under the port sidewall, but starboard is immersed

$$\begin{aligned} F_{swR} &= \zeta_w g \int_{l_c} S_{R(i)}\, d\xi - 2 \int_{l_c} N_{R(i)}\, \dot{T}_{R.1'}\, d\xi - \int_{l_c} \lambda_{R(i)}\ \ddot{T}_{R.1''}\, d\xi \\ &= F_{swR(F)} + F_{swR(D)} + F_{swR(I)} \end{aligned} \quad (8.28)$$

where F_{swR} are the total hydrodynamic forces acting on the starboard sidewall (N) and $F_{swR(F)}$ the buoyancy acting on sidewalls (N):

$$F_{swR(F)} = 0.5\rho_w\, g\, \Delta x \left[T_{RI}^2 \sum_{i=1}^{n} (\tan \beta_{1i} + \tan \beta_{2i}) + 2T_{R1} \sum_{i=1}^{n} BB_i \right]$$

where n is the number of stations along the craft length, and Δx the space between two stations (m). $F_{swR(D)}$ is the heaving damping force acting on the sidewall (N):

$$\begin{aligned} F_{swR(D)} &= 2\Delta x\, [\zeta_A\, \omega \sin (\pi B_c/L_w \cos \theta - \omega t) + \dot{p}_c/2\gamma_w - \dot{\zeta}_g \\ &\quad + (Z_{sw} \sin \theta - 0.5B_c \cos \dot{\theta})\dot{\theta}] \sum_{i=1}^{n} N_{R(i)} \end{aligned} \quad (8.29)$$

$F_{swR(I)}$ is the heave inertia force of added mass acting on the sidewall (N):

$$\begin{aligned} F_{swR(I)} &= 2\Delta x\, [-\zeta_A\, \omega^2 \cos (\pi B_c/L_w \cos \theta - \omega t) + \ddot{p}_c/2\gamma_w - \ddot{\zeta}_g \\ &\quad + (Z_{sw} \sin \theta - 0.5B_c \cos \theta)\ddot{\theta}] \sum_{i=1}^{n} \lambda_{R(i)} \end{aligned} \quad (8.30)$$

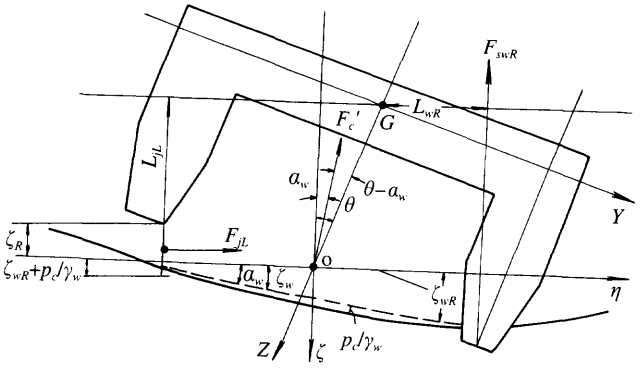

Fig. 8.2 Forces acting on SES when rolling.

$\lambda_{(i)}$, $N_{(i)}$ represent the dimensionless coefficients of heaving damping and added mass for unit length. Considering that the sidewalls are thin and located far from the roll axis, then the coefficients for roll damping and added mass of sidewalls can be obtained approximately by using the heave damping and added mass coefficient of the sidewalls. Therefore the coefficients of heave damping and added mass for conventional ships can be fully used for the calculation, i.e. the experimental results in ref. 80.

During the calculation at MARIC, it was found that the immersion area coefficient of sidewall transverse sections was between 0.6 and 1.0 and $B_n/T_{R,L}$ was about 1.2 where the B_n represented the immersed width of sidewalls and the dimensional coefficient for wave encounter frequency $(\omega_e^2 B_n)/2g = B_n/L_w << 0.2$, where L_w represents wavelength. Taking the immersion coefficients of a sidewall transverse section to be 0.8 and $B_n/T_{R,L} = 1.2$, then the dimensionless coefficients of wave damping and added mass for unit length can be expressed as

$$\lambda_{0(i)} = 1.4\text{–}3.1\ (\omega_e^2 B_n)/2g$$
$$N_{0(i)} = 1.5\ (\omega_e^2 B_n)/2g \tag{8.31}$$

The dimensional coefficient of heaving damping and added mass for unit length of sidewalls can be written as

$$\lambda_{(i)} = \lambda_{0(i)}\, \rho_w\, TB^2/8$$
$$N_{(i)} = N_{0(i)}^2\, \rho_w\, g^2/\omega_e^3 \tag{8.32}$$

Case 2: Cushion air leaks under the starboard sidewall and port side is immersed
This can be treated the same as in case 1 above, the roll angle is just reversed.

Case 3: Both port and starboard sidewalls immersed

$$F_{sw} = F_{swR} + F_{swL}$$

Assume that the hydrodynamic force on the sidewalls acts on the interception point of the sidewall centre line with its keel plane, then

$$L_{wR} = 0.5\ (B_A + B_S) \cos\theta - Z_{sw} \sin\theta$$
$$L_{wL} = 0.5\ (B_A + B_S) \cos\theta + Z_{sw} \sin\theta \tag{8.33}$$

where $L_{wR,L}$ is the hydrodynamic moment arm of the sidewall about the craft CG (m) and B_A the top width of the air cushion (m). Thus the moment of hydrodynamic force acting on the sidewall about the CG of the craft can be expressed as

$$M_{swR,L} = F_{swR,L}\, L_{wR,L} \tag{8.34}$$

Moment M_j due to the air jet from cushion to atmosphere

In this section, swaying motion is temporarily not considered, therefore the jet force will not be included in the equations of motion. However, the moment M_j caused by the jet will be the response to the equations of motion, and for this reason the jet moment can be expressed as

$$F_{jL,R} = \rho_a V_{ib} Q_{eswL,R} = 2 l_c p_c \Delta Z_{eL,R} \phi$$
$$L_{jL,R} = Z_{sw} \cos\theta - B_c/2 \sin\theta + 0.5\, \Delta Z_{eL}$$
$$M_{jL,R} = -F_{jL,R}\, L_{jL,R} \tag{8.35}$$

where $F_{jL,R}$ are the forces due to the air jet from the air cushion (N), V_{ib} the jet velocity under the sidewalls (m/s) and ϕ the flow rate coefficient.

The nonlinear differential equations of motion

The coupled roll and heave motion of craft on cushion in beam waves is taken into account in the equation, but the sway motion of craft is not. There are three variables in the motion equations. Considering that the hydrodynamic forces (moments) and the air jet force (moments) acting on the craft are different in different conditions of air leakage under the sidewall, some parameters of the equations can be simplified as follows:

1. Both sidewalls are immersed, i.e. $\Delta Z_{eR,L} \leqslant 0$, then
$$A_R = 1.0 \qquad A_L = 1.0 \qquad B_j = 0$$
2. Port sidewall is immersed, but air leaks under starboard sidewall, namely, $\Delta Z_{eL} \leqslant 0$, $\Delta Z_{eR} > 0$, then
$$A_R = 0 \qquad A_L = 1.0 \qquad B_j = 1.0$$
3. Air leaks under port sidewall, but starboard sidewall is immersed, i.e. $\Delta Z_{eL} > 0$, $\Delta Z_{eR} \leqslant 0$, then
$$A_R = 1.0 \qquad A_L = 0 \qquad B_j = 1.0$$

We can also write

$$TT_{R,L1} = A_{R,L}\, T_{R,L1}$$
$$NN_{R,L} = A_{R,L}\, N_{R,L}$$
$$\lambda\lambda_{R,L} = A_{R,L}\, \lambda_{R,L}$$
$$M_{jjR,L} = A_{R,L}\, B_j\, M_{jR,L}$$

where

$$N_{R,L} = \sum_{i=1}^{n} N_{R,L(i)}$$
$$\lambda_{R,L} = \sum_{i=1}^{n} \lambda_{R,L(i)}$$

Thus the coupled roll and heave differential equations of motion can be written as

$$[W_I]\begin{bmatrix} \ddot{\zeta}_g \\ \ddot{\theta} \end{bmatrix} = \begin{bmatrix} F_c \\ M_c \end{bmatrix} + \begin{bmatrix} F_s \\ M_s \end{bmatrix} + \begin{bmatrix} F_{swR} \\ M_{swR} \end{bmatrix} + \begin{bmatrix} F_{swL} \\ M_{swL} \end{bmatrix} + \begin{bmatrix} 0 \\ M_{jjR,L} \end{bmatrix} + \begin{bmatrix} W \\ 0 \end{bmatrix} \tag{8.36}$$

where $[W_I]$ is the matrix for coefficient of inertia force, which can be written as

$$[W_I] = \begin{bmatrix} w/g & 0 \\ 0 & I_\theta \end{bmatrix}$$

where W is the craft weight (N) and I_θ the moment of inertia of craft in roll (Ns^2m).

The suffixes c, s, sw, j in the matrix represent cushion force (moment), force (moment) acting on the skirt, on sidewalls, of course including the buoyancy, damping and inertia force and jet force (moment) blown under the side hulls respectively.

Based on equations (8.24)–(8.31), the terms in (8.36) can be written as

$$F_c = -p_c S_c \sec(\theta - \alpha_w) \cos \alpha_w$$

$$F_s = -pc/2 \,(\cot \alpha_1 + \cot \alpha_2) \int_{-Bc/2}^{Bc/2} (\,|\, \Delta Z_{es} \,|\, - \Delta Z_{es}\,)\, dy$$

$$F_{swR,L} = 0.5\rho_w g \,\Delta x \left[TT_{R,L1}^2 \sum_{i=1}^{n} (\tan \beta_{1i} + \tan \beta_{2i}) + 2TT_{R,L1} \sum_{i=1}^{n} BB_i \right]$$
$$+ 2\Delta x NN_{R,L} \,[\zeta_A \omega_e \sin(\pi B_c/L_w \cos\theta -/+ \omega_e t) - \dot{\zeta}_g + \dot{p}_c/2\gamma_w$$
$$+ \dot{\theta}\,(Z_{sw} \sin\theta -/+ B_c/2 \cos\theta)] + \Delta x\, \lambda\lambda_{R,L} \,[\, -\zeta_A \omega_e^2 \cos(\pi B_c/L_w$$
$$-/+ \omega_e t) - \ddot{\zeta}_g + \ddot{p}_c/2\gamma_w + \ddot{\theta}\,(Z_{sw} \sin\theta - B_c/2 \cos\theta)]$$

In this equation R and L correspond to (−) and (+). Thus it can be clearly seen that the first term represents the buoyancy acting on the sidewall, the second the damping force and the third the inertia force.

The equations for the moments are then as follows:

$$M_c = -p_c S_c \sec\theta \tan(\theta - \alpha_w)$$

$$M_s = -p_c/2 \,(\cot \alpha_1 + \cot \alpha_2) \int_{-Bc/2}^{Bc/2} (\,|\, \Delta Z_{es} \,|\, - \Delta Z_{es})\, y\, dy$$

$$M_{jR} = \Delta Z_{eR}\, 2\, \phi\, p_c\, l_c\, L_{jR}$$

$$M_{jL} = -\Delta Z_{eL}\, 2\, \phi\, p_c\, l_c\, L_{jL}$$

$$L_{jR,L} = Z_{sw} \cos\theta +/- B_c/2 \sin\theta + \Delta Z_{cR,L}$$

$$M_{swR,L} = +/- L_{wR,L}\, F_{swR,L}$$

$$L_{wR,L} = (B_A + B_S)/2 \cos\theta -/+ Z_{sw} \sin\theta$$

Put $x_1 = t$, $x_2 = \zeta_g$, $x_3 = \dot{\zeta}_g$, $x_4 = \theta$, $x_5 = \ddot{\theta}$ and then the equations for force and moment can be simplified as

$$[\,A\,][\,X\,] = [\,\dot{A}\,] \tag{8.37}$$

where

$$[\,A\,] = \begin{bmatrix} a_{11} & a_{12} & a_{13} & a_{14} \\ a_{21} & a_{22} & a_{23} & a_{24} \end{bmatrix}$$

$$[\,X\,] = \begin{bmatrix} \dot{x}_3 \\ x_3 \\ \dot{x}_5 \\ x_5 \end{bmatrix}$$

$$[\dot{A}] = \begin{bmatrix} a_{15} \\ a_{25} \end{bmatrix}$$

$$a_{11} = w/g + \Delta x\,(\lambda\lambda_R + \lambda\lambda_L)$$

$$a_{12} = 2\Delta x\,(NN_R + NN_L)$$

$$a_{13} = -\Delta x\,(\lambda\lambda_R\, L_{RR} + \lambda\lambda_L\, L_{ll})$$

$$a_{14} = -2\Delta x\,(NN_R\, L_{RR} + NN_L\, L_{ll})$$

$$a_{21} = \Delta x\,(\lambda\lambda_R\, L_{wR} - \lambda\lambda_L\, L_{wl})$$

$$a_{22} = \Delta x\,(NN_R\, L_{wR} - NN_L\, L_{wl})$$

$$a_{23} = I_0 + \Delta x\,(\lambda\lambda_L\, L_{ll}\, L_{wl} - \lambda\lambda_R\, L_{RR}\, L_{wR})$$

$$a_{24} = 2\Delta x\,(NN_L\, L_{ll}\, L_{wl} - NN_R\, L_{RR}\, L_{wR})$$

$$a_{15} = F_c + F_s + F_{BF} + F_p + F_{wA} + W$$

$$a_{25} = Mc + M_s + \{M_{BRF} + M_{BLF}\} + \{M_{jjR} + M_{jjL}\} + M_p + M_{WA}$$

$$L_{RR} = Z_{sw} \sin\theta - B_c/2 \cos\theta$$

$$L_{LL} = Z_{sw} \sin\theta + B_c/2 \cos\theta$$

and in term a_{15},

$$F_{BF} = -0.5\rho_w\, g\, \Delta x \left[(TT_{R1}^2 + TT_{L1}^2) \sum_{i=1}^{n} (\tan\beta_{1i} + \tan\beta_{2i}) + 2\,(TT_{R1} + TT_{L1}) \sum_{i=1}^{n} BB_i \right]$$

$$T_{R,L1} = -\Delta Z_{eR,L} + p_c/2\gamma_w$$

$$F_p = \Delta x/\gamma_w\,[\dot{p}_c(NN_R + NN_L) + \ddot{p}_c/2 - (\lambda\lambda_R + \lambda\lambda_L)]$$

$$F_{WA} = \Delta x\, \zeta_A\, \omega_e [2NN_R \sin(\pi B_c/L_w \cos x_4 - \omega_e\, x_1) - 2NN_L \sin(\pi B_c/L_w \cos x_4 + \omega_e x_1) - \lambda\lambda_R\, \omega_e \cos(\pi B_c/L_w \cos x_4 - \omega_e x_1) - \lambda\lambda_L\, \omega_e \cos(\pi B_c/L_w \cos x_4 + \omega_e\, x_1)\,]$$

now, in the term a_{25},

$$M_{BR,LF} = -0.5\rho_w\, g\, \Delta x L_{wR,L} \left[TT_{R,L1^2}^2 \sum_{i=1}^{n} (\tan\beta_{1i} + \tan\beta_{2i}) + 2TT_{R,L1} \sum_{i=1}^{n} BB_i \right]$$

$$M_p = \Delta x/\gamma_w\,[L_{wR}\,(NN_R\dot{p}_c + \lambda\lambda_R\,\ddot{p}_c) - L_{wl}\,(NN_L\,\dot{p}_c + \lambda\lambda_L\,\ddot{p}_c/2)]$$

$$M_{WA} = \Delta x\, \zeta_A \omega\ [L_{wR}\,[2NN_R \sin(\pi B_c/L_w \cos x_4 - \omega_e\, x_1) - \lambda\lambda_R \omega_e \cos(\pi B_c/L_w \cos x_4 - \omega_e\, x_1)]$$

$$+L_{wl}\,[2NN_L \sin(\pi B_c/L_w \cos x_4 + \omega_e x_1)$$
$$+\lambda\lambda_L\,\omega_e \cos(\pi B_c/L_w \cos x_4 + \omega_e x_1)]]$$

Finally, the equation can be written in standard form for numerical solution as follows:

$$D = a_{11}\,a_{23} - a_{21}\,a_{13}$$
$$D_1 = a_{15} - a_{12}\,x_3 - a_{14}\,x_5$$
$$D_2 = a_{25} - a_{22}\,x_3 - a_{24}\,x_5$$

then

$$\dot{x}_1 = 1$$
$$\dot{x}_2 = x_3$$
$$\dot{x}_3 = (a_{23}\,D_1 - a_{13}\,D_2)/D$$
$$\dot{x}_4 = x_5$$
$$\dot{x}_5 = (a_{11}\,D_2 - a_{21}\,D_1)/D$$

Initial values can be set as follows, in order to obtain the frequency domain motion response:

$$x_{10} = 0 \qquad x_{20} = \zeta_{g0} \qquad x_{30} = 0 \qquad x_{40} = 0 \qquad x_{50} = 0$$

The initial values of cushion pressure can also be given as

$$p_{c0} = p_c \qquad \dot{p}_{c0} = 0 \qquad \ddot{p}_{c0} = 0$$

Computer program logic for solving the motion equations

A computer program has been developed at MARIC to facilitate numerical solution of the motion equations, as follows:

- First we can calculate from the equilibrium equation the various equilibrium values of craft parameters (Q_0, T_0, P_{c0}) when the craft hovers static on calm water.
- Then we can calculate according to the equilibrium values the initial values of various parameters in the waves.
- Finally we can predict the time-domain motion response by solving the differential equation of motions. These equations can be solved by the Runge–Kutta method, and hence the time-domain motion response obtained from which we can consequently obtain the frequency-domain motion response.

The block diagram for this method of solving the coupled roll and heave differential equations of motion for an SES in beam seas is illustrated in Fig. 8.3. Following each time step p_c is adjusted as follows:

$$p_c^1(t + \Delta t) = p_c(t) + k_c[p_c^{(0)}(t + \Delta t) - p_c(t)] \tag{8.38}$$

During the solution of the differential equations of motion, at first we input the geometric shape and data of the craft into the computer. The initial values of the roll, heave, trim, cushion pressure and vertical height of the CG of the craft running on cushion on calm water can be calculated according to the equilibrium equation of forces (moments) flow rate continuity equation and the characteristic equation for fan and air ducts. If one inputs a given wavelength and height of beam wave, then the differential equation of motion with determined initial values, such as t_0, θ_0, $\dot{\theta}_0$, ζ_{g0}, $\dot{\zeta}_{go}$, $\ddot{\zeta}_{g0}$, p_{c0}, $\dot{p}_{c0}$, $\ddot{p}_{c0}$ can be solved by iteration.

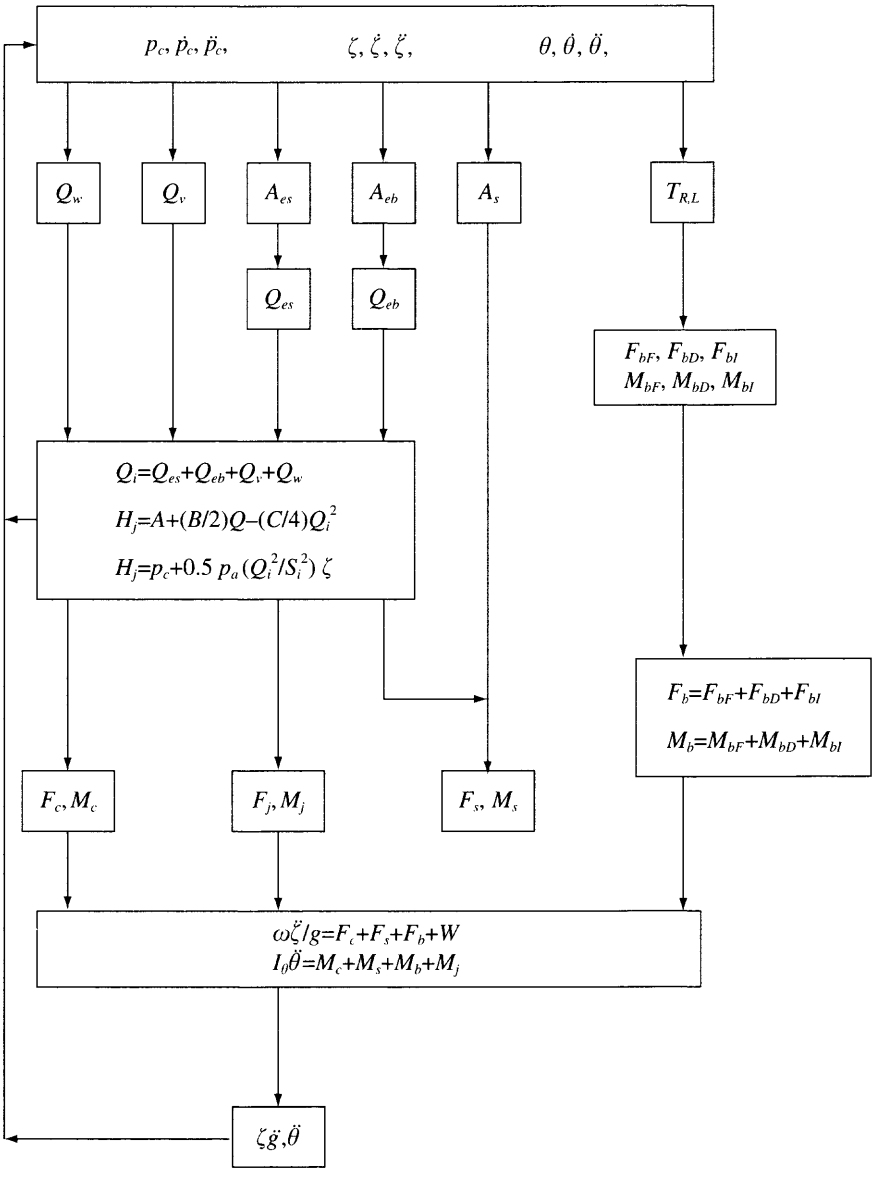

Fig. 8.3 Block diagram for solving the differential equations of coupled roll and heave motion of SES in beam seas.

Comparison of calculation results with experiments

The calculation and experiments of coupled roll and heave motion of steel hull SES version 719 in beam seas has been carried out in the case where the fan flow rate was small.

Tests showed that in the case of large fan flow rate, a large amount of cushion air

would be blown out under the sidewall. This led to a self-excitation of vibration, because the frequency of exciting force due to the jet air blown under the sidewalls was very close to the roll frequency, consequently a 'beat' occurred in the roll motion of the model. Owing to the complicated physical and mathematical model of the beat motion mentioned above, MARIC have not yet solved this problem.

The coupled roll and heave motion of model craft 719 (scale ratio $\gamma = 1{:}12$) in beam waves and its frequency-domain motion response have been predicted using the iterative method by computer. During calculation, the parameters of the craft and waves were given as follows:

Dimensionless mass of the model craft:	$\bar{m} = m/(\rho_w L_c^3) = 0.0048$
Cushion length beam ratio:	$L_c/B_c = 4$
Dimensionless wave height:	$\zeta_a/B_c = 0.0191 \sim 0.0281$
Dimensionless wavelength:	$L_w/B_c = 2.2 \sim 7.6$

Experiments with the model in static hovering mode in beam waves in the towing tank were carried out and comparisons of the theoretical prediction for vertical acceleration at the CG and roll motion amplitude of the model were made with experimental results in the frequency domain.

The responses are shown in Figs 8.4 and 8.5 respectively. One can see that a peak value at $\omega_e = 5$ in Fig. 8.5 can be found both in theoretical and experimental results. This can be considered the natural frequency of roll for the model. The average value of cushion pressure and its amplitude fluctuation in frequency domain response are shown in Figs 8.6(a) and (b). It is found that the calculated results are close to those obtained from model experiments, both having the same trend.

Further investigations required

1. In the case where the wavelengths are longer, due to the extreme fluctuation of cushion pressure, it is difficult to solve the differential equation of motions due to divergence of the calculation. It is suggested this calculation method be improved.

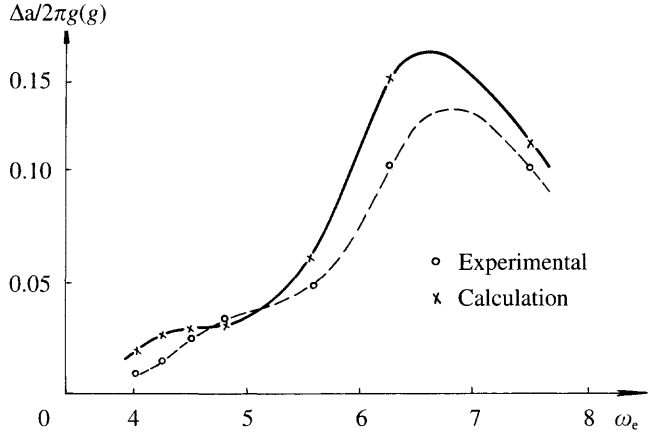

Fig. 8.4 Frequency response curves for heave acceleration at SES model CG in beam seas.

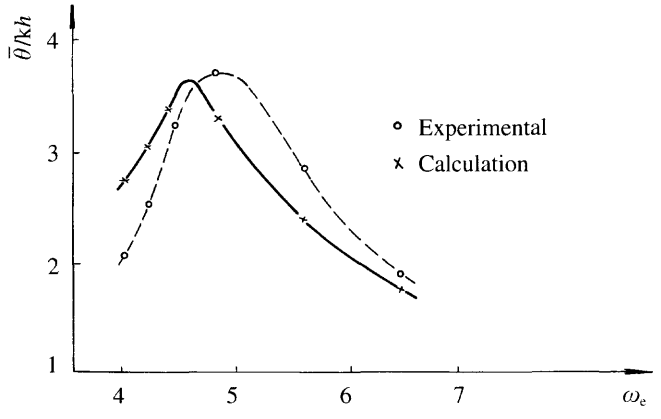

Fig. 8.5 Frequency response curves for the roll amplitude of an SES model in beam seas.

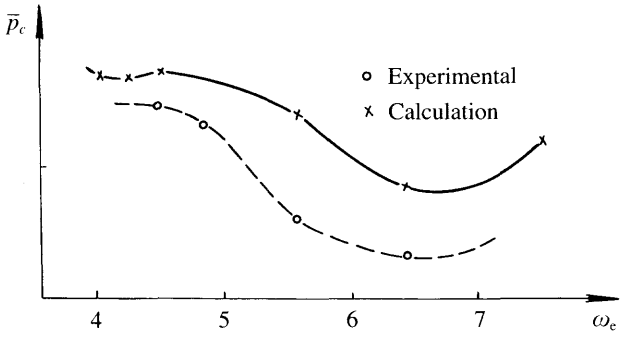

Fig. 8.6(a) Frequency response curves for the mean cushion pressure of an SES model in beam seas.

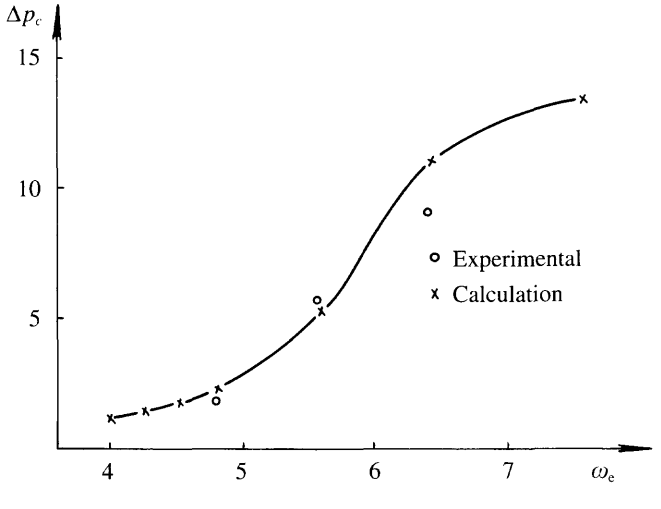

Fig. 8.6(b) Frequency response curves for the cushion pressure fluctuation of the SES model in beam seas.

2. The 'beat' phenomenon in roll of model craft with large air inflow rate can be found in the experiments. It is suggested that the air jet disturbance factor may be enhanced in such a case and cause the 'beat' phenomenon because the frequency of jet disturbance is close to the roll frequency with a little phase lag. Hence the rationale of such a physical phenomenon has to be investigated in order to obtain a more precise mathematical model for calculation.
3. Damping force and added mass due to the combined action of air cushion and sidewalls have not yet been considered in the calculation above, therefore this should be investigated in further research work.
4. Coupled roll and heave motion for small angles is derived in this chapter. In practice the motion to larger craft roll angles in waves is more important when considering craft stability from the safety viewpoint. Hence coupled motion to large rolling angles both for theoretical and test work needs to be investigated in the future.

8.3 Longitudinal SES motions in waves

In section 8.1, we introduced the seaworthiness studies of hovercraft by experts from various countries. The investigations concentrated mainly on the longitudinal (pitch) motions of ACV/SES in waves, as in refs 11, 67 to 69/71, 73 etc. These research papers present differing approaches and analytical methodology.

In this section, the various nonlinear factors associated with motion of a craft running in waves will be discussed. Skirt contact with the water makes the forces acting on the craft have strong nonlinear characteristics. From Fig. 8.7 one can see that hydrodynamic forces acting on the skirt vary sharply. It would be convenient if such conditions could be expressed in a simple manner by deriving nonlinear motion equations.

Although the restoring moment of craft is linear when the craft pitches at a small angle (Fig. 8.8), the longitudinal restoring moment increases sharply when the craft

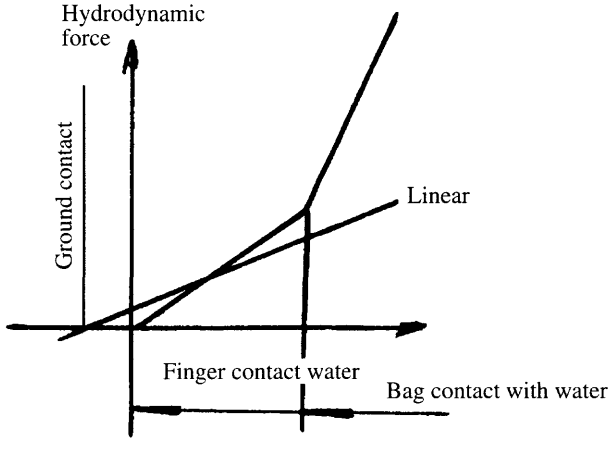

Fig. 8.7 The non-linear characteristics for hydrodynamic forces acting on skirts.

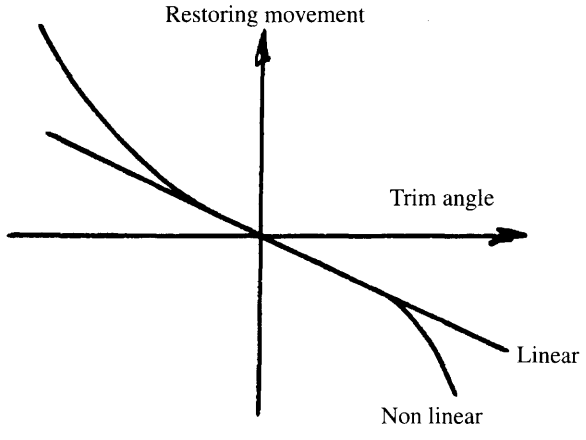

Fig. 8.8 The non-linear characteristics for transverse righting moment on hovercraft.

pitches at a large angle. So it is difficult to analyse such nonlinear characteristics by means of linear equations with adjusted coefficients. However, by applying nonlinear motion equations, the instantaneous restoring moment due to wet skirt hydrodynamic forces can be calculated. This method is more practical and convenient.

Cushion force is not only affected by skirt contact with water but also the non-linearity of fan characteristics. Fan characteristic curves as well as the characteristics of air ducts are parabolic of second order. The slope of the fan characteristic curve sharply affects stability and damping of an air cushion system. In the linear equations of motion, we assume the working point of the fan is constant, which means the slope of the fan characteristic curve stays constant. This will lead to large errors when the craft is running in high seas and the vertical motion of the craft is very large.

In such a case, we can consider air leakage gap, air cushion pressure and air flow rate as functions of time in the nonlinear equations of motion. By this means we can account for the effect of fan characteristics on damping and stability of the air cushion system. Figure 8.9 shows that the change of the curve slope is very large when the fan is operated at larger (or smaller) flow and negative flow rate. Therefore it is more convenient for us to predict craft motion response by means of nonlinear motion equations.

The nonlinearity of the hydrodynamic forces acting on sidewalls arises from the change of draft on each section along the longitudinal craft axis. Particularly when the craft is running in high seas, wave perturbations on the craft are severe and this causes local air leakage under the sidewalls. This results in nonlinearity of sidewall force and air cushion force.

In the derivation of the linear equations of motion, one assumes that the derivatives of the longitudinal stability of the sidewalls are a function of the craft in static equilibrium, in which the effect of air leakage under the sidewalls on craft motion is not taken into account, so that method applies only to the case of small perturbation. However, it would be easier if each effect is considered by the use of nonlinear equations of motion as outlined here.

When a hovercraft is running in heavy seas, it also experiences various physical phenomena such as fan reverse flow, negative air cushion pressure, wave impact on skirt

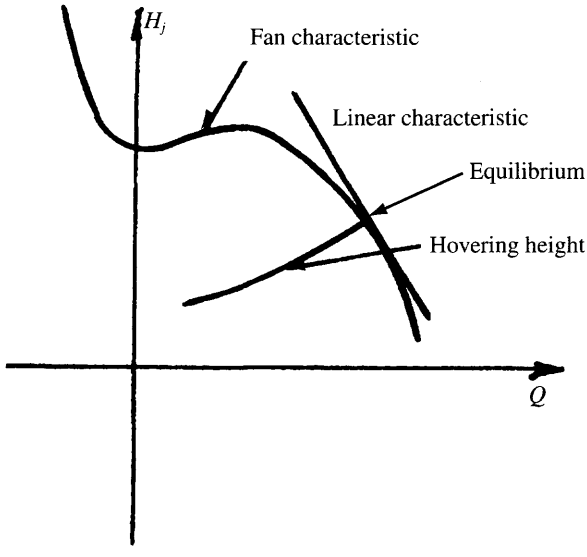

Fig. 8.9 The non-linear characteristics for pressure-flow of lift fans on hovercraft.

fingers or bag, air leakage under sidewalls, etc. One can analyse such phenomena with the aid of non-linear motion equations.

The following principal assumptions are made in order to form nonlinear motion equations:

1. The Froude–Krilov hypothesis is satisfied, which means that waves are not interfered by craft. The effect of sidewalls and skirts on waves and the effect of the air cushion on the surface deformation of waves, are neglected.
2. Uniform distribution of cushion pressure is assumed and the cushion plane is simplified as a rectangle.
3. Changes of air density and cushion pressure in the plenum chamber (air cushion) are considered to be adiabatic, but the outflow of cushion air into the atmosphere incompressible.
4. Fan speed is kept constant and the effect of dynamic response of the fan neglected.
5. Effect of skirt deformation on motions of craft is neglected.
6. Added mass and added mass moment are not taken into account in the equation.
7. The effect of external air dynamic force on the motion of craft is neglected.
8. Bow skirt fingers are regarded as absolutely flexible.
9. Effect of stiffness of stern bag on hydrodynamic forces acting on skirt is taken into account.
10. Cross-section of sidewalls is taken to be a trapezoid to simplify the calculation.

The solution logic is similar to that for solving the coupled roll and heave equations of motion as shown in Fig. 8.10. The calculation in detail can be described as follows [69].

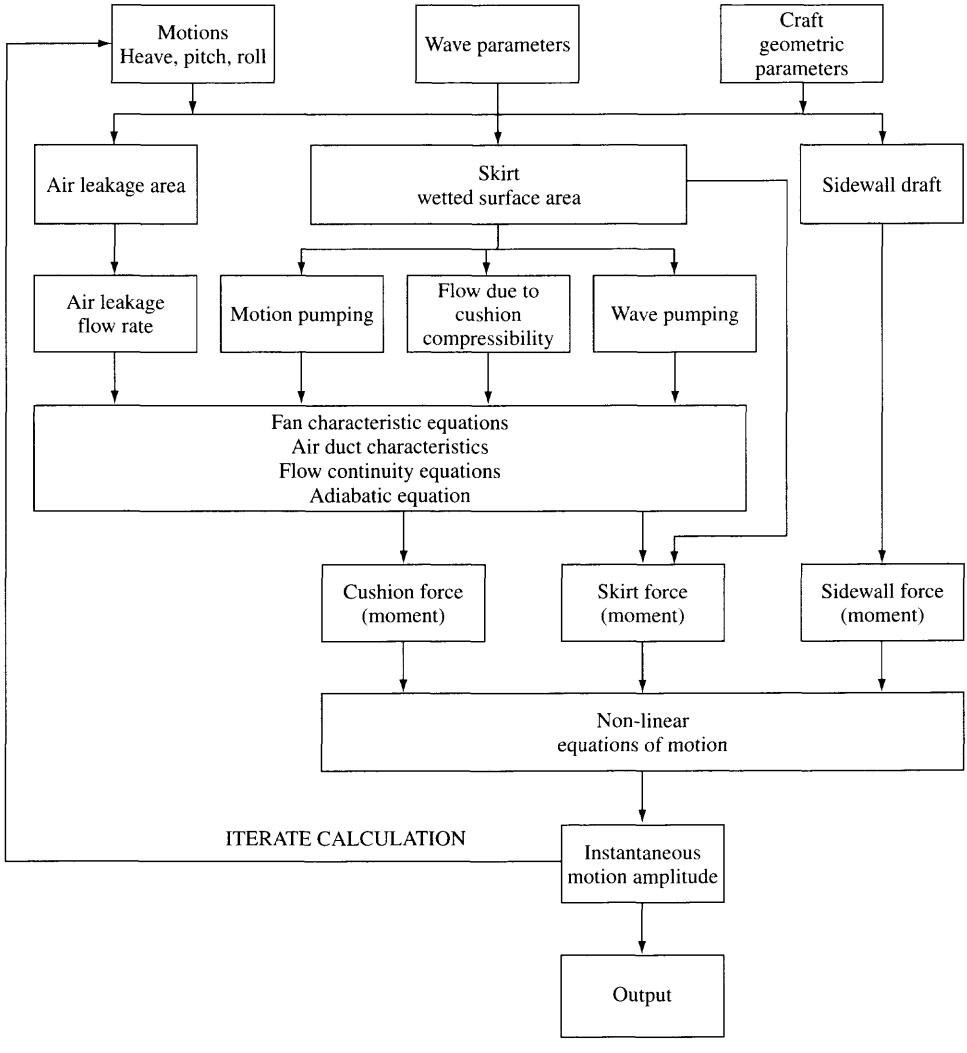

Fig. 8.10 Block diagram for solving SES non-linear differential equations of longitudinal motion in waves.

Coordinate system and geometrical dimensions of craft

Similar to section 8.2, the coordinate system $GXYZ$ fixed on the craft is chosen to be a right-hand coordinate system. The origin point is taken to go through the CG of the craft, GX is a longitudinal axis parallel to the base-line of the sidewall and the forward direction of the craft motion is positive. Along axis GY the starboard direction is positive and axis GZ is perpendicular to the GXY plane and its downward direction is taken to be positive. The outline of the craft is shown in Fig. 8.11 and the configuration of the cushion plane can be simplified as a rectangle with length of L_c, width B_c and area of A_c. There are no compartments in the cushion.

The other geometrical dimensions are illustrated as follows:

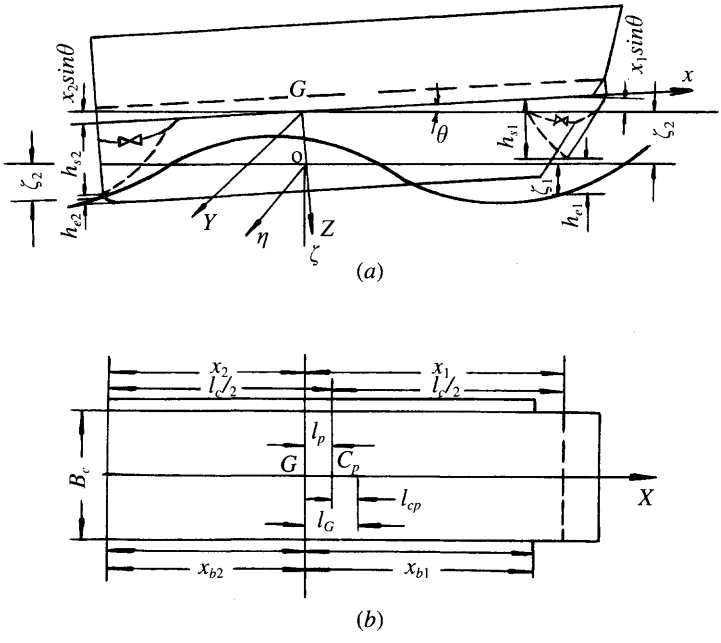

Fig. 8.11 Principal parameters for determining the longitudinal motion of SES in waves.

C_p	Position of pressure centre of air cushion
l_p	Longitudinal distance from CG to C_p (m)
l_G	Longitudinal distance from CG to mid-section (m)
l_{cp}	Longitudinal distance from C_p to midsection, i.e. $l_{cp} = l_G - l_p$ (m)
h_{s1}, h_{s2}	Vertical distances from craft longitudinal axis to lower tips of bow and stern skirt (m)
x_1, x_2	Longitudinal coordinates (on axis GX) of the lower tips of bow and stern skirt respectively; this can be written as

$$x_1 = l_c/2 + l_p \tag{8.39}$$

$$x_2 = -l_c/2 + l_p \tag{8.40}$$

X_{b1}, X_{b2}	Longitudinal GX axis coordinates of sidewall at bow/stern lower tips (m)
h_b	Vertical distance from CG to the base-line of sidewall (m)
ζ_g	Height of CG with respect to the absolute coordinate (m)
ψ	Pitch angle (bow up positive) (°)

Wave equation

With respect to the fixed absolute coordinates $0\xi\eta\zeta$ the equation for two-dimensional waves is given as follows:

$$\zeta_w = \zeta_a \sin(\pm K_w \zeta + \omega t) \tag{8.41}$$

or

$$\zeta_w = \zeta_a \sin(\pm K_w x + \omega_e t) \tag{8.42}$$

where K_w, the wave number, can be written as

$$K_w = 2\pi/L_w \tag{8.43}$$

and ω, the wave frequency, can be written as

$$\omega = [2\pi g/L_w]^{0.5} \tag{8.44}$$

where L_w is the wave length (m), ζ_A the wave amplitude (m) and ω_e the wave encounter frequency (rad/s), which can be written as

$$\omega_e = \omega(1 \pm \omega V_s/g) \tag{8.45}$$

where Vs is the craft speed (m/s).

(In this equation, we take the craft in a head wave as positive and negative in a following wave.) ζ_w is the wave elevation at the distance of x from the CG (m).

For reasons of simplification we take (cf. equation 8.43)

$$K = \pm 2\pi/L_w \tag{8.46}$$

Then the equation of the wave surface can be written as (cf. equation 8.42)

$$\zeta_w = \zeta_a \sin(Kx + \omega_e t) \tag{8.47}$$

The vertical velocity of wave motion and wave slope can be expressed as

$$\dot{\zeta}_w = \zeta_a \omega_e \cos(Kx + \omega_e t) \tag{8.48}$$

$$a_w = \frac{\partial \zeta_w}{\partial x} = K\zeta_a \cos(Kx + \omega_e t) \tag{8.49}$$

where $\dot{\zeta}_w$ is the vertical velocity of wave motion (m/s) and a_w the wave slope (°).

Then the wave elevation, vertical velocity of wave and wave slope at the CG are expressed by:

$$\begin{aligned} \zeta_{wg} &= \zeta_a \sin \omega_e t \\ \dot{\zeta}_{wg} &= \zeta_a \cos \omega_e t \\ a_{wg} &= K\zeta_a \cos \omega_e t \end{aligned} \tag{8.50}$$

The wave elevation, under the bow/stern skirt ζ_{w1}, ζ_{w2}, and wave slope a_{w1}, a_{w2}, can be expressed as

$$\begin{aligned} \zeta_{w1} &= \zeta_a \sin(Kx_1 + \omega_e t) \\ \zeta_{w2} &= \zeta_a \sin(Kx_2 + \omega_e t) \\ a_{w1} &= K\zeta_a \omega_e \cos(Kx_1 + \omega_e t) \\ a_{w2} &= K\zeta_a \omega_e \cos(Kx_2 + \omega_e t) \end{aligned} \tag{8.51}$$

Here suffixes 1 and 2 represent the position at the bow and stern.

Air cushion system

As for the case of uniform distribution of air cushion pressure, air cushion force and moment can be expressed as

$$F_c = -p_c A_c \cos\psi$$
$$M_c = p_c A_c L_p \tag{8.52}$$

Cushion pressure can be obtained by solving the equations of fan and duct characteristics as well as the equation of continuity flow, which is expressed as

$$Q_i = Q_e + \frac{1}{\rho_a}\frac{d}{dt}(\rho_a V_c) \tag{8.53}$$

where Q_i is the inflow rate of fan (m^3/s), Q_e the flow rate of air leakage (m^3/s) and V_c the cushion volume (m^3). The second term on the right of equation (8.53) represents the change of flow rate with respect to volume and density of air cushion, i.e. the sum of flow rate with respect to wave pumping, motion pumping of the craft and compressibility of the air cushion.

The flow rate of air leakage Q_e

$$Q_e = Q_{e1} + Q_{e2} + Q_{eb} \tag{8.54}$$

where Q_{e1} is the flow rate of air leakage under the bow skirt,

$$Q_{e1} = \phi_{s1} V_c A_{e1} \tag{8.55a}$$

Q_{e2} is the flow rate of air leakage under the stern skirt,

$$Q_{e2} = \phi_{s2} V_c A_{e2} \tag{8.55b}$$

and Q_{eb} is the flow rate of air leakage under the sidewall,

$$Q_{eb} = \phi_{eb} V_c A_{eb} \tag{8.55c}$$

ϕ_{s1}, ϕ_{s2} and ϕ_{eb} represent the coefficient of flow rate under the bow skirt, stern skirt and sidewall respectively.

$$A_{e1} = \begin{cases} B_c h_{e1} & \text{when } h_{e1} > 0 \\ 0 & \text{when } h_{e1} \leqslant 0 \end{cases} \tag{8.56}$$

$$A_{e2} = \begin{cases} B_c h_{e2} & \text{when } h_{e2} > 0 \\ 0 & \text{when } h_{e2} \leqslant 0 \end{cases} \tag{8.57}$$

where h_{e1} is the height of air leakage under the bow skirt and can be written as

$$h_{e1} = -\zeta_g + x_1 \sin\psi - h_{s1} \cos\psi + \zeta_{w1} \tag{8.58a}$$

and h_{e2} the height of leakage under the stern skirt, can be written as

$$h_{e2} = -\zeta_g + x_2 \sin\psi - h_{s2} \cos\psi + \zeta_{w1} \tag{8.58b}$$

where h_{s1} and h_{s2} are vertical distance between the CG and the lower tip of the stern skirt.

To simplify the calculation, equation (8.57) may be written as

$$A_{e1} = B_c(h_{e1} + |h_{e1}|)/2$$
$$A_{e2} = B_c(h_{e2} + |h_{e2}|)/2 \tag{8.59}$$

The flow rate due to mass change rate of air cushion

$$\frac{1}{\rho_a}\frac{d}{dt}(\rho_a V_c) = \dot{V}_c + \frac{V_c}{\rho_a}\dot{\rho}_a \tag{8.60}$$

where $\dot{V}_c$ is the flow rate due to the wave pumping and motion pumping of the craft, i.e. the flow rate due to the rate of change of cushion volume of craft moving in waves, Q_w, and $(V_c/\rho_a)\dot{\rho}_a$ the flow rate due to the change of density of cushion air (Q_v), i.e. due to the compressibility of the air cushion. In this case, we assume the change of air density in the cushion depends upon the law of adiabatic change and the air density in the air cushion at the static hovering condition is equal to that in atmosphere, then Q_v can be written as (assume the adiabatic coefficient $r = 1.4$)

$$Q_v = V_c\dot{\rho}_c/(1.4\,(p_c + p_a)) \tag{8.61}$$

$$V_c = B_c\int_{x2}^{x1} h_v(x)\,dx$$

where $h_v(x)$ is the depth of air cushion and can be written as

$$h_v(x) = -\zeta_g + x\sin\psi - h_{b0}\cos\psi + \zeta_w(x)$$

where h_{b0} is the vertical distance from the CG to the bottom of the craft along axis CZ. Thus

$$\dot{V}_c = \int_{x2}^{x1}(-\dot{\zeta}_g + x_c\cos\psi - \dot{\psi} + \dot{\zeta}_w)\,B_c\,dx = Q_w$$

If we integrate this expression, then

$$Q_w = (-\dot{\zeta}_g + L_p\cos\psi - \dot{\psi})\,A_c + \sin C_w/C_w\,A_c\,\omega_e\,\zeta_a\cos(KL_p + \omega_e t) \tag{8.62}$$

The first term on the right of the equation represents the flow rate due to the motion pumping of the craft and the second term represents the flow rate due to the wave pumping where

$$C_w = \pi L_c/L_w$$

Hydrodynamic forces acting on skirts

The bow skirt is assumed to be of the bag and finger type and the stern skirt of the multiple bag type. Fingers of the bow skirt are assumed to be absolutely flexible and the skirt finger will deflect as soon as it comes into contact with the water.

We consider that the hydrodynamic force acting on skirts consists of two parts. One is due to cushion pressure or bag pressure, equal to the air cushion force acting on the wetted surface before deflection. Its vertical component is the lift due to the increase in cushion area while its horizontal component is equal to the product of cushion pressure and projected area of wetted surface on the vertical plane. The second part is due to water friction. Fingers, where in contact with and subsequently lying on the waves, induce water friction force, the direction of which is parallel to the wave surface. This force is divided into vertical and horizontal components. The bow skirt bag may be impacted by waves and local deflection will take place. In that case

cushion pressure has to be altered by bag pressure in the calculation of the hydrodynamic force of the skirt bag.

Assume A_{sf}, A_{st} are the wetted area of the fingers and bag and of the skirt bag respectively. Suffix k represents projection on the vertical plane and h_{sf} represents finger height (Fig. 8.12), in the case that the fingers of the bow skirt are immersed, but the bow skirt bag is not, i.e. while $h_{e1} < 0$ and $| h_{e1} | < h_{sf}$ then

$$A_{sfk} = A_{e1} - B_c h_{e1} \quad \text{and} \quad A_{stk} = 0$$

where A_{sfk} is the projected area of the wetted surface in the vertical plane and h_{e1} the immersed height of the bow finger, or the bow finger and bag. Thus the wetted area of fingers A_{sf} can be written as

$$A_{sf} = A_{sfk} / \sin(\alpha_1 + \psi) \tag{8.63}$$

where α_1 is the inclination angle of the skirt with respect to axis GX.

When $h_{e1} < 0$ and $| h_{e1} | > h_{sf}$ (i.e. bag immersed), then

$$\begin{aligned} A_{s1} &= A_{sf} + A_{st} \\ &= B_c h_{sf} / \sin(\alpha_1 + \psi) + B_c (-h_{e1} - h_{sf}) / \sin(\alpha_1 + \psi) \end{aligned} \tag{8.64}$$

where A_{sl} is the total wetted surface of the bow skirt.

Here the vertical hydrodynamic force acting on the bow skirt F_{sr} can be written as follows:

$$F_{r1} = -(p_c A_{sfk} + p_{t1} A_{stk}) / \tan(\alpha_1 + \psi) - R_F A_{s1} \sin \alpha_{w1} \tag{8.65}$$

where α_w is the wave slope (°) and R_F the water friction force per unit area of skirt, which can be written as

$$R_F = C_f \times 0.5 \rho_w V_s^2$$

where C_f is the coefficient of friction. Thus the total hydrodynamic drag of bow skirts can be written as:

$$R_{s1} = p_c A_{sfk} + p_{t1} A_{stk} + R_F A_{s1} \cos \alpha_{w1} \tag{8.66}$$

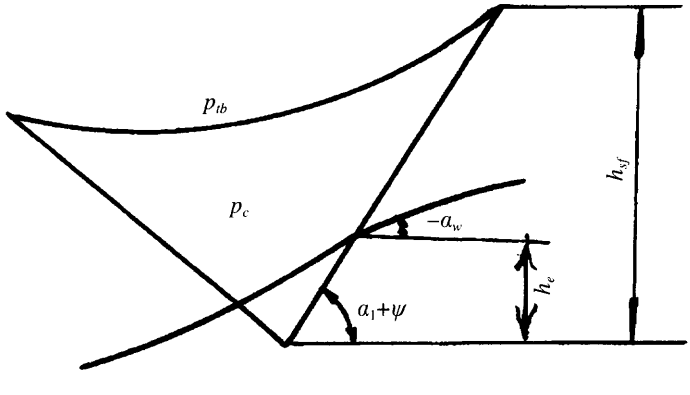

Fig. 8.12 Sketch for submergence of bow skirt.

For the same reason, the hydrodynamic forces acting on the stern seal are

$$F_{s2} = -(C_{ps} p_{t2} A_{sk})/\tan(\alpha_2 + \psi) - R_F A_{s2} \sin \alpha_{w2}$$
$$R_{s2} = C_{ps} p_{t2} A_{sk} + R_F A_{s2} \cos \alpha_{w2} \tag{8.67}$$

where F_s is the vertical hydrodynamic force acting on the stern seal, R_s the hydrodynamic drag acting on the stern seal, p_{t2} the stern bag pressure and C_{ps} the coefficient with respect to the stiffness of the bag obtained from experiments.

The sum of moments induced by vertical forces and drag about the CG can be written as

$$\begin{aligned} F_s &= F_{s1} + F_{s2} \\ R_s &= R_{s1} + R_{s2} \\ M_s &= F_{s1}(x_1 \cos \psi + R_{hs1} \sin \psi) - F_{s2}(x_2 \cos \psi + R_{hs2} \sin \psi) \\ &\quad + R_{s1}(x_1 \sin \psi - R_{hs1} \cos \psi) + R_{s2}(x_2 \sin \psi - R_{hs2} \cos \psi) \end{aligned} \tag{8.68}$$

where F_s is the sum of vertical forces acting on the bow and stern skirts (N), R_s the sum of water drag forces acting on the bow and stern skirts (N), M_s the sum of hydrodynamic moments acting on the bow and stern skirt about the CG (Nm) and R_{hs1}, R_{hs2} are the vertical distances between the axis GX and the points on the bow and stern skirts which are under the action of the hydrodynamic forces and can be written as

$$R_{hs1} = h_{s1} + h_{e1}/2$$
$$R_{hs2} = h_{s2} + h_{e2}/2$$

Hydrodynamic forces and moments acting on sidewalls

The configuration of sidewalls can be simplified as shown in Fig. 8.13. The draft h_t, buoyancy of sidewalls D_b and the restoring moment supplied by the buoyancy, M_D can be written respectively as

$$h_T = h_b \cos \psi + \zeta_g - x \sin \psi - \zeta_w \tag{8.69}$$

$$D_b = -\rho_w g \int_{xb2}^{xb1} [\,((h_T + |h_T|)/2)^2 (\tan \theta_{b1} + \tan \theta_{b2}) + (h_T + |h_T|) B_2\,]\, dx$$

$$M_D = \rho_w g \int_{xb2}^{xb1} [\,((h_T + |h_T|)/2)^2 (\tan \theta_{b1} + \tan \theta_{b2}) + (h_T + |h_T|) B_2\,]\, X\, dx \tag{8.70}$$

where the geometrical parameters $\overline{BB}_1$, $\overline{BB}_2$, θ_{b1}, θ_{b2} are shown in Fig. 8.13.

The outflow rate under the sidewalls can be expressed by

$$Q_{eb} = 2\phi_{eb} V_e \int_{Xb2}^{Xb1} (-h_T + |h_T|)/2\, dx \tag{8.71}$$

in which ϕ_{eb}, the coefficient of air flow leaked under the sidewall with respect to the wave damping force and added mass induced by the sidewall–air cushion system, can be obtained by experiments as in the introduction to this chapter in section 8.2.

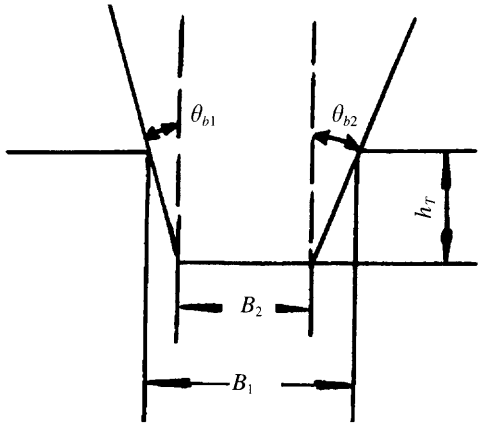

Fig. 8.13 Transverse section of sidewall.

The nonlinear differential equations of motion

The coupled pitch and heave nonlinear differential equations of motion can be written as

$$[W_I]\begin{bmatrix} \ddot{\zeta}_g \\ \ddot{\psi} \end{bmatrix} = \begin{bmatrix} F_C \\ M_C \end{bmatrix} + \begin{bmatrix} F_s \\ M_s \end{bmatrix} + \begin{bmatrix} F_b \\ M_b \end{bmatrix} + \begin{bmatrix} W \\ M_0 \end{bmatrix} \tag{8.72}$$

in which

$$W_I = \begin{bmatrix} W/g & 0 \\ 0 & I_\psi \end{bmatrix}$$

where M_0 are the moments of both drag and thrust about the CG of craft running at given speed and I_ψ the pitch moment of inertia of the craft.

Solution of equations and comparison with experiments

Similar to the procedure described in section 8.2, the coupled pitch and heave are nonlinear differential equations which can be solved with the aid of computers, the block diagram for which is shown in Fig. 8.14.

A comparison of theoretical predictions with experiments in the frequency domain response is made below:

1. The test model is model 719 and its non-dimensional coefficients are the same as that in section 8.2, the wave parameters can be obtained as

$$\zeta_a/L_c \text{ (non-dimensional wave height)} = 0.025$$

$$L_w/L_c \text{ (non-dimensional wavelength)} = 1.0\text{–}7.5$$

   The tests were carried out in a towing tank of MARIC (test in head waves).
2. Figure 8.15(a) shows the response of heave motion; it is found that the maximum value of response does not exceed unity because of the high damping coefficient of

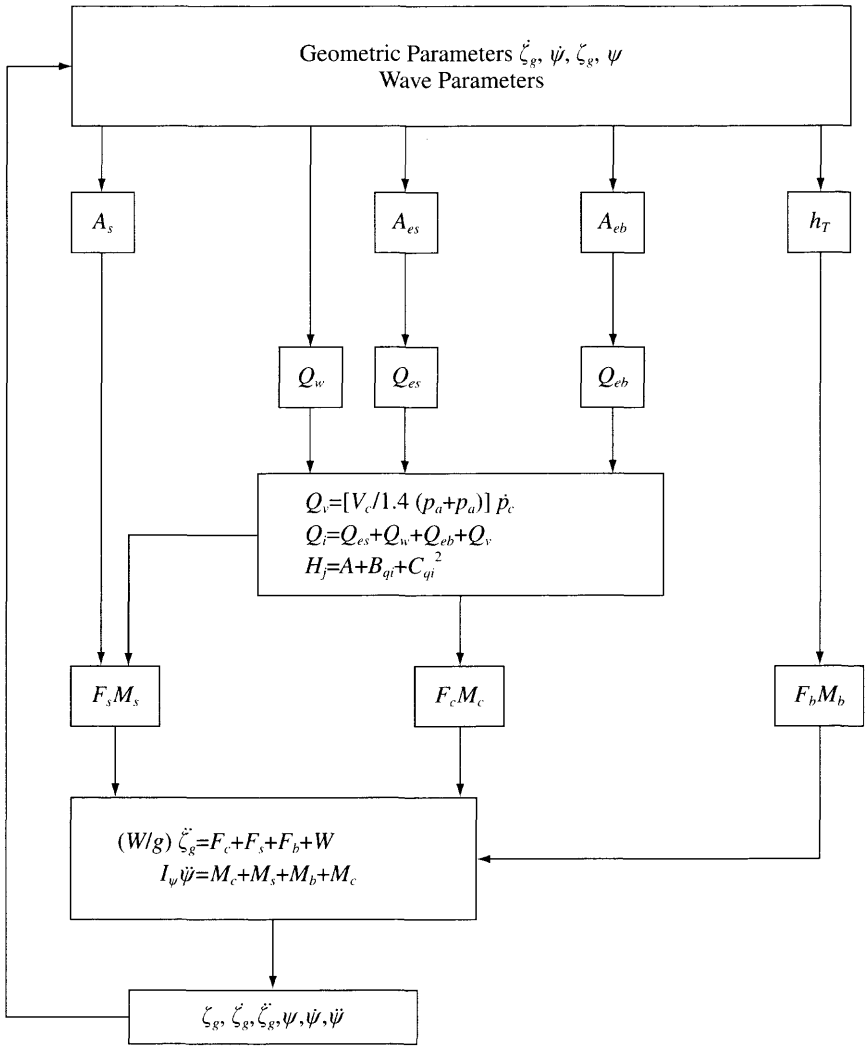

Fig. 8.14 Block diagram for solving the differential equations of longitudinal motion of SES in waves.

motion. It is noted that the heave response depends strongly upon the cushion system characteristics. The calculated values are larger than the experimental results, but both have the same trend. The figure shows a small step at the point corresponding to non-dimensional frequency of 4 due to the coupled pitch–heave motion and wave pumping. The figure also shows a peak at higher frequency, where the wavelength is approximately equal to the craft length.

Figure 8.15(b) indicates that the perturbation force of the wave, the peak of which corresponds to the peak of heave response, has a strong influence on the heave motion response. The response indicates that the heave motion has high heave stability and damping.

3. Figure 8.16 shows the pitch response ψ_{ζ_a} to the wave amplitude as it varies with

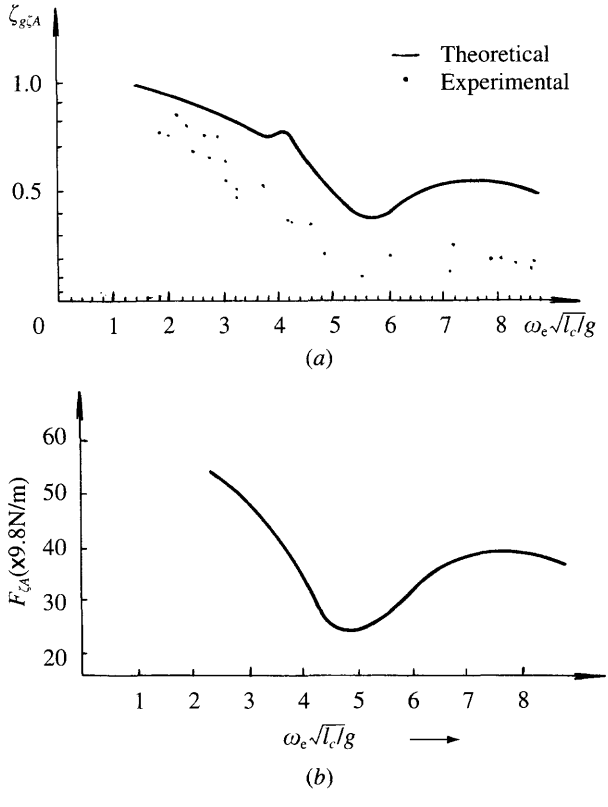

Fig. 8.15 Unit (response/m waveheight) frequency response for heave motion: (a) frequency response for heave amplitude; (b) frequency response for heaving exciting force.

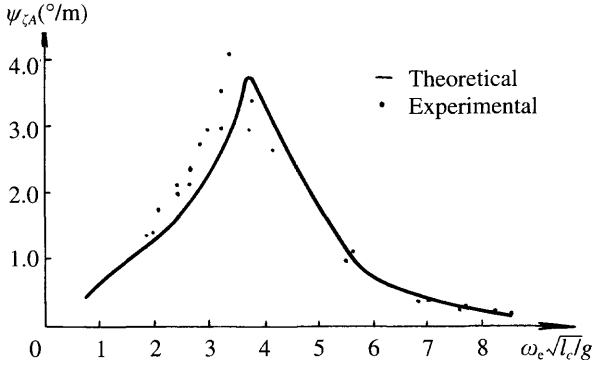

Fig. 8.16 Unit frequency response for pitch angle of SES in waves.

encounter frequency. It is shown that the theoretical prediction is close to the experimental results. Figure 8.17 gives the pitch perturbation moment. It may be noticed that the peak is at the point of non-dimensional frequency of 4, at which the wavelength is about twice the craft length and so the wave perturbation

moment is maximum. To sum up, the peak at about non-dimensional frequency of 4 is due to pitch and heave motion and the peak at higher frequency is due to heave perturbation. The peak on the pitch response curve is rather steep, which shows that the pitch moment has low damping .

4. Figure 8.18 shows the bow acceleration response. The peak at non-dimensional frequency of 4 is induced by both heave and pitch motion. Due to the vertical acceleration of the craft increasing in square proportion with encounter frequency, the vertical acceleration of the craft increases rapidly. The hollow on the curve is due to the superposition of hollows caused by both heave and pitch motion.

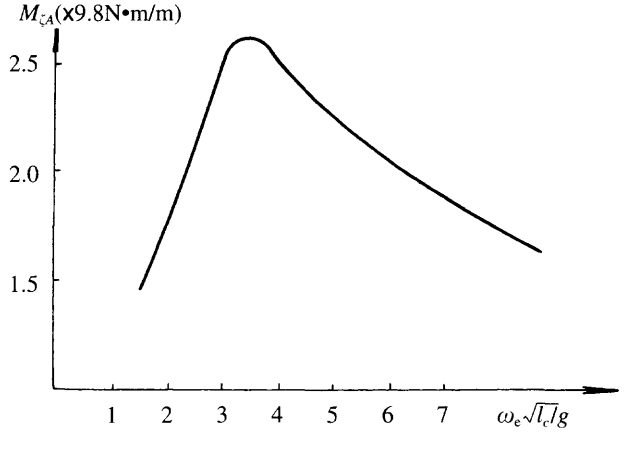

Fig. 8.17 Unit frequency response for pitch exciting moment.

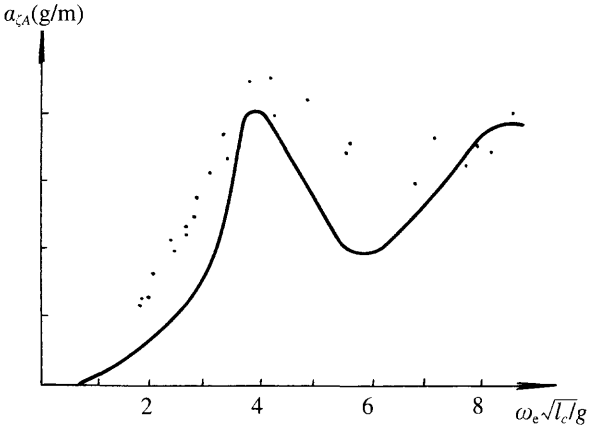

Fig. 8.18 Unit frequency response of bow acceleration for SES in head seas.

8.4 Longitudinal motions of an ACV in regular waves

Seaworthiness motions analysis of ACVs is similar to that of SESs. In this section, we will introduce the linear differential equations of motion for an ACV in regular waves. As mentioned above, although this method is rather artificial, the results obtained by this method are more directly understood and so one can estimate the effect of changes in various parameters of the linear differential equations of motion.

For a typical ACV, the cushion moment will be the predominant restoring moment due to the cushion compartmentation or skirt of deformation. It is normally possible to neglect the effect of hydrodynamic force (moment) acting on the skirt. References 11, 67 and 71 discussed this subject with respect to the linear equations of motion. Here we introduce the linear equations concerning coupled heave and pitch motion [70]. In this approach the hydrodynamic force (moment) acting on the skirt and the wave surface deformation due to the motion of cushion air are not considered, but we take the Froude–Krilov hypothesis and effect of cushion air compressibility into account.

In the course of deriving the equations, one still adopts the assumptions in section 8.3 above, namely recognizing the Froude–Krilov hypothesis; simplifying the cushion plane as a rectangle; taking the change of pressure and density in the air cushion to comply with the adiabatic principle; neglecting the dynamic response of air cushion fans; not considering the added mass force and damping force due to the motion of the air cushion; and considering the distribution of cushion pressure in fore and rear cushion to be uniform.

Craft dimension and coordinate system

As in sections 8.2 and 8.3, the fixed coordinate system $0\xi\eta\zeta$ and body coordinate system $GXYZ$ are both used. We introduce the following dimensions in this section (see Fig. 8.19):

l_1, l_2 Length of fore and rear skirts respectively

A_{c1}, A_{c2} Area of fore/rear air cushion, which can be written $A_{c1} = B_c\, l_1$, $A_{c2} = B_c\, l_2$

X_{p1}, X_{p2} Centre of pressure of fore/rear air cushion respectively

$$X_{p1} = (X_1 + X_g)/2$$

$$X_{p2} = (X_2 + X_g)/2 \tag{8.73}$$

h_{ss1}, h_{ss2} Vertical distance from the GX axis to the lower tip of fore and rear skirts

h_{s1}, h_{s2} Vertical distance from the GX axis to the lower tip of bow and stern skirts

h_{sg} Vertical distance from the base plane to the lower tip of the transverse stability skirt

p_{c1}, p_{c2} Cushion pressure of fore and rear cushion

Calculation of ACV dynamic trim over calm water

Craft trim including static hovering air gap, trim angle, etc., can be obtained by the equilibrium of forces, fan air duct characteristic and the air flow continuity equation detailed from Chapter 5. The difference of this paragraph from Chapter 5 is that for

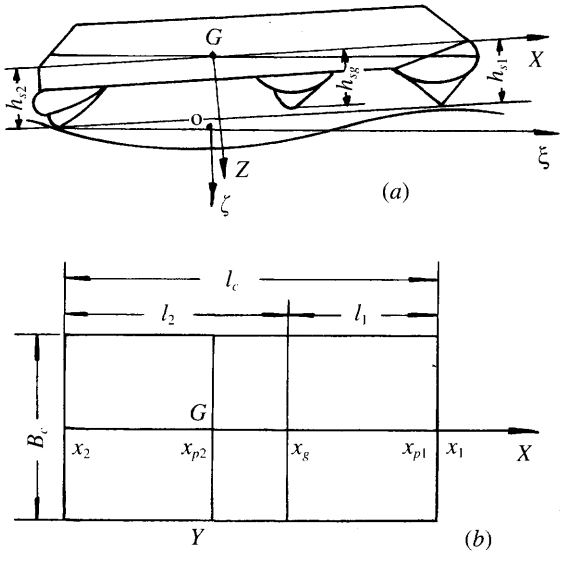

Fig. 8.19 Geometric dimensions and co-ordinate system of ACV.

the purposes of determining dynamic response, the effect of water deformation induced by wave-making on the trim is neglected for simplification of the equations. It may be noted that the SES trim running on calm water is also considered as the initial value in the case of solving the nonlinear differential equations of motion of an SES, as has been described in sections 8.2 and 8.3.

Static forces equilibrium

The static equilibrium equation for the vertical force and its moment with respect to the CG can be written as

$$A_{c1}\, p_{c1} + A_{c2}\, p_{c2} = -W$$
$$A_{c1}\, p_{c1}\, X_{p1} + A_{c2}\, p_{c2}\, X_{p2} = -M_0 \tag{8.74}$$

where M_0 is the moment induced by the drag and thrust of the craft about its CG and W the craft weight. This equation can be expressed as a matrix and written as

$$[A_n][p_{ci}] = [W_n] \tag{8.75}$$

where $[A_n]$ is the geometric matrix for the air cushion:

$$[A_n] = \begin{bmatrix} -A_c & -A_{c1} \\ N_{y1} & N_{y2} \end{bmatrix}$$

$$N_{y1} = A_{c1}\, X_{p1}$$

$$N_{y2} = A_{c2}\, X_{p2}$$

$$[p_{ci}] = \begin{bmatrix} p_{c1} \\ p_{c2} \end{bmatrix}$$

$$[W_m] = \begin{bmatrix} -W \\ -M_0 \end{bmatrix} \quad \text{(the weight matrix)}$$

if

$$[A_{n1}] = [A_n]^{-1}$$

then

$$[p_{ci}] = [A_{n1}][W_m] \tag{8.76}$$

Fan air duct characteristic

The fan air duct characteristic equation can be written as

$$H_j = A_f + B_f Q - C_f Q^2 \tag{8.77}$$

where H_j is the total pressure of the fan, Q the inflow rate of the fan, and A_f, B_f, C_f the dimensional coefficients for the fan. We also assume that one fan is mounted on the ACV and supplies the pressurized air from the outlet of the fan via skirt bags and holes into the air cushion.

Then put

$$\begin{aligned} D &= (k\rho_a)/2A_{fk}^2 \\ E_1 &= \rho_a/(2C_{j1}^2 A_{j1}^2) \\ E_2 &= \rho_a/(2C_{j2}^2 A_{j2}^2) \end{aligned} \tag{8.78}$$

where A_j is the area of the bag holes (subscripts 1, 2 represent the fore and rear cushion respectively), C_j the flow rate coefficient, A_{fk} the characteristic area of the air duct and k the coefficient due to the energy loss of the air duct. Then the bag pressure, cushion pressure in the fore/rear cushion and flow rate can be written as

$$\begin{aligned} p_t &= H_j - DQ^2 \\ p_{c1} &= p_t - E_1 Q_1^2 \\ p_{c2} &= p_t - E_2 Q_2^2 \\ Q &= Q_1 + Q_2 \end{aligned} \tag{8.79}$$

From equations (8.77) and (8.79) we have

$$p_t = A_f + B_f Q - (C_f + D)Q^2 \tag{8.80}$$

If p_{c1} and p_{c2} are given, then the bag pressure, flow rate Q, Q_1, Q_2 and total pressure head of fan H_j can be obtained as the solution of these combined equations.

Flow rate continuity

The flow rate leaked from the fore/stern cushion can be written as

$$\begin{aligned} Q_1 &= Q_{e1} + Q_{i2} \\ Q_2 &= Q_{e2} - Q_{i2} \end{aligned} \tag{8.81}$$

where Q_{e1}, Q_{e2} are the flow leaking out from the fore/rear cushion and Q_{i2} the flow leaking from fore to rear cushion.

Assume h_{eb}, h_{es} represent the air gaps under the bow/stern and side skirts respectively and can be written as

$$\begin{aligned} h_{es1} &= -\zeta_g + x\,\psi - h_{ss1} \\ h_{eb} &= \zeta_g + x_1\,\psi - h_{s1} \\ h_{es2} &= \zeta_g + x\,\psi - h_{ss2} \\ h_{es} &= -\zeta_g + x_2\,\psi - h_{s2} \end{aligned} \tag{8.82}$$

The air leakage area under the fore cushion can be written as

$$\begin{aligned} A_{e1} &= A_{eb} + 2A_{es1} \\ A_{es1} &= \int_{xg}^{x_1} (-\zeta_g + x_\psi - h_{ss1})\,dx = -l_1\,\zeta_g + l_1\,x_{p1}\psi - h_{ss1}\,l_1 \end{aligned} \tag{8.83}$$

where A_{es1} is the air leakage under the side skirt of the fore cushion and A_{eb} the air leakage under the bow skirt, $A_{eb} = B_c\,h_{eb}$. Air leakage area under the side skirts of rear cushion A_{es2} and air leakage area from the rear cushion A_{e2} can be written as

$$\begin{aligned} A_{e2} &= B_c h_{es} + 2A_{es2} \\ A_{es2} &= -l_2\,\zeta_g + l_2\,x_{p2}\,\psi - h_{ss2} l_2 \end{aligned}$$

The flow from the fore/rear cushion Q_{e1}, Q_{e2} can be written as

$$\begin{aligned} Q_{e1} &= \phi_e A_{e1}\,(2p_a/\rho_a)^{0.5} \\ Q_{e2} &= (\phi_{es} A_{es} + 2\phi_e A_{es2})\,[2p_{c2}/\rho_a]^{0.5} \end{aligned} \tag{8.84}$$

where A_{es} is the air leakage area under the stern skirt, ϕ_{es} the flow rate coefficient under the stern skirt and ϕ_e the flow rate coefficient at other places.

The rate of cross flow between the fore/rear air cushion via the transverse stability skirt is

$$Q_{12} = \phi_{eg}\,(2(p_{c1} - p_{c2})/\rho_a)^{0.5}\,\mathrm{sgn}\,(p_{c1} - p_{c2})\,A_{eg} \tag{8.85}$$

where ϕ_{eg} is the flow rate of cross-flow (m^3/s), A_{eg} the air leakage area of the cross-flow (m^2), $A_{eg} = B_c\,h_{eg}$, and h_{eg} the air gap under the transverse stability skirt (m), where

$$h_{eg} = -\zeta_g + x_g\psi - h_{sg} \tag{8.86}$$

In these equations we assume the cross-flow rate from fore to rear cushion is positive.

Substitute equations (8.82)–(8.86) into equation (8.81), then

$$[Q_i] = [A_Q]\,[\zeta_\psi] + [A_h] \tag{8.87}$$

where

$$[Q_i] = \begin{bmatrix} Q_1 \\ Q_2 \end{bmatrix}$$

$$[\zeta_\psi] = \begin{bmatrix} \zeta_g \\ \psi \end{bmatrix}$$

$$[A_Q] = \begin{bmatrix} A_{Q11} & A_{Q12} \\ A_{Q21} & A_{Q22} \end{bmatrix}$$

$$[A_h] = \begin{bmatrix} A_{h1} \\ A_{h2} \end{bmatrix}$$

where

$$A_{Q11} = -\phi_e V_{e1} (2l_1 + B_c) - \phi_{eg} V_{e12} B_c$$

$$A_{Q12} = \phi_e V_{e1} (B_c x_1 + l_1 x_{p1}) + \phi_{eg} V_{e12} B_c x_g$$

$$A_{Q21} = -V_{e2} (\phi_{es} B_c + 2\phi c\, l_2) + \phi_{eg} V_{e12} B_c$$

$$A_{Q22} = V_{e2} (\phi_{es} B_c x_2 + 2\phi_e l_2 x_{p2}) - \phi_{eg} V_{e12} B_c x_g$$

$$A_{h1} = -\phi_e V_{e1} (h_{s1} B_c + 2h_{ss1} l_1) - \phi_{eg} V_{e12} B_c h_{sg}$$

$$A_{h2} = V_{e2} (\phi_{es} B_c + 2\phi_e h_{ss2} l_2) + \phi_{eg} V_{e/2} B_c h_{sg}$$

where

$$V_{e1} = (2p_{c1}/\rho_a)^{0.5}$$

$$V_{e2} = (2p_{c2}/\rho_a)^{0.5}$$

$$V_{e12} = (2\,(|\, p_{c1} - p_{c2}\,|)p_a/\rho_a)^{0.5} \operatorname{sgn}(p_{c1} - p_{c2})$$

From equation (8.87), put

$$[A_{q1}] = [AQ]^{-1} \quad \text{and} \quad [QA_h] = [Q_i] - [A_h]$$

Then the running attitude of the craft can be written as

$$[\zeta_\psi] = [AQ_1]\,[QA_h] \tag{8.88}$$

Wave equation

With respect to coordinates 0, $\xi\eta\zeta$, the two-dimensional wave surface can be written as

$$\zeta_w = \zeta_a \sin(Kx + \omega_e t) \tag{8.47}$$

The vertical velocity of wave motion and wave slope can be expressed as

$$\dot{\zeta}_w = \zeta_a \omega_e \cos(Kx + \omega_e t) \tag{8.48}$$

If we put

$$\Delta\zeta_w = \zeta_a \sin \omega_e t$$

and

$$\Delta\dot{\zeta}_w = \zeta_a\, \omega_e \cos \omega_e t \tag{8.89}$$

then

$$\begin{bmatrix} \zeta_w \\ \dot{\zeta}_w \end{bmatrix} = \begin{bmatrix} \cos Kx & \sin Kx/\omega_e \\ -\omega_e \sin Kx & \cos Kx \end{bmatrix} \begin{bmatrix} \Delta\zeta_w \\ \Delta\dot{\zeta}_w \end{bmatrix} \tag{8.90}$$

Longitudinal linear differential equations of motion of ACVs in regular waves

Longitudinal linear differential equations of motion with small perturbation are

$$[W_I]\begin{bmatrix} \Delta\ddot{\zeta}_g \\ \Delta\ddot{\psi} \end{bmatrix} = [A_n]\begin{bmatrix} \Delta p_{c1} \\ \Delta p_{c2} \end{bmatrix} \tag{8.91}$$

in which the inertia matrix is

$$[W_I] = \begin{bmatrix} W/g & 0 \\ 0 & I_y \end{bmatrix}$$

where I_y is the pitch moment of inertia of the craft.

Air cushion system

Flow rate–pressure head linear equation with small perturbation

Under small perturbations the change of both cushion pressure and flow rate are small, thus the nonlinear equation due to the fan characteristic can be dealt with as a linear equation. From equation (8.80)

$$\Delta P_t = P_{tQ}(\Delta Q_1 + \Delta Q_2) \tag{8.92}$$

where

$$P_{tQ} = B_f - 2Q(C_f + D)$$

From equation (8.79), the fore/rear cushion pressure can be written in matrix form, as

$$\begin{bmatrix} \Delta p_{c1} \\ \Delta p_{c2} \end{bmatrix} = \begin{bmatrix} \Delta p_t \\ \Delta p_t \end{bmatrix} + \begin{bmatrix} -2E_1Q_1 & 0 \\ 0 & -2E_1Q_1 \end{bmatrix}\begin{bmatrix} \Delta Q_1 \\ \Delta Q_2 \end{bmatrix} \tag{8.93}$$

Substitute equation (8.92) into (8.93) and after straightening out, we obtain

$$\begin{bmatrix} \Delta p_{c1} \\ \Delta p_{c2} \end{bmatrix} = [p]\begin{bmatrix} \Delta Q_1 \\ \Delta Q_2 \end{bmatrix}$$

The elements of matrix $[p]$ are as follows:

$$[p] = \begin{bmatrix} p_{11} & p_{12} \\ p_{21} & p_{22} \end{bmatrix}$$

where

$$p_{11} = p_{tQ} - 2E_1 Q_1$$

$$p_{12} = p_{21} = p_{tQ}$$

and

$$p_{22} = p_{tQ} = 2E_2 Q_2$$

Considering $[P]^{-1}$ as the inverse matrix of $[P]$, then

$$[P]^{-1} = [Q_p]$$

i.e.

$$\begin{bmatrix} \Delta Q_1 \\ \Delta Q_2 \end{bmatrix} = [Q_p] \begin{bmatrix} \Delta p_{c1} \\ \Delta p_{c2} \end{bmatrix} \tag{8.94}$$

Small perturbation equation for flow rate of air leakage and cross-flow

Differentiating the variables Q_{e1}, Q_{e2}, Q_{j2} in equations (8.84) and (8.85), putting the summation together and considering the effect of waves on the air leakage area, we have

$$\begin{bmatrix} \Delta Q_{e1} + \Delta Q_{12} \\ \Delta Q_{e2} + \Delta Q_{22} \end{bmatrix} = [\Delta Q] \begin{bmatrix} \Delta \zeta_g \\ \Delta \psi \end{bmatrix} + [A_p] \begin{bmatrix} \Delta p_{c1} \\ \Delta p_{c2} \end{bmatrix} + [A_w] \begin{bmatrix} \Delta \zeta_w \\ \Delta \dot{\zeta}_w \end{bmatrix} \tag{8.95}$$

where A_Q can be obtained from equation (8.87),

$$[A_p] = \begin{bmatrix} A_{p11} & A_{p12} \\ A_{p21} & A_{p22} \end{bmatrix}$$

where the elements of the matrix can be written as

$$A_{p11} = \frac{Q_{e1}}{2p_{c1}} + \frac{Q_{12}}{2(p_{c1} - p_{c2})}$$

$$A_{p12} = -\frac{Q_{12}}{2(p_{c1} - p_{c2})}$$

$$A_{p21} = A_{p12}$$

$$A_{p22} = \frac{Q_{e2}}{2p_{c2}} + \frac{Q_{12}}{2(p_{c1} - p_{c2})}$$

The elements of matrix $[A_w]$ can be obtained by assuming the sums of flow from bow to stern and longitudinal flow due to the vertical displacement of waves are Q_{ew1} and Q_{ew2} so that

$$Q_{ew1} = Q_{ewb} + Q_{ews1} + Q_{ew12}$$

$$Q_{ew2} = Q_{ews} + Q_{ews2} + Q_{ew12}$$

where Q_{ewb}, Q_{ews} are the flow rate under the bow/stern skirts due to the waves, Q_{ews1}, Q_{ews2} the flow rate under the side skirts of fore/rear cushion due to the waves and Q_{ew12} the longitudinal flow due to the waves. Then

$$Q_{ew1} = \phi_e V_{e1} \left[B_c \zeta_a \sin(Kx_1 + \omega_e t) + 2 \int_{x_g}^{x1} \zeta_a \sin(Kx + \omega_e t)\, dx \right] + \phi_{eg} V_{e12} B_c \zeta_a \sin(Kx_g + \omega_e t)$$

$$Q_{ew2} = \phi_e V_{e2} \left[B_c \zeta_a \sin(Kx_2 + \omega_e t) + 2\phi_e V_{e2} \int_{x_g}^{x1} \zeta_a \sin(Kx + \omega_e t)\, dx \right] + \phi_{eg} V_{e12} B_c \zeta_a \sin(Kx_g + \omega_e t)$$

If we integrate this equation and put $C_{w1} = \pi l_1/L_w$ and $C_{w2} = \pi l_2/L_w$, then

$$\begin{bmatrix} Q_{ew1} \\ Q_{ew2} \end{bmatrix} = [A_w] \begin{bmatrix} \Delta\zeta_w \\ \Delta\dot{\zeta}_w \end{bmatrix} \tag{8.96}$$

$$\begin{aligned}
A_{w11} &= \phi_e V_{e1} B_c \cos(Kx_1) + 2\phi_e V_{e1} l_1 [\sin C_{w1}/\sin C_{w2}] (\cos Kx_{p1}) \\
&\quad + \phi_{eg} V_{e12} B_c \cos(Kx_g) \\
A_{w12} &= \phi_e V_{e1} B_c [\sin(Kx_1)]/\omega_e + 2\phi_e V_{e1} l_1 \sin C_{w1}/C_{w1} + [\sin(Kx_{p1})]/\omega_e \\
&\quad + \phi_{eg} V_{e12} B_c [\sin(Kx_g)]/\omega_e \\
A_{w21} &= \phi_{es} V_{e2} B_c \cos(Kx_2) + 2\phi_e V_{e2} l_2 [\sin C_{w2}/C_{w2}] (\cos Kx_{p2}) \\
&\quad - \phi_{eg} V_{e12} B_c \cos(Kx_g) \\
A_{w22} &= \phi_e V_{e2} B_c [\sin(Kx_2)]/\omega_e + 2\phi_e V_{e2} l_2 [\sin C_{w2}/C_{w2}] (\sin(Kx_{p2}))/\omega_e \\
&\quad + \phi_{eg} V_{e12} B_c [\sin(Kx_g)]/\omega_e
\end{aligned}$$

Flow continuity equation for small perturbations

In previous paragraphs we have developed the linear equations for change of flow rate. In this section we will use these to derive expressions for the change of flow rate due to the wave pumping, motion pumping and compressibility of the cushion air, which can be expressed as

$$\begin{bmatrix} \Delta Q_1 \\ \Delta Q_2 \end{bmatrix} = \left(\frac{\Delta Q_{e1} + \Delta Q_{12}}{\Delta Q_{e2} - \Delta Q_{12}} \right) + \frac{\Delta Q_{e1}}{\Delta Q_{e2}} \tag{8.97}$$

where ΔQ_{e1}, ΔQ_{e2} represent the total change of flow rate due to the wave pumping, motion pumping and the density change of cushion air induced by its compressibility and which can be expressed as

$$\Delta Q_{e1} = 1/\rho_a \frac{d}{dt} (\rho_a V_{c1}) = \Delta \dot{V}_{c1} + \frac{V_{c1}}{\rho_a} \dot{\rho}_a$$

$$\Delta Q_{e2} = 1/\rho_a \frac{d}{dt} (\rho_a V_{c2}) = \Delta \dot{V}_{c2} + \frac{V_{c2}}{\rho_a} \dot{\rho}_a$$

Therefore

$$\begin{bmatrix} \Delta Q_{e1} \\ \Delta Q_{e2} \end{bmatrix} = \begin{bmatrix} \Delta \dot{V}_{c1} \\ \Delta \dot{V}_{c2} \end{bmatrix} + [Q_{pd0}] \begin{bmatrix} \Delta \dot{p}_{c1} \\ \Delta \dot{p}_{c2} \end{bmatrix} \tag{8.98}$$

The first right-hand term of this equation represents the flow rate due to the wave pumping and motion pumping of the craft and the second term represents the flow due to the compressibility of the cushion air. The same as in sections 8.2 and 8.3, this flow rate can be expressed as (cf. equations 8.61 and 8.62)

$$\Delta \dot{V}_{c1} = \int_{xg}^{x_1} [-\dot{\zeta}_g + x \Delta\dot{\psi} + \zeta_a \omega_e \cos(Kx + \omega_e t)] B_c \, dx$$

If we integrate this expression, then

$$\Delta \dot{V}_{c1} = (-\dot{\zeta}_g + x_p \Delta\dot{\psi}) A_{c1} + \sin C_{w1}/C_{w1} A_{c1} \omega_e \zeta_a \cos(Kx_{p1} + \omega_e t)$$

and similarly

$$\Delta\dot{V}_{c2} = (-\dot{\zeta}_g + x_{p2}\Delta\dot{\psi})\, A_{c2} + \sin C_{w2}/C_{w2}\, A_{c2}\, \omega_e\, \zeta_a \cos(Kx_{p2} + \omega_e t)$$

Thus the sum of flow rates due to the wave pumping in fore/rear cushions can be expressed in matrix form as

$$\begin{bmatrix} \Delta\dot{V}_{c1} \\ \Delta\dot{V}_{c2} \end{bmatrix} = [Q_{zD}] \begin{bmatrix} \Delta\zeta_g \\ \Delta\psi \end{bmatrix} + [V_w] \begin{bmatrix} \Delta\zeta_w \\ \Delta\dot{\zeta}_w \end{bmatrix} \tag{8.99}$$

where $[Q_{zD}]$ represents the motion pumping matrix, in which the various elements are

$$\begin{aligned} Q_{zD11} &= -A_{e1} \quad Q_{zD12} = A_{e1}\, x_{p1} \\ Q_{zD21} &= -A_{e2} \quad Q_{zD22} = A_{e2}\, x_{p2} \end{aligned} \tag{8.100}$$

$[V_w]$ represents the wave pumping matrix, in which the elements are

$$\begin{aligned} V_{w11} &= -(\sin C_{w1})/C_{w1}\, A_{e1}\, \omega_e \sin(Kx_{p1}) \\ V_{w12} &= (\sin C_{w1})/C_{w1}\, A_{e1} \cos(Kx_{p1}) \\ V_{w21} &= -(\sin C_{w2})/C_{w2}\, A_{e2}\, \omega_e \sin(Kx_{p2}) \\ V_{w22} &= (\sin C_{w2})/C_{w2}\, A_{e2} \cos(Kx_{p2}) \end{aligned}$$

We assume the change of air cushion complies with the adiabatic principle, therefore its matrix expression is

$$[Q_{pD0}] = \begin{bmatrix} V_{c1}/(1.4\,(p_a + p_{c1}) & 0 \\ 0 & V_{c2}/(1.4(p_a + p_{c2}) \end{bmatrix}$$

Now we can substitute the matrix of flow rate into the air cushion (8.94), the matrix of flow rate due to air leakage from the cushion, the wave pumping, motion pumping and matrix representing the flow rate due to the compressibility of cushion air (8.98) into the matrix representing the flow rate continuity equation (8.97) and after straightening out, then

$$[Q_{pc}] \begin{bmatrix} \Delta p_{c1} \\ \Delta p_{c2} \end{bmatrix} + [Q_{pD}] \begin{bmatrix} \Delta\dot{p}_{c11} \\ \Delta\dot{p}_{c21} \end{bmatrix} = [A_Q] \begin{bmatrix} \Delta\zeta_g \\ \Delta\psi \end{bmatrix} + [Q_{zD}] \begin{bmatrix} \Delta\dot{\zeta}_g \\ \Delta\dot{\psi} \end{bmatrix} + [Q_{zw}] \begin{bmatrix} \Delta\zeta_w \\ \Delta\dot{\zeta}_w \end{bmatrix}$$

where

$$\begin{aligned} [Q_{pc}] &= [Q_p] - [A_p] \\ [Q_{pD}] &= -[Q_{pD0}] \\ [Q_{zw}] &= [A_w] + [V_w] \end{aligned}$$

Put $[p_{cQ}] = [Q_{pc}]^{-1}$ and multiply the left/right terms of equation (8.100) by $[p_{cQ}]$, then

$$\begin{bmatrix} \Delta p_{c1} \\ \Delta p_{c2} \end{bmatrix} + [T_c] \begin{bmatrix} \Delta\dot{p}_{c1} \\ \Delta\dot{p}_{c2} \end{bmatrix} = [p_{zc}] \begin{bmatrix} \Delta\zeta_g \\ \Delta\psi \end{bmatrix} + [p_{zD}] \begin{bmatrix} \Delta\dot{\zeta}_g \\ \Delta\dot{\psi} \end{bmatrix} + [p_w] \begin{bmatrix} \Delta\zeta_w \\ \Delta\dot{\zeta}_w \end{bmatrix} \tag{8.101}$$

where

$$\begin{aligned} [T_c] &= [p_{cQ}]\,[Q_{pD}] \\ [p_{zc}] &= [p_{cQ}]\,[A_Q] \end{aligned}$$

$$[p_{zD}] = [p_{cQ}]\,[Q_{zD}]$$

$$[p_w] = [p_{cQ}]\,[Q_{zw}]$$

Put equation (8.101) in Laplace transformation, then

$$\{[T_c]S + [I]\}\begin{bmatrix}\Delta p_{c1}(S)\\ \Delta p_{c2}(S)\end{bmatrix} = \{[p_{zD}]S + [p_{zc}]\}\begin{bmatrix}\Delta\zeta_g(S)\\ \Delta\psi(S)\end{bmatrix} + \{[p_{wD}]S + [p_{wc}]\}\Delta\zeta_w(S) \quad (8.102)$$

where $[I]$ is the unit matrix and S the Laplace operator.

Solution of the linear differential equations of motion

Applying Laplace transformation to the linear differential equations of motion (8.91) and substituting into expression (8.102), the motion equations can be expressed as

$$[A(S)]\begin{bmatrix}\Delta\zeta_g(S)\\ \Delta\psi(S)\end{bmatrix} = [B(S)]\,\Delta\zeta_w(S) \quad (8.103)$$

where $[A(S)]$ is the matrix representing the characteristic coefficients for the craft, which can be written as

$$[A(S)] = [A_0]S^3 + [A_1]S^2 + [A_2]S + [A_3] \quad (8.104)$$

where

$$[A_0] = [A_n]\,[T_c]\,[A_{n1}]\,[W_I]$$

$$[A_1] = [W_I]$$

$$[A_2] = -[A_n]\,[p_{zD}]$$

$$[A_3] = -[A_n]\,[p_{zc}]$$

$[B(S)]$ is the matrix representing the coefficient of wave perturbation force and can be written as

$$[B(S)] = [B_0]S + [B_1] \quad (8.105)$$

where

$$[B_0] = [A_n]\,[p_{wD}]$$

$$[B_1] = [A_n]\,[p_{wc}]$$

From equation (8.103), the transfer matrix of motion can be written

$$[D\,\zeta_g(S)] = [A(S)]^{-1}\,[B(S)] \quad (8.106)$$

Substitute $S = j\omega_e$ into the foregoing matrix, then the frequency response characteristics for craft motion and wave perturbation force can be obtained.

So far, we have introduced the formation of the linear differential equations of motion of ACVs in regular waves. Although the deformation of the wave surface induced by the air cushion and the hydrodynamic force acting on the skirts have not been taken into account, the equations are expressed in matrix form and use the Laplace transformation to obtain the simplified equation, which is similar to that for conventional ships and is easy to solve and analyse.

However, it may be noted that there are some differences between the theoretical method and the practical situation, particularly for modern coastal ACV/SES with responsive skirts. This will lead to some prediction errors.

Calculation results and analysis

Reference 69 described the calculation of longitudinal motion response of an ACV of 5, 20, 60, 200 and 400 t to regular waves and predicted the seaworthiness qualities of an ACV in sea state 3 in the East China Sea with the aid of spectral analysis in order to analyse its seaworthiness and the effect of compressibility of cushion air. The main parameters used were:

Froude number	Fr	$= 1.6$
Cushion length–beam ratio	l_c/B_c	$= 2$
Non-dimensional mass coefficient of craft	$W/(\rho_w g l_c^3)$	$= 6.6 \times 10^{-3}$
Non-dimensional inertia coefficient of craft	$I_y/(\rho_w g l_c^5)$	$= 5.2 \times 10^{-4}$
Non-dimensional length of skirt	h_s/l_c	$= 0.078$
Non-dimensional horizontal location of transverse stability skirt	X_g/l_c	$= 0.023$
Non-dimensional area of skirt holes in fore air cushion	A_{j1}/l_c^2	$= 0.0136$
Non-dimensional area of skirt holes in fore air cushion	A_{j2}/l_c^2	$= 0.0111$

The analysis and comparison between the calculation and experimental results can be summarized as follows:

Heave response

The frequency responses of heave amplitude for the ACVs weighing 5t(A) and 400 t(B) in waves are shown in Fig. 8.20. The trend of the curves is similar to that for an SES, in which an amplitude peak exists at low frequency ($\omega_e[l_c/g]^{0.5} \approx 5$), which is induced by the coupled pitch–heave motion. Figure 8.21 shows the frequency response of pitch amplitude for the ACVs in waves.

In the case where the pitch motion response is smooth, a small step of amplitude will appear here, otherwise there will be a peak and the relative amplitude will be greater

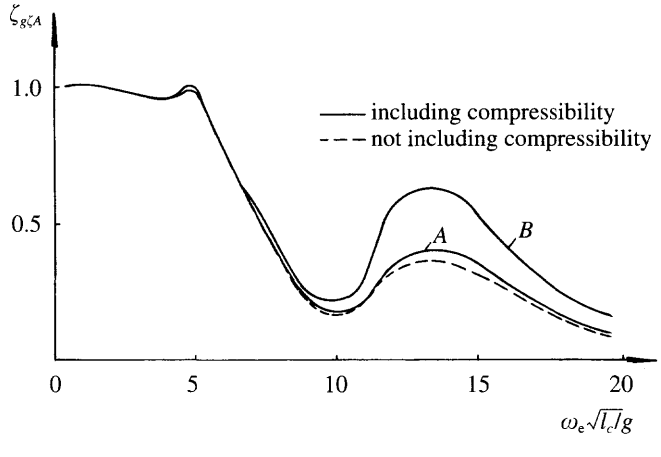

Fig. 8.20 Unit frequency response of heave amplitude for ACV in waves. A: 5 t craft, B: 400 t craft.

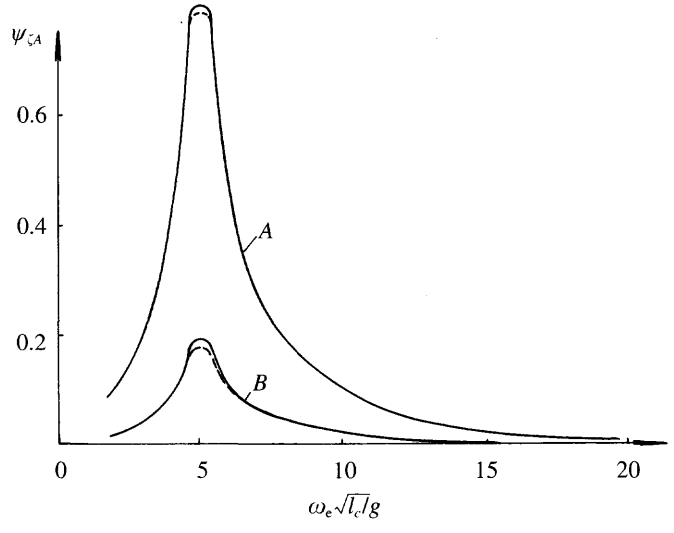

Fig. 8.21 Unit frequency response of pitch amplitude for ACV in waves (see Fig. 8.20 for key).

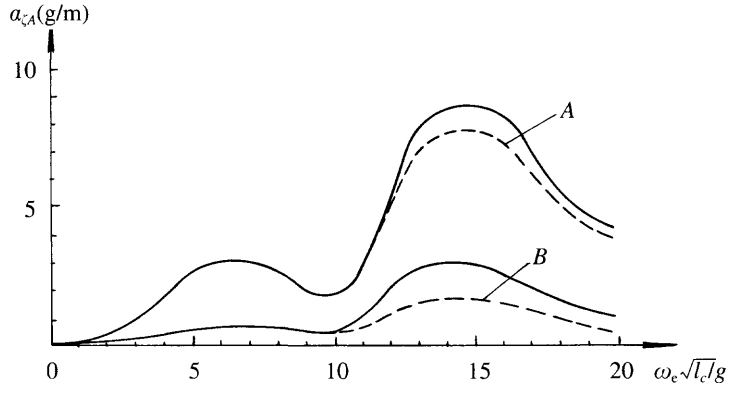

Fig. 8.22 Unit frequency response of heave acceleration for ACV in waves (see Fig. 8.20 for key).

than 1. The formation of a peak amplitude of heave at high frequency, and a hollow at medium frequency is closely related to the wave perturbation force as shown in Fig. 8.23.

When the relative period length ratio $\omega_e[l_c/g]^{0.5} \approx 10$ and L_w $(1.25 \sim 1.5)l_c$, the wave-pumping effect and wave perturbation force will be so small as to form the hollow on the curve of the wave perturbation force. But when the relative period length ratio $\omega_e[l_c/g]^{0.5} \approx 14$ and $L_w \approx 0.9l_c$, then the wave perturbation force will be so large as to form the peak on the curve of wave perturbation, at which the heave natural frequency is situated.

Pitch response

Figure 8.21 shows the curve of frequency response of pitch motion; it can be seen that the steep amplitude peak is situated at $\omega_e[l_c/g]^{0.5} \approx 5$, namely at the pitch natural

frequency. The figure shows the characteristics of a system with low damping, low stability and low natural frequency of pitch motion. The peak disturbance moment occurs at $\omega_e[l_c/g]^{0.5} \approx 8 \sim 10$, where the wavelength $L_w \approx 1.5l_c$ (see Fig. 8.24). Sometimes a small peak also exists at this relative frequency.

Vertical accelerations

Figure 8.22 shows the frequency response of vertical accelerations, in which the peak vertical acceleration is estimated to be induced by pitch motion, but peak vertical acceleration at high frequency is caused by heave motion. Thus it can be seen that the vertical acceleration at the bow will be reduced considerably if the pitch motion damping rate can be increased and the quasi-static stability in heave motion can be decreased.

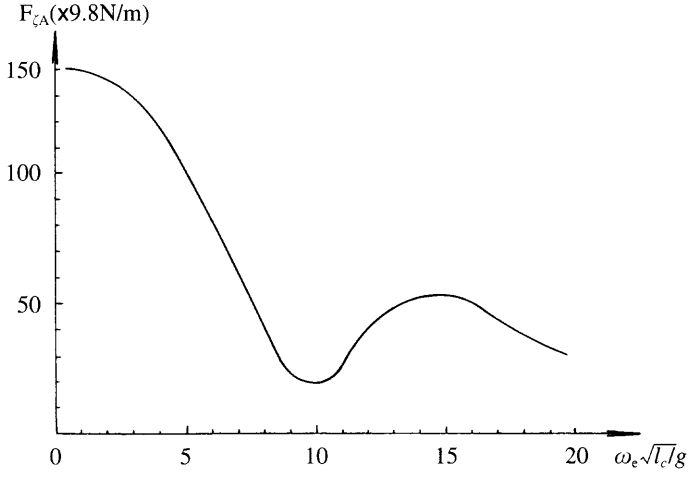

Fig. 8.23 Unit frequency response for wave exciting force.

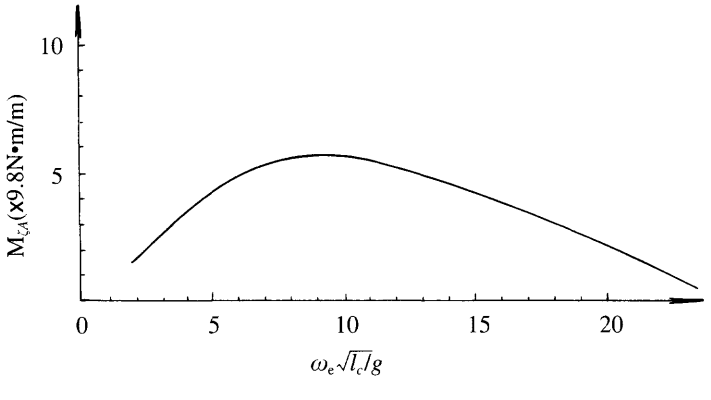

Fig. 8.24 Unit frequency response for wave exciting moment.

Compressibility

All the figures mentioned above from Fig. 8.20 to 8.26 include the effect of compressibility on the motion, thus it can be seen that the effect of compressibility increases with the all-up weight of the craft. Figure 8.25 shows that if K_p represents the percentage increase of significant bow vertical acceleration due to the effect of cushion air compressibility, then it can be seen that $K_p = 2.5\%$ for the craft of 5 t ($l_c \cong 10$), i.e. the effect of compressibility of cushion air can be neglected, but $K_p = 41\%$ for the craft of 400 t, which means that in this case the cushion air compressibility cannot be neglected.

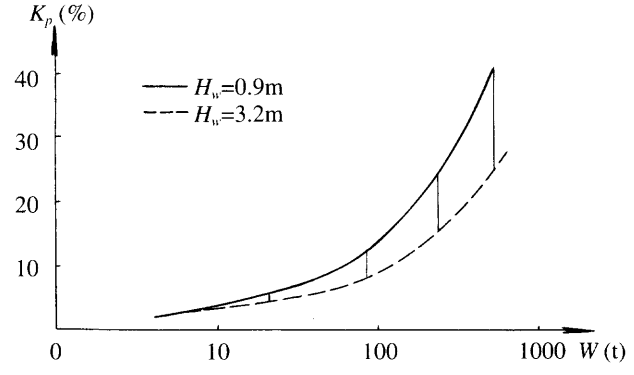

Fig. 8.25 Influence of cushion air compressibility on ACV seaworthiness.

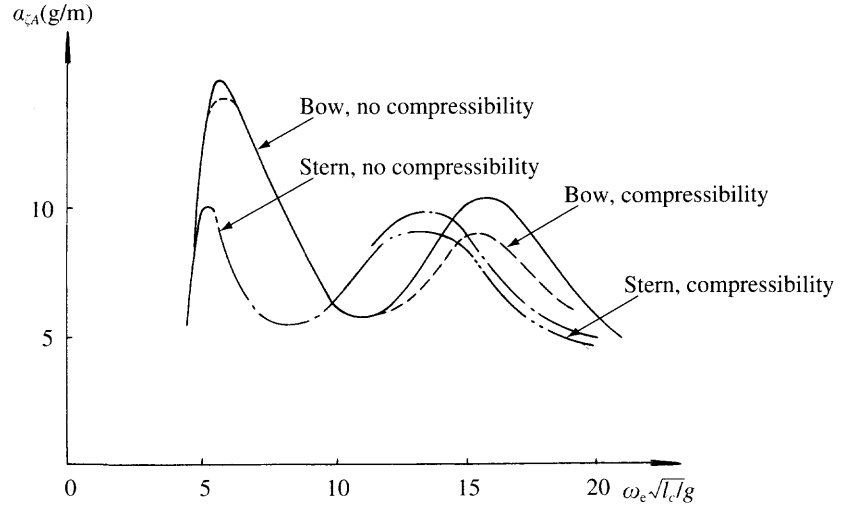

Fig. 8.26 Unit frequency response for acceleration at bow/stern.

We have now introduced the coupled motion for both longitudinal/transverse directions of ACV/SES in waves. Strictly speaking, the calculations are not perfect for the following reasons:

1. Response of the skirt to the waves has not been considered.
2. Wave surface deformation due to the air cushion pressure pattern has not been taken into account.
3. The calculations do not take the dynamic response of the fans into account, where ACV/SES are heaving and pitching while moving through the waves, particularly in the case of high craft speed.
4. The damping coefficient and added mass due to wave-making caused by the motion of the hovercraft, and the interference between the air cushion and side-walls are also not taken into account.

All of these problems should be eased in further research work in the future.

8.5 Motion of ACV and SES in short-crested waves

Both ACVs and SESs will be excited at high frequency when they are running over short-crested waves (or three-dimensional waves), just like an automobile running on a road surface with a lot of cobblestones. Thus this physical phenomenon is called the 'cobblestone effect' and which upsets the crew and passengers. The Chinese SES 7203 had such an experience when the craft was on the Wang Puan river, but the phenomenon disappeared when the craft left the river and entered the mouth of the Yangtze, a wider and deeper waterway. Because the motion response is an ultra-short one, such a phenomenon is therefore very difficult to describe by theoretical methods.

Of course this phenomenon can be simulated in a towing tank for qualitative analysis, but the theoretical basis for it is not yet fully understood. The rationale, cause and solution of the cobblestoning effect are not clear, therefore we are obliged to analyse this physical phenomenon qualitatively, as below.

Compressibility effect of air cushion air

When the ACV/SES are running in short-crested waves, the compressibility effect will be considerable although the waves are not high. Only the SES version 7203 of all of the ACV/SES designed by MARIC is strongly sensitive to the cobblestoning effect with large vertical acceleration. In our experience, this is expressed by the slamming or the higher upward vertical acceleration; and it is rather different with the craft running in long waves, in which the craft will be accelerated downward, i.e. the crews or equipment will suffer from a sense of loss in weight.

This effect will probably be due to the sudden increase of cushion pressure. From Fig. 8.20, it is found that a peak vertical acceleration is located at high encounter frequency with the influence of compressibility. Figure 8.20 shows the operation of the ACV running in regular waves compared with the craft running in the three diagonal waves, the instantaneous flow rate of the craft is probably equal to zero ($Q_c = 0$); in this case, the effect of air cushion compressibility will be enhanced. In order to simplify the estimation, we assume the change of air condition in the cushion complies with Boyle's law, i.e. PV = constant, in which P represents the cushion air pressure and V the cushion volume.

In the case where the cushion volume reduces by 10% because of the craft's

heave motion, without any outflow of air, then $p = p_a + p_c = 103\,300 + p_c$ (N/m^2), in which p_a represents the atmospheric pressure and $p_c = 3000$ N/m^2, then the relative cushion pressure will be increased to five times the initial pressure. Of course, this is an extreme condition for estimation, but it can be demonstrated that the large heave motion in the case of a sealed air cushion will induce a large vertical acceleration.

Effect of slope of fan air duct characteristic

Although the characteristic curve of the Chinese fan model 4.73 is quite flat, the combined characteristic curve will be steep in the case where the air duct inlet or outlet is narrow, causing an increase in the flow damping coefficient.

The interference of waves

The interference of waves to the bow and stern seals will not only influence the change of air leakage area, but will also build up the response of skirts to waves because of the change of bag-cushion pressure ratio. Sometimes it will cause the sealing action of air leakage and thus present the effect mentioned in the paragraph on compressibility.

In order to improve the vertical acceleration due to the cobblestoning effect, the following measures may be adopted.

A number of measures may be taken to improve ACV ride, as follows.

Decrease of the effect of cushion air compressibility as little as possible

For instance, the delta area for air leakage between the fingers should be preserved in order to reduce the sealing effect of air leakage under the action of the waves.

Careful skirt geometry design

The bow/stern skirts have to be designed with a suitable 'yieldability' – particularly to avoid bounce or sealing effect. Of course this problem has still not been understood perfectly, but the balanced stern seal of SES version 713 had good results, because the cobblestoning effect was seldom encountered.

Use of the damping effect of cushion depth

High sidewalls, thus the deep cushion and large volume of the air cushion will reduce the cobblestoning effect dramatically. For instance, the sidewall depth of SES version 719G is double that on SES version 7203. Probably this is one of main reasons for no cobblestoning effect having been found on the craft version 719.

Use of flat lift fan and duct system characteristics

The fan air duct characteristic curves have to be as flat as possible, for instance, the air ducts of air inlet/outlet should be as large as possible to reduce the inflow and outflow velocity, which had not been possible to satisfy on SES version 7203. In addition, the parallel operation of multiple fans can also flatten the fan characteristic, e.g. there are two double inlet fans operating in parallel on SES version 719G and 713 but only a single inlet fan on SES version 7203, which is more sensitive to the cobblestone effect.

Figure 8.27 shows the time history for vertical acceleration of a certain SES running on three-dimensional waves at a speed of 28 knots. The wave height is rather small, only 0.2–0.3 m (1/10 highest waves) and the measured encounter frequency is about 2 Hz, vertical acceleration reaches up to 0.3 g. Perhaps this is a typical result of the cobblestoning effect.

The higher acceleration in long periods of operation causes discomfort for crew and passengers. For this reason the cobblestoning effect has to be considered seriously in ACV/SES design.

8.6 Plough-in of SES in following waves

Sometimes the plough-in phenomenon also occurs to an SES. It does not normally happen in the case of following winds as for an ACV, but it does occur in the case of following waves, particularly at the early stage of development of SES. For instance this phenomenon used to occur with the experimental SES version 711-III (weighing 2 t) of MARIC, in the case of following waves with significant wave height $h_{1/3}$ = 0.45 m, i.e. $h_{1/3}/W^{0.33} > 0.3$, where W is the displacement of the craft (m^3).

Sometimes, the plough-in phenomenon even happened to craft running over stern waves induced by large tugs, while overtaking them. Figure 8.28 shows a damaged lift fan caused by plough-in of the craft; furthermore one can find that the forward guide blades are also damaged. In addition, plough-in also happened to the passenger SES version 713 in following waves with $h_{1/10}$ = 0.8–1.0 m, i.e. $h_{1/10}/W^{0.33}$ = 0.26–0.33. It also happened to an SES model in the towing tank of the China Ship Scientific Research Centre (CSSRC) during the seaworthiness experiments in following (regular) waves with $h/W^{0.33}$ = 0.22 as shown in Fig. 8.29. Similarly, plough-in has happened to the SES version 717C when running over a ship's stern waves in cases where the cushion air supply to the bow bag was insufficient.

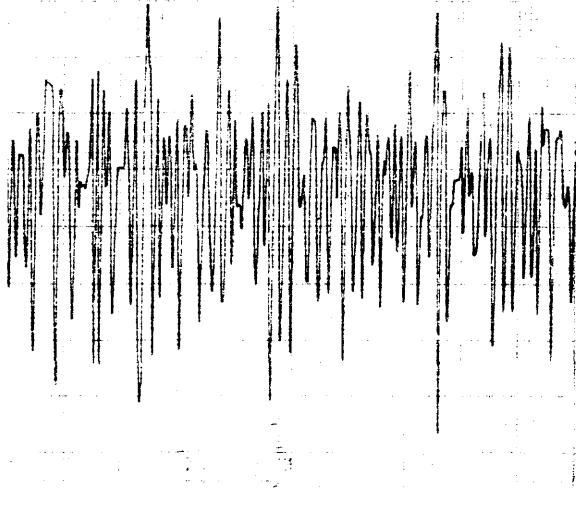

Fig. 8.27 Time history of cushion pressure fluctuation due to the 'cobblestoning effect' measured on an SES running in light waves.

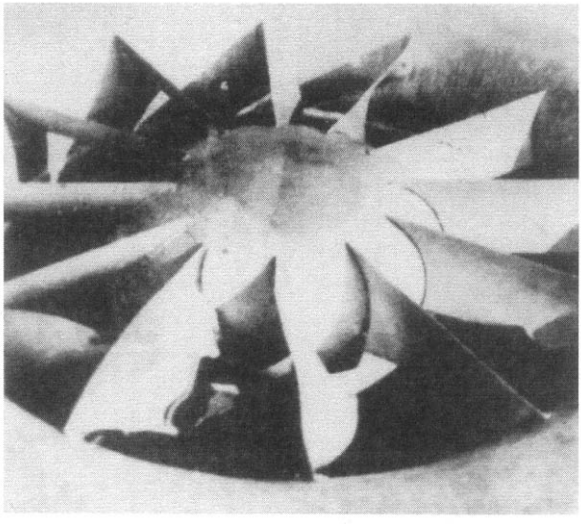

Fig. 8.28 The broken wooden fan caused by plough-in of an SES in following seas.

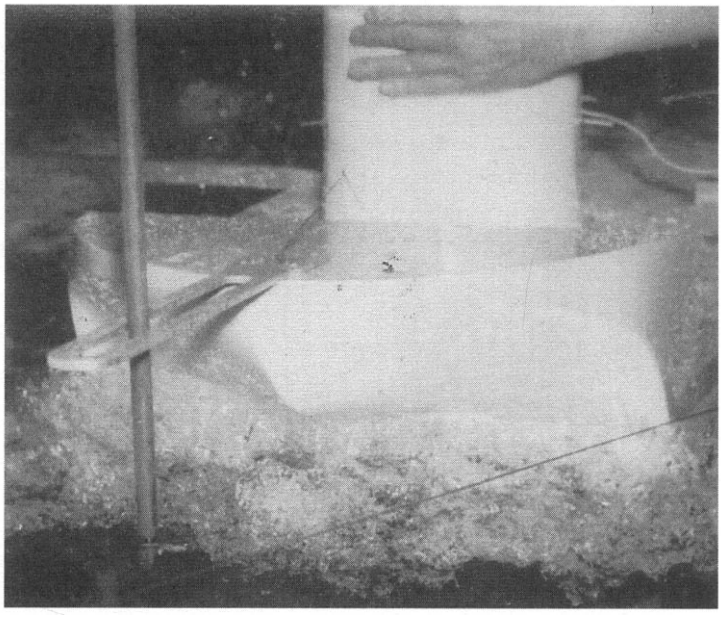

Fig. 8.29 'Plough-in' phenomenon of a SES model simulated in a towing tank.

To sum up, with respect to the SES, the plough-in phenomenon when running in following waves is very important and we will therefore present some analysis in the following subsection as a guide to the reader.

Internal reasons for plough-in

Skirt tuck-in at bow skirt

In the same way as on an ACV, tuck-under of the SES bow skirt has to be prevented. Originally, when the flexure is inward to the bow skirts, the craft will experience a bow-up moment because of increasing the bow cushion area as long as the cushion pressure can be kept constant. But actually the oncoming water flow will stick to the bow skirt to build up the internal vortices and disturb the cushion air, which will cause a drop in cushion pressure and a bow-down moment as shown in Table 8.1. The bow skirt with the long fingers, which are fitted on the SES version 711-III, is sensitive to tuck-under and has a poor pitching stability.

From Table 8.1, it is found that the craft was pitching bow down when the bow cushion pressure was dropping, causing plough-in of the craft. It may be noted that the skirt with long fingers is poor at preventing plough-in.

Lift system insufficiency

The craft lift system has to provide enough heave stability and restoring force (moment). Now in most craft of Chinese construction the industrial fan model 4–73 is fitted, with $H_{jmax}/H_{jd} \approx 1.2$ where H_{jmax}, represents the maximum total head at $Q = 0$ and H_{jd} the designed total pressure of the fan. In the case where Q_e increases, the restoring force due to the lift system decreases.

Lift system ducting problems

When the outlets of lift fans are mounted vertically, such as the arrangement of lift fans on passenger SES model 713 and experimental SES model 711-III, in cases where the craft was dropping down, then the water spray would be raised to impact the fans leading to a decrease in the revolution of the fans, subsequently causing the craft to plough-in.

Matching of bow/stern seal equipment

In the case where the heave stiffness of the bow and stern seal equipment does not match closely that of the bow seal and is softer at the bow, then the craft may present

Table 8.1 The test results of cushion pressure of SES version 711-III during craft plough-in

Running attitude	Cushion pressure (Nm^2)				Remarks
	Bow	Front cushion	Rear cushion	Stern	
From take-off course to post-hump speed of 40 kph	1500	1500	1400	1400	Cushion pressure steady, trim approx. +5°
Running through a ship's stern wave	1400	2000	1600	1800	Trim approx. +4.5°
Another take-off course	1400	1500	1600	1600	Trim approx. +6.5°
During operation of the craft, some people were asked to move from amidships to the bow so as to cause bow-down trim	0–1500	0–2500	1300	1600	Trim approx. −4° (plough-in occurred)

a bow-down pitching moment while it is heaving down. Therefore as the balanced type stern seal matched with the long finger-type bow seal, similar to the bow/stern seal arrangement on the SES versions 71-III and 713, then the plough-in phenomenon often occurred on these craft because the heave stiffness of the stern seal was much larger than that of the bow seal.

External response

In the case where the SES is running in following waves, then the wave encounter period will increase considerably. For example, if the SES model 713 is running at speed of 30 km/h in following waves with wavelength of L_w = 20 to 25 m, then the wave encounter period T_e = 10 s, but T_e = 2 s in head seas. Therefore the craft has enough time to leak air in the case of running in following waves, and thus build up to plough-in.

This phenomenon can be explained practically. In the case where the SES is running in following waves, the air was initially leaked under the stern seal and rear sidewalls, then the air leakage or spray gradually moved forward. The time for air leakage at a fixed location will lengthen as the wave encounter period elongates, especially when the craft speed is close to wave velocity. Thus plough-in would occur as the location of air leakage was moving to the bow. This is why the plough-in phenomenon has occurred to SESs running in following waves, but never happened to SES in head seas.

Methods for preventing plough-in

Stiffen geometry of bow skirt area relative to stern

The bow skirt of the bag and finger type, higher bag–cushion pressure ratio and D-type bag are suggested to be mounted on SES, which can prevent tuck-under of the skirt due to the high tension on the fabrics of the bow skirt. The resistance to plough-in of SES type 717 improved considerably once this type of skirt had been mounted on the craft.

Increase fan curve gradient

Increasing the steepness of the fan air duct characteristic curve would be in conflict with the need to prevent cobblestoning, so perhaps using a winding outlet of fans is a better measure for preventing the water spray from impacting directly on the fan blades.

Adjust bow finger tip line

It suggests mounting the bow fingers flatter with respect to the base-line of the craft, which can not only reduce the water drag of the fingers, but also increase the restoring moment of pitching.

Use anti-plough-in hydrofoils

Anti-plough-in hydrofoils may be mounted at the bow as shown in Fig. 1.32, which was mounted on the experimental SES model 711-III.

Adjust relative stiffness of bow and stern skirts

The heave stiffness for bow/stern seals has to be suitably selected. In general, the heave stiffness for the bow should be greater than that for the stern seal in order to present a bow-up restoring moment in the case of heaving down, which can be obtained by means of adjusting the bag–cushion pressure ratio and responsiveness of the bow and stern bag.

Adjust air supply to bow skirt area

The air supply to the bow skirt has to be carefully taken into account. In the case where a separate bow lift fan is adopted, then the heave stiffness of the bow area can be adjusted to keep a constant bag pressure to prevent tuck-under of the bow skirt and plough-in of the skirt in following seas. In general it is advised to feed the majority of cushion air flow through the bow skirt area.

8.7 Factors affecting the seaworthiness of ACV/SES

In this section we will discuss the various factors affecting the seaworthiness of ACV/SES with a view to improving performance. Similarly as with conventional ships, the problems concerning the seaworthiness of craft to which we pay particular attention are as follows:

1. the motion amplitude and acceleration of craft running in waves, such as ζ_g, $\ddot{\zeta}_g$, ψ, $\ddot{\psi}$, θ, $\ddot{\theta}$, etc. and the superposition of coupled motion, which presents a combined vertical motion amplitude and acceleration, transverse and longitudinal motion amplitude and acceleration;
2. speed degradation of craft in waves;
3. the ability for taking off and maintaining high speed cushion-borne operation of craft;
4. the problems concerning the manœuvrability and stability of craft in waves;
5. the reliability of instruments, equipment, engines and hull structure on craft operating in waves.

Some problems not only concern the theory of hovercraft, but also the design methods. These aspects will be discussed in later chapters, after Chapter 10. Some problems detailed above are the problems which are under study at present, and the references concerned with these problems are fewer, such as (3) and (4). Therefore we will discuss problems (1) and (2) above and analyse these problems approximately based on some experimental data.

Effect of skirts on seaworthiness of ACV/SES

Effect of skirt height

According to [4], the drag of ACV skirts in waves can be expressed as

$$R_{rw}/(q_w l_c S_c^{0.5} = f\{2h_w/[h_c + h_f]\} = 20 \times 10^{-5} (2h_w/[h_c + h_f])^{5/3} \qquad (8.107)$$

where R_{rw} is the skirt drag in waves (N), l_j the peripheral length of air cushion (m), S_c

the cushion area (m), h_w the half-wave height (m), h_c the cushion height (m), h_f the finger height (m) and

$$q_w = 0.5\,\rho_w V_s^2$$

where V_s is the craft speed (m/s) and ρ_w the water density (Ns^2/m^4). This equation can also be expressed graphically as in Fig. 8.30, which demonstrates the effect of cushion depth and finger height on the wave drag: the deeper the cushion, the smaller the wave drag.

Effect of skirt type

With respect to the ACV, inclined responsive skirts with low natural frequency obtain a clear effect for improving seaworthiness. So-called inclined skirts are those with higher bow skirt than stern skirt. Thus the high bow skirt fingers and bag could reduce the wave drag. As a matter of fact, this effect has been seen on SES and the matching of higher bow skirt with a lower stern skirt was adopted on passenger SES in 1969.

The responsive skirt can decrease its natural frequency, thus it is equivalent to mounting a damper on hovercraft, which not only improves vibration at high frequencies, such as the cobblestone effect, but also improves heave motion in long waves, which causes deformation of the skirt and reduction of the vertical motion of the hull so as to move closer to platforming operation. The vertical acceleration and skirt drag will be reduced significantly.

Figure 8.31 shows the improvements in speed degradation of the craft model SR.N4 Mk 1 of BHC running in head waves and beam wind. Thanks to mounting an improved skirt on Mk 3 craft, speed loss in rough seas was reduced by 30–40%. In the case of using the new standard skirt design, then the improvement in speed loss will be less, even though the craft model Mk 3 has higher cushion length to beam ratio and larger all-up weight than the Mk1. The speed degradation has improved due to well-designed skirts.

Thanks to the improvements in skirts and elongation of cushion length/beam ratio of the Mk 3 craft, the bow vertical acceleration of SR.N4 Mk 3 in waves with

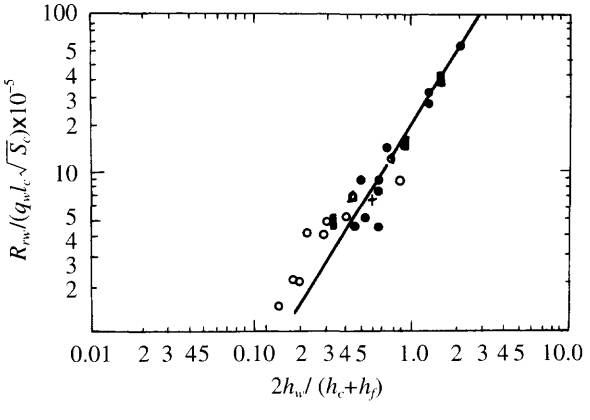

Fig. 8.30 Influence of skirt height / wave height on the skirt wave drag of ACV in waves.

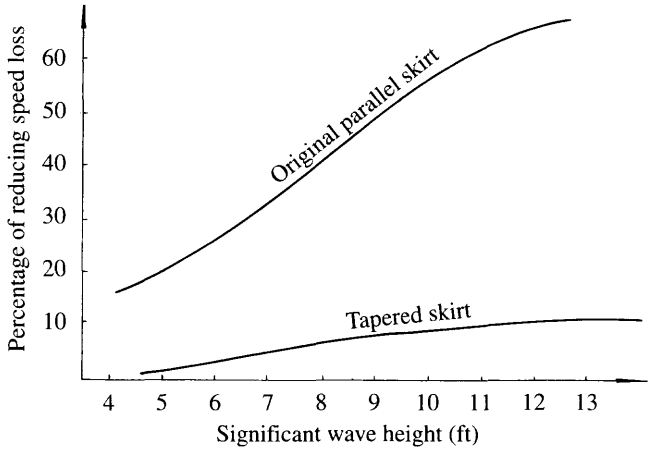

Fig. 8.31 Reduction of speed loss of SR.N4 Mk3 relative to SR.N4 Mk1 in head seas and beam winds.

significant wave height of 1.2 m reduced to 0.1 g, pitch angle (double amplitude) dropped to 1.5°, decreasing by a factor of 50% over Mk 2, vertical acceleration at the CG dropped to 0.07 g, decreasing by 25% over the Mk 2, and craft speed increased from 45 knots decreasing to 54 knots. All of these should be attributed to the success of the inclined responsive skirt with low natural frequency skirt cloth thickness.

Effect of material thickness

There are no definite conclusions on such problems, but it may be seen that a reduction of skirt cloth thickness will reduce the inertia drag of skirts, induced by flagellation of the skirt in waves. Therefore thinner skirt cloths were applied to the British military ACV model BH.7. Of course, it may influence the skirt life, particularly if the craft are often operated along sandy beaches. Since the BH.7 is a military test craft therefore the thinner skirt cloths were applied to the craft after a design trade-off.

Effect of principal dimensions on seaworthiness

Effect of l_c/b_c

The increase in l_c/b_c can always improve the seaworthiness and the speed degradation of craft both for ACVs and SES. The relation of frontal area may be one of the reasons for reducing water drag of skirts; reduction of longitudinal motion of the craft due to the increase in cushion length may be another reason for improving speed degradation.

Figure 8.32 shows a speed comparison between the SR.N4 Mk1 and Mk3 craft models. Keeping cushion pressure constant, the SR.N4 Mk1 was stretched by 16.74 m, increasing the speed in waves by 10–20% while increasing all-up weight by 44%.

Figure 8.33 shows the improvement of British SES model HM-2 by stretching of the cushion length/beam ratio from 2.45 to 2.95 and 3.58 respectively, keeping the

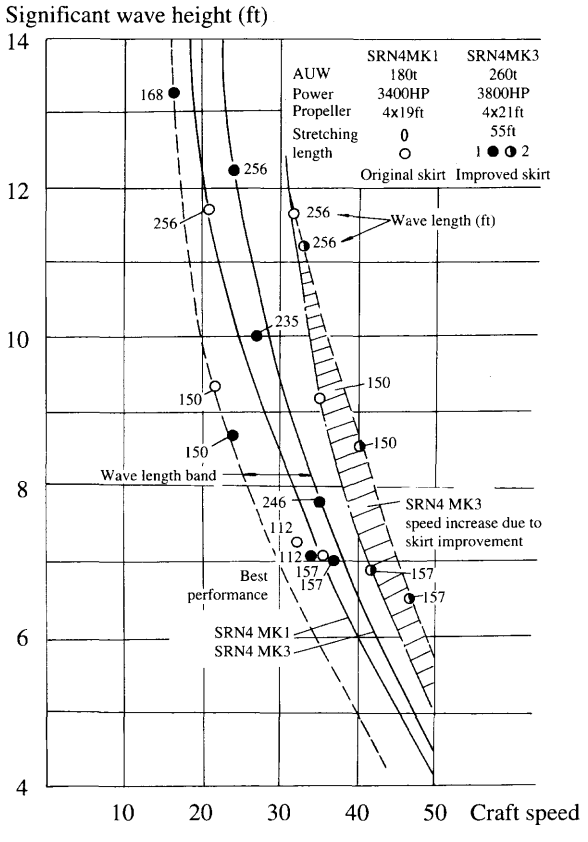

Fig. 8.32 Comparison of ship speeds between SR.N4 Mk3 and Mk1 in head seas and beam winds.

cushion pressure constant. This change was based on the original design HM.216 keeping cushion beam constant, then stretching the cushion length and thus the all-up weight of the craft, while keeping engine output approximately constant. Thus it is found that the speed degradation of the craft improves greatly in waves with significant height of 0.8–1.0 m. Meanwhile, the calm water performance, particularly at low and medium speeds, drag hump, overload capability and economy of the craft are also significantly improved.

For this reason, the stretching of ACV/SES is the modern way to improve craft performance. With the stretching of the Chinese SES craft 717 and 719, the speed performance, seaworthiness and economy of both craft were also very much improved.

Figure 8.34 demonstrates the speed degradation of various craft in waves. It is seen that the speed loss of craft with high cushion length/beam ratio is lower than those with low length/beam ratio at different ratios.

Figure 8.35 shows the comparison of pitch response factors between the craft model SR.N4 Mk 1 and SR.N4 Mk 3 in waves; thanks to the improvement of the skirt and elongation of the cushion length/beam ratio of the craft model Mk 3, the pitch attitude response decreased by 50–100%.

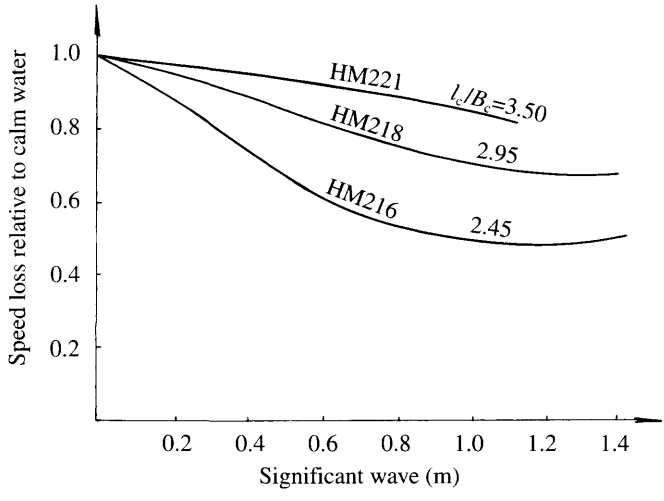

Fig. 8.33 Speed improvement of British SES in waves due to the increment of cushion length-beam ratio.

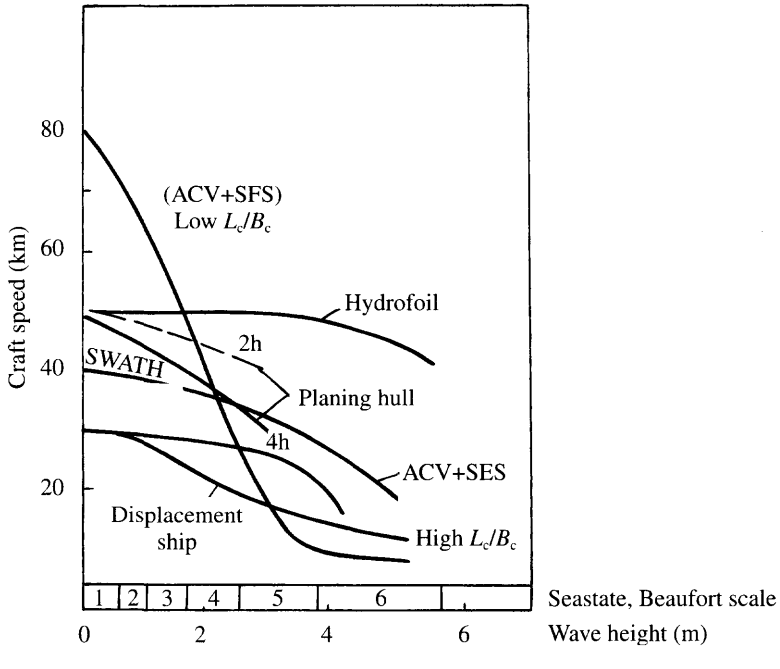

Fig. 8.34 Comparison of sustainable ship speed in different sea states between various types of ships weighing 200 t.

Effect of sidewall thickness ratio B_{sw}/B_c

An increase in the sidewall thickness ratio B_{sw}/B_c (where B_{sw} is sidewall thickness, B_c is cushion beam) will improve the seaworthiness, reduce vertical acceleration and

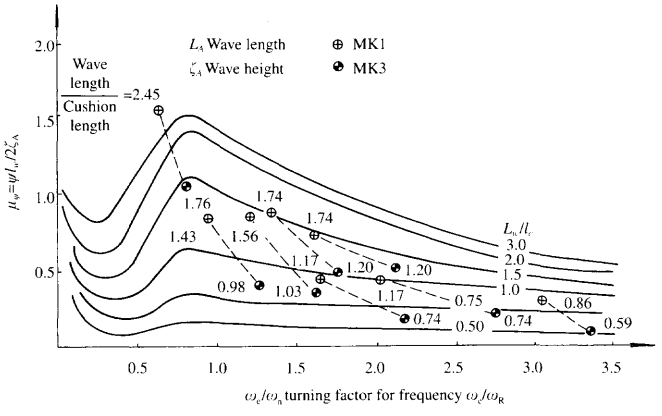

Fig. 8.35 Frequency response of pitch amplitude for SR.N4 Mk1 and SR.N4 Mk3 models in waves.

improve speed loss in waves, because the fluctuation of cushion pressure will decrease in the case of thicker sidewalls, which then reduces the heave acceleration.

One must be careful not to increase sidewall width too far, since if more than about 30% of the craft weight is taken by sidewall planing pressure on the sidewall lower surface, then motions begin to be controlled by these hydrodynamic forces rather than be supported from the cushion, and drag forces will increase greatly.

Effect of sidewall depth H_{sw}

Increased H_{sw}, thus increase in cushion depth and cushion volume, will decrease the effect due to the wave pumping, motion pumping and compressibility of the cushion air, thus will decrease the perturbation of waves on the hull motion and improve seaworthiness. Therefore sidewall depth and skirt depth will be increased in the case of craft with good seaworthiness.

Effect of inner draft of sidewall

Increase of the inner draft of the sidewall will decrease the nonlinear air leakage (Q_{esw}) in waves, so as to decrease the wave perturbation force (moment), therefore the seaworthiness will be improved in the case where the skirts can be adjusted automatically.

Effect of damping on seaworthiness

Besides the change of motion natural frequency to avoid resonance with the wave encounter frequency, the increase of motion damping may be one of the most efficient measures to decrease the motion amplitude at the resonance frequency, particularly in the case of pitch motion, because the latter has the characteristic of small damping and small stability with respect to the heave motion. Specific measures are as follows.

Pitch damping

The bow hydrofoils can be fitted at the bow of an SES to increase damping pitch, thus improving the seaworthiness efficiently. Figure 8.36 shows the effect of hydrofoils with different dimension ratio on the seaworthiness of an SES model [75].

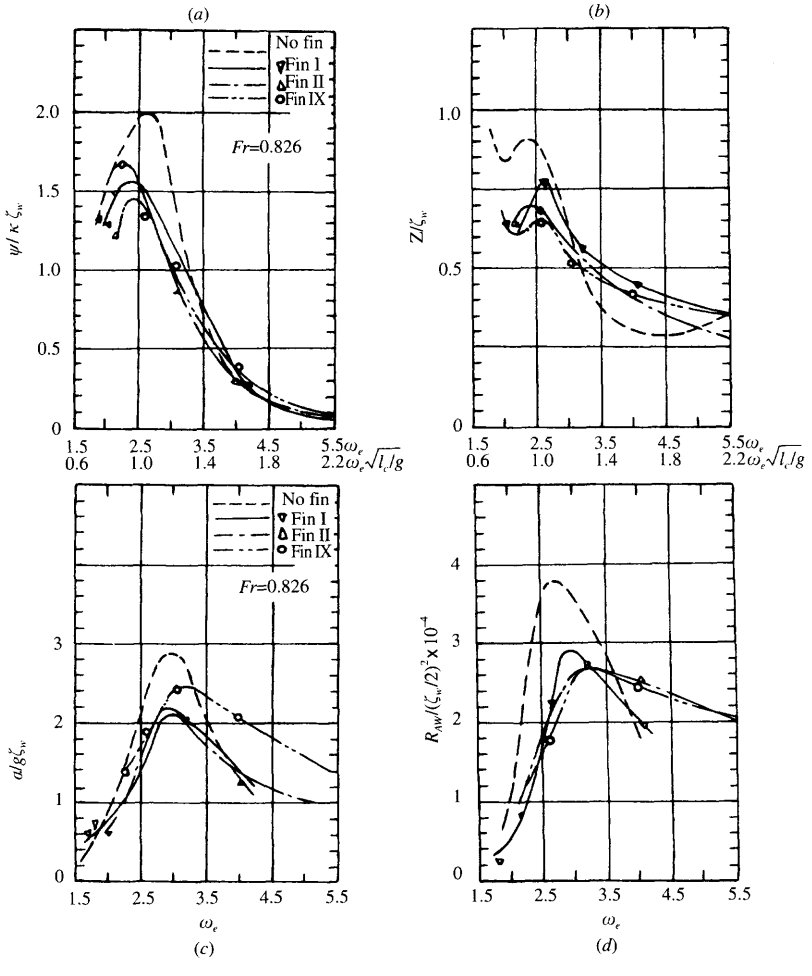

Fig. 8.36 Influence of bow hydrofoil of SES model on its seaworthiness. (a) Relative pitch angle versus relative encounter wave frequency; (b) relative heave amplitude versus relative encounter wave frequency; (c) relative vertical acceleration versus vertical acceleration at bow; (d) relative average drag increment of craft in waves.

Among them, on type I, i.e. the bow hydrofoil with side plates at an aspect ratio of 2 and an area ratio of 2% (namely the ratio of foil area to cushion area), mounted at inside of sidewalls, will be the better choice, which reduces the heave amplitude by 8–30%, pitch amplitude by 10–30%, vertical acceleration by 20–30% and wave drag by 15–45%. Meanwhile the bow hydrofoil was also mounted on SES test model 711-III in 1967 as shown in Fig. 1.32; the test proved that the bow hydrofoil could prevent plough-in and improve the seaworthiness of the craft.

Cushion flow rate

Increase the air flow rate into the bow/stern skirt and bag cushion pressure ratio so as to increase the pitch damping moment. The lift power will be increased following this measure.

Sidewall chines

The anti-spray plate on sidewalls for increasing pitch damping moment may also be a suitable measure for improving the seaworthiness of an SES. Figure 8.37 shows the test results of bow anti-spray plates on British SES HM.5. It can be found that bow acceleration can be reduced. With same reasoning, hard chine on sidewalls can also obtain the same results, just as the double hard chine on the sidewall lines of British SES HM.5.

Passive or active heave attenuation system and anti-roll systems

The fluctuation of cushion pressure of ACV/SES is unavoidable, as hovercraft run in waves; therefore some automatic control system for keeping cushion pressure constant will be the essential measure for improving the seaworthiness and reducing the vertical acceleration of ACV/SES. Some experiments for automatic discharge of cushion air have been carried out on the skirt test rig of MARIC and satisfactory results obtained. An automatic heave attenuation system was developed in the USA in the 1970s and produced the same results for reducing the cushion pressure fluctuation of an SES in waves follows:

1. automatic cushion air discharge apparatus to reduce the fluctuation of cushion pressure will be followed by an increase of fan air flow, otherwise the craft speed will drop down;
2. fan inlet/outlet valve regulation to adjust the cushion pressure;
3. automatic control of fan blades.

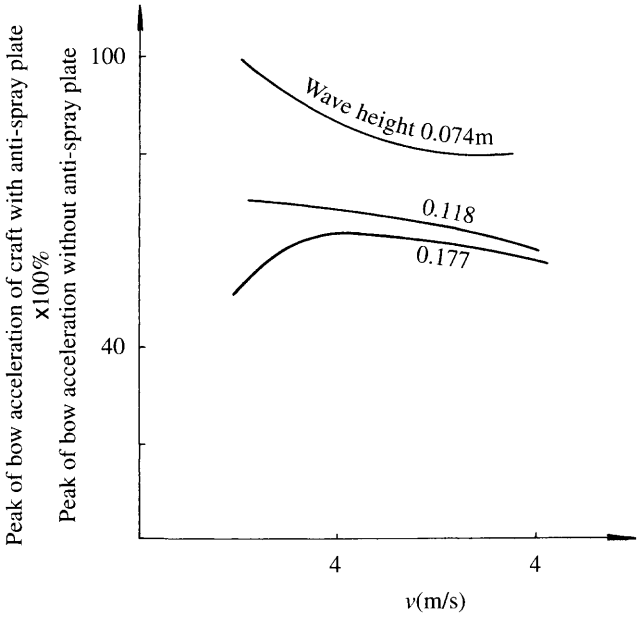

Fig. 8.37 Decrease of vertical acceleration of British SES due to the anti-spray plate on bow sidewall.

The latter two methods will save some lift power due to the lower flow rate consumption. Figure 8.38 shows the reduction of vertical acceleration in the navigation cabin of SES-200 by means of the ride control system (RCS). Thanks to the extreme reduction of pressure fluctuation, vertical acceleration was reduced significantly.

From Fig. 8.38 it can be seen that vertical acceleration was decreased to a satisfactory level, but accompanied by an increase of lift power of 15%. Figure 8.39 shows the improvement of seaworthiness of a high-speed test SES model SES-100A by means of an automatic control system. This equipment is also based on the theory of overpressure discharge and has the advantage of simple configuration, low cost and high efficiency. The figure shows that vertical acceleration can be decreased by ~50%.

Ability to maintain cushion-borne operation of ACV/SES in high waves

With respect to an ACV, since the aerodynamic momentum drag, aerodynamic profile drag and skirt drag comprise the most part of craft total drag, these drags will be significantly increased in the case of head-wind operation of craft. Under such conditions the craft will experience speed degradation not only due to the drag increase but also the light load of the air propellers, if they are fixed pitch propellers.

Thus the power output and thrust will be reduced with the same propeller revolutions. Combining the effect of both drag and thrust, the craft speed will be degraded even though under hump speed. Figure 8.40 shows this situation. Using controllable pitch air propellers, increasing the reserve power and improving the skirt design mentioned above are the most efficient correction measures.

The additional drag of craft in waves can be calculated. Because the wind speed is given, the aerodynamic profile and aerodynamic momentum drag can be calculated.

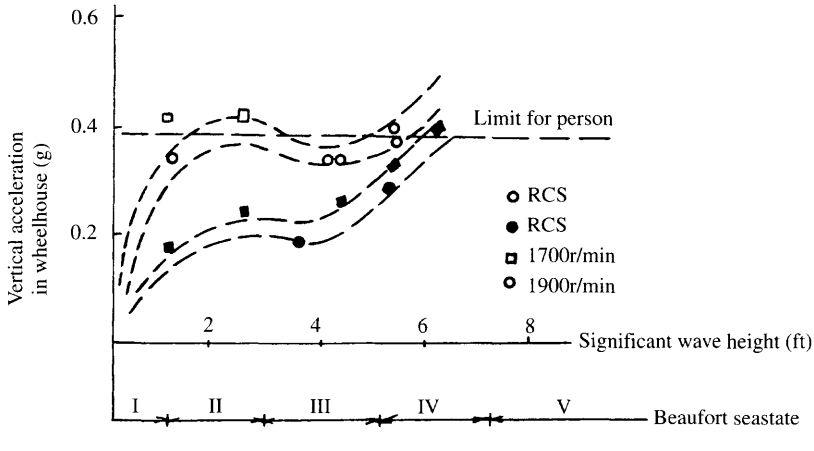

Fig. 8.38 Reduction of vertical acceleration in navigation cabin of SES-200 by operation of the ride control system (RCS).

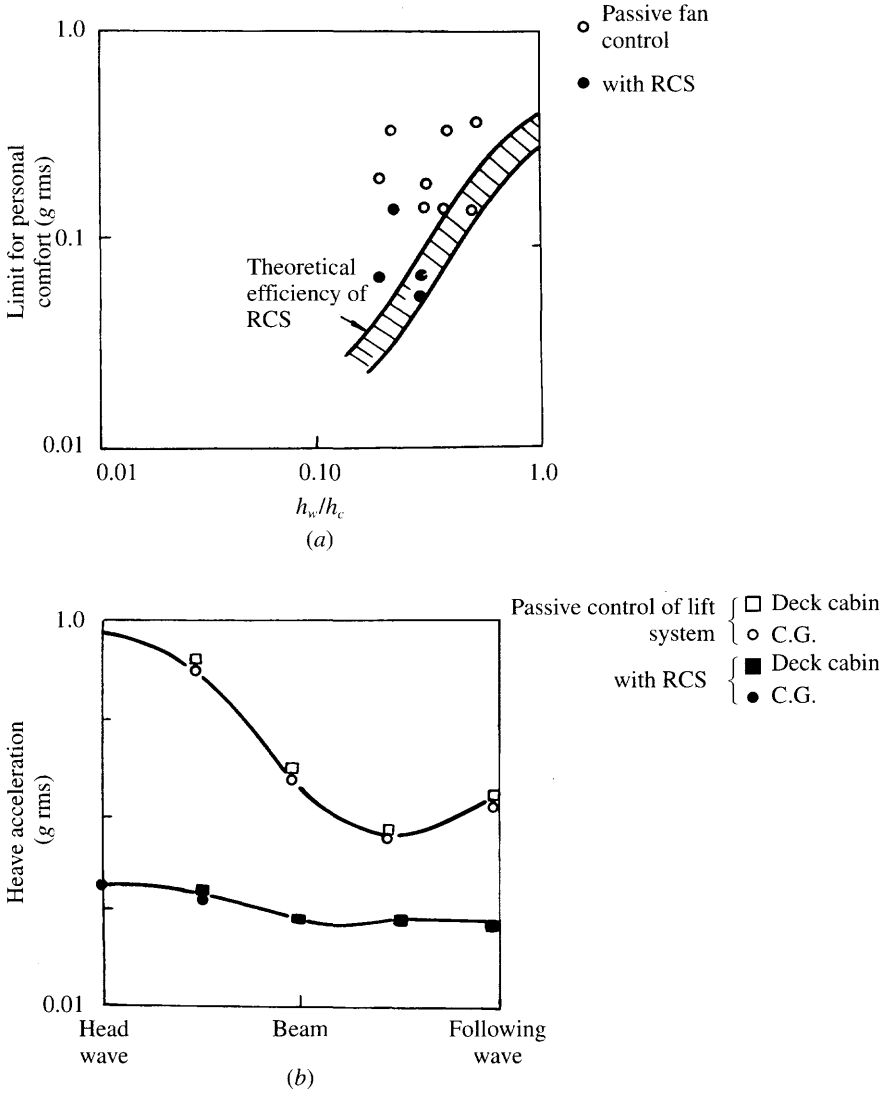

Fig. 8.39 Influence of RCS on seakeeping quality of SES-100A.

With respect to the wave drag, it can be calculated by the foregoing expressions. The additional drag of skirts in waves and can also be estimated by Fig. 8.41.

It is suggested that with respect to the ACV, particularly for small ACVs, the ability to maintain the cushion-borne operation of craft in waves has to be seriously considered, given that small wind and waves will affect the ability to maintain the cushion-borne operation, and the reserve power (or reserve thrust of the propellers) has to be considered in design.

From Fig. 8.40, it can be seen that it is impossible for the craft to take off in wind speed 5. Sometimes users ask for a lower designed calm water speed for some business

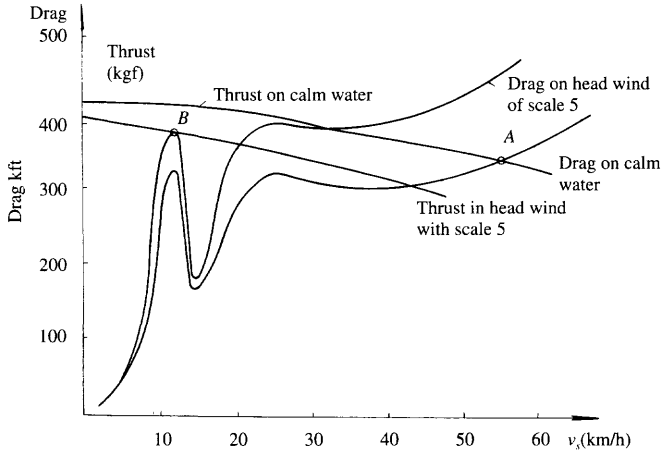

Fig. 8.40 Drag and thrust of an ACV in head seas.

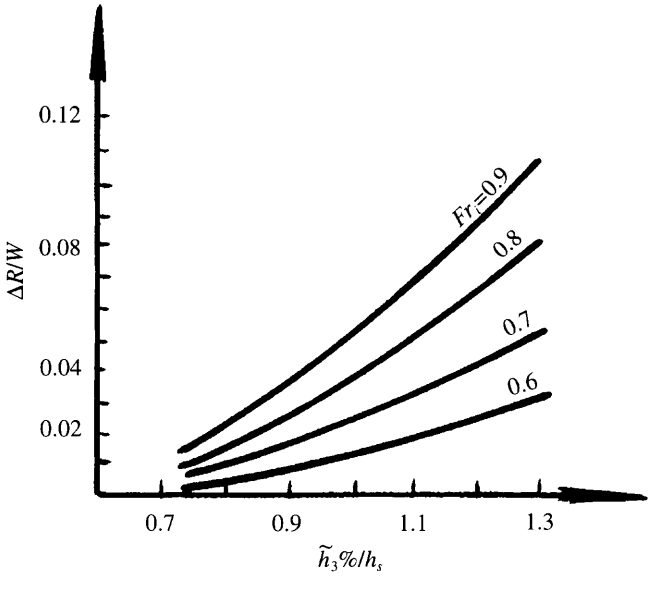

Fig. 8.41 The variation of relative additional drag of ACV in waves as a function of Froude Number and relative wave height.

consideration, but again demand the high weather limitation, namely the ability to maintain the cushion-borne operation in head wind. Then the two requirements contradict each other. The craft will have a given calm water speed to satisfy the user's requirements, but cannot maintain the cushion-borne operation under the given wind. Designers are most likely to have such experience with the design of small ACVs.

Effect of air flow rate and its distribution on seaworthiness

Effect of air flow rate

Air flow rate greatly affects the seaworthiness for both ACVs and SES, because the wave pumping, motion pumping, change of air leakage and compressibility of cushion air will affect the change of cushion pressure and flow rate. Figure 8.42 shows such dependency between the craft drag and air flow rate, but unfortunately we do not have concrete calculation methods to predict such a relation.

Perhaps such an influence can be obtained by means of a model test, when the principal dimensions of the craft, skirt configuration and lift system have been determined. Thus the influence of air flow rate on wave drag and also on the craft motion amplitude and acceleration can be estimated so as to determine the reserve power to meet the seaworthiness design requirement.

Effect of distribution of air flow rate

The distribution of air flow affects the seaworthiness of an SES, particularly on an SES running at high speed and in rough seas. The distribution of air flow on US SES-200B can be expressed as follows:

			Per cent of total
Cushion pressure	4423	Pa	
Total flow rate	181.7	m^3/s	100.0
Flow rate blown directly into the cushion	113.0	m^3/s	62.0
Flow rate blown directly into the bow seal	22.6	m^3/s	12.5
Flow rate blown directly into the stern seal	45.0	m^3/s	25.5

These data were obtained by experiments.

With respect to craft at low speed, it is doubtful whether it is necessary. MARIC also has such experiments. Experiments of an SES model with two air ducts from the air outlet of the fan have been carried out in the towing tank. Part of the outflow may be led directly into the cushion and another part via air ducts, the bow/stern bag and through into the air cushion. The distribution of air flow can be regulated by a valve. The experiments did not obtain a clear conclusion. With such experiments with three parts of the air flow coming from the same source it might be difficult to get the expected results. But actually the air flow rate of bow/stern skirt on the Chinese SES-717 7203, 719, etc. are very small, sometimes even zero or a negative value.

Due to the lack of precise experiments and analysis as well as a suitable theoretical approach, it is difficult to estimate the influence of air flow distribution on seaworthiness. However, following the application of bow/stern responsive skirts to hovercraft, we are sure the air flow will have a definite effect on seaworthiness and maybe it is an important research theme for us in the near future.

Key observations

Seaworthiness of ACVs and SES plays a very important role in their performance. Assessment, particularly by analysis, is very complex and at present not completely developed and validated. If ACV and SES are to be developed further for operation

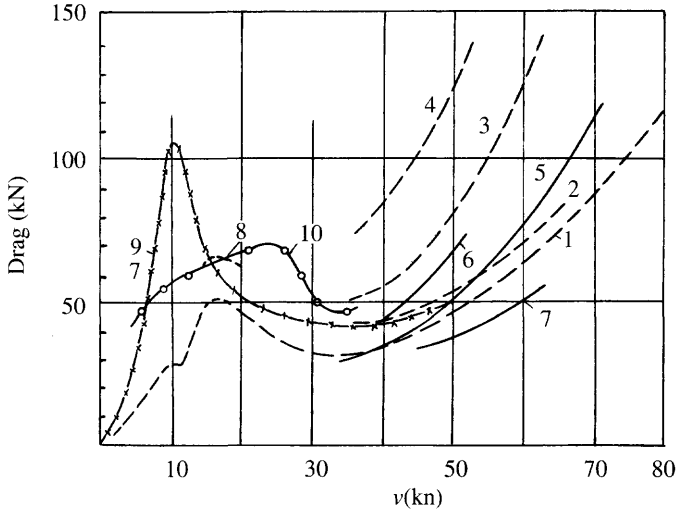

Fig. 8.42 Influence of air flow rate and wave height of SES weighing 80.7 t on craft drag: (1) on calm water; (2) in waves with height of $H_w = 0.33$; (3) $H_w = 0.5$; (4) $H_w = 0.7$; (5) $H_w = 1.4$; (6) $H_w = 0.3$, with the air flow rate $Q = 99$–113 m^3/s; (7) $H_w = 0.6$, $Q = 99$–113 m^3/s; (8) on calm water, $Q = 165$ m^3/s; (9) the peak drag in waves with $H_w = 0.73$m; (10) passing through the peak drag for non acceleration operated mode of craft; (11) passing through the peak drag for accelerated operation of craft.

on open ocean seaways, further work to improve responsiveness is required. The following issues should be borne in mind by designers.

Pitch motions

Both ACVs and SES have small pitch damping and low pitch stability, therefore it is recommended to pay attention to resonance frequency for pitch motions. For example, according to calculation and experiments, the resonance relative pitch frequency of an SES weighing 100 t, $\omega_e(l_c/g)^{0.5} \approx 1.5$–$3.0$, i.e. $\omega_e \approx 3$–6. If the craft are running in waves with wavelength of 15–30 m at a speed of 35–40 km/h, then the craft are operating below resonance pitch frequency, hence craft are seldom over the critical condition when the craft are running in rough seas, and may develop significant response.

With respect to an ACV, although the craft can run at high speed, the inherent pitch frequency is also higher due to the larger pitch stiffness. Here, the resonant pitch relative frequency $\omega_e[l_c/g]^{0.5} \approx 5$. For an ACV weighing 70t at the speed of 40 knots, sometimes such an ACV also operates at critical or supercritical conditions, but due to the speed degradation of the ACV in waves, it also probably operates at subcritical conditions.

Thus it can be seen that increasing the pitch damping may be the critical measure for improving seaworthiness. Additional hydrofoils, anti-spray plates and bow sidewall configuration with a hard chine can solve such problems for an SES. Change of bag–cushion pressure ratio of the bow/stern skirt, the tightness of diaphragm of the D-type bag, area ratio of bag holes and various geometric parameters of responsive

skirts can also solve such problems for an ACV. Such parameters are best experimented with at model scale, or on full scale prototypes.

Heave motions

Both ACVs and SES possess large heave damping and heave stiffness, thus the amplitude peak will be located both on the high and low encounter frequency on the frequency response curve of heave (Figs 8.15(a) and 8.20), where the relative heave frequency $\omega_e[l_c/g]^{0.5} \approx 4$–8 (for SES) and 5 up to 15 (for ACV), which causes the high vertical acceleration associated with the cobblestoning effect which is also observed at high encounter frequency. For this reason, heave stiffness may need to be reduced by the following measures:

- using an automatic cushion pressure regulating control system, such as ride control systems (i.e. automatic air flow discharge system);
- using responsive skirt with low inherent frequency, i.e. positive control system, to improve the heave motion of craft;
- reducing the heave stiffness by means of using a rather flat fan characteristic curve and decreasing the air inlet/outlet pressure losses.

Speed degradation

Speed loss is always a troublesome problem faced by designers for both ACV and SES, because while the skirt components are in contact with the waves, they do not form a fine streamline, which induces significant wave drag. Figure 8.34 shows that speed degradation of ACV and SES is larger than deep submerged hydrofoil craft with automatic control systems and SWATH, therefore such problems are still an important research subject; perhaps the responsive skirt with large deformability will improve this problem.

Performance in head winds

Speed loss or even losing the above hump speed cushion-borne operation of an ACV running in head wind may be the most troublesome problem faced by designers and operators. This is due to the increase of drag and decrease of thrust; therefore designers have to pay serious attention to the problem to select engine, principal dimensions, to design propellers and skirt well as well as the lift system, etc. to keep the capability of cushion-borne operation of the ACV at given wind speed which is required by users.

9

Model experiments and scaling laws

9.1 Introduction

Hovercraft (ACV or SES), like ships, have a complex interaction with the surface they travel over. In previous chapters we have reviewed the theoretical background to hydrodynamic drag components and the response of these craft to waves. Many of the parameters in the equations are nonlinear, so creating complex problems for direct analysis.

Direct measurement of the drag or motions at model scale can be used as a means of identifying non-dimensional coefficients in the appropriate analytical equation. So long as a reliable relation between the model-scale behaviour and full-scale performance is available, the full-scale data can be generated and used to complete the craft design.

Since models are specific, if parametric data are required then a series of tests during which the parameter of interest is varied has to be carrried out. For example, tests may be with increasing cushion pressure, changes of centre of gravity, or perhaps changes to the skirt geometry, all for the same set of environmental conditions of speeds, sea conditions, etc.

Scaling criteria between model and full-scale craft have to be considered carefully during tests on hovercraft. There are many similarities as well as a number of differences in the scaling criteria for experimental data between hovercraft and conventional planing boats.

Similarly to conventional ships, it is difficult in model experimental conditions to scale all the needed parameters at the same time. A typical example is that many parameters follow Froude's scaling relationship (inertia-dominated loadings such as wave-making drag) while others follow Reynolds' law (skin friction and other velocity-dominated drag components). Experiments therefore have to be designed to scale the most important parameters and if necessary multiple tests carried out to investigate different loading components. An example is that the aerodynamic drag of a craft would be tested in a wind tunnel scaled according to Reynolds' law, while the wave-making drag would be investigated in a towing tank scaled according to Froude's law.

Hovercraft provide some additional challenges, since skirt wetting drag is rather complex, being an air-lubricated compliant surface, partly influenced by the generated spray. Such drag terms are generally treated as 'residuals' from experiments and a conservative approach to scaling adopted.

A (large) hovercraft design will usually require both 'static' testing and 'dynamic' testing. Examples of static tests are model skirts in skirt test boxes, static hovering models from which stability measurements are taken and fixed models of the above water part of a hovercraft in a wind tunnel used for aerodynamic drag and stability tests. Examples of dynamic tests are towing tank tests for drag in calm water or waves, trim, motions and accelerations. In addition dynamic tests may be carried out on a lake or the sea with radio-controlled models to obtain motions data in spread rather than unidirectional random sea states. Open sea testing can be very helpful to evaluate turning and control performance and if a fairly large-scale model is used, plough-in performance. Instrumentation becomes rather more complex than in a towing tank, as it requires on-board recording of the parameters, or remote telemetry.

We will consider first the scaling laws based on dimensional similarity, and then static and dynamic testing in turn, giving guidance on planning and analysis.

9.2 Scaling criteria for hovercraft models during static hovering tests

Test classification

There are three types of test normally carried out on hovercraft models or full-scale craft hovering statically and running on rigid surfaces as follows:

1. *Static hovering tests.* Static hovering tests of ACV or SES models and full-scale craft on rigid surfaces or platforms are carried out to investigate the static hovering performance at various fan speeds, including measurement of static cushion stability, internal air ducting characteristics, the geometry and tailoring of skirts, heave, stiffness, and craft pitch and roll damping.
2. *Experiments with skirts in skirt test boxes.* Testing scale model skirts of full scale craft or of models in small or large skirt boxes are carried out to investigate the static shaping, the dynamic response of skirts, flow and loss characteristics of air ducts, aerodynamic performance of the internal cushion, pressure head loss coefficients due to the skirt holes, heave motion characteristics of skirts, hysteresis effects and the heave attenuation characteristics of air control systems.
3. *Wind tunnel tests.* Wind tunnel testing is carried out to measure various coefficients of aerodynamic drag, static force derivatives, the performance of air propellers, the internal aerodynamic characteristics of models, and its influence on pressure distribution in the cushion.

Scaling laws and criteria

Table 9.1 shows the dimensional ratios for the main variables between the models and full scale craft based on the geometrical similarity, in which λ denotes the linear dimensional ratio.

Cushion pressure ratio (H_q) (Euler number)

In order to correctly simulate air leakage from an air cushion and external aerodynamics of full-scale craft, as well as the spray caused by the cushion acting on the water surface, the scaling criteria of cushion pressure ratio H_q, the Euler number, can be written as

$$H_q = p_c/(0.5\,\rho_a\,V_a^2) \tag{9.1}$$

where p_c is the cushion pressure (N/m^2), ρ_a the air density (Ns^2/m^4) and V_a the velocity of air leakage, (m/s). According to Table 9.1, V_a can be written as

$$V_a \propto \lambda^{0.5} \tag{9.2}$$

If V_a denotes the velocity of the craft model, then expression 9.2 is similar to the Froude number, which is normally used for ship models running on water. Thus the dimension ratio of some corresponding variables can be given as in Table 9.2.

Reynolds number at jet nozzles, Re_j

In the case where hovering experiments are carried out on hovercraft models, the Reynolds number at the jet nozzles Re_j has to be in the range for turbulent flow, namely $Re_j = V_j\,t/\gamma \geqslant 1 \times 10^5$, as was described in Chapter 2, where γ denotes the kinematic viscosity coefficient, t the equivalent nozzle width and V_j the average velocity of the jet at the nozzle. In the case of $Re_j \geqslant 1 \times 10^5$ then the aerodynamic characteristics of the air jet at the nozzle can be considered independent of the Reynolds number.

Table 9.1 The dimensional ratio of various physical variables between the models and full-scale craft with geometric similarity

Physical variables	Nomenclature	Dimensional ratio
Length	l_c	λ
Cushion area	S_c	λ^2
Force and weight	F	λ^3
Acceleration of gravity	g	Constant
Air density	ρ_a	Constant*
Cushion pressure	p_c (height of water head)	λ
Time		$\lambda^{0.5}$

* Note: Air density can vary significantly with altitude and temperature. Take care to choose the appropriate value.

Table 9.2 The dimensional ratio of air cushion related physical variables

Physical variables		Dimensional ratio
Air flow rate	$Q = V_j\,S_j$	$\lambda^{2.5}$
Lift power	N_p	$\lambda^{3.5}$
Frequency	$\omega\,(s^{-1})$	$\lambda^{-0.5}$

Non-dimensional characteristic curves of fans and air ducts

The Reynolds number for model air ducts is rather small because the dimensions of the model decrease with the dimensional ratio λ. This will influence the air duct friction drag. However the air friction drag losses are usually small; the main losses of air pressure in air ducts are due to the curved or sharp bends in the ducts and sudden expansion of air flow into the cushion. Thus the air pressure loss in ducts can be considered independent of *Re*. Calculation of losses is similar to analysis of heating and ventilating systems.

Hovering performance parameters such as heave stiffness, damping, etc. are closely linked to the fan characteristic curve. On small models the fan characteristic may be distorted, because of its small dimensions and thus small *Re* and non-similarity of fan-specific speed (which will be introduced in detail in Chapter 12, Fan design).

The non-dimensional pressure coefficient H_j and non-dimensional flow rate coefficient Q can be written as

$$\bar{H}_j = H_j/[\rho_a\, n\, D^2] \tag{9.3}$$

$$\bar{Q} = Q/[n\, D^3] \tag{9.4}$$

where $\bar{H}_j$ is the fan non-dimensional pressure coefficient, $\bar{Q}$ the non-dimensional flow rate coefficient, H_j the total pressure head (N/m^2), n the fan revolutions (1/s), D the fan diameter (m) and Q the flow rate (m^3/s). Thus the specific speed of the fan is

$$N_s = Q^{0.5}/H^{0.75} \tag{9.5a}$$

If H_j can be expressed by the height of water head, then this expression can be written as

$$N_s = n\, Q^{0.5}/[g\, H]^{0.75} \tag{9.5b}$$

For craft models, $[D] \propto [l]$, $[n] \propto 1/[s]$. Thus the speed of a model fan should increase compared with that of full-scale craft by a factor of $\lambda^{0.5}$, i.e. less than linear scaling. High-speed electric motors are often used as power units for hovercraft models, so the specific speed of models, N_{sm}, *Re* and consequently the fan characteristics, differ from that of full-scale craft.

While it would be possible to install reduction gears with some penalty in weight on a model, the local aerodynamics in a model fan creates further difficulties in scaling and thus normally some trial and error is used to manufacture fans which have pressure/flow characteristics as close as possible to the desired curve, rather than modelling the fan itself.

When a section of the craft skirt is mounted on a test rig as a test skirt, the corresponding flow rate at the test rig should be smaller than that on full-scale craft, i.e. $Q_{sb} = Q/n_{sb}$ where Q_{sb} denotes the air flow rate of the fan on the skirt test box, Q denotes the air flow rate on full-scale craft (or model if the scaling is between the box and a model) and n_{sb} denotes a given value of flow reduction, which is according to the size of test box.

However, the overall pressure head has to comply with the linear dimension, i.e. $[H_j] \propto [l]$. Thus there is a great difference in the specific speed between the fans of a skirt box and full-scale craft. In fact, a test rig fan cannot be suitable for all craft (models),

due to its fixed characteristic. Normally the fan system in a skirt test box is not changed for each test! For this reason, the skirt test box is more suitable for experiments to optimize static shaping of skirts and will create large errors needing correction in the case of skirt dynamic response characteristic testing unless the fan and air speed system are also specially modelled.

Skirt weight per unit area

Skirt weight is directly related to its static geometry and surface area, since it is essentially a membrane, so scaling between model and full scale has to satisfy

$$W_{ss}/W_{sm} \propto \lambda \tag{9.6}$$

where W_{ss} is the weight per unit area of skirt (including the connections) of full-scale craft (N/m^2) and W_{sm} the weight per unit area of skirt (including connections) of models (N/m^2). The problems concerned with the elastic aerodynamics of skirts have to be considered during the investigation of the dynamic shaping of skirts; however, this does not greatly affect the skirt shaping and can therefore be neglected.

Strouhal number S_r

Strouhal's number is closely related to the elastic aerodynamic characteristics of the skirt fingers. It characterizes the ratio of inertia force due to the air pressure and the elastic modulus of skirt materials and can be expressed as

$$\begin{aligned} S_r &= \sqrt{[\rho_a V_a^2/E]} \\ &= V_a/\sqrt{[E/\rho_a]} \\ &= V_a/a \end{aligned} \tag{9.7}$$

or

$$\omega\, l/\sqrt{[E/\rho_a]} = \omega\, l/a \tag{9.8}$$

where v is the velocity of air flow (m/s), a the velocity of sound in skirts or other structural materials (m/s), ω the vibration frequency of skirts (1/s) and l any linear length.

In the case where the skirt material of the full-scale craft has the same characteristics as those of the model, then the model skirts' S_r is not scaled correctly compared to the full-scale craft. Thus it may be noted that in the calculation of skirt shaping described in Chapter 7, the skirt bag membrane tension and stresses of both the model and craft are not similar, even though the skirt geometric scaling with the same specific weight can be satisfied.

The tension in the skirt bag membrane is represented by $T = p_t R \propto \lambda^2$, where p_t denotes the bag pressure and R the radius of curvature of the skirt bag at that position, i.e. the dimensions of $[T]$ = [N/m]. Meanwhile the tension stress of the skirt membrane $\sigma = T/\delta$, where δ denotes the thickness of the skirt material.

According to this theory, the elastic modulus E of a full-scale craft skirt should be λ times E of the model skirt, i.e. $[E] \propto [l]$, but actually the experiments demonstrate rather different results as shown in [81]. The elastic modulus of skirt material for both model and full-scale craft are shown in Table 9.3.

In general the linear ratio between full-scale craft and models is approximately equal to 10, but Young's modulus of skirt materials for both models and full-scale craft are much closer (model skirts are too stiff relative to the linear scale). In addition, the thickness of model skirt materials is usually too great in comparison with

Table 9.3 The elastic modulus E and coefficient of elongation ε for both models and full-scale craft

Skirt material	E_{warp} (N/cm^2)	E_{weft} (N/cm^2)	ε_{warp} (%)	ε_{weft} (%)
6408 (for full-scale craft)	3 970	1 770	5.5	12.1
1533 (for models)	12 700	6 900	7.3	13.3
9514 (for models	10 900	10 900	6.0	10.0

that of full-scale craft on a basis of direct scaling, i.e., $\delta_s/\delta_m < \lambda$, and the materials are also relatively stiff.

This will affect the test results for inertia drag and frequency of vibration, especially for seaworthiness tests. Reference 9 recommends the parameter Γ which characterizes the ability to straighten the skirt under pressure of the air cushion. Γ can be written as

$$\Gamma = E \delta l_s/[\rho_a v^2 S] \tag{9.9}$$

in which δ denotes the skirt cloth thickness, E, l_s and S denote Young's modulus, equivalent length and skirt material area respectively. Due to the fact that $E_s \approx E_m$, $\Gamma_s < \Gamma m$, the deformability of model skirts is less than that of a full-scale craft skirt. For this reason, skirt bag bounce and the flagellation motion of the skirt fingers in the water, which occurs at full scale and is also observed in the bag skirt test box, seldom happens to model craft and to skirts in small skirt test boxes.

Scaling conditions for wind tunnel model tests

In the case where the craft model tests are carried out in a wind tunnel to determine the aerodynamic resistance coefficients at various heading angles, the R_e of jet flow at nozzles has to be equal to or in excess of the critical R_e (i.e. the R_e for turbulent flow).

In addition, the linear velocity of any moving supporting plate in the wind tunnel has to be equivalent to the craft speed, namely $V_g \propto \lambda^{0.5}$, in which V_g denotes the linear velocity of the supporting plate. Otherwise, the wind tunnel tests cannot correctly simulate the internal and external aerodynamic characteristics. Unfortunately, these test conditions are difficult to satisfy.

In general, supporting plates representing the ground are static and are difficult to move with a high linear velocity to simulate the operational environment of craft. In order to investigate the external aerodynamics and static force derivatives during the wind tunnel tests, ACV models generally have to be in static hovering condition. It is also very difficult to model internal flows, because the flow and specific revolution of model fans are very difficult to scale, as has been discussed above.

For this reason, in general ACV tests in wind tunnels are carried out on solid models, perhaps also with fan and propulsor flows modelled according to Reynolds' law and not in static hovering condition. This certainly leads to errors in the data measured. Determination of the basic body drag and lift coefficients will be accurate enough for normal design purposes. Reference is also normally made to Hoerner's fluid dynamic drag [23] as a starting point. This book gives a wealth of information concerning aerodynamic modelling practice.

Air cushion adiabatic stiffness coefficient, C_b

The coefficient which characterizes the adiabatic stiffness of air cushion can be expressed by

$$C_b = V_c/(\gamma(p_a+p_c)) \tag{9.10}$$

where V_c is the cushion volume (m^3), p_a the atmospheric pressure (N/m), p_c the cushion pressure (N/m) and γ the adiabatic constant for air (m^2/N). This coefficient characterizes the adiabatic change of cushion air in compression due to the heaving, pitch and roll motion of hovercraft running at high speed, which affects heaving stiffness and damping.

The cushion pressure denotes the excess pressure of cushion air, i.e. the difference value between the absolute cushion pressure $|p_c|$ and the atmosphere. At model scale, $p_c \ll p_a$ and so $|p_c|$ can be neglected compared with atmospheric pressure, which suggests that the effect of cushion air compression is too small to change the air flow rate and fluctuate the cushion pressure. This is not true for full-scale craft, especially for larger hovercraft at high speed, because in this case the fluctuation of cushion pressure is large enough that $|p_c|$ is not a small value in comparison with p_a and therefore cannot be neglected.

In practice, therefore, it is very difficult to make the adiabatic stiffness coefficient of models equal to that of full-scale craft, so compressibility of cushion air for models is not similar to that for full-scale craft and will lead to some differences in the seaworthiness results for models compared with full scale. This difference should not be very important except in very large ACV/SES (displacements of several hundred tonnes).

9.3 Scaling criteria for tests of hovercraft over water

Test classification

There are three types of hovercraft test carried out hovering or running on a water surface:

1. *Static hovering test.* Static hovering tests, longitudinal/transverse stability tests of full-scale craft/models on water.
2. *Skirt tests in skirt test boxes with water supporting surface.* Static shaping and dynamic response tests of full-scale craft or model skirts on big/small skirt test boxes.
3. *Experiments of hovercraft in towing tank, etc.* Drag and seaworthiness tests.

Scaling conditions and criteria

Froude number Fn

According to Chapter 3, the wave-making resistance of hovercraft R_w can be written as

$$R_w = [p_c^2 B_c/\rho_w g]\, \boldsymbol{f}(F_{ni}, l_c/B_c) \tag{9.11}$$

or

$$R_w = p_c/[\rho_w\, g\, l_c]\, f(F_{nl},\, l_c/B_c) \qquad (9.12)\ (3.3)$$

where F_{nl} is the Froude number, l_c the cushion length (m) B_c the cushion beam (m) and ρ_w the water mass density (Ns^2/m^4).

Equivalent to the methods used in fast boat research, the Froude similarity has to be considered at first during the tests in water tank, i.e. $F_{nls} = F_{nlm}$. Thus $V_s/V_m = \sqrt{\lambda}$, which is actually the same as the Euler similarity. The other scaling criterion p_c/l_c = constant is also to be considered in experiments.

Reynolds number Re

During hovercraft experiments, just as for conventional ships, the Reynolds similarity or $Re_m > Re_c$ (where Re_c denotes the critical Reynolds number) has to be satisfied in order to accurately predict the friction drag. For this reason, stimulation threads or pins should be mounted on the outside of the bow sidewalls during towing tank experiments with an SES to induce turbulent flow over the whole model sidewall. Such stimulation threads are difficult to mount on the side of the bow skirt of an ACV, but it is found that the disturbance due to jet air escaping under the skirt segment or finger tips creates very turbulent conditions close to the water surface; therefore it is impossible to build up a laminar boundary layer along the side skirt.

Weber number W_e

During consideration of skirt drag and spray formation, we have to estimate the relation between the inertia force of water flow and surface tension of water. The generation process of spray and its size as well as its direction can be determined by the Weber number, which can be written as

$$W_e = [\rho_w\, V^2\, l]/\sigma_t \qquad (9.13)$$

where V is the water flow velocity (m/s) and σ_t the surface tension of water (N/m). Due to the ρ_w and σ_t being constant for both model and full-scale craft, then $W_e \propto \lambda^2$ and $W_{es} \gg W_{em}$, therefore the spray induced by the full-scale craft will be greater than that by models, due to the size of spray particles caused by full-scale craft being relatively smaller than those caused by models.

In one respect, this suggests that the hump drag of full-scale craft will be less than that of models; in another, it demonstrates that a thicker mixed water-air layer might be blown out under the stern lower bag to reduce the stern drag. This spray layer can be seen on full-scale craft, but it cannot be found on models running in towing tanks because of the small Weber number.

Skirt weight per unit area

The dissimilarity of specific weight and Young's modulus of skirts between the full-scale craft and models will cause a distortion of skirt geometry, different skirt dynamic response and added wave drag predicted by the test results. For this reason the repeatability of test results by towing tanks can be poor.

The same craft model with same specific fan speed, tested by the same methods, will obtain different values of drag at different dates and with different test facilities. Sometimes the difference will be as high as 20%. Figure 9.1 shows experimental results

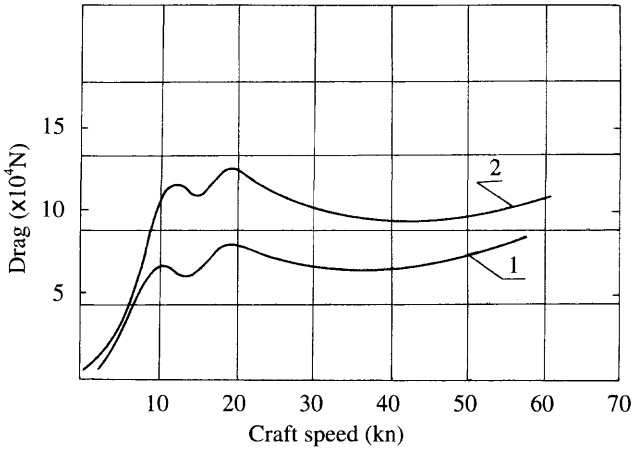

Fig. 9.1 Drag test results for US AALC 150-50 model in different towing tanks: (1) AALC 150-50 model in Davison Laboratory; (2) same model in DTNSRDC Laboratory.

for the same model in different towing tanks at different dates illustrating such differences. It is also possible for different experimental results to be obtained on the same model and same facility; the different condition might only be that the model skirt was straightened before later experiments.

This was also a troublesome problem which faced researchers during the early phase of study in China. In the 1970s, the plastic membrane which was used as model skirt material easily aged and changed the skirt geometry, thus affecting the drag of craft running on calm water and in waves. Thus it could be found that different test results were obtained from the same model, or might be obtained from a different towing tank and at a different date. This is not the case now, as polyurethane-coated fabrics of very fine nylon or aramid woven material are available. These are flexible while being very strong and stable. The scaling problem still remains to a lesser extent, but the ageing and stretching should not be a problem for model tests today.

Non-dimensional characteristics of fans and air ducts

Similar to the experiments with hovercraft models on rigid surfaces, owing to the difference of the non-dimensional characteristic of fans and air ducts, as well as the specific speed between full-scale craft and models, the damping coefficient and natural frequencies are rather different between full-scale craft and models. This affects the motion performance of craft in vertical, longitudinal and transverse directions.

MARIN in Holland have found that for SES models, the dynamic characteristics of the cushion chamber can be modelled more accurately by adding a flexible membrane to what would normally be the hull hard structure between the sidewalls. This allows the cushion natural frequency and damping in heave to be tuned to the expected scaled response.

Table 9.4 Scaling criteria and conditions for use in hovercraft research, design and tests

Item	Scaling criteria	Applicable tests	Applicability of criteria	Influence	Remarks
1	Constant pressure ratio {1}	All tests	Possible	High	
2	Constant *Re* at the jet nozzle {2} or higher than 10^5	All tests	In general cannot be obtained	Low for craft with small flow rate	
3	Dimensionless characteristic of the air ducts	All tests	In general cannot be obtained	Medium	Usual method is to increase revolutions of the fan to make constant Q_i c.f. full scale, i.e. equal flow coefficient
4	Fan constant dimensionless characteristic, or constant fan revolutions {3}	All tests	Cannot be obtained for b, or SES models, but OK for ACV	Medium	As 3
5	Similarity for specific weight of skirt materials {4}	a, b, d, e	Possible	High, should make an effort to obtain it	If no suitable material available then thin glue may be coated on it as balance weight
6	Constant Strouhal number {5}	a, b, d, e	Impossible	Influences the dynamic response of skirt bag and finger so it is very difficult to simulate flagellation and bounce in small models	Also influences the seaworthiness quality of models
7	Constant Π {6}	a, b, d, e	Impossible	As for 6	As for 6
8	Constant *Re* above 10^5 for external flow	a, d, e	Possible	Medium	This condition has to be satisfied during wind tunnel tests
9	$V_g \propto \lambda^{0.5}$ where V_g is the speed of movable model support plate	e only	Impossible	High in the case of simulating internal and external aerodynamic characteristics, particularly at high speed	
10	Constant cushion air adiabatic stiffness coefficient {7}	d, e	Impossible	Less influence for craft with small weight and low speed, otherwise high influence	Tests of intermediate scale test craft have to be carried out if studying large hovercraft
11	Constant *Fn*	d, e	Possible	Serious influence on model test results	
12	Reynolds correlation	d, e	Possible	Serious influence on model test results	In towing tank tests, the Reynolds correlation has to be kept for predicting friction drag from model to full scale
13	Constant Weber's number {8}	d, e	Impossible	Serious influence on spray formation in model tests	

Test types: a static hovering; b skirt box; c wind tunnel; d towing tank, calm; e seaworthiness tests.

Scaling relations: {1} $H_q = p_c/(0.5\ \rho_a\ V_a^2)$ i.e. $V_a \propto \lambda^{0.5}$. {2} $Re_j = V_j t/\gamma$. {3} $N_s = n\ Q^{0.5}/(g\ H_j)^{0.25}$ = constant. {4} $\bar{W}_s = W_s/S \propto \lambda$. {5} $S_r = v/a = \omega l/a$ = constant. {6} $\Pi = E\ \delta\ l_s/\rho_a\ v^2\ S$). {7} $C_b = V_c/(p_a + p_c)\ \gamma$ = constant. {8} $W_e = p_w\ V^2\ l/\sigma_v$ = constant.

Scaling conditions for model seaworthiness experiments

In general, test instruments for seaworthiness are used to measure the amplitude of pitch/heave/surge and the additional wave resistance during seaworthiness tests of hovercraft models in towing tanks. The other three degrees of freedom of yaw, sway and roll are generally fixed. In addition, during experiments the craft are towed at a constant speed but not free flying, therefore the running attitude of models may differ from that of full-scale craft.

When full-scale craft are running in waves, the direction of the propulsor thrust line is fixed with respect to the craft base-line. In the case of towing tank model experiments, the thrust line direction is actually affected by the trim angle of the craft and an additional trim moment acting on the craft may therefore exist, which is very difficult to regulate by balance weights, because the pitching angle of craft running in waves is variable. The result of all this is that motions measured on a model in a towing tank may be different from those measured from free running models in an open tank, or on a lake. Care is needed for interpretation of these results. In general it may be expected that the tank tests will give conservative results for heave and pitch. The surge motions may not be realistic due to the nominal constant speed of the carriage.

9.4 Summary scaling criteria for hovercraft research, design and tests

The scaling criteria and conditions, which should be followed in the experiments mentioned above, are summarised in Table 9.4, in which λ denotes the linear dimensional ratio.

10

Design methodology and performance estimation

10.1 Design methodology

In the next seven chapters we will introduce design methodology for ACV and SES craft. This includes selection of equipment for the major craft subsystems, which forms an essential part of the design process.

In principle, ACV and SES design does not differ substantially from that of conventional ships. Some hovercraft subsystems are also very similar to those in conventional ships, particularly on SES. In the following chapters, we will concentrate on the design features of ACV and SES which differ from the norm. Readers are referred to [21], [129] and [207] as starting points for reference data on craft which have been constructed.

It is assumed that readers will have an appreciation of the general design philosophy and methods for some conventional ship subsystems, such as propeller design, power plant specification, hull structural design, design of ship's outfit and systems, etc. The content of the following chapters will thus be limited to the special needs of ACVs, with appropriate reference to suitable standard naval architecture texts for the remainder, to simplify the treatment here. A number of specialist texts are also listed in the references section following Chapter 16.

In the course of describing the design method for ACV/SES, the subjects which have been introduced in Chapters 2–9 form the basic input, such as air cushion performance, drag, stability and manœuvrability, the force analysis for skirts and the calculation of skirt geometry, etc. which form the basic theories of ACV/SES.

ACV and SES initial design requires three sets of requirements to be input:

- user requirements, such as craft speed, payload, range, economy, weather limitations;
- statutory requirements to be satisfied by the craft, such as stability and safety criteria;
- the main features of ACV/SES which control their principal dimensions, including the lift power, propulsion power and type of propulsors, as well as the main structural style of the hull and skirt, etc.; these are selected by the designer as he/she proceeds.

The various performance parameters and required installed power of a craft can be predicted using the analytical and model test methods presented in Chapters 2–9, once the principal dimensions and some key requirements for performance of craft have been chosen. For this reason, the initial design process of ACV/SES may be grouped in sections as follows.

Stage 1: Establish key design parameters

Specification of criteria and standards for use during the design of ACV/SES are provided as general guidance by national authorities such as the IMO [215], the UK Civil Aviation Authority [200], Canadian Coastguard, US Coastguard, Classification Societies [223], etc. The following criteria are normally specified:

- intact stability criteria;
- damaged stability and buoyancy compartmentation requirements;
- requirements for seaworthiness;
- weather limitation capability;
- requirements for manœuvrability;
- requirements for habitability, such as internal/external noise and vibration level, etc.
- requirements for machinery and control system redundancy.

The initial craft design is checked against these requirements and adjusted as required, prior to completion of the detail design of the craft for construction purposes.

Stage 2: Determination of principal dimensions

- payload specification;
- craft overall dimensions;
- craft weight estimate and distribution;
- parametric studies (as required for optimization purposes).

At this stage general relationships for required power (SHP/tonne knot), craft sizing, etc. are used, based on past experience. The necessary data for this are presented in Chapter 11.

Stage 3: Principal subsystem design

- skirt and cushion system
- lift system
- propulsion system
- selection of main equipment
- initial design of hull structure, etc.

The initial subsystem data will be revised based on data generated for the craft being designed. The methods described in Chapters 2–9 are used to prepare the system analyses.

In this chapter, we will introduce typical criteria and standards for the various design parameters, which allow the designer to continue with determination of principal dimensions in Chapter 11. Some of the design criteria for hovercraft have been discussed in Chapters 2–9, such as relative transverse metacentric height (h/B_c), to characterize the transverse stability of an SES, and the shifting distance of the centre of cushion pressure to characterize the transverse/longitudinal stability of ACVs etc.

There is no single consistent set of standards for ACV and SES design, therefore we take the following documents as the main references during design of hovercraft:

1. some design rules and regulations such as the UK CAA BHSRs and IMO rules [200], [215];
2. safety requirements for dynamically supported marine vehicles [106], [94];
3. some provisional safety requirements and rules published by some countries as [202], [97], [95], etc.

The following discussions mainly concern hovercraft in cushion-borne operation. The craft also have to satisfy the requirements from the rules and regulations for hull-borne operation, which we will not detail because this is similar to the design of conventional ships.

10.2 Stability requirements and standards

In the various rules and regulations available at present, requirements are often not specific to dynamically supported and high-speed craft, the category which includes hovercraft. A large amount of information from model experiments and craft trials is already available which allows us to propose criteria for the safe operation of hovercraft. We outline these below, followed by some discussion of the principal rules available internationally at present, the IMO requirements and the UK BHSRs .

Principal dimensions and parameters

ACV – stability and cushion height

Reference 52 considered that if the air cushion can be compartmented reasonably and a flexible skirt with bag cushion pressure ratio $p_c/p_c = 1.3$ can be adopted, then the skirt height should meet the following expressions:

$$h_{sk}/B_c \leq 0.17 \tag{10.1}$$

$$(z_g + h_{sk})/B_c \leq 0.33 \tag{10.2}$$

where h_{sk} is the height of flexible skirt (m), z_{cg} the vertical height of the CG (m) and B_c the cushion beam (m). In addition, based on statistical data from existing craft, allowable skirt height can be determined as in Fig. 10.1.

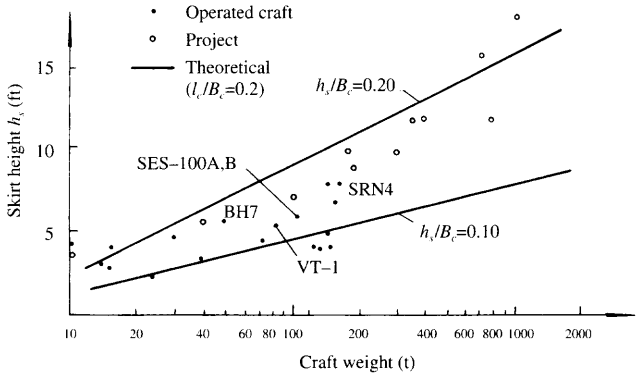

Fig. 10.1 ACV/SES skirt height statistics.

SES – stability and cushion height

The transverse stability of an SES on cushion is closely related to the cushion length/beam ratio, as described in Chapter 5. Based on statistics from previous craft, this should comply with Fig. 10.2. These relationships can be used at the concept design stage, in which the craft principal dimensions have not yet been determined. Figure 10.2 shows that the sidewall thickness ratio of Chinese SES with high L_c/B_c is rather small, but practice proved that these craft, such as the 717-II and -III, have good transverse stability while they are operating in the upper stream of the Yangtze River. For this reason, it is found that the sidewall thickness ratio (B_{sw}/B_c) is not the only criterion to characterize the transverse stability of the SES, but can still be used as a reference for designers during preliminary design.

Transverse and longitudinal metacentric heights

These are very important criteria to characterize the stability of craft, particularly in the case of craft with large cushion beam and at small heeling angles; therefore, in general, designers always take this as the parameter for characterizing the transverse and longitudinal stability. According to [52], they can be written as follows. For ACVs

$$\bar{h}_\theta = h_\theta/B_c \geqslant 0.3\text{–}0.4$$
$$\bar{h}_\psi = h_\psi/l_c \geqslant 1.0\text{–}1.5 \qquad (10.3)$$

For British ACVs, ref. 19 recommended

$$h_{\theta g}/B_c = 0.6\text{–}1.2$$
$$h_{\psi g}/l_c = 1.2\text{–}2.4$$

where $h_{\theta g}$, $h_{\psi g}$ denote the dimensionless transverse and longitudinal metacentric heights of an ACV hovering on a rigid supporting surface.

For SESs, typically the Hovermarine HM-2 for example,

$$h_\theta/B_c = 0.36$$
$$h_\psi/l_c = 0.69$$

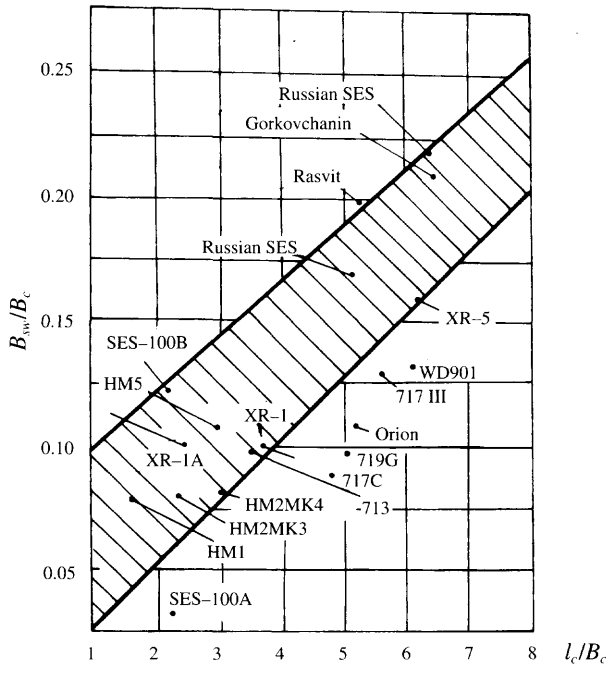

Fig. 10.2 Relative sidewall thickness B_{sw}/B_c and cushion length/beam ratio of SES on cushion. [4]

In Chinese practice during development of ACV/SES, it has been found that the values of these criteria are quite flexible. At the early stage of SES development (1966–79), owing to lack of a calculation method for predicting stability, the SES stability criteria used were wholly dependent upon the relative sidewall thickness (B_{sw}/B_c) as shown in Fig. 10.2. This criterion for characterizing the stability does not uniquely characterize the craft stability, because it does not consider the sidewall draft, the ratio of sidewall displacement and all-up weight, air flow rate and sidewall geometric configuration. For example, the Chinese SES-719G has $l_c/B_c = 5.05$, $B_{sw}/B_c = 0.088$, while SES-717C has $l_c/B_c = 4.94$ and $B_{sw}/B_c = 0.077$, but the transverse stability of the former is far better than the latter, which was proven in the craft trials.

In the early stage of design and manufacture of hovercraft in China, particularly SES, due to the use of thin sidewalls for reducing drag and pursuing high speed, the craft's transverse stability was not satisfactory for open water operation. However they could be operated safely in inland rivers, upstream of the Yangtze River for example, but not the more demanding environment such as in the estuary of the same river.

MARIC has much experience of the effect of various factors on the transverse stability and the operational performance of SES with poor transverse stability. In the beginning of the 1980s, they developed a calculation method for predicting the transverse stability (see Chapter 4, section 2) and subsequently developed comparative evaluation methods to build on this experience.

The relative transverse metacentric heights for Chinese SES are listed in Table 10.1. It can be seen from this table that for SES operating in inland rivers h_0/B_c should be

Table 10.1 Relative transverse metacentric height for several Chinese SES

	Type of craft				
	717C	711-III	719G	717-III	713
Year constructed	1980	1966	1982	1981	1969
Cushion length/beam ratio l_c/B_c	4.94	3.5	5.05	5.7	3.5
Transverse metacentric height h_0/B_c	0.17	0.08	0.306	0.398	0.38
Relative sidewall thickness B_{sw}/B_c	0.077	0.062	0.088	0.13	0.086
Calculation method for transverse metacentric height	Computer. Close to experimental results	Computer analysis	Computer analysis	Computer analysis	Experience method *
Operating experience during trials	Poor	Very poor	Good	Fine	Good

*Offered by Andrew Blyth of UK.

greater than 0.25–0.30 and for SESs running in river estuaries (more exposed conditions), it is suggested that h_0/B_c should be greater than 0.40.

David R. Lavis [57, 92] also presented some statistical material demonstrating the stability of ACV/SES and the capsizing of various ships as shown in Fig. 10.3, in which the hatched zone denotes the capsized conventional displacement ship and hovercraft. It can be seen that the Chinese experimental craft 711-III and 717C are also included in this area. It is possible this is realistic; if these craft are operated at a rivermouth or coast then they would be insufficiently stable.

From Fig. 10.3, it is seen that the suggestion offered by the CAA in the UK, [93] namely all craft have to meet the requirements of $h_0/B_c > 0.4$–0.5, is close to MARIC's experience.

The ratio of skirt height with the cushion beam is not the sole criterion to characterize the stability for ACVs, and designers also have to consider the configuration of both peripheral skirts and stability skirts.

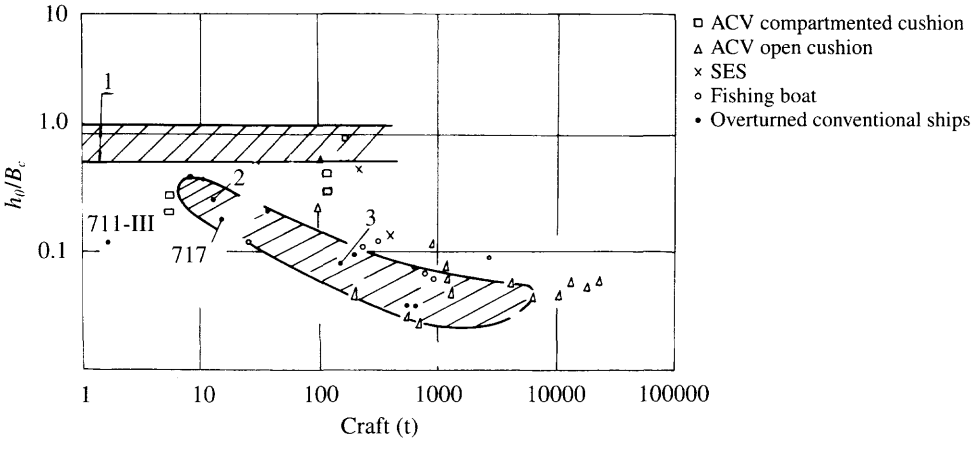

Fig. 10.3 Comparison of initial static transverse stability between conventional ships and ACV/SES: (1) stability range for ACV/SES suggested by CAA; (2) range for overturned ACV/SES (hatched area); (3) range for overturned conventional ships (hatched area).

In the early stage of hovercraft development the main criterion for stability was the craft's skirt height. It was considered that the craft would be safe if $h_{sk} < 0.2B_c$, where h_{sk} denotes skirt height. The designer generally determined skirt height according to statistical references, for instance, the skirt height can be determined by Fig. 10.1 according to the craft weight. From Fig. 10.1, it is seen that the data, which include craft both from China and elsewhere, are closely concentrated. Fig. 10.4 shows the relation between height of craft CG and skirt height. The data points are very concentrated here also. It seems from this that general arrangements for the various ACVs are similar.

Figure 10.5 shows the relation between rolling stiffness of hovercraft with the cushion depth–beam ratio, in which S_R denotes the rolling stiffness, i.e. the relative shifting distance at cushion centre of pressure per degree of heeling angle, which is also related to the relative transverse metacentric height. This is because we have $h_\theta/B_c = S_R \times 57.29$ (shown in Chapter 4).

In Fig. 10.5, curve 1 shows the stability requirements of the UK Civil Aviation Administration (CAA). Curve 2 shows the envelope for relative skirt height, below which no overturning of craft has occurred to date. It can be seen that the CAA requires the ratio of skirt height to cushion beam to be smaller than 0.2. For 'ordinary' skirts, we consider that this requirement is reasonable and practical, but if a responsive skirt with large deformability is adopted, the requirements have to be seriously reconsidered, because responsive skirts generally have lower transverse stability. It is suggested that it is better to judge the stability by relative metacentric height in this case.

Calculation of initial stability for both ACV/SES is obtained by the methods presented in Chapter 4. The stability for a number of craft which have been built are as listed in Table 10.2. Based on this table the following requirements for an ACV may be considered reasonable:

$$h_{sk}/B_c < 0.2 \tag{10.4}$$

$$h_\theta/B_c > 0.35\text{–}0.4 \tag{10.5}$$

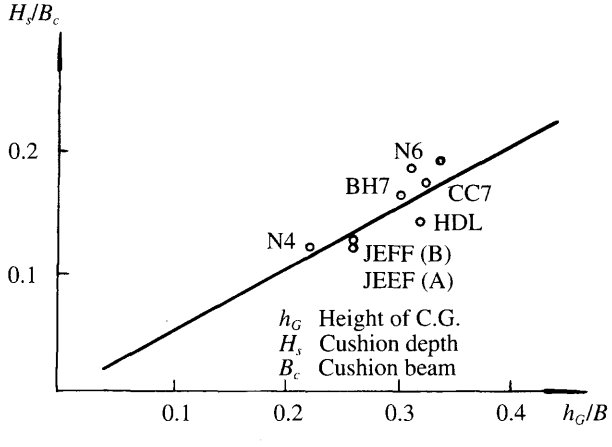

Fig. 10.4 Vertical CG position compared to ACV cushion heights.

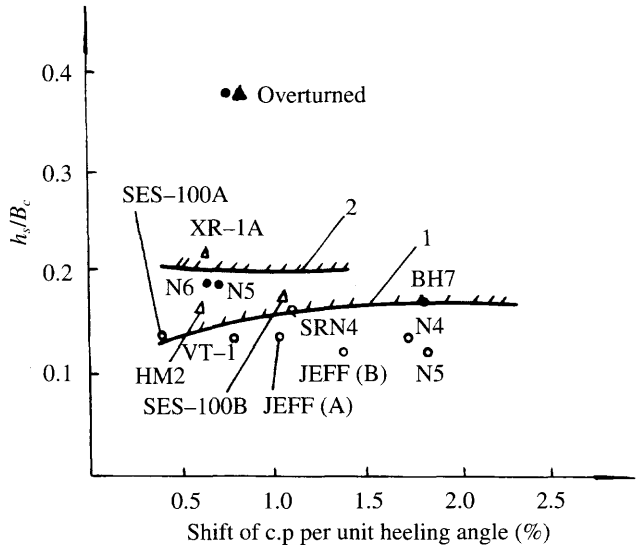

Fig. 10.5 Transverse roll stiffness versus cushion height/width ratio H_s/B_c: (1) stability requirements for ACV/SES proposed by UK CAA; (2) the boundary line for transverse roll stiffness with respect to relative skirt height.

Meanwhile initial stability has to comply with the following conditions:

1. *The requirements for extreme transverse rolling angle.* The transverse stability of a craft has to be checked for all relevant intact and damaged operational conditions on waterways within a distance of 100 nautical miles from the home port. The safety requirement for dynamically supported craft [215] issued by the Intergovernmental Maritime Consultative Organization (IMO) proposes the following:

   > The stability of ACVand SES should be such that the heeling angle should not be larger than 8° with respect to the sea level at any direction of craft at the maximum permitted load running on calm water and wind condition. The initial stability of a craft should be determined in the worst operational environment.

2. During craft turning at high speed, the heeling angle should not exceed 8°.

Table 10.2 Static transverse initial stability of various ACVs

	Craft								
	HD.2	VT.2	CC.7	SR.N6 Mk 1	SR.N4 Mk 2	SR.N4 Mk 3	BH.7	7202	711-III
Country	UK	UK	UK	UK	UK	UK	UK	China	China
h_φ/B_c	0.206	0.286	0.326	0.716	0.475	0.510	0.596	0.470	0.578
h_φ/l_c	0.791	0.573	0.393	2.290	1.140	1.776	1.530	??	0.750
Stability measures	b	b	b	a	a	a	a	a	a

a = Cushion compartmented and skirt lifting system.
b = Cushion not compartmented, horizontal skirt shift system installed.

Requirements for stability at large heeling angles

During estimation of the effect of beam wind on ACV/SES stability designers have to consider the combined action of both wind and waves on craft. In general the wind force is considered as the controlling force. The heeling moment arm due to the wind force can be written as

$$l_m = KV_w S_B (l_w - 0.5T) / (W_v \cos^2\theta) \tag{10.6}$$

where l_m is the arm of heeling moment due to the wind force (m), l_w the arm from base plane to centre of area of wind pressure (m), v_w the wind speed (m/s), S_B the area under the action of wind force (m^2), θ the heeling angle (°), T the draft (m), K the coefficient, it is normal to use $K = 0.726 \times 10^{-4}$, and W_v the volume displacement (m^3).

The SES, due to its large craft beam and the presence of sidewall buoyancy at a large moment arm, is impossible to roll to large angles, therefore 15° rolling angle can be considered as the extreme heeling angle for calculation in the upwind direction, compared to 25° normally used for conventional single-hull ships.

The transverse stability of an ACV under the action of heeling moment due to the wind pressure can be calculated by plotting the data as in Fig. 10.6, which shows the stability curve and heeling moment curve of ACVs SR.N4 and SR.N6, which should satisfy the following conditions:

1. During heeling, the balance angle θ_0 between heeling moment and static stability righting moment does not exceed 60% of the maximum restoring moment arm.
2. $S_1 \geqslant 1.4S_2$.

Reference 52 gave these requirements for craft stability during hull-borne operation, which also defined the requirements for transverse stability of hull-borne craft during loading and lifting cargo. However, hovercraft which capsize are often in

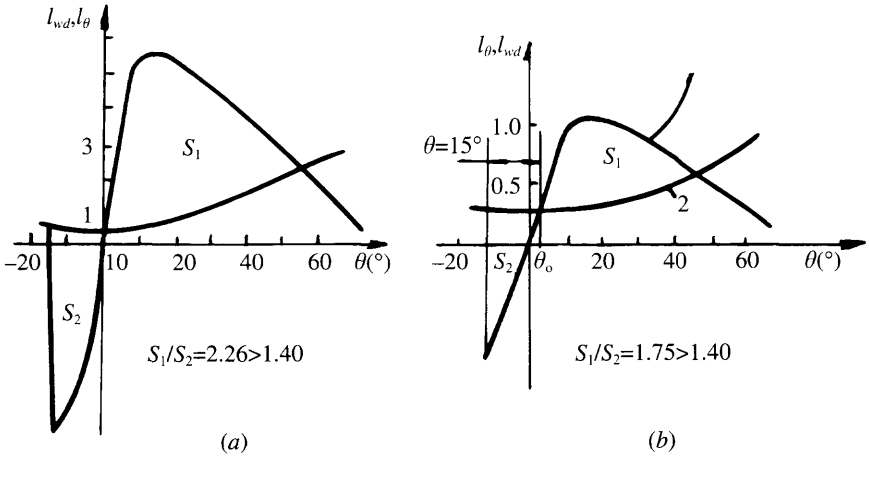

Fig. 10.6 Static stability curves of SR.N6 and SR.N4 in winds, with speed of 28.3 and 33.5 m/s respectively: (a) SR.N4 (weighing 182t); (b) SR.N6 (weighing 9.1t). 1: static stability; 2: heeling moment.

cushion-borne operation as shown in Fig. 5.54, particularly under the action of combined winds and waves, for the following reasons:

1. The transverse stability is lower in cushion-borne operation compared with floating mode.
2. Moment due to the centrifugal force of craft will be increased at high speed.

Research is ongoing on the effect of combined wind and waves action on hovercraft on cushion. This research is not complete; however, the calculation method predicting the roll angle of an SES on cushion in waves can be carried out according to the methods in Chapter 8.

During the investigation of stability, craft with icing on the surface of the craft superstructure may have to be checked. According to the IMO it is suggested that on offshore hovercraft the thickness of the icing layer may be 30 kg/m^2 on all unsheltered surfaces, such as the deck and the top of navigation cabin, etc. and 7.5 kg/m^2 on all perpendicular sides of superstructures. In order to estimate the icing on ropes, handrails and other deck-mounted items it is suggested that the thickness of icing on such surfaces will be the perpendicular icing layer plus 5%, and an increase 10% in moment, caused by such weights.

These standards may be decreased to half in the case where the ACV/SES operates in navigation regions where icing seldom occurs. Owing to the large width of hovercraft, the extreme rolling angle, which is closely related to the relative cushion height (cushion depth/cushion beam) is small, about 15° as shown in Fig. 10.7, because the transverse stability increases rapidly once the wet deck (lowest hull surface) is immersed in the water.

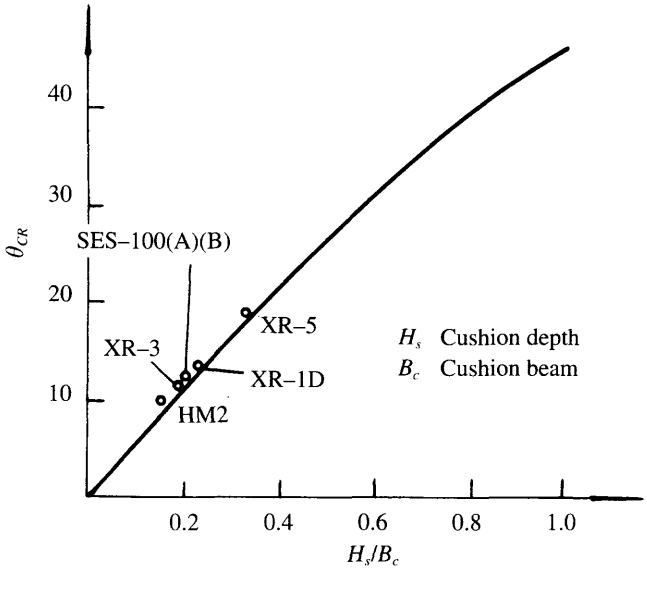

Fig. 10.7 Limiting roll angles of ACV/SES versus relative cushion height.

10.3 Requirements for damaged stability

Calculation of damaged length, width and depth

According to the IMO, hovercraft have to have positive stability and buoyancy from the water surface in the case where the bottom and/or side of craft are damaged. In addition, the heel or trim angles are not to exceed 8° and the final craft freeboard, over any holes which may enter the water shall be at least 75 mm [215, 93]. Based on these requirements, the following data can be used in calculations:

Side damage:	
Longitudinal direction:	$0.1L$ or $[0.03L + 3\text{ m}]$ or 11 m
Depth direction:	No less than 0.2 × width of buoyancy tank for an ACV or $0.2B$ (or 5 m) for an SES,
Vertical direction:	Whole depth of sidewalls
Bottom damage:	
Longitudinal direction:	$0.1L$ or $[0.03L + 3\text{ m}]$ or 11 m
Transverse direction:	$0.2B$, where B is craft width, or 5 m, or less than the space between the sidewalls
Depth direction:	$0.02B$ (or 0.5 m)

The buoyancy of an ACV is provided by the buoyancy tank. When calculating buoyancy, it is suggested that the superstructure is not included as part of the watertight region.

Calculation of damaged stability

Damaged stability and floodability can be obtained with the aid of classification regulations and construction rules of the inland river ship rules of the USSR [86]. The following checks are proposed to be carried out:

1. Based on damaged conditions from 10.3, calculate the floodability of craft in the case of damage.
2. During calculation of craft floodability, the free volume coefficient should be considered as 0.95 in passenger and crew cabins, 0.80 in machinery areas and 0.6 in cargo holds.
3. According to this calculation, the craft have to float and the distances between the waterline and upper deck (or holes) are no less than 75 mm.
4. The transverse metacentric height of a damaged craft should be no less than 0.05 m and the area under the envelope of the transverse stability curve should be positive. The maximum transverse stability arm should be no less than 0.01 m, the range of positive transverse stability should be larger than 30° in the case of symetric immersion and no less than 20° in the case of asymmetric immersion.

10.4 Requirements for seaworthiness

In general, users base the requirements on the weather restrictions limiting hovercraft operations. Thus a route or mission requirement may demand a craft to operate in a certain sea state and wind force.

Stability of craft in waves

The stability requirements of craft under the action of a given combination of wind and waves can be obtained with the aid of calculation methods presented in Chapters 4 and 5, model test results and statistics from existing craft. While there are some simple guidelines which control craft design due to waves (planing surface angles for ACV buoyancy tank side and bow to be greater than 5° when the skirt at one side or bow has collapsed, for example), the majority of requirements are linked to craft performance or passenger comfort.

Speed degradation and craft's ability to accelerate though hump

The speed degradation and hump transition speed of craft in wind and waves are very important, particularly for an ACV. The expression 'craft can be operated in a certain scale of wind and waves' implies that the craft can be operated at an acceptable post-hump speed on cushion in the defined wind and waves, even though the speed may be far less than that on calm water. The speed loss and the ability for cushion-borne operation can be calculated according to Chapter 8 or model experiments to check if the design can satisfy the requirements desired by the users. This will generally determine the required reserve power of the craft.

Slamming forces in waves

Slamming is normally designed by interpolation from special model tests, or from data presented in references such as the BHSRs [79], Chapter B4–2. The slamming pressures of ACV hulls are typically 50% less than that of conventional planing hull, while those at the bow of SES sidehulls are similar.

Du Cane [87] suggests that for planing boats a typical design peak pressure may be about 3.45 bar acting over a small area of 0.1–0.2 m^2, based on measurements from fast patrol craft. Such pressures occur in the forward 30% of a craft's length. Structural members supporting a significant area of the bottom panels, i.e. deep longitudinal or transverse frames, should be designed on the basis of 2.07 bar pressure. Pressures are assumed to fall away linearly to 25% at the stern.

The BHSRs give a rather more detailed analysis procedure based on the following equation:

$$p = 0.0324\, K_2\, V_v\, V$$

where p is the pressure (lb/in^2), K_2 the empirical hull station weighting factor (2.0 at bow, 1.0 at 22.5% craft length from bow), V the craft overwater speed (ft/s), V_v the relative vertical velocity (ft/s) and is

$$V_v = 2.26\,\pi H/(l_w^{0.5}) + V_s$$

where H is the wave height (ft), l_w the wavelength (ft) and V_s the rate of sink (ft/s) (use 2.0 ft/s unless better data are available).

The vertical acceleration is often considered to be the limiting condition for the crews and passengers; however, most damage to mountings, pipe systems, equipment and passenger chairs arises from slamming accelerations and mechanical vibration. Therefore the design requirements have to be chosen carefully; check the slamming acceleration and use this as the limiting condition if appropriate. Vibration dampers are selected according to the requirements discussed in Chapter 14.

During preliminary design, limitations to be considered by designers may be similar to those offered by ref. 52 for ACVs:

1. A well-designed ACV may travel safely on cushion in the waves with maximum wave height of $(1.3–1.5)h_{sk}$, where h_{sk} denotes the height of the flexible skirt. The significant, or 'visible' wavelength will be in the range 0.80-1.0 h_{sk}. However, the speed loss will be high, up to 50% of calm water maximum speed, dependent on wind direction.
2. In the case where maximum wave height is approximately equal to $0.8h_{sk}$ the ACV should be able to travel normally at any course with respect to the direction of the waves, but with a speed loss of about 25%.
3. Due to the $h_{sk}/B_c \leqslant 0.17$ for meeting the stability requirements, so ACVs are able to operate normally on cushion in waves with height of less than $(0.22–0.25)B_c$, i.e. at normal angles of yaw and rates of sideslip

10.5 Requirements for habitability

Habitability criteria directly influence the comfort of crew and passengers and operability of instruments and equipment. Motion amplitude and accelerations control the design of equipment. For example, seat mountings, engine mountings, etc. need to be designed to accept loadings of up to $4g$ [79, 88] due to accelerations and slamming loads, while resilient mountings for instruments need to provide damping for vibration from wave period and cushion natural period oscillations.

Due to the high craft speed and lightweight hull structure, high power plant output and high speed of various rotating machines, such as lift fan, propellers, gear boxes, hydraulic pumps and motors, hovercraft have in the past been characterized by significant on-board vibration, high noise level and large vertical accelerations. Such factors reduce the craft's habitability, which mean the crews and passengers find it difficult to travel, work and live on the craft. Meanwhile, they also influence the operational condition of equipment and apparatus of the craft. Here we will discuss mainly the effect of vertical acceleration and internal as well are external noise levels on the habitability of craft for personnel.

Vertical acceleration

Passenger craft have to satisfy the requirements stipulated by the IMO and the International Standards Organization (ISO), which are based on a large amount of test and statistical information. Figure 10.8 shows thc vertical acceleration data for

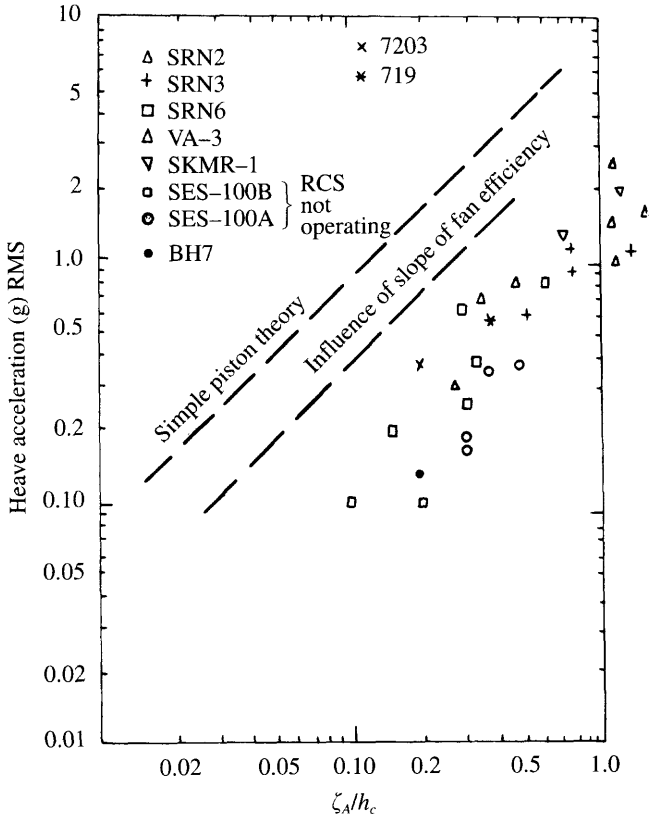

Fig. 10.8 Vertical acceleration of ACV/SES in waves.

various hovercraft (models) collected by Peter Mantle of the USA [4] and stipulates approximately the permitted vertical acceleration for SESs operating within 30 minutes and 1 day. Figure 10.9 shows the test data plotted over the ISO recommendations for human exposure to vibration. Figure 10.10 shows the vertical acceleration frequency response of a typical SES.

The so-called 'cobblestone' effect, i.e. the vertical motion of craft at high speed with high frequency, can be clearly seen. This motion tends to annoy passengers. Figure 10.11 shows the physiological response of a human being at various vibration frequencies and accelerations, which reflect the seasickness sensitivity of humans. Figure 10.12 shows the ISO regulation with respect to the vibration frequency and vertical acceleration, namely ISO standard 2631. Many users take this as the criterion to evaluate habitability of ACV/SES, namely, the operators or users may demand that the hovercraft should meet the requirements of ISO 2631 (certain acceleration level at a given operation).

Designers have to make efforts to satisfy this condition in the calculation of vertical acceleration for designing craft. Figure 10.9 shows the statistical values of vertical acceleration of some British, American and Chinese ACV/SES. From the figure one can see that the ride comfort of ACV/SES (i.e. the vertical acceleration of craft) is

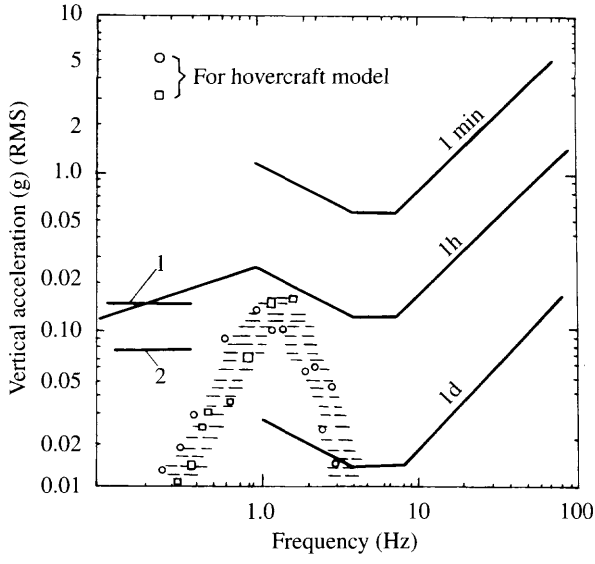

Fig. 10.9 The criteria for ride characteristics: (1) acceptable maximum accleration for SES operating on 30 min journey; (2) acceptable maximum acceleration for SES operating for 1 day.

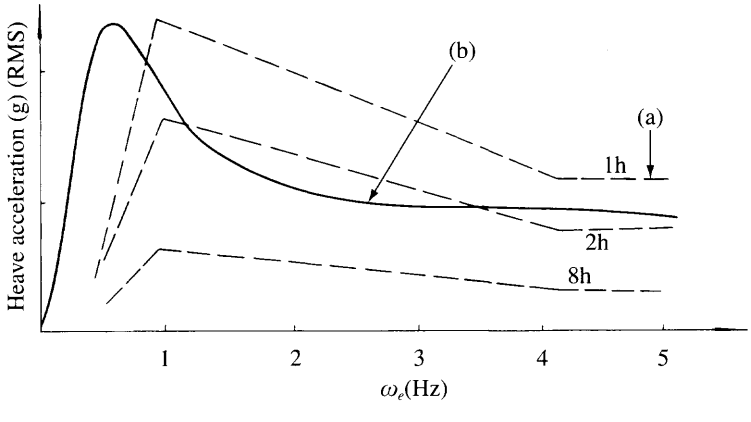

Fig. 10.10 Vertical acceleration for a typical SES in waves: (a) fatigue and efficiency reducing boundary proposed by ISO; (b) response for a typical SES in waves.

rather unsatisfactory at present for journey durations longer than 1 hour, compared with the requirements proposed by the ISO. Further development of responsive skirts for ACVs and ride control systems for SES is therefore required to enable such craft to be fully comfortable for long duration missions.

So far as ACV/SES operating in coastal or estuarine areas are concerned, such as craft weighing 30–100 t, cushion depth 1.5–2.0 m operating in a significant wave height of 0.8–1.0 m (AP1.–88, HM.2, HM.5 of UK and 719-II, 716-III and 7203 of China), the extreme vertical acceleration will be up to 0.2–0.4g and according to the requirement of the IMO, they can therefore only be operated at short range or in

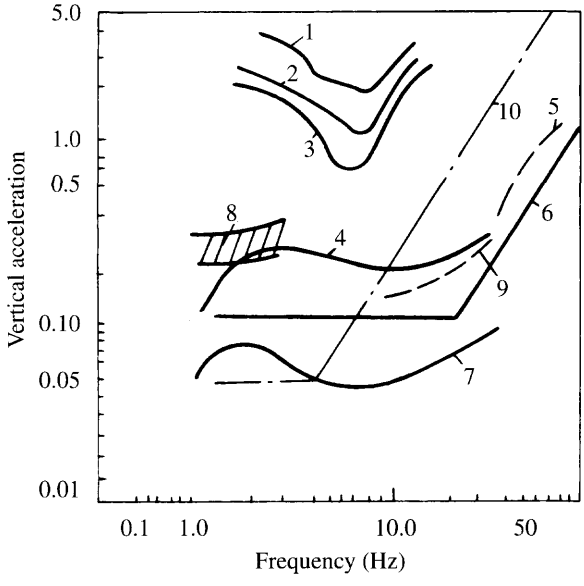

Fig. 10.11 Comfort boundaries of vibration for human being: (1) acceptable level for short time duration; (2) for 1 min; (3) for 3 mins; (4) for 4–20 mins; (5) sight quality reduced rapidly; (6) tolerable for long time duration; (7) comfort limit; (8) vertical acceleration of a typical military ACV in two sea states (weighing 50t); (9) reduced aiming; (10) reduced attention (traced photo).

protected environments, i.e. at the range of 1–2 hours, otherwise passengers will find the motion one uncomfortable.

However, the cobblestone effect also seriously influences the habitability of ACV/SES and thus affects the users' acceptance of hovercraft, because on conventional ships and high-speed catamarans motions are very small while they are running in short waves.

If automatic control systems for improving seaworthiness are applied to the craft, such as the heave attenuation system of US Navy SES-200 or Norwegian Navy MCM SES craft or the automatic control system based on inclined rudders for reducing the roll amplitude of British SES ferry HM.5, then the situation can be improved significantly. For this reason, automatic control systems form an integral part of the design of modern SESs.

Table 10.3 shows the passenger numbers with seasickness on ACV SR.N4 and Table

Table 10.3 The percentage of passengers with seasickness on SR.N4 in operation [89] (measured value)

Wave height	Acceleration (g)	Seasickness among passengers (%)
0.00–0.27	0.0–0.1	0.05
0.31–0.58	0.1–0.14	0.0
0.61–0.88	0.14–0.20	1.1
0.92–1.19	0.20–0.35	0.22
1.22–1.49	0.35–0.50	0.54
1.53+	0.52+	10.3

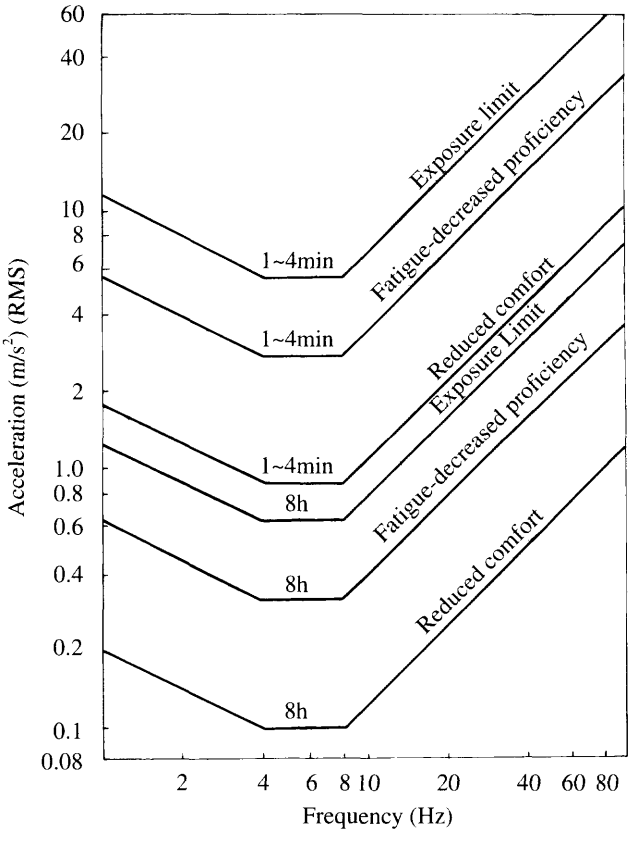

Fig. 10.12 ISO 2631 for toleration limits for acceleration/frequency.

Table 10.4 Motion standards for the surface warships

Subsystem	Motion	Significant single amplitude	Location
Crew	Roll	8°	LCG
	Pitch	3°	LCG
	Vertical acceleration	0.4g	Bridge/wheelhouse
	Lateral acceleration	0.2g	Bridge/wheelhouse
Helicopter	Roll	5°	LCG
	Pitch	3°	LCG

10.4 shows the motion standard for surface warships; thus it can be seen that the seaworthiness of ACVs needs careful design by incorporation of responsive skirts.

Noise

Nowadays there are no regulatory requirements for ACV/SES, but the high internal/external noise level of ACV/SES in comparison with conventional ships has been and still is one of the principal reasons for preventing or limiting ACV/SES penetration into the market [190]. This is why ACVs cannot operate in Hong Kong, Germany and the Netherlands without special dispensations being granted by the authorities.

Figure 6.4 shows the slogan protesting at the arrival of the British AP1.88 ACV in Germany when it went on trials for a ferry company.

Hong Kong island is so small that the ACV terminal could only be set up close to downtown Hong Kong, therefore ACVs will be not permitted by the Hong Kong government to operate near the island. Fortunately after making considerable design efforts through the 1980s and early 1990s, both the internal and external noise levels have been significantly reduced for amphibious ACVs.

The following factors influence noise levels in cabins.

General arrangement

The internal noise level can be reduced if the noise source, such as the main engines, fans and air propellers, can be separated from the passenger cabins either by isolation or by distance.

The isolation of cabins

Machinery bays with remote control and passenger cabins with noise insulation are suggested to improve noise levels.

Insulation (1). Fine noise damping and noise-absorbent material have to be used as isolation material in passenger cabins.

Insulation (2). Some noise isolation and vibration isolation measures should be adopted in the cabin areas close to the propellers.

The noise source in cabins should be decreased as low as possible

If some noise source might be located in passenger cabins, for example gearboxes and hydraulic pipelines, then they have to be isolated with a noise insulation.

Vibration damping

Mounting of main and auxiliary engines by vibration dampers should be considered.

After making efforts to reduce noise level, such as reducing the noise level of gearboxes and hydraulic pipelines, vibration isolation for the main engines, packing the volute of centrifugal fans with isolation material, etc. the cabin noise level can be reduced to under 70 dBA (Table 10.5).

After making efforts to reduce noise, the cabin noise of SES version 717 also dropped more than 10 dBA to 79 dBA. If the bow fan is not operated then the cabin noise in the navigation cabin and the fore part of passenger cabins can be reduced to

Table 10.5 The noise level at various positions on a number of craft

	Craft					
	HM.2 Mk 2	HM.2 Mk 3	717A	717C	719	719-II
Measurement position						
Middle of passenger cabin	94	83.5	93	75	85	73
Front of passenger cabin	96	83		83		
Rear of passenger cabin	93	86.5		80		
Bridge/wheelhouse	92	80.5	94	89	80	65

under 70 and 76 dBA respectively. Thanks to installing carpets, sound-absorbing plates and other sound-absorbing measures in passenger cabins, thc noise level was reduced 5 dBA from the rear part to side part of cabins with only 2.5 m of space between them.

So far as the passenger SES with steel hull version 719 is concerned, after a series of measures had been taken, the noise level of passenger cabins and navigation cabin was reduced by 12 and 15 dBA respectively, to reach the low noise level of 65 dBA. Such measures included packing the volute of lift fans by isolation material, sound-insulated passenger cabins, vibration isolating engine mountings and thickening the sound-tight layer of passenger cabins, etc.

These noise levels may be compared with modern high-speed catamarans for passengers and vehicles, in the 40–70 m class. Typically passenger cabin noise levels are 70–75 dBA. When sound levels are at this level in passenger areas, the vibration of engines and gearboxes becomes more noticeable than the noise. Once the cabin has a significant number of passengers, the noise of their conversation will tend to mask machinery vibration.

With respect to the ACV, thanks to the use of such measures and in addition using ducted air propellers and coating the duct with viscous elastic sound-absorbent material, the noise level in passenger cabins also drops noticeably.

Noise levels in the passenger cabins of small ACVs version 711-IID, 7202, etc. are approximately 90–95 dBA, but with the measures mentioned above implemented, the noise levels of passenger cabins of updated Chinese ACV versions 7210 and 716-II (ACV weighing 20 t) etc. dropped to approximately 80 dBA. While acceptable for short journeys, these noise levels need further reduction. Recent studies by some manufacturers of utility ACVs have shown that by attention to detail, noise levels in the range of 75 dBA are practical for an amphibious ACV. This progress on noise reduction is encouraging and demonstrates that the disadvantages of ACV/SES with high internal noise level can be lessened with effort.

Figure 10.13 shows the comparison of noise level in cabins between hovercraft and other forms of transport, thus it can be seen that they are close to each other. With respect to the external noise level, there are no large differences between SES and conventional high-speed craft, but the external noise of an amphibious ACV is higher than other craft because it uses air propellers. The critical problem is reducing the air velocity at the propeller blade tips. For example, originally the velocity at blade tips of British ACV version SR.N6 was about Mach 0.86. After taking some measures such as replacing the single air propeller by double propellers to reduce the blade loading, the velocity at blade tips dropped to Mach 0.49, which resulted in the air noise level reducing by about 15 dBA. In addition, the uniformity of inflow to the air propellers and distributions in the downstream of the air propellers will also affect the propeller noise. In recent years ducted air propellers have been more widely used on ACVs and give a reduction of about 6 dBA of noise. In beam winds additional noise due to the non-uniformity of air inflow may result.

As yet there are no definite standards for the noise level in cabins of ACV/SES and designers normally take the requirements from operators into account in design, together with ship's rules. Table 10.6 shows the rules for cabin noise of various ships for reference. Table 10.7 lists the noise level in the passenger cabin of some Chinese and Western ACV/SES.

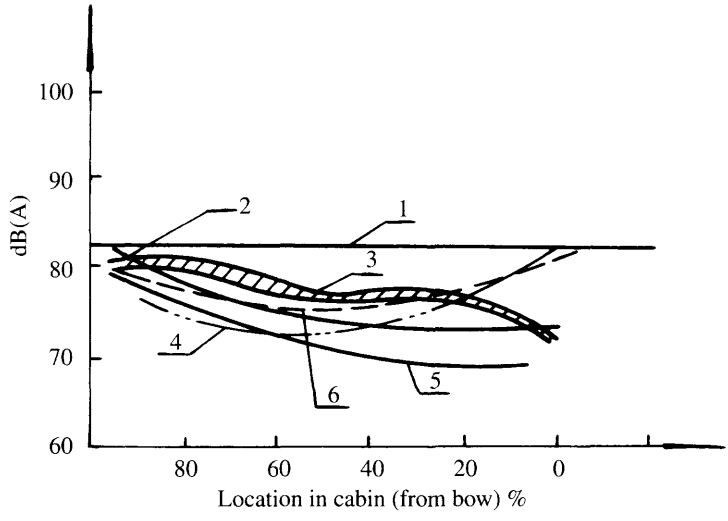

Fig. 10.13 Comparison of internal noise between hydrofoil craft, ACV/SES and various transportation forms: (1) internal noise for bus with 47 seats at speed of 90 km/h; (2) noise in the lower cabin of a jetfoil; (3) cabin noise for four-engine wide body aeroplane at cruising speed; (4) internal noise for 1980 Mazda station wagon at 90 km/h; (5) noise in upper cabin of jetfoil; (6) cabin noise for SES model 717.

Table 10.6 The rules for cabin noise level on the ships of various countries

	Country			
	UK	Japan	USA	Germany
Effect date		01.07.75	01.03.68	01.06.68
Suitable range	Shipping	Ships < 3000 t	Merchant ships	Ships with German crews
M/C room control area continuous	75	75		
M/C area non-continuous	110			110
M/C area continuous	90	85	90	90
Accommodation	60	60–65	56	65
Navigation cabin	65		65	60
Bridge	68			65
Radio room	60			60
Kitchen	70			
Recreation areas	75			
Dining rooms	75			65
Unsheltered deck	75			
Corridors	80		61	

Table 10.8 lists the requirement for external noise level in the UK. The external noise levels for Chinese ACV model 711-IID are 95 dBA at 80 m from the air propellers, and 62 dBA at 150 m, thus it can be seen that 711-IID is able to meet the UK requirement, because of the low tip velocity of the air propeller blades.

Table 10.7 The passenger cabin noise level for some high performance vehicles (dBA)

Craft	Hydrofoil	Hydrofoil	717C	719	719-II	711-IID	Griffon	AP1.88	W 120		
Type	Built 1960	Design	SES	SES	SES	ACV	ACV	ACV	Catamaran	Rules	Rules
Country	China	China	China	China	China	China	UK	UK	Norway	USSR	Japan
Measurement position											
Machinery bay	118	118		122	114		102			90–95	95
Front of passenger cabin	105–107	73	83	85	73	95		88	72	50	70–80
Rear of passenger cabin	110	80	80	98	80			88	79		
Bridge/wheelhouse		63	89	80	65		85	78		55–60	65

Table 10.8 Classification for external noise level in the UK

Location for measured points	Noise level (dBA)	Classification
152 m from ACV	70	Quiet
	80	Medium
	100	Noisy
	105	Very noisy

10.6 Requirements for manœuvrability

Since there is no difference in the manœuvrability between the SES and conventional fast boats as well as catamarans, the requirements discussed in this paragraph are for ACVs. The design issues for manœuvrability of an ACV are outlined below.

The turning diameter of an ACV at high speed

It is normal for an ACV to have sufficient turning moment from its rudders to spin the craft while travelling in a given direction. Turning is therefore a matter of generating a given side-slip while maintaining power. Assuming that this does not create stability problems, the turn radius is controlled by the thrust as a proportion of the craft total mass. The main design issue is for the designer to determine the safe envelope of operation for the craft (speed, sea state, wind, maximum safe rate of turn). If a craft may be operated safely at maximum speed with a side slip of 90°, the thrust will determine turn radius at the given speed. Determination by analysis or model tests of the maximum safe angle of side-slip in the design sea state will therefore give advice on the craft's safe operation envelope.

The course-keeping ability and handling of craft at post-hump speed

ACV downwind and down-wave performance is the most critical issue. Since control forces depend on propulsor thrust level and an ACV is normally aerodynamically stable facing into the wind, it will normally tend to broach to if power is reduced, and come off hump. The ability to trim the craft well bow up helps minimize this, so elevators can be useful in this respect. Intermittent application of power can assist, as can tacking across the wind.

In calm conditions above hump speed, ACVs are sensitive to application of control forces. If a prototype shows instability (not able to travel in a steady straight line) it may be necessary to increase the effective vertical fin area at the stern (see guidelines in Chapter 6).

The course-keeping ability of an ACV under quartering or beam winds

In side winds an ACV will operate with a steady yaw angle (or rotated pylons in the case of craft such as the SR.N4). This is not usually a problem until the craft has to perform slow-speed manœuvring at a hoverport or other special requirements, for example, the capability of an ACV running into landing craft dock, etc. Improvements for slow-speed manœuvring can be made by installing rotating bow thrusters, or rotating propeller pylons. Hoverport design can also assist craft operation [91].

Table 10.9 Capability for obstacle clearance, climbing banks and clearing canals [48]

	Obstacle width/L_c	Obstacle height/H_c	Required speed Fr
I Landing on bank			
1. Steep bank, approach vertical bank from at least 5 craft lengths	Unlimited	0.8	0.6–0.8
2. As 1, but slope 1/ 1.4	Unlimited	1.0	0.6–0.8
3. As 1, but slope 1/ 2	Unlimited	1.6	0.6–0.8
4. As 1, but slope 1/ 3	Unlimited	2.5	0.6–0.8
II Launch from bank to water			
1. Sharp bank approach vertical bank from at least 6 craft lengths	Unlimited	1.2	0.8–1.1
2. As 1, but slope 1/ 1.4	Unlimited	1.6	0.8–1.1
3. As 1, but slope 1/ 2	Unlimited	2.5	0.8–1.1
4. As 1, but slope 1/ 3	Unlimited	3.3	0.8–1.1
III Obstacle clearance			
1. Steep obstacle	Unlimited	0.7	0.6–0.8
2. Smooth bump	Unlimited	0.6	0.6–0.8
IV Clearing Ditches			
1. Rectangular ditches	0.00–0.05	Unlimited	0.6–1.7
	0.05–0.1	1.6	0.8–1.3
	0.1–0.3	0.8	0.8–1.3
	0.3–0.5	0.7	0.6–1.1
	0.5–1.2	0.4	0.6–1.1
	1.2–1.4	0.7	0.6–1.1
	1.4 +	0.8	0.6–1.3
2. Ditches with sides sloped about 1/6	0.0–0.1	0.5	1.1–1.3
	0.1–0.7	0.8	1.1–1.3
	0.7–1.0	1.0	1.1–1.3
	1.0–1.3	1.5	1.1–1.3
	1.3 +	1.6	1.1–1.3
3. As 2, but slope 1/12	0.0–0.1	0.4	1.1–1.3
	0.1–0.7	0.6	1.1–1.3
	0.7–1.0	0.8	1.1–1.3
	1.0–1.3	1.0	1.1–1.3
	1.3–2.3	1.2	1.1–1.3
	2.3 +	1.6	1.1–1.3

The manœuvrability of an ACV operating on ice

ACV drag over ice is governed by aerodynamic drag. Reduced skirt drag can allow much higher maximum speeds. This can also affect trim, due to aerodynamic lift effects. The control surfaces will be relatively more powerful and so the craft will be more sensitive to drive. Slowing and stopping will also take longer. Once again the principal design issue is to identify the safe operational envelope for craft rate of turn, side-slip, etc.

In recent years, the development of control surface design has been very innovative, so a number of control surface types and mechanisms are available for designers' selection. The requirements of manœuvrability of an ACV are a trade-off since additional installed power tends to reduce transport efficiency. Designers can select several optional layouts based on the requirements of users, then make computer analysis and free-flying model tests to make a final decision.

10.7 Obstacle clearance capability

The obstacle clearance capability of an ACV is almost completely dependent on the skirt height; ref. 48 gave some test data for reference as shown in Table 10.9. Based on these data and the requirements for obstacle clearance capability of prospective users, designers can specify the skirt height of an ACV.

11

Determination of principal dimensions of ACV/SES

11.1 The design process

Initial determination of principal dimensions and key design parameters is the core of overall craft design. We will introduce here a methodology for this using a number of relationships which have been arrived at by successful experience. Once these initial data have been defined, the vehicle general arrangement, initial performance estimation, power plant selection and design of lift systems, skirt, propulsor and hull structure can be started.

Hovercraft design is similar to that of conventional ships, as also is the process of progressive approximation, namely a sequence of initial concept design, preliminary design, detail design and preparation of production drawings and documents. This chapter aims at the first stage – identification of the basic concept.

The design requirements are dependent on the craft's role. It might be military, commercial, a special utility role, or recreation. The controlling parameters will also differ according to the performance requirements for stability, damage resistance, heavy weather performance, seaworthiness, manœuvrability, restrictions on engine selection and limitations on principal dimensions.

There is no one universal approach to vehicle design, but we recommend the following sequence:

1. Define the role parameters (including payload, performance, any special requirements).
2. Make initial weight estimate (using experience-based rules).
3. Select dimensions.
4. Estimate powering and performance.
5. Check standards, rules and regulations.
6. Compare to suitable existing craft.
7. Begin design optimization through detailed analysis.

11.2 Role parameters

To make a start, consider some key attributes for craft within the different major roles:

Commercial

An ACV or SES for commercial use will require to deliver a given quantity of passengers or cargo between two points at the highest possible transport efficiency (payload × speed / installed power). Since payload such as passengers is of low density, the space requirements are most important to define.

In addition, the craft should be able to deliver the payload with maximum efficiency throughout the year, i.e. performance degradation in heavy weather should be within acceptable limits for the particular route (if it can be better than the competition, so much the better). It is not sufficient to have high calm water speed; rather, performance must be matched to the route characteristics so that a regular timetable can be maintained.

Craft route length is another important parameter, since this will control the fuel load and requirements associated with passengers such as catering, shopping facilities for larger craft and both passenger and crew accomodation if the route is associated with overnight travel.

Finally, commercial craft may require aesthetic appeal in order to attract customers and retain them. This requires attention to quality of internal outfitting and to external styling. At the definition stage of an ACV or SES this means including a margin of weight.

Military

Military craft have similar requirements to commercial vehicles, except that a round trip may well be measured in days rather than hours and include periods of operation at different speeds. It is necessary therefore to define the mission profile rather than simply the cruise and maximum speed requirements as for a commercial craft. Some craft may have multiple missions, in which case each one needs to be defined and the controlling mission identified for initial dimensioning purposes.

The functional payload for a military craft is defined by its permanent outfit plus consumables required for a particular mission, and operating crew. Permanent outfit may include military 'hardening' in the form of shell proof panels, additional structural compartmentation, stealth adjustments to the structure etc. At the initial stage, a margin of weight should be identified.

Utility

Utility craft generally have a low utilization, so that transport efficiency is not so important as the ability to deliver the payload for the defined task or range of tasks in a reliable manner and to have lowest practical annual fixed operating cost. A simple craft needing little maintenance is desirable.

Utility craft will be used at times beyond normal design capacity, perhaps extreme

weight (in lighter weather), more bulky load, or in extreme environmental conditions. At the initial stage of design it is therefore best to maintain a substantial margin for powering and to check the performance outside the normal envelope.

Such craft are also often used in the floating mode. Deck space, access to the deck edge, stability for lifting equipment on board and off-cushion manœuvring are all parameters which need specification at an early stage.

Recreation

Craft in this category are normally specified by the extreme performance within a particular role. A racing craft will require much higher installed power than a craft used for cruising or expeditionary purposes. On the other hand, the latter craft will have space, payload and stability requirements which a racing craft is not limited by.

Small craft are greatly affected by the mass introduced by enclosed cabins. At the same time it is likely to be difficult to provide full standing accommodation. Personnel access to such craft will normally be by climbing over the side deck structure. This may be the highest loading for that area. The designer will need to look at a number of alternatives to balance these requirements and obtain the most effective ACV design. At the initial stage, include a margin for unknowns, and refine at a later design stage. Experience-based guidelines are given in reference 201.

11.3 Initial weight estimate

In designing a craft, the first task is to identify all the relevant components of weight:

$$W = \sum_{i=1}^{n} W_i \tag{11.1}$$

where

$$W_i = f_i(L_c, B_c, H, N_e, R, p_c, \ldots)$$

where W is the all-up weight of the craft, W_i the weight of various subsystems, L_c, B_c, H the cushion length, beam and height of the craft and N_e, R, p_c the engine power, range of the craft and cushion pressure respectively.

Once the designer has listed out the key design parameters, it is possible to estimate these components with reference to previous practice. Example data are presented in the tables later in this chapter. It should be noted that since these data are based on earlier craft, they should be considered the starting point with which the actual design data will eventually be compared.

We begin by introducing a number of different classifications of weight components and data for craft which have been built which should serve as a benchmark to start a craft design. We will continue by showing a number of methods used by different design groups to prepare initial estimates using such historical data. Some expressions for predicting the weight of various groups and items obtained by the regression method in some references may be suitable for the Western world, but not in China or other

countries. Care should therefore be taken in using this information. In addition the classifications of craft weight are different for various design groups in different countries. For this reason, at first one has to understand their different approaches to weight classification of ACV/SES in order to analyse and use the information obtained from them. So we summarize different weight categorisations below

The procedure to follow is first to check through the weight category listings and identify the major known components. Initial craft sizing will be based on a simple fraction of craft total weight, so at this stage it is a matter of checking the difference between the known weights and the weight fractions. The detailed item weights can gradually be added in as the design progresses. At the end of the preliminary design, a detailed list should be available and the first estimate of available weight margin prepared. If this is felt insufficient at this stage, it can be arbitrarily increased before optimization is carried out.

Weight classification of hovercraft in MARIC

The weight classification below is used by MARIC:

$W1$ hull weight including main hull structure, superstructure, bow/stern ramp structure, landing pad, air propeller ducts and their mountings, engine mountings and their strengthened structure, various bearings and mountings, etc.;

$W2$ outfit weight including anchoring equipment, rudder and their handling equipment, mast, ladder, etc., cover of windows and doors, retractable equipment for ramp, life-saving and fire-fighting system, cabin equipment, floor and isolation, painting, etc.;

$W3$ power plant: including main engine, machinery equipment such as the main reduction gearboxes of the main engine, reduction gearbox for lift fan, radiator for lubrication oil system, air filter, remote control system, fuel supply tank, pipeline, hydraulic and propeller pitch controlling system, shaft system, propellers, lift fans, etc.;

$W4$ electric system: including batteries, electric generators, electric transmission and distribution system, starting system for engine, illumination system, communication equipment, navigation equipment, rectification equipment, cables, etc.;

$W5$ weight of skirt and joints;

W' light weight of craft, where:

$$W' = W1 + W2 + W3 + W4 + W5 \tag{11.2}$$

$W6$ weight of weapons, passengers and luggage in the payload:

$W7$ weight of crew and luggage, provisions, fresh water, supplies, etc.;

$W8$ weight of fuel, lubrication oil;

$W9$ liquid load on the craft, such as bilge, fuel, oil and water in the pipelines and engines;

$W10$ reserve displacement.

W_{op} operating weight of craft, including disposable loads:

$$W_{op} = W' + W7 + W8 + W9 + W10 \tag{11.3}$$

Weight classification of hovercraft in USSR [52]

Since ACVs are made in aircraft manufacturers' plant and SES are made in shipyards in Russia, two different kinds of weight specification have developed.

Weight classification of hovercraft in shipbuilding industrial ministry of the former USSR

$$W = W1 + W2 + W3 + W4 + W5 + W7 + W9 + W11 + W12 + W13 + W14 + W15 + W16 \quad (11.4)$$

where

- $W1$ hull weight: metal hull, strengthening structure, mountings, deck equipment coating, painting, isolation and cabin furniture and equipment;
- $W2$ weight of ship equipment: rudder, anchor, mooring, life-saving and crane equipment, mast, rigging, flexible skirt, ramp, etc.;
- $W3$ weight of systems: bilge system, fire-fighting system, water supply system, sewage system, sanitary system, air conditioning, air duct system, heating system, hydraulic system;
- $W4$ machinery: main engine, transmission system, starting system, auxiliary engine, propulsor and other system for power plant;
- $W5$ electric system: internal communication system, handling system;
- $W7$ weight of communications equipment: radio technical equipment, telecomunication and navigation equipment;
- $W9$ weight of spare parts carried on board;
- $W11$ reserve weight for displacement and stability;
- $W12$ fixed weight of liquid: residual liquid in hull, fuel oil tanks and in engines as well as in the pipes of various systems;
- $W13$ weight of provisions;
- $W14$ weight of crew, provisions, fresh water and other consumables;
- $W15$ weight of cargo or passengers;
- $W16$ weight of fuel, oil and fresh water.

Weight classification of hovercraft in aviation industrial ministry of the former USSR

$$W = W1 + W2 + W3 + W4 + W5 + W6 \quad (11.5)$$

where

- $W1$ weight of hull structure: wing, fuselage, landing gear, coating;
- $W2$ power plant: engine, propeller, pylon, engine system, exhausts and silencers, air intake, drive system;
- $W3$ weight of equipment and handling systems: electric apparatus, hydraulic system, pneumatic system, aviation navigation equipment, telecommunication equipment, control system of aircraft, safety system, ice and fire-protection system, oxygen system, air conditioning, noise and heat isolation facilities and cabin furnishing;
- $W4$ equipment weight and working load: crew, fresh water, provisions, life-saving

equipment used in $W2$; the fuel weight includes residual fuel oil and working liquid, i.e. $W8$ and $W9$ from classification 1 are considered together and payload includes spare parts and tools, giving the simplified definitions. Items $W1$ to $W4$ are the same as used at MARIC.

$W5$ fuel weight including operational and supplying fuel;

$W6$ payload including passengers, luggage and cargo (≡ MARIC $W6$, $W7$, $W10$).

Weight classification of high-speed marine vehicles in Western countries

Hovercraft weight terms [4]

$W1$ hull (or structure): base structure, plate, frame, stringers scantling, decks, foundations, fittings, superstructure, doors and closures ($W1$);

$W2a$ auxiliary systems: fuel, heating, ventilation, fresh water, ship's controls, rudder, cushion seals, plumbing, oil, fire extinguishing, drainage, ballast, mooring/anchoring ($W2$);

$W2b$ armament: weapons, mounts, ammunition stowage, handling system, special plating (part of $W2$ for a military craft);

$W3$ propulsion and lifting systems: engines, turbines, propeller fans, gearboxes, shafting, drive systems, associated controls, nuclear plant, associated fluid ($W3$);

$W4a$ electric: power generator, switching, lighting, load centres, panels, cables ($W4$);

$W4b$ communication and control: communication (internal, external) and navigation equipment, military electronic computers, displays ($W4$);

$W2/5$ outfit and furnishing: hull fittings including skirt system, marine hardware, ladders, furnishing, boats and rafts, life jackets, storages, lockers, painting, deck covering, hull isolation, insulation, commissioning equipment, radiation shielding ($W2 + W5$).

The total of these items is equal to the light displacement or 'empty' weight of the craft including all fixed equipment (W').

$W6/10$ variable load or useful load: operating personnel and effects, cargo, freight, fuel, passengers, luggage, water, ammunition, aircraft, stores, troop provisions ($W6$ to $W10$).

Full load displacement or load displacement or gross weight or all-up weight are the sum of empty weight plus the useful load.

This breakdown is very similar to the MARIC listing (see item numbers in brackets), splitting items in more detail which relate to military equipment, while combining the skirts with outfitting and not breaking down the payload.

Weight classification used for high-speed boats

This may be defined as follows:

standard bare weight + customer equipment weight	=	basic weight
+ variable loads + expendable loads + payload	=	operating load
+ usable fuel	=	all-up weight

The detailed breakdown of these items, which need to be defined, are as listed below:

1. *Standard bare weight (equivalent to hovercraft terms W1 + W5 part of W2, W3, W4)*
   Weight of structure, power plant and systems
   Oil (turbine engine only)
   Full hydraulic/pneumatic/cooling systems, etc.
   Essential standard equipment common to all customer requirements
   Unusable fuel and other non-consumable liquids (ullage)
   (assume includes all items under MARIC *W*1, identified items under *W*2, *W*3, *W*4 and the skirt systems, *W*5)
2. *Customer equipment weight (part of W2, W3 and W4)*
   Flight crew seats
   Flight crew emergency equipment
   Soundproofing, trim, partitions, floor, covering, etc. in payload areas
   Passenger seats, tables, lockers and other furnishings
   Heating, ventilating and air conditioning
   Toilet and washing facilities
   Galley facilities
   Domestic water supply (in toilet)
   Fire precautions in payload areas
   Marine equipment
   Life rafts and containers stowage, life-jackets and stowage
   Radio, radar and navaids
   Intercommunication and internal broadcasting
   Electrical racking
   Signalling equipment
   Weapons
   Environmental equipment
   Long range tankage and system
3. *Variable load (W7)*
   Crew
   Crew baggage and equipment, purser's equipment, role equipment
   Non-consumable liquid ballast, oil (piston engines only)
4. *Expendable load (other than usable fuel) (W9)*
   Domestic, humidifying, windscreen water
   Other liquid or gaseous consumables
   Ammunition
   Food, drink, bonded stores, etc.
   Boarding parties and their equipment
5. *Payload (W6)*
   Passengers, vehicles, freight
6. *Usable fuel (W8)*
   Main fuel, reserve fuel, long-range fuel

This breakdown distributes the components of the light weight differently and since it is derived from fast boat practice, does not define the skirts specifically. The payload components are defined in a very similar way to MARIC.

The weight distribution of some British ACV/SES and US SES are shown in Tables 11.1–11.3. Principal dimensions and features of some Western ACVs are shown in Table 11.4. The weight breakdown of a Chinese SES and ACV are listed in Table 11.5. All of these can be referred to and analysed by readers during preliminary design, to obtain estimates for the various weight components identified above. It is recommended that where a component is known to be needed, if relevant reference data are not available, then a simple estimate should be made. To aid this process a checklist is included at the end of this chapter, based on the MARIC weight breakdown (see Table 11.7).

11.4 First approximation of ACV displacement (all-up weight), and estimation of weight in various groups

The first approximate calculation of craft all-up weight (displacement) is carried out by determining the payload and relating this as a percentage of the all-up weight. The logic illustrated in Table 11.6 may then be used to develop the design. Where possible, the relationships presented below are referenced to the weight breakdown descriptions in section 11.3.

Payload fraction (*W6* and *W7* combined)

At the initial stage of hovercraft design, it is difficult to separate the components of *W6* and *W7* and so a combined estimate is given here. The designer will usually prepare a more refined estimate at the detailed design stage.

$$W6 = K14 \times \text{AUW} \tag{11.6}$$

where $K14$ is a coefficient. Typical values are

0.15	for small ACV	(AUW < 10 000 kg)
0.16	for medium ACV	(AUW < 30 000 kg)
0.20	for large ACV	
0.20	for small SES	(AUW < 60 000 kg)
0.25	for large SES	

An initial cross-check can be made here against the designer's desired payload. For passenger craft it is reasonable to use 200 kg per passenger including luggage. Other payloads should be directly defined, for example cars, trucks or container masses. For fuel payload, initially use $0.25W6$ for craft with limited range, $0.5W6$ for long-range craft. This can be refined once the first estimate of power has been made and based on mission profile.

An alternative to using the above relationship is to set up a list of the expected total weight components, fill in the weights of the known components and generate the AUW by determining the expected remaining value, using data from the tables as a

Table 11.1 The weight distribution of a number of British ACVs [52]

Weight item (t)	Description	SR.N5	SR.N6 Mk1	SR.N2	SR.N3	SR.N4 Mk1
Hull structure	Riveted aluminium	2.3	2.7	6.3	9.2	57.5
Flexible skirt	Bag and finger	0.4	0.5	0.8	1.6	3.5
Power plant	Gas turbine	0.8	0.8	3.8	4.0	23.7
Equipment	Passenger ferry outfit	1.2	1.6	5.5	8.3	21.9
Dry weight		4.3	5.1	15.6	21.5	103.1
Crew		0.1	0.2	0.2	0.2	0.5
Fuel		0.9	0.9	4.1	3.8	12.2
Payload		1.5	3.05	7.5	12.2	51.6
Full displacement		6.8	9.25	27.2	37.5	167.4
Payload and fuel % of displacement		35	42	42.5	43	38.5

Table 11.2 Typical weight distribution of British SES [52]

Weight item	% all-up weight
Hull (including equipment and bow/stern seals)	30–33
Public systems of craft	2–3
Power plant	8–10
Electric system, communication, navigation	3–4
Liquid load	2–6
Crew and provisions	2–4
Fuel	20–30
Freight (inc. passengers and luggage)	10–23
Reserve displacement	5–6

Table 11.3 The weight distribution of US SES-100 A and B and 2KSES

Weight item	2KSES		SES-100A		SES-100B	
	Weight (t)	% AUW	Weight (t)	% AUW	Weight (t)	% AUW
Metal hull structure	617	28.04	34.50	30.16	31.7	33.44
Power plant	168	7.64	22.30	19.49	12.69	13.38
Propulsion system			14.70	12.85	7.37	7.77
Lift system			7.60	6.64	5.32	5.61
Electric system	48	2.18	1.74	1.52	0.65	0.63
Control system	54	2.45				
Auxiliary equipment	211	9.59	5.81	5.08	3.07	3.24
Public systems			4.21	3.68	1.41	1.49
Weapons	12	0.54				
Reserve displacement	147	6.68				
Provision	111	5.04				
Empty displacement	1368	62.18	68.56	59.95	49.52	52.24
Crew			0.42	0.37	0.49	0.52
Provisions			0.25	0.22	inc. crew	inc. crew
Liquid payload			0.05	0.04		
Payload inc. experimental facilities			9.06	7.92	10.30	10.86
Ammunition	50	2.68				
Fuel	773	35.14	35.16	31.60	34.50	36.69
Undefined	9	0.41				
Full displacement	2200	100	114	100	98.4	100

Table 11.4 Principal dimensions and features of available and planned ACV [81]

	Name	Country	Weight (t)	Length (m)	Beam (m)	L/B	p_c (kg/m^2)	p_c/L (kg/m^3)	S_c (m^2)	q_v/p_c	Power (shp)	Speed (knots)	$M_t = WV/P$
1	SR.N4 Mk 3	UK	300	56.4	23.2	2.43	257	4.56	1168	0.272	18 000	65	7.43
2	N500	France	265	50.0	23.0	2.17	315	6.3	840	0.257	17 000	70	7.48
3	Aist	Russia	260	47.8	17.5	2.73	360	7.53	725	0.225	26 000	70	4.80
4	SR.N4 Mk 2	UK	200	39.7	23.2	1.71	257	6.47	780	0.315	17 000	70	5.65
5	SR.N4 Mk 1	UK	180	39.7	23.2	1.71	230	5.79	780	0.351	17 000	70	5.08
6	JEFF (A)	USA	157	28.0	13.4	2.09	469	16.75	335	0.127	22 500	60	2.87
7	JEFF (B)	USA	150	24.2	13.1	1.86	484	19.84	310	0.131	22 500	62	2.84
8	VT-2	UK	100	30.2	13.3	2.27	305	10.10	328	0.229	7 600	63	5.87
9	Lebed	Russia	90	23.3	10.2	2.27	390	16.81	230	0.128	7 200	55	4.72
10	BH.7 Mk5A	UK	55	23.1	11.2	2.04	268	11.60	205	0.208	3 800	58	5.76
11	Bell AL30	USA	52	23.0	10.0	2.30	267	11.61	195	0.155	3 600	50	4.95
12	BH.7	UK	50	23.1	11.3	2.04	244	10.56	205	0.244	3 800	60	5.42
13	MV.PP15	Japan	50	25.1	11.1	2.26	217	8.65	230	0.322	4 400	65	5.07
14	Voyageur	Canada	35	20.0	10.0	2.00	213	10.65	166	0.171	2 600	47	4.39
15	AP1-88	UK	29	21.5	10.1	2.13	200	9.30	145	0.250	1 500	55	7.29
16	N300	France	27	24.0	10.5	2.29	169	7.04	160	0.367	3 000	62	3.83
17	Gus	Russia	27	21.3	7.3	2.92	193	9.06	140	0.214	2 340	50	3.95
18	Vosper 18m ACV	UK	25	18.4	9.3	1.98	185	10.05	135	0.322	2 500	60	4.12
19	MV.PP5MkII	Japan	19.3	17.6	7.6	2.32	186	10.60	104	0.240	1 050	52	6.56
20	Viking 7505	Canada	19	16.5	6.7	2.16	193	11.70	90	0.220	1 700	50	3.89
21	SR.N4 Mk 6	UK	17	17.1	6.6	2.59	155	9.06	110	0.267	1 125	50	5.18
22	MV.PP5	Japan	16.3	15.4	7.6	2.03	185	12.10	88	0.270	1 050	55	5.86
23	Viking 7501	Canada	14.7	13.2	6.7	1.97	193	14.62	76.3	0.214	1 700	50	2.97
24	SR.N6	UK	10	14.8	6.6	2.47	128	8.65	78	0.350	900	52	3.96
25	SR.N5	UK	6.7	11.8	6.6	1.97	129	10.93	52	0.462	900	60	3.06
26	SH2-4	UK	3.1	8.0	4.4	1.82	110	13.75	28.3	0.265	200	42	4.46
27	SH2	UK	1.8	5.9	4.4	1.34	90	15.25	20	0.372	200	45	2.80
28a	Skima 12 (12)	UK	1.9	7.2	2.8	2.57	101	14.03	18.8	0.120	250	27	1.41
28b	Skima 12 (9)	UK	1.675	7.2	2.8	2.57	89	12.36	18.8	0.164	250	30	1.37
28c	Skima 12 (6)	UK	1.45	7.2	2.8	2.57	77	10.69	18.8	0.225	250	32	1.29
28d	Skima 12 (3)	UK	1.225	7.2	2.8	2.57	65	9.03	18.8	0.363	260	38	1.27

Table 11.4 (continued)

	Name	Country	Weight (t)	Length (m)	Beam (m)	L/B	p_c (kg/m^2)	p_c/L (kg/m^3)	S_c (m^2)	q_v/p_c	Power (shp)	Speed (knots)	$M_t = WV/P$
29a	Skima 4 (4)	UK	0.475	4.0	2.0	2.0	95	23.75	5.0	0.081	25	22	2.82
29b	Skima 4 (3)	UK	0.40	4.0	2.0	2.0	80	20.00	5.0	0.150	25	27	2.96
29c	Skima 4 (2)	UK	0.325	4.0	2.0	2.0	65	16.25	5.0	0.224	25	30	2.65
29d	Skima 4 (1)	UK	0.250	4.0	2.0	2.0	50	12.50	5.0	0.292	25	30	2.04
30a	Skima 4 Mk 2	UK	0.550	5.03	2.08	2.42	78	15.51	7.0	0.085	40	20	1.89
30b	Skima 4 Mk 3	UK	0.330	5.03	2.08	2.42	47	9.24	7.0	0.310	40	30	1.68

Notes:
1. M_t is a non-dimensional coefficient, therefore the physical units in this expression are: W in N; v in m/s; P in Nm/s.
2. $q = 0.5\,\rho_a\,V_s^2$ has units of m/s.

Table 11.5 Weight distribution of a Chinese ACV and SES

	Key	Craft version			
		7313		7202	
		Design weights (kg)	%	Final weights (kg)	%
Type		SES		ACV	
Date completed		September 1969		October 1980	
Manufacturer		Wu Dong shipyard		MARIC	
			$\%W'$		$\%W'$
Hull structure	$W1$	7 796	39.6	641	31.2
Outfit	$W2$	2 605	13.3	289	14.1
Power plant	$W3$	8 540	43.4	734	35.8
Electric system	$W4$	735	3.7	117	5.7
Skirts	$W5$	Included in 'Hull'		270	13.2
			% AUW		% AUW
Empty weight	W'	19 676	73.2	2 051	78.2
Passengers and crew (including luggage)	$W6,7$	6 400	23.8	520	19.8
Liquid load (water, oil, etc.)	$W9$	Included in 'Hull'		32	1.2
Fuel	$W8$	800	3.0	20	0.8
All-up weight	AUW	26 876	100	2 623	100

guide. Remember that this is simply an initial step, all the data will need to be refined at a later stage.

With this as a starting point, it is useful to determine a number of the basic dimensions for the craft such as l_c, B_c, S_c, p_c, Q', H_{sk}, H_{sw} and B_{sw} as in section 11.4 and Table 11.6. Start with:

$$p_c = K_p W^{0.333} \tag{11.7}$$

$$K_p = 50 \text{ kg/m}^2 \quad \text{(low-density craft)}$$
$$100 \text{ kg/m}^2 \quad \text{(high-density craft)}$$

then

$$S_c = W/p_c \tag{11.8}$$
$$l_c = p_c/(p_c/l_c)$$

where

$$p_c/l_c = 10\text{–}15 \quad \text{(low-density craft)}$$
$$15\text{–}20 \quad \text{(high-density craft)}$$

then

$$B_c = l_c B_c/l_c \tag{11.9}$$

where

$$B_c/l_c \quad 2.0\text{–}2.8 \quad \text{(amphibious ACV)}$$
$$3.0\text{–}3.5 \quad \text{(SES)}$$

Table 11.6 Determination of principal dimensions and weight of ACV (taking the given engine type as the constraint, as this is the normal situation)

Item	Dimensioning value	Calculation method	Remarks
1	W	W	Initial starting estimate
2	B_c	$B_c = (W/[(p_c/L_c)\,(L_c/B_c)^2])^{0.333}$	L_c/B_c ratio and p_c/L_c initially chosen from Table 11.4
3	L_c	$L_c = B_c/(B_c/L_c)$	According to given L_c/B_c ratio chosen from Table 11.4
4	p_c	$p_c = W/(L_c\ B_c)$	According to given L_c/B_c ratio chosen from Table 11.4
5	H_{sk}	$H_{sk} = (H_{sk}/B_c)\ B_c$	According to given H_{sk}/B_c from Chapter 10 (requirements for stability)
6	The various weights can be calculated as follows:		Coefficient in weight calculation from this chapter
	I. Hull weight		
	1. Metalic structure	$W_s = K_s\ S_c$	
	2. Deck equipment and paint	$W2\text{-}2 = K2\text{-}2\ W$	
	3. Ship equipment	$W2\text{-}4 = K2\text{-}4\ W^{0.666}$	
	4. Life-saving equipment	$W2\text{-}5 = K2\text{-}5\ S_n$	S_n – passenger numbers determined by role
	5. Other items in hull group	According to prototype	
	II. Power plant	$W3 = K3\ .\ N$ N = designer choice	Lift and propulsion engines can be obtained according to the AUW of craft in the first approximation, craft speed and some coefficients. Then designers can select the type of lift and propulsion engines and thus determine the power plant weight
	III. Fuel weight	$W8 = q_c\ \Sigma\ N\ R/V_s\ K8$	
	IV. Electric equipment weight	$W4 = K4\ W^{0.666}$	
	V. Skirt weight	$W5 = K5\ B_c\ h_s\ p_c$	SES or
		$W5 = K5\ (L_c + B_c)\ h_{sk}\ p_c$	ACV
	VI. Provision weight	$W10 = K10\ W$	
	VII. Passenger weight	$W6 = K6\ P_n$	S_n is number of passengers or seats. $K6$ will vary a little in different parts of the world
		$K6$ = 140 kg passenger only 200 kg with luggage	
7	Calculation of craft weight	$W_c = \Sigma\ W_i$	If this relation does not hold, then the process should be iterated until the difference is small enough to be ignored (say less than 5% at estimating stage)
8	Calculation of speed	V_s	Iteration. See Chapters 10 and 3, Fig. 12.5
	I. Wave-making drag	$R_w = f\ (L_c/B_c,\ P_c/L_c,\ W,\ F_r\ \ldots)$	Use method in Chapter 3
	II. Air momentum drag	$R_m = f\ (\bar{Q},\ Fr,\ W\ \ldots)$	
	III. Air profile drag	$R_a = f\ (S_a,\ Fr,\ \ldots)$	S_a is frontal area of craft
	IV. Skirt drag	$R_{sk} = f\ (\bar{Q},\ Fr,\ \ldots)$	
	V. Trim drag	$R_\psi = f\ (\ldots)$	

Table 11.6 (continued)

Item	Dimensioning value	Calculation method	Remarks
9	Estimation of lift power	$N_l = Q\,H/(\eta_F\,\eta_M)$ where $Q = Q'S_c\,(2p_c/\rho_a)^{0.5}$ $H = p_t/\zeta_h,\ p_t = \bar{p}_t\,p_c$ $\bar{p}_t$ = bag/cushion pressure ratio	H is fan overall pressure head ζ_h is the coefficient due to loss of head in ducts, obtained from prototype
10	Estimation of engine power propulsion power	$N_p = V_s\,\Sigma\,R_i/(\eta_p\,n_m)$	η_p is efficiency of air propeller
	Total power	$N = N_l + N_p \leq \varepsilon$	If this expression is not satisfied it has to be revised and repeated until it is
11	Estimation of transverse stability	$h_{\theta}/B_c = f(H_{sk}/B_c,\ L_c/B_c, \ldots)$	Determined as in Chapter 5. During this initial estimate, skirt responsiveness is not considered
12	Estimation of speed of craft in wind and waves		Note: head wind and oncoming waves
	I. R_{wmax} (drag peak in calm water)	$R_{wmax} = f(L_c/B_c,\ p_c/L_c,\ Fr \ldots)$	Use Chapters 3 and 8
	II. R_m	$R_m = f(\ldots$	The wind speed has to be taken into account for calculation of II–V then . . . $R'_{wmax} = \Sigma R$ V_w is wind speed
	III. R_a	$R_a = f(\ldots$	
	IV. R_{sk}	$R_{sk} = f(\ldots$	
	V. R_{ψ}	$R_{\psi} = f(\ldots$	
	VI. Thrust reserve	$T = (T - R'_{wmax})/R'_{wmax}$ where $T = f(N, [V_w + V_s]/V_s, Fr \ldots)$	
13	Seaworthiness I. Maximum vertical acceleration at CG, $\ddot{\zeta}_{gmax}$	$\ddot{\zeta}_{gmax} = f_g\,(Fr_l,\ \bar{Q},\ L_c/B_c,\ p_c/L_c,\ h_w/H_{sk},\ L_w/L_c \ldots)$ where h_w = wave height L_w = wavelength	For Passenger craft, the main check targets are the vertical acceleration in a wave, which can be calculated by the method in Chapter 8 and according to the seaworthiness requirements for craft given in Chapter 10
	II. Maximum vertical acceleration at bow	$\ddot{\zeta}_{bmax} = f_b\,(Fr_l,\ \bar{Q},\ L_c/B_c,\ p_c/L_c,\ h_w/H_{sk},\ L_w/L_c \ldots)$	
14	Area of passenger cabin S_{ca}	$S_{ca} = L_{ca}\,B_{ca}$	L_{ca} and B_{ca} denote cabin length and width respectively, which are related to L_c, B_c and the relation between them can be determined

It is also helpful to estimate the installed power at this point, which can be found from

$$N_e = K_n\,W^{7/8} \quad \text{kW} \tag{11.10}$$

where

$$K_n = 135$$
$$W = \text{AUW in tonnes}$$

This expression is representative of efficient craft of all sizes through the late 1980s assuming speed and size follow existing norms. High-speed craft would require additional power, low-speed craft less. This also applies to SES as well as ACVs.

Table 11.7 Weight Estimate Checklist

Item	Sub-items	Check comments
*W*1	*Hull weight* including: Main hull structure, including basic raft or hull structure plate, frames, stringers and other scantling,decks, sandwich panels Superstructure Bow/stern ramp structure Doors and hatches Landing pads Air propeller ducts and mountings Engine mountings and their strengthened structure Bearings and mountings, etc. Integral tankage Fins (vertical or angled stabilizers) Horizontal fixed aerodynamic stabilizers	The hull includes the primary structure (buoyancy tank area for ACV, sidehulls and central buoyant connecting structure for SES) superstructure and all main secondary structures
*W*2a	*Basic Outfit weight* including: Rudder and their handling equipment Mast Ladders Windows and doors Retractable equipment for ramp Floors and coverings Isolation, insulation, sound proofing, trim, partitions, etc. Painting Flight crew seats Flight crew emergency equipment Passenger seats Fire precautions in payload areas Marine equipment, including anchoring Life-saving and fire-fighting system Life-rafts and containers stowage Life-jackets and stowage	The items included here will be very dependent on the craft mission and safety regulations for the area of operation
*W*2b	*Customer-specified equipment* which may be considered optional, including: Passenger tables, lockers and other furnishings and cabin equipment Heating, ventilating and air conditioning Toilet and washing facilities Galley facilities Domestic water supply (in toilet) Long-range tankage and system	These items should be checked individually, since most of them will not normally be installed Do not assume they are included in the historical reference data, unless clearly identified
*W*3	*Power plant* including: Main engine(s) Machinery equipment such as: Main reduction gear boxes of main engine Reduction gearbox(es) for lift fan(s) Radiator(s) for lubrication oil system Air filters Hydraulic and propeller pitch controlling system Transmission shaft system Remote control systems	
*W*3a	Lift and propulsion equipment and auxiliaries, including: Propellers Lift fans Fuel supply tanks (if not integral with hull) Pipelines	

Table 11.7 (continued)

Item	Sub-items	Check comments
*W*4a	*Basic Electric system* including: Batteries Electric generators Electric transmission and distribution system Engine starting system Illumination system Voltage rectification equipment Cabling and cable trays Navigation equipment, inc. radio, radar, Navaids	
*W*4b	*Cockpit communications equipment* Intercommunication and internal broadcasting Electronic enclosures and racking Signalling equipment Environmental equipment	These items should be checked individually, since most of them will not normally be installed. Do not assume they are included in the historical reference data, unless clearly identified
*W*5	Weight of skirt and joints including Loop or bag Bag stabilizer diaphragms Segments or fingers or jupes Rear double segments or anti scoop flap Rear multi loop skirt (SES) Longitudinal stabilizer skirt Athwartships stabilizer skirt Skirt shift mechanism Segment ties Loop attachments	 Estimate loop surface area Estimate one finger and total number off Estimate loop surface area Estimate loop surface and individual cones × number
*W*6	*Weight of payload* including: Weapons, passengers and luggage, vehicles, freight	Define as unit weights, number and distribution
*W*7	Weight of crew and luggage, Provisions Bonded stores and sales stores Fresh water supplies Boarding parties and their equipment Spares carried on board	
*W*8	Weight of fuel, Main fuel, reserve fuel, long-range fuel Lubrication oil	
*W*9	*Liquid load on the craft* such as: Bilge, water in the pipelines and engines	
*W*10	*Reserve displacement* This item should include : Project weight estimating reserve	 Do not start with less than 15%

An alternative to this expression is to use installed power/tonne knot :

$$N_e = K_n W V_s \tag{11.11}$$

where V_s is the design craft service speed, W the weight (t) and

K_n = 0.7 (light large craft)
0.9 (light small craft > 5 t)

2.0 (dense large craft)
3.0 (recreational and small utility craft)

We can now move on to develop further estimates for the craft weight components and begin to refine the parameters.

Weight of hull structure

According to ref. 4, the weight of the hull structure for an ACV, W_s can be written as

$$\frac{W_s}{W} = 0.29\,(W^{0.33}/p_c)^{0.60} \tag{11.12a}$$

or

$$\frac{W_s}{W} = 0.6/p_c\ W^{0.33} + 0.015\ W^{0.33} \tag{11.12b}$$

where W_s is the weight of the hull stucture (t), W the weight of craft (t) and p_c the cushion pressure (lb/ft^2). (*Note*: 1 Pa = 0.02 lb/ft^2 = 1 N/m^2.) This expression can be seen plotted in Fig. 11.1 and the structural weight of some hovercraft is shown in Fig. 11.2.

Based on data from some SES designed and built in China, the weight of the hull structure can be estimated by the following equation [11]:

$$W_s = 8.8\ K\,[1 + 0.045(V_s/L)^{0.666}]\,[L\,(H + B_c)/100]^{1.25} \tag{11.13}$$

where W_s is the weight of the hull structure (kg), L the length of the hull structure (m), V_s the design speed (knots), B_s the cushion beam (m), H the cushion depth (m) and K a coefficient, which can be taken as

K = 750–800	for welded aluminium alloy structure
= 900–950	for GRP structure
= 830–860	for the combined structure of GRP and aluminium (GRP sidewalls)
= 1100–1500	for combined structure of steel and aluminium (aluminium superstructure)
= 1200	for whole steel structure

Weight of metallic structure for an ACV, W_s (or $W1$)

$$W_s = K'_s\,S_c \tag{11.14}$$

where S_c is the cushion area (m^2) and K'_s a coefficient (taken from the prototype or reference craft, see Tables 11.1 and 11.4).

Weight of deck equipment and painting $W2$-1

$$W2\text{-}1 = W\,K2\text{-}1 \tag{11.15}$$

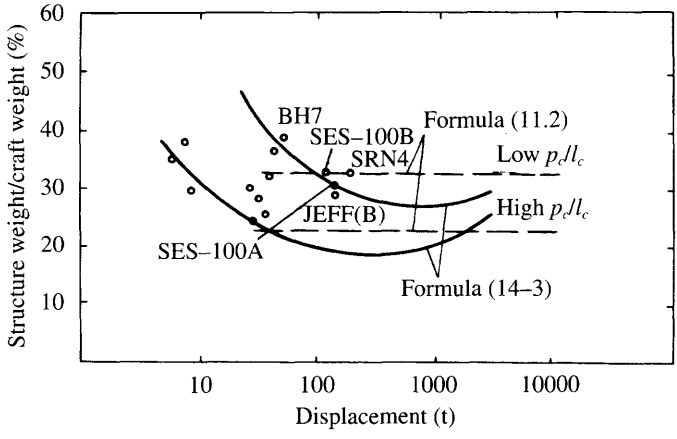

Fig. 11.1 Weight trends for ACV/SES structures with displacement.

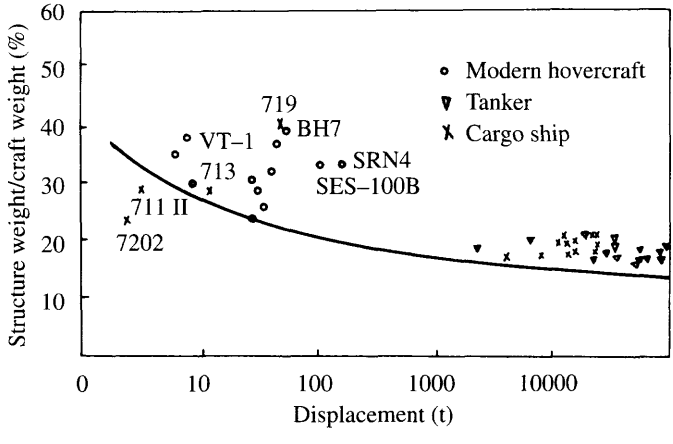

Fig. 11.2 Hovercraft and ships' structure weight statistics with displacement.

where W is the craft weight (t) and $K2$-1 a coefficient. Typical values are 0.12 for an ACV and 0.1 for an SES.

Weight of ship's equipment *W*2-2 (rudders, anchors, mooring, towing, lifting equipment, etc.)

$$W2\text{-}2 = K2\text{-}2\ W^{0.666} \tag{11.16}$$

where $K2$-2 is a coefficient. Typical values are 0.08 for an ACV and 0.1 for an SES.

Life-saving equipment *W*2-3

In the case where the weight of the craft is similar to that of a prototype, then W2–3 is

$$W2\text{-}3 = K2\text{-}3\ S_n \tag{11.17}$$

where S_n is the number of passenger seats (should also be the same as the number of passengers) and $K2$-3 a coefficient. Typical values are 3.0 (kg) for an ACV or an SES, covering life vest and weight component of life-raft and fittings installed.

Weight of ship's systems *W*2-4

$$W2\text{-}4 = K2\text{-}4\ W \tag{11.18}$$

where $K2$-4 is a coefficient. Typical values are

0.05	for small ACV	(AUW < 2000 kg)
0.05	for medium ACV	(AUW < 20 000 kg)
0.02	for large ACV	
0.02	for small SES	(AUW < 20 000 kg)
0.01	for large SES	

Weight of power plant *W*3

$$W3 = K'\ K3 \sum N \tag{11.19}$$

where $K3$ is a coefficient according to the specific weight of the given power plant. Typical values, in kg/kW, are

0.5	Gas turbine engines
2.5	High speed diesels
5.0	Medium speed diesels

and $\sum N$ is the total installed power (lift, thrust and auxiliaries) (kW). For engine weight, with respect to the total weight of the power plant, the coefficient K' has to be found in this equation; for example for gas turbines $K' = 2$–3, while for high-speed diesels $K' = 1.5$–2.5. This is to account for gearbox weights, etc.

Note: Cooling systems additional outfit weights (in addition to K')

0	for air cooled (though maybe there will be an oil cooling system)
0.1	for water cooled diesels
0.2	for recirculated cooling water

It should be noted at this point that it may be best to check the available power plants to provide the power. A number of design choices may have to be taken at this point, since if it is decided to use separate power systems for lift and propulsion, an estimate of the required cushion system power is needed. This will mean making a preliminary cushion system design (Chapters 2, 6 and 12) and then revisit the engine selection, before going on. Power system selection has a strong influence on the whole craft layout, so it is worth while spending some time on this aspect. Since engines are

only available in discrete sizes, some flexibility in design is required in order to avoid underpowering or overpowering a given design.

Weight of electrical equipment *W4*

$$W4 = K4\ W^{0.666} \quad \text{(based on dry weight)} \tag{11.20}$$

where $K4$ is a coefficient (non-dimensional). Typical values are

0.10 SES
0.14 ACV
0.10 additional component for military craft

Skirt system weight of ACV *W5*

$$W5 = K5\ (L_c + B_c)\ h_{sk}\ p_c \tag{11.21}$$

where h_{sk} is the skirt height (m), p_c the cushion pressure (Pa) and $K5$ a coefficient. Typical values are 0.02 for an ACV depending on cushion depth.

Skirt system weight of SES *W5*

$$W5 = K5\ B_c\ h_s\ p_c \tag{11.22}$$

where h_s is the height of sidewalls (m), B_c the cushion beam and $K5$ a coefficient. Typical values are 0.023 for an SES.

Weight of fuel and oil *W8*

$$W8 = q_e \sum N\ R/V_s\ K8 \tag{11.23}$$

where R is the range (nautical miles), V_s the craft speed (knots), $\sum N$ the total power (kW), q_e the specific fuel consumption of main and auxiliary engines (kg/kwh) and $K8$ the additional oil and water consumption coefficient (approx 1.07).

Liquid Load *W9*

This will vary somewhat, dependent on whether a static ballasting system is used rather than a skirt shift system (a), and whether water (b) or fuel (c) is used for the trimming ballast.

$$W9 = K9\ W \tag{11.24}$$

where $K9$ is a coefficient. Typical values (a/b/c) are

0.05 / 0.1 / n.a.	for small ACV	(AUW < 2000 kg)
0.06 / 0.12 / 0.08	for medium ACV	(AUW < 20 000 kg)
0.07 / 0.12 / 0.10	for large ACV	
0.05 / 0.10 / 0.08	for small SES	(AUW < 20 000 kg)
0.05 / 0.10 / 0.08	for large SES	

Estimating margin for hull weight *W10*

$$W10 = K10\ W \tag{11.25}$$

where $K10$ is a coefficient. At the initial design stage, use 0.15, reduce to 0.05 once the structure is designed, and fabrication drawings are available for a detailed weight take-off.

11.5 Parameter checks for ACV/SES during design

Role requirements

The tactical and technical/economic validation for military and civil hovercraft designs for specific routes or roles is often commercially confidential, or the subject of defence secrecy laws. From data publicly available it is possible to identify the key parameters which control the economy of these vehicles. Here we introduce some commonly used criteria.

Transport efficiency η_1

$$\eta_1 = \frac{\text{payload} \times \text{speed}}{\text{total power}} = \frac{\text{payload}}{\text{AUW}} \quad \frac{\text{AUW}}{\text{overall equivalent drag}} \times \frac{\text{overall equivalent drag} \times \text{speed}}{\text{total power}}$$

$$= \text{payload factor} \times \text{equivalent lift/drag ratio} \times \text{propulsor efficiency} \tag{11.26}$$

where overall equivalent drag is the sum of various hydrodynamic drag, aerodynamic drag and equivalent drag due to the lift power; therefore the transport efficiency not only denotes the hydrodynamic characteristic of the craft, but is also related to the payload factor and propulsor efficiency.

Payload factor η_2 [= K14]

$$\eta_2 = \frac{W_6}{\text{AUW}} \tag{11.27}$$

Payload is related to the structure, material, power plant and outfit which not only affect the cost, but also the operational cost.

Fuel consumption per unit passenger and unit nautical mile η_3

$$\eta_3 = \frac{\text{fuel consumption} \times \text{block route time}}{S_n \times \text{route length}} \tag{11.28}$$

where fuel consumption is in litres or kg/h, route length is in nautical miles, S_n is number of seats/passengers and block route time is in hours.

Total construction cost per unit seat η_4

$$\eta_4 = \frac{\text{total construction cost}}{S_n} \tag{11.29}$$

η_4, quoted in \$US here, denotes the cost of craft per unit seat, which characterizes the first investment of the craft, at delivery from manufacturer. It must be noted that for larger craft, the cost of delivery to site, initial training of crew, investment in terminal and maintenance facilities and spares inventory, can add significantly to the craft's construction investment. It is suggested that in evaluating different sizes and types of craft for a given service or role, the effect of the different craft on these other investments should be evaluated in parallel, to identify the most economic overall solution to the transportation project.

It should also be noted that the construction costs can vary widely between different countries. The data given as example below are representative for Europe or Japan, while in China the costs are between a quarter and a half of these values (1995 data).

Power per unit seat η_5

$$\eta_5 = \frac{\text{total installed power (kW)}}{S_n} \tag{11.30}$$

This is a simple coefficient for comparison of hovercraft with conventional transport vehicles.

Once an initial estimate has been made for craft dimensions, weight and powering,, it is useful to calculate the performance indicators above. Typical values which should be reached for craft designed for construction now (mid 1990s) are

η_2 = 20–30	for ACV	25–35	for SES	
η_3 = 0.1–0.15	for ACV	0.02–0.05	for SES	(diesel)
η_3 = 0.2–0.25	for ACV	0.15–0.25	for SES	(gas turbine)
η_4 = 4000–5000	for ACV	2000–4000	for SES	(\$ US)
η_5 = 25–30	for ACV	10–15	for SES	

If the initial estimate is far removed from these data, an unrealistic combination of design parameters may have been selected and so these should be reviewed. Once the initial design has been prepared, there should be some improvement in the factors compared with the initial estimate.

Other design checks

Based on the role requirement, operational region and use of the craft, design requirements may be specified which play an important role during the determination of principal dimensions of the craft, for example:

Required minimium craft speed
This can be determined according to the craft-specified block speed for ferries or role requirement by other users.

Required minimum range
This can be determined based on the route length and required minimum number of trips for ferries, or the role requirement for minimum endurance time for the craft by other users.

Power plant limitations (main engine)
The power plant selection may be determined according to the choice of main engines available to the constructor, considering the cost of delivery to the construction yard. Power plant selection is very important in practice since it influences many of the other craft design parameters.

Requirements for stability
Requirement for stability can be obtained from Chapter 10 to comply with the requirements of the IMO [215] or the rules for merchant ships. The simplest criterion for the stability is h/B_c (for an SES) or the percentage of shifting distance of C_p to cushion beam per degree of heeling angle (for an ACV).

Requirements for seaworthiness
Requirements for seaworthiness can be obtained from Chapter 10 to comply with the criteria specified by ISO 2638 and 2633 or the specifications from operators.

Accommodation space requirements
According to the number of passenger seats and the specific area for every passenger, the passenger cabin floor area can be determined. Typical space per passenger for seating and aisles for entry will be about 0.6 m^2 per passenger.

Limitations to principal dimensions
The limitation to craft beam due to transport requirements for the craft on a ship or road trailer, the limitation to draft due to port conditions and the limitation to the craft beam for getting into landing ship, dock, etc. may be required by users.

The designer should review each of the above possible restrictions on the craft design, as relaxation could enable improvements in other performance indicators. In general this would be done after the initial design has been completed as described below.

11.6 Determination of hovercraft principal dimensions

Determination of principal dimensions is begun by using the ratio of principal dimensions from past experience. In the first and second approximation of general design it is not possible to choose too many ratios of principal dimensions, because of the need to keep the design process simple. This then enables the designer to consider changes in some of the parameters to study possible improvements to the initial choices.

In such a case, it is possible to plot systematic changes in the parameters chosen to find the extreme value as a function of multiple variables. Since the functional relations between the parameters concerned with the craft performance and the ratio of principal dimensions have not been established analytically, and in addition, nowadays, it is straightforward to create a spreadsheet on a computer, such problems can be solved fairly simply and quickly. Therefore, the variation method may rapidly home in on an optimum craft design, based on the restrictive parameters and role functions above, using parameters such as those discussed below. The parameters that have the greatest effect on the performance of craft are as follows:

Cushion length-beam ratio (l_c/B_c)

The ratio l_c/B_c greatly affects the ship's speed, engine power and seaworthiness. In the case of low speed, increasing l_c/B_c will improve the seaworthiness, decrease the drag at medium speed, increase the range and decrease the drag peak. Therefore, during the 1980s, there was a general tendency to increase the cushion length/beam ratio. Clearly there is a trade-off to make it dependent on the desired operational speed for the craft.

A typical starting point for an ACV would be 2.0, assuming a basic rectangular plan-form with rounded or hexagonal corners. Craft as small as single seat ACVs up to medium size ferries stay close to this geometry. An l_c/B_c increasing to 2.5 is used on larger craft than this. SES normally have l_c/B_c in the range 3.0–5.0, though the most commonly used is 3.5–4.5.

Cushion pressure/length ratio (p_c/l_c)

In general, craft with large deck area and low load density are required for passenger craft; in contrast, craft with high load density are required for landing craft with tanks. There is a wide range in this ratio, as shown in Table 11.4, though for ACVs the starting point should be somewhere between 10 and 15 kg/m^3, or up to 20 if space constraints require high density such as for amphibious landing craft. The higher this parameter, the noisier the craft will be. SESs generally operate at values between 13 and 30 kg/m^3. Figure 11.3 shows this parameter plotted for a number of craft and some projected trends for reference. This parameter greatly influences the speed, seaworthiness, structural strength of the hull, craft weight and principal dimensions.

Sidewall depth ratio for an SES (H_{sw}/B_c)

The sidewall depth ratio affects the transverse stability, seaworthiness and hull weight, etc. Typical values of H_{sw}/B_c for an SES would be 0.25–0.333. Start with 0.25 and if stability is fine, try deepening the cushion a bit and check the stability parameters.

Skirt height ratio for an ACV (H_{sk}/B_c)

The effect of H_{sk}/B_c for an ACV is equivalent to that of H_{sk}/B_c for an SES. It should be noted that we are addressing the skirt height measured to the hull keel, not the upper loop attachment. The position of the upper loop attachment both vertically

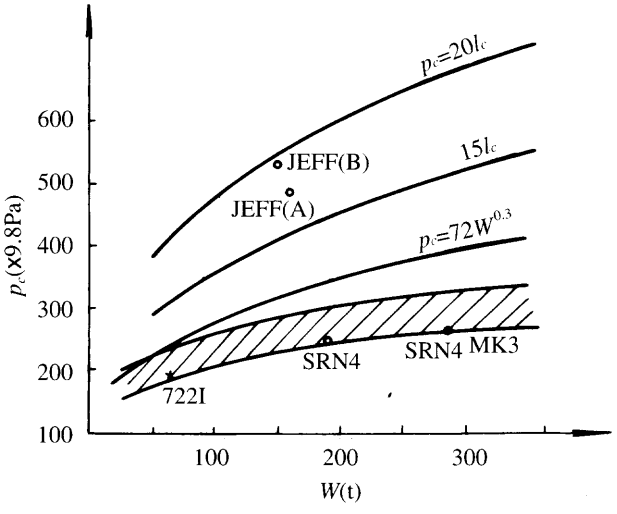

Fig. 11.3 Cushion pressure trends for hovercraft (hatched area for passenger hovercraft).

(hull depth) and horizontally (hull sidebody width) can be adjusted to tighten or loosen the loop tension and so stiffness. If the required underkeel clearance results in low stability, these skirt geometrical parameters should be varied first, together with the position of the skirt tip (toe-in or toe-out relative to the upper loop attachment) before reducing H_{sk}.

Typical values for H_{sk}/B_c for an ACV would be 0.11–0.18. Start with the higher value, as ACVs generally need all the clearance they can get.

Cushion flow coefficient $\bar{Q}$

$$\bar{Q} = Q / [S_c (2p_c/\rho_a)^{0.5}] \tag{11.30}$$

This coefficient influences the speed performance, seaworthiness and speed loss over different terrain. The higher the relative flow rate, the larger the air gap under the skirt. Choice of the base value, and thus the lift system requirements, is key to a successful hovercraft. It is best to start with a high number and if power requirements seem excessive, reduce the flow. Refer to Chapter 2 for guidance. Remember that if a reserve of cushion flow is available, the pilot can always operate at a 'cruising' level and if the sea state picks up, he can increase lift and so minimize speed loss.

It is important to remember that cushion air thrusters for ACVs, and cushion venting systems in the case of SES, absorb part of the cushion air flow or lift power if separate fans are used, and should be taken into account at the preliminary stage by adding a percentage to the cushion flow, power etc. Typically SES will use 30% for ride control systems, while ACVs will use 20–25% for rotating thrusters.

Sidewall thickness ratio B_{sw}/B_c

B_{sw}/B_c influences the transverse stability, seaworthiness, speed and general arrangement. Therefore, it is a very important parameter for an SES. In the case of craft with medium speed (Fr = 0.7–0.9), it is suggested thicker sidewalls are adopted. Start with B_{sw}/B_c at 0.08–0.125 as an average to start, assuming that the main engines will be housed in midships flared areas if diesel power is used.

The designer should concentrate on a few of these parameters at any one time. For ACVs, l_c/B_c, p_c/l_c and Q can be selected as the variables, while for SES, l_c/B_c, p_c/l_c and B_{sw}/B_c can be selected as the variables and H_{sk}/B_c, H_{sw}/B_c, etc. can be taken as the given values according to the requirement of stability and seaworthiness. More precise values for such parameters can be determined at the next design phase for determining the principal dimensions, namely in the preliminary design phase which follows the initial estimation of dimensions.

Thus, three variables for one parameter can be taken and in total there are 27 variants to be assessed. In the case of four variables for one parameter, then 81 total variants need assessment. This is not too much for computer analysis and such calculation can be undergone as in Table 11.6.

In this example, we take the general condition of design into account, namely the role stipulates not only the number of passengers, range, speed of craft, requirement

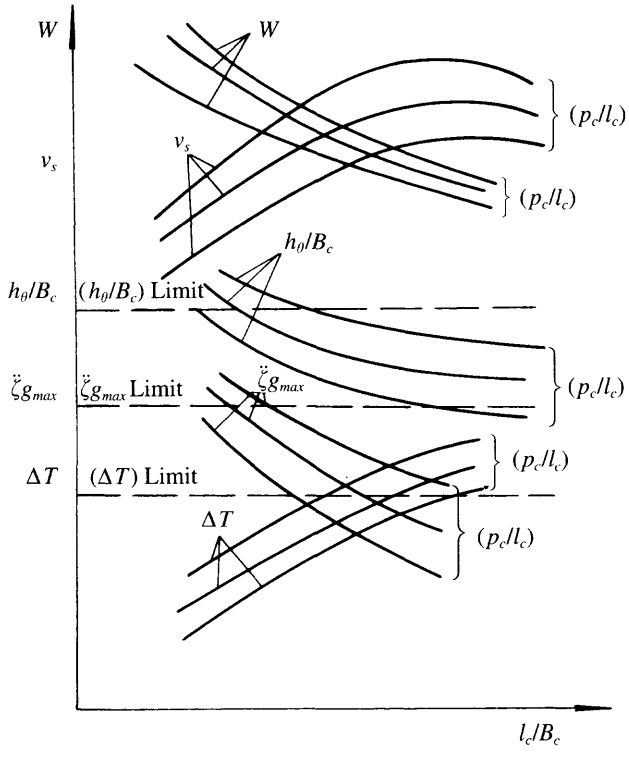

Fig. 11.4 Optimization plots of craft leading particulars selection prior to design.

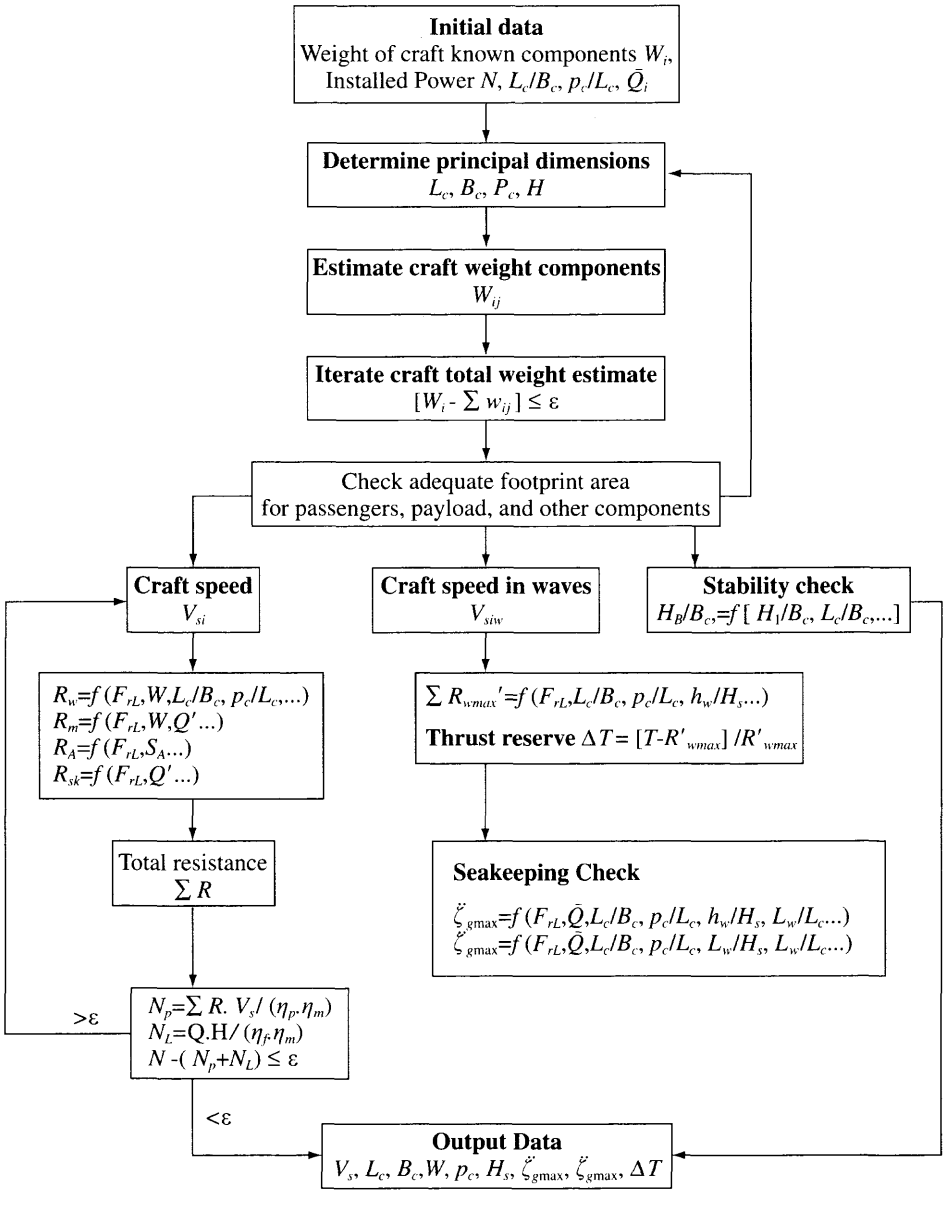

Fig. 11.5 Block diagram for determination of principal dimensions and weight of an ACV.

for seaworthiness, but also the type of engine which can be chosen in design. In this case, we take an integrated air propeller–lift system as the designing type of power systems, because this is the general case for ACVs, particularly for craft using gas turbine propulsion.

Once the data are gathered based on Table 11.6, varying the design parameters within a range, it is possible to construct a plot of the data such as shown in Fig. 11.4.

In the case of three parameters such as $\bar{Q}$, p_c/l_c, l_c/B_c, then three drawings can involve all of the data for the 27 groups of data. From the figure it can be seen that h_θ/B_c, ζ_{max} and ΔT are the limits for transverse stability, seaworthiness (according to the IMO requirements) and the thrust reserve of craft in waves respectively.

It is suggested to select the alternative which gives the maximum craft speed or minimum displacement and also meets these restrictions. The method expressed by Table 11.6 can also be illustrated by a block diagram as shown in Fig. 11.5.

12

Lift system design

12.1 Introduction

In Chapter 2 we introduced air cushion theory and its development to date. Modern air cushion systems are based on the plenum chamber principle, though generally using lower skirt fingers or segments which encourage an element of air jet sealing to improve free air gap and so reduce drag. The normal starting point for lift system design is to assume a cushion system which includes segments or fingers as the primary cushion seal and an upper skirt including a bag or loop which acts as an air distribution duct, and spring/damping system. If another system (e.g. extended segment system) is used, then the same cushion system elements have to be provided by other means.

Thanks to improvements in the design of flexible skirts, the air gap under the segment tips necessary for minimized drag, and thus the required air inflow rate, is small. The lift power of modern hovercraft is not excessive in proportion to the total craft installed power compared with hovercraft built in the 1960s. The decrease in bag pressures used (typically down from 1.4 p_c to 1.1 p_c), which lead to the development of more responsive skirts, also results in minimized fan total pressure and therefore reduced power.

The specific power of ACV/SES, i.e. lift power plus propulsion power divided by craft all-up weight, has been reduced significantly, from 90 kW/t for SR.N1 in 1960, to 50 kW/t for SR.N4 in 1970 and 30 kW/t for both SR.N4 MK 3 and AP1.88 in 1982. Since that time the specific power for lift systems has stabilized.

Meanwhile, lift system design must be approached carefully, because for an ACV, the lift power is still approximately 1/3 of the total craft installed power. Figure 12.1 shows the typical distribution diagram for the lift system and the pressure distribution of the lift system, in which q_0 denotes the pressure recovery of air inflow of the craft in motion, $k_1 q_1$ denotes the inflow pressure loss and H_j denotes the overall pressure head of the fan. Airflow is through air ducts with a diffusion loss in section (3), then into a skirt bag with head loss due to sudden diffusion, and to the bag pressure p_t (since the air velocity is very small, therefore the dynamic pressure in the skirt bag is also very small); subsequently the air flows via the skirt bag and into the cushion, at cushion pressure p_c.

G. H. Elsley [92] investigated the power distribution of small high-speed ACVs operating at the speed of 1.5 times hump speed. From Table 12.1 it can be seen that

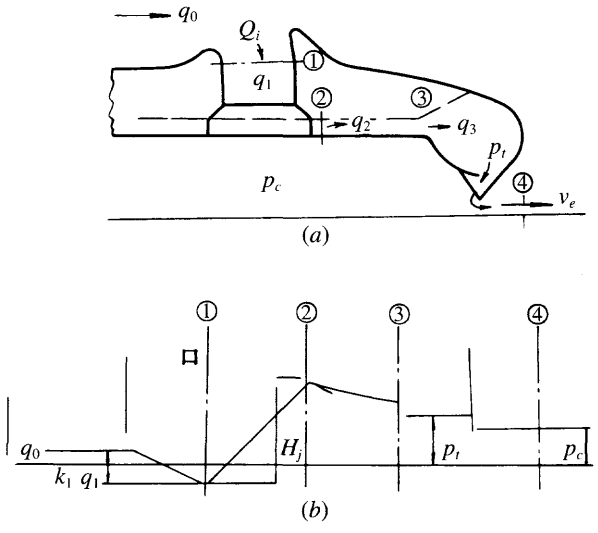

Fig. 12.1 Layout of a typical ACV lift system and the distribution of pressure in different positions.

Table 12.1 Power analysis for three small ACVs at 1.5 × hump speed in head winds and waves [100]

No.	Power consumption item	% Installed power	% Cumulative power saving from 10% reduction in this item	Related items
1	Cushion flow losses	14	4.3	1, 2, 3, 7, 8
2	Skirt drag	24	4.0	4, 8
3	Propeller/propulsor loss	25	2.5	8
4	Intake, fan and ducting losses	15	1.5	1
5	Wave-making drag	6	1.0	5, 8
6	Skirt pressure loss	7	0.8	1, 3
7	Profile drag	5	0.8	6, 8
8	Momentum drag	4	0.7	7, 8

saving cushion flow and skirt drag will obtain the best results, because it not only saves on the power of this item but also other items, e.g. 1, 3, 7 and 8, etc. This illustrates the important role which cushion air flow has for saving flow rate.

In this chapter our aim is to define the cushion as an air supply and ducting system, so as to be able to select an appropriate type of lift fan (axial, mixed flow or centrifugal) to feed it. Fans can then be designed and built to the required specification by specialist suppliers, or a standard unit selected from an existing range. Standard fans used for hovercraft are generally units designed for ventilation systems for buildings. There are a number of suppliers world-wide of axial and mixed flow fans with non-metallic lightweight blades which are reasonably efficient. Centrifugal fans suitable for ACV/SES on the other hand are usually built to specification, since for industrial use steel is used rather than the aluminium which is preferred for an ACV.

We will discuss the following aspects:

1. the determination of cushion parameters concerned with the performance of the craft, e.g. the relative flow rate $\bar{Q}$, the bag cushion pressure ratio p_t/p_c and the cushion pressure/length ratio p_c/l_c;
2. design of air inlet and outlet, as these seriously affect the loss of total pressure head;
3. air duct design;
4. air fan design.

12.2 Determination of air flow rate, pressure and lift system power

Determination of air flow

Reference is made to sections 2.3–2.5 for background.

The flow coefficient $\bar{Q}$, can be written as

$$\bar{Q} = \frac{Q}{S_c\,(2p_c/\rho_a)^{0.5}} \tag{12.1}$$

where Q is the air flow rate (m^3/s), S_c the cushion area (m^2), p_c the cushion pressure (N/m^2) and ρ_a the air density ($N\,s^2/m^2$). The value of $\bar{Q}$ is dependent upon the design requirements for the craft speed, speed loss in waves and control of heaving acceleration. It has to be taken into account comprehensively in the overall design of a craft. The effect of air flow on overall performance of a craft has been described in earlier chapters, but can be estimated as follows in preliminary design or initial project design stages.

Statistical method

Based on craft actually constructed, a statistical analysis can be made as follows (ref. 15, see also section 2.5):

$$\bar{Q} = 0.015\text{–}0.030 \quad \text{(ACV) [15]} \tag{12.1a}$$

$$\bar{Q} = 0.005\text{–}0.010 \quad \text{(SES)} \tag{12.1b}$$

which can also be written as follows [108]:

$$Q/W = 5.0\text{–}10.0\ m^3/s/t \quad \text{(ACV) [93]} \tag{12.1c}$$

$$Q/W = 0.5\text{–}1.3\ m^3/s/t \quad \text{(SES)} \tag{12.1d}$$

The flow should be assumed to be at the upper limit of this expression to start with, while the flow rate coefficient for river hovercraft will be rather lower as shown in Table 12.2.

Model experimental method

In a towing tank, the calm water drag and vertical acceleration in waves at different $\bar{Q}$ can be measured and the optimum flow rate (or range, for a craft operating

envelope) selected. Figure 12.2 shows the drag curve of British SES model HM-2 at different flow rates.

Designers can also make decisions using full-scale prototype test results on calm water and waves. This method is rather more costly and time-consuming than building a scale model. It is normally used if the original skirt design gives different results from the model tests, as a method to optimize craft performance.

Approximate equations

An initial estimate of the cushion flow rate required for an ACV at project design stage can be obtained according to the required equivalent hovering height H_e/l_c, based on past experience from completed ACVs. H_e/H_c can be determined statistically as in equation (12.2) [4, 93]:

$$H_e/l_c = 0.05/W^{0.5} \tag{12.2a}$$

Table 12.2 Flow coefficient for various Hovercraft

Craft	Country	Type	Cushion length l_c (m)	Cushion area S_c (m^2)	Craft weight W (t)	Cushion pressure p_c (N/m^2)	Flow rate Q (m^3/s)	$\bar{Q}$ bar
HM.216	UK	SES	11.95	58.29	18.38	3570	29.80	0.0067
HM.218	UK	SES	14.39	70.19	27.30	3390	21.50	0.00412
HM.221	UK	SES	17.44	85.07	37.20	3339	26.80	0.00427
713	China	SES	17.5	87.30	28.00	3200	50.00	0.008
711-IIA	China	ACV	10.09	52.32	6.40	1290	51.70	0.0217
SR.N6	UK	ACV	14.8	78.00	10.00	1280	75.10	0.0213
SR.N4	UK	ACV	39.7	780.00	200.00	2570	453.40	0.00906
JEFF (A)	USA	ACV	28.0	335.00	157.00	4690	362.70	0.0124

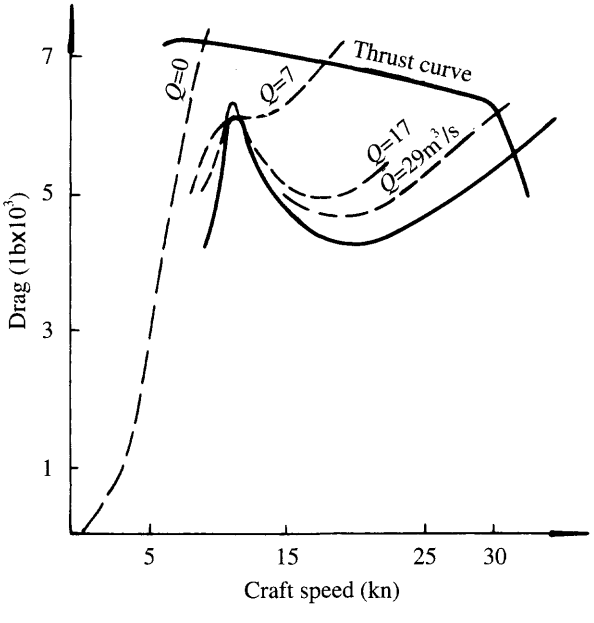

Fig. 12.2 Influence of flow rate Q on drag of SES model HM-2.

or

$$H_e/l_c = k_1 (p_c/l_c)^{0.5} \tag{12.2b}$$

where H_e is the equivalent air gap under the skirts, including delta between fingers (ft), $l_c = S_c/B_c$, W is the craft weight (t), p_c/l_c the cushion pressure/length ratio (lb/ft^3), S_c the cushion area and k_1 a constant, which we can take as $0.0035 < k < 0.0046$ or as shown in Fig. 12.3.

After obtaining the equivalent air gap, the air outflow Q can be calculated as

$$Q = \phi\, l_j\, H_e\, (2p_c/\rho_a)^{0.5} \tag{12.3}$$

where l_j is the peripheral length of air leakage (m) and ϕ the flow coefficient (take $\phi = 0.6$).

Flow rate for minimum calm water drag Q_{minR}

Owing to momentum drag of the cushion air increasing with flow rate and skirt drag increasing inversely with flow rate, ref. 98 proposed the following relation for the flow rate Q_{minR}, for minimum drag:

$$Q_{\text{minR}} = [0.34\, b/a]^{0.75} \tag{12.4}$$

$$a = \rho_a V_s$$

$$b = C_{dsk}\, l_j^{1.68}\, (2p_c/\rho_a)^{0.17}\, S_c^{0.5}\, 0.5\rho_w\, V_s^2$$

where C_{dsk} is the skirt drag coefficient of craft on calm water,

$$C_{dsk} = 1.5 \text{ (typically)}$$

Meanwhile, the flow at which the minimum total installed power can be obtained [98] can be written as

$$Q_{\text{minp}} = [0.34b/(a + (p_c\, \eta_p/V_s\, \eta_l))]^{0.75}$$

where η_p is the overall propulsion efficiency and η_l the overall lift efficiency.

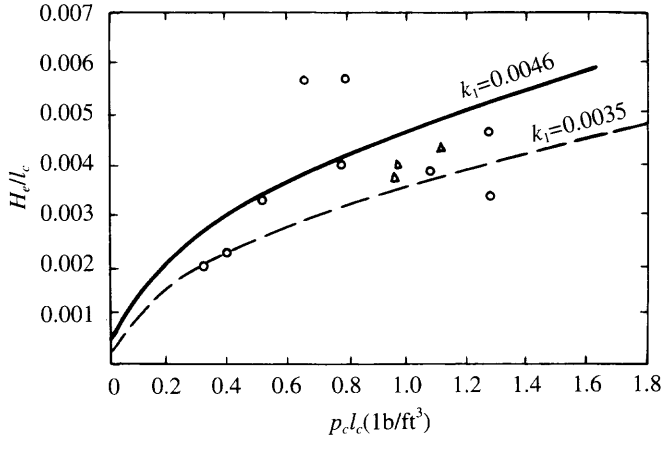

Fig. 12.3 Relative air clearance vs p_c/l_c.

These equations should only be used for reference as a starting point in determination of ACV cushion air flow. Meanwhile it may be noted that all of the physical values in these expressions are imperial dimensions, e.g. ft for length and lb for weight, etc., while the equivalent in SI units is given on the right-hand side.

Determination of overall pressure head of fans

The determination of overall pressure at the fan requires the calculation of the various pressure drops in the 'pipe' system. To begin this, at first one has to determine the bag cushion pressure ratio p_1/p_c of the skirt to meet the requirements for stability and seaworthiness. Early hovercraft designs, in order to prevent the plough-in of craft, in general had a high bag/cushion pressure ratio.

In the early 1980s, once the mechanism of skirt deformation in the bow area was fully understood, it was shown that plough-in could be prevented by means of improving the type and configuration of skirts and air ducts as well as regulating the ACV dynamic trim. Therefore designers now often adopt a low bag/cushion pressure ratio, such as 1.09 for ACV model 7202.

With respect to the bag/cushion pressure ratio of SES, in order to minimise the losses in air ducts and lift fan system, sometimes an air duct or bow/stern fan might be deleted, and the bag/cushion pressure ratio may be even lower, as the air duct system will be greatly simplified. A typical calculation for the air ducts of ACV/SES can be written as follows.

Air duct calculation for ACVs

The arrangements of ACV fans and air ducts differ greatly and dependent on the passenger cabin arrangement, machinery bay, transmission shaft system, fans and propellers. The calculation of air duct head loss and the flow distribution have to be analysed for the specific craft design. A typical example can be seen in Fig. 12.1. This figure shows that one fan blows the pressure air via the pressure chamber into the bags (such air ducts have been used on Chinese ACVs 711-IIA, 716-II, 7206 and 7210 for example). Sometimes the air ducts of skirt bags are connected with each other, so the overall pressure in various bags is basically equal, thus the problems are simplified. An arrangement is shown in Fig. 12.4, namely the air duct system becomes a parallel pipeline system and its branch pipes are:

1. via the air feed holes of the bow and fore side bag into the cushion;
2. via the air feed holes of the stern and rear side bag into the cushion;
3. via the air feed holes of the longitudinal stability skirt bag into the cushion;
4. via air feed holes of the transverse stability skirt bag into the cushion.

According to the Bernoulli equation and knowing the cross-section area of the duct sections, the flow rate in air ducts Q_1, Q_2, Q_3, Q_4, etc. can be calculated as shown in section 8.4.2.

During the initial performance analysis, before the craft geometry is fixed, the calculation can be worked out according to the different bag/cushion pressure ratios in various air ducts, in order to get different skirt stiffnesses. The equation will have multiple degrees of freedom, so the flow equation is best solved by an iteration method.

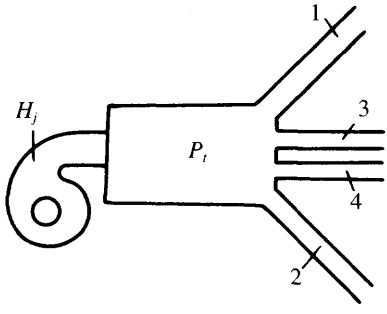

Fig. 12.4 Layout of simulated pressure distribution of typical lift systems (H_j = fan pressure, P_t = bag pressure): (1) air from bow and fore bag, via its bow into cushion; (2) air from stern and rear bag, via its hole into cushion; (3) air from longitudinal stability skirt bag and via its holes into cushion; (4) air from transverse stability bag and via its holes into cushion.

In order to reduce the work, during the preliminary design, the overall fan pressure on an ACV can be estimated by simplified expressions as follows [94]:

$$H_j = p_c\,(p_t/p_c) + k_d\,(Q/d_2^2)^2 + k_E q_E - k_R q_A \tag{12.5}$$

where d_2 is the diameter of the fan impeller, k_d the air duct head loss coefficient from outlet of fan to skirt bag (as shown in Table 12.3), k_E the head loss coefficient of fan air inlet (as shown in Table 12.4), k_R a coefficient due to the head recovery of air inlet (as shown in Table 12.5), q_E the dynamic head of fan air inlet, which can be written as

$$q_E = 0.5\rho_a\,[4Q/(\pi d_E^2)]^2 \tag{12.6}$$

d_E is the diameter of the fan inlet and Q the air inflow rate,

$$q_A = 0.5\rho_a\,(V_s + V_w)^2 \tag{12.7}$$

where V_s is the craft speed and V_w the wind speed (it is shown above as in head wind condition). The first item of the right-hand side of equation (12.5) represents the bag

Table 12.3 Loss coefficient in air ducts k_d [94] (including SES)

Year	Craft weight (t)	Type of air flow distribution (air duct system)			
		Free diffusion into pressure chamber (on craft SR.N4, BH.7)	Mixed controlled and free diffusion (on craft SR.N6)	Centrifugal fans with short outlet diffusers (on craft JEFF(A), VT 1, 3KSES)	Axial fans with conical diffusers (on craft HD.2)
1980	100	0.037	0.0114	0.0063	0.0035
	10 000	0.037		0.0055	0.0030
1990	100	0.035	0.0110	0.0055	0.0032
	10 000	0.035		0.0045	0.0028
2000	100	0.033	0.0105	0.0050	0.0030
	10 000	0.033		0.0042	0.0026

Table 12.4 Loss coefficient of fan inlet k_E (including SES)

Year	Craft weight (t)	Configuration of fan inlet		
		Opening inlet, integrated fan system (on craft SR.N6, SR.N4, BH.7)	Opening inlet, circular inlet (on craft JEFF(B), HD2, N300, N500)	Air ingested from diffusion (on craft JEFF(A), VT1, VT2, CC-8, 3KSES, SES-100A, SES-100B)
1980	100	0.016	0.01	0.016
	10 000	0.014	0.009	0.014
1990	100	0.012	0.009	0.012
	10 000	0.011	0.008	0.011
2000	100	0.010	0.008	0.010
	10 000	0.009	0.007	0.009

Table 12.5 Pressure recovery coefficient at inlet of fan k_R (including SES)

Year	Craft weight (t)	Configuration of fan inlet				
		Rearwards facing fan inlet (on craft HD.2)	Integrated fan and propeller system (on craft SR.N6, SR.N4, LACV–30, BH.7)	Flush inlet (on craft JEFF(A)&(B), VT 1 and 2, SES–100B, N300 and 500, 3KSES, CC–7, MV-PP5, Aist, etc.)	Scooping inlet (on craft SES-100A)	Fan forward inlet (on craft HM.2, Gus)
1980	100	− 0.2	0.4	0.5	0.7	1.0
	10 000	− 0.2	0.5	0.6	0.8	1.0
1990	100	− 0.2	0.45	0.55	0.8	1.0
	10 000	− 0.2	0.55	0.65	0.85	1.0
2000	100	− 0.2	0.5	0.6	0.85	1.0
	10 000	− 0.2	0.6	0.7	0.9	1.0

pressure, the second the head loss between the fan outlet to the skirt bag, the third the head loss at the air inlet and the fourth item denotes the head recovery at the fan inlet.

Calculation of overall pressure and lift system power for SES

The typical air duct system of an SES is shown in Fig. 12.5(a) (similar to that on craft 717) and an equivalent pipe system is shown as Fig. 12.5(b), i.e. the parallel pipeline of the air supply system. The equation, similar to that in the ACV lift system, can also be solved by the Bernoulli equation. Thus according to the required air flow and the configuration of air ducts, the overall head H_j and lift power N_{el} (in kW), can be written

$$N_{el} = H_j\, Q_i/[1000\eta_F\, \eta_M] \tag{12.8}$$

where H_j is the fan overall pressure (N/m^2), Q_i the air inflow of the fan (m^3/s), η_F the fan efficiency and η_M the transmission efficiency. The calculation concerning the fan

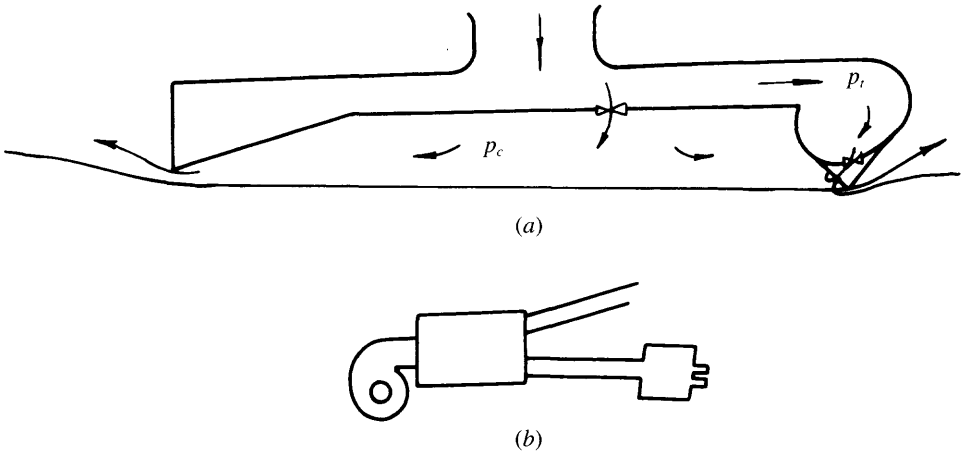

Fig. 12.5 A typical equivalent air duct system for SES: (a) air duct configuration; (b) equivalent parallel air network for calculations.

recovery pressure coefficient and pressure loss at inlet, etc. can be calculated as detailed above.

12.3 Design of fan air inlet/outlet systems

Inlet system

From Figure 12.4, it can be seen that the air inlet pressure recovery will play a very important role for an ACV with large lift air flow rate, and so a significant saving can be obtained by using a well-designed air inlet. It will be less important for SES due to the lower lift system air flow rates.

The British Hovercraft Corporation has carried out much research work [95] in this area. The ACV series SR, such as SR.N4, SR.N5, SR.N6, all used an integrated system for lift system fans and air propellers mounted above the cabin structure, as shown in Figs 12.7 and 12.8. Reference 96 specially introduced the effect of the geometrical parameter of the inlet on the air inlet pressure recovery. They investigated the effect of inclination angle of the inlet and lip configuration on the air pressure recovery, as shown in Fig. 12.10. Figure 12.9 shows the effect of inlet position on the lift power.

All of these factors can give a reference for inlet design, which may be summarized as follows:

1. During design of the lift fan inlet, the advantage of an air scooping inlet should be considered. Figure 12.8 shows the effect of air inlet position on the lift power. The difference of lift power between a positive air recovery inlet and negative inlet will be up to 5–8%.
2. The ingestion effect of air in the laminar layer close to craft structure surfaces

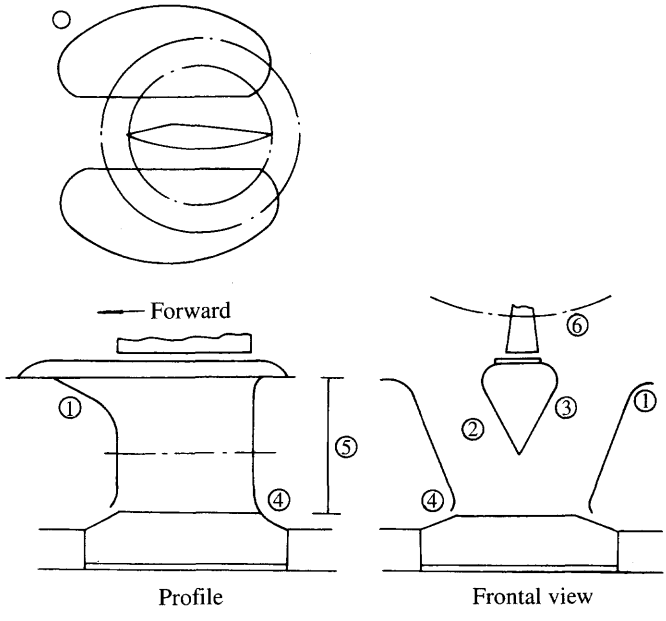

Fig. 12.6 Design considerations for air inlets of integrated lift/propulsion systems. 1: increased forward lip radius; 2: air inlet fairings; 3: centre body for smooth flow; 4: close fitting inlet to fan; 5: height of air inlet duct; 6: influence of air propeller/pylon.

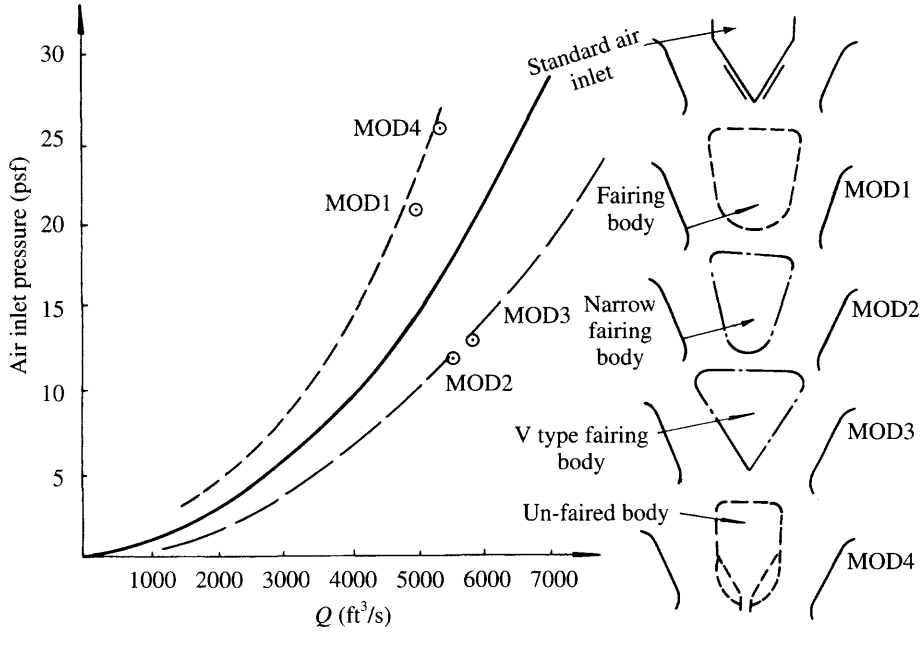

Fig. 12.7 Influence of gearbox shape on air inlet systems pressure losses.

should also be considered. In general, the inlet front lip should be designed with a larger radius of curvature, as 1 in Fig. 12.6 and the foreward part of A in Fig. 12.9, and slightly protruding in order to increase the air pressure recovery coefficient. Figure 12.9(c) is a typical example investigating the air inlet pressure recovery [96].

The researchers in this reference carried out three projects, two types of inlet foreward lips A, C and one inlet rear protruding part B compared to the standard symetrical fan inlet. The maximum air inlet recovery of the combination of these three parts could therefore be obtained. The figure shows that the second project, namely the standard inlet plus foreward lip A and rear lip B, is found to be the optimum. Moreover, it will be better for the angle between the centre line of fan inlet and the oncoming flow angle α to be smaller than 90° in order to obtain better ram pressure recovery. This is not necessary in the case of small craft and at large inlet ram pressures, i.e. at higher values.

3. A definite height of inlet tunnel is required to obtain straight air streamlines in the inlet to enhance the fan efficiency. Too high an inlet tunnel will increase the craft height, therefore it is a trade-off between the two requirements, as shown at 5 in Fig. 12.6.
4. In general, the transmission gearbox is located in the fan inlet, for practical reasons. It is therefore suggested that the gearbox is carefully designed to reduce its size and thus minimize air inflow blockage, particularly at the contracting section of the inlet. MARIC have experience with a gearbox and fan arranged exactly at the contracting section of the fan inlet of an ACV model, which consequently could not hover up. This was improved after raising the position of the gearbox.

Designers are also recommended to pay attention to the shape of the centre body of the gearbox. Figure 12.7 shows results from study work carried out by BHC. The difference of inlet pressure loss is 10% between the non-smooth gearbox model

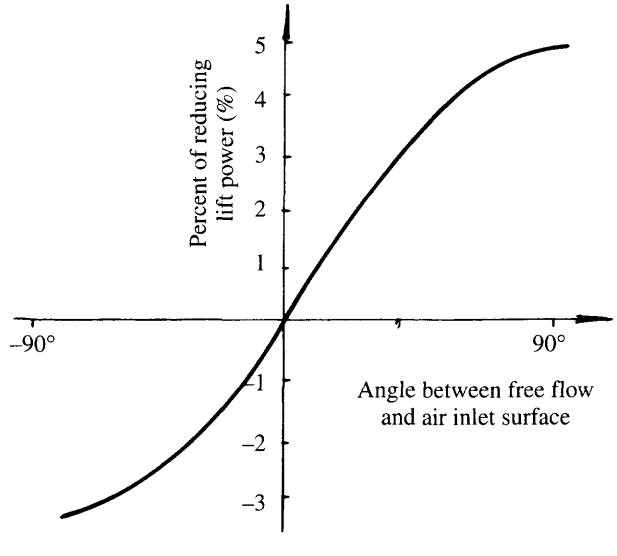

Fig. 12.8 Lift power versus air inlet location.

MOD 4, blocking at the contracting section of model MOD 1, and the narrow centre body with less blockage at contraction section model MOD 3. Thus it can be seen that about 10% of lift power may be saved.

5. Increasing the air inlet duct area to decrease the velocity of air inflow will give a significant reduction of inlet losses, because the dynamic pressure at the air inlet increases in square proportion to the inflow velocity, thus increases inversely in

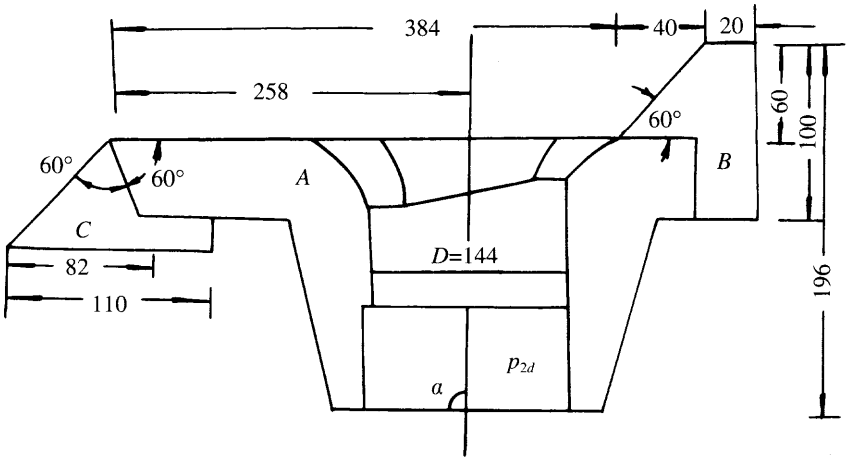

Fig. 12.9 (a) Influence of inclination angle of air inlet on ram air pressure recovery: (a) dimension and variations of air inlet geometry.

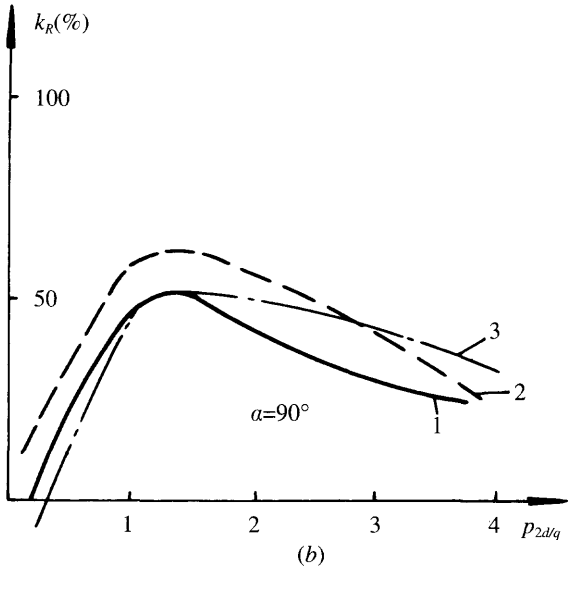

Fig. 12.9 (b) ram air pressure recovery coefficient vs air inlet configuration. 1: standard air inlet plus A; 2: standard air inlet plus B; 3: standard air inlet plus A and C.

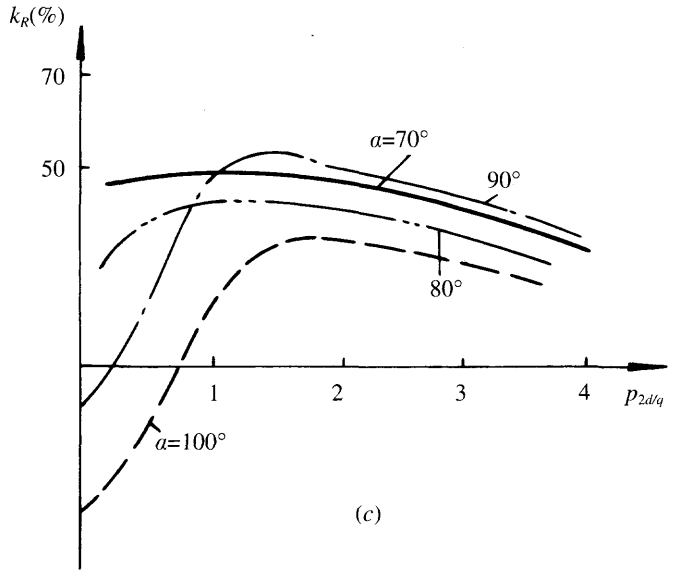

Fig. 12.9 (c) ram air pressure recovery vs inclination angle of air inlet.

fourth proportion with the diameter of air inlet. Moreover, discontinuity of section area for inflow should be avoided as far as possible in order to reduce pressure losses, as shown in Fig. 12.6.

6. Continuity of cross-section of the fan inlet in the axial direction should be preserved with the foreward disc of the fan impeller in order to avoid air flow separation and leakage of pressurized air as well as reduction of fan efficiency as shown in Fig. 12.10.
7. In general, the fan air inlets might be arranged at the craft rear or stern in order to reduce the craft aerodynamic form drag. If this arrangement is used the distribution of air inflow between the fans and air propellers has to be considered carefully.

In our experience, if some care is taken this problem can be solved successfully and vibration of shaft systems, engine mountings, air ducts and air propellers due to the non-uniformity of air inflow avoided. This is because air density is less than water density, so as to make a smaller vibration exiting force. However, it is better to carry out model test investigations in a wind tunnel with the actual arrangement in order to avoid violent vibration at this part.

ACV fan air outlet system

At the fan air outlet, the air flow velocity and dynamic pressure are highest. In addition the air flow will be very turbulent unless a downstream volute and guide vanes are fitted. For this reason, it must be designed carefully.

Outflow has to be led with no air blockage due to sudden changes of cross-sectional area and diffused gently to the craft air duct system. Air blockage sometimes may occur to the craft, because of a large amount of pipeline arranged in the plenum chamber, but it is unlikely to be a problem in the case where the blocking structures

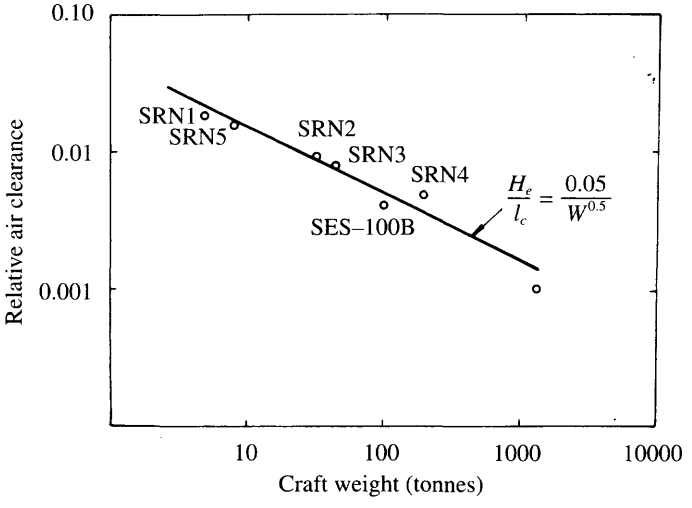

Fig. 12.10 Relative air clearance H_c/L_c for ACV vs craft weight.

are slight and far from the fan outlet. Therefore the fan outlet has to be designed carefully with the aid of model experiments for measuring loss of pressure.

The skirt bag can also be used as the plenum chamber for diffusion of pressurized air. MARIC has a lot of experience on this subject. Due to the lack of care during design and construction of some craft, there were pipes and frames blocking the outflow, which caused reduction of pressure and air clearance under the skirt so as to lead to deterioration of take-off through hump speed. The craft sometimes lost speed as low as to hump speed in the case of head wind, overload and incorrect handling.

In general there are three air outlet system designs which may be used on an ACV, these are as follows.

Vertical arrangement of fans

In this case, the fan is arranged perpendicular to the ground or waterline. The air is blown out from the fan outlet directly into the skirt bag or air cushion and uses the skirt as the diffusion duct. Since the fan can diffuse the pressurized air in the volute system, then the air velocity at the outlet can be decreased significantly in order to reduce the pressure loss, which can also be calculated accurately. This system can obtain a high air outlet efficiency.

Horizontal arrangement of fan (without volute)

This is an arrangement such as used for the BHC SR.N4 and SR.N6. The key requirement of such an arrangement is that the corridor from the air duct has to be roomy not only in the tangential direction, but also in the radial direction. All stiffeners or frames, pipes, cables, etc. have to be arranged far from the outlet. Although these fans are without a volute to diffuse air progressively into the cushion, the streamline is diffused freely in an intermediate plenum chamber formed by the craft buoyancy tank and hull structure. Experiments prove that this system can give high air duct efficiency due to the low air velocities.

Horizontal arrangement of fan with part volute (or guide plate)

Often due to various requiremnts for craft layout, the air streamline in the horizontal arrangement of fans cannot provide free diffusion, but needs to be diffused smoothly via a part volute or flow-guide plates. In this case particular attention has to be paid by designers, because the existence of machines, equipment and structure will affect the layout of volute and flow guide plates so as to reduce the air duct efficiency and so skirt air gap, stability, seaworthiness, anti-plough-in capability, etc.

SES fan outlet system

The lift fan flow rate of an SES is smaller than that of an ACV, thus the size of fans for an SES is also smaller. For this reason, SES fans are generally accommodated in the machinery bay and sometimes include the inflow system in the engine bay. Differing radically from an ACV, only enough area of air inflow for the engine bay has to be regarded in order to avoid high velocity of air inflow and too large a pressure loss.

Noblocking objects or plates should be arranged in front of the fan air inlet in order to avoid inflow blockage, particularly in the case where the craft is running on rough seas, as the air inlet blockage will affect the air inflow and increase the loss of pressure at the air inlet. Consequently, it will affect the fan characteristic indirectly, making it steeper, which strengthens the cobblestone effect in the case where craft are running in short-crested waves.

To meet these requirements for the design of air outlet systems, a number of measures may be taken. They can be summarized as follows:

1. A minimum distance of the air outlet from the water surface has to be maintained in order to prevent the water causing damage to the fan impellers. It is best if some guide plates are arranged at the fan outlet which can act as green water deflectors, or the air duct from the outlet can be curved in order to prevent spray hitting the fan blades.
2. The area of the outlet is suggested to be widened as far as possible in order to avoid sudden air diffusion at the outlet, leading to a large pressure loss. A efficient diffuser shape also will flatten the fan air duct characteristic and reduce the cobblestoning effect.
3. Action should be taken to optimize the bow and stern bag cushion/pressure ratios and the flow distribution for the bow/stern bag and air cushion. It is difficult to give general recommendations. Definite conclusions can be determined according to the craft size, craft speed and requirements for seaworthiness.

   An SES may have a separate air feed to the stern skirt loops, or adjustable (during maintenance) feed holes into the loop. If the stiffness of this skirt is too high, problems may be encountered with acceleration through hump speed and cavitation or air injestion of the propulsors in heavier seas.

   It is normal for most of the cushion air to be fed through the bow bag or into the segments at their top, from holes positioned similarly to the optimum for feed from a loop above the segments.

12.4 Lift fan selection and design

The function of the lift fan is to provide:

- sufficient pressurized air to support the craft weight on the cushion;
- the required flow rate in order to maintain the design skirt tip air gap, and in addition meet the requirements due to wave pumping, heave motion pumping and the change of cushion air requirements as the craft moves over differing terrain;
- a suitable fan pressure/flow characteristic curve so that it will not stall during craft operation. The characteristic has to meet the slope of overpressure with respect to flow rate at the design point, and also to consider the characteristics at off design points, which will affect the seaworthiness at larger heaving amplitudes.

Before selecting and/or designing the fan(s), one first has to consider how to select the appropriate type, i.e. which type of fan will be suitable for the craft design, whether axial, mixed flow or centrifugal flow.

The considerations are introduced below, followed by a discussion of the design characteristics of each lift fan type.

Selection of fan type

There are three generic types of fans which may be used for ACVs and SESs. The centrifugal fan possesses the feature that high pressure head may be maintained at small flow rates. The axial fan produces a large flow and relatively low pressure head. Mixed flow fans have characteristics in between the centrifugal and axial fan types. Typical characteristics of these types of fan are shown in Fig. 12.11.

Each of the three types can be adopted for ACVs, as they normally have a cushion with low to medium pressure. SESs and air cushion platforms tend to operate with higher cushion pressures and so generally centrifugal or mixed flow fans are most appropriate. The application ranges defined by the specific speed of the fan at design flow (N_s) are

$$\begin{aligned} N_s &< 3 \quad \text{Suitable for centrifugal fans} \\ 2 < N_s &< 4 \quad \text{Suitable for mixed flow fans} \\ N_s &> 3 \quad \text{Suitable for axial fans} \end{aligned}$$

However, the selection of a lift fan is also strongly dependent upon the tradition and custom of the research institutes and manufacturers. For example, the former Soviet Union and France more often use the axial fan, while in the UK the centrifugal fan is used for ACVs except small recreational craft, and centrifugal or mixed fans for SES. In China it is usual to install an industrial centrifugal fan, partly due to its easy procurement.

The non-dimensional specific speed of a fan can be written as

$$N_s = nQ^{0.5}/(gH)^{0.75} \tag{12.9}$$

where N_s is the specific speed, H the overall pressure of the fan (metres of water head), Q the flow rate of the fan (m^3/s) and n the speed of the fan impeller (revolutions/s). Meanwhile the non-dimensional specific speed can also be written as

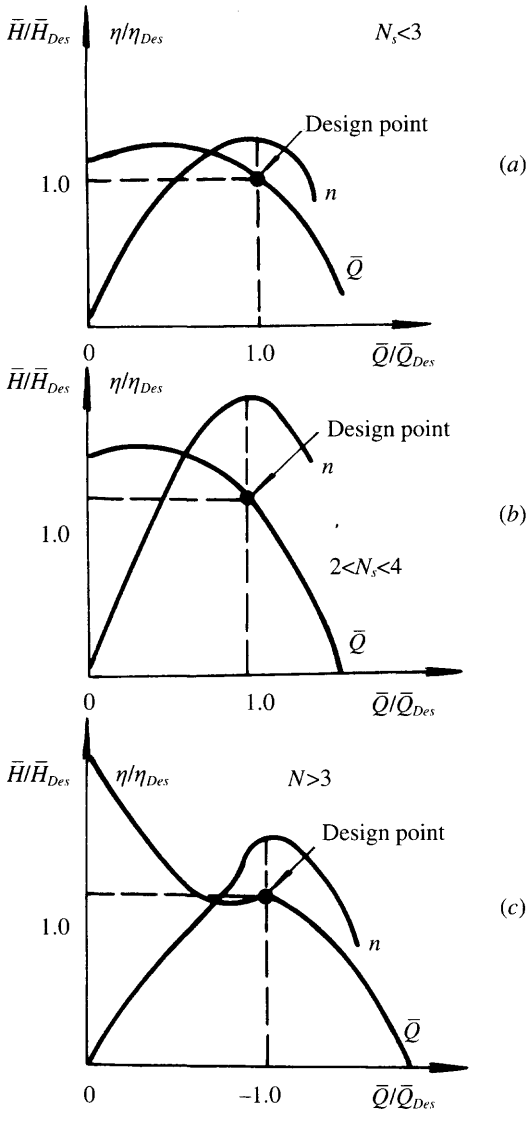

Fig. 12.11 Characteristics of three types of fans: (a) centrifugal fan with backward inclined blades; (b) mixed flow fan; (c) axial fan.

$$N_s = \bar{Q}^{0.5}/\bar{H}^{0.75} \tag{12.9a}$$

where $\bar{Q}$ is the flow rate coefficient

$$\bar{Q} = \bar{Q}/nD^3$$

and $\bar{H}$ the pressure coefficient

$$\bar{H} = H/[\rho_a n^2 D^2]$$

where D is the diameter of the fan impeller (m), H the overall pressure head (N/m^2) and ρ_a the air density (Ns^2/m^4).

Considerations for off-design operation

Due to the flat fan pressure-inflow characteristic of a centrifugal fan, it will also be generally suitable for off-design operation. A typical centrifugal fan design is shown in Fig. 12.12.

Blade vibration may occur to an axial fan at low air flow rates due to the separation of flow at the blade surface. This causes a peak and hollow on the pressure/flow characteristic of the fan, i.e. $dH/dQ > 0$, which means that in this region the operation mode is unstable. This is the disadvantage of the axial fan. Certainly craft motions in a seaway can cause vibration and eventual fatigue to an axial fan blade.

Most small craft use this type of fan for their lift system, as their cushion pressure is relatively low (around 5–20 psf or 240–960 N/m^2). The fans used have polypropylene or nylon (PA-11) blades, which are relatively light. Extreme pressure fluctuations can cause the fan to burst, but due to the low mass of the blades, damage to the craft structure is normally minimal. In contrast, burst of a centrifugal fan is likely to be a major event and needs careful design of the surrounding ducting to prevent damage to the craft and personnel.

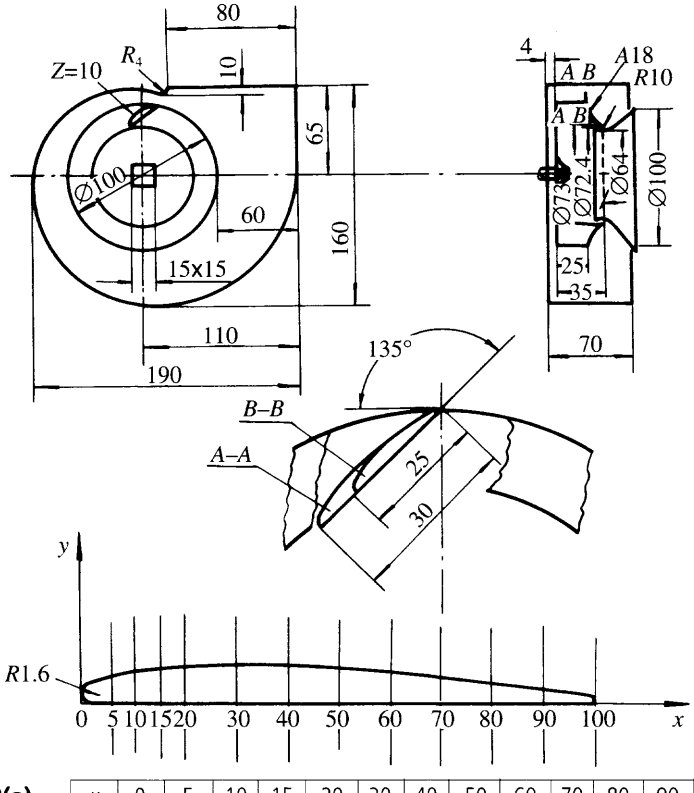

Fig. 12.12(a)

x	0	5	10	15	20	30	40	50	60	70	80	90	100
y	16	4.6	6	6.8	7.25	7.6	24	6.85	6.08	5.1	3.95	2.65	1.2

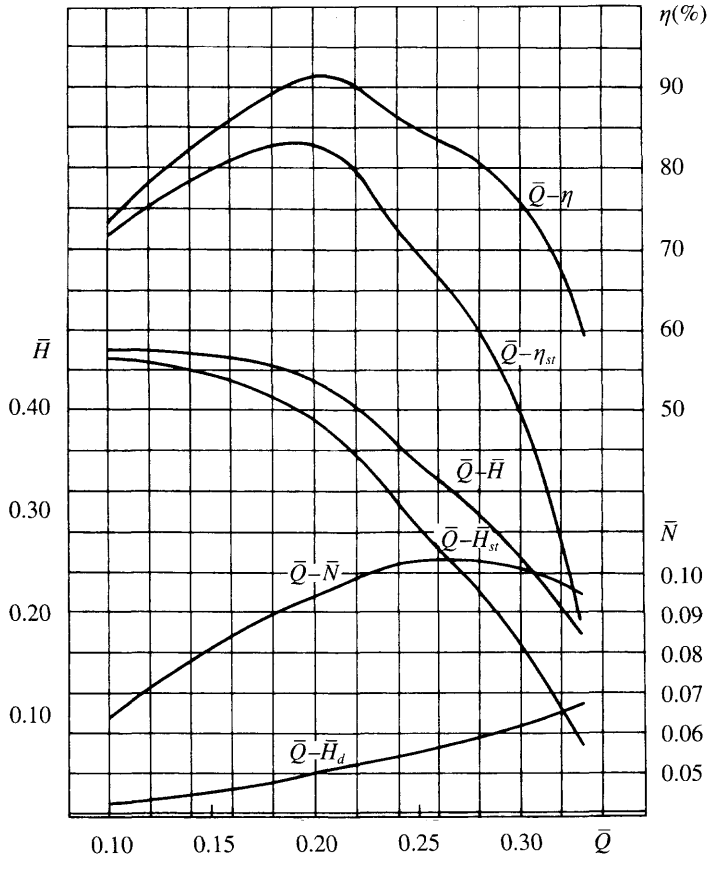

Fig. 12.12(b) Aerodynamic characteristics of Chinese centrifugal fan model 4-72, its configuration and streamlined blade offsets.

Fan choice

The principal choice for an ACV or SES designer is likely to be which commercially available fan type will be used. The major source of fans is the heating and ventilating industry. The first task therefore is to investigate what fans are locally available, whether direct from local manufacturers or from distributors, which are of a size which appears applicable to the initial craft design. Currently, fans of all three major types are available, though the ACV designer may have to uprate the fan, either by allowing increased stresses compared with building industry practice, or by building a completely new hub to hold the blades in the case of some axial fans.

Since the HVAC industry design considerations are normally related to system noise and efficiency, fans in HVAC systems are normally very lightly loaded. Use of higher specific speed can normally provide the requirements for an ACV. Care should be taken to select fans which are designed around aerofoil blades and not flat plate

blades. Also steer away from blades cast in aluminium as these will be sensitive to vibration and fatigue.

A fan burst of a cast aluminium fan is generally very dangerous due to the large energy stored in the blades themselves. Steel fans (normally centrifugal, formed from plate) are generally too heavy for ACVs and select themselves out. Should a fan in either material be selected, then care must be taken to install a guard around the fans which can retain the energy of a failed blade. In the case of an axial fan, a mesh guard at the intake is required, and a duct with walls sufficient to absorb the energy. An aluminium sheet ring around the fan blade tips, or additional woven roving layers in the GRP ducting, will normally be sufficient. A centrifugal fan would require a steel plate ring around the volute.

GRP moulded blades can also be sensitive to fatigue and cannot be recommended for axial fans, though there have been several successful applications for centrifugal and mixed flow GRP fans. Attention has to be paid to finishing these fans, by sealing all surfaces with gel coat, so as to prevent water being drawn into the fan along glass strands and putting the fan out of balance.

Axial and centrifugal fan blades of PA-11 impregnated with short glass strands have been successfully applied. These blades are stiffer than PA-11 alone. They can shatter more easily than the basic polymer in temperatures below zero. Craft which are to be used in cold climates therefore need to use materials such as polypropylene and polyurethane.

After selection of fan type, the fan, air duct and air clearance characteristics have to be drawn out as shown in Fig. 12.13. Based on the non-dimensional characteristics and size of the selected fan as well as the fan speed, one can determine the dimensional characteristics of the fan, subtract the pressure loss in air ducting, then obtain the characteristic of the air cushion. The logic for this procedure is shown in a chart form as Fig. 12.14.

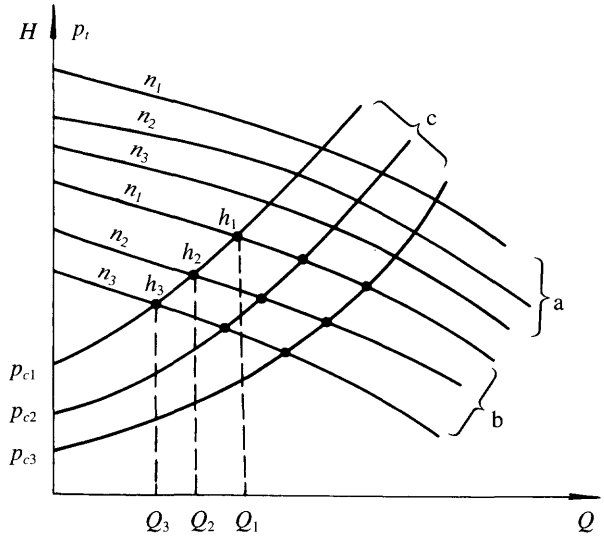

Fig. 12.13 Fan, air duct and air clearance characteristic curves of ACV/SES: (a) fan; (b) air duct; (c) air clearance (under-skirt gap).

Meanwhile, based on Chapter 2 and previous sections of this chapter, the relation can be obtained between the bag pressure and flow rate at different cushion pressures p_c, i.e. the characteristics related to differing air clearance. Thus from the intersection point of clearance and air duct characteristic curves, one may obtain the air clearance under the skirt (or flow rate) at different craft weight and engine speeds. This group of curves is very important for checking the performance of craft.

We introduce here the fan characteristics and configurations widely used in China, i.e. the characteristic of industrial fan model 4-73, 4-72 and modularized fan design. A comparison between foreign and Chinese fans is also made. Table 12.6 shows the fans mounted on some ACV/SES.

Modularized design of centrifugal fans

The industrial centrifugal fan models 4-73, 4-72, etc. have been widely used in China and a large amount of experimental results and data have been obtained which verify

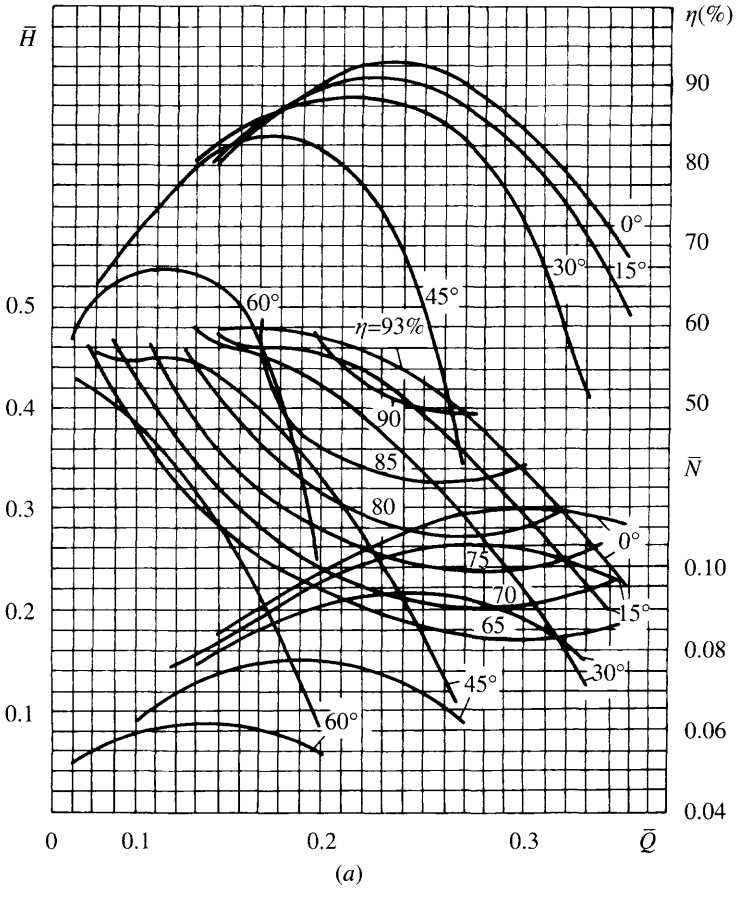

Fig. 12.14(a) Aerodynamics characteristics of Chinese centrifugal fan model 4-73, its configuration and streamlined blade offsets.

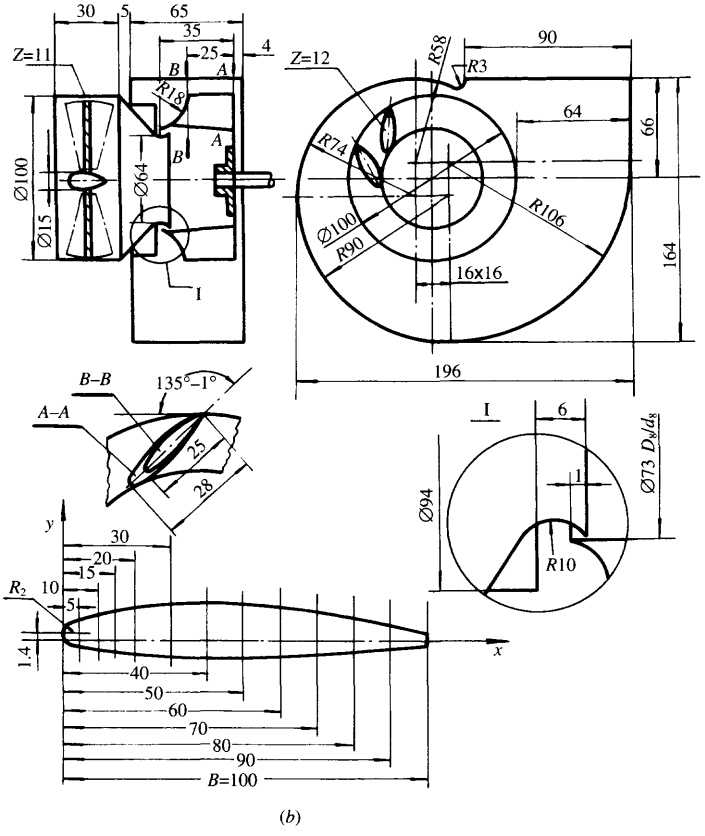

(*b*)

Fig. 12.14(b) Chinese fan model 4-73 geometric data.

x	5	10	15	20	30	40	50	60	70	80	90	100
y	4.6	6	6.8	7.25	7.6	7.4	6.85	6.08	5.1		2.65	1.2
$-y$	1.15	1.5	1.7	1.81	1.9	1.85	1.71	1.52	12.8	0.99	0.66	0.3

that the characteristics of these fans are suitable for the ACV and SES, so in general we apply the modularized design method and take the industrial centrifugal fan as the prototype to design ACV fans [97, 98]. Some fans, those on ACVs with high load density, or air cushion platforms with special requirements, are outside the range of such standard fan types. Then new fans have to be designed.

During the modularized design of a centrifugal fan, the following steps should be taken.

Selection of fan type by means of specific speed

The dimensional specific speed of lift fan can be written as follows:

$$N_s = n\, Q^{0.5}/H^{0.75} \tag{12.10}$$

where n is the fan speed (r/min), Q the inflow rate of the fan (m^3/s) and H the overall pressure of the fan (kg/m^2). Thus the dimensional specific speed can be obtained according to the required Q, H and speed of fan. Then designers can select the characteristic curve of an available industrial fan and check to see if the design point is

Table 12.6(a) Lift fans mounted on some ACV/SESs [4] – basic data

Craft	Builder	Fans (No.)	Fan type	Tip diameter (m)	No. blades	Design speed (RPM)	Overall pressure (Pa)
VA-1	Dowty Rotol	2	Centrifugal	1.31	17	875	1250
VA-2	Dowty Rotol	2	Centrifugal	1.67	17	870	3400
VA-3	Dowty Rotol	2	Centrifugal	3.35	19	430	3112
HM.2	Hovermarine	5	Mixed Flow	0.61	11	2900	3351
HM.2			Centrifugal				2394
SKIP	General Dynamics	1	Axial	1.65			
SKMR–1	Bell Aerospace	4	Axial	1.98	10	1200	2973
VRC-1	British Vehicle Research Corporation	2	Centrifugal	0.99	8	1140	962
SES 100B	Bell Aerospace	8	Centrifugal	1.22	12	1700	5745
SES 100A	Aerojet General	3	Axial	1.21	19	2500	7804
SR.N6	BHC	1	Centrifugal	2.13	12	800	3591
SR.N4	BHC	4	Centrifugal	3.50	12	700	5745
N-500	Sedam	4	Axial	1.85	12	900	2968
		2	Axial	3.60	12		
VT.1	Vosper Thornycroft	8	Centrifugal	1.54	12	1050	
JEFF-A	Aerojet General	8	Centrifugal	1.22	12	2450	8139
Sormovich	Krasnoye Sormovo	1	Axial	2.74	12		4309
713	Shanghai HDSY	2	Centrifugal	1.0	12		4400
717C	MARIC	4	Centrifugal	0.6	12		4900
711-II	Shanghai HDSY	1	Centrifugal	1.8	12		2900

Table 12.6(b) Lift fans mounted on some ACV/SESs [4] – statistics

Craft	Builder	Flow rate (m^3/s)	Fan efficiency	Fan Shp kW/0.735	Specific speed (N_s)	Impeller weight (kg)	Cushion pressure (Pa)	Overall pressure (Pa)
VA-1	Dowty Rotol	22.6	0.86	55	2.43	27.6	820	1250
VA-2	Dowty Rotol	21.8	0.78	128	1.11	59.0	958	3400
VA-3	Dowty Rotol	75.6	0.79	400	1.09	304.0	1518	3112
HM.2	Hovermarine	5.61		30	2.34	8.2	2202	3351
HM.2		5.1						2394
SKIP	General Dynamics					28.5		
SKMR-1	Bell Aerospace	73.6	0.79		3.20		2250	2973
VRC-1	British Vehicle Research Corporation	8.86				58.1	814	962
SES 100A	Aerojet General	18.4	0.76		2.95		4549	5745
SES 100B	Bell Aerospace	66.0	0.68	195	1.35	95.2	4788	7804
SR.N6	BHC	75.0	0.83		1.82		1675	3591
SR.N4	BHC	113	0.75		1.38	680.0	2394	5745
N-500	Sedam	481	0.75		3.99			2968
VT.1	Vosper Thornycroft			175	1.75			
JEFF-A	Aerojet General	45.3	0.80	785	2.35	59.0	4596	8139
Sormovich	Krasnoye Sormovo	113					1963	4309
713	Shanghai HDSY	12.5	0.85	190			3120	4400
717C	MARIC	5	0.85	30			2500	4900
712-II	Shanghai HDSY	51.7	0.84	239			2160	2900

located at a high efficiency region. If not an alternative choice may be made and rechecked, as an iterative process.

Determining the type of fan, the non-dimensional flow and head as well as the fan efficiency at the design point can then be calculated (H, Q, η, etc.):

$$\bar{H} = H/[\rho_a u_2^2] = 3600H/[\rho_a \pi^2 n^2 D_2^2] \tag{12.11}$$

$$\bar{Q} = Q/Fu_2 = 240Q/[\pi^2 n D_2^2] \tag{12.12}$$

where F is the area of the fan impeller disc (m^2),

$$F = \pi/(4D_2^2)$$

u_2 is the circular velocity of the fan impeller (m/s),

$$u_2 = (\pi D_2 n)/60$$

and D is the impeller diameter (m). Meanwhile the power output of the fan can be obtained as

$$N_f = QH/[1000 \eta_f](\text{kW})$$

where η_f is the fan efficiency.

The calculation mentioned above is suitable for selecting the fan type. During the calculation of circular velocity u_2, it is suggested that designers have to take the strength of the impeller blade and the noise of the fans into account. For the blades with an aerofoil profile, in general we take $80 < u_2 < 110$ m/s.

Selecting the impeller diameter

After selecting the fan type one can select the impeller diameter to position the design point of the fan according to the fan characteristic, required air inflow, overall pressure head of the fan and given fan speed. It may be noted that the actual operation points of a lift fan are not often situated at the design point.

In general only a small air flow is needed when the craft is running on calm water, in order to obtain the optimum craft running attitude. In the case where craft are operating in waves, captains often throttle up the lift engine in order to reduce the vertical acceleration of the craft, i.e. reduce the vertical motion and the wave pumping effect. For instance, the fan speed of SES model 713 operating on calm water is 1250 r.p.m., but 1400–1500 r.p.m. in waves.

As a general rule, fan flow rate increases in linear proportion to the speed, while pressure increases in square proportion and the power increases in cubic proportion; thus the flow rate of the fan in waves will increase 1.12 times, pressure increase 1.25 times and power increase 1.4 times, taking SES-713 as the example.

Craft weight is always nearly constant, so that the cushion pressure also approximately stays constant. The main change is fuel usage, making the craft gradually lighter. The operation point on the dimensional characteristic curve will therefore slip to the right-hand side of the curve, i.e. at larger inflow condition.

The operation points will in general not be located at the design point of curves, since this is normally set for calm water, or for a small sea state rather than the maximum. Therefore during the design of a lift fan, designers have to take off-design points into account to locate these off-design operation points also within the region of high efficiency, moreover at a flattening section of the H–Q characteristic curve so as to reduce vertical motion.

Designers can select several impeller diameters, D_2, to get the corresponding u_2, $\bar{Q}$, $\bar{H}$, then choose a suitable D_2 and consequently plot the operational characteristic

curve of the fan. Using the characteristic of the fan, one can recalculate the characteristic curve of the air duct and compare this with the characteristic of air clearance, then the operation point at various craft weights and fan speeds can be obtained as shown in Fig. 12.13.

Figures 12.12 and 12.14 identify the fan configuration, aerodynamic characteristics and blade offsets for the streamline type of centrifugal fan models 4-73 and 4-72. One can carry out the design (selection) of fans based on these figures.

Technical issues to take into account for lift fan design and manufacture

Choice of impeller speed and diameter

It is very important to select the optimum speed and diameter of impellers. From the point of view of craft general arrangement, the impeller diameter should be decreased for higher craft design speeds, to minimize frontal area. However, the decrease of diameter will need to be compensated by an increase in the number of fans to produce the same airflow volume and their speed will have to be increased so as to support the required pressure head. For this reason, designers have to make a tradeoff between the number, diameter and speed of lift fans to select the most suitable combination.

Fan characteristics at low flow rate

Because the required flow of fans on hovercraft operating over calm water (particularly for SES) is small, i.e. at small Q and sometimes may be $\bar{Q} < 0.1$, complementary experiments with very small flow have to be carried out if unstable operation is suggested by the fan H/Q characteristic. From the point of view of safety and plough-in resistance of craft running in waves, it is suggested setting the pressure characteristic at low flow at twice that at the design point [94]. This cannot be obtained on many hovercraft, as this would require the fan to be operated too far down its efficiency curve and so a compromise must be reached.

Fan balancing

It is not enough to carry out static balancing of a fan. Owing to the wide impeller blades and the lower speed used in steady-state fan tests ($\approx$ 500 rev/min), it is important to check the fan balance at a range of speeds, if possible up to the operating conditions on the craft. MARIC have a lot of experience on this point. By not carrying out fan dynamic balancing carefully enough, some fans, shaft systems and air propellers have been damaged after a period of operation, causing the deterioration of equilibrium of rotating machines. For example:

1. By not carrying out dynamic balancing tests of fans for the craft model 719, fan vibration amplitude was very large at the speed of 1200 rev/min, causing hull vibration and alarm in crews and passengers.
2. With respect to the air impeller composed of GRP of the ACV model 722, the dynamic equilibrium of propeller was destroyed after a time of operation, because water and oil were absorbed into the air propeller blades non-uniformly, thus causing damage to propeller bearing mountings, etc.

Similar experience has been had with fans on craft in the UK through the 1970s and 1980s.

Installation of lift fan

Lift fans have to be mounted carefully according to the specified geometry between impeller and volute (Figs 12.13 and 12.14). Attention should be paid to the size of clearance between the air inlet and impeller (tip clearance and uniformity) as shown in Fig. 12.15. This has been proved in the test of fan model 4-72. For instance, the reduction of radial clearance from 0.5 to 0.3% will give an efficiency increase from 87 to 89% and efficiency will enhance to 91% if the clearance was decreased further to about 0.1%. This latter is probably not practical for fans on large craft.

Air flow rate for fans with double inlet

Due to the difficulty of arrangement of fans, sometimes two lift fans will be fitted on to one backplate to become a fan with a double inlet. To our knowledge, the flow will be 90% of the sum of flow of two fans, i.e. $Q_1 = 1.8Q_0$, where Q_1 denotes the flow of a double inlet fan and Q_0 denotes the flow of a single fan inlet and the corresponding overall pressure will stay unchanged, which was validated by a test of fans on SES model 713. This fan arrangement has also been successfully used on craft such as the VT.1, VT.2, AP1–88, LCAC, etc.

Noise reduction

In order to reduce fan system noise it is suggested to put isolation material on fan volutes. This has been tested on the SES model 719-II and gave good results.

Fan characteristic curves

As is mentioned above, it is better to install fans with a flat pressure–flow characteristic curve in order to get small heaving stiffness and damping, thus minimized motion of craft in waves, particularly the cobblestoning effect of craft running in short-crested waves at high craft speed.

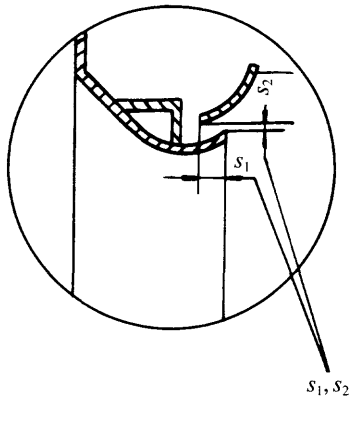

Fig. 12.15 Data for clearance between fan impellers and air inlet casing, which has to be considered carefully during installation of fans.

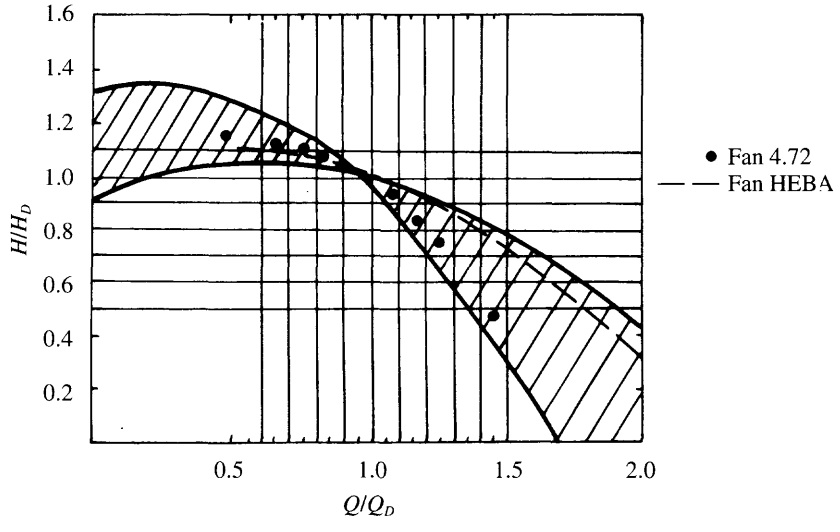

Fig. 12.16 Fan overall pressure-flow rate characteristics of fans used in China and abroad.

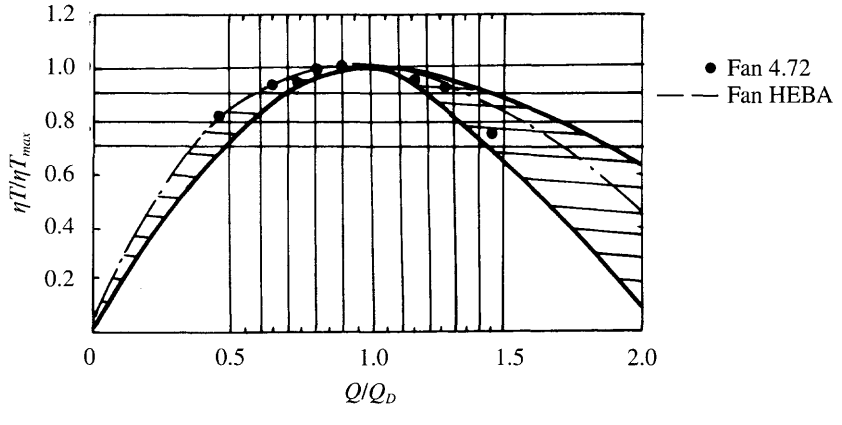

Fig. 12.17 Fan efficiency-flow rate characteristics of fans adopted in China and abroad.

Figures 12.15 and 12.16 [94] introduce the high efficiency HEBA fan which is widely used in Western countries for ACV/SES. It is surprising that the characteristic curves for these characteristics are so close to each other (the shaded area shown in the figures). The high efficiency fan type HEBA-B, as shown in the figures, is typical and shows the flat H–Q curve and η–Q curve.

Characteristic curves for Chinese manufactured industrial fans, which are used as the lift fans of ACV/SES, are shown in Figs 12.17 and 12.16 with black points. It can be seen that the overall pressure head/flow rate characteristics are rather steep and the proportion of overall pressure at the maximum efficiency region with the maximum overall pressure of the fan is about 0.83, but not 0.5, which leads to the following results:

1. Due to the steep characteristic at the region near the design point, heave stiffness and damping are larger, thus causing larger vertical acceleration which will be strongly sensitive to the 'cobblestone effect'.
2. Once the flow rate reduces, the craft has a lack of vertical restoring force and is easy to plough in.

The efficiency of fan models 4-72 and 4-73 is high and with a wide region for high efficiency, but the high efficiency fan (HEBA) will be better due to the aspects mentioned above.

13

Skirt design

13.1 Introduction

Skirt service life is an important factor in the successful application of hovercraft and their credibility for users. At the early stage of hovercraft development, skirt life was as low as several hours of craft operation. The first task for the members of the trials team of the Chinese test craft model 711-II after tests was repair of the flexible skirt damage before testing on the next day.

Twice in a month, tearing of the bow bag occurred to the SES model 719 weighing 70 t, which not only cost a large amount of labour and money and affected the credibility of ACV/SES, but also caused great inconvenience for the users when looking for a dock to undertake the skirt repair. This caused the ferry operators to refuse to use the hovercraft because of lack of skirt repair facilities.

Such problems are not normal for present-day ACV/SES. Bag and loop components generally last many thousands of hours with general wear and tear, while segments and fingers may be left in place for up to 1500 hours operation before replacing the lower half only. It is nevertheless important that segment tip wear is monitored, since uneven wear can cause a significant increase in skirt drag and thus loss of performance. Luckily segment damage is visible as increased spray while hovering over water, and so can easily be observed.

A review of the types of wear and damage experienced is presented below to assist designers to minimize the sensitivity of a given skirt to the causes, so improving operational life.

13.2 Skirt damage patterns

There are many patterns of damage to skirts, which can be summarized as follows.

Delamination

The delamination of outer/inner rubber coating from the nylon fabric, which leads to water ingress to the fabric, decreasing its strength and accelerating damage.

Abrasion and corrosion

During the operation of ACV/SES, the skirt materials are abraded with sea-water, sand, stones and concrete, which cause the fabric to wear and sea-water to be taken into the fabric, as well as delamination and corrosion of the elastomer.

Tearing

In general, nylon fabric possesses higher tension strength but unsatisfactory tearing strength (*see* Table 13.2). This is because tension will be borne uniformly by the fibres of cloth layers, but during tearing of the fabric, the high concentrated load will cause the fibre of cloths to be broken layer after layer. For this reason, the most significant skirt damage, particularly of skirt bags, will be caused by the unsatisfactory tearing strength of the fabric. Thus designers have to pay great attention on this point to the stress concentration.

The principal failure pattern of skirts and its related major factors are listed in Fig. 13.1. It can be seen that three patterns of skirt damage, i.e. delamination, abrasion and tearing of the skirt fabric are each closely related to the operational environment, the fabric coating of rubber, the weave method of the nylon fabric and the joining of skirt cloths, therefore designers have to pay attention to the selection of skirt fabric, coating and the joining method of skirt cloths during design. These subjects we will introduce in the next section.

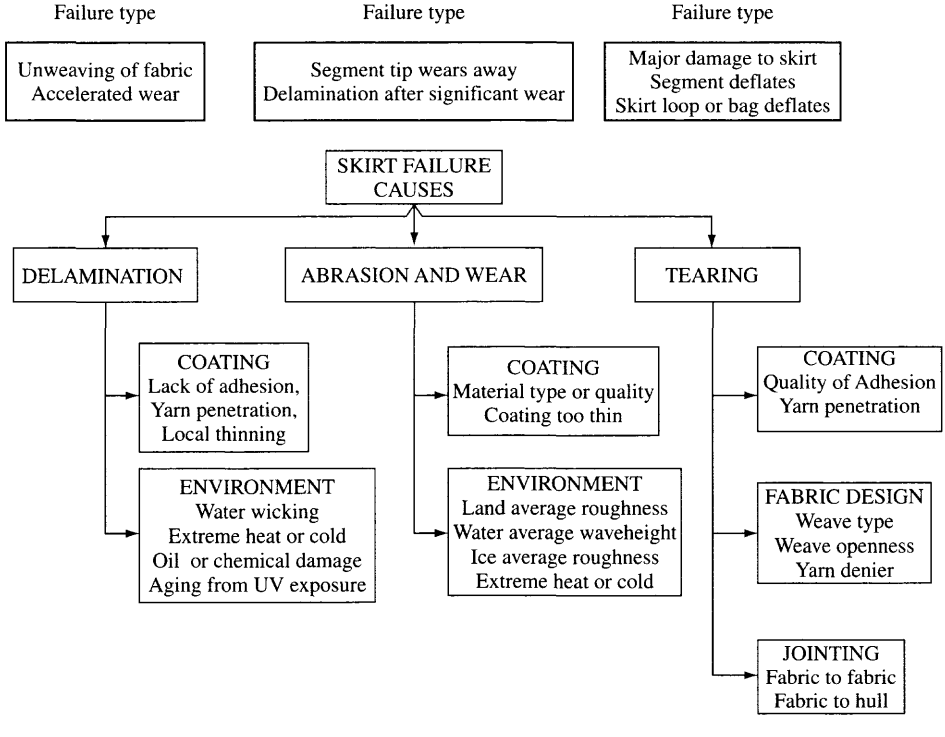

Fig. 13.1 Factors affecting the three modes of skirt damage.

13.3 Skirt failure modes

The actual failure modes of skirts from craft in operation can be found listed in Table 13.1 and may be summarized as follows:

1. So far as the small and medium-size ACV/SES are concerned, tearing of the skirt bag will seldom occur, because of the favourable operational environment and satisfactory skirt material for such craft.
2. With respect to the ACV/SES of medium and large size, tearing of the skirt bag will still be a serious problem, particularly for larger SES, because repair of the skirt bag will have to be carried out in dock or floating dock, which will cost a large amount of money. Therefore the improvement of skirt bag life is still a very important study theme for designers and skirt manufacturers. Rip stops are very helpful.
3. The upper and lower bag of the longitudinal stability trunks of ACVs will be easy to wear out or tear during landing or launch of the craft because of the craft trim.

Table 13.1 The failure mode of hovercraft skirts

Craft	Skirt outer loop or bag	Stability trunks	Bow finger	Side finger	Stern bags
SR.N4	Occasional tearing	Occasional tearing	Delamination Abrasion Fabric wrinkle and wear	Abrasion Fabric wear Delamination Tearing	Abrasion Fabric wear
Voyageur Coastguard	Tearing	Abrasion Tearing	Delamination Abrasion Fabric wear	Tearing Abrasion Fabric wear Joint crimp	Abrasion Fabric wear
SES–100B	Joint wear Seam delamination Rubber breakdown	N/A	Flagellation Abrasion Rubber breakdown	N/A	No damage
Voyageur Arctic Ops	Tearing Rubber breakdown	Tearing	Abrasion Tearing Finger tearing and detachment	Abrasion Tearing Finger tearing and detachment	Abrasion Conical bag tearing and detachment
722-I ACV	Tearing	Abrasion Tearing at stern	Delamination Fabric wear Crimp	Finger tearing and detachment Delamination caused bag tearing	Tearing and abrasion at stern corner Fabric wear
719-G SES	Tearing	N/A	Delamination Fabric wear Crimp	N/A	Fabric wear Tearing
7203 SES	Finger life longer than 600 hours	N/A	Delamination Fabric wear Crimp	N/A	Life longer than 600 hours for lower bag
7202 ACV	Tearing	Abrasion Tearing	Delamination Fabric wear	Abrasion Tearing over ice	Abrasion Tearing over ice

For this reason, great attention has to be paid during the installation of the trunk. It is suggested that too low installation of such a trunk is unsuitable. Moreover, repair of the stability trunk is particularly difficult unless there is a facility to lift the craft. This is the one reason for JEFF(A) to replace the bag and inner skirt with the peripheral cell so as to eliminate the stability trunks.

4. The abrasion, delamination and wrinkling of flexible inner membranes often occur to bow and side skirts. Fortunately, local damage of the skirt finger probably does not substantially affect the performance of the craft. For example, the operational time and range for some Chinese SES are as long as to 1000–2000 hours and 40 000–90 000 km respectively, with several finger/lower bags damaged, but still in operation. They can be replaced by fixed time duration maintenance, or by underwater replacements (for SES).
5. At the stern, particularly at the stern corners, owing to the water scooping of skirts of poor design, the skirt fingers or lower bags of the skirt at this part are often damaged. We obtained test results for the force acting on the attachment bolts joining the rear part of the skirt fingers with the bag of an ACV weighing 70 t. It showed about 4.8–9.8 kN of impact force acting on one bolt. It seems that it would damage the skirt bag in the case where the bolts were connected to the skirt bag. Figure 13.2 shows the inner and outer connection of a typical skirt finger and its components.
6. The skirt fingers and stern lower bag are easy to tear or wear when operating ACVs on ice. Therefore this is also a serious problem faced by designers. Use of inner drape membranes and sacrificial elements can reduce this problem.

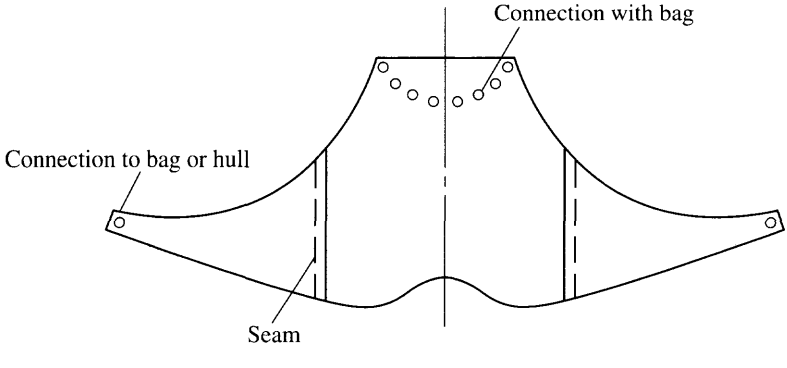

Fig. 13.2 Development of a typical skirt fingers and attachments.

13.4 Skirt loading

The loads acting on skirts are shown in Fig. 13.3. We summarize these below.

Pressure force

This includes static and dynamic pressure forces as well as the impact pressure force due to the action of waves and heave/pitch motion. Some data suggest that the impacting pressure is higher than static pressure by up to 8–10 times. However, this impacting pressure is supported by the tension of the skirt membrane. The skirt material deflects locally in response to impact, so damping out the pressure transients.

Vibration forces

This includes the fluttering and flagellation forces. The first is often associated directly with the high-frequency vibration of the edge of the fingers themselves, due to air escaping past them, which produces low stress but very high strain rates in the coating material and is accompanied by heat build-up due to coating hysteresis and friction between the fabric fibres, therefore the flagellation causes the finger damage.

The flagellation is associated with the contact of a finger edge with either a wave or some obstacles on land. The resulting spring-back and low-frequency oscillation of the finger, due to the pressure forces driving it back into an equilibrium position, provide stresses and moments which are sufficient to cause material degradation and failure. When a coated fabric is subjected to cyclic vibration of stress or strain, a certain proportion of the input deformation energy is non-recoverable. The non-recovered energy, termed the hysteresis loss, has in general four components:

1. internal losses in the fibres;
2. internal losses in elastomer coating;
3. frictional losses associated with relative movement at fibre-to-fibre contact point;
4. frictional losses at the fabric/elastomer interference.

All these energy losses convert to heat, because of the low thermal conductivity of rubber, and the heat at the coating/fabric interface at the finger tip is not readily

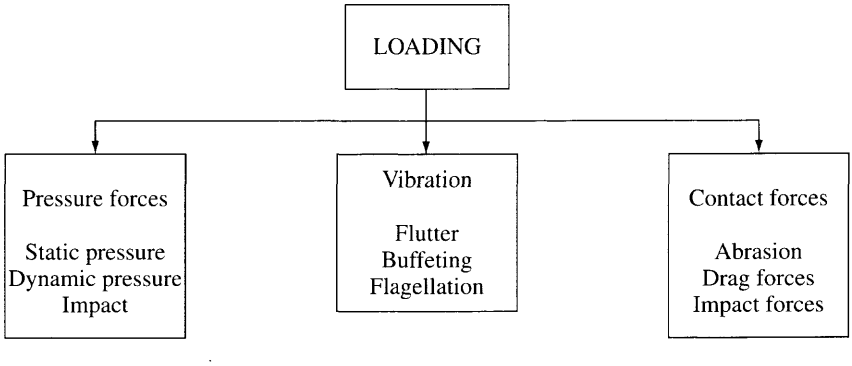

Fig. 13.3 Loads acting on skirts.

dissipated, resulting in a rise in internal temperature and corresponding deterioration of tensile and/or adhesion strength of the coating.

The internal temperature of a specimen rose rapidly and could be measured at 150 °F at the highest frequency of 17.5 Hz as shown in Fig. 13.4 [99] which shows the acceleration and internal temperatures of the flagellation test specimen. The experiment [99] showed that the fatigue life of a test specimen of coating fabric will be decreased to 10% when the temperature increased from 38 to 54 °C, and fatigue life will be decreased to 1% when the temperature increased from 38 to 57.5 °C. The high acceleration and high temperature during the high-frequency vibration of the fabric specimen are the main causes of the damage of the lower edge of the skirt fingers.

Since the life of a skirt finger decreases rapidly due to the high acceleration and high temperature during the vibration of skirt fingers at high frequency, it will therefore deteriorate as the craft weight increases with craft speed, because the velocity of air leakage will be increased with the craft weight and speed. From Fig. 13.5, one can see that the skirt life will decrease to 10% as the craft speed doubles.

Elastomer or rubber delamination caused by high-frequency vibration is the main cause of skirt finger damage. In order to study the loads experienced and to predict skirt life, research institutes and other organizations associated with ACV/SES are

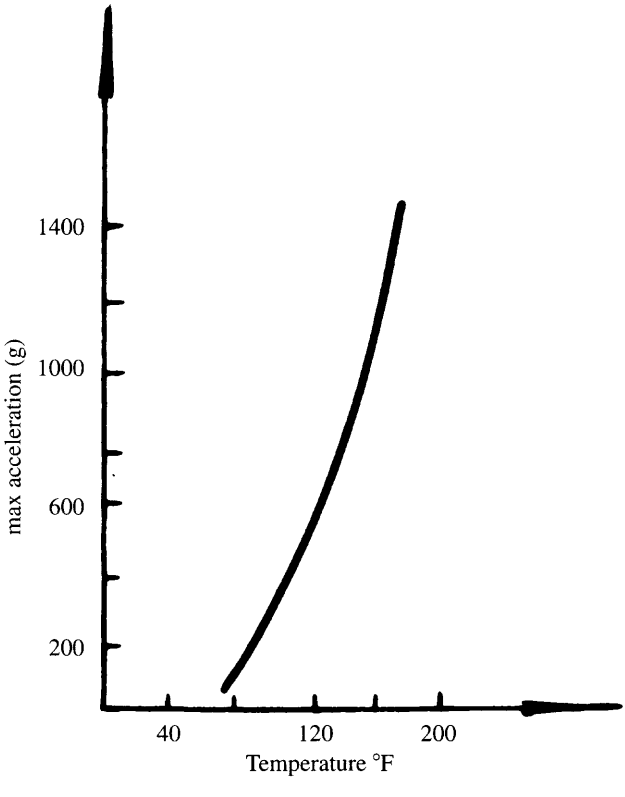

Fig. 13.4 (a) Relations between various parameters in case of vibration on the tip of skirt fingers: (a) relation between the maximum acceleration on tips of skirt fingers and flow rate

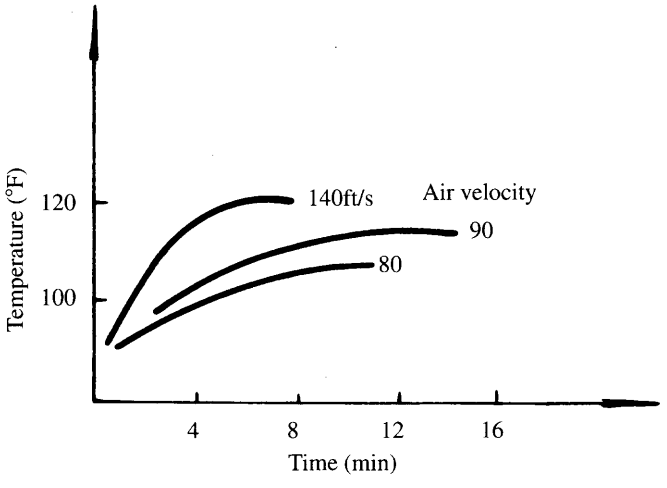

Fig. 13.4 (b) Relation between the temperature rise of fingers and flow rate.

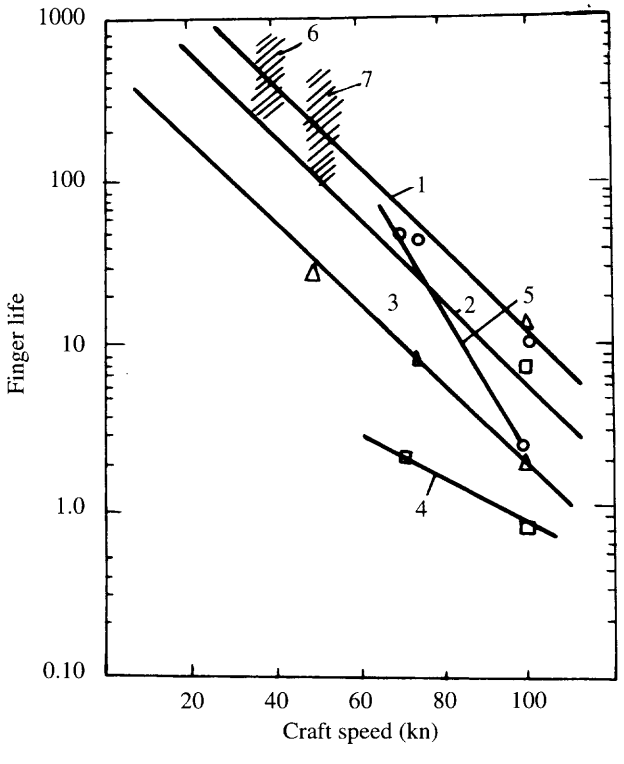

Fig. 13.5 Relation between the finger life, ship speed and the coating of skirts. 1: natural rubber 2.48 kg/m^2; 2: neoprene 3.37 kg/m^2; 3: neoprene 2.5 kg/m^2; 4: neoprene 1.63 kg/m^2; 5: neoprene 2.21 kg/m^2; 6: VT–1 1.36 kg/m^2; 7: SRN–4 4.76 kg/m^2.

making great efforts to study this area and provide various experimental facilities as follows:

1. 'flutter' test facility,
2. 'flagellation' test facility;
3. skirt test facility for water-jet impact testing;
4. abrasion tests for skirt finger materials;
5. fatigue tests due to the vibration of skirt joint, etc.

Figure 13.6 shows the kind of tests that can be carried out using skirt material samples, and air or water jets to create the vibrational loadings.

Some experts consider [4] that the best way to test the skirt material is by use of large scale self-propelled models or the full scale sections of skirt. The small-scale test facilities listed above can identify or quantify the main parameters in skirt wear,

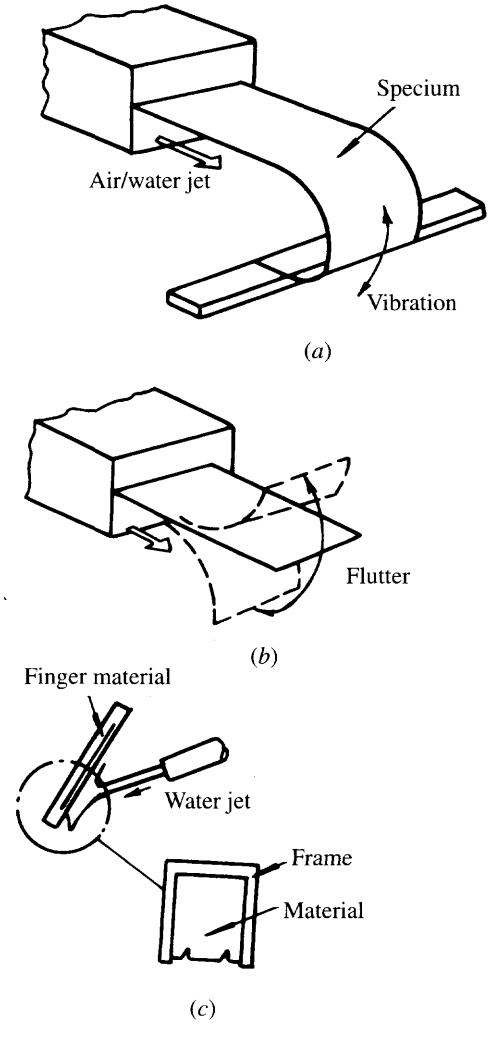

Fig. 13.6 Test facilities for skirt materials. (a) vibration, (b) flutter, (c) impact.

allowing service life predictions to be made or design modifications to be proposed; nevertheless, unless some full-scale service data are logged, even full-scale tests can only approximate the expected life. An integrated approach is therefore needed if skirt segment lives are to be improved from the current norms listed earlier in this chapter.

13.5 Contact forces

In this respect, there are three forces as follows.

Abrasion force

This is the friction of the skirt fingers (and stern lower bag or loop) with sand, concrete and ice. With respect to the passenger ACVs operating in the English Channel, e.g. SR.N4, the wearing out of skirt fingers mainly comes from the direct contact of skirt finger material with the sand and concrete.

In addition, the metal joints connecting the bag with fingers, bag with hull structure and so on (as bolts had been widely used on ACV/SES in the early stage of hovercraft research in China) often cause self-damage of skirt material due to the internal abrasion between the hard metal joints and flexible skirt material, particularly in the case of landing/launching of ACVs. This is an important reason causing short life of skirts in the case of poor design and assembly of the skirts.

Drag force

During hull-borne operation, the drag due to the skirt (particularly of the skirt bag) is large, and the drag force for hull-borne operation which is different from that for cushion-borne operation, is balanced by the tearing force of skirt cloths. The drag force for cushion-borne operation is balanced by the tension of skirt cloths,

The tearing strength of skirt cloths is far lower than the tension strength of skirt cloths, therefore towing operations of hovercraft hull-borne for a long time should be avoided; for example, the ACV model 716-II was towed hull-borne after the craft was launched, causing local tearing of the skirt to occur before it arrived at its destination.

Slamming, water scooping and plough-in may occur to a hovercraft in cushion-borne operation, particularly in rough seas. Skirt fingers may also be scooping water during the turning of hovercraft at high speed.

All such phenomena will lead to large instantaneous hydrodynamic forces so as to tear the skirt cloths or lead to tremendous bag pressure to burst the skirt bag and lead to plough-in. The SR.N4 hovercraft ferry tore a large split of 30 m in its bag while trying to go through the entrance to Dover harbour. Such a split with a large area also happened to the ACV 722–1 operating in waves at high speed. A split bow bag also occurred to model 711-II during plough-in tests. The stern bag of SES model 719 was also broken during craft take-off, caused by mud and rubbish filling the stern bag, causing very large hump drag.

Impact force

During operation of hovercraft, floating objects or obstacles are likely to be encountered, which will cause local impact; for example, during a landing operation of ACV 722–1 downwind, the craft was landing at high speed, the pilot was obliged to throttle down suddenly and caused the stern bag and stern longitudinal stability trunk to split. Such impact force is tremendous and large enough to destroy the skirt bag. However, the skirt can protect the hull.

Such force is difficult to estimate and simulate; it is exactly the main consideration of designers during the selection of materials and configuration of skirts. Figure 13.7 denotes the typical wreck mode of skirt fingers.

13.6 Selection of skirt material

The following issues have to be considered during selection of skirt materials:

1. tension strength of material;
2. tearing strength of material;
3. anti-delamination capability of coating fabric;
4. flexibility and anti-ageing capability of skirt cloths (nylon fabric coating);
5. the low temperature characteristic of skirt materials for situations where the craft are operating on ice.

The tensile strength of skirt cloths is dependent on the tension strength of the woven fibre, and is related to the specific weight of the fibre material. Generally speaking, the heavier the material the higher the tension strength as shown in Fig. 13.8. But tearing strength does not comply with this rule as shown in Fig. 13.8. A–G show the tearing strength of the samples made from various materials with different weaving

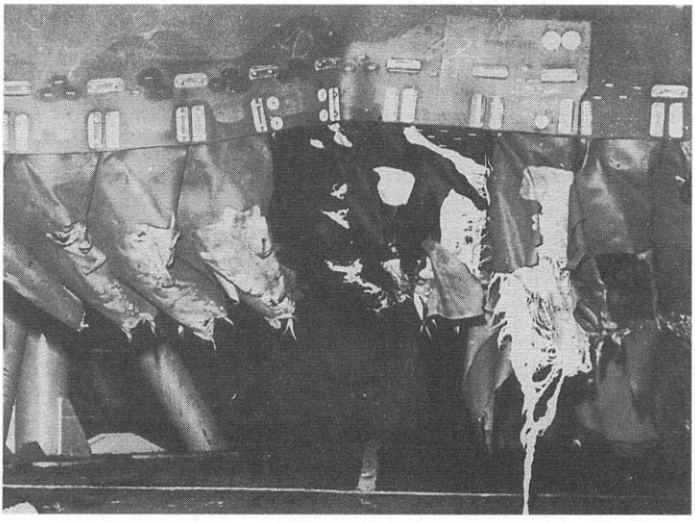

Fig. 13.7 Typical damage on skirt fingers.

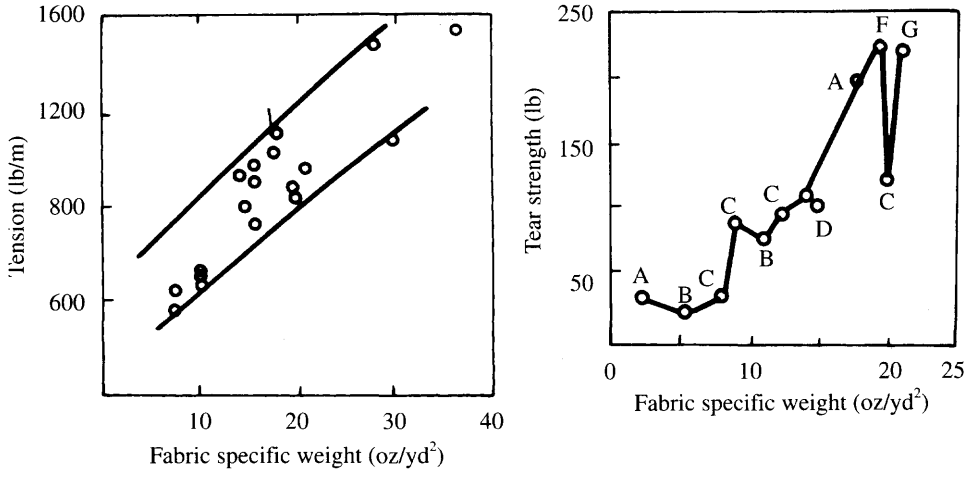

Fig. 13.8 Tension and tear strength of skirt materials.

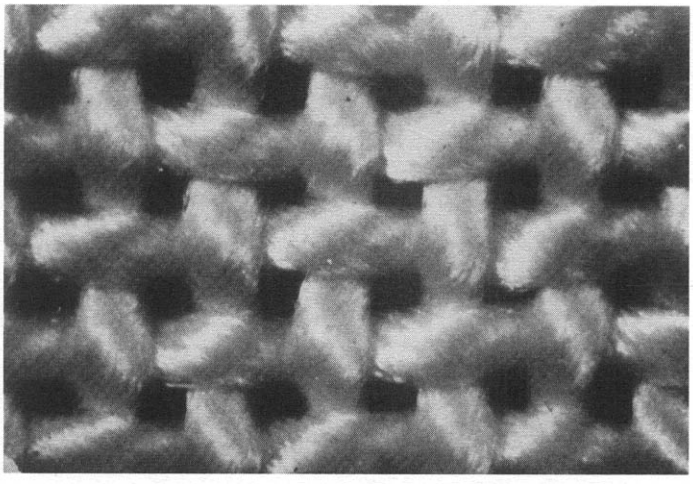

Fig. 13.9 Open weave skirt cloth.

methods. In general the fibres are twisted in ply to become the open weave as shown in Fig. 13.9. Thus the rubber coating actually will be adhesive, through the gap between both sides of the fabric; obviously the adhesive ability of open weave is higher than that on close weave, because the adhesive force between the rubber is larger than that between the fabric and rubber.

Open weave will not only improve the anti-delamination strength as mentioned above, but also increase the tearing strength of the fabric, because the ply twisted by the fabrics will have higher tension strength, thus improving its tearing strength, because the tension strength of skirt cloths is subject to the tension strength of all fibres per unit width of cloths, whereas the tearing strength of cloths is subject to the tension strength of unit fibre ply.

Table 13.2 Data for some skirt coating fabric produced in China [100]

Skirt fabric designation	Units	6408–1	57703
Width of coated fabric	mm	810	830–840
Thickness of coated fabric	mm	2	2.5
Specific weight of coated fabric	kg/m2	2.19	2.57
Peel strength – Original	N/ (5 cm)	660	980
Peel strength – 1 week's soak in fresh water	N/ (5 cm)	160	
Peel strength – 20 days' soak in fresh water	N/ (5 cm)	160	920
Peel strength – 1 week's soak in 10% salt water	N/ (5 cm)	350	
Peel strength – 20 days' soak in 10% salt water	N/ (5 cm)	260	
Breaking strength of coated fabric – warp	N/ (5 cm)	7100	4920
Breaking strength of coated fabric – weft	N/ (5 cm)	6270	6200
Tearing strength of coated fabric – warp	N	770	1490
Tearing strength of coated fabric – weft	N	910	1300
Application		Small and medium-size ACV or SES	Medium-size ACV and SES

Table 13.3 The coated fabric characteristics for Chinese and foreign ACV/SESs

Craft name		Craft weight (t)	Maximum craft speed (knots)	Cushion pressure (Pa)	Skirt height (m)	Coated fabric (kg/m^2)	Tension strength (N/cm^2)	Tear strength (N)	Skirt life (hours)	Notes
SR.N4	b	200	70	2521	2.4	2.9–4.6			5000 +	
Mk 2	f					4.5	8722	1875	100–400	
VT.1	b	110	46	2992	1.68	2.4	5690	893	5000 +	
	f					1.36			300–1200	
VT.2	b	106	60	2900	1.68	2.44	5690	863	5000 +	
	f					1.36			300–1000	
SR.N6	b	10.8	54	1256	1.22	1.36				
Mk.1	f					3.0	5690	893	200–750	
HM.216	b	20	35		1.0	3.0			2000 +	
	f					1.2		893	300–1500	
BH.110	b	138	35							
	f								700	
7202		2.8	24	981	0.5	1.5	2943	932	300	58021 fabric
711-1I		5.0	52	1170	0.75	2.1	5886	883	250	6408 fabric
716		15.0	50	1471	1.0	2.1	5886	883		6408 fabric
722-I		65.0	50	2453	1.6	2.6	4905	1177		57911 fabric

b = bag, f = finger.

The quality of Chinese skirt coating fabric has been dramatically improved, the data of some of which are shown in Table 13.2. Table 13.3 shows the characteristics of some coating fabric applied to foreign and Chinese ACV/SES. Fortunately thanks to the adoption of adhesives for joining the coating fabric, the joint strength has been greatly improved so that bolts and even more the stitching thread for joining seams of coating fabric does not have to be used, because bolts destroy the strength of the coating fabric and the joining strength of the latter is unsatisfactory. It should be noted here that for smaller amphibious ACVs, skirt materials used are light enough that stitched seams are adequate and are less expensive as an assembly method than glued or welded joints.

With respect to the coating, in general, natural rubber or neoprene are the most commonly adopted materials. The former is soft, elastic and has good resistance to delamination, so some ACV/SES manufacturers use natural rubber (at high cost) as the material for the bow fingers. On the other hand neoprene has outstanding resistance to wear and fine low-temperature performance. In China neoprene mixed with natural rubber is generally used as the coating material giving a good low temperature performance.

During selection of skirt material, the following aspects have to be considered. Different material should be applied to different locations. In general, the material for the skirt bag should have high tearing and tension strength, but not with good abrasion characteristics. For this reason, the fabrics of skirt bags should be of good strength and thin coating thickness. The fabric for fingers should be of low stiffness, but with a thick coating for larger commercial craft. Table 13.4 shows the specific weight of coating and nylon fabric for skirt fingers.

There are two points of view for the selection of skirt finger material: one is that the heavier material has to be chosen to meet the requirement of abrasion resistance; the other is that designers prefer to select material to reduce the inertia force acting on the skirt finger due to acceleration during skirts flutter, consequently preventing delamination of the elastomer, reducing the added resistance of craft in waves and so extending the skirt life. It is difficult to judge clearly which approach is correct, since the application itself has an influence. As far as air cushion ferries are concerned, since they often operate on sandy beaches, designers tend to specify a thicker coating in order to increase the abrasion resistance. With respect to military ACVs the speed performance and seaworthiness of craft are given higher priority than the abrasion quality of skirts, therefore the light-coated cloths will be better. Figure 13.5 shows the overall life of skirt fingers on ACV SR.N4 and VT.1.

Fig. 13.10 shows the relation between the specific weight of the bag–finger skirt of operated hovercraft and craft weight. It is very interesting that the points are not scattered, for this reason, ref. [4] suggested the expression as follows:

$$W_s = 15\, W^{0.333} \tag{13.1}$$

where W is the weight of craft (t) and W_s the skirt weight (oz/yd^2) (1 oz/yd^2 = 0.034 kg/m^2). The kinds of skirt material which can be selected by designers is rather limited. In general, there are three kinds of material to be adopted on ACV/SESs, i.e.

Table 13.4 The specific weight of skirt material for home and foreign ACVs

Craft	Country	Material location	Specific weight of coated fabric (kg/m^2)	Specific weight of nylon fabric (kg/m^2)
SR.N6	UK	Bag	1.36	0.407
		Finger	2.9–3.4	
SR.N4	UK	Bag	2.89	0.68
		Finger	4.6	
7202	China	Bag + finger	1.6	0.8
711 II	China	Bag + finger	2.1	

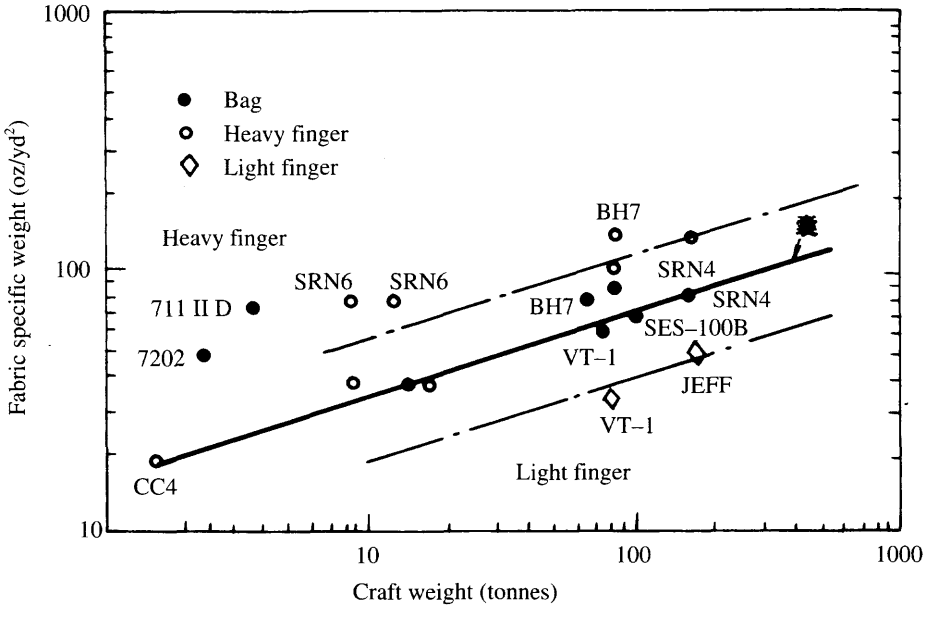

Fig. 13.10 Specific weight of skirt material and statistical relation with craft weight.

Mini ACV (or air cushion jeep),	W < 10 t
Small ACV,	W = 10–30 t (and SES)
Medium ACV,	W = 30–100 t

In order to improve the strength of the skirt bag, it is suggested flexible stiffeners (rip stops) are used on the coating fabric. Thus it will increase the tension and tearing strength greatly and can also prevent the extension of splitting, which has been validated on the Chinese SES 719G, 719-II with good results.

Figure 13.11 shows the relation between the total weight of the skirt system and the

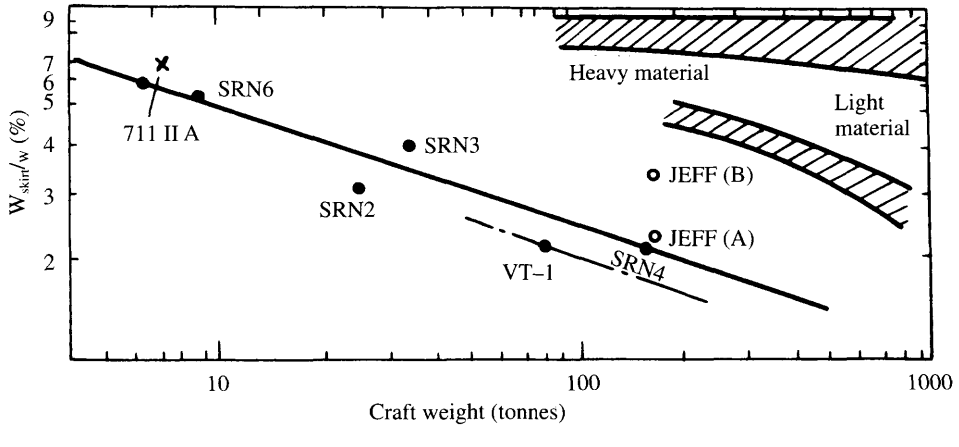

Fig. 13.11 Total weight of skirt system and relation to craft weight (hatched area denotes the material in research).

weight of the craft. Since the thickness of skirt material is impossible to increase with the linear dimension of the craft, therefore the proportion of skirt weight will decrease as size of craft increases.

13.7 Selection of skirt joints

The type of skirt joints is very important, because much skirt damage starts from the skirt joints, including those between the coating fabrics and the coating fabric and the hull. Therefore the requirements for the joints should be as follows:

1. High joining strength for joints themselves.
2. The joints should not injure the strength of coated fabric, otherwise the joints may be strong enough.
3. No self-damage will occur to the fabrics, owing to the flutter, flagellation and abrasion of skirts; so that the joints do not cause wear out or wrecking of the skirt fabric.
4. Light weight so that they do not cause corrosion or erosion of aluminium hull plates.

Table 13.5 lists and compares some typical joints, which are widely applied to Chinese and western hovercraft. Figures 13.12 and 13.13 show some types of skirt joints applied

Table 13.5 Comparison between the various joints (see also Figs 13.12 and 13.13)

Items	Name of joints	Placing	Merit	Limitations	Recent applications
1	Nylon thread	Coated fabric with coated fabric	Light	Low strength	Recreation craft
2	Belt bolts	Coated fabric with coated fabric, bag and finger	Cheaper	Poor anti-corrosion capability and also occasionally injures the skirt fabric	Obsolete
3	Steel bolts and washers	Bag and hull structure	Cheaper and easier assembly	Poor anti-corrosion capability	Apply to ACV/SESs
4	Nylon bolts	Bag and bag and fingers	Light	Low strength, very expensive	Recreation craft
5	Piano hinge joints	Bag and hull structure	Easy to assemble	Complicated manufacture	Used widely in BHC
6	Cap-like joint (Bonio's)	Bag and bag and fingers	Fine joining strength, low self-damage possibility	Complicated manufacture	Used widely in China and BHC
7	Aluminium plates plus steel bolts (or nylon plates plus steel bolts)	Bag and bag	Fine joining strength, low self-damage possibility	Difficult assembly	Used in China for ACVs and SESs
8	Compression plates joint	Bag and hull	Easy to assemble	Unsatisfactory joining strength for ACV/SESs of medium size	Used in China for ACVs and SESs

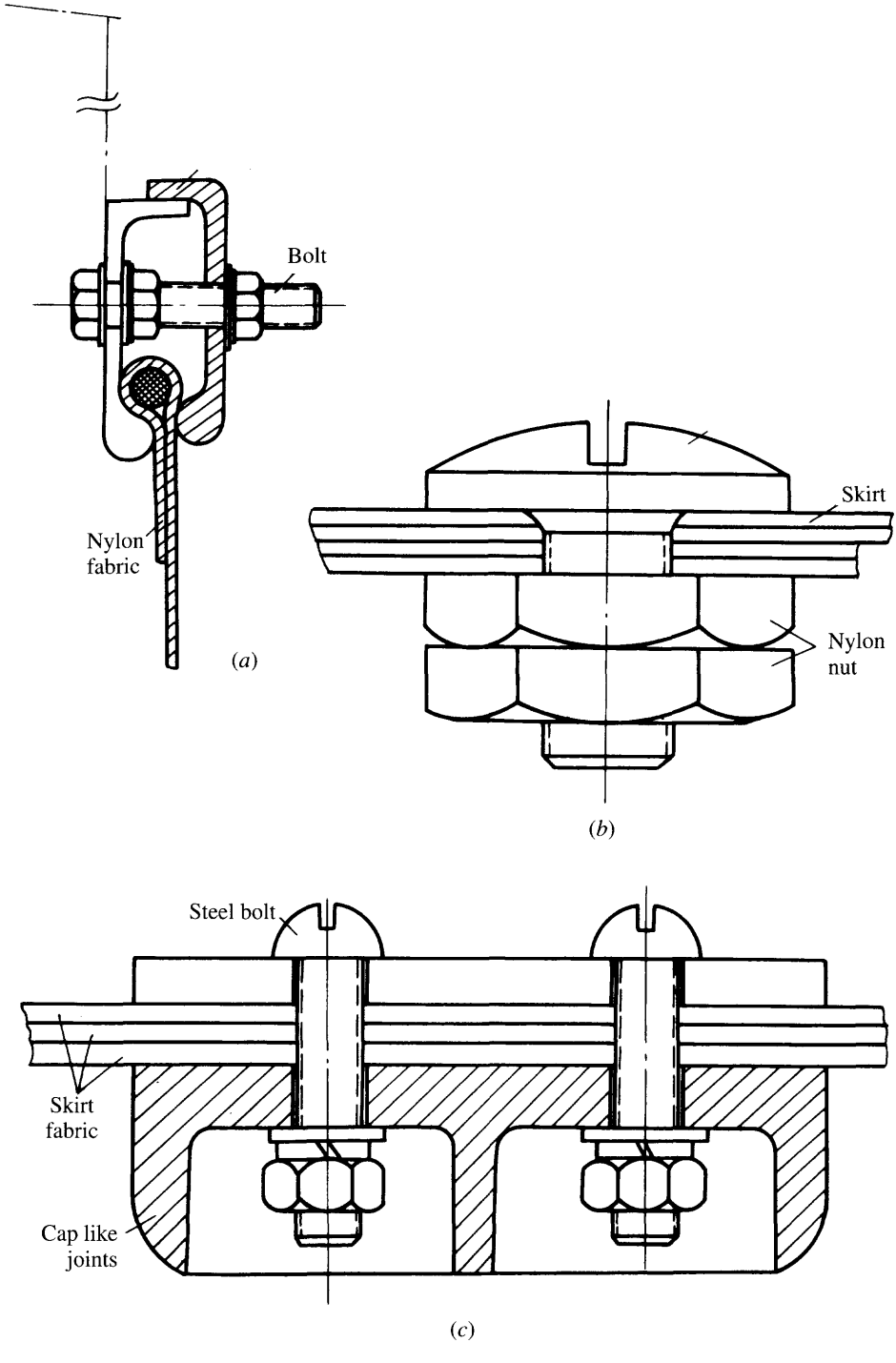

Fig. 13.12 Several types of skirt joints. (a) Clamped joint for bag/hull; (b) nylon bolt for bag and finger panel constructions; (c) steel bolts and plates for bag/finger panels.

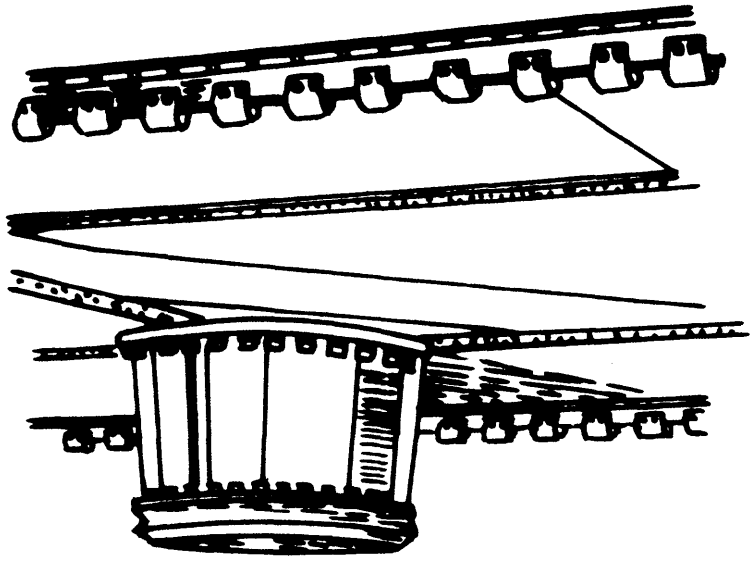

Fig. 13.13 Skirt attachments of piano hinge type on hull, which is normally used by BHC.

to the hovercraft. Items 2, 3 and 5–8 in Table 13.5 are widely used on Chinese hovercraft, item 6 among them is very similar to the 'Bonio's' of BHC, which are widely used on the BHC ACVs. The material of such joints is nylon 1010, but the material of Bonio's is rubber or neoprene, which is softer and more suitable to avoid self-damage of skirts.

13.8 Assembly and manufacturing technology for skirts

Assembly and manufacturing technology is dependent on attention to detail for success. Many skirt failures in the past have been due to the poor assembly and manufacturing technology of skirts. Skirt life may be demonstrated to improve by a factor of 10 just due to improvements in assembly or manufacturing technology of skirts, as has been experienced between the skirts of SES 717-II and SES 717-III. For this reason, we would like to introduce some examples, which are considered instructive to the designer.

Skirt tailoring and cutting of skirt air feed holes

It is suggested not to use scissors or a knife to cut skirt materials, because this will tend to part the the rubber coating from the fibres and encourage capillary suction of salt water into the fabric, which will become a key cause of rubber delamination. According to ref. 101, BHC earlier used a laser beam to cut the skirt. The disadvantage of this is a reduction in static strength of 15% of the fabric and a reduction of fatigue strength of 20% of the skirts. BHC therefore replaced this method with a water jet with a 0.15 mm diameter of jet of water at 345 kpa, which was sufficiently powerful to cut though skirt material, GRP and other laminates. They also used computer-aided manufacture as shown in Figs 13.14 and 13.15. In China, we use the

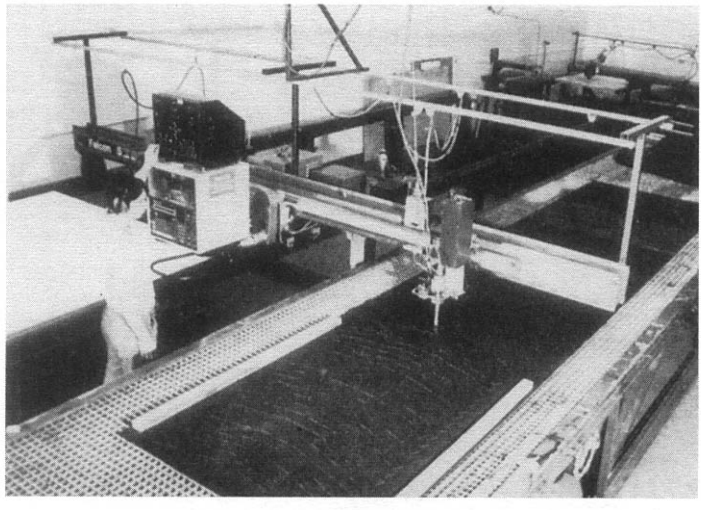

Fig. 13.14 The waterjet punching and cutting facility for skirt processing in BHC.

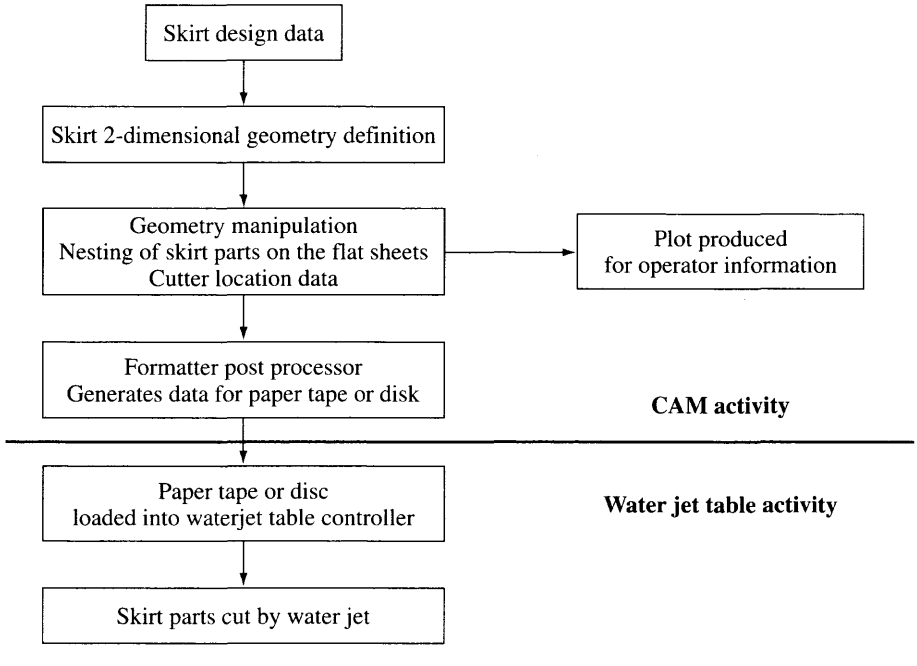

Fig. 13.15 The flow chart of CAM for the manufacture of skirts in BHC.

electric thermo-knife, which possesses the function of edge sealing. This has given good results for operational craft.

Avoid direct joining of skirt fingers with the bag

This is because the fabric might be ruined in the case of sideslip or reverse operation of craft, consequently large splits might be made in the bags.

Avoid building in assembly stresses

For example, owing to the poor manufacture of the bow skirt of SES version 719, large assembly stress existed, and as a result the overhaul life of the skirt was less than 20 hours! Assembly stresses can usually be seen from uneven geometry of the skirt.

Installation of diaphragms

With respect to bag diaphragms, there are two points of view. The skirt bag without a diaphragm has the advantage of uniform tension of the bag sheet and good formation of the skirt bag geometry. However, the skirt bag with a diaphragm will be restrained, with a concentrated stress exerting on the diaphragm, but it will improve resistance to skirt bounce and can also avoid interference between the water propellers and the stern skirts in the case of reverse motion of an SES on hull-borne operation.

13.9 Skirt configuration design

Skirt design begins by determining the various parameters and geometric relationships of the skirt sections at side bow and stern, such as X_A, X_c, a_E, Y_A Y_c Y_E, etc., as shown in Figs 13.16 and 13.17.

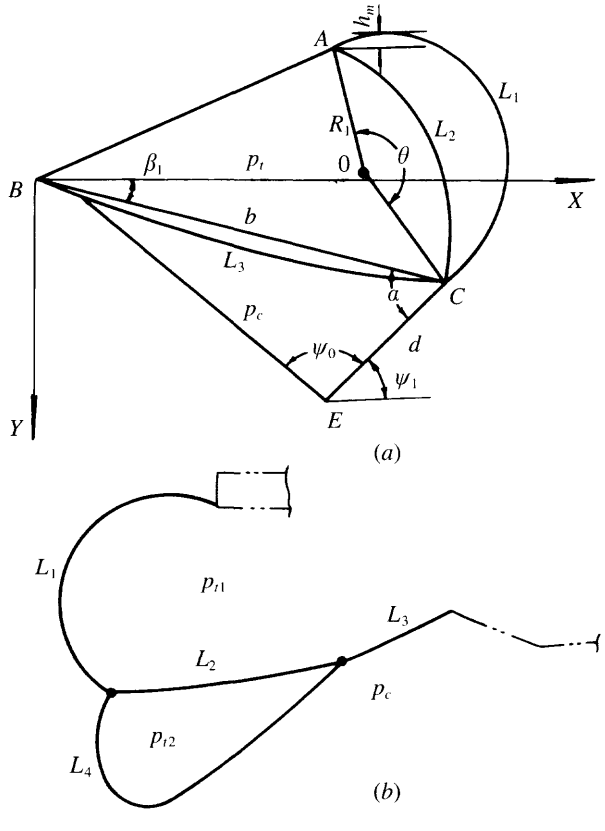

Fig. 13.16 Geometric features of skirts. (a) Skirt of bag and finger type; (b) Skirt of twin bag type.

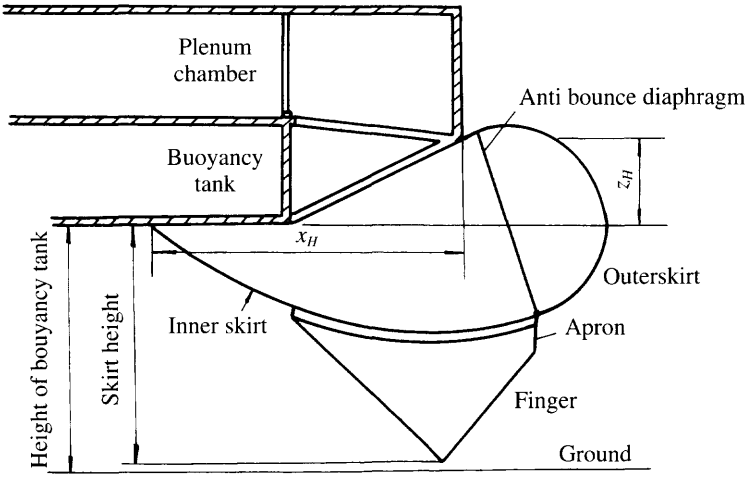

Fig. 13.17 Some geometric features of skirts.

Based on the requirements of craft performance, the size of the hull structure and the method for analysing the forces acting on skirts, designers can determine the skirt dimensions mentioned above, thus draw the static formation of the required skirt and begin the laying-off.

Skirt design is somewhat complicated due to the three-dimensional geometry of the membrane and the many parameters which have to be satisfied, including control or limitation of flutter, flagellation, bounce, etc. Skirts also affect craft performance parameters, such as tuck-under resistance, plough-in, speed performance, stability and seaworthiness. Skirt design should therefore be optimized in stages by using progressive refinement.

Statistical analysis method

Owing to the lack of comprehensive design methods for skirts in the 1970s some hovercraft manufacturers and designers, such as the British Hovercraft Corporation, Hovermarine International Limited, Hovercraft Development Limited and Vosper Thornycroft Limited, accompanied by some register units, as UK CAA, under the leadership of British Department of Industry, prepared the guidance document *Stability and Control of Hovercraft, Notes for Commanders* [48]. Table 13.6 defines the design factors affecting the leading side skirt tuck-under boundary, design factors affecting the craft's reserve against capsizing and the considerations on overall skirt geometry and craft parameters from this reference.

Design and analysis methods for skirts

So far there are no systematic and complete analytical design methods for skirts, so we introduce some design considerations on skirts and the determination of some skirt parameters for the reader's reference, as follows.

Determination of height of the bow/stern skirts

We can determine the height of the bow/stern skirts according to the requirements for seaworthiness. With respect to coastal hovercraft the slope of bow/stern skirt can be obtained from

$$\text{arc tan}\ \frac{(H_{skb} - H_{sks})}{L_c} \cong 0.4\text{–}0.55^\circ \tag{13.2}$$

where H_{skb} and H_{sks} denote the height of bow and stern skirts respectively. This is not necessary for river hovercraft.

Bag and cushion pressure ratio (p_t/p_c)

This can be determined dependent upon the requirements for plough-in resistance

Table 13.6(a) Design factors affecting leading side skirt tuck under boundary [48]

Sectional geometry parameter	Comment	Current practice
$\frac{Z_h}{X_h} = \frac{\text{Hinge vertical spacing}}{\text{Hinge horizontal spacing}}$	High value favourable	0.15–1.0
$\frac{L_j}{X_h} = \frac{\text{Bag perimeter}}{\text{Hinge horizontal spacing}}$	High value favourable at lower pressure ratio of p_j/p_c	1.75–3.5
$\frac{B_c}{X_h} = \frac{\text{Cushion beam}}{\text{Hinge horizontal spacing}}$	Low value favourable	5.0–7.5
Finger depth per cent hull clearance	Low value favourable in theory, but some minimum value (>20%) probably optimum in practice due to better drag characteristics of finger than bag, even in purely beam-on condition	0.5–1.0
Overall skirt geometry and craft parameters		
Compartmentation	Centre keel with different pressure in roll favourable unless p_j/p_c for leading side skirt becomes low and Z_h/X_h and/or l_j/X_h are low	
$\frac{H_{sk}}{B_c} = \frac{\text{Skirt depth}}{\text{Cushion beam}}$	Low value favourable	0.10–0.2
$\frac{p_b}{p_c} = \frac{\text{Bag pressure}}{\text{Cushion pressure}}$	High value favourable	1.0–2.0
C_Δ = Cushion loading	High value favourable, usually	0.01–0.03
$\frac{H_{bt}}{H_{sk}} = \frac{\text{Buoyancy tank clearance}}{\text{Skirt depth}}$	High value favourable	0.80–1.1
$\frac{B_c}{le} = \frac{\text{Cushion beam}}{\text{Effective cushion length}}$	Low value favourable, in conjunction with H_{sk}/B_c and C_Δ, but only $(B_c/l_c)^{0.5}$ is as powerful as these	0.40–0.75

Table 13.6(b) Design factors affecting hovercraft's reserve against capsizing (up to tuck-under point)

Parameter	Comment	Current practice
Differential pressure rate less CG height moment parameter $\frac{\partial(\Delta p_c/p_c)}{\partial\theta}\frac{h_g}{B_c}$	A high value is favourable in this context, but will be offset by an adverse adjustment to the tuck-under merits if hinge spacing and bag perimeter ratios are not good (unless initial pressure ratio is high)	−0.3–0.6
$\frac{H_{bt}}{H_{sk}} = \frac{\text{Buoyancy tank clearance}}{\text{Skirt depth}}$	The importance of this parameter is modified by the size of the drag moment parameter, but a high value is favourable.	0.8–1.1
$\frac{H_g}{B_c C_\Delta} = \frac{\text{CG height ratio}}{\text{Cushion loading}}$	Drag moment parameter, low value favourable	10–25
$\frac{L_j}{X_h} = \frac{\text{Bag perimeter}}{\text{Horizontal hinge spacing}}$	Affected by beam increase. High value favourable	1.75–3.5
$\frac{p_t}{p_c} = \frac{\text{Bag pressure}}{\text{Cushion pressure}}$	Affects bag pressure moment, high value favourable	1.0–2.0
$\frac{B_c}{X_h} = \frac{\text{Cushion beam}}{\text{Horizontal hinge spacing}}$	Relates skirt contact moment to cushion beam dependent and other moments. Low value favourable	5.0–7.0

capability, seaworthiness and minimum lift power etc. In the past it might be taken as $p_t/p_c = 1.2$–1.5 for ACVs. So far, thanks to improvement in skirt design, the plough-in resistance of craft is greatly improved. For this reason, in order to save lift power, it can be taken as 1.0–1.3 for ACVs and 1.0–1.15 for SESs.

Finger height ratio h_f/h_{sk}

Here, h_f denotes the finger height and h_{sk} the overall height of the skirt, i.e. the vertical height of the bottom plates over the ground. Higher finger height gives better seaworthiness and obstacle clearance but worse stability. In general we take h_f/h_{sk} at around 0.5–0.8 This is a realistic value where pressurized bag skirt designs are used. Where an open loop design is used h_f/h_{sk} is normally between 0.85 and 0.95.

Inclination angle of fingers ψ_1 (Fig. 13.16)

According to the theory developed in Chapters 4 and 7 the smaller this angle, the better the static stability of craft accompanied with small drag, but if this angle is too small it will cause the decrease of cushion area to be too rapid for acceptable stability. In general we take ψ_1 to be between 40 and 50°.

Inward inclination angle ψ_0 (Fig. 13.16)

Too small ψ_0 will cause the wrinkling of skirt fingers at their front edge under the action of cushion pressure, but too large will use too much skirt material and weight; in general $\psi_0 \geqslant 90°$.

Determination of deformability or stiffness of skirts

The main parameters for study of skirt deformability are as follows:

1. the static deformability in vertical and horizontal direction

$$\Delta X_E/\Delta p_c \qquad \Delta Y_E/\Delta p_c \quad (\text{mm}/(\text{N}/\text{m}^2))$$

2. the inherent frequency and damping coefficients.

So far, there are no clear analytical theories of how skirt deformability improves hovercraft performance, however it is mainly dependent on the operational environment for a particular craft. For this reason, according to the requirements for the seaworthiness of craft, designers generally select two or three different deformabilities of skirts and study the performance of craft with such skirt deformability with the aid of experimental tank results or computer analysis.

Designers can then judge from the test results and select the optimum deformability of the designed skirt. The inherent frequency of a responsive skirt (one with lower stiffness of the bag geometry) should be lower than the wave encounter frequency of the component wave on which the peak wave energy of the irregular wave spectrum occurs.

With respect to small ACVs operating on rivers, it is suggested not to use the responsive skirt with low natural frequency, because the anti-plough-in capability of this design is degraded and may cause plough-in. Similar to the ACV, the SES so far also adopts stiffer skirt geometries with small deformability.

As far as the coastal ACV, or ACV with good seaworthiness are concerned, it is suggested to adopt the responsive skirt, but the deformability of the bow skirt should be smaller than that of the side skirt in order to prevent tuck-under of the bow skirt during operation of the craft in a following wind. The deformability of the stern skirt should be larger than that of the side skirt in order to improve the take-off performance and seaworthiness of craft in waves.

During preliminary and project design, the calculation mentioned above generally cannot be carried out because of lack of required data. The following two geometric parameters, which greatly affect the deformability of skirts, are offered for judging the responsiveness of the designed skirt at this stage, i.e., if

$$\frac{X_E}{X_A} > 1.0$$

then the skirt obviously becomes a responsive skirt (the larger this value the more deformable the skirt), and if

$$\frac{h_m}{R} > 0$$

then this skirt will also be a responsive skirt. The larger this value, the more deformable the skirt, therefore the responsive skirt is also often called a skirt with protruding shoulder.

The parameters mentioned above are very important and become the main criteria characterizing the responsiveness of skirts. When adopting the responsive skirt the designers have to check the tuck-under capability of the skirts, namely to estimate if

tuck-under might occur to the skirt while the craft has negative trim angle and significant immersed depth of the bow skirt (H_w), at any given craft speed.

In order to improve the tuck-under resistance and anti-bounce capability, in general the D-type skirt bag (with inner membrane) will be fitted on bow skirts and longitudinal anti-bounce diaphragms on the side skirt. These membranes are needed where bag pressures above $1.3p_c$ are used.

Special attention has to be paid to the design of ACV/SES corner skirts, since the skirts there are in three dimensions and have to be designed and calculated according to the three dimensional principle of skirt formation, otherwise the air gap under the skirts in this area will be non-uniform and cause a large amount of air leakage and spray.

With respect to the SES, in general, the 'rigid' (i.e. with less responsiveness) bag–finger skirt, or simple deep segments, may be mounted at the bow in order to obtain anti-tuck-under and anti-plough-in capabilities, leaving control of pitch motion to the sidewall lines and perhaps damping mechanisms such as bow foils.

As far as the stern skirt is concerned, the twin bag or triple bag with large responsiveness (i.e. low p_l/p_c ratio) may be mounted on both ACV/SES as discussed in Chapter 7. Owing to lack of a suitable method to predict the formation of the stern skirt, determination and checking of the geometry of the skirts is normally by means of model experiments, in a skirt box and subsequently in a towing tank.

After determination of the responsiveness, the various geometric dimensions may thus be designed. This is followed by possible additional skirt components as outlined below.

Longitudinal and transverse stability trunks

The height and type of arrangement in plan (+ type or T type) of longitudinal and transverse stability trunks can be obtained according to the methods in Chapter 4. Positive trim angles of craft have to be considered in order to avoid excessive wear of longitudinal trunks at the stern during landing of craft. It is also normal to make a 20–30° back inclination angle on transverse stability trunks during installation of the skirt in order to reduce the craft drag in waves.

Spray suppression skirts

In order to suppress spray, a spray apron or skirt can be mounted at the bow and side skirts of amphibious ACVs. Experience shows that this skirt is especially effective when mounted on low-speed air cushion platforms.

There are two main types of spray skirt normally used, the external inflated tooth and the 'apron'. The US Navy LCAC craft are fitted with the spray suppression teeth (see Fig. 7.38(b)) to depress spray when manœuvring at slow speed around a landing ship, or close to shore. They are similar to a double segment and may be inflated either from the loop, or from the outer face of the segment to which they are attached at its outer hem.

An apron skirt is more commonly used by utility craft. Many AP.1-88 craft have these fitted, (see Fig. 7.38(a)). A shaped apron of medium-weight skirt material simply lies over the outer part of the bow and side bag/loop skirts. Tethers attach it to the upper loop hem line. At its outside the apron hangs vertically to a level about mid-height of the finger or segment, when the craft is at full hover height. This skirt

will tend to flap somewhat, which does not improve the attractiveness of the ACV's looks, but especially for operations over ice and snow this helps to maintain the skirt clear of ice. If the apron is too long, it can affect craft dynamic behaviour and speed loss in waves. If this should prove to be the case when a craft is put on trials, a careful programme of trimming will allow optimization of the spray suppression and minimize effect on performance in a seaway.

A recent modification of the AP.1-88 'maxi-apron' is to attach a smaller apron to the segment or finger upper attachment point. This short apron hangs approximately half the segment height. Some holes should be punched in the upper part of the apron to reduce the pressure build-up.

14

Structural design

14.1 ACV and SES structural design features

In this chapter specific aspects concerned with structural design of ACV/SES will also be discussed, as follows:

1. a brief introduction of the determination of external forces acting on hovercraft;
2. determination of safety factors during the calculation of internal stresses;
3. calculation of hull structure strength;
4. determination of plate thickness during hovercraft structural design (scantlings);
5. evaluation of ACV/SES vibration and its attenuation.

The structure of ACV/SES can be designed in a similar way to conventional ships, based on the following general procedure:

1. selection of material;
2. selection of safety factors;
3. determine external forces acting on the hull during the operation and maintenance of craft;
4. structural analysis of ACV/SES hull:
   (a) on cushion in waves;
   (b) off cushion in waves;
   (c) moored at its berth;
   (d) lifting strength;
5. optimization of scantlings.

The procedure is similar to that on most high-performance vehicles. The hull is generally constructed of aluminium alloy, GRP or marine grade steel. Further, the main design considerations after selection of the main structural dimensions are motion accelerations, impact loading due to waves and landing, fatigue of highly stressed areas and stresses induced by vibration.

Both ACV/SES have a large volume compared with their displacement and so have a large area of shell plate, i.e. high $\bar{S}$, where $\bar{S} = S/(W_v)^{0.66}$, where S represents the area of shell plates in m^2 and W_v the volumetric displacement of the craft in m^3.

SES

An SES hull is similar to a catamaran with wider beam and thinner hulls. Thus, at the same displacement it has a larger area of shell plate and a heavier structure weight compared with that of a conventional monohull.

Hull weight is related closely to the principal dimensions of an SES and thus also with the cushion pressure/length ratio p_c/l_c. Due to support of the major part of the craft weight by the cushion, an SES structure is less highly loaded and can therefore be designed as a lighter structure per unit area. Materials which lend themselves to SES structures are GRP and welded aluminium alloy due to their low density. It has not been found necessary to use aircraft design techniques to minimize structure weight, for example using carbon fibre reinforcement to GRP, or using high-tensile-strength grades of aluminium. A satisfactory structure can be fabricated from weldable marine aluminium alloys, or glass reinforced polyester or vinylester plastic.

Since ACV/SES operate in a salt water environment, the structural material is required to have good corrosion resistance. In this respect GRP or marine grade aluminium alloy has advantages. If steel is used, corrosion protection has to be applied and regularly maintained.

Steel is less expensive to fabricate than the other materials but incurs a considerable weight penalty. Some use of HT steels can mitigate this. To date there are very few SES, e.g. the 719-II, which have successfully applied a steel hull structure. Steel hull structures may find useful application for larger SES (above 100 m in length) where its higher modulus may allow improved optimization, particularly if the normal approach for Navy frigates is used where the lower-loaded superstructure is constructed in aluminium.

ACV

Since passenger hovercraft have to have low p_c/l_c in order to obtain good take-off performance, small wave-making resistance, added wave drag and roomy passenger cabin, in general designers adopt smaller p_c (i.e. low-density craft) for passenger ACVs and take larger p_c (high-density craft) for military landing craft, which are required to have small overall dimensions for entering into the landing ship's stern dock area and where operational economics are not so sensitive to installed power.

Due to the low density requirements in order to achieve low p_c, designers were earlier obliged to use material with high specific strength, e.g. riveted aluminium alloy and sandwich panel construction, in a similar manner to aircraft. High construction costs follow this approach. Since the early 1980s, as skirt technology has allowed higher p_c values to be adopted, GRP construction has been used in ACVs as well as SES, and welded aluminium structures similar to catamarans have been successfully designed. The normal approach is now to use these lower-cost structural design.

It is useful to note that when designing with high-strength materials, as for aircraft, it is often the case that stiffness rather than strength is the controlling design criterion (cabin floor panels for example). The transition to lower-strength materials therefore also leads to a change to strength governing stiffness as the main structural design criterion. Both criteria should nevertheless be checked during design!

The welding of aluminium structures can be a serious problem for the aluminium

plates applied to the structure, particularly for upward and vertical welding. In certain areas manufacturers and designers have been obliged until recently to continue to use riveted or adhesive jointed structures based on aviation technology. So long as this is minimized, the effect on total cost need not be significant.

Summary

The current state of development of hovercraft structures may be summarized as follows:

1. Welded aluminium structures are now widely used on hovercraft (e.g. AP.1-88) to replace the riveted and adhesive structure based on aviation technology (SR.N series), leading to decreased construction cost. Marine grade aluminium alloy is generally of lower strength than aircraft grades. The welds are relatively low strength, since no work hardening can be applied. Shell plates of SES or ACV structures are therefore thicker than a riveted design, resulting in a higher structure weight.
2. With respect to small ACV/SES, thin plates would normally be sufficient for the structural loading requirements. These plates are difficult to weld in some cases and this together with the stiffness requirements for the structure may oblige the designer to replace thin plating with over-thick plates, or use riveted, glued or fibre-reinforced plastic structures. As an alternative, in order to save labour, weight and overall dimensions it is possible to consider alternative structural arrangements to the traditional buoyancy tank approach, or to replace part of the rigid structure with an inflatable structure.
3. It is possible to construct the structure with welded aluminium or GRP. The latter is easy to maintain or repair with simpler construction technology, but it has lower stiffness than aluminium, which prevents the material being used to construct larger craft (above 50 t approx). In the case of large medium-speed SES, marine steel can also now be used as the material in order to reduce the construction cost. The Chinese SES 719-II is an example.
4. With respect to smaller hovercraft, the most significant problem is minimizing structural weight based on extreme external loads such as wave 'slamming' at high speed. In other respects, small hovercraft are dimensioned from stiffness requirements rather than strength.
5. Due to the low structural density, high installed power and high-speed rotating machinery with wide distribution of exciting frequencies (engines, fans, propellers and transmission gearboxes), vibration problems can become very important. Vibration and noise analysis therefore has to be included in the overall design of the craft, to minimize the vibration, and apply appropriate vibration isolation design.

14.2 External forces on hull – introduction to the strength calculation of craft

Determination of external forces

Structural design should start with assessment of the quasi-static trim and equilibrium of forces at maximum speed. Designers normally estimate the external loads while the ACV/SES runs in the required sea state at maximum cushion-borne speed. From the point of view of strength calculation, the estimation of such loads is critical. The distribution of wave-impacting load in longitudinal and transverse directions can be determined by empirical methods, using data from model tests or previously constructed craft and thus the dynamic bending moment acting on the craft can also be determined in a similar way to the method used for the strength calculation of planing hulls [90].

In order to determine external loads accurately, a great deal of model and full-scale ship experiments, similar to those on planing hulls, have to be carried out. So far such data are limited; the main reference to which one can refer for information is the calculation method for determining external loads in the rules for safety requirements of civil hovercraft originally issued in 1962 by the British Aviation Authority [4,115,] which was based upon the calculation method for external loads of sea-planes and the unskirted ACV model SR.N1. Therefore correction for the impact absorption of skirts and the air cushion should be incorporated (see below).

In a similar way to a planing hull, the external loads acting on an ACV or SES are mainly the vertical impact acceleration acting on the hull running in waves and the slamming pressure of waves acting on the bottom frame of the craft. Superposing the dynamic bending moment caused by these loads upon the static bending moment, we can calculate the overall bending moment and shear, according to which the required local strength and overall longitudinal, transverse and torsion strength can be calculated.

Determination of design inertial loads

According to [115], a factor may be defined, η_w, where η_w may be calculated as the relative vertical acceleration, that is, the vertical acceleration divided by gravitational acceleration at point A located at a distance of l_2 from the CG of the craft:

$$\eta_w = (p_w/gW)\,(1 + l_1 l_2/r_y^2) \tag{14.1}$$

where p_w is the impacting force acting on the hull by the waves (N), W the craft weight (kg), l_1 the distance from the impacting force to the CG of the craft (m), J_y the transverse moment of inertia through the CG of the craft (kg m^2) and r_y the radius of inertia of the hovercraft (m), $r_y = (J_y/W)^{0.5}$. The wave-impacting force can also be written as

$$(p_w/gW) = (K_1 V_{zk} V_s)/[W^{0.333}\,(1 + r_y^2)^{0.666}] \tag{14.2}$$

where K_1 is the coefficient due to the wave-impacting force, and can be written as (Fig. 14.1) [4]

$$K_1 = \begin{cases} 1 + l_1/l_2 & l_1 > 0, \text{ impact occurring forward of LCG} \\ 1 & l_1 < 0, \text{ impact occurring aft of LCG} \end{cases}$$

and V_{zk} is the relative vertical velocity due to the craft and wave motion, at the section on which the impact force acts (m/s),

$$V_{zk} = \pi\, V_w\, \zeta_a/L_w + V_z \tag{14.3}$$

where L_w is the wavelength (m), V_z vertical velocity of hull section on which impact force acts (m/s). In the case of lack of experimental data, $V_z \approx 0.6$ m/s. V_s is the craft speed (m/s) and ζ_a the wave height, which can be written as

$$\left.\begin{array}{ll} \zeta_a = 0.1L_w & \text{when } L_w < 38 \text{ m} \\ \zeta_a = 0.10L_w^{0.5} & \text{when } L_w > 38 \text{ m} \end{array}\right\} \tag{14.4}$$

V_w is the wave speed (m/s):

$$V_w = 1.25L_w^{0.5} \tag{14.5}$$

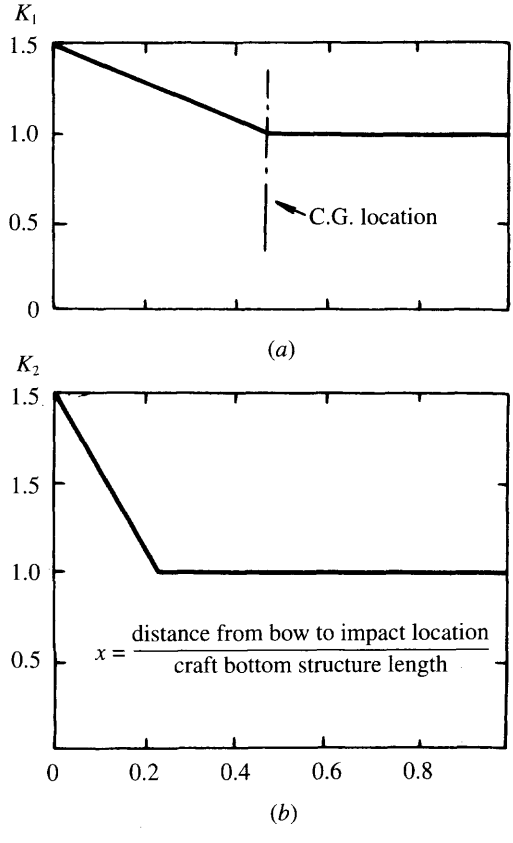

Fig. 14.1 Wave impact loading and pressure coefficients: (a) loading coefficient; (b) pressure coefficient.

J_y is the ACV/SES moment of inertia which can expressed in simplified form as

$$J_y = (W/12)\,(L^2 + 4z_g^2) \tag{14.6}$$

where $L^2 >> 4\,z_g^2$, then expressions can be written as

$$\left.\begin{aligned} J_y &\approx W\,L^2/12 \\ r_y &\approx 0.3L \end{aligned}\right\} \tag{14.7}$$

where L is the craft length (m) and z_g the vertical height of the CG of the craft over the base-line (m).

Determination of wave impact pressure [4][52]

When hovercraft are running at high speed in waves, the impacting pressure due to waves at the acting centre of the waves (e.g. the maximum hydrodynamic pressure) can be written as

$$p_{max} \approx K_3 K_2 \rho_w\, V_s \tag{14.8}$$

where K is an empirical coefficient, take $K_3 = 4.6$–4.9, ρ_w is the water density (Ns^2/m^4) and

$$K_2 = \left\{\begin{array}{ll} 2 - x/(0.22L) & \text{when } x \leqslant 0.22L \\ 1 & \text{when } x \geqslant 0.22L \end{array}\right\} \tag{14.9}$$

The data can also be obtained in Fig. 14.1(b).

Reference 4 discussed the linear relation between the wave-impacting force acting on the bow and the craft speed, as in expression (14.8). It was validated by the test results on the ACV SKMR-1 (without skirt) in 1963. With respect to the bow slamming condition, if one uses $K = 2.0$, then we have

$$P_{max} \cong V_s \tag{14.10}$$

where V_s is the craft speed (knots) and P_{max} the maximum slamming pressure, lb/in^2 ($\times$ 6894.76 in Pa).

Expression (14.10) is the well-known 1lb–1 knot rule, in other words, the slamming pressure acting on the bottom plate of the bow increases with the speed in the proportion to 1 lb/in^2 per knot of speed. This formula has been used for the design of many early hovercraft.

The calculation of pressures for shell plates of US JEFF(A), JEFF(B) landing craft ACVs and SES-100A and SES-100B are shown in Fig. 14.2. The design conditions for the US ACV are the craft operated at speed of 50 knots in sea state 5, while for the SES it is 60 knots, sea state 5.

British designers took a different point of view on ACV structural design in the 1970s. They proposed that the air cushion and skirt attenuated slamming and that the design slamming pressure could be reduced by a factor of 50%. For the SR.N4 hovercraft ferry, maximum slamming pressure for design of the bow structure was taken as 22–23 lb/in^2 at a speed of 35–40 knots and in sea state 5. It was later found that the bow bottom plates of SR.N4 had been damaged in sea state 5 conditions and as a result, BHC's experts offered a revised attenuation coefficient, i.e. 30% reduction of hydrodynamic pressure, as shown in Fig. 14.3. Table 14.1 shows the calculated conditions for some ACVs during the calculation of hull bow strength.

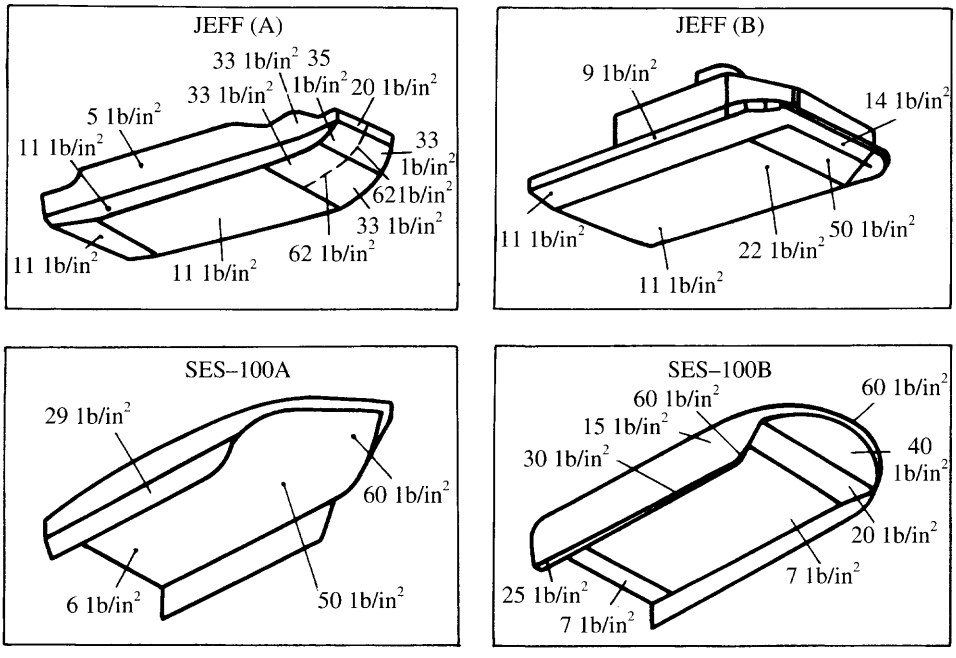

Fig. 14.2 Calculated hydrodynamic pressure on plates of US SES craft due to wave impact.

Having obtained the external load, i.e. the inertial load factor and slamming pressure acting on the bottom plates and frames of the craft, one can check the strength (including the fatigue strength) of structure and mountings for various machines, equipment and instruments as follows:

1. The overall strength of the craft in the case where the wave exerts an impact force at the CG or other longitudinal portions of the craft.
2. The overall longitudinal strength, torsion and transverse strength of craft under the action of wave slamming at one side of the bow or other portion of the craft. Hovercraft and SES structures normally comprise a relatively thin buoyancy tank

Table 14.1 Calculated conditions adopted in calculating the strength of hull of ACV [4]

Features	Unit	SKMR–1 (no skirt)	SR.N2	SR.N4	SR.N4	SR.N5	SR.N6	JEFF(B)
Weight	t	20.40	25.90	168.00	168.00	6.80	9.55	147.00
Craft speed	knots	50.00	55.00	70.00	60.00	60.00	50.00	50.00
Wave height	m	1.50	0.90	0.76	0.37	0.61	0.61	1.98
Maximum slamming pressure	MPa							
Bow		0.415	0.103	0.155	0.155	0.155	0.124	0.345
Stern		0.206	0.041	0.033	0.033	0.033	0.083	0.152
Inertial load factor	*g*							
Bow		2.00	0.83	0.83	0.45	1.00	1.00	1.00
Midship		1.00	1.80	1.80	0.80	2.00	2.00	2.00
Stern		1.00	0.75	0.75	0.40	0.75	0.75	0.75

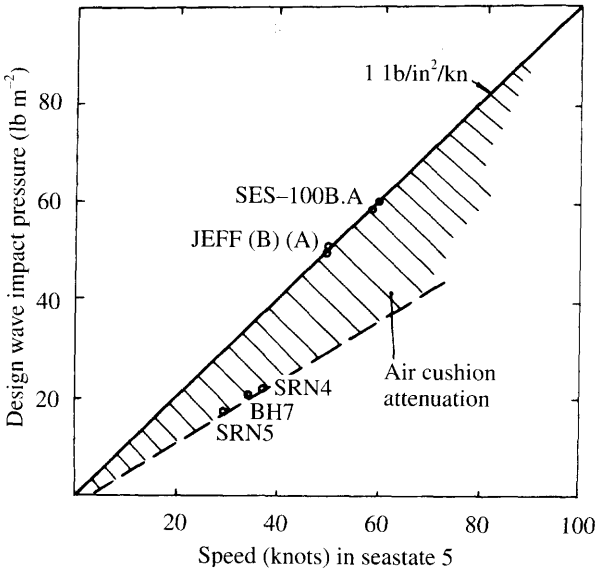

Fig. 14.3 Cushion attenuation coefficient vs craft speed.

above their wet deck, and the main transverse strength is provided by a number of watertight bulkheads and transverse web frames.

On small SES, the overall longitudinal strength is provided by the two sidewalls, while the transverse strength, being controlled by the transverse bulkheads, may require more than that needed to provide damage stability. This may lead to cabin spaces being divided. A large proportion of SES transverse bulkheads are above the upper deck, which moves the centre of area upwards relative to the sidewalls. This results in a further increase in structural scantlings. The effect is inbuilt into the catamaran cross-section of an SES, enhanced by the deeper sidewalls of an SES.

3. Owing to the craft operating in waves at a high speed, hydrodynamic impacts, clearing vertical obstacles, landing and launching and emergency landing etc, during the design of mountings for various instruments and equipment the acceleration acting on the equipment in three directions X,Y, Z has to be considered carefully.

14.3 Brief introduction to the structural calculation used in MARIC[102][103]

Parameters and conditions

During the analysis of the local and overall strength of the craft structure, the following conditions are considered at MARIC:

1. ACV lifted by crane;
2. ACV static on the ground (rigid surface, normally three-point loading);
3. ACV/SES operating cushion borne over ground (ACV) or water surface (ACV and SES);
4. ACV/SES operating on cushion in waves at high speed, including wave slamming, when the following slamming conditions have to be considered:
   (a) wave slamming at the CG of craft;
   (b) slamming at bow/stern instantaneously;
   (c) slamming at bow only.
5. ACV/SES on hull-borne operations:
   (a) in sagging condition;
   (b) in hogging condition.

The conditions listed under (4) and (5) are similar to those applied to conventional ships. The differences between them are the dynamic bending moment acting on the hull caused by the wave slamming of the craft and the hydrodynamic impacting force acting on the shell plates. This requires a different method of calculation for the overall and local strength of craft, so we will introduce briefly the procedure and conditions for strength inspection of hovercraft.

ACV/SES operating on cushion at high speed in waves – wave slamming at the CG or bow/stern instantaneously

In this case, the craft can be considered as not heaving or pitching, therefore the equilibrium conditions for the vertical force are as follows (taking an ACV as the example):

$$W + F_i = A_c p_c + p_w$$

where W is the craft weight, F_i the inertia force of the craft, $A_c p_c$ the total cushion lift and p_w the impacting force of waves, from equation (14.2) and Fig. 14.1. In the above equation, the inertia force can be taken as the weight at the different longitudinal position (ordinate) times the vertical acceleration acting on this position, i.e. the inertial load times the gravitational acceleration g. In general, the craft length can be divided into 20 ordinates for calculation. In the case where the wave slamming is acting on the CG, the impacting acceleration will be constant along the longitudinal axis and without pitching, then we have

$$p_w = \eta_w W \tag{14.11}$$

The impacting length can be taken as (0.145–0.16) l_c, symmetric about the craft's CG. In the case where wave slamming impacts on the craft at the bow/stern instantaneously, then

$$p_{wb} + p_{ws} = p_w = \eta_w W \tag{14.12}$$

where p_{wb} is the wave impacting force at bow (N), p_{ws} the wave impacting force at stern (N), W the craft weight (N), l_s the impacting length at stern (m), l_f the length of front body of craft before the CG (m), l_a the length of rear body of craft before the CG (m) and l_b the impacting length at the bow (m):

$$l_s = (2.34\, l_c\, l_f)/(1.2\, l_f + l_a)$$

$$l_b = (1.95\, l_c\, l_a)/(1.2\, l_f + l_a)$$

For impact at the bow/stern instantaneously, the craft is not pitching, the resultant of both bow/stern impacting force acts on the CG. The equilibrium condition for this force can be written as

$$p_w + \int_{lc} p_c\, B_c\, dl = \sum_{i=1}^{n} (1 + \eta_w) W_i \tag{14.13}$$

where p_c is the cushion pressure (Pa), l_c, B_c the cushion length and beam respectively (m) and W_i the craft weight sharing on ith space (N) and the craft is divided into n spaces along its length. The shear and longitudinal bending moment can be obtained according to this equation,.

Craft operating on cushion at high speed in waves – hull strength in the case of wave slamming at bow

In the case where slamming occurs at the bow, pitching motion will occur and the vertical acceleration is not uniformly distributed along the longitudinal axis; the law of distribution can be calculated according to equation (14.1) and Fig. 14.1, being linearly distributed as follows:

$$p_w + \int_{lc} p_c\, B_c\, dx = \int_{lc} (1 + \eta_x)\, W(x)\, dx \tag{14.14}$$

$$L_b = 0.1 L_c$$

According to this equation and applying the gravitational force, cushion force, inertia force and hydrodynamic impacting force on each longitudinal space, the longitudinal bending moment and thus strength inspection can be obtained. Meanwhile, the local strength analysis also can be carried out based on the wave-impacting pressure. With respect to the inertial loads (η_{wi}) acting on the mechanical and electrical equipment as well as their mountings at various positions along the longitudinal axis can be obtained according to this equation and Table 14.2. During craft landing, the force acting on the landing pads can also be obtained from Table 14.2; this table was obtained from tests and statistical analysis.

14.4 Calculation methods for strength in the former Soviet Union

Analysis of structures is specified by these methods for adequate reserve while floating or on cushion in the design wave conditions, while moored at its berth and while being lifted for maintenance. The analysis methods have been found useful and realistic and can be recommended where the craft type and operational mission are applicable.

Table 14.2 Maximum acceleration acting on hovercraft engines and equipment and the forces acting on landing pads of hovercraft [104]

1	Maximum acceleration acting on engines and equipment	Upward		$3g$
		Down		$4g$
		Forward		$6g$
		Backward		$3g$
		Lateral		$5g$
		Resultant		$6g$
2	Force acting on landing pads	SR.N2, middle pads,	vertical	1.0 × craft weight (W)
			lateral	$0.5W$
		SR.N5, all pads,	vertical	0.5–$0.6W$
			horizontal	$0.17W$
		SR.N4, fore pads,	vertical	$0.5W$
			horizontal	$0.25W$
		SR.N4, other pads,	vertical	$0.4W$
			horizontal	$0.2W$

Useful range of the calculation

This calculation is suitable for craft operating on waterways in (O), (P) and (L) classes. The craft can be operated cushion-borne and hull-borne as passenger, auxiliary transport, or cargo ACV/SES. The classifications O, P and L are for river boats as stipulated by the Soviet government, which corresponds to the A, B and C classes of boats operating in China, on rivers and in estuary waters. The calculations of wave height h (the 1% highest waves) are equal to:

For craft operating on O class waterways $h_w = 2.0$ m
For craft operating on P class waterways $h_w = 1.2$ m
For craft operating on L class waterways $h_w = 0.6$ m

The stiffness of hull and relative speed F_r of such hovercraft should satisfy the following conditions:

$$\left.\begin{aligned} EI/(DL) &> 1.3 \\ V/(gL)^{0.5} &> 2.0 \end{aligned}\right\} \tag{14.15}$$

where E is the elastic modulus on the normal direction (tf/m^2), I the section moment of inertia of the hull structure (m^4) – this only includes the section moment of inertia of the main hull structure in the case of no strong superstructure, otherwise it must include the section of inertia of the superstructure. D is the displacement of craft (t) and L the craft length (m).

The ratio of principal dimensions of an SES has to satisfy the following conditions:

$$\left.\begin{aligned} L/H &< 20 \\ L/B &= 3\text{–}6 \\ H/H_{sw} &= 2\text{–}3 \end{aligned}\right\} \tag{14.16}$$

where H is the depth of the upper deck (m) and H_{sw} the depth of sidewalls (m).

Design loads for craft structure, overall bending and torsion

The loads acting on the craft structure during the calculation of overall bending and torsion can be determined using the maximum inertial load coefficient measured at the craft's CG. The inertial load coefficient operating in waves can be obtained from prototype or experimental results of models in various operation modes and various modes of overall deformations. The loads acting on locations other than the CG can be determined as follows:

$$\eta = \{1 + \mu_1 [(x_1 - x_g)(x - x_g)/\rho_1^2 + (y_1\, y)/\rho_2^2] + \mu_2 [(x_2 - x_g)(x - x_g)/\rho_1^2 + (y^2\, y)/\rho_2^2]\}\eta_g \tag{14.17}$$

where μ_1, μ_2 are coefficients, determined from Table 14.3, x_1, x_2, y_1, y_2 are the coordinates of external force as shown in Fig. 14.4, x_g the longitudinal ordinate of the CG of the craft (m), ρ_1 the radius of inertia of the hull weight about the transverse axis through the CG (m), ρ_2 the radius of inertia of the hull width about the longitudinal axis through the CG (m), η_g the inertial load coefficient acting at the CG of the craft in the case of lack of information during the preliminary design phase. The inertial load coefficient for calculating longitudinal strength can be determined as follows (for cushion-borne operation):

$$\eta_g = 1 + (0.085\, h^{0.5} + 0.04 V/D^{0.333}) \tag{14.18}$$

The external force can be written as

$$\left.\begin{aligned} P_1 &= \mu_1\, D\, \eta_g \\ P_2 &= \mu_2\, D\, \eta_g \end{aligned}\right\} \tag{14.19}$$

Based on these inertial load coefficients, the longitudinal and transverse bending moments can be obtained in a similar way. The location and area of action of the hydrodynamic impacting force during slamming at the CG or bow/stern can be obtained from Fig. 14.4 and Table 14.3.

The torsion moment M_t can be determined by integrating the torsion moment intensity, which is the algebraic sum of the moment intensity m_1, m_2 and distribution moment m_3, induced by the supporting force P_1, P_2 and the mass inertia of the craft about the longitudinal axis respectively, i.e.

$$\left.\begin{aligned} m_1 &= \mu_1\, D\, \eta_g\, y_1/l_1 \\ m_2 &= \mu_2\, D\, \eta_g\, y_2/l_2 \\ m_3 &= -W(x)\,(\mu_1\, y_1 + \mu_2\, y_2) \end{aligned}\right\} \tag{14.20}$$

The distribution of moment intensity m_1, m_2 along the craft length can be determined as in Fig. 14.4 and Table 14.3. Moment m_3 distributes along the whole length of the craft. $W(x)$ represents the distribution of craft weight along the longitudinal axis.

Overall bending moment acting on the midship section

In preliminary design, the overall bending moment acting on the midship section M_o can be determined as follows.

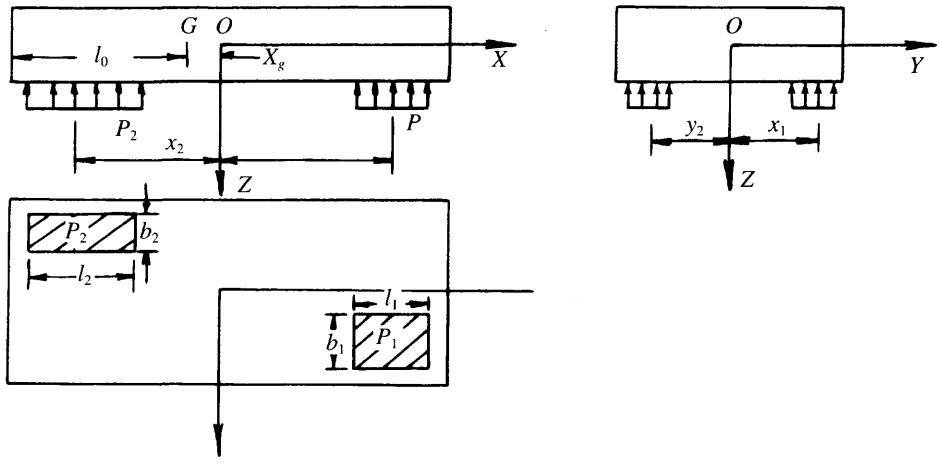

Fig. 14.4 Some parameters for determining overall bending moment and torsion load of SES.

Table 14.3 Some parameters for determination of overall bending and torsion moment acting on a structure

Characteristic value	Cushion-borne operation in waves				Hull-borne operation in waves			
	Longitudinal bending		Transverse bending	Torsion	Longitudinal bending		Transverse bending	Torsion
	Sag	Hog	Sag		Sag	Hog	Sag	
$L1$	$0.2L$	$0.4L$	$2\,l_o$	$0.2L$	$0.2\,L$	$0.4L$	$2\,l_o$	$0.2L$
$L2$	$2\,l_o$	$2\,l_o$	$2\,l_o$	$0.2\,l_o$	$0.2\,L$	0	$2\,l_o$	$0.2\,L$
$b1$	B	B	ε_1	ε_2	B	B	ε_1	ε_2
$b2$	B	B	B	B	B	0	ε_1	ε_1
$x1$	$0.4\,L$	x_g	x_g	$0.4L$	$0.4L$	x_g	x_g	$0.4L$
$x2$	x_g	x_g	x_g	x_g	$-0.4\,L$	0	x_g	$-0.4\,L$
$y1$	0	0	ε_2	ε_2	0	0	ε_2	ε_2
$y2$	0	0	0	0	0	0	$-\varepsilon_2$	$-\varepsilon_2$
μ_1	$(\eta_g - 1)/\eta_g$	$(\eta_g - 1)/\eta_g$	$(\eta_g - 1)/\eta_g$	$(\eta_g - 1)/\eta_g$	2/3	1	1/2	2/3
μ_2	$1/\eta_g$	$1/\eta_g$	$1/\eta_g$	$1/\eta_g$	1/3	0	1/2	1/3

Note:
For ACV: $\varepsilon_1 = 0.2B$, $\varepsilon_2 = 0.4B$.
For SES: $\varepsilon_1 = B_{sw}$, $\varepsilon_2 = 0.5\,(B - B_{sw})$.
B_{sw} = width of sidewalls at the bow, and
B = width of midship section at design water-line.

ACV and SES cushion-borne operation

$$M_o = [K_s \pm 0.5\,(0.15 \pm K_s)\,(\eta_g - 1)]\,D\,L \tag{14.21}$$

where K_s is the coefficient for longitudinal bending moment in calm water, (+) represents the hogging mode, (−) represents sagging mode, and η_g the inertial load coefficient, which can be determined by equation (14.18), or using prototype and model test results.

ACV hull-borne operation

$$M_o = \pm 0.5\,(0.15 \pm K_s)\,\eta_g\,D\,L \tag{14.22}$$

SES hull-borne operation

$$M_o = [K_s \pm 0.5\,(0.15 \pm K_s)\,(\eta_g - D_{sw}/D)]\,D\,L \pm 5.1 B_{sw}\,(L/10)^2\,h \tag{14.23}$$

where D_{sw} is the displacement provided by the sidewalls and h the wave height.

The maximum shear can be written as $N_o = 4\,M_o/L$. The overall bending moment and shear for every section of a craft can then be determined as in Fig. 14.5.

Determination of transverse bending moment of ACV/SES in preliminary design

This can be determined as follows.

ACV/SES cushion-borne operation

$$M_o' = [K_s' - 0.5\,(0.15 - K_s')(\eta_g' - 1)]\,DB \tag{14.24}$$

ACV hull-borne operation

$$M_o' = -0.5\,(0.15 - K_s')\,DB\,\eta_g' \tag{14.25}$$

SES hull-borne operation

$$M_o' = -0.5\,[0.25 - 0.5\,(B_{sw}/B - K_s')]\,DB\,\eta_g' \tag{14.26}$$

where K_s' is the coefficient for transverse bending moment in calm water,

$$K_s' = M_{os}'/DB$$

M_{os}' the transverse bending moment in calm water (tm), B the width of midship section at designing water-line (m) and η_g' the inertial load coefficient, determined by prototype or model test. The maximum shear can be written as

$$N_o' = 4M_o'/B \tag{14.27}$$

Calculation for local loading

The local load acting on the bottom and sidewalls of an ACV/SES can be determined according to the following conditions:

1. air cushion pressure (in the case where water does not contact the structure directly);
2. hull slamming ;
3. reaction force of supports.

These forces can be calculated as follows.

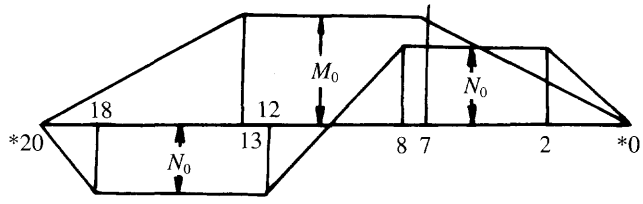

Fig. 14.5 Distribution of overall bending moment and shear forces at different craft stations.

Air cushion pressure

In the case where the hull does not contact the water surface, the distribution of pressure under the bottom along the craft length can be expressed as in Fig. 14.6 and along the transverse direction can be written as a uniform distribution:

$$\left.\begin{aligned} P_1 &= 2D\,\eta_g/S_c \\ P_2 &= D\,\eta_g/S_c \end{aligned}\right\} \tag{14.28}$$

where S_c is the cushion area (m^2). The design cushion pressure should be at least 30% greater than the cushion pressure supplied by the lift fan in the case of no air leakage.

Distribution of wave impact force along the craft length

During slamming on the craft bottom, the distribution of hydrodynamic pressure along the craft length can be determined as in Fig. 14.7, but it is uniformly distributed along the transverse direction. The impact force acting on section 0, 10, 20 (bow, midships and stern) can be taken as

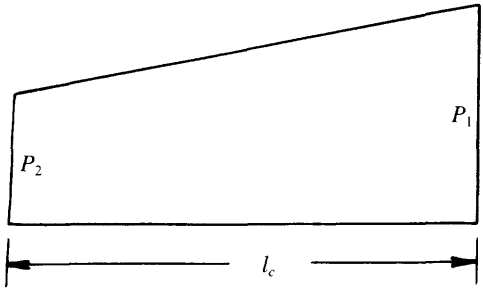

Fig 14.6 Distribution of cushion pressure in longitudinal direction due to slamming in waves.

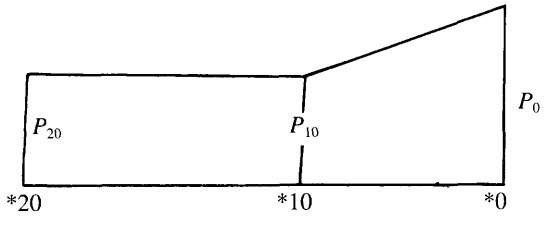

Fig. 14.7 Pressure distribution in longitudinal direction due to slamming of craft bottom in waves.

$$P_0 = KD\eta_g/(0.3\ LB)$$
$$P_{10} = KD\eta_g/(0.4\ LB) \qquad (14.29)$$
$$P_{20} = KD\eta_g/(0.4\ LB)$$

where K is the coefficient due to non-uniformity, and can be written as

K= 1 for the calculation of frames
K= 3 for the calculation of stiffness and frames between station 0 and 10
K= 1.25 for the calculation of stiffness and frames at station 20

Hydrostatic pressure acting on the bottom P_b and the sidewalls P_{sw}

$$P_b = T + h/2 - h_{sw} \qquad (14.30)$$
$$P_{sw} = T + h/2 - z$$

where h is the design wave height (m), z the vertical height from the base-line to the design location of the side plates (m), T the draft of craft in hull-borne operation, which can be measured from the lower edge of the bottom plates of the sidewall (or from the bottom in the case of no sidewall) to design water-line (m), P_b the hydrostatic pressure acting on the bottom, water head in metres (1m H_2O = 9.8 kPa) and h_{sw} the sidewall depth (m).

Cushion pressure

This can be calculated as a uniform distribution along the vertical direction and the distribution along the longitudinal axis can be calculated as shown in Fig. 14.6.

Design load on deck plates

The following pressure head values are recommended:

Passengers and crew spaces in a craft, walkways, etc.	0.50 m H_2O
The deck area where passenger chairs are accommodated	0.35 m
Superstructure deck plates and stiffeners	0.30 m
Superstructure deck beams	0.10 m
Design uniform load of front of deck house and window are:	
For 'O' class craft	2.00 m
For 'P' class craft	1.00 m
For 'N' class craft	0.50 m
Design uniform load on side plates and windows on first floor of superstructure	0.30 m

Calculation of strength for craft in docking and lifting situation

During the calculation of strength for craft in docking and lifting situations, the vertical velocity of the craft affecting the mounting or block and the dynamic load caused by cranes have to be taken into account. In general, the inertial load coefficient should be taken as $\eta_g = 1.25$.

14.5 Safety factors

Practical experience with hovercraft is much less than that of conventional ships, therefore, as yet there are no fully consistent calculation rules and regulations for

Table 14.4 Typical safety factor applied to the strength calculation of structure of ACV/SES [4]

Load condition	Safety factor cf. yield strength	cf. ultimate strength
On cushion	1.0–1.5	1.5–2.0
Emergency	1.0	1.5
Damaged	1.0	1.0
Towing, lifting, pushing	1.5–2.0	2.0–3.0

designers' reference. Reference 4 suggests that the safety factors for strength calculation of structure can be written as in Table 14.4.

Reference 105 suggested the following factors, which are summarized in Table 14.5.

14.6 Considerations for thickness of plates in hull structural design

In general, ACV/SES are constructed of stiffened plate structures. A key parameter in determining the dimensions is to determine minimum plate thickness; here we will discuss methods to determine the necessary thickness of plates.

Step 1

At first, designers have to determine the minimum thickness of plates. Particularly for small ACV/SES, the plate thickness is not determined according to the strength of the structure, but to other requirements related to stiffness, practical construction requirements, operational durability, overhaul life of craft and corrosion of plates, etc. Reference 105 recommended that minimum thickness of plates should be as shown in Table 14.6, in which the plate thickness of some SES are also listed.

Step 2

The local thickness of plates in the region of engine mountings, propeller supports, water-jet installations and other regions in which plates will experience serious corrosion, should be thickened by at least 40%.

Step 3

In the case where the thickness of plates is less than 3 mm the frame spans should not be greater than 300 mm. Spans should not be greater than 400 mm in other conditions.

Step 4

In the lower regions of sidewalls, the thickness of plates has to be thickened or strengthened in addition to other requirements so that after strengthening the thickness should not be less than double the thickness of the shell plates.

Table 14.5 The safety factors suggested by Ref. 105

Item	Name and character	Character of calculation stress under action of the loads	Ratio between admissible and maximum stress
1	Hull and superstructure framing participating in longitudinal or transverse overall bending (including window frames)	Normal stress and shear stress due to the overall longitudinal and transverse bending	0.5
		Resultant normal stress and shear stress due to the overall longitudinal and transverse bending	0.7
2	Longitudinal framing participating in the overall longitudinal bending and resisting local load (longitudinal cargo deck and bottom panel)	Resultant normal and shear stress due to the overall longitudinal bending and bending on single stiffeners, mid-span/at supports.	0.75/0.90
3	Beam participating in the overall bending and resisting local load (framing of cargo deck, bottom, and sidewalls)	Resultant normal stress due to the overall bending moment and local bending of panel and stiffeners, mid-span/at supports	0.80/0.90
4	Shell plates and bulkhead plates of the hull and superstructure. Tank bulkheads	Normal and shear stresses due to the local loads, mid-span/at supports	0.80/0.90
5	Stiffeners of hull and superstructure not participating in the overall bending	Normal and shear stresses due to the local loads, mid-span/at supports	0.75/0.90
6	Hull structure and superstructure beams not participating in overall bending	Normal and shear stresses due to the local loads, mid-span/at supports	0.80/0.90
7	Watertight and tank bulkhead stiffeners	Normal and shear stresses due to the local loads, mid-span/at supports	0.80/0.95
8	Watertight and tank bulkhead stiffeners	Normal and shear stresses due to the local loads, mid-span	0.85
9	Pillar and bracing stability	Normal stresses due to local loadings. Single frames/cross braces	0.5/0.75 but not $> \sigma_{0.2}$

Notes:

1. In this table maximum stress can be taken as

$$\sigma_0 = K\sigma_{0.2} \quad \text{while in extension}$$
$$\sigma_0 = \sigma_{kp} \quad \text{while in compression}$$

where $\sigma_{0.2}$ is the assumed yield point of material equivalent to the residual deformation of 0.2%; σ_{kp} the critical stress of stiffeners considering the correction of the elastic modulus, K a coefficient,

$K = 0.9$ riveted structure
$0.6 \quad 2 < t < 3$ mm
$0.7 \quad 2 < t < 3$ mm } welded structure
$0.8 \quad 2 < t < 3$ mm

and t is the thickness of the connecting plates (mm).

2. In this table maximum shear stress $\tau_0 = 0.57\,\sigma_0$.

Table 14.6 Comparison of minimum plate thickness recommended by the registers of former USSR [105] with that of Chinese hovercraft

Item		Craft											
		$L \leq 20$ m; craft class:			$20 \leq L \leq 40$ m; craft class:			$L > 40$ m; craft class:		Chinese river SES with aluminium hull			28 m SES with steel hull
		L	P	O	L	P	O	P	O	Bow	Mid	Stern	
1	Bottom plates	1.5	2.0	2.5	2.0	2.5	3.0	3.0	3.5	4	3	2.5	3.0–2.5
2	Side plates	1.5	2.0	2.5	1.5	2.0	2.5	2.5	3.0	2.5	2.5	2.5	3.0–2.5
3	Deck plates	1.5	1.5	2.0	1.5	2.0	2.5	2.5	3.0	2.5	2.5	2.5	3.0
	Cabin floors	1.5	1.5	2.0	1.5	2.0	2.5	2.5	3.0	2.5	2.5	2.5	3.0
4	Sidewall plates	2.5	3.0	3.0	3.0	3.5	4.0	4.5	5.0	3.0	3.0	3.0	2.5
5	Plenum chamber plates	1.0	1.0	1.5	1.5	1.5	2.0	2.5	3.5				
6	Superstructure shell plate	0.8	0.8	1.0	1.0	1.0	1.5	1.5	1.5				

14.7 Hovercraft vibration

The importance and complexity of hovercraft vibration

Hovercraft vibration is a complicated problem, for the following reasons.

Vibration with a severe and superharmonic excitation source

The installed power is high for ACV/SES even though the displacement is small, hence the specific power is as high as 15–60 kW/t and with a high harmonic exciting force. For instance, on ACVs with turbine propulsion, the speed of a gas turbine is about 10 000 r.p.m. and the speed of air propeller about 1000 r.p.m. and lift fan about 500–1500 r.p.m. There are also other power transmission gearboxes and shafting systems mounted on the craft, therefore the out-of-balance exciting force (moment) induced by the engines and other non-equilibrium dynamic forces provided by some machinery will cause exciting forces (moments) on an ACV.

After a period of operation the dynamic equilibrium of air propellers and lift fans may deteriorate because of some wear or minor damage to the complicated shaft system, owing to installation errors and inaccurate centring. All of these will be vibration sources and complicate the problems of vibration.

Low natural frequency

Owing to the relatively flexible hull structure, superstructure and machinery mountings of hovercraft, the natural frequency of such structures is low. For this reason the natural frequency of mountings is low even though the mountings themselves are strong enough. Meanwhile the static and dynamic stresses on the structure are also large.

High operational speed

Hovercraft with low specific weight often operate at high speed and in high seas in comparison with conventional ships. The propeller blades of Chinese air-cooled diesel propelled ACVs have broken twice during operation. Break-up of cooling fan blades, engine mountings and thrust ring mountings has also happened to ACVs, due to violent vibration of the main engines and air propellers.

Failure of lift fan mountings, the break-up of transmission gearboxes and universal joints has also occurred to SES. With respect to oil and water pipes, the failure of these used to happen to the ACV/SES because of vibration and fatigue. Table 14.7 lists the malfunction of various machines and components due to the vibrations, summarized from practical operations.

The situation of hovercraft in the past was that during demonstrations users were always interested in ACV/SES special characteristics, but once the craft were used in service, the users would get very annoyed, as a lot of malfunctions occurred to the early craft, mainly due to the vibration. These vibrations have been the main problems facing almost all design, manufacture and operation units concerned with the ACV/SES in China. In the case where the vibration problems can be solved smoothly, not only will the rate of sorties be greatly enhanced, but also the noise level will be reduced thus improving the ride comfort of hovercraft.

Table 14.7 The malfunctions often occurring to ACV/SES caused by vibration

Items	Malfunction	Craft type	Frequency of occurrence	Main reason for malfunction
1	Exhaust pipe breakage	ACV/SES	Medium	Weak exhaust pipes, lack of elastic supports and jointing
2	Hydraulic, fuel and lubrication system piping failure	ACV/SES	High	Violent vibration, lack of elastic joining on pipes
3	Lubricating oil radiator damage	ACV	High	Poor anti-erosion and anti-vibration capability of radiators
4	Transmission gearbox damage	ACV/SES	Medium	High vibration, particularly high vibration with low frequency at starting of engines
5	V drive power transmission damage	SES	Low	
6	Engine and bearing mountings damage	ACV/SES	Medium	High vibration of engines, weak hull and mounting strength
7	Air propeller GRP blade root failure	ACV	Low	Comprehensive factors of vibration
8	Air propeller GRP blade high vibration	ACV	Medium	Rupture of dynamic equilibrium on air propellers
9	Electrical system malfunctions	ACV	Medium	Induced by erosion and vibration
10	Rudder bearing mounting failures	ACV/SES	Low	High vibration at stern, weak structure
11	Water leakage at window and door seals	ACV/SES	Medium	High vibration and weak structure, unsuitable seal designs
12	Cracking of passenger chair mounts	ACV/SES	Medium	High vibration and weak structure

Note: Weak = not stiff enough.

The problems mentioned above can be solved as soon as careful design, manufacture and maintenance are in place, as is the case for many ACV/SES made in China and in the West. The vibration problems discussed here do not imply there are specific vibration problems concerning the shaft system or structure on ACV/SES. Rather, there are comprehensive problems which have to be mastered and paid more attention to by designers during design, construction and even operation. This is similar to the design problems faced by designers of high-speed warships and monohull or catamaran fast ferries.

Such problems most often concern the vibration of the structure, main engine and shaft systems, reduction gears, mountings of bearing and engines, various equipment and instruments, pipelines and their joints, etc. which includes the selection and determination of permissible standards for vibration, the co-ordination between mechanical and structural designers in order to avoid high vibration levels during the selection of main engines, drawing the general arrangements, construction profile and deck plans and the design of various subsystems such as propellers and shaft systems. This is the so-called general design of vibration absorption.

So far we do not have an accepted common vibration standard for ACV/SES. ACV/SES differ from conventional ships, aeroplanes or helicopters and wheeled vehicles. The permissible vibration standard is more difficult to define. Here we list some vibration standards specified for marine vessels and wheeled vehicles for reference. Table 14.8 summarizes the vibration standard ISO 2372 and ISO 3945.

It would be best if ACV/SES could meet the requirement C of class IV. Figure 14.8 shows the vibration standard for conventional ships published by the Bureau Veritas of France [106], in which (a) shows the vibration standard for diesel engines and (b) that for rotating machinery. As far as ACV/SES with flexible structure, elastic mountings and couplings are concerned, it is clear that this standard level is high, but can be used as a reference. Table 14.9 details the technical standards for vibration in classification rules and construction regulations for former Soviet marine vehicles (1974) [107]; these standards are also high for ACV/SES.

We could propose the vibration standard for helicopters and perhaps such standards will be lower, considering the measurement of external force acting on helicopters. Installation of main engines in the helicopter is at the stern and the design of vibration absorption is more precise for the helicopter than the ACV/SES, which are now constructed in shipyards in China. For this reason, we do not recommend the aviation standard. We prefer to use the vibration standards for conventional ships for reference and then make engineering decisions based upon test results of prototypes.

Design for vibration absorption

Owing to the importance and complicated nature of hovercraft vibration, the considerations for vibration absorption should take in the whole course of craft developments from preliminary design, construction to sea trials. Thus it can be called the general design for vibration absorption.

It is difficult to calculate the natural frequency of bearing mountings, because the boundary conditions of supports are complex. Taking the intermediate shafts of the propeller shaft system as an example, they are only a section of the propeller shaft system, which are supported on the bearing mountings, then to the panel of superstructure, to the main structure of hull and finally supported by the buoyancy tank.

Table 14.8 The vibration standard ISO 2372 and ISO 3945 of the International Standard Organization [108]

Ranges of radial vibration severity		Quality judgement for separate classes of machines			
Range	RPM velocity in the range 10–1000 Hz at the limiting mm/s	Class I	Class II	Class III	Class IV
0.28					
	0.28				
0.45		A			
	0.45				
0.71					
	0.71		A		
1.12					
	1.12	B		A	
1.8					
	1.8		B		A
2.8					
	2.8	C		B	
4.5					
	4.5		C		B
7.1					
	7.1			C	
11.2					
	11.2	D			C
18					
	18		D		
28					
	28			D	
45					
	45				D
71					

Note:
Machine classes are defined as follows:
Class I Small machines to 20 hp
Class II Medium-size machines 20–100 hp
Class III Large machines 600–1200 r/min, 294 kW and larger, mounted on rigid supports
Class IV Large machines 600–1200 r/min, 294 kW and larger, mounted on flexible supports
Acceptance classes:
A=Good; B=Satisfactory; C=Unsatisfactory; D=Unacceptable.

Thus analysis of vibration will be best determined by progressive approximation, i.e. beginning from the analysis of arrangement of the main engines, transmission shaft system and longitudinal structure arrangement as well as the vibration conditions and progress to calculation of shaft system vibration natural frequency, engine mountings and structure and finally the tests of vibration on such systems during construction and sea trials.

Only at sea trials can designers fully determine the characteristics of vibration of a particular hovercraft. Sometimes, in order to reduce vibration, local revision (stiffening) of the structure and mountings might be carried out during the sea trials. Prototype hovercraft trials therefore always play a very important role.

(a) For diesel and reciprocating engines:
  (1) For slow engines up to 150 rpm check that $\Delta s < 0.5$ mm at the bearings and foundations.
  (2) For piping mounts and miscellaneous units $\alpha < 1.5g$.
  (3) (A) Good
    (B) Normal operating condition
    (C) Requires survey to check
    (D) Not admissible.

	v(mm/s)	A	B	C	D
Slow	< 750 kW		4.8	11	18
Fast			4.8	11	18
Slow	< 750 kW		4.8	11	30
Fast			7.0	18	50

(a) For rotating engines and line shafting measured at the bearings or foundations:
  (1) For low-speed line shafting to 150 rpm it should be checked that $\Delta s < 0.5$ mm (vibration amplitude).
  (2) For the piping mounts and miscellaneous units acceleration $\alpha < 1.5g$

	v(mm/s)	A	B	C	D
Slow	< 15 kW				
Fast	< 75 kW		1.1	2.8	7.0
Slow	< 750 kW		1.8	4.5	11.0
Fast	> 750 kW		2.8	7.0	18.0

Fig. 14.8 Acceptable vibration levels for conventional ships proposed by Bureau Veritas of France [104].

The following three considerations have to be borne in mind with respect to vibration study:

1. investigation and analysis of the exciting force;
2. calculation of natural frequency for various structural components, in order to avoid resonance with rotating components;
3. vibration isolation.

In the whole course of vibration absorption design the three issues mentioned above have to be considered as shown in Fig. 14.9, a block diagram for general design for vibration absorption of hovercraft as explained below.

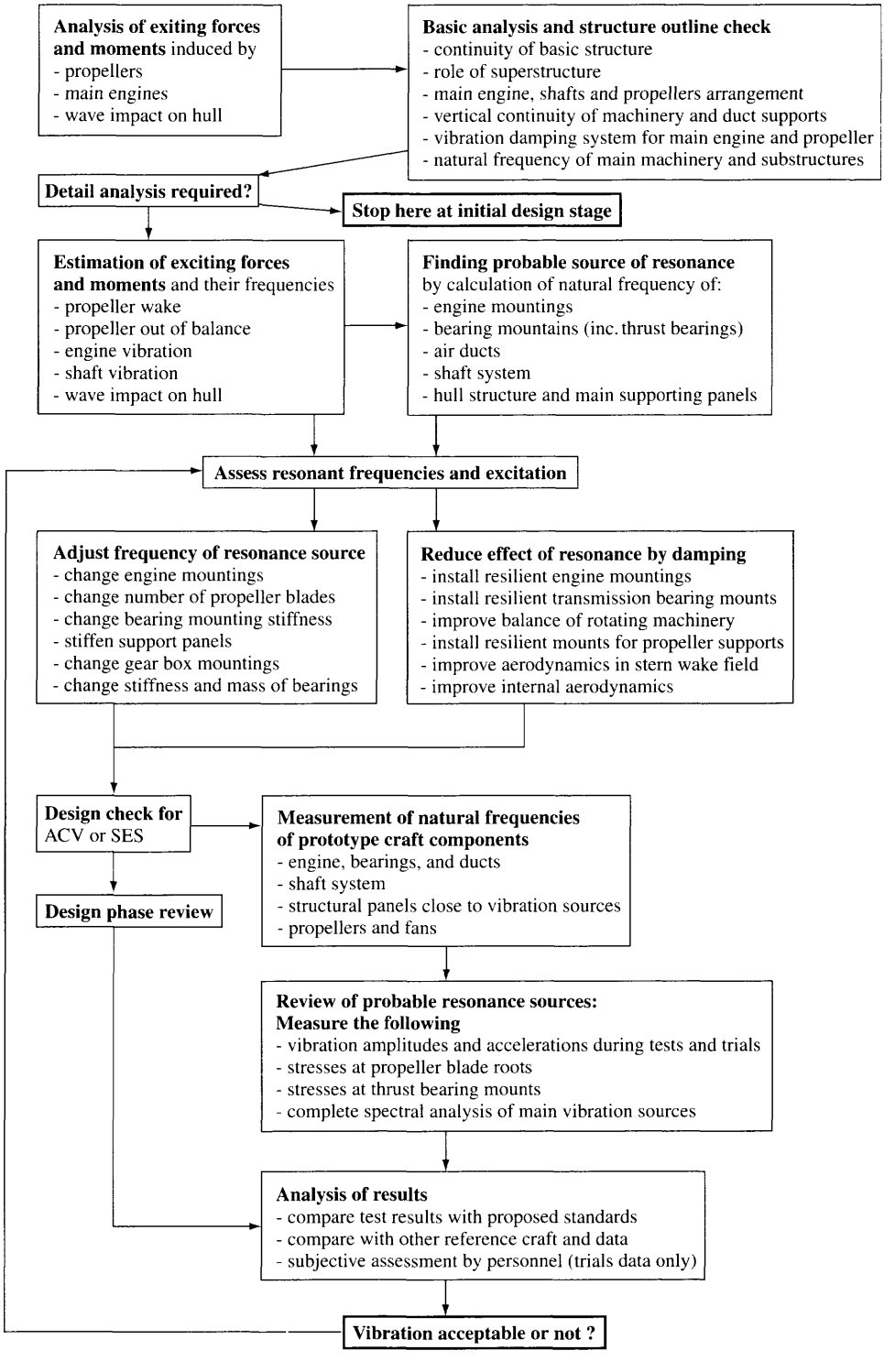

Fig. 14.9 Block diagram for vibration damping design ACV/SES.

Table 14.9 The permissible vibration and construction rules of marine vehicles in USSR [107]

Name of structure machine and equipment	Vibration axis	Frequency range (cycles/min)	Permissible amplitude (mm)	Remarks
Rigid member at stern	X, Y, Z	< 200	0.8	
			$[1.5 \times 10^4 + 85n]/n^2$	
Propeller and intermediate shafts	Y, Z	< 1500	$0.5–2.8n \times 10^{-4}$	
Gas turbine with reduction gearbox	X, Y, Z	< 850	0.35	Vibration frequency tuned to propeller revolutions
(top of reduction gearbox and bearings of turbine) and thrust bearing (top part) of turbine and diesel engines		> 850	$[0.25 \times 10^8]/n^2$	
Auxiliary machinery and heat exchangers				
Without vibration isolation	X, Y, Z		0.25	
With vibration isolation	X, Y, Z		0.5	
Navigation and radio equipment	X, Y, Z	< 300	1.0	
		300–1500	$300/n$	
Diesel engine without vibration isolation (top of diesel)	X, Y, Z	< 1000	0.5	Vibration frequency tuned to propeller revolutions
		> 1000	$[0.5 \times 10^6]/n^2$	
Diesel engine with vibration isolation (top of diesel)	X, Y, Z	< 1000	0.3	Vibration frequency tuned to shaft revolutions
		> 1000	$300/n$	
Rotating machine with vibration isolation	X, Y, Z	400–2000	$0.2–6.5 \times 10^{-5}\, n$	
		> 2000	$[0.28 \times 10^6]/n^2$	

Notes:
1. X, Y, Z denote the longitudinal, transverse and vertical vibration respectively.
2. n represents the frequency of vibration (cycle/min).
3. In the case of machine and equipment with vibration isolation, the vibration amplitude of alternative deformation of vibration isolation should not exceed the permissible value proved by the former USSR Register Bureau.
4. The vibration frequency for this standard begins from 30 cycles/min.

Preliminary design phase (or extended preliminary design)

In the preliminary design phase, the following principles have to be considered.

Exciting force

At first, designers have to consider whether the craft will operate in rivers or along a coast at sea, at low speed or high speed; if the wave-impacting force (moment) should be studied; what kind of engine will be installed in the craft, petrol, diesel or gas turbine; the degree of non-equilibrium; the exciting force induced by propellers and lift fans, etc. Based upon such considerations, designers then judge the vibration problems and whether they are likely to be troublesome or ordinary problems to solve.

General arrangement

Based on the initial craft design, the configuration of machinery within the structural arrangement, particularly the supports and foundations, the natural frequency and magnitude of forces acting on mountings of bearings, need to be reviewed, to assess the possibility of vibration isolation, and prepare a specification. It is normal

on hovercraft to mount at least the main and auxiliary engines resiliently and sometimes the main gearboxes (see Chapter 16 for more details about local mechanical design). Since the calculation for vibration is very difficult, in this phase empirical rules are normally followed, based upon the analysis of previous craft prototype vibration.

Detail design phase

The following sequence of analysis is followed :

1. Estimation and analysis of exciting forces.
2. Calculation of natural frequency of various members, such as the overall vertical vibration of the hull at full loaded and light displacement; the local vibration of stiffeners, panels, shell plates, deck plates and bulkhead plates; calculation of natural frequency of mountings of main engines, bearings, gearboxes and air propeller ducts, etc.; natural frequency of shaft systems.
3. Referring to the critical operational frequency as shown in Fig. 14.10, it can be seen that during calculation of the frequency of the exciting force, the speed of transmission shaft, i.e. shaft frequency, double of shaft frequency, the speed of shaft times the number of blades and so on need to be considered. The probability of resonance vibration between the exciting force and various mountings is high, but can be avoided at the operational range of engine speed as long as it is given careful consideration.
4. In this calculation, the following profile of vibration resonance between the various exciting forces and mountings and components have to be checked.
   (a) The allowance between the shaft speed and the natural frequency of vibration of the shaft system at the first mode is at least 20%.
   (b) On cushion-borne and hull-borne operation, the natural vibration frequency at the first mode of the hull structure should exceed the frequency of the exciting force.
   (c) The natural frequency of bottom plates and stiffeners at the stern should be higher than propeller speed by 50 and 30% respectively. The natural vibration frequency of plates and stiffeners at engines should be greater than the speed of the crankshaft and double that of crankshaft speed plus 50% and 30% respectively.
   (d) The propeller shaft speed times the number of blades should avoid the natural frequency of vibration of the stiffeners in the region where the propeller is located.
   (e) In the region of the lift fan, the natural frequency at the first mode of the local stucture of the hull should avoid the speed of the lift fan times the number of blades and so on.
   (f) The allowance between the natural frequency at the first mode of bearing mountings and the shaft frequency should be at least 30–50%.
   (g) The allowance between the natural frequency at the first mode of thrust bearing mountings and the shaft frequency of the propeller should be at least 30–50%.

(h) The blade frequency of the propeller should avoid double shaft speed and n times shaft speed with the number of blades and so on.
The frequency of the foregoing calculation should include the vibration frequency in vertical, transverse and longitudinal directions.

5. In the case of resonance, the frequency adjustments should be made first, i.e. changing the stiffness of mountings at resonance, since this is the simplest job, then changing the mass of the rotating component, thus changing the general arrangement, or shaft arrangement, which it is preferable to avoid.

Changing the stiffness of structure at which the resonance occurs, for instance in the case where the resonance occurs to the panel of the bottom structure at the stern, then the stiffness of such a structure should change and so on.

If the frequency adjustments fail to provide the desired effect, then designers are obliged to take measures to reduce the exciting force :

- changing the number of propeller blades;
- implement vibration absorption for main engines and shaft system;
- use elastic coupling;

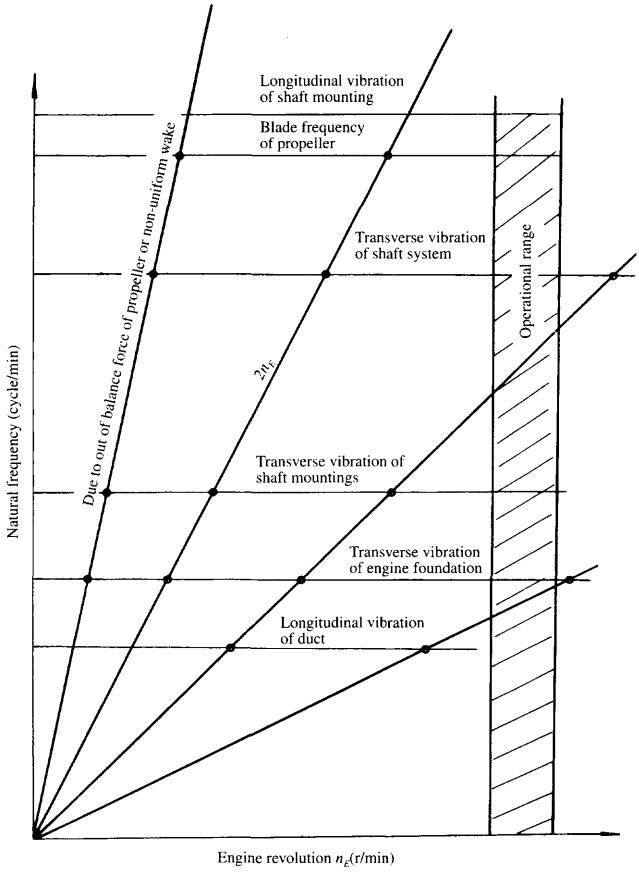

Fig. 14.10 Critical operational frequencies for certain systems on ACVs.

- belt transmission and so on can be adopted on the shaft system in order to dampen the exciting force.

Construction

In the case where the problems mentioned above have been solved, or it is predicted that these problems might be solved, then the production design and construction can be undertaken. If the designers anticipate that trouble may occur in the vibration absorption design, such as large exciting forces being in existence, frequency difficult to adjust and vibration absorption difficult to measure, etc. then attention has to be paid during construction to the static and dynamic balance, strict centering and vibration isolation of equipment and instruments and mounting of pipelines.

Table 14.10 Assessment of mechanical vibration [40]

Frequency of vibration	Primary reasons	Secondary reasons
Shaft frequency	Shaft not properly balanced	1. Eccentric gear journals 2. Poor shaft centring 3. Shaft not straight 4. Faulty transmission belt 5. Resonance 6. Unbalanced attached components 7. Problems with electrical systems
Shaft frequency × 2	Eccentricity for mechanical loosening	1. In the case of large axial vibrations then the eccentricity will be the main reason 2. Unbalanced attached components 3. Resonance 4. Faulty transmission belt
Shaft frequency × 3	Eccentricity	In general it is due to the out of centre and excessive slack in the axial direction
< Shaft frequency	Vibration on oil membranes, normally at 0.43 × shaft frequency	1. Faulty belt transmission 2. Background vibration 3. Low mode harmonic response 4. Beat vibration
Shaft frequency harmonics	1. Gear failure 2. Poor belt transmission 3. Aerodynamic action 4. Hydrodynamic action 5. Electric problems 6. Roller bearing failure 7. Air pressure fluctuation 8. Mechanical loosening 9. Reciprocating inertia forces 10. Combustion force	1. The number of teeth of failed gear × shaft frequency 2. 1 to 4 × shaft frequency, for defective belts 3. Number of fan blades × shaft frequency 4. Number of impeller blades × shaft frequency 5. In the case of mechanical loosening, 2, 3, 4, × shaft frequency and other harmonics 6. Imbalanced force at high order at inertia moment
Harmonic vibration frequencies not related to shaft harmonics	Failure of journal bearing	1. Unstable vibration on bearing 2. Vibration due to the friction of poorly lubricated journal bearing 3. Vibration with high random due to cavitation, turbulence and backflow 4. Vibration due to friction

Static hovering tests, and during trials

During tests of craft hovering statically and on trials, tests also have to be carried out and compared with the vibration standard mentioned above. In the case where the test results are not satisfactory, then the vibration source should be found by spectral analysis with attempts to adjust frequency by changing mounting characteristics, etc. to reduce the exciting force once again. Failure diagnosis can be undertaken according to Table 14.10 [44]. Meanwhile, the overall and alternating stress at the blade roots of air propellers, mountings and bearings and engines should be measured as good practice.

15

Propulsion system design

15.1 Introduction

In this chapter we will summarize the fundamentals for ACV and SES propulsor selection. We will also discuss issues which need to be considered when selecting supporting components to achieve the designer's overall objective – an efficient and readily manœuvrable craft.

ACV propulsion

ACVs are generally propelled by free or ducted air propellers, or by ducted fans. Air propulsor types are illustrated in Fig. 15.1. Available thrust is strongly affected by wind speed, so a designer has to consider carefully the requirements for thrust at hump speed as well as at design operating speed. It is normal to aim at minimum 20% thrust margin when transiting hump, to provide reasonable acceleration against the wind and sea. This is not usually an issue for craft with design speeds of greater than 55 knots, while it may become the controlling factor for utility craft with operating speeds in the 30–50 knots range.

The main design issue for air propulsion is to minimize the propulsor diameter (and so the system weight), while obtaining the desired efficiency for minimized power and an acceptably low emitted noise level. Propeller or fan blade tip speeds tend to be high. At speeds above 200 m/s the induced pressure field at blade tips creates significant noise. Open propellers adapted from aircraft often have tip speeds higher than this and so craft designed in the 1960s became known for their high noise signature. Since the mid 1970s craft have been developed with ducted propulsors, which are able to use lower tip speed to develop the same thrust, as the blade loading can be kept much higher in the outer 25% of the radius rather than tapering off to zero at the tip. Reduction of the tip vortices due to the presence of a duct also results in lower external noise.

Ducted propellers or fans are optimized as a system. Air flow around the duct, typically an aerofoil section, can provide additional thrust. If a fan is used, then flow straightener vanes are usually installed to maximize the developed thrust and remove the asymmetrical response to rudders which is otherwise present from the rotating slipstream. The duct also acts as a fin, providing directional stability for the craft.

SES propulsion

SES use water screws (open propellers) or water jets for propulsion, see Fig. 15.2. A subcavitating fixed pitch propeller is the simplest installation, relatively light and inexpensive. This has limitations though. Subcavitating propellers are very efficient at low speeds. Installation under the sidehulls of an SES often requires considerable shaft angles and possibly a vee gearbox to the engine.

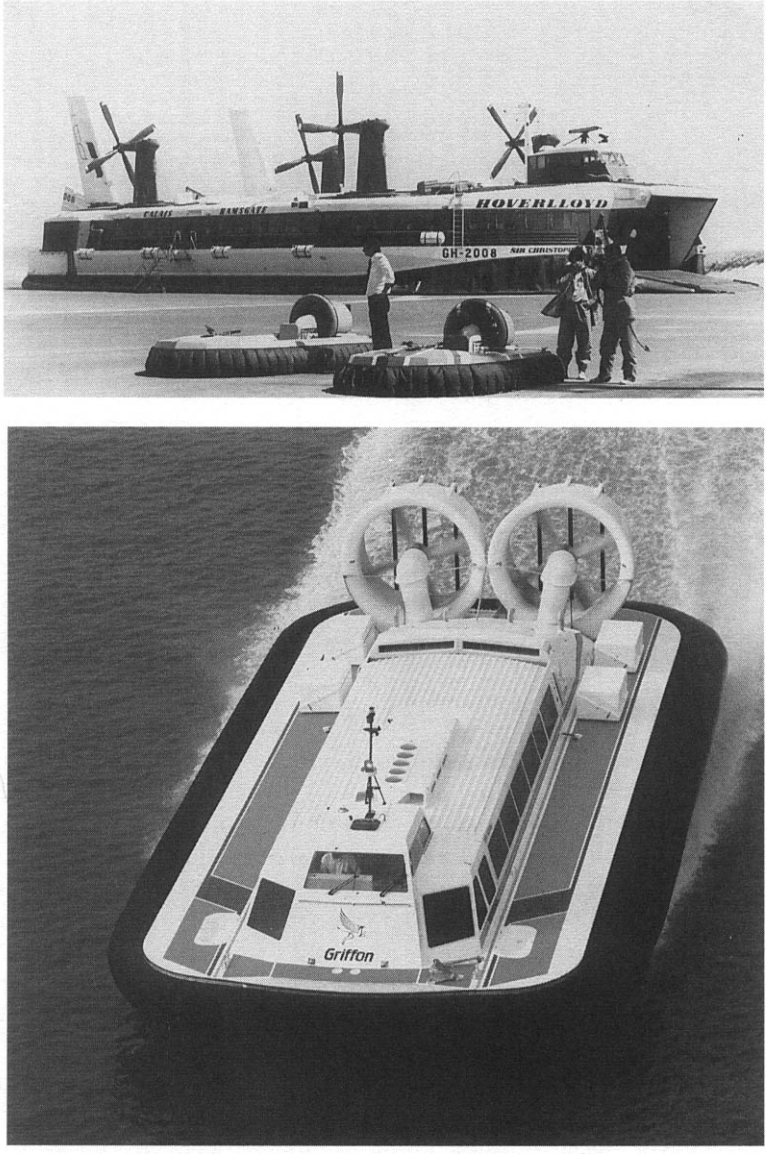

Fig. 15.1 Air propulsion types. (a) Pylon mounted open propellors on Hoverlloyd SRN-4 at Calais. The two integrated ducted fan craft in the foregound had just crossed the channel on the 25th anniversary of the first crossing by SRN-1. (b) Twin ducted propellers in the Griffon 2500TD.

The loading on a propeller blade is controlled by the suction pressure on the upper surface. As blade loading is increased this drops to water vapour pressure, causing cavities to form containing water vapour and air from solution. Cavitation starts at the blade tips and spreads inwards to eventually cover the whole blade forward surface.

In the speed range up to 35 knots it is possible to use subcavitating propeller blades which are designed to avoid suction pressures which may cause cavitation. Some cavitation at the blade tips is unavoidable due to vortices from the circulation, though this is usually over less than 2% of the blade area. Significant cavitation is unavoidable for

(c)

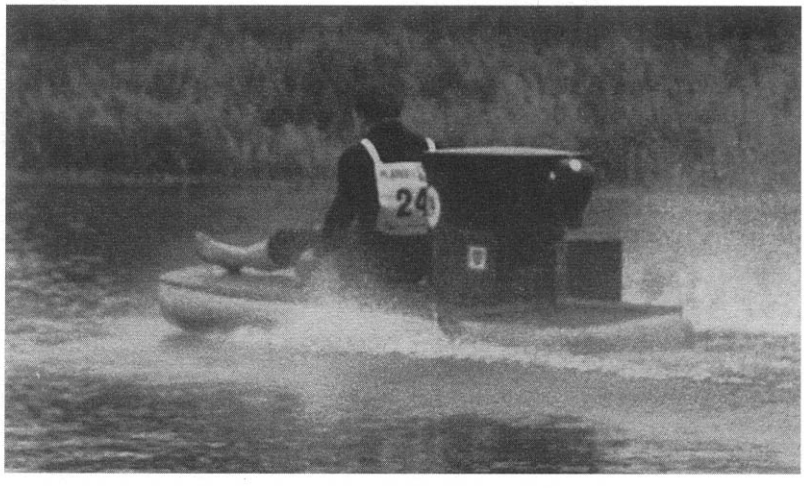

(d)

Fig. 15.1 (c) Integrated lift/thrust from single axial fan on the Griffon 375TD. (d) Air jet propulsion an an 'amateur' hovercraft racing in 1967.

propellers installed on craft designed for service speeds higher than about 35 knots. To stabilize the cavitation, fully cavitating or ventilated blade sections need to be used.

Several 'series' of cavitating blade sections have been developed, for example the Newton–Rader [109] and DTMB [82,85] series designs. Propellers using these sections have been successfully developed for SES with speeds up to 90 knots. Efficiency in the region 0.6–0.7 is typical for these propellers, compared with 0.65–0.75 for subcavitating propellers.

(a)

(b)

Fig. 15.2 (a) Model of Hovermarine HM.5 showing subcavitating propeller and rudder arrangement. (b) Close-up view of Hovermarine HM.2 subcavitating propeller.

Water jets have developed greatly since the early 1970s when units typically had efficiencies in the range 0.45–0.6. This has recently been driven by demands from catamaran ferry builders, though the initial impetus was for hydrofoils and SES due to potential simplification of the machinery and transmission arrangements. Units with system efficiency in the range 0.65–0.8 are now available, see Fig. 15.3, which plots achieved efficiency for KaMeWa installations. They offer lower vibration than a water screw, but require careful design of the inlet system.

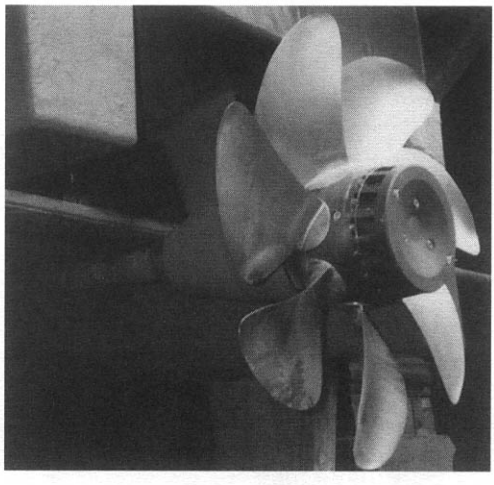

(c)

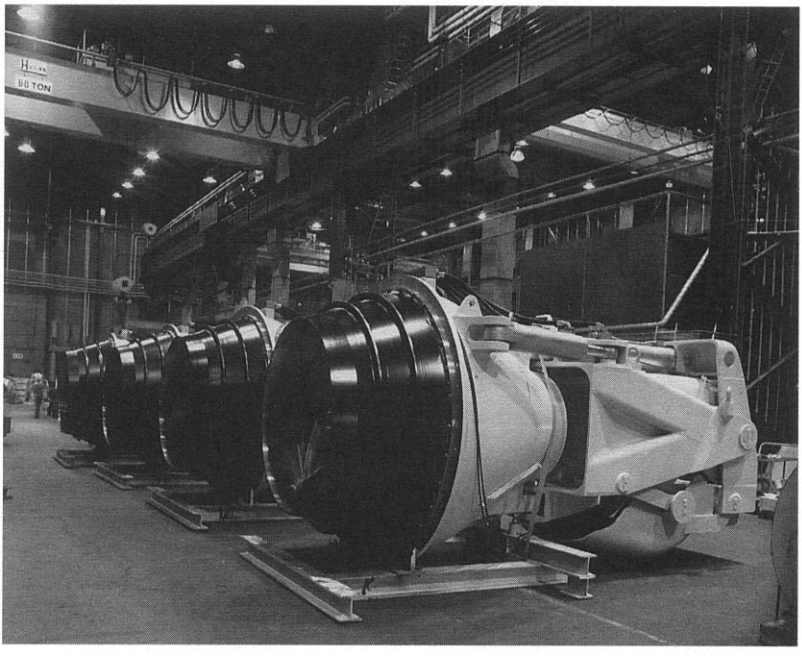

(d)

Fig. 15.2 (c) The Mekat supercavitating/superventilating propeller. (d) A group of large KaMeWa waterjet units type 125 prior to installation.

Efficient water jets for service speeds of up to 60 knots have been developed so far. While demand in the fast ferry market continues to press for increasing service speeds, it may be expected that units with similar efficiency for the speed range towards 100 knots will appear in the near future.

Other propulsion systems

Various other propulsion systems have been experimented with, mainly surface contact devices for propulsion of load-carrying platforms, see Fig. 15.4. Examples are hydraulic powered wheel units, winching systems and tracked propulsion. Platforms have also been towed by tractors, tugs and helicopters. The main challenge for design of these systems has been reliable traction over the usually difficult terrain and control of vehicle track when it is on a slope. Brief guidelines for these devices are given later in this chapter.

Basic theories

Before looking at selection for a particular craft, it is useful to review the physical phenomena which apply to both air and water propellers. Our purpose is to give an insight into the efficiency with which power (torque) is translated into thrust at various speeds and to discuss the basis on which blade geometry and number are best selected. This information should allow initial sizing of propulsors without reference to design of the units themselves, allowing realistic enquiries to suppliers prior to selection of candidates and optimization. Propulsor selection and design aspects are then discussed in more detail in following sections of this chapter.

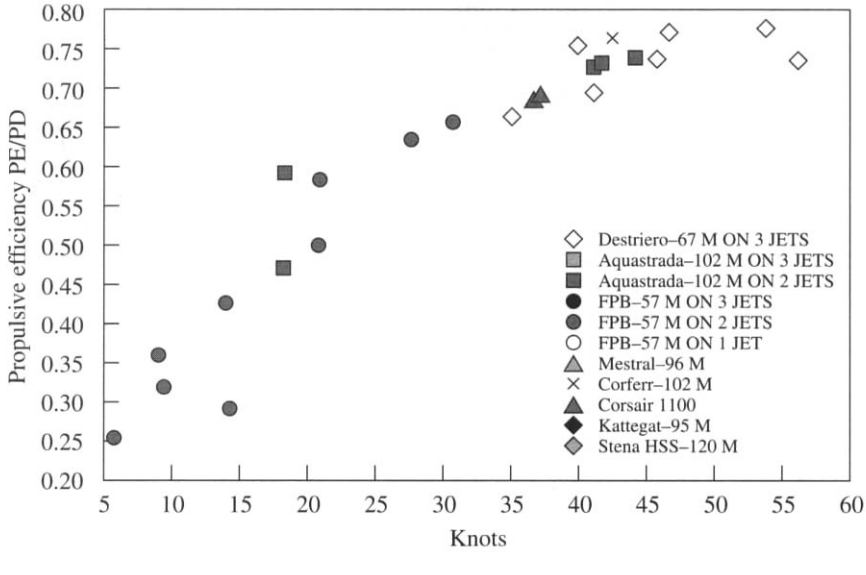

Fig. 15.3 Water-jet efficiency in practice, KaMeWa recent experience.

Momentum theory

Air propellers, ducted fans, water screws and water jets all deliver their propulsion as a reactive force to the momentum in the mass of air or water which is accelerated – they are momentum exchange devices. The fluid is accelerated by the action of the rotating blades. The lift and drag forces generated by air or water flow over the blades may be resolved into a thrust in the direction of craft motion and a torque which is the force required to rotate the impeller, see Fig. 15.5(a).

Without considering the air or water interaction with individual blades, momentum theory treats the propeller as a disc providing acceleration to the fluid in the direction of its movement. The principle is illustrated in Fig. 15.5(b). Incoming fluid at V_0 (the forward speed of the impeller, which is the craft speed plus/minus the wind speed or water current speed) is accelerated at the impeller disc to V_d. The streamlines continue to contract until flow has reached V_j. The velocity is assumed uniform over the disc area, implying a discontinuity at the outer diameter.

$$\begin{aligned} V_0 &= V_c +/- V_w \\ V_d &= V_0 (1 + a) \\ V_j &= V_0 (1 + b) \end{aligned} \tag{15.1}$$

(a)

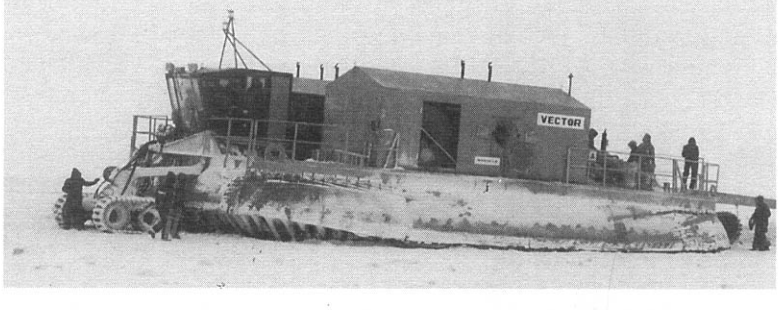

(b)

Fig. 15.4 Air cushion platform propulsion. (a) Direct propulsion by hydraulic powered wheels/tracks on the Wartsila Vector. (b) Winch propulsion along wires across the Peace river in Alaska during pipeline construction.

(c)

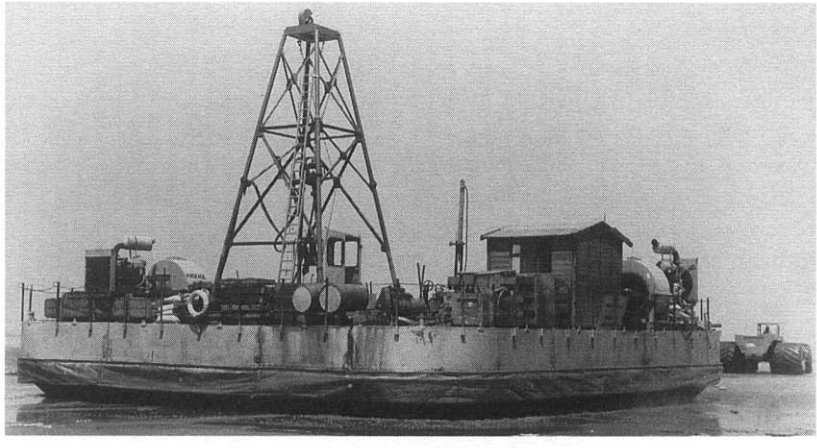

(d)(i)

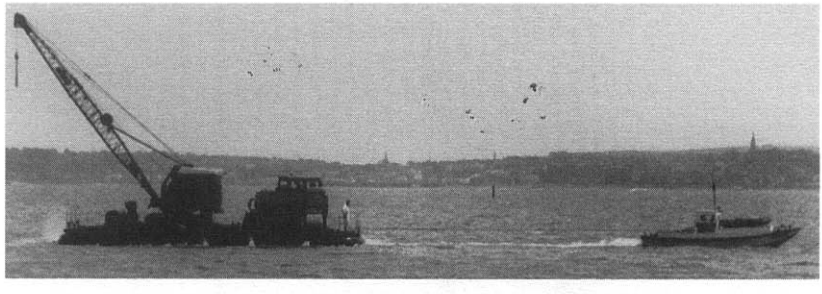

(d)(ii)

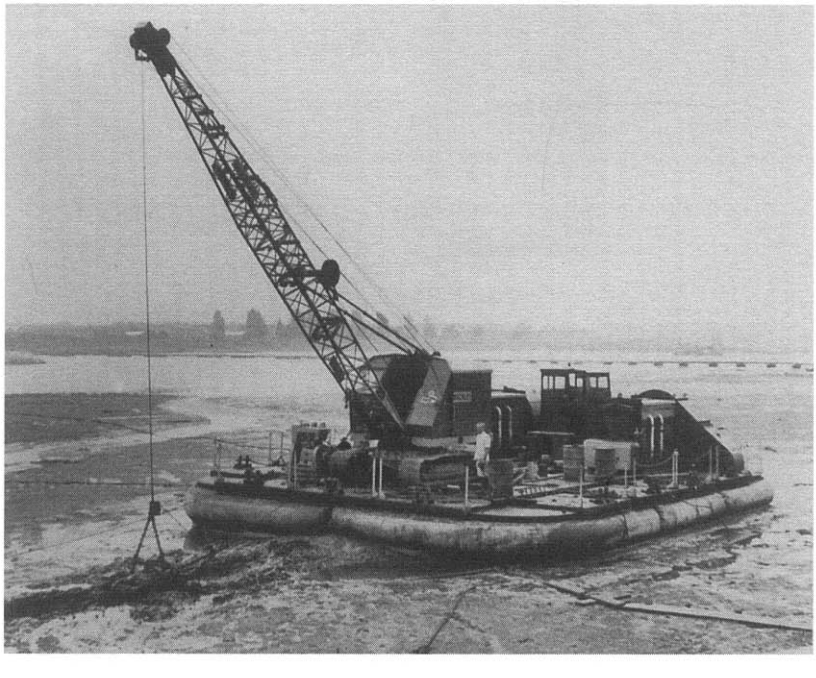

Fig. 15.4 (c) Overland towing of a soil sampling rig. (d)(i) Overwater tow of an outfall pipe dredging rig at high tide. (d)(ii) The rig at work.

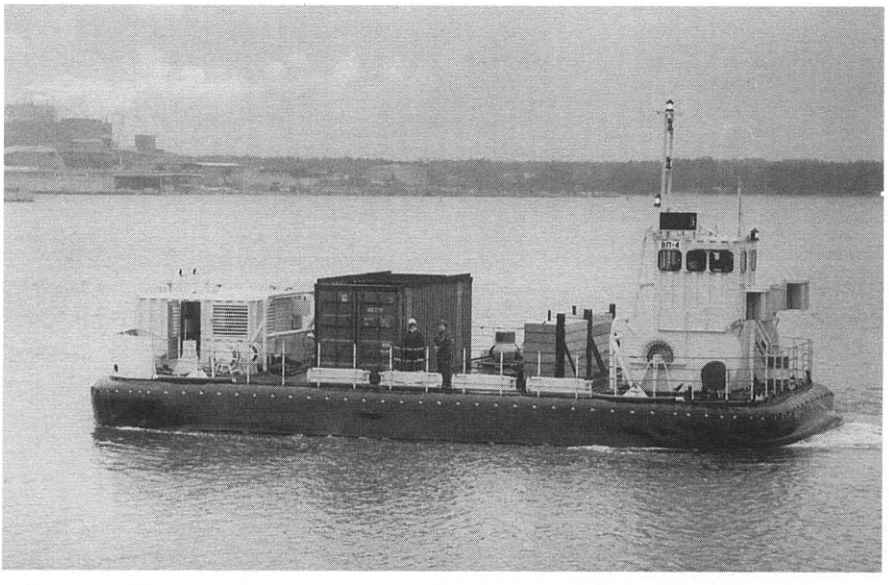

(e)

Fig. 15.4 (e) Wartsilla TAV.40 arctic resupply hoverbarge with air jet vents for slow speed propulsion/control.

The mass flow through the impeller is

$$\dot{m} = \rho_a/g \; A_d \; V_d \tag{15.2}$$

where $\rho_a = 1.293$ kg m/m^3 and $g = 9.81$ m/s^2, and the thrust developed is

$$T = \rho_a/g \; A_d \; V_d \; [V_j - V_0] \tag{15.3}$$

The thrust at the impeller disc is equal to the static pressure increment across it:

$$T = A_d \; (p_2 - p_1) \tag{15.4}$$

where p_2 is the static pressure just downstream of the impeller disc and p_1 the static pressure just upstream of it. Using Bernoulli's equation we can show by considering flow either side of the disc, that for a free propeller $b = 2a$ in equation (15.1), as follows. Upstream:

$$p_0 + 0.5\rho_a/g \; V_0^2 = p_1 + 0.5 \; \rho_a/g \; V_d^2 \tag{15.5}$$

downstream:

$$p_2 + 0.5\rho_a/g \; V_d^2 = p_0 + 0.5 \; \rho_a/g \; V_j^2 \tag{15.6}$$

thus

$$p_2 - p_1 = 0.5 \; \rho_a/g \; [V_j^2 - V_0^2] \tag{15.7}$$

so

$$T = A_d \; 0.5\rho_a/g \; [V_j^2 - V_0^2] \tag{15.8}$$

Equating to (15.3) we obtain

$$V_d \; [V_j - V_0] = 0.5 \; [V_j^2 - V_0^2]$$

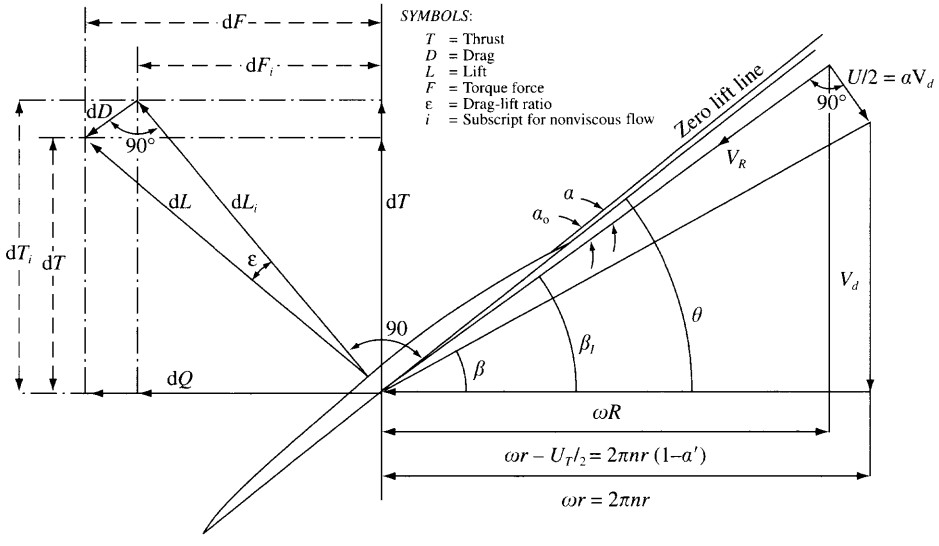

Fig. 15.5(a) Blade velocity vector diagram.

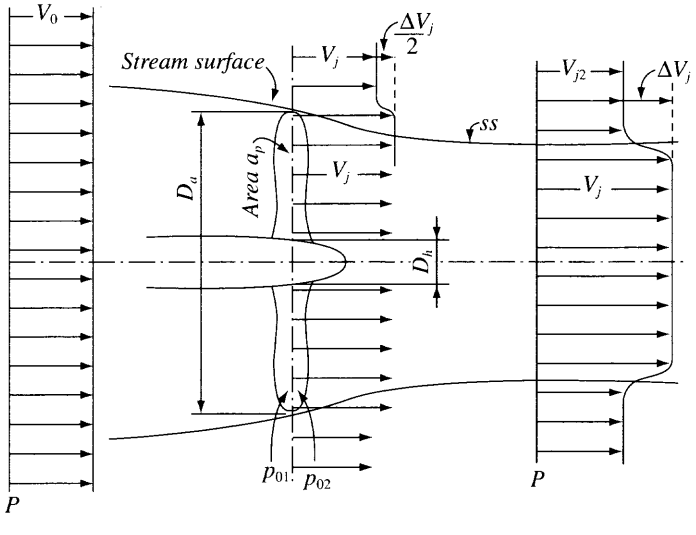

Fig. 15.5(b) Momentum exchange principle diagram.

Using the relations in (15.1)

$$[1 + a]\, b = 0.5\, [(1 + b)^2 - 1] = 0.5\, [b^2 + 2b]$$

on reduction this becomes

$$a = 0.5\, b$$

The useful work done by the impeller moving at V_0 is

$$T V_0 = \rho_a/g\, A_d\, V_d\, [V_j - V_0]\, V_0 \tag{15.9}$$

The kinetic energy applied to accelerate the flow to V_j across the disc is

$$E = 0.5\, \rho_a/g\, A_d\, V_d\, [V_j^2 - V_0^2] \tag{15.10}$$

The ideal efficiency is the ratio of useful work to the applied kinetic energy, thus

$$\begin{aligned} \eta_i &= T V_0/E \\ &= 2\, [V_j - V_0]\, V_0/[V_j^2 - V_0^2] \\ &= 2V_0/[V_j + V_0] \end{aligned} \tag{15.11a}$$

since $V_j = V_0\,(1 + 2a)$, the ideal efficiency is

$$\eta_i = 1/(1 + a) \tag{15.11b}$$

Now the power absorbed by the impeller is

$$N = T V_0/\eta_i \tag{15.12}$$

$$N = N\, g/550 \quad \text{shp (where } T \text{ is lbf = lb. ft/s)}$$

$$N = N\, g/1000 \quad \text{kW (where } T \text{ is kgf = kg. m/s)}$$

so the unit thrust developed is

$$T/N = 746/[(1 + a)\, V_0]\ \text{kgf/kW} \tag{15.13}$$

the disc loading varies with craft forward speed and a, which is a measure of the kinetic energy or velocity increment generated by the propeller. This may be expressed as

$$\begin{aligned} T/A_d = p_2 - p_1 &= 0.5\, \rho_a/g\, [V_j^2 - V_0^2] && \text{(from 15.7)} \\ &= 0.5\, \rho_a/g\, V_0^2\, [(1 + 2a)^2 - 1] && (15.14) \end{aligned}$$

If we take as an example an ACV at $V = 50$ kt (84.4 ft/s, 25.75 m/s) in still air; as V_j is increased this gives trends tabulated in Table 15.1 and shown in Fig. 15.6 for ideal thrust/power against disc loading for an air propeller. A water screw has a similar relationship between ideal efficiency and disc loading, theoretically displaced by the increase in water density, a factor of 835. Cavitation prevents water screw efficiency

Table 15.1 Variation of ideal efficiency with slipstream jet velocity

V_j	V_j/V_0	a	η_i	T/N (kgf/kW)	T/A_d (kgf/m^2)	η_i Ducted	T/N Ducted
36.05	1.4	0.2	0.833	24.14	41.95	0.909	26.34
41.20	1.6	0.3	0.769	22.28	68.17	0.870	25.19
46.35	1.8	0.4	0.714	20.69	97.88	0.833	24.14
51.50	2.0	0.5	0.667	19.31	131.09	0.800	23.17
64.38	2.5	0.75	0.571	16.09	251.69	0.727	21.07
77.25	3.0	1	0.500	14.48	349.58	0.667	19.31
128.75	5.0	2	0.333	9.65	1048.73	0.500	14.48

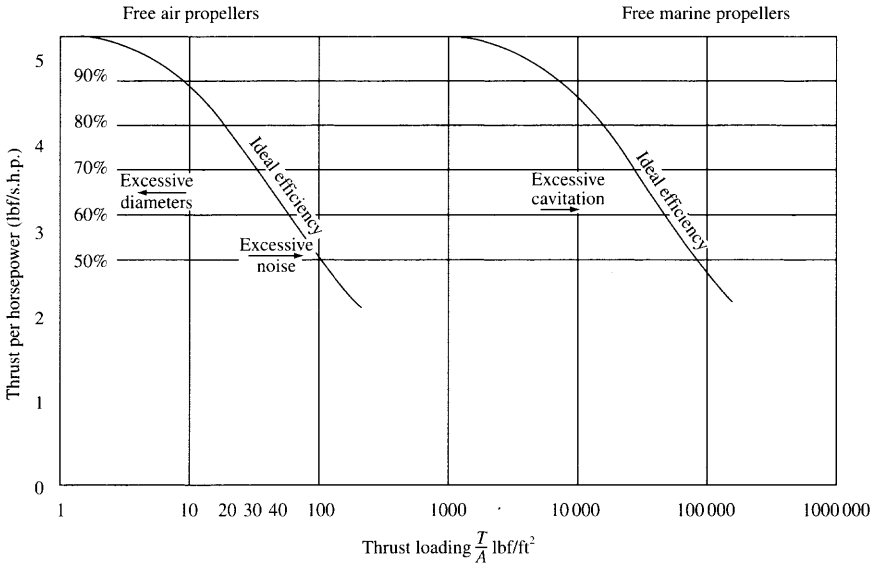

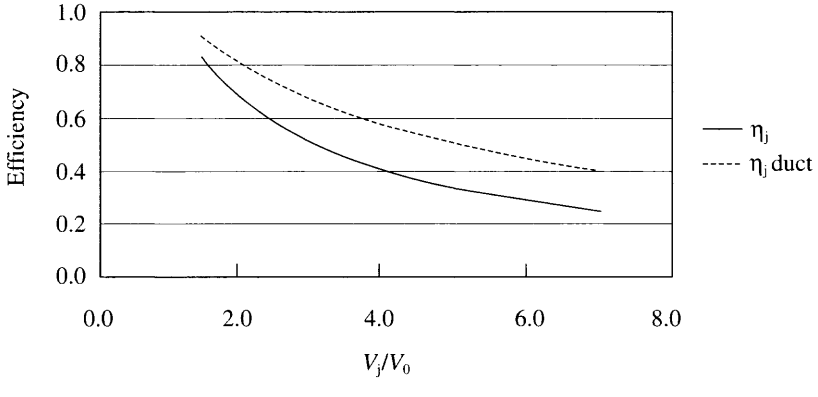

Fig. 15.6 Trends of ideal efficiency with disc loading and jet velocity: (a) trends with disc loading; (b) trend with jet velocity.

approaching the ideal curve as closely as an air propeller; see section 15.4 for a detailed discussion.

It can be seen that as disc loading is increased, η_i drops away. To minimize installed power, a value of a between 0.2 and 0.5 appears desirable. The thrust for a ducted propeller is also given for comparison, see section 15.3 for further discussion.

Blade element theory

Our discussion has so far ignored the form of the propeller itself. The ideal efficiency and therefore the characteristics discussed above are based on the assumption that the only loss of energy is that represented by the kinetic energy of the slipstream along the propeller axis. In addition to this there are three main sources of energy loss:

- drag forces on the propeller blades (see Fig. 15.5(a));
- variation of the pressure distribution radially along the blades, and circumferentially between blades;
- kinetic energy losses due to the slipstream rotating vortex.

In order to derive realistic performance curves of absorbed power and produced thrust against craft speed, the individual aerofoil blades must be taken into account. The blades must be designed with an appropriate form and angle of attack along their length to provide the lift force which accelerates the fluid to provide the thrust.

The lift generated by a propeller blade tapers to zero at its tip. In addition, the blades create parasitic and pressure-induced drag as well as lift. Absorbed power will therefore be increased compared to an ideal impeller due to the drag forces, and the total thrust developed will be less. This will reduce efficiency by 15% or so compared to the ideal for an air propeller. Water screws face a more difficult problem with cavitation, which limits the effective lift force as well as limiting the lift which can be generated close to the blade tips, reducing efficiency by as much as 30% compared to the ideal.

Consider each blade of a propeller rotating around its axis with angular velocity Ω, in an airstream velocity of V. At any section, the element creates a lift force due to the circulation around the section. This will vary along the blade and will create vortices at the axis and the tip of the blade similar to those at the root and tip of a wing and which pass downstream in the propeller wake following helical paths. These vortices create an interference flow which alters the circulation around the blade section.
The blade element thrust may be represented by

$$dT/dr = 4\pi r \rho V^2 (1 + a) a \tag{15.15}$$

and torque by

$$dQ/dr = 4 \pi r^3 \rho V \Omega (1 + a)a' \tag{15.16}$$

where a is the interference flow axially (same as for momentum theory) and a' the interference flow in rotation. The forces on a blade element are therefore

axial $= V(1 + a)$ at disc (note also that $V = V(1 + 2a)$ in propeller slipstream)
rotational $= r \Omega (1 - a')$

The resultant, W is at angle ϕ to the rotation disc plane, where

$$\tan \phi = [V/r\Omega] (1 + a)/(1 - a') \tag{15.17}$$

If we resolve lift and drag to thrust and torque, then

$$\delta T = C_L \cos \phi - C_D \sin \phi \tag{15.18}$$

$$\delta Q = C_L \sin \phi + C_D \cos \phi \tag{15.19}$$

so that

$$dT/dr = \delta T \times 0.5\,\rho\, W^2\, c\, dr \tag{15.20}$$

$$dQ/dr = \delta Q \times 0.5\,\rho\, W^2\, c\, r\, dr \tag{15.21}$$

If we consider the propeller disc rather than a single blade, then in place of the area of the blade, we need to integrate to the effective area of all blades, so a non-dimensional quantity s is introduced, the solidity, where

$$s = nc/(2\,\pi\, r)$$

then

$$dT/dr = \pi\, s\, r\, \rho\, v^2\, (1 + a)^2\, \delta T \operatorname{cosec}^2 \phi \tag{15.22}$$

or

$$\pi\, s\, r^3\, \rho\, v^2\, (1 - a')^2\, \delta T \sec^2 \phi$$

and

$$dQ/dr = \pi\, s\, r^2\, \rho\, v^2\, (1 + a)^2\, \delta Q \operatorname{cosec}^2 \phi \tag{15.23}$$

or

$$\pi\, s\, r^4\, \rho\, v^2\, (1 - a')^2\, \delta Q \sec^2 \phi$$

Comparing with the earlier expressions for dT/dr and dQ/dr it can be shown that

$$a/(1 + a) = 0.5\, s\, \delta T/(1 - \cos^2 \phi) \tag{15.24}$$

and

$$a'/(1 - a') = 0.5\, s\, \delta Q/\sin^2 \phi \tag{15.25}$$

the efficiency of the blade element is therefore

$$\eta = \frac{V}{\Omega}\frac{dT}{dQ} = \frac{V}{r\Omega}\frac{\delta T}{\delta Q} = \frac{1 - a'}{1 + a}\frac{\tan \phi}{\tan (\phi - \gamma)} \tag{15.26}$$

where $\tan \gamma = C_D/C_L$. This can be compared to the ideal efficiency from momentum theory of $1/(1 + a)$, illustrating the additional losses from the slipstream rotation a' and the effect of profile drag of the blades γ.

The characteristics of a blade element can be calculated knowing r/R, s, θ and the aerofoil characteristics (α, C_L, C_D). Starting with a series of α, the values of a, a', J and η can be calculated. It can be seen in Fig. 15.7(a) that η typically eaches a maximum at J of 0.5–0.6 whereas if the drag force were zero then efficiency would increase to 1.0 at J of 1.0. If the blade angle is increased or decreased, this will alter the efficiency curve as shown in Fig. 15.7(b), due to the blade lift coefficient changing as its angle of attack is changed. High blade pitch gives the highest efficiency. For a given propeller diameter, this will also lead to the smallest number of blades.

A two-bladed propeller is the simplest to construct. At the forward speeds typical of an ACV, a two-bladed propeller would require relatively large diameter to produce the desired thrust. While this may be accommodated on very small craft (Fig. 15.8), propellers with between three and six blades are generally selected for larger ACVs. The most common design is a four-bladed propeller.

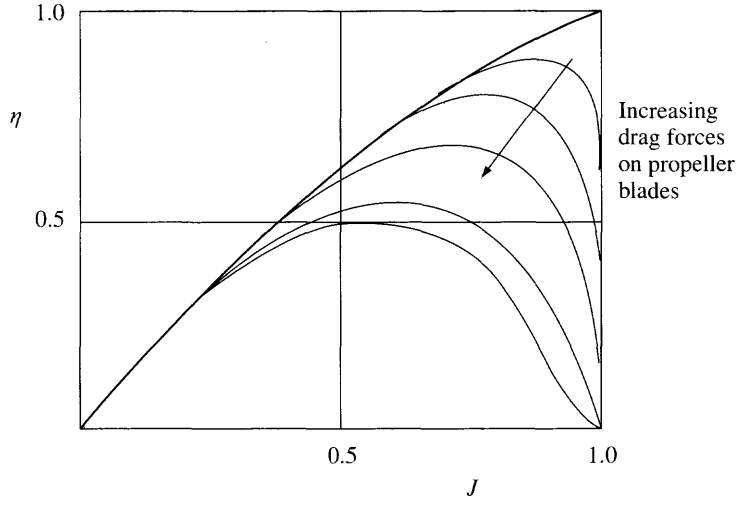

Fig. 15.7(a) Propeller efficiency vs speed of advance, *J*.

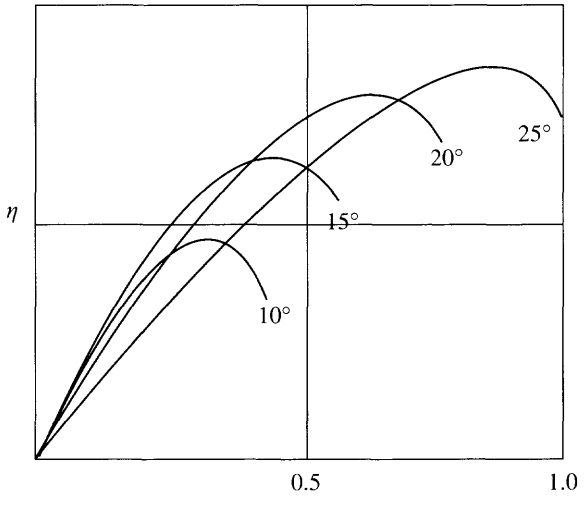

Fig. 15.7(b) Efficiency variation at different blade angles.

Static thrust

Propellers, fans and water jets operating when a craft is static or at very low speed will have streamlines looking something like those shown in Fig. 15.9. Air or water flow in the area of the blade tips will move forward before travelling through the impeller. Flow contraction will be rather different from the momentum theory presented above and so the generated thrust will not be as high.

Fig. 15.8 View of a small craft with large two-blade propeller, the Universal Hovercraft UH-15P.

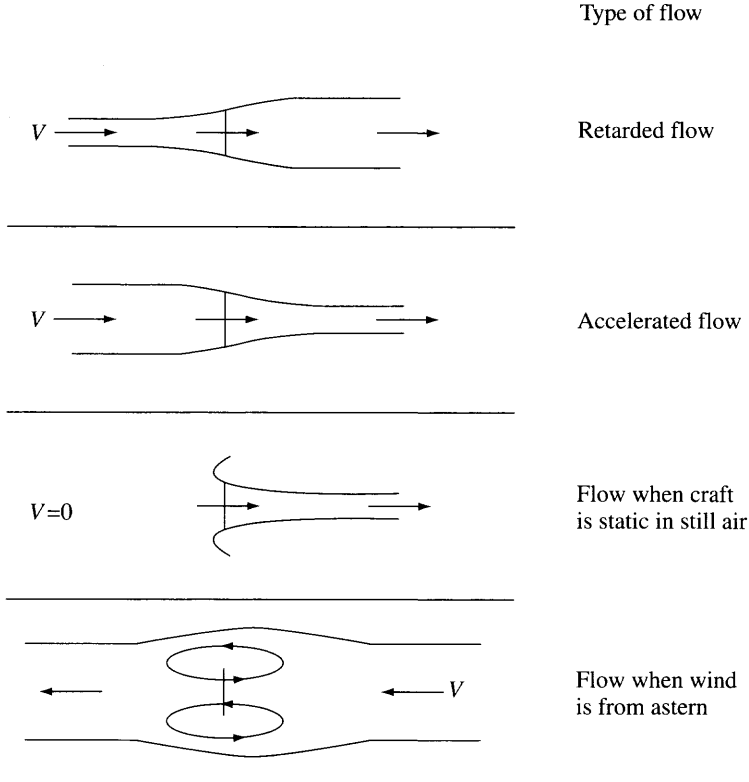

Fig. 15.9 Velocity streamlines at low speed.

An open propeller will experience turbulent flow over the outer part of the blade. Ducted systems can be designed with these outer radius streamlines in mind, so maximizing thrust at low speeds, but then at high speed the bell-shaped intake will not be optimum. Clearly a compromise is required. The duct nose geometry is generally developed using a camber line which forms a bell radius forward of the impeller plane. A thick section, of 12–18% chord is used, to minimize flow breakaway, both at high forward speeds and when the craft is yawed.

Based on experience gained from helicopter rotors, ACV designers often use a figure of merit (FoM) to characterize a propeller performance at a particular speed of advance into the fluid V_0, defined as the ratio of ideal power input to actual power input, i.e.

$$\text{FoM} = N_i/N_a = \eta_i/\eta_a \tag{15.27}$$

Real propeller characteristics are determined from wind tunnel or cavitation tunnel testing, where thrust and power coefficients C_T, C_N are determined at given rotational speeds, n. Dimensional analysis may be used to verify the following relationships:

$$C_T = T/[\rho_a n^2 D^4] \tag{15.28}$$

$$C_N = N/[\rho_a n^3 D^5] \tag{15.29}$$

now

$$\begin{aligned} T &= \rho_a A V_{act} V_j = m V_j \\ &= \rho_a A V_{act}^2 V^* \end{aligned} \tag{15.30}$$

where

$$V^* = V_j/V_{act}$$

also

$$V_{act}^2 = T/(\rho_a A V^*)$$

(If craft forward speed is V_0 this must be deducted from V_{act} and V_j when determining the thrust.) Now

$$\begin{aligned} N_i &= 0.5\rho_a V_{act} A V_j^2 \\ &= 0.5\rho_a V_{act}^3 A V^{*2} \\ &= 0.5\rho_a A V^{*2} [T/(\rho A V^*)]^{3/2} \end{aligned} \tag{15.31}$$

so

$$T = N_i^{2/3} [2 \rho_a A]^{1/3} \tag{15.32}$$

or

$$N_i = T^{3/2}/[2 \rho_a A]^{1/2} \tag{15.33}$$

thus

$$\begin{aligned} \text{FoM} &= N_i/N \\ &= [C_T^{3/2} \rho_a n^2 D^4]^{3/2}/\{[C_N \rho_a n^3 D^5] [2 \rho_a A]^{1/2}\} \\ &= [C_T^{2/3}/C_N] \{2/\pi\}^{0.5} \end{aligned} \tag{15.34}$$

also

$$\text{FoM} = T^{2/3}/\{N [2 \rho_a A]^{1/2}\} \tag{15.35}$$

so

$$T = \text{FoM}^{2/3}\, N^{2/3}\, [2\, \rho_a\, A]^{1/3} \tag{15.36}$$

thus

$$T/N = \text{FoM}^{2/3}\, [2\, \rho_a\, A/N]^{1/3} \tag{15.37}$$

from which it can be seen that thrust per unit power is inversely proportional to the cubed root of the disc loading. Since

$$A = \pi\, D^2/4$$

$$T = \text{FoM}^{2/3}\, N^{2/3}\, [\pi\, \rho_a/2]^{1/3}\, D^{2/3}$$

and

$$T/N = \text{FoM}^{2/3}\, [\pi\, \rho_a/2]^{1/3}\, D^{2/3}\, (1000/g)^{2/3}\, 1/N^{1/3} \quad \text{in kW} \tag{15.38}$$

or

$$T/N = \text{FoM}^{2/3}\, [\pi\, \rho_a/2]^{1/3}\, D^{2/3}\, (550)^{2/3}\, 1/N^{1/3} \quad \text{in hp} \tag{15.39}$$

These expressions can be reduced as follows:

$$T/N = 1.26891 \times \text{FoM}^{2/3}\, [D^2/N]^{1/3} \quad \text{in kW} \tag{15.40}$$

or

$$T/N = 1.04216 \times \text{FoM}^{2/3}\, [D^2/N]^{1/3} \quad \text{in shp} \tag{15.41}$$

which allows a plot of thrust/power against $[D^2/N]^{1/3}$ for a given FoM, as shown in Fig. 15.10. Typical FoM for four-bladed open propellers may be between 0.7 and 0.75, so that T/N may be estimated for a given diameter.

From momentum theory (see section 15.3) the relationship between ideal thrust available from a ducted propeller compared to a free propeller at zero forward speed can be shown to be approximately

$$T_{sp}/T_{fp} = 1.26\, (D_s/D_f)^{2/3} \tag{15.42}$$

where D_s is the duct inside diameter, ignoring the blade tip clearance, for the ducted propeller. If the shroud section thickness is 15% of diameter and outer diameters are the same (shrouded propeller diameter 85% of free propeller, which is typical) T_{sp}/T_{fp} is 1.13062, so that T/N becomes

$$T_{sp}/N = 1.43466 \times \text{FoM}^{2/3}\, [D^2/N]^{1/3} \quad (N \text{ in kW}) \tag{15.43}$$

If FoM is again assumed as between 0.7 and 0.75 then the static thrust exclusive of induced thrust from the duct itself can be estimated for given powers, to gain some idea of the appropriate duct diameter for a given craft. It should be noted this assumes a duct which has ideal inflow and no flow contraction in the slipstream.

Air jet propulsion

If we consider alternatives to a propeller to create a jet of air for propulsion or manœuvring of an ACV, the following might be used:

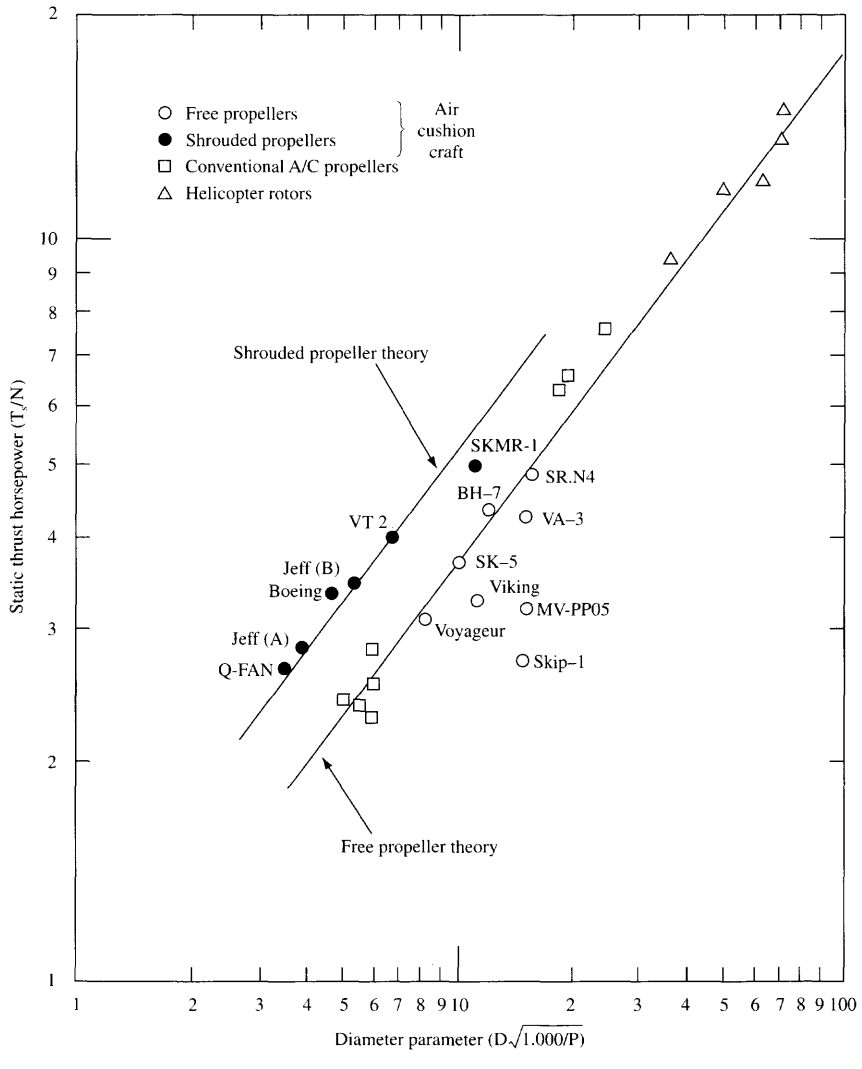

Fig. 15.10 T/N vs $D/N^{0.5}$ [4].

- cushion air
- air ducted from a mixed flow or centrifugal fans
- ducted axial fans

A small component of thrust is often present from the gap under stern skirts. To prevent scooping through hump speed a positive gap under stern segments is desirable anyway, usually about 10% of the segment height. The thrust developed from this air jet is

$$T = Q\,\rho_a\,(V_j - V_c) \tag{15.44}$$

where V_c is the craft speed air speed and V_j the air jet speed

$$V_j = [2\, p_c/\rho_a]^{0.5}$$

$$Q = A\, C_j\, V_j$$

where C_j is the discharge coefficient for the air jet under the skirt segments. At zero speed in still air equation (15.44) reduces to

$$T = A\, C_j\, 2\, p_c \tag{15.45}$$

Cushion static pressure is converted to kinetic energy at free stream pressure to develop thrust. The V_j available from typical cushion systems is shown in Fig. 15.11. At zero speed, the discharge coefficient for the skirt 'nozzle' reduces the available thrust. At increasing craft forward speeds, the thrust simply diminishes, in contrast to

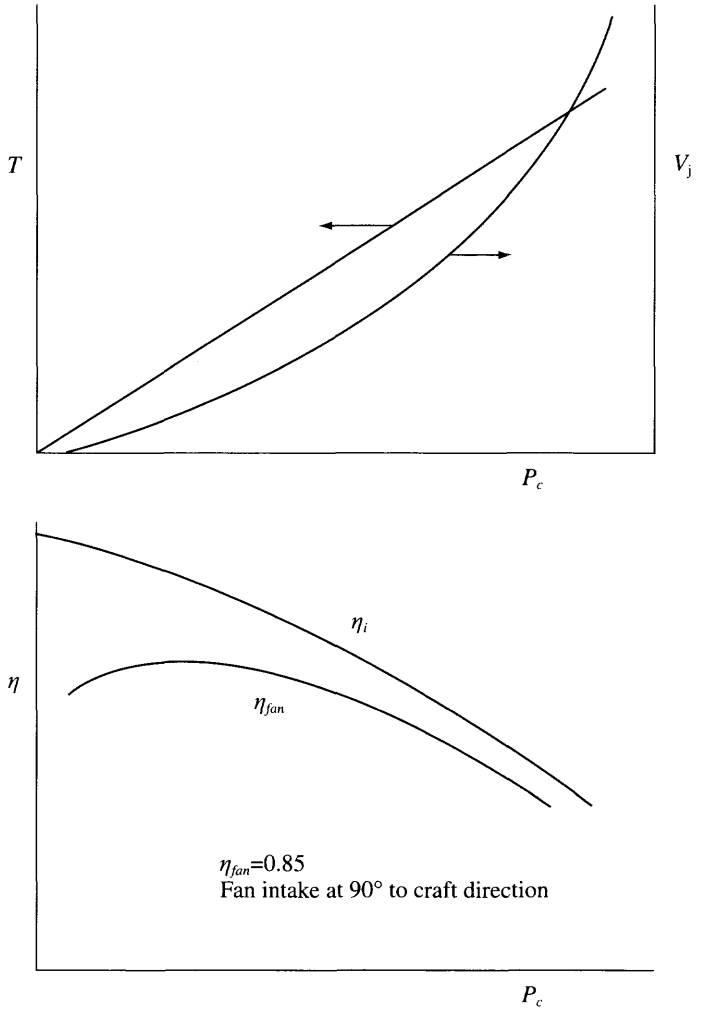

Fig. 15.11 V_j from cushion systems.

a propeller or ducted axial fan, which may be designed for a given forward speed. This loss may be correlated with acceleration of lift fan intake air to craft forward speed, which is normally calculated as momentum drag and represents a comparative efficiency loss of 50%.

Cushion system fans are selected for maximum efficiency when at mean cushion flow, at cushion pressure. In order that the lift fans operate at their most favourable point, the cushion system design should account for the desired stern skirt discharge.

Rather than using cushion air, it is more convenient to use dedicated air ducts and fans. The SR.N1 in its original configuration used a system with ducts to each corner of the craft, see Fig. 1.9. In the 1960s this was developed further on a number of craft, for example the Cushioncraft CC5, Fig. 15.12, used centrifugal fans for propulsion. The primary design objective for this craft was a low noise signature. In this case the fan operating point is adjusted to a discharge pressure sufficient to balance the intake and diffuser duct losses. A fundamental problem exists, which is that at craft forward speeds there is an intake loss as the air is first accelerated to craft forward speed and in addition centrifugal fans have low efficiency at high flow rates. While not the most power efficient, fan jet craft were extremely quiet.

More recently, ducted air has been used for rotatable bow thrusters on the LCAC, and AP1.88, for example, see Fig. 15.13 and Fig. 6.9. Optimization follows the same logic as for a centrifugal fan propulsion system, at craft speeds close to zero. While the thrust at high speed is low, this can be used to assist control of yaw in side winds. Low efficiency is accepted based on the utility of the control forces made available. The air jet exhaust velocity should be selected to be higher than the craft cruise speed, so as not to create unnecessary additional drag force in normal operation.

Ducted axial flow fans are discussed further below. For the purposes of ACV design these may be considered a subset of ducted propellers with higher solidity.

15.2 Air propellers

It is assumed at this point that the designer has used momentum theory with approximate values of expected efficiency to estimate his desired propeller diameter, as in Fig. 15.14. The propeller design itself is now to be selected, including the number of

Fig. 15.12 The Cushioncraft CC5 – a very quiet centrifugal fan propelled craft.

Fig. 15.13 A rotating thruster unit (AP1.88).

blades and their form. We will first give some background, before discussing propeller selection itself. Example data for hovercraft propellers are given in Table 15.2.

Table 15.2 Hoffman air propeller summary data

Propeller	No. blades	Pitch change mechanism	Power (kW max.)	RPM (max.)	Diameter (max. m)	Weight (kg)	Application
HO-V123O-DOR	3	H/M	225	2400	1.8	32	SAH 1500, Hovertrans PH11, PH12
HO-V1440-DOR	4	H/M	300	2500	2.0	45	Griffon 2000 TDX
HO-V1550-DO	5	H	300	3600	1.5	34	
HO-V1830-DO	3	H ground adjustable	320	2500	2.2	42	
HO-V194P-DFR	4	H	640	2200	4.0	173	Wartsila Larus
HO-E214	4	ground adjustable	800	2200	2.75	108	BHC AP1-88
HO-V225Q-VR	5	H	1200	1200	4.0	220	Chaconsa SA36
HO-V254P2-DFR-0	4	H	640	2200	3.0	150	BHC AP1-88 ABS
HO-V285	5	H	2450	960	3.6	600	Korea Tacoma Marine

Design methodology

A design methodology has been developed over many years for aircraft propellers, based on interpretation of results from wind tunnel testing, in a similar way to the original development of data on aerofoil forms. Non-dimensional coefficients C_T (thrust coefficient), C_N (power coefficient) and J (advance ratio) are determined

experimentally in the wind tunnel by propeller designers, based on a given blade angle at a station 70% of the propeller diameter from the centre.

$$C_T = T/[\rho_a/g\, n^2\, D^4] \tag{15.46}$$

$$C_N = N/[\rho_a/g\, n^3\, D^5] \tag{15.47}$$

$$J = V_0/[n\, D] \tag{15.48}$$

where T is the propeller thrust (kg), ρ_a the air density (kg/m^3), n the propeller speed, rps (l/s), D the diameter (m), N the propeller power (kg m/s) and V_0 the free stream velocity (m/s). Propeller efficiency can be determined as

$$\eta = T\, V_0/N = C_T\, J/C_N \tag{15.49}$$

The propeller characteristics are normally plotted against variations in the propeller diameter, number of blades, the activity factor AF and blade-integrated design lift coefficient $C_{L,Di}$ [104] where

$$\mathrm{AF} = 10^5/D^5 \int_{r\,=\,0.1D}^{r\,=\,0.5D} \mathrm{c}\, r^3\, \mathrm{d}r \tag{15.50}$$

where c is the local blade chord

$$C_{L,Di} = 10^4/D^4 \int_{r\,=\,0.1D}^{r\,=\,0.5D} C_{L,D}\, r^3\, \mathrm{d}r \tag{15.51}$$

where $C_{L,D}$ is the local lift coefficient at zero blade incidence for the aerofoil. Activity factors for propellers which have been used on existing hovercraft are usually in the range 100–150 and have $C_{L,Di}$ values in the region 0.55–0.7.

Blade types and efficiency

High activity factor blades (above 150) have more of a paddle appearance, while low AF (e.g. SR.N4 at 108) blades are tapered. High AF propellers are more suited to lower tip speed, 120–170 m/s, which also helps limit emitted noise. High $C_{L,Di}$ blades are more cambered and so give very little reverse thrust if constructed as a variable pitch propeller.

Early ACVs used low AF propellers direct from aircraft, which had high tip speeds. Experience has shown that unless tip speed is kept below about 50% of the speed of sound (C = 330 m/s) then propeller noise can be a nuisance to the environment, with external levels in excess of 90 dBA at 150 m from the source. If we consider the desired propeller speed for a moment, if we limit tip speed to 175, 165 and 150 m/s, this gives the results shown in Table 15.3, for different diameters.

It can be seen that above around 1.5 m diameter, reduction drive is required for high-speed diesels. For installations up to around 400 kW (550 shp) toothed belt drives may be used to achieve the reduction, while above this, a gearbox is unavoidable.

The noise limitation requirement effectively limits the power which may be absorbed by a propeller of a given diameter. The designer then has a choice between increasing blade number or changing the blade geometry to maximize efficiency. If a

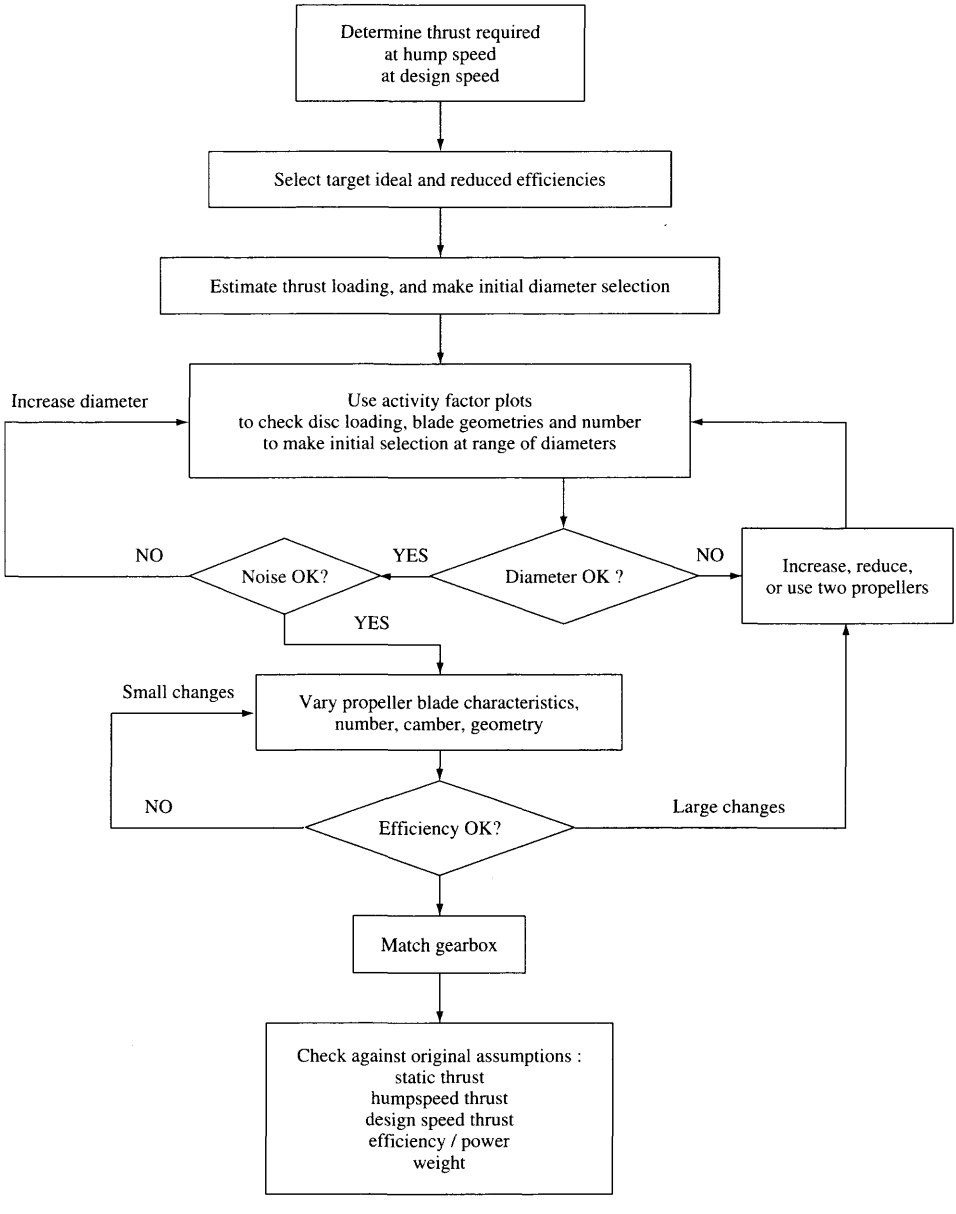

Fig. 15.14 Air propeller selection.

variable pitch propeller is to be selected, to give reverse thrust, then blades with low camber (low $C_{L,D}$) need to be chosen. With camber of around 4% and lift coefficient 0.7, similar to SR.N4 propellers, reverse thrust of 45–50% can be generated. If camber is increased to 5%, with lift coefficient at 0.9, then reverse thrust drops to 35–40%, for the same forward thrust rating. If the propeller is a fixed pitch unit, then higher camber may be selected, to reduce the blade number or dimensions for a given power rating.

Table 15.3 Propeller diameter/tip speed relationship

Diameter (m)	RPM at tip speed			Typical power	
	175 m/s	165 m/s	150 m/s	kW	shp
0.5	6685	6303	5730	13	17
1.0	3342	3151	2865	51	68
1.5	2228	2101	1910	115	154
2.0	1671	1576	1432	204	274
2.5	1337	1261	1146	319	428
3.0	1114	1050	955	459	616
4.0	836	788	716	817	1095
5.0	668	630	573	1276	1711
6.0	557	525	477	1838	2464
7.0	477	450	409	2501	3353

Selection procedure

The starting point to select a propeller for a given craft is to consider two forward speed conditions, hump speed into a wind of say 25 knots and the desired maximum operating speed, e.g. 60 knots in a head wind of 10 knots or so. At hump speed, sufficient thrust margin for acceleration is required, between 20 and 50% depending on the design maximum speed. Propeller selection is shown diagramatically in Fig. 15.14.

Propeller power loading in the region 50–75 kW/m^2 is typical of ACVs which have been built to date. Choice of diameter is dictated by available blades and hub assemblies from the specialist suppliers. If a practical efficiency level for a typical propeller is assumed as 15% below the ideal curve to estimate thrust, this will provide a start for sizing and enable initial enquiries to be made to suppliers.

Typically characteristic plots for propellers with three to six blades should be available. A good starting point will be to use the data for a four-blade propeller and check first how close this is to the desired characteristics. Once AF, C_N, C_T and J data plots have been obtained it is possible to select a series of AF and check the C_N and C_T at differing J. A sample plot is shown in Fig. 15.15 for the Dowty LCAC propeller. From these data a compromise for propeller speed, blade angle and shape may be chosen to fit the craft operating envelope.

Some experimentation between blade number and blade chord is usually necessary before the desired combination of propeller speed and diameter can be selected. Normally four-blade propellers provide a realistic selection, while ducted propellers for high powered craft may require six blades to limit diameter and emitted noise.

This approach assumes that the ACV designer will select a propeller from a range of standard components available from a specialist supplier (Messier-Dowty, Hoffman, Hamilton Standard or Air Vehicles for example). Development by these suppliers of a new propeller is very expensive, partly because the new design would be required to be prototype tested for certification by authorities prior to use on a commercial ACV. Several propeller designs are now available based on standard hubs and blades, which can be assembled to fulfil a range of possible requirements. Designers should nevertheless bear in mind that in most cases, the selection of a propeller will be between a series of available units, in the same way as selecting an engine.

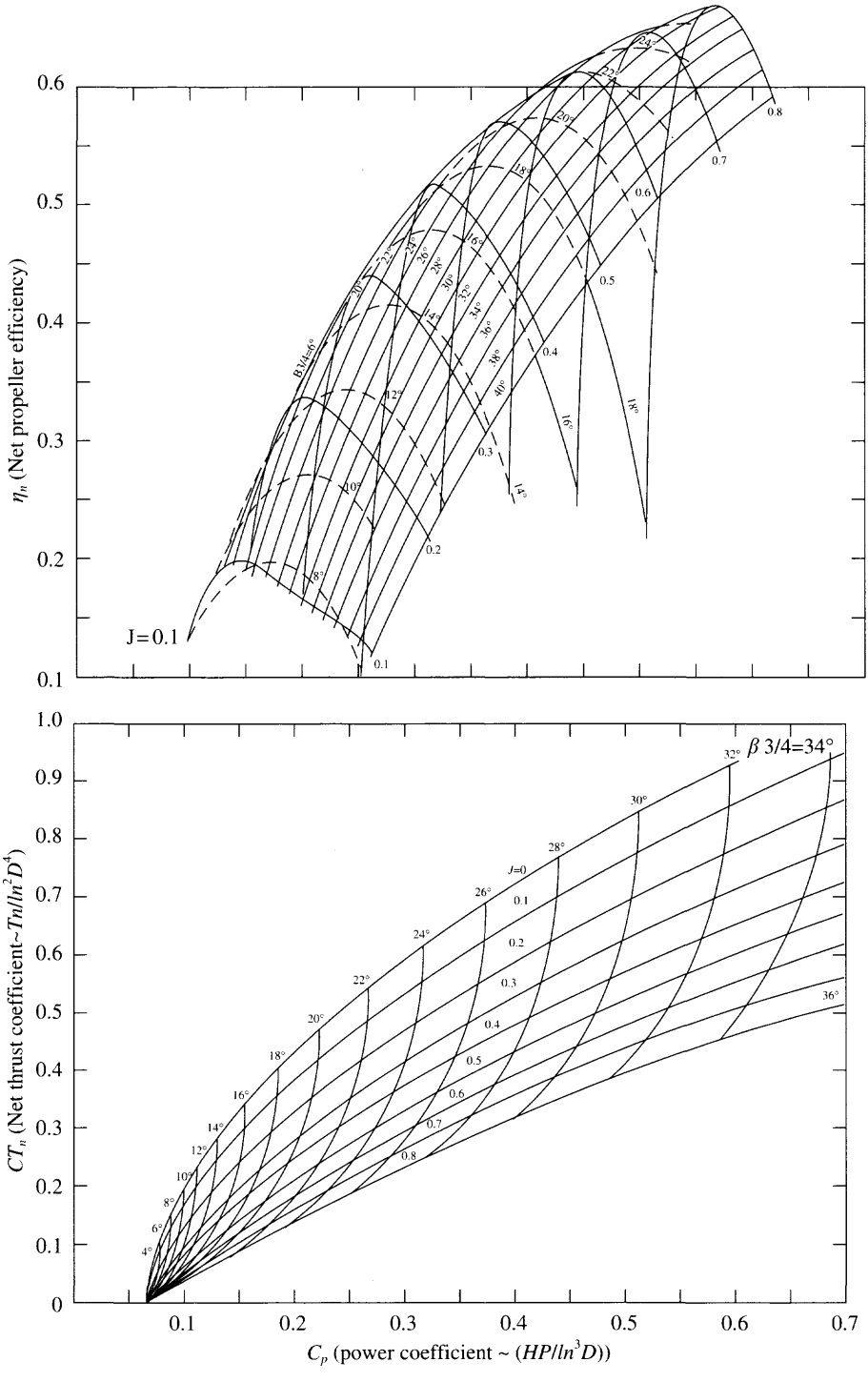

Fig. 15.15 Example plots of efficiency and CT_n against varying blade angle for the Dowty LCAC ducted propeller with exit area ratio 1.18, stator vanes and blade erosion protection.

Construction and weight

Air propellers are constructed in three ways. Fixed pitch propellers for smaller craft can be manufactured in wood laminated with epoxy resin. Larger propellers used to be made from solid aluminium alloy forgings, while very large propellers, for example the 5.8 m diameter SR.N4 propellers, are made from an inner aluminium alloy spar surrounded by a blade section formed from polyurethane foam with a glass/epoxy outer sheath. Since the mid 1980s, composite propeller blade design has been developed and this is now the most likely candidate for a utility ACV, in 'ground adjustable blade angle' form, or as variable pitch propellers. Such propellers are significantly lighter than aluminium propellers. Due to the complexity of their construction aluminium and composite propellers are expensive to procure, particularly in variable pitch form. Dependent therefore on the craft size and mission, fixed pitch propellers combined with air-jet thrusters may be considered as a first option, and variable pitch propellers if craft manœuvring demands this choice.

Propeller weight may be estimated from the diameter. An initial estimate for craft design purposes may be based on:

4-blade VP propellers	100 kg/m diameter in aluminium
	75 kg/m diameter in epoxy composite
6-blade VP propellers	120 kg/m diameter in epoxy composite
4-blade fixed pitch	20 kg/m diameter in wood laminate (to 3 m)
2-blade fixed pitch	10 kg/m diameter in wood laminate (to 3 m)

Variable pitch propellers have a hub structure and control system such as that shown in Fig. 15.16(a) and (b), a Dowty propeller hub. A system of hydraulic pistons is used to rotate the blades via crank pins. Fig. 15.16(b) shows a Hoffman ground adjustable propeller hub which allows static optimization of a fixed pitch propeller to a craft.

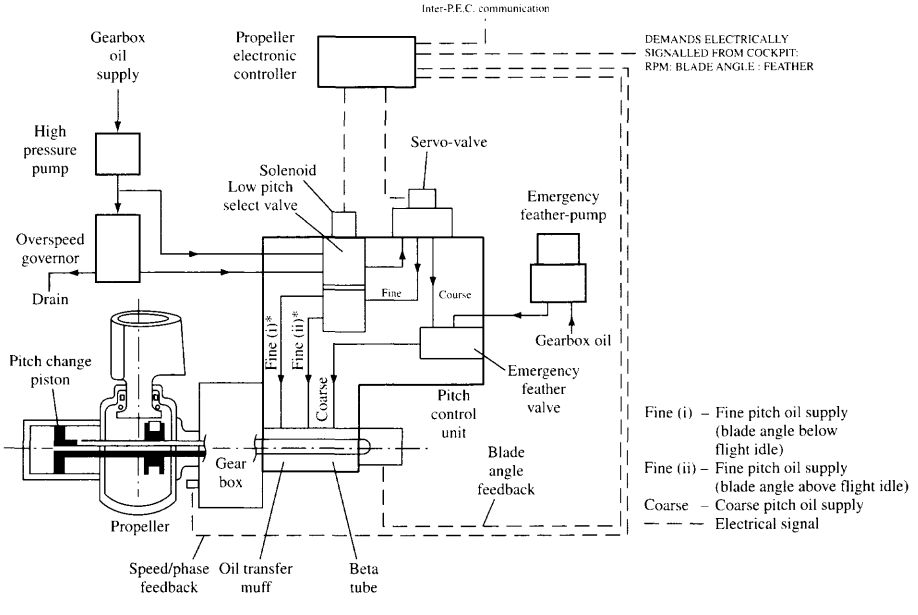

Fig. 15.16(a) Variable pitch air propeller control system schematic.

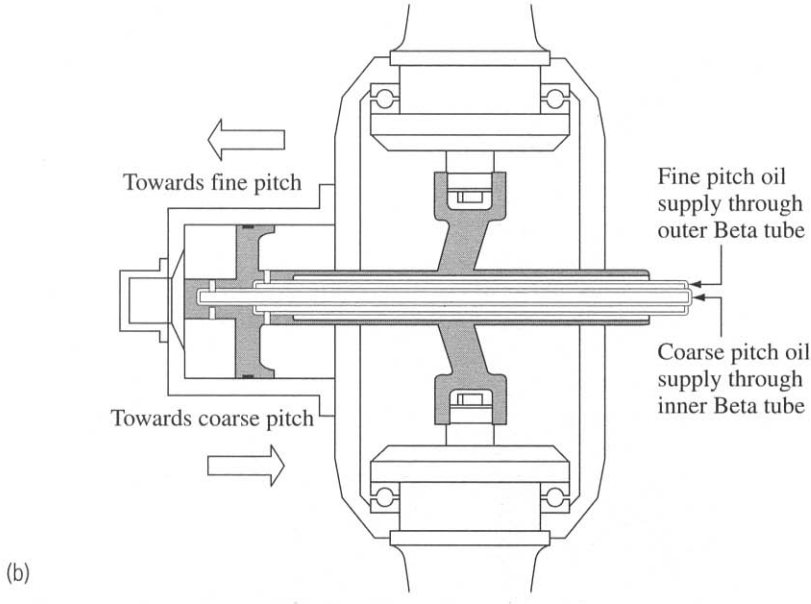

(b)

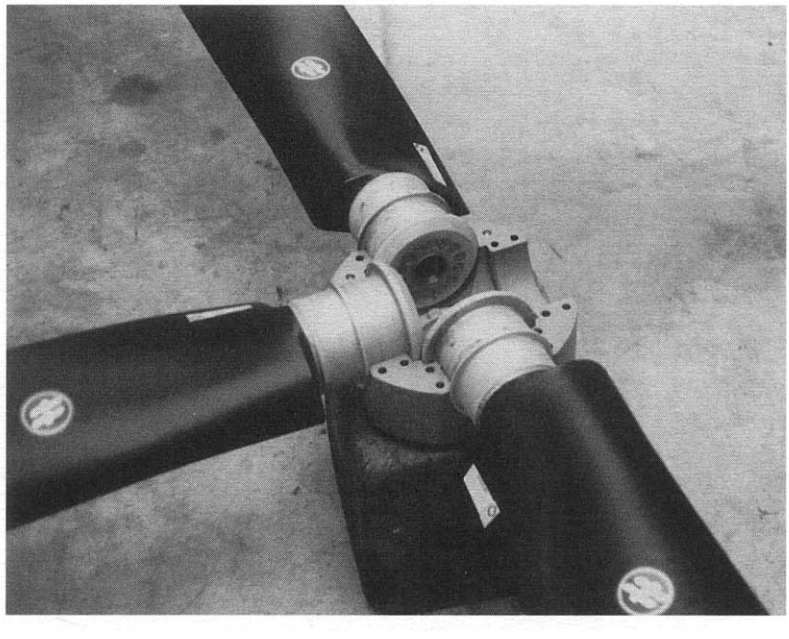

(c)

Fig. 15.16 (b) Variable pitch propeller hub construction and control system; (c) Hoffman ground adjustable hub from an API-88 propeller.

Blade erosion and its mitigation

Sand and salt water can cause rapid leading edge erosion to propeller blades unless protective strips are fitted. Wooden blades are normally protected by a thin metal

plate over the outer half of the blade length. Aluminium blades require nickel-plated leading edges, while composite blades are usually fitted with thin metal plates bonded into the resin.

15.3 Ducted propellers and fans

The primary purposes for installing ducted air propulsors are to reduce diameter so as to reduce noise level for a given thrust and to provide higher thrust levels at low speeds giving greater thrust margin for acceleration through hump speed.

The penalty is that of duct weight. With efficient cushion systems now making the use of heavier hull structures and diesel engines practical, this should not be a significant penalty and the advantages can be maximized. Other benefits include the physical protection of the propulsor afforded by the duct.

Ducted propellers

If a propeller is installed in a duct, the inflow conditions are changed so that the jet velocity behind the duct is the same as velocity at the impeller disc (or possibly slightly below, if the duct has an internal flare), i.e.

$$V_j = V_0 (1 + a) \tag{15.52}$$

In this case the ideal efficiency may be derived again from equation (15.11a)

$$\eta_i = 2/[2 + a] = 1/(1 + a/2) \tag{15.53}$$

Table 15.1 illustrates the variation of η_i with V_j in comparison with open propellers. It can be seen that as V_j increases, the relative gain from installing a ducted propeller also increases.

Ducted fans

The main difference between a ducted fan and a ducted propeller is that a fan generally has much higher solidity, operates at lower J values and employs static flow straightener vanes behind the impeller to remove the swirl imparted to the air flow, recovering the energy which would otherwise be wasted. A ducted fan with stator system should therefore give higher T/N than a ducted propeller of the same diameter.

Since the stator blades are fixed, the designer has to make a choice of what craft operating condition should be optimized. Craft cruising conditions may be taken as a start. At lower craft speeds there will be some residual swirl in the slipstream, while above cruising speed thrust will simply diminish since there will be no additional power available.

Ducted fan propulsion has been developed to the greatest extent for small craft, based on using industrial HVAC fan components, in the power range between 15 and 150 kW (20 and 200 shp). The commercial availability of a variety of aerofoil cross-section moulded plastic blades and hub designs in this power range allows acceptable efficiency to be achieved while maintaining minimum cost and installed weight. The designer may then concentrate on design of an effective stator system and duct in order to maximize craft performance.

Fig. 15.17(a) The VT2 hovercraft propelled by Dowty variable pitch ducted fans.

Fig. 15.17(b) The Dowty T2 ducted fan impeller.

At the opposite end of the size scale, Vosper Thornycroft and Dowty Rotol co-operated together in the mid 1970s to design a ducted fan propulsion system for the 100 t VT2 hovercraft, see Fig. 15.17. These fans, designed to absorb 3000 shp each from Rolls-Royce Proteus gas turbines, were installed in integrated lift and propulsion power trains. The fans had variable pitch mechanisms on the impeller blades to allow thrust variation while maintaining cushion lift and to give some reverse thrust capability.

When operating a fan and stator system in reverse flow, it is clear that efficiency will be relatively low and so the obtainable thrust will be lower than from a variable pitch ducted propeller. Due to the number of blades, the pitch change mechanism will also be very complex.

In general, if a designer selects a ducted fan propulsion system, the initial approach will be to look at fixed impeller designs, with separate powering to the cushion system, and consider alternative means for reverse or manœuvring thrust. Where installed power is higher than around 150 kW, a ducted propeller is more likely to offer the best balance of design parameters.

Fan selection

Fan characteristics of power, pressure and efficiency are normally determined by fan manufacturers in relation to the volume flow at a given diameter and speed of rotation. Dimensional analysis [110] can be used to show that the laws relating volume flow and pressure are

$$Q = k_q d^3 n \tag{15.54}$$

$$p = k_p \rho_a d^2 n^2 \tag{15.55}$$

and

$$N = p\,Q = k_N \rho_a d^5 n^3 \tag{15.56}$$

where k_q, k_p and k_N should be constant for geometrically similar units. Once the values of these coefficients have been obtained from a manufacturer for a given fan, it is then possible to plot power and thrust curves against rotational speed, at a pressure equal to the free stream dynamic pressure. Since

$$T = Q \rho_a V$$

and

$$V = (2\,p/\rho_a)^{0.5} \quad \text{if we assume fan total pressure can be used as basis.}$$

It is assumed here for simplicity the craft is static and that a stator system is installed such that slipstream swirl is removed.

Axial fans are normally designed with hubs which allow the blades to be set at a range of different angles, measured at the blade root, commonly between 20 and 50°. Each blade design will have an optimum root angle where the characteristics are most favourable, which will be evident from inspection of the characteristic curves. Data are often presented also for different numbers of blades in a given hub, 3 blades in a 6-blade hub, 4 out of 8, 5 from 10, etc.

Fan hubs are considerably larger than propeller hubs, between 0.1 and 0.3D rather than 0.05–0.15D and require nose and tail fairings to avoid significant loss of efficiency due to turbulence.

Stators

Consider the velocity triangle diagram for an axial fan shown in Fig. 15.18. The aerofoil blade operates at an angle of attack relative to the ideal vane and imparts a mean velocity of w_∞ to the flow which is the mean of the entry and exit velocities w_1 and w_2 at a vane. The induced rotational velocity V_u is therefore

$$V_u = w_\infty C_L 0.5c/s \tag{15.57}$$

where c is the individual blade chord and s the blade spacing, $= 2\pi r/z$, where z is the number of blades.

If drag forces on the aerofoil blade are included, then it can be shown [110] that

$$V_u = w_\infty C'_L 0.5c/s \tag{15.58}$$

where

$$C'_L = C_L [1 + C_D/C_L \cot(\beta - \alpha)]$$

Typically the value of C_D is of order 0.015 to 0.02 [111] while C_L is between 0.7 and 1.0 and the design angle of attack would be 4–6°.

The stator vane or aerofoil will have a velocity triangle as shown in Fig. 15.18 where the induced rotational velocity is $-V_u$. The stator blades will require significant camber and in order to avoid turbulence problems at off-design conditions it is advisable to use a reasonably thick aerofoil section.

In order to avoid problems of 'beating' between impeller and stator and the associated noise generation, it is advisable to use an odd number of blades (if impeller has 6 blades, stator should have 5, 7 or 9).

Design of stator systems requires fan blade aerodynamic data to be available to the designer for the design conditions. This can be obtained from the manufacturer, or calculated based on direct measurement of the fan blade geometry, so long as the aerofoil is a known design, for example one of the NACA series [111]. Where the fan used as basis for the propulsion system is an industrial unit, an improvement of between 10 and 20% in developed thrust compared to a unit without stators is normally achievable.

Stators should be located as close to the trailing edge of the impeller blades as possible. There are limitations to this in order that stator blade geometry is practical to fabricate. Blade flexure and vibration in service mean that an average of 20% of impeller chord is a likely minimum, while if the gap exceeds the impeller blade chord, then the stator effectiveness will be significantly reduced.

Duct design

Ideally a propulsor duct should be as short as possible, to minimize weight, but there are practical limitations to this. The duct section is an aerofoil formed around a camber line which follows a parabolic or hyperbolic curve in front of the impeller and either a cylinder behind, or an expanding cone with angle of 5–10°.

A realistic dimension for the intake section will be between 10 and 15% of the diameter. The impeller should be located at the aerofoil ordinate with maximum suction, which is usually just ahead of the maximum camber, at about $0.3c$, thus the chord

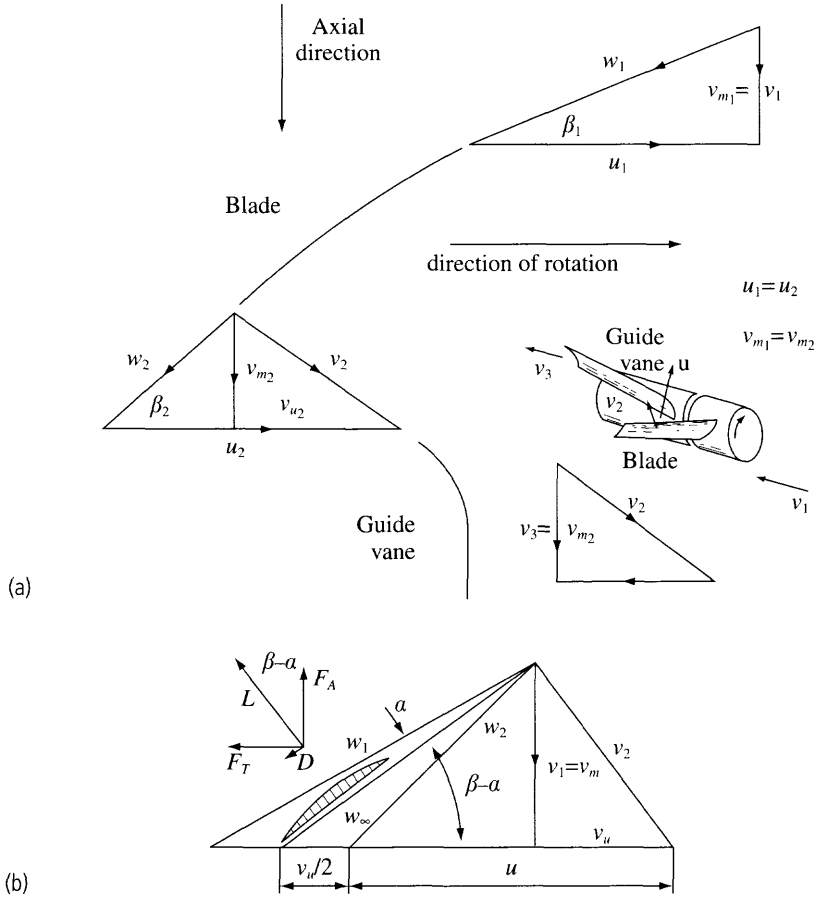

Fig. 15.18 Axial fan velocity diagrams, ideal vane and aerofoil. [110]

should be between 0.3 and 0.5D. If stators are installed, the duct may be between 0.4D and 0.6D in length. NACA 63 series aerofoils are a useful starting point [111].

The intake bell-mouth geometry will require some thought regarding the craft speed for which it is optimized. The camber line cone angle for inflow to the leading edge is related to the chosen value of a for the impeller. If a is 0.2 then the the cone angle should be $\tan^{-1} 0.2$, i.e. 11.5°, while at $a = 0.5$ the angle should be 26.5°. At zero speed, when a is infinite, the inflow streamlines will converge from a wide angle, so that the ideal geometry is a radius, typically of 0.1–0.2D. The intake clearly has to form some compromise between these two conditions.

Experience suggests that if the designer begins with a cone convergence angle of 15° for high-speed craft and 30° for low-speed craft and fits a camber mean line similar to NACA 63, followed by a 63-012, 015 or 018 basic thickness form, this should provide an efficient aerodynamic basis for a duct; this is because of the favourable pressure profiles of both the mean line and aerofoil. The final form is likely to be altered slightly from this so as to optimize fabrication.

Integrated controls

Ducted propulsors have rudders and elevators directly mounted to the trailing edge of the duct. This minimizes supporting structure, but places stresses on the duct which need to be accounted for when designing the duct structure.

Interaction with ACV hull form

ACV propellers operate in a non-uniform air flow caused by disturbance from the hull form. The lower part of the propeller or fan will be operating in a region of lower velocity and will produce less thrust than predicted above. The reduction depends very much on the ACV hull and superstructure profile.

The most practical approach to account for this effect is to consider the loss of thrust in the same way as a naval architect considers the wake deduction for a marine propeller behind the hull of a ship. Propellers mounted on pylons, such as those of the SR.N4, may have a thrust reduction factor of around 2–5%, while units mounted behind a superstructure, such as the AP1.88 may have slightly higher losses of order 4–8% compared to the free stream performance. This should be accounted for by a designer when first specifying the desired thrust and installed power to avoid the final craft performance being less than that contracted with the customer.

15.4 Marine propellers

Marine propeller design developed from the same momentum and blade element theories reviewed above [88]. The denser fluid in which they operate allows the blades to have much higher chord length and solidity than an air propeller. Marine propellers have total blade area which is between 50 and 120% of the disc area (solidity, or blade area ratio 0.5–1.2). The blade pressure distributions interfere with each other, reducing lift force compared to isolated aerofoil theory. Chord length at $0.7R$ and blade length are of similar dimensions and the chord itself varies rapidly and so the pressure distribution over a marine propeller blade is therefore very much three-dimensional.

Marine propeller design has therefore been founded on tests of propeller designs in closed circuit water tunnels ('cavitation tunnels') to provide correction coefficients to the available theory. As an example, ref. 109 details testing of a parametric series of propellers for operation at high speeds characteristic of SES.

Marine propellers most often have three or four blades. Two-blade propellers are difficult to balance and the pressure variations tend to create vibration under the hull. Larger numbers of blades tend to require a larger boss which reduces efficiency for high-speed propellers. At forward speeds below about 35 knots it is possible to achieve efficiency levels in the range of 70%, but this drops sharply as suction pressure on the blade back surface reduces towards the local vapour pressure. Figure 15.19 shows a plot of approximate efficiency which may be expected from different types of marine propellers and water jets.

Subcavitating propellers must operate with a blade tip speed constrained below a limit (approximately 170 fps or 52 m/s) to maintain the suction side pressure above the

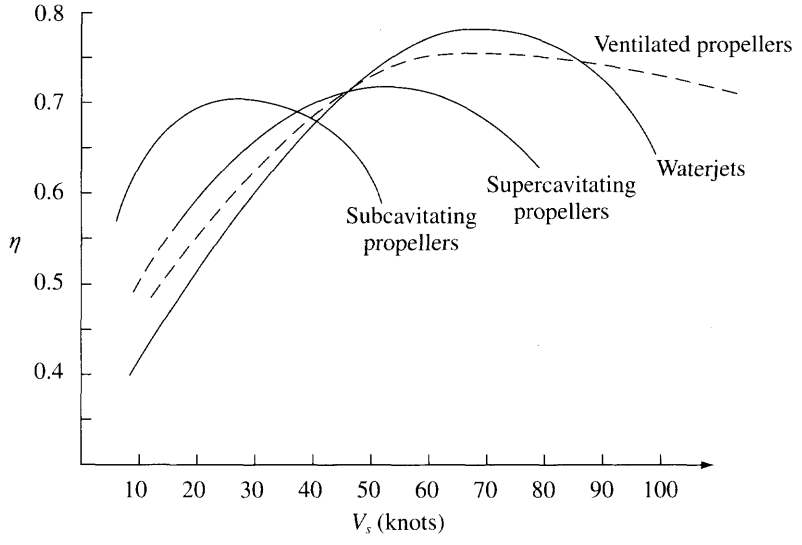

Fig. 15.19 Marine propeller and water-jet efficiency.

level where cavitation begins, while supercavitating propellers should have a minimum tip speed to ensure cavity formation (approximately 300 fps or 92 m/s). If a propeller is to reliably operate in the fully cavitating regime (often also referred to as 'supercavitating'), the suction pressure must be low enough to generate a steady cavity over the full blade forward surface.

Marine propeller blade sections are thinner than air propellers. Leading edge geometry and orientation are critical to whether turbulence in the real fluid will cause local cavitation. The three-dimensional flow regime combined with this sensitivity created many challenges for analysts until computing power was sufficient to allow calculation based on lifting surface theory rather than two-dimensional analysis. Development of successful blade geometries has therefore been by derivation from parametric series tested in cavitation tunnels.

Marine propellers are normally installed on inclined shafts at an angle of 5–15° (see Fig. 15.27 showing example SES installations). The propeller disc will have a clearance below the SES hull which is minimized in order to give least floating draft. The exposed shaft, shaft supports and rudder mounted behind the propeller all create drag forces (see section 3.10, Figs 15.2 and 7.15) which reduce the propulsive efficiency of the system. They also affect the propeller inflow and so its efficiency directly. At high speeds, these effects become much more significant. Figure 15.19 shows fully submerged cavitating propeller efficiency reducing above about 65 knots. This is because of the rapidly increasing propeller shaft and boss drag.

To reduce this problem the propeller boss may be ventilated, or the propeller may be placed behind the transom with its centre-line closer to the water surface and most or all of the shaft internal to the hull. The blades may be designed to emerge from the water over part of their rotation, in which case propeller sizing has to be carried out for the immersed blades area. Such propellers can be efficient at speeds as high as 100 knots. This design technique is typical of racing craft such as hydroplanes.

Water jets have no external appendages and so can offer higher system efficiencies than supercavitating propellers in the speed range to 65 knots. This is also partly due to the same effect as with ducted air propellers whereby loading on the outer part of the blade may be higher, more closely approximating the assumptions of momentum theory. At present there is not enough experience to clarify whether water jets or ventilated propellers provide the optimum propulsor for ultra-high speeds. The challenge for cavitating or ventilated propellers is structural design, while for water jets design of the intake duct system and a change to inducer-type impellers are the main issues.

In the following paragraphs we will outline the main issues affecting propeller selection for SES, beginning with propellers in the subcavitating regime. Examples of propellers designed for SES are shown in Table 15.4.

Table 15.4 Marine propellers

Craft	Propeller manufacturer or design	Type	Dia (m)	No. off	No. blades	RPM	SHP	Thrust (kg)	Weight (kg)	Material	Remarks
HM.2	Gawn Burrill	Sub FP	0.385	2	3	2600	300	818		Stainless steel	
HM.5	Gawn Burrill	Sub FP		2	3					Stainless steel	
VT.1	KaMeWa	Super VP	0.640	2	3	2200	1100			Ni Al bronze	Outboard rotation
SES-100B	Hydronautics	Semi VP	1.067	2	6	1900	class.	class.	1045	Titanium	Inboard rotation
BH.110		Super Super FP	1.067	2	3	1335				Stainless steel	
Mekat	Escher Wyss	Semi VP		2	7					Stainless steel	
Norcat		Super Trans FP		2	3					Ni Al bronze	

Sub: subcavitating; Super: supercavitating; Semi: semisubmerged design; FP: fixed pitch; VP: variable pitch; class.: classified data (US Navy).

Cavitation

Marine propellers for SES are likely to be subject to cavitation. Variation in local pressure at the blades due to proximity of the hull surface and varying advance coefficient due to shaft inclination will also make cavitation more likely due to the unsteady flow regime.

Dissolved air in the water tends to come out of solution as bubbles (cavities), as pressure reduces towards atmospheric over a propeller blade upper surface. The cavities are initially water vapour saturated. Cavitation damage occurs when the local pressure reduces below the saturation pressure of the water at that depth so that water vapour in the cavities recondenses. The rate at which this happens is sufficient to cause mechanical damage to the propeller blade surface.

The propeller cavitation number is given by the ratio of local static pressure ($P_a + \rho gh$), normally measured at the propeller centre-line, to the local water vapour pressure P_v, divided by the dynamic pressure through the propeller plane:

$$\sigma_p = \frac{P_a + \rho gh - P_v}{0.5\rho V_p^2} \tag{15.59}$$

where h is the immersion of propeller centre-line to static water level, P_v the water

vapour pressure (36 lbf ft^2 or 176 kgf/m^2 approximately), P_a the atmospheric pressure (2116 lbf/ft^2 or 10348 kgf/m^2),

$$V_p = V_a + U'_a$$

where U'_a is the induced axial velocity component at the propeller plane and V_a the free stream velocity. Since U'_a is a function of propeller loading, so σ_p reduces as propeller loading is increased. If the calculation of cavitation number is extended to include the induced velocity at a blade section represented by $\sigma_{0.7}$ (see Figs 15.20 and 15.26) rather than simply the induced axial velocity, it can be stated that below $\sigma_{0.7} = 0.05$ the blade section will fully cavitate, while above $\sigma_{0.7} = 0.12$ cavitation should be limited to vortex shedding from blade tips.

At values of advance coefficient J typical of fast craft, between 0.6 and 1.4, the cavitation number based on free stream velocity, σ_0, should be above the upper line of Fig. 15.20 for subcavitating propellers. As craft speed increases, it becomes more difficult to restrict blade loading to achieve this.

In the central zone of Fig. 15.20 it is particularly important to consider measures to mitigate the effects of cavitation, including selection of materials with good cavitation resistance, application of cavitation-resistant coatings and improvements to the hydrodynamic design of the hulls. Titanium alloys, followed by stainless steels, are the most resistant, but also the most expensive. The most widely used material, aluminium bronze, has reasonable resistance, but has shown insufficient life for SESs and so it is normally recommended to use stainless steel as a minimum specification, unless operations can allow regular change-out of propellers.

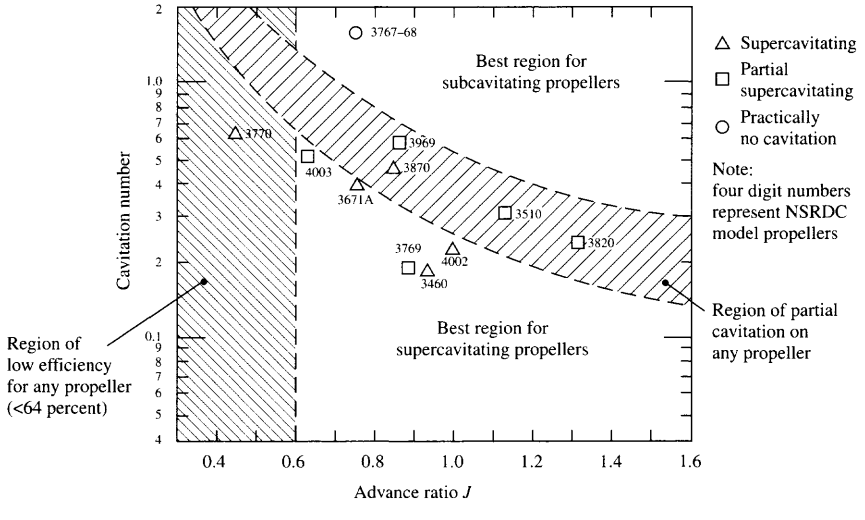

Fig. 15.20 Subcavitating >> fully cavitating regions vs J. [4]

Momentum theory

Momentum theory as developed in section 15.1 can be used to carry out initial selection of propeller diameter based on a scheme such as shown in Fig. 15.23.

Blade element theory

Blade element theory for marine propellers needs to account for the much lower aspect ratio of the blades than air propellers. Subcavitating marine propellers commonly use flat-faced circular arc blade sections, or thin aerofoil sections such as NACA 16 or 66 series which have a relatively fine leading edge profile [111].

Determination of lift and drag by integration of properties along the length of the blade is straightforward, except that for a marine propeller, the blade chord changes rapidly with diameter and blades form a cascade where interference is significant. The consequence of this is that significant corrections are needed to the blade lift coefficients both with diameter and along the chord at each station of the blades, based on the vortex theory.

Vortex theory

The concept of lift force being generated as a function of circulation around a body developed by Lanchester and expanded later by Prandtl, was applied to propeller design by Helmbold and Goldstein. It was found that marine propellers designed using this theory had too low blade pitch in practice (assumed efficiency as a lifting surface was too high) and so empirical corrections were developed from testing, later followed by theoretical treatments. This work produced correction functions for the inflow and for the effective characteristics of the propeller blades for lightly loaded propellers.

If we consider the lift produced by a propeller's blades:

$$L = \rho V \Gamma \tag{15.60}$$

where Γ is the circulation of a blade element, and if we integrate along the blade, the thrust and power coefficients for the whole propeller may be represented as

$$C_{Ti} = 4Z \int_{x=x_h}^{x=1} G\,(x/\lambda - U_t/2V_a)\,\mathrm{d}x \tag{15.61}$$

$$C_{Ni} = 4\,Z/\lambda \int_{x=x_h}^{x=1} G\,(1 + U_a/2V_a)\,\mathrm{d}x \tag{15.62}$$

where Z is the number of blades, initially assumed infinite, λ the advance ratio (becomes λ_i for finite number of blades), U_t the tangential induced velocity in slipstream ($U_t/2$ at propeller disc), U_a the axial induced velocity in slipstream ($U_a/2$ at propeller disc), V_a the axial velocity at propeller plane and G the non-dimensional circulation, $G = \Gamma/\pi\, D\, V_a$. For a finite number of blades, G must be modified to account for the non-uniform velocity over the circumference. Goldstein derived a relation for this as follows:

$$\Gamma_z = \{2\,\pi\,K(r)/Z\}\;U_t \tag{15.63}$$

so

$$G = \{2\,K(r)\;x/Z\}\;U_t/2V_a \tag{15.64}$$

The Goldstein function for three-blade propellers is shown in Fig. 15.21. For an optimum propeller, the axial and tangential induced velocities at the propeller blades are

$$\begin{aligned} U_a/2V_a &= [\cos\beta_i \sin(\beta_i - \beta)]/\sin\beta \\ &= \{[1-\eta_i]/\eta_i\}\;\{x^2/(x^2+\lambda_i^2)\} \end{aligned} \tag{15.65}$$

$$\begin{aligned} U_t/2V_a &= [\sin\beta_i \sin(\beta_i - \beta)]/\sin\beta \\ &= \{[1-\eta_i]/\eta_i\}\;\{\lambda_{ix}/(x^2+\lambda_i^2)\} \end{aligned} \tag{15.66}$$

Kramer solved these equations to obtain λ_i as a function of $\lambda\,(J/\pi)$ and C_{Ti}. The results for a three-bladed propeller are shown in Fig. 15.22. The area relevant to propellers for high-speed craft is indicated.

If the effects of viscosity are added in the expressions for C_T and C_P become

$$C_T = \int_{x=xh}^{x=1} \frac{dC_{Ti}}{dx}\,(1 - \varepsilon\tan\beta_i)\,dx \tag{15.67}$$

$$C_N = \int_{x=xh}^{x=1} \frac{dC_{Ni}}{dx}\,(1 - \varepsilon/\tan\beta_i)\,dx \tag{15.68}$$

where ε is the lift/drag ratio for each blade section, which may be approximated by using the value at $r = 0.7R$ to characterize the blade performance. The efficiency can be expressed as

$$\eta = C_T/C_N = \eta_i\,\eta_\varepsilon \tag{15.69}$$

where η_ε is the blade element efficiency due to viscous flow. If an approximation for ε at the blade element at $0.7R$ is used ($\bar{\varepsilon}$):

$$\eta_\varepsilon = (1 - 2\,\bar{\varepsilon}\;\lambda_i)/(1 + 2\,\bar{\varepsilon}/3\lambda_i) \tag{15.70}$$

These relations allow a lightly loaded propeller to be assessed by representing the propeller by its performance at the $0.7R$ ordinate. Assumptions implicit in the method so far are those of two-dimensional theory. The effects between adjacent blade elements with rapidly changing chord, both radially and tangentially, cascade interference and the highly curved flow of the fluid through the propeller all alter the blade element performance. Computer programs have been developed to carry out iterative solution of the pressure distribution over the blade surfaces. These have improved the analytical predictions, but still require calibration with cavitation tunnel tests to avoid errors. The unsteady fluid dynamics of cavitating propellers further increases the dependence on test data.

The consequence of the additional three-dimensional effects is in general to reduce the lift which is generated and to increase the drag forces, making it necessary to adjust the blade incidence and allow for reduced efficiency. The changes will vary with advance coefficient λ and blade loading C_T for a given propeller.

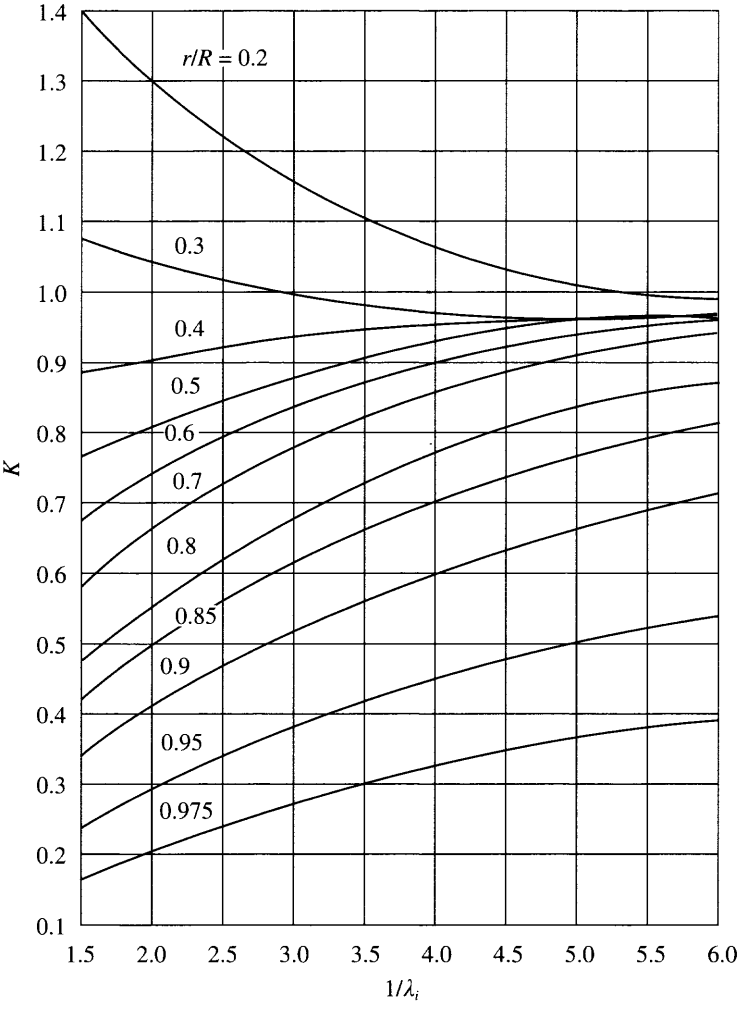

Fig. 15.21 Goldstein function plot for three-blade propellers. [88]

Propeller selection procedure

We consider first a subcavitating propeller. The designer follows a procedure similar to that in Fig. 15.23. An initial estimate of propeller diameter from momentum theory is made, by first determining the required thrust

$$T_r = R_{tot}/(1 - t) \tag{15.71}$$

where t is the thrust deduction factor, often assumed at 0.92 for twin propeller installations. Approximate data for high-speed craft, based on FoM = 0.7, are given in Fig. 15.24. The propeller speed can be estimated from a formula given by Burtner [88]

$$n = [50 \times 0.2\, N/D]\, 1.667 \tag{15.72}$$

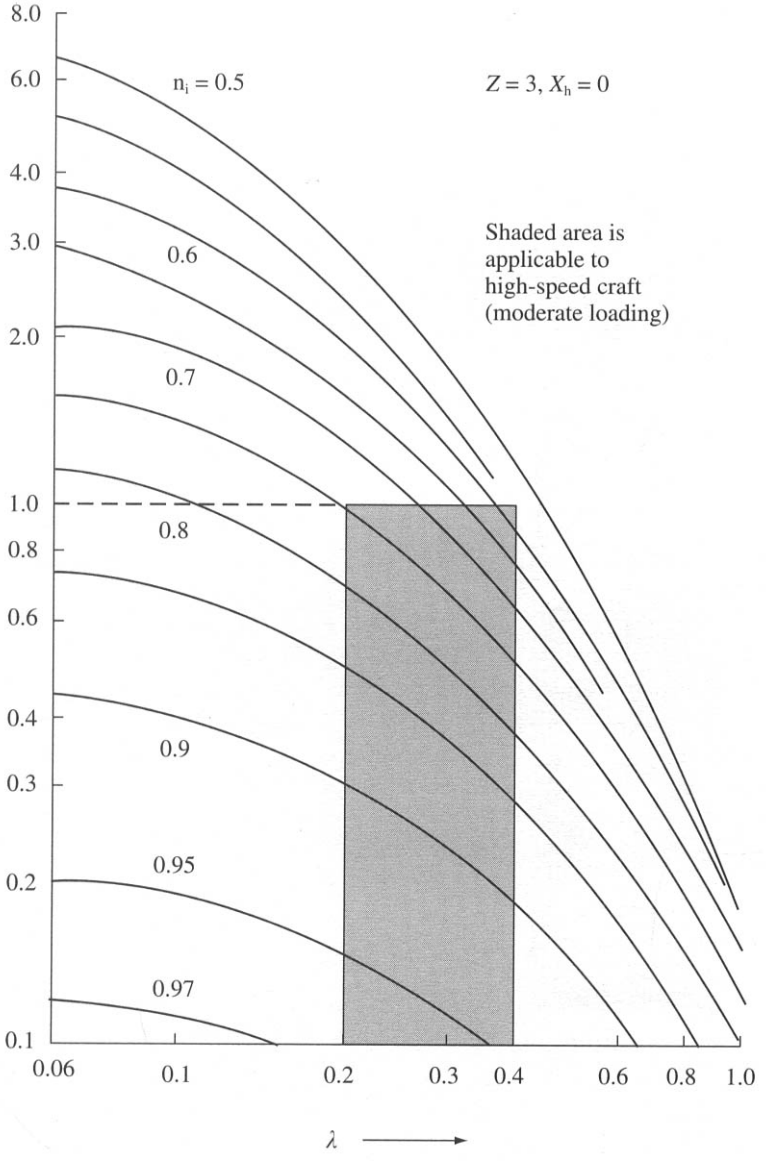

Fig. 15.22 Kramer's chart for three-blade propellers. [88]

where D is the diameter in feet and N the power in shp. If the tip speed ($n\,D$) is below 55 m/s (180 fps) and the advance ratio ($J = V_s/n\,D$) is in the region of 0.8–1.0 a successful start has been made.

Propeller blade pitch needs to be adjusted from the advance ratio J, which represents the ideal situation, to include the blade angle of attack necessary to develop lift. This is referred to in propeller design as the slip. High-speed propellers operate with slip in the range 10–15%. During initial design 15% is recommended to be used. The flow regime past SES hull aft bodies is not significantly decelerated

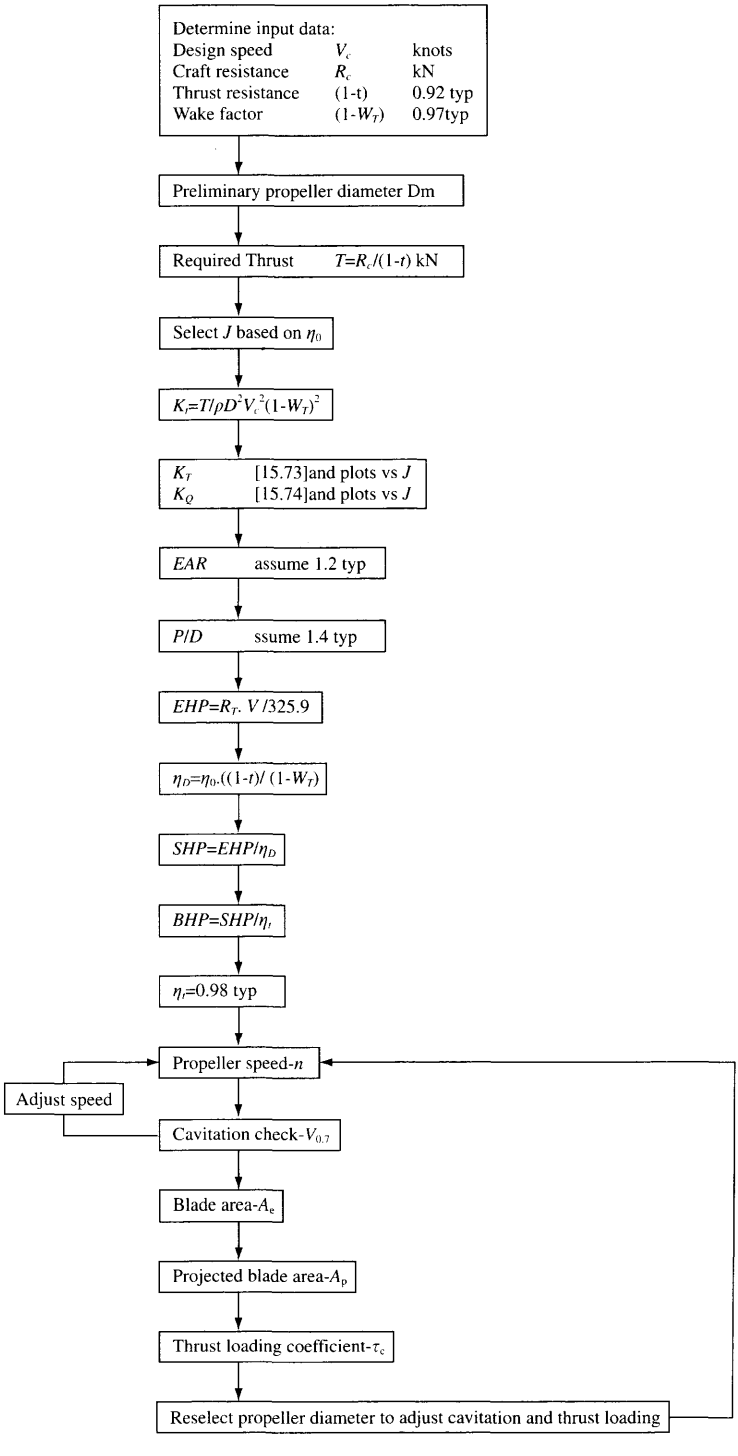

Fig. 15.23 Marine propeller selection procedure.

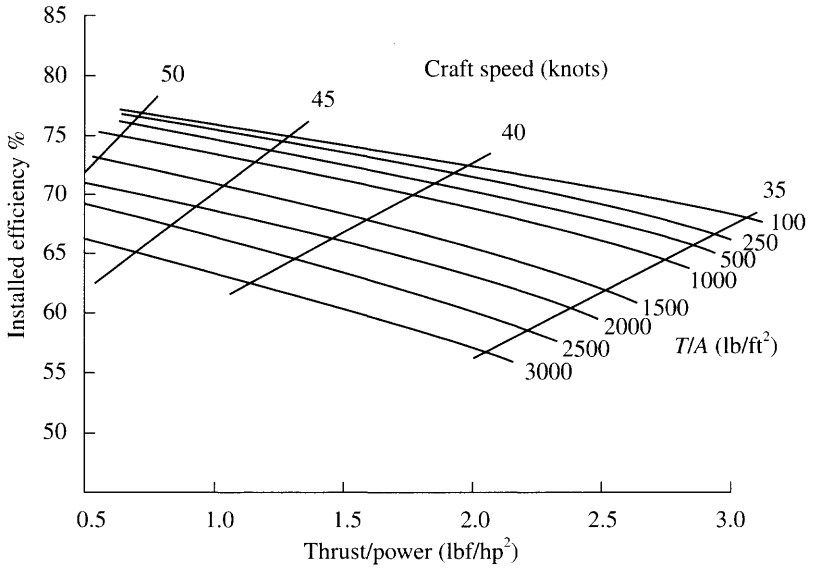

Fig. 15.24 Table of effective *T/A*, *T/HP* for FoM 0.7 for 35–50 knots.

as for displacement vessels and so the effect of wake fraction on propeller design can be ignored for the moment.

The next step is to check the performance of standard blade series for which data are available, for example Gawn–Burrill [87, 112], Newton–Rader [87, 109], or the Troost [142] series. The values of K_T and K_Q can be investigated for different blade area ratios and the related values of J, D, N and η determined. An example plot for a three-blade subcavitating propeller is shown in Fig. 15.25. More extensive data are presented in the reference papers.

K_T and K_Q are related to C_T and C_N as follows:

$$K_T = (\pi J^2/8)\, C_T \tag{15.73}$$

$$K_Q = (J^3/16)\, C_N \tag{15.74}$$

$$\eta = C_T/C_N = K_T/K_Q\, J/2\pi \tag{15.75}$$

A designer will often have limited options for engine selection and reduction gearbox ratio. The propeller selection will therefore be a matter of iteration to an acceptable diameter, pitch ratio and blade area ratio which will develop the required thrust within the available engine power rating.

Propeller suppliers will perform this matching process, possibly offering alternative blade sections which may improve efficiency. Previous experience with similar craft can also be used to advise the SES designer on minimum advisable clearance between the sidehull keel and the propeller tip, which as a starting point should not be less than $0.1D$.

Use of standard series, or similar data via propeller suppliers, has the advantage of obtaining a reliable solution quickly, but has limitations. The blade pressure

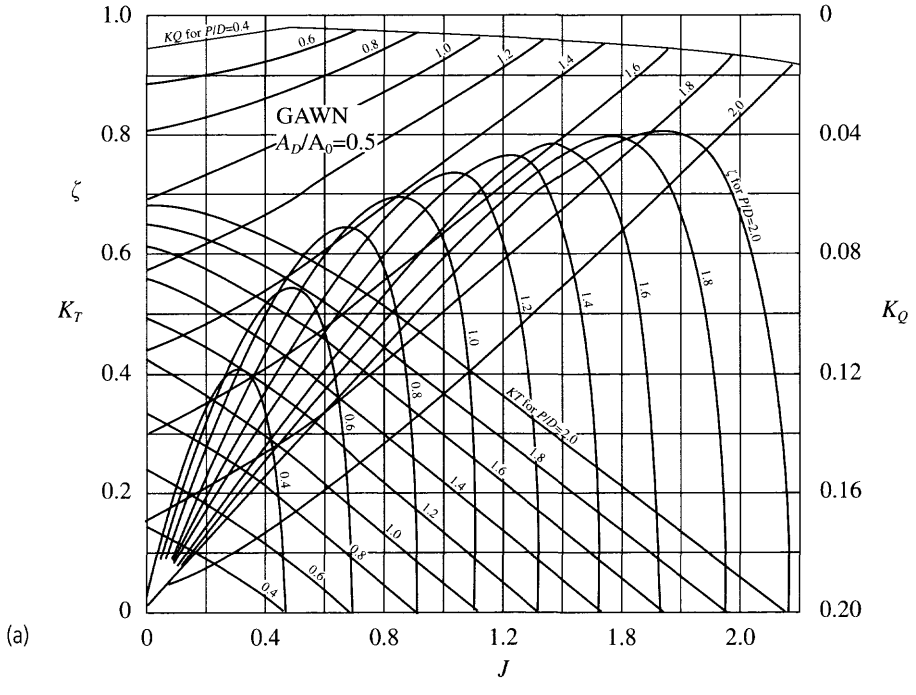

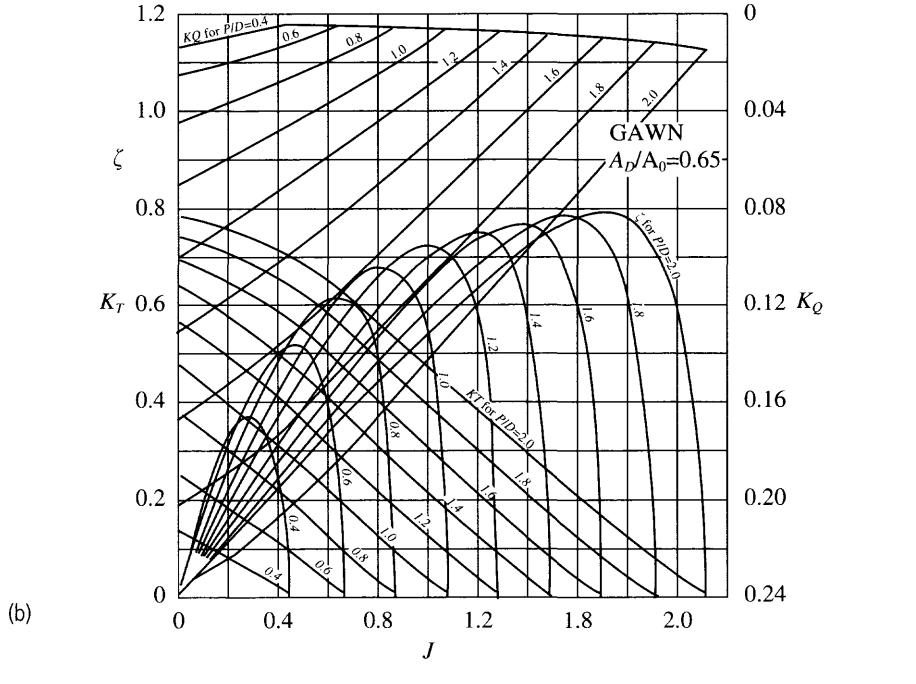

Fig. 15.25 K_T and K_Q diagrams for marine propellers. [112]

distribution for these propeller series is developed generally with high cavitation number in mind. For high-speed craft a different distribution may be more appropriate, with lower loading towards the blade tips.

The design method for such propellers [88] involves determining C_{Ti} and C_{Ni} based on assuming $\eta_i = 0.75$ and $\varepsilon' = 0.08$ as a starting point and subsequently calculating the forces on each blade element using aerofoil section data having derived the hydrodynamic pitch β and the blade angle of attack $(\beta_i - \beta)$. The blade chord at any section can be determined from the relation

$$C_L\, C/D = (4\,\pi\, K/Z) \sin \beta_i \tan (\beta_i - \beta) \tag{15.76}$$

where K is the Goldstein function (Fig. 15.21). The cavitation number at any section should be kept above the critical level. For deeply submerged propellers this may be approximated to

$$\sigma_x = \sigma_0 [1 + (x\,\pi/J)^2] \tag{15.77}$$

The blade camber should be restricted to ensure shock-free flow. For NACA sections this is approximately $(0.06\ C_L\ c)$, where C_L is typically 0.8 and C_D about 0.015 for angles of attack between 6 and 8°.

Having determined an acceptable pressure distribution over the blades, a check on the blade strength is made using cantilever beam theory and adjustments made to section thickness if this indicates problems of fatigue at the blade root.

Supercavitating propellers

Where craft speed is higher than 35 knots and so σ_0 is below 0.5, cavitation will be impossible to avoid and so a different approach needs to be taken. Propeller blade section and geometry are chosen with the aim of developing a steady cavity over the leading surface of the propeller.

First consider the development of cavitation over a propeller blade as speed is increased. In the subcavitating regime thrust increases with J in relation to speed squared. A single K_T vs J characteristic can be defined. Once σ_0 is low enough that cavitation begins to grow from the blade tip in towards the root as shown in Fig. 15.26, K_t will be reduced. At a given σ_0 (craft speed), as propeller speed is increased (reducing J), cavitation will grow across the blade until the K_T characteristic again forms a single curve. This characteristic for a fully cavitating section has an optimum K_T in the region of $J = 0.55$–0.6.

A fully developed cavity creates a blockage to flow between the blades, reducing the inflow on the pressure side of the adjacent blade, so reducing lift generated. A higher propeller speed, compared with a subcavitating propeller, is thus needed to generate similar thrust. The cavity developed will depend on the propeller speed and the blade characteristics.

Momentum theory can be used to develop equivalent expressions for efficiency to the non-cavitating regime, by introducing a term η_c to represent the effect of the cavities on inflow and η_b to represent the efficiency of the blades in cascade flow, giving an expression of the form

$$\eta = 2/(1 + (1 + C_T/\eta_b)^{0.5})(1 + C_T/\eta_b\eta_c)/[\eta_b\,(1 + C_T/\eta_b)] \tag{15.78}$$

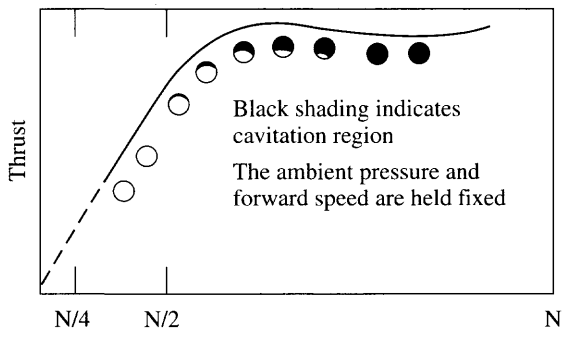

Cavitation development and its effect on thrust (after Smith, 1937)

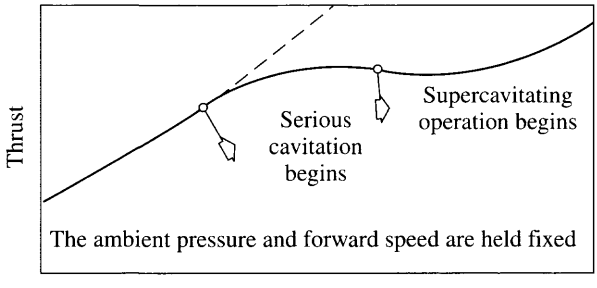

Schematic of thrust variation with rotative speed, carried into the supercavitating regime

Fig. 15.26(a) Growth of cavitation across propeller blade. [88]

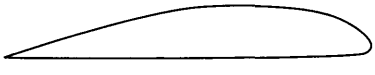

Subcavitating blade section

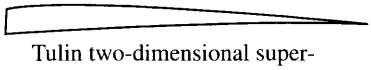

Tulin two-dimensional supercavitating section - TMB (1954)

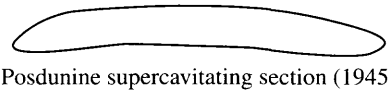

Posdunine supercavitating section (1945)

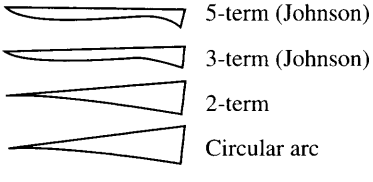

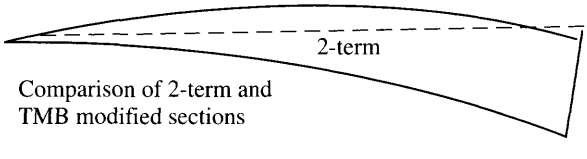

Comparison of 2-term and TMB modified sections

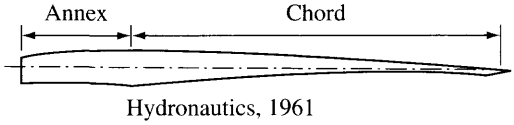

Hydronautics, 1961

Fig. 15.26(b) Examples of supercavitating blade sections.

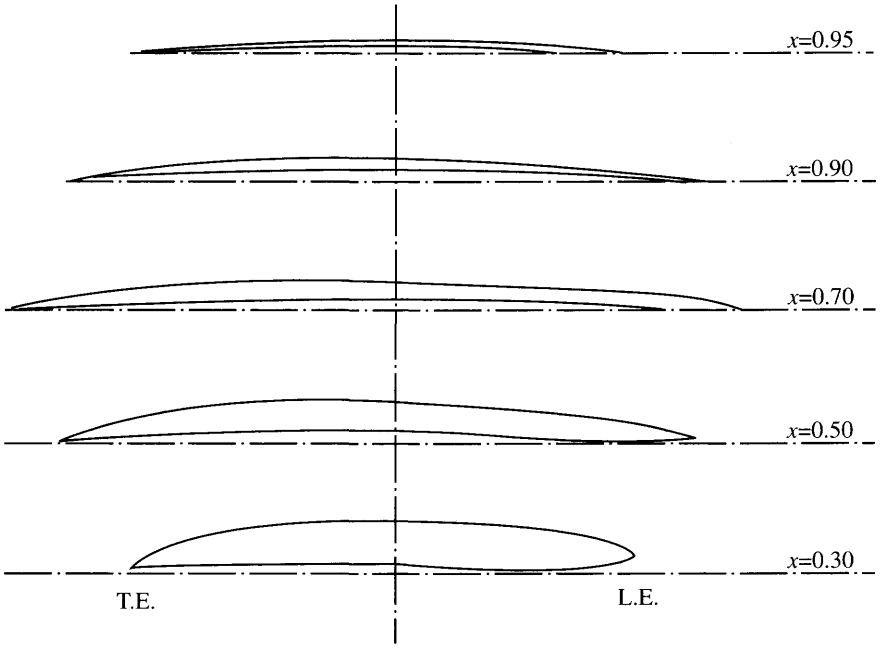

Newton–Rader blade sections

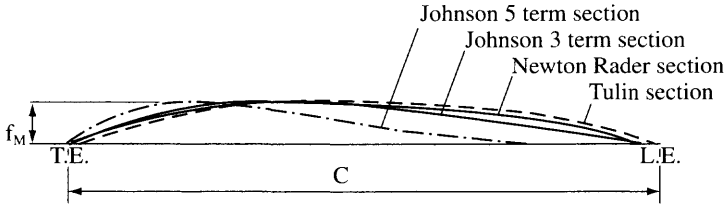

Comparison of camber lines

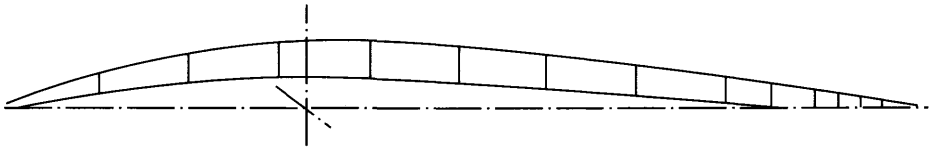

Sulzer–Hydro ventilated partially submerged propeller
installed on Mekat SES

Fig. 15.26(b) cont. Examples of supercavitating propeller blade sections.

which reduces to the expression

$$\eta = 2/(1 + (1 + C_T)^{0.5}) \tag{15.79}$$

for non-cavitating flow, where η_c and η_b are both 1.0.

Newton and Rader [109] carried out tests of a parametric series of three-bladed propellers at σ_0 values down to 0.25 (craft speed of approximately 55 knots). The blade sections used were an elliptic section profile based on a NACA $a = 1.0$ mean camber line, covering blade area ratios of 0.48, 0.71 and 0.95 and P/D of 1.05, 1.25, 1.66 and 2.05. The base design had BAR of 0.71 and P/D of 1.25.

The leading edge profile of the base propeller had to be modified during initial trials so as to remove face cavitation (Fig. 15.26(b)). A sharp leading edge section is needed so as to encourage clean cavity initiation, while at low angles of attack this can lead to cavities on either side of the section.

Principal conclusions from Newton and Rader's work were:

1. The efficiency of cambered blade sections in cavitating conditions approach that of non-cavitating sections, in contrast to flat-faced sections which have much lower efficiency.
2. The optimum blade incidence range is similar between cavitating and non-cavitating conditions.
3. When fully cavitating, obtained when $\alpha_{0.7} = 2.5°$ and $\sigma_{0.7} < 0.08$ for the series, the lift coefficient depended only on the angle of incidence, the face shape and the local cavitation number and not on the thickness form, in conformation with the theory of cavitating flow.
4. The drag–lift ratio followed an increasing trend with t/c, which is in conflict with theory, probably due to the finite thickness of the leading edge. The ratio was also higher than that for non-cavitating sections. This was attributed to the need for high camber ratio to achieve the necessary lift, which in turn necessitated higher angles of incidence to achieve sheet cavitation from the leading edge. These angles are higher than consistent with minimum drag. Further experimentation with the leading edge profile was proposed as a means to reduce the drag.

This work demonstrated that in the range to 55 knots it is possible to design open propellers with efficiencies close to that of subcavitating units and provided performance data for selection which have been successfully applied to a number of fast craft.

For higher speeds, a further investigation of hydrofoil sections is required. Since it is the face geometry which controls the section performance, researchers have investigated a number of possible forms, usually as isolated foils. Examples of these are the Johnson '3 term' and '5 term' sections [88] as shown in Fig. 15.26(b). While the lift coefficient can be optimized somewhat, the main challenge in development of these forms has been the leading edge geometry, the thinness of which is limited by strength considerations. In practice therefore, the designer has to accept reduced efficiency in order to achieve high craft speeds.

The reduced efficiency can in part be accommodated by raising the shaft close to the water-line and designing the propeller to be only partially submerged. While this introduces higher varying stress amplitudes at the blades, it reduces the appendage drag, which will be significant at high speeds. Design of partially submerged propellers follows the approach for a fully submerged propeller except that the thrust

developed is assumed proportional to the immersion. For SES such propellers have the advantage that at low speeds, higher thrust can be generated by increasing immersion (reducing lift) to assist acceleration through hump speed.

Performance data for a number of propellers are now available from the main international hydrodynamics laboratories such as DTNSRDC in the USA and MARIN in the Netherlands. DTNSRDC has for example extensively tested a propeller designated No. 4281 at a range of P/D, J, σ, shaft inclination and yaw, blade skew, rake and shaft immersion. For craft with speed requirements above 55 knots, consultation with these institutions is a useful starting point.

Outline design procedure

Design of supercavitating propellers is an iterative process. A typical procedure will include the steps shown in Fig. 15.23. Differences compared with subcavitating propeller design include:

1. greater sensitivity of the blades to both radial and chordwise stress distribution, so that development of the blade profile using blade element analysis may require some iteration before an acceptable profile is achieved for both hydrodynamic and structural criteria;
2. 'off design' conditions, including SES hump speed require full analysis since σ changes, rather than the check which can be carried out for subcavitating propellers.

Special considerations for SES

A propeller mounted at the stern of an SES hull is influenced by the proximity of the air cushion water surface and of the stern skirts, see Fig. 15.27. For lower speed craft (35 knots or less), fully submerged propellers need to be checked against free stream cavitation number based on the cushion water-line and cushion pressure to ensure this does not change the predicted performance. Propellers may become ventilated in a seaway due to craft motion if the rear seal is soft and so either the seal stiffness may need to be high, which is generally not optimum, or propeller immersion might be increased, or performance when ventilated may need to be investigated.

Higher-speed craft will generally require variable pitch propellers so as to optimize the power absorbed at both hump speed and service speed. In this case a further iteration of the design process is required for the hump speed condition. If partially submerged propellers are to be used, then the designer also has the choice of varying this relationship between hump and full speed.

Large high-speed craft with partial immersion propellers at the stern may require wider sidewall width than optimum from the resistance point of view in order to accommodate the propeller transmission and afford some physical protection during manœuvring. The design problem becomes progressively more difficult as SES size increases. Above around 1000 t displacement, the advantages of internal arrangement for water jets encourage the designer to consider these in preference to supercavitating propellers.

Open propellers are most suited therefore to low- and medium-speed SES in the

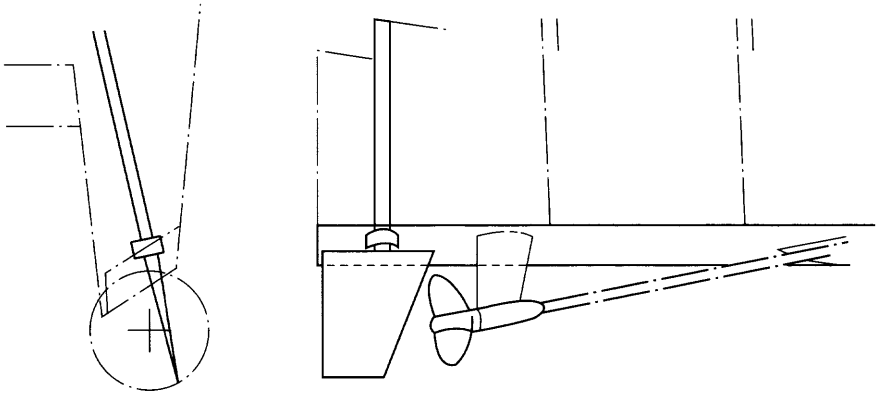

Fig. 15.27(a) Bell Halter BH 110 propeller arrangements [88].

range 20–55 knots and for sizes up to 1000 t displacement. Within this application range, propulsive efficiency between 0.65 and 0.75 should be achievable and propeller designs sourced from a number of suppliers. Where fixed pitch propellers can be selected, the installation will be relatively simple, lightweight and of low cost. Careful selection of blade geometry can achieve surprisingly high efficiency at speeds up to 55 knots. Beyond this speed, reduced efficiency has to be accommodated. Given that this is compatible with the mission, for example fast military strike craft, ventilated partially submerged propellers can offer effective propulsion to speeds in excess of 100 knots.

15.5 Water jets

Water jets for marine propulsion have a similar background to marine screw propellers. Reference 113 gives a comprehensive description and bibliography for water-jet history. The British Navy carried out parallel trials of a water-jet powered and a water screw driven vessel, the Waterwitch vs the Viper, in 1863. At that time pumps used as water jets were found to be less efficient than screw propellers and so the British Royal Navy concentrated on water screw development as an alternative to paddle wheels.

Development in the recent past was initially encouraged by a market for very shallow draft small pleasure craft in the 1950s and for propulsion of larger high-speed hydrofoils during the 1960s. Since then development has been primarily driven by applications for SES and a rapidly expanding high-speed ferry market in the 1980s and 1990s.

In the early 1970s the US Navy carried out initial design of a 3000 t water-jet propelled high-speed SES. This followed competitive trials of two 100 t displacement prototypes, the SES-100A (water jets) and SES-100B (supercavititating propellers). The programme was taken as far as preliminary design of water jets for the ship, aimed at a power rating of 40 000 kW, and a design ship speed of 80 knots. The project

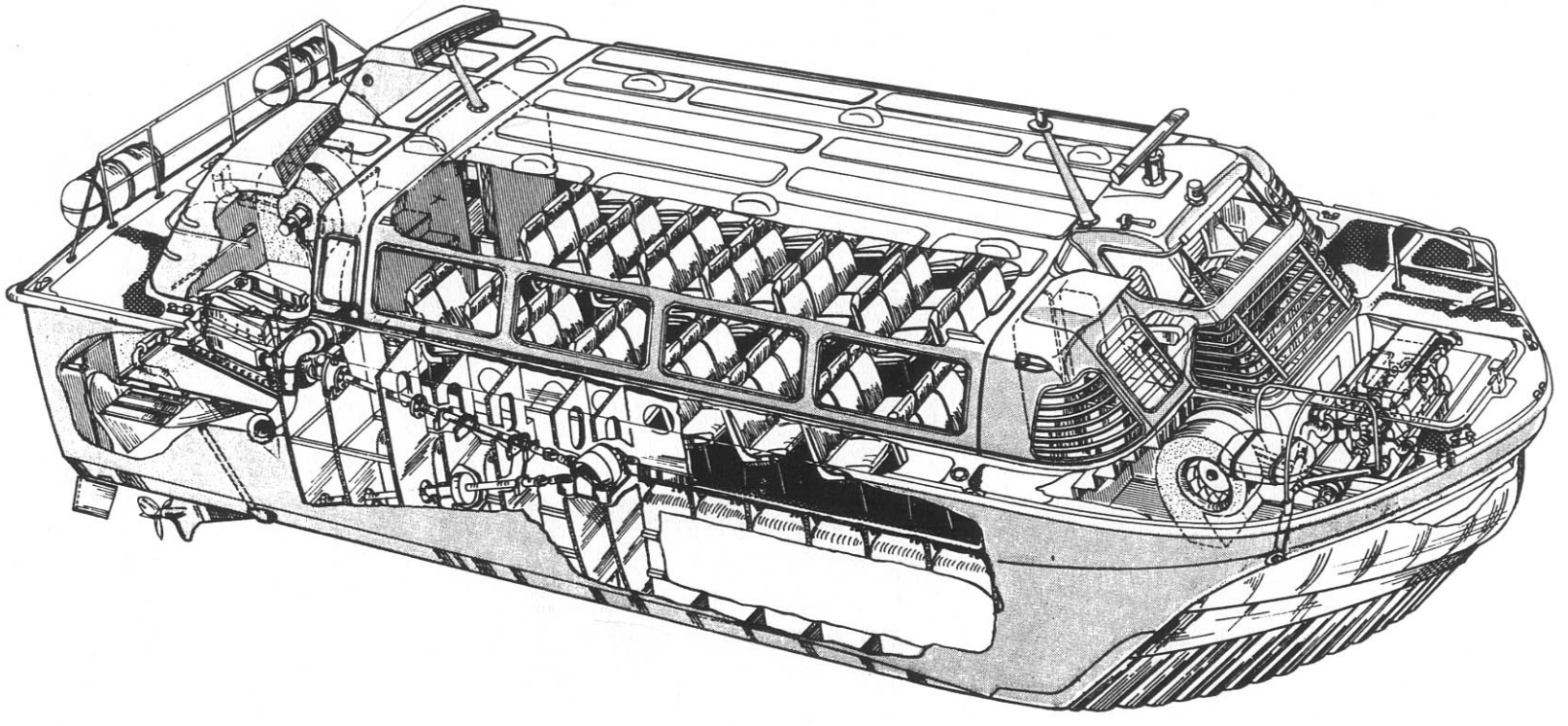

Fig. 15.27(b) Hovermarine HM 216 SES showing propulsion shaft and propeller arrangement.

was cancelled before ship construction started, but significantly improved the understanding of technical requirements for large water-jet units for high-speed craft. The water-jet system designed by Rocketdyne still represents the highest power rating attempted to date.

Overall propulsive efficiency (OPC) of between 0.45 and 0.55 were a realistic expectation at that time, using centrifugal pumps (USN hydrofoil Tucumcari), or inducer pumps such as proposed for the 3KSES, both designed for high jet exit velocity compared with craft speed.

It can be shown (see below) that if the jet velocity can be reduced closer to ship speed the efficiency can be much increased. There are two problems with this. Firstly, similarly to air propellers, the propulsor diameter has to increase exponentially as design ship speed is lowered. The second problem is that for craft operating at above about 40 knots cavitation begins to become a problem just as for marine propellers, unless the inlet pressure to the main pump can be maintained above that at which cavitation occurs.

For applications in the speed range 30–50 knots it has been found that water-jet systems with mixed flow pump impellers can give OPC in the range 0.5–0.75 (Fig. 15.3). This is clearly most attractive for designers compared to open propellers, particularly when a number of other advantages are accounted for:

- Flush inlet water jets have no appendage drag (shafts, supports, rudders).
- Steering is achieved by deflection of the jet itself, which is much more powerful than rudders.
- Reverse thrust is achieved by jet deflection rather than via a gearbox or variable pitch blades.

Other advantages associated with water jets include:

- reduced draft;
- reduced underwater noise, see Fig. 15.28 for an experimental comparison;
- reduced vibration and inboard noise from water-jet impeller, see Fig. 15.29 for a comparison;
- high power able to be applied at low ship speeds.

Water jets are products procured from specialist suppliers. Development of a new jet system from scratch is a process only open to large projects such as the US 3KSES programme. This section is therefore aimed at outlining for the SES designer the typical characteristics of water-jet systems, what opportunities there are for optimization relative to SES hulls and what may also be expected from the water-jet supplier.

Suppliers, see for example Table 15.5, have developed their ranges in a stepwise manner as the market has grown. The basic building blocks of inlet, pump and stators, nozzle and steering gear are scalable within a range of speeds, which has assisted improvements over the current speed range of 30–50 knots. At higher speeds where different pump types are required, a similar approach will need to be taken.

SES hulls lend themselves to the flush-type water-jet inlet (see Figs 15.30 and 15.31 for example), so long as some measures are taken to guard against ingestion of cushion air in heavy seas. Many detailed studies have been carried out by the suppliers for this type of inlet, through model testing and analysis.

SES designers will most likely make an initial selection of candidates based on their

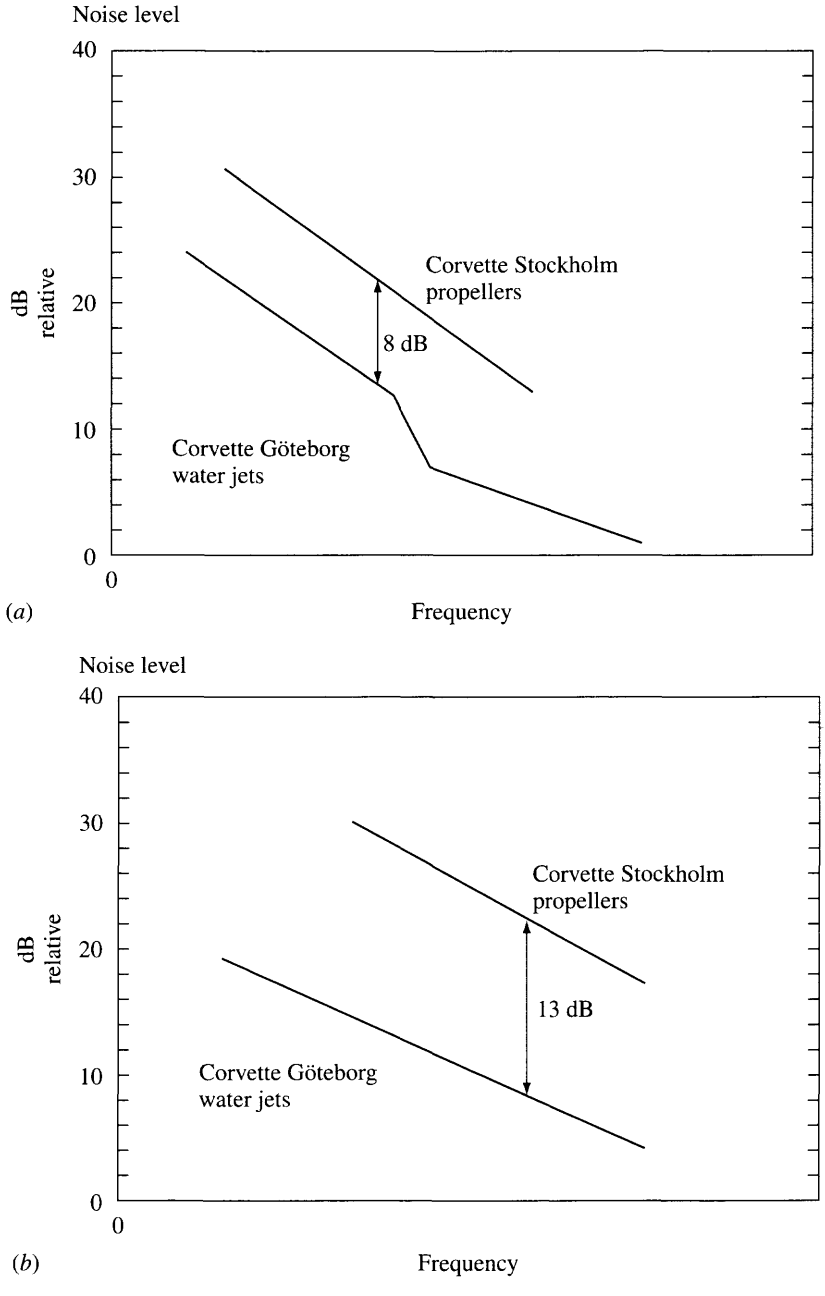

Fig. 15.28 Underwater noise comparison for water jets vs open propellers.

own powering estimates. The supplier will then need hull lines, resistance curves, predicted wake and craft dynamic trim through the speed range in order to begin the optimization process. The SES designer can expect that a water-jet supplier will provide a recommended geometry for the system based upon the craft hull lines together

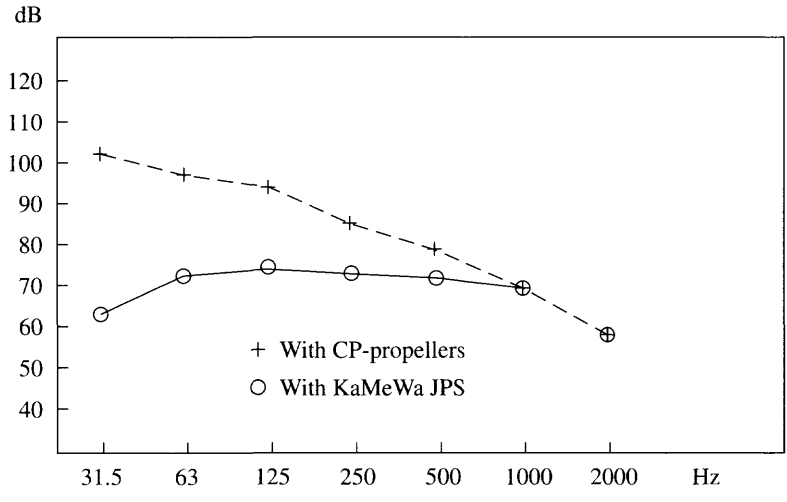

Fig. 15.29 Internal noise and vibration comparison for water jets vs open propellers.

with an indication of the allowable power input at the range of craft speeds, and the predicted thrust performance of his unit. Final integration of the SES hull and water-jet design will be an iterative process from this point, as SES detail design proceeds.

A summary of physical dimensions for various waterjet units is shown in Table 15.5(a) and (b). The designer can determine required water-jet performance using the logic shown in Fig. 15.32 by calculating:

Table 15.5a KaMeWa water jets

Size	A	B	C	D	E	F	G	H	J	K	L	M
40	1095	2530	440	300	20	75	415	480	790	900	480	2000
45	1400	3350	493	350	20	80	410	640	840	1220	540	2200
50	1520	3750	550	375	25	100	635	695	945	1350	600	2200
56	1670	4200	620	395	35	110	635	760	1030	1510	670	2500
63	1900	4700	695	465	35	120	675	860	1120	1700	760	2500
71	2115	5300	772	535	35	130	745	965	1280	1900	850	2900
80	2395	5970	875	535	40	140	810	1085	1450	2140	960	3300
90	2615	6720	972	630	50	165	1030	1185	1610	2410	1080	3500
100	3000	7470	1100	670	50	180	1020	1360	1820	2680	1200	4130
112	3360	8360	1230	750	60	200	1140	1520	2030	3000	1350	4620
125	3750	9390	1370	840	65	220	1270	1700	2230	3350	1500	5160

A Overhang length from transom.
B* Minimum length transom to forward foot of intake.
C Nozzle outlet behind transom.
D Location of interface between intake and pump inlet casing.
E Minimum transom plate thickness.
F Nominal shaft diameter.
G Extended depth of reversing bucket in stowed position.
H Maximum width when jet deflected 30°.
J Diameter of transom mounting flange.
K* Minimum distance of intake rear lip from transom.
L Height of pump centre-line from keel.
M Distance from transom to shaft connection.

* These dimensions will vary with craft installation. In general the intake will be longer.

Table 15.5b MJP Mark II water jets

Size	Nom. kW	Max. kW	A	B	C Dia.	D Dia.	E	F	G	H	Weight steerable	Weight booster
500	1200	1800	510	1290	855	500	2050	3400	575	460	815	57
550	1500	2250	560	1412	940	550	2250	3790	630	505	1090	71
650	2100	3150	665	1680	1120	650	2675	4510	750	600	1560	103
750	2800	4200	765	1900	1255	750	3075	5180	860	690	2105	146
850	2700	5550	880	2100	1440	850	3540	5890	990	795	3145	212
950	4900	7350	1010	2460	1610	950	4070	6590	1100	915	4330	300
1100	6950	9750	1200	2845	1890	1100	4820	7630	1350	1090	6040	408
1350	9200	13800	1355	3490	2110	1350	5560	9370	1555	1250	8450	583
1550												

Dimensions in mm.
Weights in kg, including hydraulics, but excluding intake duct and shafting.
All data are nominal, and would be adjusted based on client discussions.

- required thrust by determining and applying the thrust deduction factor to the drag;
- velocity approaching the inlet by applying the wake factor to the ship speed;
- inlet/jet velocities and mass flow to achieve required thrust, via momentum theory;
- initial estimates for system component efficiencies;
- net positive suction head and pump head based on assumed inlet and nozzle efficiencies;

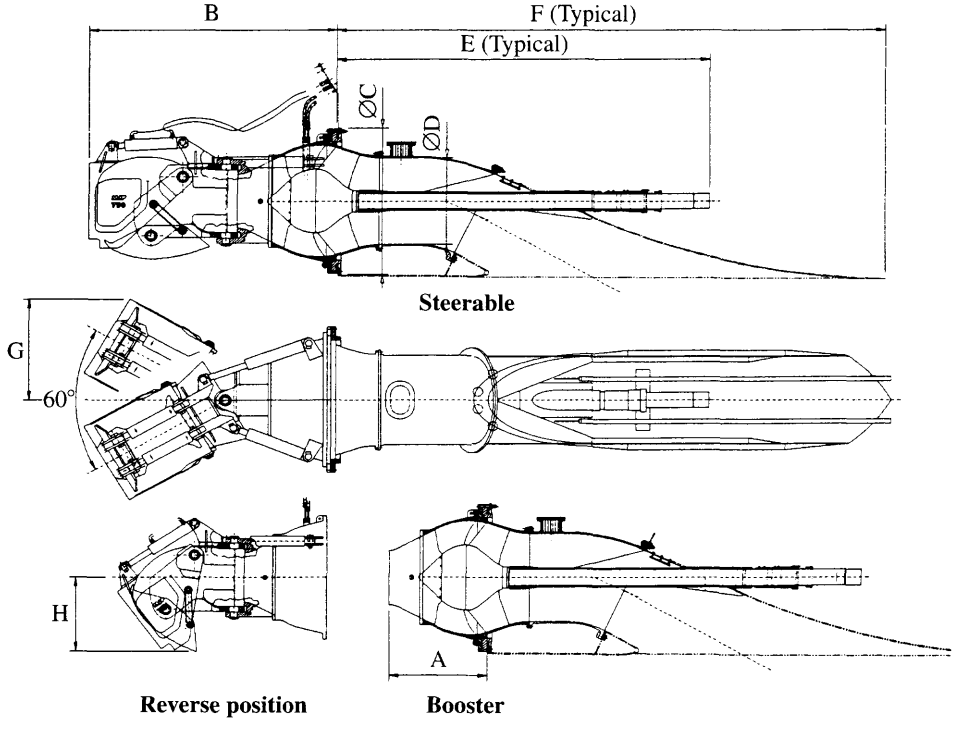

Fig. 15.30 Water jet geometries (MJP designs).

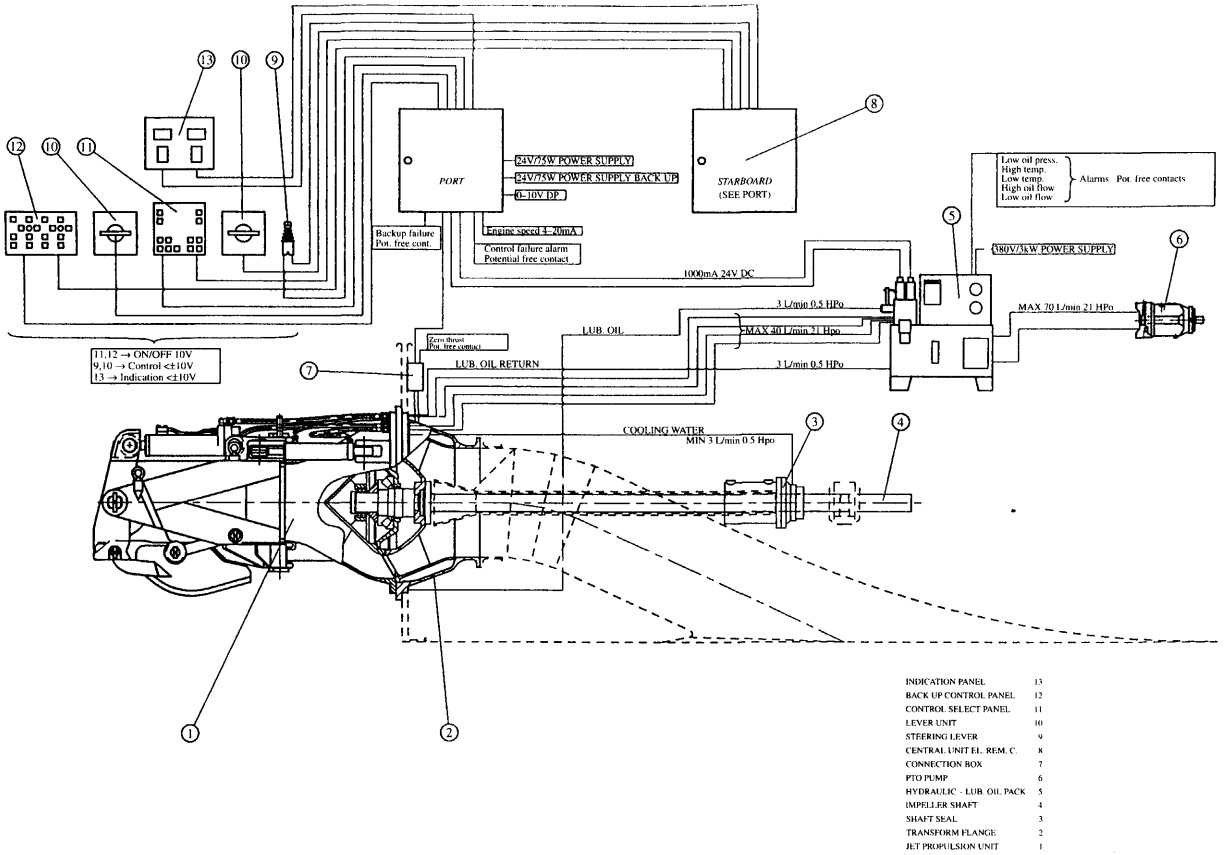

Fig. 15.31 KaMeWa waterjet system drawing.

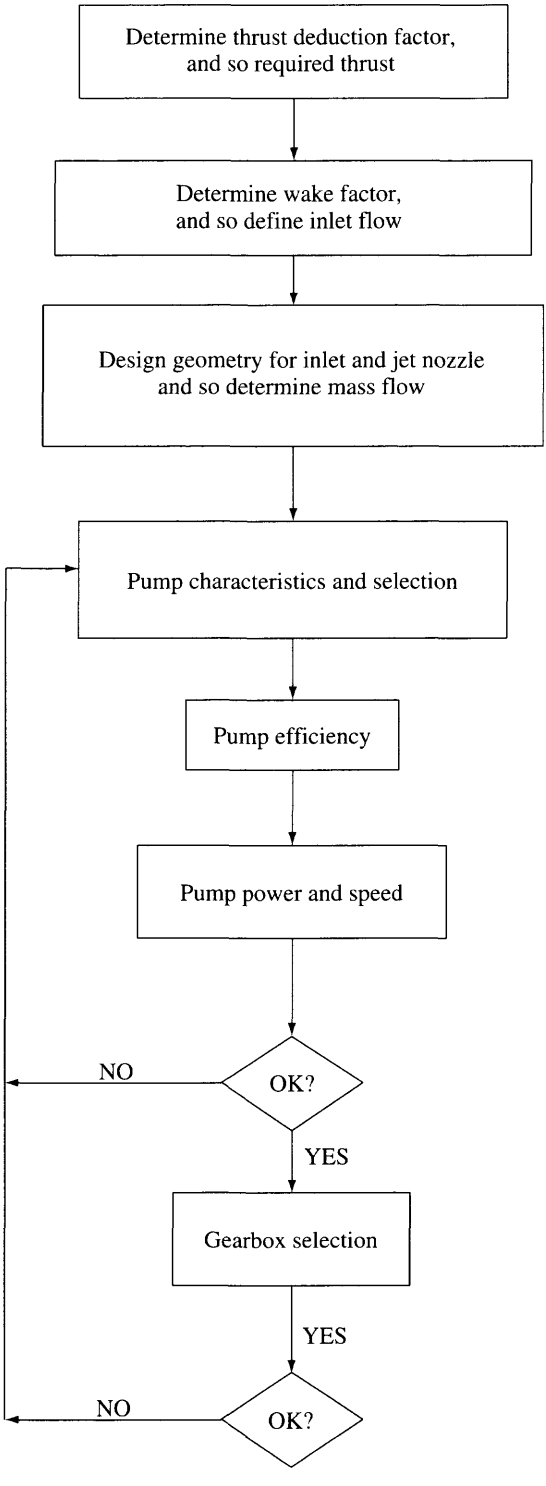

Fig. 15.32 Water jet selection procedure.

- non-dimensional operating point for the pump (ϕ, ξ, η_p);
- pump dimensions and rotation speed;
- system component efficiencies and therefore installed power, as a cross-check.

Once the desired characteristics have been determined, a selection can be made of units with closest performance and physical dimensions checked to ensure they will fit to the SES hull dimensions. At this point the designer may choose to revise the hull lines if the selection of water jet, transmission and engine are not fully compatible and so may repeat powering predictions before involving the suppliers in the design. Advice can then be sought of the suppliers to take the next step of verifying or revising the selection and optimizing the system. This will include adjustments to the inlet geometry and position in the sidehull, optimization of the pump itself, design of the power train, the nozzle installation outboard of the transom, and the water-jet control system.

We will look at each of the steps above in turn beginning with a review of system losses, including some discussion of their effect on component and system design.

Thrust deduction and wake factors

Ship resistance is normally determined from scale model test data or analysis of the basic hull form. The actual required thrust will normally differ from this due to unaccounted scale effects. In addition, appendages will add drag components to the overall resistance. These components are particularly important for propeller-driven craft. The effect of this increase in overall resistance is accounted for as a thrust deduction factor during initial design, where

$$T = R_p/(1 - t)$$

The thrust deduction factor $(1 - t)$ for a water-jet propelled craft with flush type inlets is normally in the range 0.97–1.03. Pod inlets have a higher drag and will result in $(1 - t)$ of between 0.9 and 0.97.

At low speeds a water-jet inlet will accelerate flow in the region of the intake in a similar manner to the velocity field behind a propeller (see Fig. 15.9), except that part of the boundary layer will be ingested, reducing the thrust deduction compared to open propellers. At higher speeds flow will be gathered from a much smaller volume and the flow behind the intake will be at close to free stream velocity so that the overall effect will be a reduction in required thrust. During the initial design stage of an SES it is recommended to use 1.0 for $(1 - t)$.

The hull wake factor $(1 - w)$ ranges between 1.02 and 0.8. At the upper bound of this range, the water jet is assumed to remove or reduce the boundary layer under the hull by accelerating water into the inlet duct rather than the deceleration which is normal in the afterpart of a fast semi-displacement or planing craft hull. This will be most effective at slow speeds and for SES where the hulls themselves are very slender. At design operational speed the effect will be governed by the jet velocity ratio. Since water-jet systems for high-speed craft tend to have high V_j/V_c, the wake factor will still be close to 1. During initial design a value of 0.97 is recommended for SES.

In the same way as for propeller design, the required thrust to be developed takes account of these two factors by

$$T = T_i (1 - w)/(1 - t) = T_i \eta_H \tag{15.80}$$

where η_H is often equated to 'hull efficiency'.

Inlet losses

If we consider the flow into an open propeller, as craft speed is reduced from the design conditions, streamlines will enter from a widening area (see Fig. 15.9). Water-jet systems face the same issues as ducted air propellers for design of the intake system. The duct centre-line normally follows an S curve from the hull base-line, while the duct geometry itself is a parabolic or hyperbolic curve, with an intake lip having similar geometry to an aerofoil leading edge at the front and a sharper edge on the aft part, similar to a supercavitating propeller leading edge.

Water-jet inlets normally have a geometry based on the normal operating condition (SES cruise speed), so that below this speed flow velocity will be higher at the inlet intake and losses will increase relative to the ideal. Inlet losses will reduce the available head at the pump suction and the practical limit for thrust developed will be controlled by the net positive suction head (NPSH) below which the pump starts cavitating. Above normal operating speed, flow into a fixed inlet geometry will be decelerated over the initial part of the duct, producing a similar effect to hull wake.

While a variable geometry inlet would optimize flow into the pump, removing turbulence at the intake lip at low speeds and in the throat at high speeds, the costs of such an installation are normally prohibitive. Instead, water-jet manufacturers have found from model testing that inlet geometries can be defined which minimize the turbulence in off-design conditions, particularly at lower speeds.

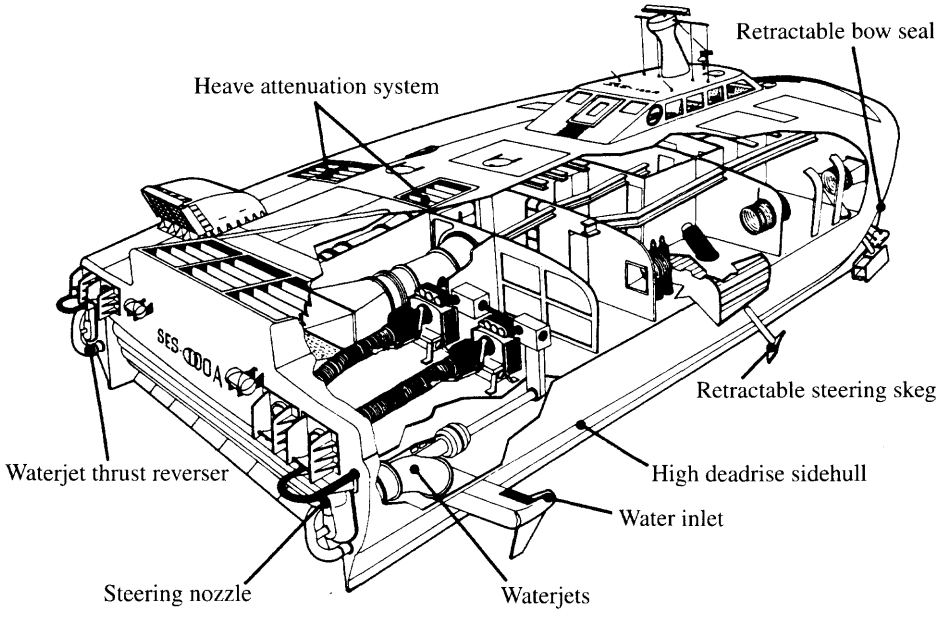

Fig. 15.33 Water jet inlet with secondary slow speed intake.

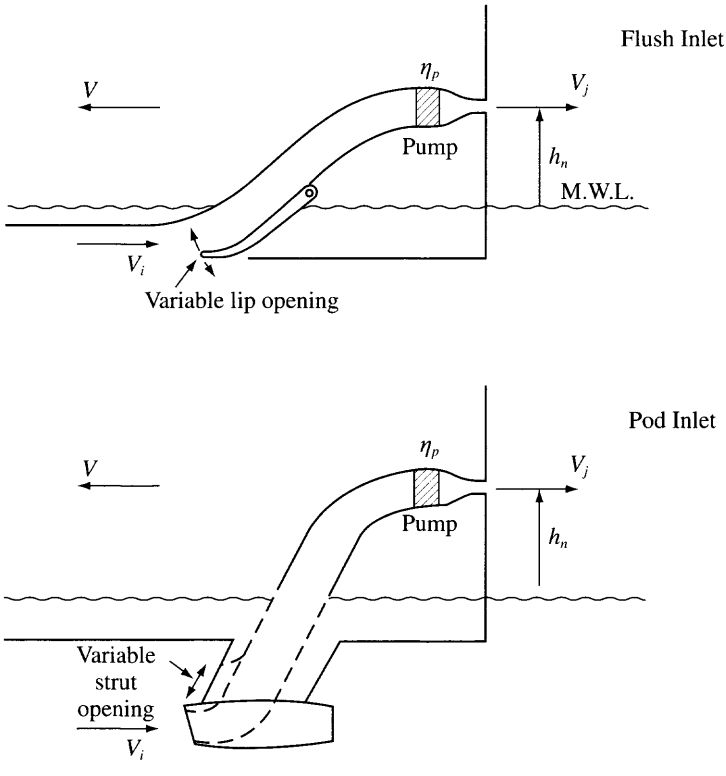

Fig. 15.34 Variable area water jet inlets.

Water-jet inlets can either be flush to the base-line of the SES hull, or extended as a 'pod' to capture flow from the area undisturbed by the hull boundary layer. Pod inlets are used on hydrofoils. The SES 100A test craft was originally fitted with pod inlets (see Fig. 15.33). These comprised a main high-speed intake and auxiliary inlets allowing greater flow at lower speeds. Performance was less than projected and so the craft was retrofitted with variable area flush inlets. These initially had problems with air ingestion in a seaway and so various geometries of 'fence' between the intakes and the sidehull lower chines were experimented with until performance was satisfactory. Further studies were then carried out on the variable geometry inlets, which did not behave according to design predictions. It was found to be very difficult to set the ramp position for optimum thrust and at the same time avoid cavitation either internally or externally. Eventually it was found that a round fixed area inlet could give a reasonable compromise without the complexities of the variable ramp operating mechanism and so this design was selected for the 3KSES as a design basis.

At craft speeds of 30 knots, V_i/V_c variation between 0.5 and 0.95 can occur without cavitation on a typical well-designed flush type inlet (see Fig. 15.41). This range narrows to V_i/V_c of 0.66–0.82 at 70 knots and further to 0.7–0.8 at around 100 knots. Below the lower boundary cavitation occurs under the rear intake lip, while above the upper boundary, flow separates from the intake roof or the inside of the lower lip.

It can be seen therefore that if a craft is designed for V_i/V_c to be 0.66 at 70 knots, this will become 1.54 at 30 knots and cavitation will occur on the inside of the inlet unless the pump flow is reduced to about 60% of design. This may be acceptable so long as the SES drag hump is not too high, i.e. for high L/B craft. For craft with higher hump drag and those with very high design speed (above 60 knots), it may be beneficial to install a secondary inlet system which can be closed above hump speeds, along the lines of Fig. 15.34. For craft speeds in the 40–60 knot range, it is realistic to design the inlet based on the design speed and accept reduced efficiency at lower speeds.

The inlet for an SES will generally be constrained in width by the sidewall. Ideally, the transition forwards from the pump impeller to the inlet should be as smooth as possible, with an elliptical cross-section at the entrance. If the width is restricted, the elliptical entrance will naturally be extended forward and aft. If this becomes too extreme, there may be a tendency to flow breakaway at the sides of the inlet, so if necessary the SES hull width should be adjusted to give a greater beam at the keel.

If smooth geometry can be achieved for the inlet system and the inlet width can be kept wide, approximately 1.0–1.2 times the impeller diameter, it is realistic to expect efficiency between 0.8 and 0.9 for a flush inlet system. A starting point for initial design may be 0.825 for craft speed 30 knots inceasing to 0.9 at about 55 knots. Above this speed cavitation problems may reduce inlet efficiency again so that at 100 knots 0.85 might be assumed as a starting point.

Nozzles and efficiency η_n

Nozzles may be of two types. The Pelton type has an exhaust duct outer wall which follows the geometry of the stator hub fairing as used by MJP (Fig. 15.30) and KaMeWa (Fig. 15.31). In this case the vena contracta of the jet will occur just downstream of the nozzle. Alternatively the duct may be extended as a parallel section, in which case there will be no external vena contracta. The latter nozzle is more often used on small water jets used for pleasure boats and jet ski craft.

Nozzle design, including flow though the system of stators behind the pump and the duct formed by the hub rear fairing and the outer casing, is aimed at uniform axial flow. In fact there will be some variation due to the boundary layers at the casing and hub fairing, see Fig. 15.35, but these effects are usually very small and the nozzle efficiency should be close to 99% at design condition.

Nozzle elevation h_n

The water which travels through a water-jet system is elevated before entering the pump, incurring a head loss. This suction head loss is significant for a hydrofoil where the jet is located in the hull, but for an SES generally amounts to just a metre or so above the keel. This suction head must be taken into account when determining pump NPSH, see Fig. 15.34.

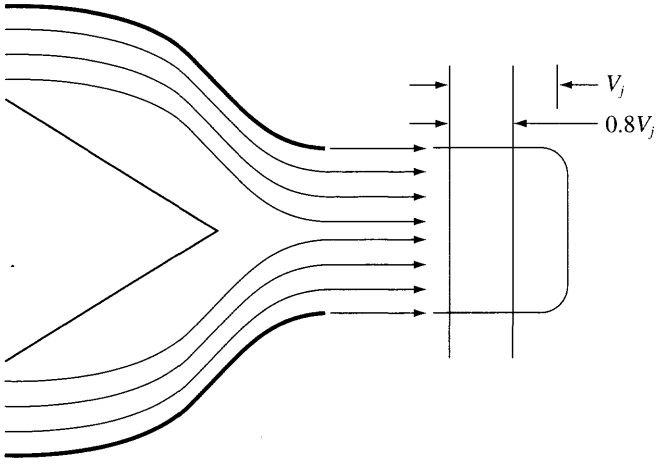

Fig. 15.35 Water jet vena contracta.

Momentum theory and jet efficiency

Having considered the main system losses, excepting the pump, we first consider the efficiency of a jet system, before looking at the pump itself in a little more detail.

Water entering the water-jet system is considered to be accelerated to the forward speed of the vessel, V_c before being accelerated through the pump and nozzle to V_j. The net thrust developed by a water jet is therefore

$$T = \dot{m}\ V_j - \dot{m}\ V_c \tag{15.81}$$

the energy applied by the pump to the water mass is

$$E = 0.5\ \dot{m}\ (V_j^2 - V_c^2) \tag{15.82}$$

The propulsive efficiency is therefore

$$\eta_j = T\ V_c/[0.5\ \dot{m}\ (V_j^2 - V_c^2)] \tag{15.83}$$

which reduces to

$$\eta_j = 2\ V_c/(V_j + V_c) \tag{15.84}$$

if we equate V_c/V_j to μ then dividing terms in equation (15.83) by V_j:

$$\eta_j = 2\,\mu/(1 + \mu) \tag{15.85}$$

which has a similar form to the equations for ideal efficiency of air propulsors. This is shown as the top curve of the series in Fig. 15.36. If losses are considered as a single factor ζ related to the inlet energy, i.e.

$$E = 0.5\ \dot{m}\ (V_j^2 - V_c^2) + \zeta\ 0.5\dot{m}\ V_c^2$$

then

$$E = 0.5\ \dot{m}\ (V_j^2 - V_c^2\,(1 - \zeta)) \tag{15.86}$$

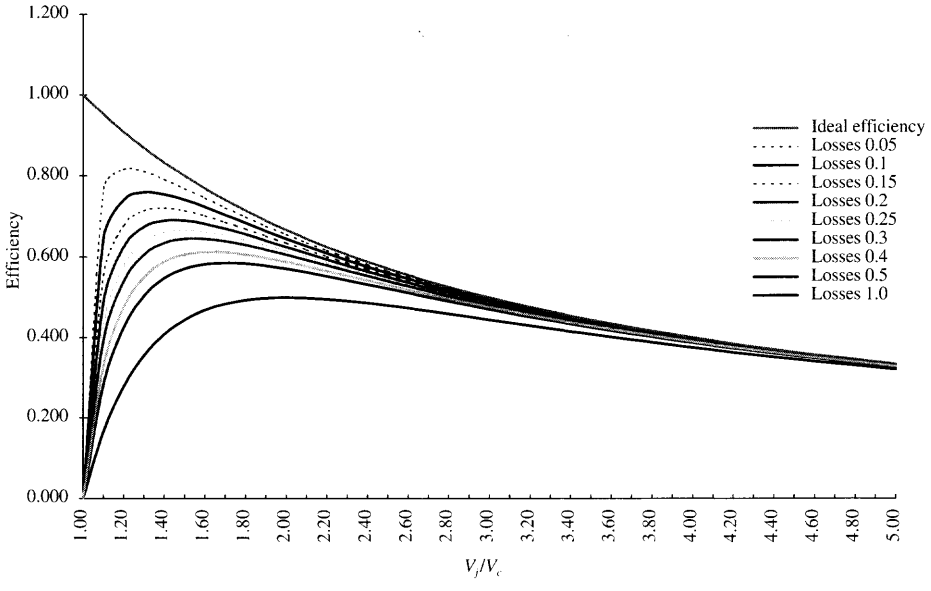

Fig. 15.36 Water jet efficiency.

since

$$\eta_j = T\,V_c/E$$

so

$$\eta_j = T\,V_c/[0.5\,\dot{m}\,(V_j^2 - V_c^2\,(1 - \zeta))]$$

or

$$\eta_j = 2\,\mu(1 - \mu)/[(1 - \mu^2)\,(1 - \zeta)] \tag{15.87}$$

This is shown in Fig. 15.36 for values of ζ up to 1.0, where the inlet energy is completely lost.

It can be seen that if the system is to be efficient, losses from the inlet must be relatively low, of order 5–15%. The optimum jet velocity ratio is 1.2–1.4. Water jets with jet velocity ratios in this range would be relatively large, somewhat larger than an equivalent open propeller in fact, due to the relatively high boss diameter (see Fig. 15.30 for example).

In fact it is possible to design water jets to have pump outer diameters similar to that of open propellers, while maintaining high efficiency, as demonstrated by the KaMeWa performance data, Fig. 15.3. KaMeWa recommended selection of water-jet sizes for initial design as shown in Fig. 15.37. We need therefore to investigate interaction of a water jet with the hull, which can mitigate the losses which are apparent from momentum theory.

If the efficiency is expressed as a relation to thrust loading coefficient rather than the velocity ratio the following expression for ideal efficiency results. If

$$C_t = T/[0.5\,\rho_w\,A_j\,V_c^2] \tag{15.88}$$

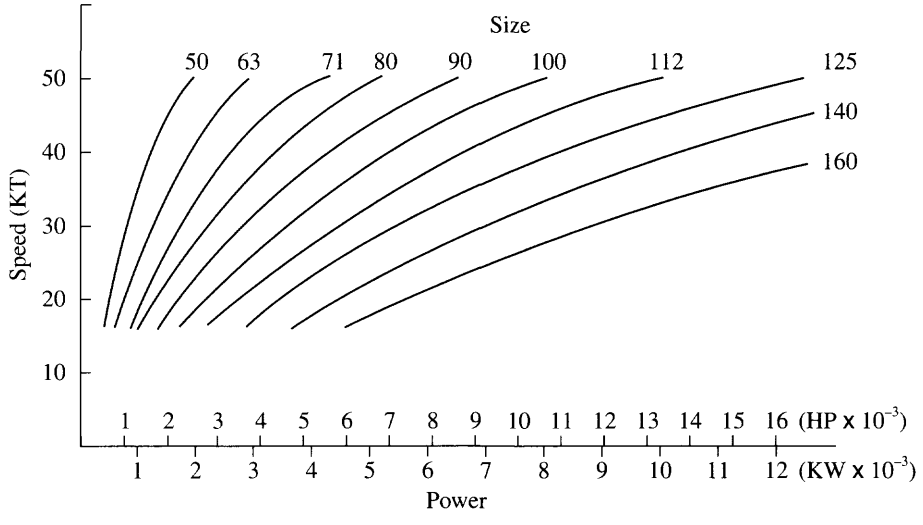

Fig. 15.37 KaMeWa water jet selection chart.

then

$$\eta_j = 4/[3 + (1 + 2\,C_t)^{0.5}] \tag{15.89}$$

which may be compared with the equivalent expression for an open propeller; where

$$\eta_i = 2/[1 + (1 + C_t)^{0.5}] \tag{15.90}$$

this is shown in Figs 15.38 and 15.39. Clearly a water jet has improved performance at higher thrust loading, a result equivalent to the ducted propeller, suggesting that reduced disc area is possible while maintaining efficiency equivalent to an open propeller.

If we include system component losses in the expression for efficiency (15.87), i.e.

$$\eta_i = (1 - \zeta) \text{ inlet losses}$$

$$\eta_n = (1 + \psi) \text{ nozzle losses}$$

$$W_c = \dot{m}\, g\, h_j \text{ head loss due to nozzle elevation}$$

then the expression for expended energy becomes

$$E = 0.5\,\dot{m}\,[(1 + \psi)V_j^2 - (1 - \zeta)\{(1 - w)V_c\}^2 + 2\,g\,h_j] \tag{15.91}$$

now

$$\eta_j = T\,V_c/E$$

$$= \dot{m}\,(V_j - (1 - w)\,V_c)\,V_c/E \tag{15.92}$$

if we divide through by V_j^2 and set $\mu = V_c/V_j$ as earlier, this expression becomes

$$\eta_j = \frac{(1 - (1 - w)\,\mu)\,\mu}{0.5\,[(1 + \psi) - (1 - \zeta)\{(1 - w)\mu\}^2 + 2\,g\,h_j/V_j^2]} \tag{15.93}$$

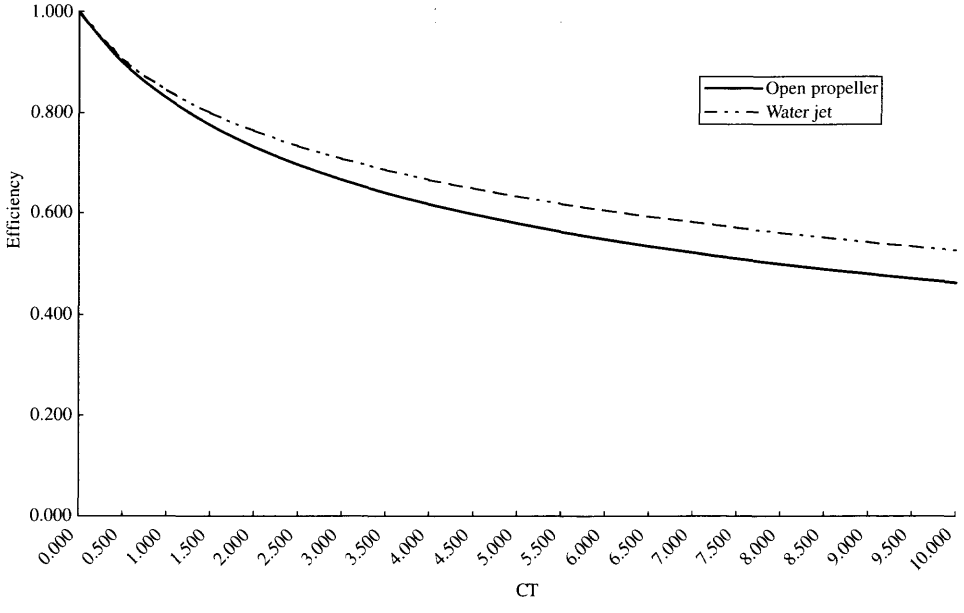

Fig. 15.38 Efficiency comparison: open propeller vs water jet.

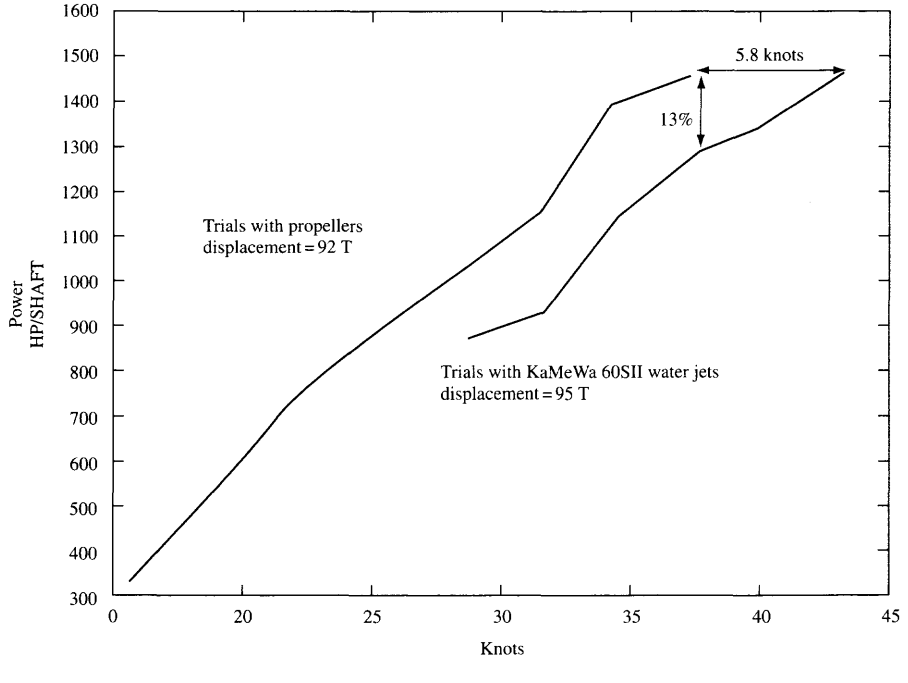

Fig. 15.39 Comparison between propellers and water jets from trials with SES Norcat.

If μ is considered relative to wake velocity at the jet intake, i.e $\mu_w = (1 - w)V_c/V_j$ instead of relative to the craft speed, this becomes

$$\eta_j = \frac{2(1 - \mu_w)\,\mu_w/(1 - w)}{(1 + \psi) - (1 - \zeta)\mu_w^2 + 2gh_j/V_j^2} \tag{15.94}$$

This formulation is convenient to allow cavitation tunnel testing of a water jet in a facility similar to Fig. 15.40. When combined with the inclination of the jet pump this becomes

$$\eta_j = \frac{1}{(1 - w)} \cdot \frac{2\mu_w(\cos\alpha\cos\phi - \mu_w)}{(1 + \psi) - (1 - \zeta)\mu_w^2 + 2g\,h_j/V_j^2} \tag{15.95}$$

since

$$T_{eff} = \dot{m}\,V_j \cos\alpha \cos\phi$$

where α is the pump centre-line inclination to horizontal water-line (should include vessel trim) and ϕ the pump centre-line horizontal inclination to ship centre-line.

If the effect of inlet drag is included (this is more pronounced for pod type inlets) then, first

$$\begin{aligned} D_i &= C_{Di}\,0.5\,\rho\,A_i\,V_i^2 \\ &= C_{Di}\,0.5\,\dot{m}\,V_i \text{ since } \dot{m} = \rho\,A_i\,V_i \end{aligned} \tag{15.96}$$

We define an inlet velocity ratio (IVR) in terms of the wake velocity, where

$$\text{IVR} = V_i/V_w$$

then

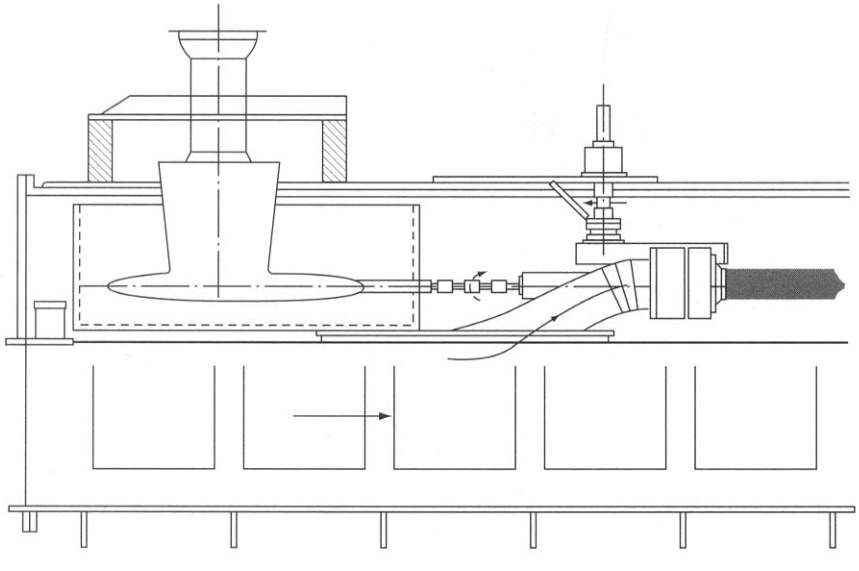

Fig. 15.40 Water jet model in cavitation tunnel (KaMeWa diagrammatic).

$$V_i = \text{IVR } V_w = \text{IVR } V_c (1 - w)$$

thus

$$D_i = C_{Di}\, 0.5\, \dot{m}\, \text{IVR } V_c (1 - w) \tag{15.97}$$

If an inlet is truly flush and the flow around the rear inlet lip causes no turbulence, then D_i may be assumed as zero. Since for an SES it is likely that fences may be needed around the inlet and the rear lip will create drag, it is prudent to assume some losses. A value of C_{Di} between 0.008 and 0.03 may be considered representative of well-designed installations. Now

$$\eta_j = (T - D_i)\, V_c/E \qquad \text{(from 15.91)}$$

$$= \dot{m}\, [V_j - (1 - w)\, V_c - C_{Di}\, 0.5\, \text{IVR } V_c (1 - w)]\, V_c/E \tag{15.98}$$

so by following the steps from (15.93) to (15.96), we obtain a revised expression as follows:

$$\eta_j = \frac{1}{(1 - w)} \frac{\mu_w\{2(\cos a \cos \phi - \mu_w) - C_{Di}\, \mu_w\, \text{IVR}\}}{1 + \psi - (1 - \zeta)\, \mu_w^2 + 2g\, h_j/V_j^2} \tag{15.99}$$

Finally let us consider the local pressure effects around a water-jet intake, see Fig. 15.41. Based on physical measurements, Svensson [56] has shown that flow in the region behind a flush inlet produces an increased pressure which may exceed wake-affected stream pressure, causing a lifting force on the hull. This is the opposite to the flow field behind a propeller, which is accelerated, creating a relative suction on the hull compared to wake-affected stream pressure.

This effect is rather complex, varying with craft speed, IVR for the intake design, and the extent of the bottom plate behind and on either side of the intake. The altered velocity field will effectively reduce hull drag locally, so increasing jet efficiency. If the hull geometry is optimum in the region of the intake, then the velocity field itself will also be so, minimizing turbulence. It may be seen that optimization of the hull stern geometry and the jet intake position, together with the intake geometry itself, is important to a water-jet system. If we consider the pressure difference in the inlet area:

$$P_s - \rho g\, h_i = C_p\, 0.5\, \rho\, V_c^2 \tag{15.100}$$

where P_s is the representative value of static pressure for the inlet flow field and h_i the water depth at inlet. At low craft speeds $P_s < \rho g h_i$ due to the large inflow capture area and so C_p will be negative, suggesting a reduced efficiency. At normal operating speeds the intake may be designed so $P_s > \rho g h_i$, whereby C_p becomes positive. A value of C_p of approximately 0.1 may be expected for optimized water-jet/hull combinations operating at design speed [113]. The term to be added into (15.100) will be a deduction from E. The form is similar to that for inlet drag (15.96) except that C_p is measured relative to craft speed rather than inlet velocity. Since the flow field around the outside of the inlet is a complex one, this is a logical approach. Equation (15.99) then becomes

$$\eta_j = \frac{1}{(1 - w)} \frac{\mu_w\{2(\cos a \cos \phi - \mu_w) - C_{Di}\, \mu_w\, \text{IVR}\}}{1 + \psi - (1 - \zeta)\, \mu_w^2 + \dfrac{2g\, h_j}{V_j^2} - \dfrac{C_p\, \mu_w^2}{(1 - w)^2}} \tag{15.99a}$$

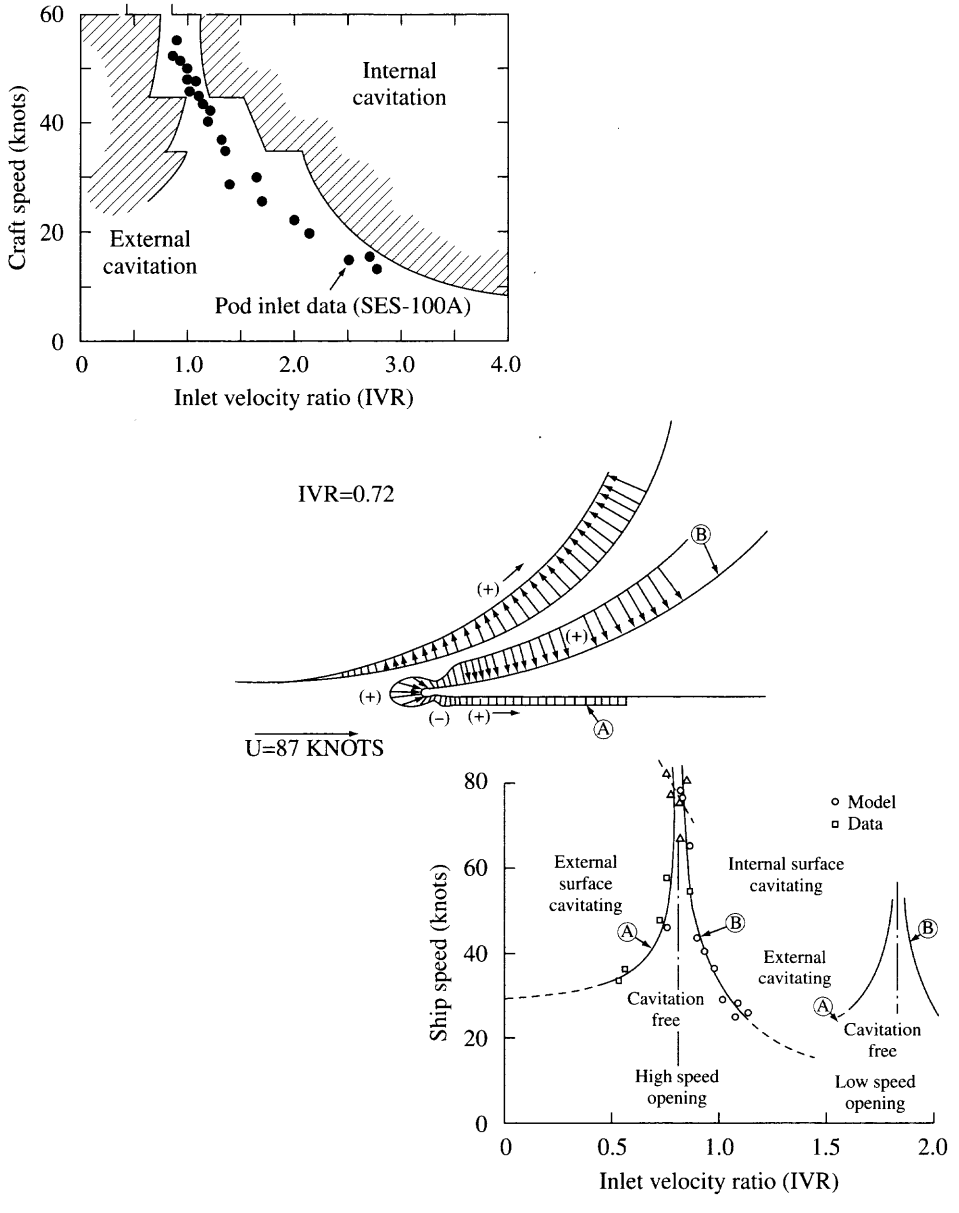

Fig. 15.41 Water jet inlet cavitation charts with craft data included. [4]

An expression for OPC including all significant loss components may now be stated as

$$\text{OPC} = \eta_p \, \eta_r \, \eta_t \, \eta_j \, (1 - t) \tag{15.101}$$

where η_p is the pump impeller efficiency, η_r the pump relative rotative efficiency and η_t the transmission efficiency.

At the initial stage of design, the designer will generally exclude inlet drag and the hull interaction effects, using the form in equation (15.95) to estimate power and size the propulsors. These other effects can then be tested as sensitivities.

Pump characteristics, types and selection

Pumps may be of radial flow (centrifugal) type, axial flow or mixed flow. By considering the momentum theory, it has been shown above that a small velocity increment over the ship speed gives greatest efficiency. High flow rate with low-pressure head pumps are in principle the most efficient as water jets. The optimum pump type will vary according to the craft design speed. With exception of high speed craft, above about 60 knots, it is likely that the main design constraint will be the pump physical size inside the SES sidewall geometry.

A pump has the objective to deliver a specified flow Q, at a particular fluid pressure. The fluid pressure is equated to a static head of the fluid ρgH. Thus, the ideal pumping power is

$$N_i = Q\rho gH \tag{15.102}$$

and

$$N = N_i/\eta \tag{15.103}$$

Pumps are generally characterized by non-dimensional parameters which affect their efficiency, to allow scaling [114]. In general for a pump

$$\eta = f(Q, gH, \rho, n, D) \tag{15.104}$$

we can reduce the number of independent variables by dimensional analysis so that

$$\eta = f(\Phi, \Psi) \tag{15.105}$$

where

$$\Phi = Q/n\,D^3 \quad \text{(non-dimensional flow coefficient)} \tag{15.106}$$

and

$$\Psi = gH/(n^2\,D^2) \quad \text{(non-dimensional head coefficient)} \tag{15.107}$$

Characteristic plots of Ψ vs Φ, or η against Φ should overlay one another for geometrically similar pumps. We may combine Φ and Ψ to obtain a non-dimensional power coefficient:

$$\Pi = \Phi\Psi = N/(\rho\, n^3\, D^5) \tag{15.108}$$

In viscous fluids, the Reynolds number Re should be the same. Since $Re = VD/\upsilon = nD^2/\upsilon$ for a rotating machine, then the pump speeds should be related by $n_a/n_b = (D_b/D_a)^2$.

Two other dimensionless groups may be defined and are widely used in pump and fan selection, known as specific speed and specific diameter:

$$N_s = n\,Q^{0.5}/[gH]^{0.75} \tag{15.109}$$

where n is the pump speed (rps), Q the flow (m^3/s) H the pressure head (m), g is gravity = 9.81 m/s^2, and

$$D_s = D\,(gH)^{0.25}/Q^{0.5} \tag{15.110}$$

Pump characteristics of N_s and D_s may be plotted together. Assembly of a wide range of data has led to a plot similar to that in Fig. 15.42, known as the Cordier diagram, showing regions where different rotating machines may be expected to have best possible efficiency.

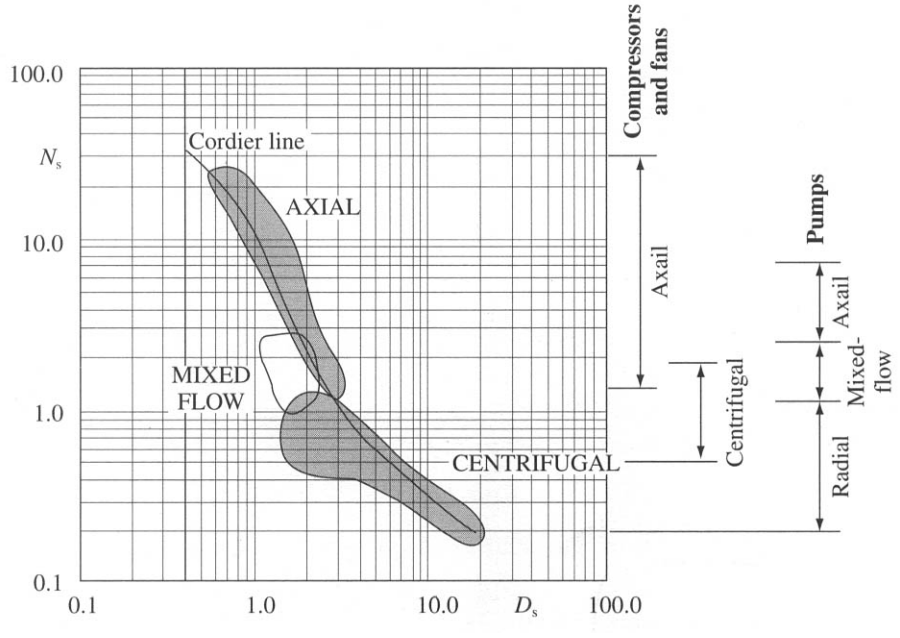

Fig. 15.42 N_s–D_s diagram [222].

Cavitation

A given water jet will cavitate and lose thrust if too much power is applied at low ship speed. An operating point marginally below this therefore defines the limiting thrust available at a given speed. Since jets are designed for maximum efficiency at the normal operating speed it is possible to plot contours of equal efficiency against craft speed and thrust, see Fig. 15.43. An important requirement for water-jet pumps is therefore that the suction head should not fall below the level at which cavitation would occur. Net positive suction head at the pump inlet is defined as follows:

$$\text{NPSH} = H_{pi} - H_v \tag{15.111}$$

where H_{pi} is the total head available at the entrance to the pump and H_v the water vapour pressure head. The total head in the free stream at SWL

$$H_{fs} = H_{at} + V_w^2/2g \tag{15.112}$$

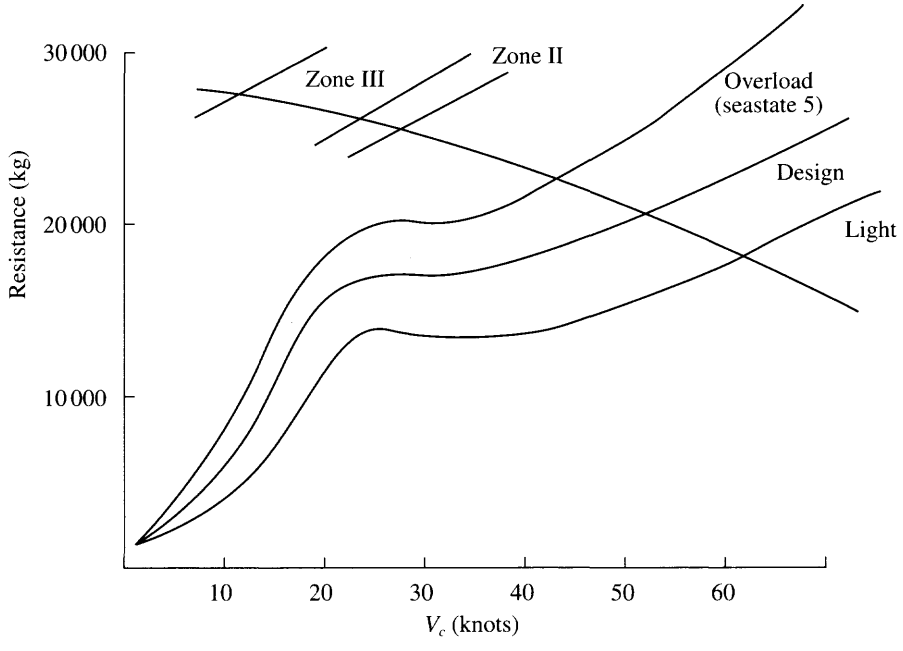

Fig. 15.43 Water jet efficiency vs V_c and T.

At the pump entrance this becomes

$$H_{pi} = H_{at} + (1 - \zeta)\, V_w^2/2g - H_i \tag{15.113}$$

where H_{at} is the atmospheric pressure (at SWL $H_v \sim 0.15H_{at}$) and H_i the height of pump inlet above SWL.

The water-jet inlet duct must be designed to supply an acceptable NPSH at design conditions and where possible allow the pump to operate close to its optimum at the lowest possible craft speed. Clearly from equation (15.113) a high duct efficiency is most important to maximize available NPSH. As craft speed reduces, if pump maximum power is maintained, the NPSH will drop below cavitation limits and the pump would overspeed as cavitation spread if power were not reduced. In cavitation tunnel tests, this point is determined by reducing fluid flow through the tunnel for constant pump speed, to the point where pump pressure head starts to fall off, typically by about 2%. The specific speed at this point is then defined as the suction specific speed, N_{ss}:

$$N_{ss} = n\, Q^{0.5}/(g \times \text{NPSH})^{0.75} \tag{15.114}$$

or

$$N_{ss} = n\, Q^{0.5}/[g\,(\eta_i\, V_w^2/2_g - H_i - H_v)]^{0.75}$$

Limits of N_{ss} for operation without cavitation are around 1 for mixed flow pumps and as high as 3 for inducer type pumps. Water-jet pumps may be operated for short periods outside this limit so long as the pump is not allowed to reach severe cavitation

where overspeed may occur. Water-jet suppliers may provide plots similar to Fig. 15.44 showing lines of constant N_{ss} defining these regions. The limit for safe emergency operation may be in the region of N_{ss} = 75, with a red line limit at 80–90 for mixed flow units.

Centrifugal and radial flow pumps

These were used in early hydrofoil craft because of availability of pump units and have been successfully used for thruster units designed for low craft speed (Schottel units). They offer a compromise in that while the pump head is high, the unit is very compact for the static thrust generated.

Mixed flow pumps

The majority of water jets in use today use mixed flow pump units. The ratio of radial to axial flow varies between different manufacturers' designs. The range of pump specific speed N_s varies between 0.2 and 0.8. Mixed flow pumps can be optimized for craft speeds of 30 knots up to at least 50 knots.

There are a number of manufacturers now offering water-jet ranges of this type which extend up to 32 000 shp. Developments are currently ongoing to extend this as far as 50 000 shp, encouraged largely by the market for large fast catamaran ferries.

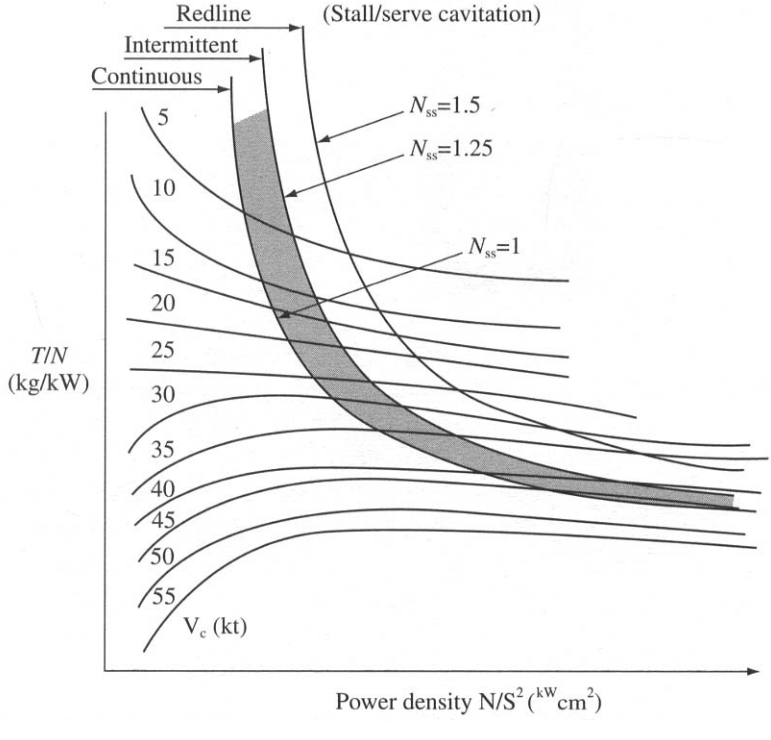

Fig. 15.44 N_{ss} boundaries on plot of water jet thrust vs craft speed.

Some mixed flow water jets use an inducer first stage to reduce the sensitivity to cavitation at high craft speeds.

Axial flow pumps

Axial flow pumps are high specific speed, high flow, low head machines. These pumps are often used for smaller units for pleasure boats in the power range 20–1000 shp. Higher power units generally use an inducer first stage or two axial stages in series where higher head is required.

Inducer pumps

The impeller for inducer pumps looks a little like an Archimedes screw. Pumps of this type were first developed for rocket motors, to increase the head sufficiently to prevent cavitation in the main impeller, of axial or mixed flow design at very high suction specific speeds ($N_s > 2$). Inducer pumps are less efficient than mixed flow pumps, typically $\eta_D = 0.5$–0.65 compared to 0.65–0.9 for mixed flow pumps. The optimum application is where an inducer is used to enable a mixed flow pump efficiency to be maximized for hump and operational conditions on a craft with design speed of 80–90 knots.

Pump efficiency η_p

Mixed flow pumps design for water-jet applications typically have hydraulic efficiency in the range 0.85–0.92. Inducer pumps may be expected to have efficiency in the region of 0.8. Axial flow pumps generally operate at efficiencies of 0.75–0.85, while centrifugal pumps may be expected to operate between 0.85 and 0.93. All pump types will normally be designed with downstream guide vane systems which recover energy by eliminating swirl from the jet flow.

These generalized data may be found useful for initial selection purposes, though information from the manufacturers themselves is recommended to be used during detailed design. There is a strong interaction between the impeller design and both the intake and the nozzle, so several iterations may be required before the optimum total system is found.

Water-jet selection

Preliminary assessment can be made using the procedure in Fig. 15.32. Having identified the desired thrust and power input, the pump characteristics need to be checked, so as to allow matching with power plant and gearboxes. Approximate sizing may be carried out based on charts such as the preliminary selection chart from KaMeWa, Fig. 15.37. A summary listing of larger jet units from the main suppliers is given in Table 15.5.

The ideal water-jet system should have the following characteristics:

- high hydraulic efficiency at design flow rate;
- freedom from cavitation over the desired range of operating craft speed and power;

- minimum pump diameter and so weight for a given nozzle size;
- pump speed to match standard (lightweight) gearboxes;
- tolerance to unsteady flows.

These requirements normally result in selecting a high specific speed N_s and also high suction specific speed N_{ss}. The procedure is best illustrated by an example.

Example

Consider selection of a water jet to power the SES with resistance curves as shown in Fig. 15.44. Two waterjet units will be selected, one in each sidehull, so craft resistance/2 is used for selection.

Required thrust at design operating point of 50 knots (25.7 m/s) is

$$T_{pi} = 40\,000 \times 0.5 \times 0.95/1.0 = 19\,000 \text{ kg}$$

where $(1 - w) = 0.95$ and $(1 - t) = 1.0$. Assume the following system efficiencies for first pass estimating:

η_i	= 0.85	inlet efficiency
η_n	= 0.99	nozzle efficiency, leading to a first pass
η_j	= 0.72	jet efficiency (Fig. 15.31)
η_p	= 0.91	pump hydraulic efficiency
η_r	= 0.99	relative rotative efficiency
η_t	= 0.97	transmission efficiency

$$\text{OPC} = \eta_p \eta_r \eta_j \eta_H \eta_t = 0.662 \text{ (based on } \mu \text{ rather than } \mu_w)$$

Then

$$T_p = T_{pi}/(\eta_p \eta_r \eta_j)$$
$$= 19\,000/0.65 = 29\,230 \text{ kg required}$$

Power required is then

$$N = T_p V_c/(1000/9.81\ \eta_t) \text{ kW}$$
$$= 29\,230 \times 25.7/(1000/9.81 \times 0.97) = 7770 \text{ kW}$$

The thrust per kW, $T/N = 19\,000/7770 = 2.44$. From Fig. 15.37, at this power loading and craft speed, a pump loading of 3100 kW/m^2 is appropriate, which suggests a pump inlet diameter of 2.25 m. The thrust loading can be estimated from Fig. 15.44 following a line of constant power loading. This line is shown in Fig. 15.43. It can be seen that between 23 and 25 knots for this craft, cavitation is likely at full power and so full power should not be applied until the craft has accelerated beyond 25 knots.

To check the validity or our original efficiency assumptions we may proceed as follows. Let nozzle area be 40% of inlet area, which is typical,

$$A_j = 0.4\ \pi/4 \times 2.25^2 = 1.59 \text{ m}^2 \quad (D_j = 1.423 \text{ m})$$

The inlet velocity to the water jet is

$$V_w = (1 - w)\ V_c = 0.95 \times 25.75 = 24.46 \text{ m/s}$$

From

$$T = \dot{m}\ (V_j - V_w) = \rho\, A_j\, V_j\, (V_j - V_w)$$

we can derive

$$V_j = 0.5\ (V_w + [V_w^{\ 2} + 4\ T/\rho\ g\ A_j]^{0.5} \tag{15.115}$$

so

$$V_j = 48.8 \text{ m/s} \qquad \mu = 0.5266$$

and

$$\eta_j = 2\,\mu/(1 + \mu)$$
$$= 0.69 \quad \text{which compares to the 0.72 assumed initially}$$

The actual jet efficiency will be slightly reduced by the height of the water jet above the keel, but is likely to be enhanced by the hull interaction effects so that the originally assumed 0.72 might be achieved after optimization.

The impeller diameter will be approximately 1.4 times the inlet diameter, i.e. 3.15 m. If cavitation is to be avoided then tip speed should be less than 46 m/s and so the pump speed should be less than 278 rpm (4.63 rps).

$$Q = V_j\, A_j$$
$$Q = 48.8 \times 1.59 = 77.6 \text{ m}^3\text{/s}$$

The pump head is

$$H = V_j^2/2g\ \eta_n - \eta_i\ V_w^2/2g + h_j \text{ m} \tag{15.116}$$
$$= 0.99 \times 48.8^2/2g - (0.95 \times 25.7)^2\ 0.85/2g + 1.0 = 94.34 \text{ m}$$

or

$$H = 1000/g\ \text{N}\ \eta_p\ \eta_r/\dot{m} \text{ m} \tag{15.117}$$
$$= 1000/g \times 7770 \times 0.91 \times 0.99\ /\ (77.6 \times 1000/g) = 90.2 \text{ m}$$

We use $H = 90.2$ m. The pump dimensionless specific speed is then

$$N_s = n\ Q^{0.5}/(gH)^{0.75} \tag{15.109}$$
$$= 4.63\ (77.6)^{0.5}/(g \times 90.2)^{0.75}$$
$$= 0.25$$

Now

$$\text{NPSH} = \eta_i\ V_w^{\ 2}/2g - h_i - H_v \tag{15.118}$$

We take $h_i = h_j$, so

$$\text{NPSH} = 0.85 \times 30.5 - 1 - 0.15 = 24.78 \text{ m}$$

where h_i is the height of inlet above SWL, assumed at 1m for this calculation, and H_v the vapour pressure head of water, approximately 0.15m above atmospheric ($H_a \sim 10$m); then

$$n_{ss} = n\,Q^{0.5}/(\mathrm{g} \times \mathrm{NPSH})^{0.75} \tag{15.114}$$
$$= 278\ (77.6)^{0.5}/(g \times 24.78)^{0.75} = 39.8$$

also

$$\sigma_p = \mathrm{NPSH}/H \tag{15.119}$$
$$= 24.78/89.57 = 0.28$$

Based on these data we can conclude that the pump is in a stable region for normal operation. As craft speed reduces, while H will remain almost constant at constant power, NPSH will reduce and the cavitation number will gradually reduce to the point where cavitation is unavoidable at the impeller. For our example this occurs at approximately 25 knots.

The water-jet unit weight for this example will be in the range 8000–9000 kg, see Fig. 15.45 which presents generic data which are applicable to the main manufacturers. For initial selection, the middle of the weight range may be used, until a design check against specific supplier pumps has been carried out.

Overall propulsive efficiency

If we consider the results of the calculation above and compare with open water propellers and the likely range for water jets, the following data are relevant:

Propeller	35 knots	Water jet typical	30–50 knots	Example 50 knots
η_0	0.663	η_{inlet}	0.80–0.95	0.85
		η_{jet}	0.70–0.85	0.72
		η_{pump}	0.85–0.95	0.91
		η_{nozzle}	0.99	0.99
η_t	0.97	η_t	0.97	0.97
η_H	0.985	η_H	1.052	1.052
for $w = 0.05$, $t = 0.065$		for $w = 0.05$, t = 0		
η_D	0.633	η_{opc}	0.495–0.795	0.662

It can be seen that water jets have a large range of possible efficiency dependent on the system component performance. Careful integration of system components into the SES hull design is necessary, aimed at optimization of the intake geometry and jet nozzle velocity, in order to achieve OPC in the range 0.65–0.7 for an SES.

Once a typical water-jet sizing and OPC have been assessed, the designer should be in a position to make an assessment of the powering needs for the craft, including selection of reduction gearboxes and review candidate water jets from published information. Detail design would continue by making detailed studies in liaison with the suppliers.

Steering and reversing gear

Water-jet systems may be fitted with rotatable nozzles and deflector vanes to redirect the jet forwards under the hulls to give reverse thrust, see Figs 15.30 and 15.31. On large craft fitted with four water jets, it is normal to install this steering equipment on the outer jets only. This is because a relatively small deflection of a water jet produces

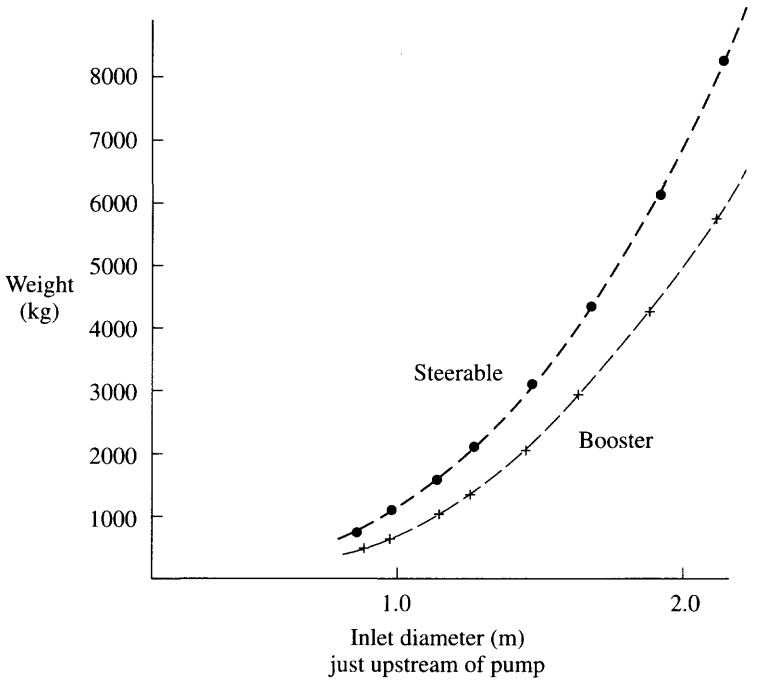

Fig. 15.45 Water jet weight vs inlet diameter.

high turning forces in comparison to a marine rudder. In addition, considerable weight is saved by installing non-steerable jets (see Fig. 15.45).

At full power, the side force generated by a jet deflected by 6° will be 10%. The available reverse thrust may be expected to be 30–40% of the maximum static thrust for the system. Reverse thrust can be selected at high speed, for rapid deceleration, though as the vessel slows, power must be reduced, to avoid cavitation at the impeller.

Reversing is achieved by a bucket or deflector plate system, depending on the supplier. Examples of two different approaches which both deflect flow under the hull transom can be seen in Figs. 15.30 and 15.31. Hydraulic cylinders are used to rotate the deflector bucket components about their hinge joints. Since relatively high forces are generated – the reactive force on the bucket itself may be as high as twice the design thrust – these components must be carefully designed. These loads are transmitted directly back to the transom flange mounting via the pump casing, thus the hull structure in this area must also receive careful attention.

If the deflector system is partially deployed, jet flow can be distributed so as to give zero net forward thrust, while engine power is set at the maximum allowable for the craft speed. Since operation of the deflectors is rapid, maximum thrust can be obtained very quickly, giving high craft acceleration to cruising speed.

Integrated control systems

Water-jet units are remotely operated from the wheelhouse via an electro-hydraulic system, an example of which is shown in Fig. 15.31. Operation can be designed

around combined thrust/steering levers, steering wheel, tiller, or a single joystick for all the water jets on a vessel controlling the units via a programmable system. Digital electronics are used to control engine/pump speed and monitor status of the system components. Back-up systems for operation of individual units by on/off levers and push buttons for steering, reversing and engine power are also provided. Examples of these systems are shown in Fig. 15.46.

While it is possible to control engine speed, thrust and steering manually, the convenience of a computer-controlled integrated control system has made it the primary choice for designers. These systems form an integral part of the water-jet system and so are designed by the same suppliers as the water-jet units themselves. It is now also possible to link this control system to an autopilot.

Prior to completing detailed design therefore, the SES designer will need to identify the hydraulic power, electrical power and electronic systems requirements for the units, to be included in the specification of auxiliary power and electrical services.

15.6 Power transmission

The power transmission system in an SES or ACV should be designed with minimum weight in mind. This approach implies that engine and fan, propeller or water jet are as close together as practical. The greater the distance between the two, the greater the challenge of providing transmission shafting which is stiff (to avoid whirling) and light (to minimize the problems of dynamic balancing).

There is often a trade-off between reduced distance and introduction of gearboxes in an SES for main propulsion engines, particularly for propeller-driven craft due to the narrow sidehull width. Where a reduction gear is needed anyway, this is not a particular problem. The design of smaller SES is also challenged by the vertical CG if engines have to be located above the sidehulls. It is common practice therefore to widen the hull towards amidships to accommodate engines within the hull depth. Water-jet systems require a significant keel width to optimize flush inlet design. This eases design of hull lines to accommodate engines immediately forward of the jet units.

ACVs are particularly sensitive to changes in CG. Since main engines are the largest mass apart from the passengers or cargo, their positioning influences the sizing of the ballast system for trim. Craft with separate lift and thrust engines are easier to optimize in this respect. The optimum position for propulsion devices is at the craft stern, while engines located towards the craft centre reduce required trimming ballast and craft rotational inertia so making it more manœuvrable.

Designers will investigate different machinery arrangements at an early stage, to identify the sensitivity of their concept to payload variations and high/low fuel payload. The effect of layout changes on transmission arrangements may then be checked and an optimum chosen.

Before discussing transmission components, the design criteria should be stated. If the maximum operating torsional stress is q, the following factors for limiting stress design have been specified in the UK British Hovercraft Safety Requirements (the BHSRs) [115] (Table 15.6). The reasoning behind these design factors is to give an acceptable margin against unsteady stresses due to engine start-up and acceleration/

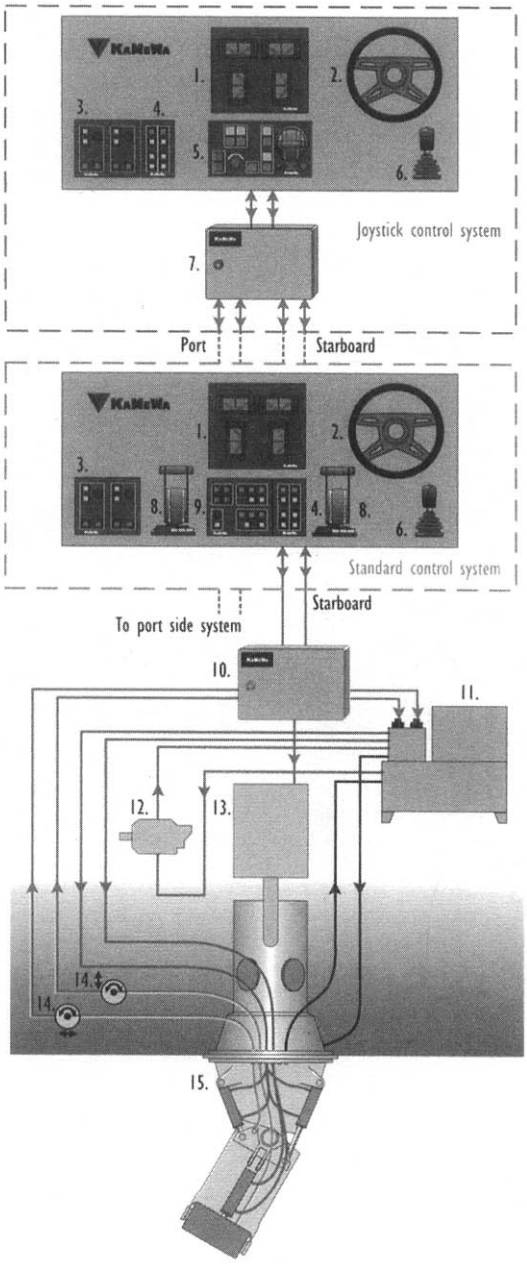

Fig. 15.46 KaMeWa control system components.

Table 15.6 Transmission shaft design factors

Engine type	Proof stress factor at q	Ultimate stress factor at q
4-cylinder engines	0.50	0.33
5-cylinder engines and greater	0.67	0.44
Gas turbine engines	0.75	0.50

deceleration of the propulsion device against its rotational inertia as power is increased or reduced. The response of reciprocating engines is much faster than a gas turbine, so exerting higher accelerations, demanding a higher design factor. In addition it is necessary to build in design margins against the uncertainty of material properties, approximately 15–20% of the 25% margin allowed for gas turbine engines in this case.

These factors are likely to control the design for steel transmission shafts, while for aluminium or composite shafting it may be found that fatigue will govern the dimensions. Lloyds, in their Special Service Craft rules, Part 13 – Shaft vibration and alignment [116], give empirical formulae for shaft design stresses including different couplings and bearings which will be useful to the designer at the detail stage.

Design stresses

A shaft is designed to transmit torque, where

$$T_q = \frac{N \times 746\, g}{2\pi n} \text{ kg m} \quad \text{or} \quad \frac{N \times 33\,000}{2\pi n} \text{ lb ft} \tag{15.120}$$

where T_q is the torque and N the transmitted power in kW or shp. The maximum stress in the outer fibre of the shaft is determined from

$$q = T\, r/J \tag{15.121}$$

where q is the maximum shear stress, r the shaft outside radius and J the polar moment of inertia of shaft cross-section,

$$J = \pi\, r^4/2 \qquad \text{for a solid shaft} \tag{15.122}$$

$$= (r^4 - r_i^4)\, \pi/2 \quad \text{for a tubular shaft with inner radius } r_i \tag{15.123}$$

Since the polar moment of inertia is related to r^4, clearly tubular shafts will be much more efficient than solid shafts. Larger diameter thin-walled shafts also have the benefit of greater stiffness. If high strength material (aluminium or steel) is used to further save weight, it is likely that welded joints may not be practical as the weld strength would control the design. In this case, shafts machined from solid may be required, with the consequent costs involved. Unless weight is critical, a compromise is usually reached between shaft diameter and material and the design of end connections.

A number of design cases need to be analysed for each section of shafting to establish acceptable dimensions from the quasi-static design approach, see Fig. 15.47, based on the design factors in Table 15.6. This will lead to a table similar to Table 15.7. The dimensioning load case will be identified by inspection, generally cases (3) or (5). Other load cases are needed for subsequent fatigue analysis. This analysis must be

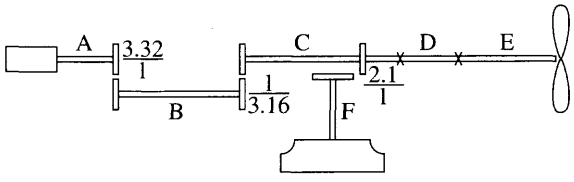

(*a*)

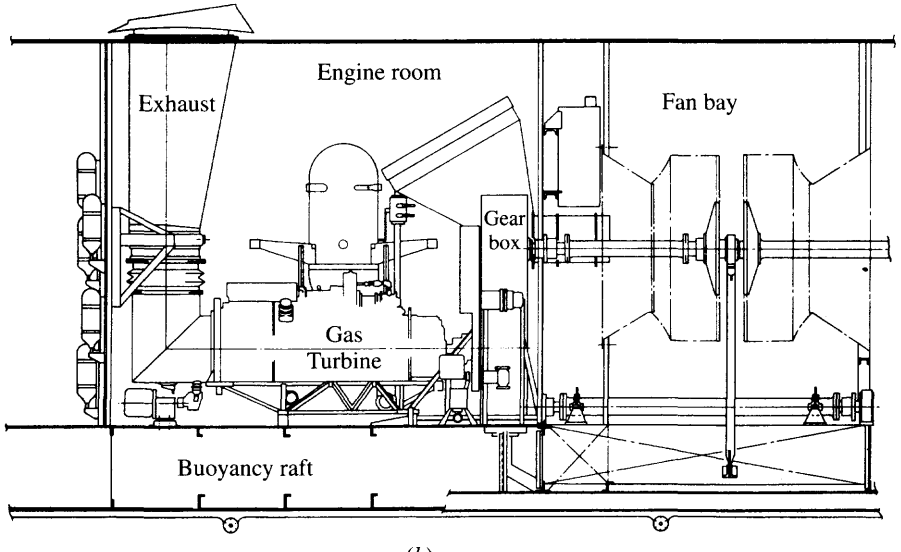

(*b*)

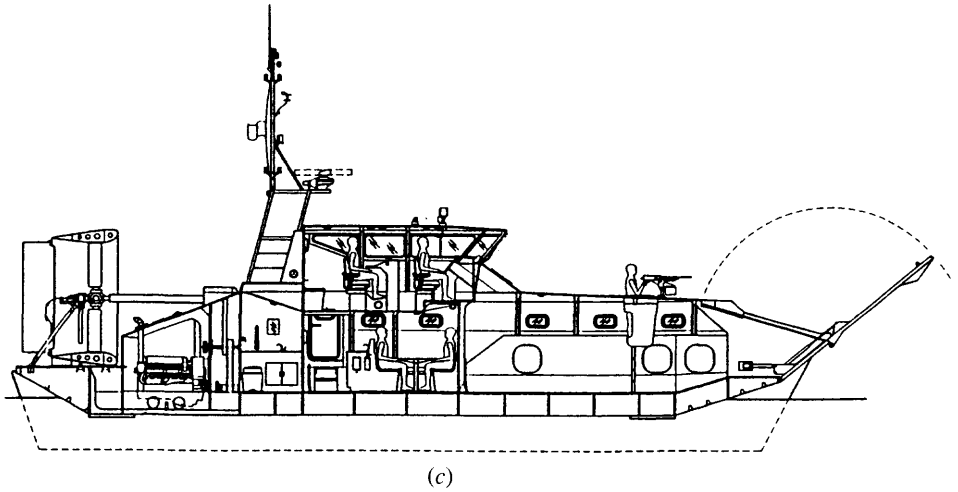

(*c*)

Fig. 15.47 Shaft sections for analysis: (a) BHC SR.N6; (b) Vosper Thornycraft VT.1; (c) ABS M10.

Table 15.7 Shaft design load case matrix

Load case	Engine (RPM)	Shaft (RPM)	Power (kW)	Shaft torque (kg. m)	Maximum stress (unfactored)	Running (Hours)
1 Static hovering						
2 Slow manœuvring						
3 Near hump						
4 Cruise light seas						
5 Cruise design seas						
6 Maximum speed calm						
Total						

repeated for each section of shafting between an engine and the fan, propeller, pump, or combination being driven. During detailed analysis once bearings and gearboxes have been selected, the power absorption by these devices can also be included.

Whirl speed

If a shaft is not exactly concentric, or has out of balance weights attached to it, a force will be generated as the shaft rotates, creating a bending moment along the shaft between its supports (the bearings). The shaft will deflect due to the force and this will increase the bending moment, so further increasing the deflection. The resistance generated by the shaft will be linear with deflection and proportional to its stiffness EI. The out of balance force due to a mass m, distance x from the shaft centre is

$$F = m\, x\, (2\, \pi\, n)^2 \tag{15.124}$$

The force generated increases as shaft speed squared, so it may be seen that at low speed the deflections will be small and the shaft stiffness will enable a stable condition to be reached. It is normal to assume that the shaft behaves like a simply supported beam with pin joints to calculate the resisting forces. If the force is increased beyond the point where stresses generated in the shaft from its deflection reach yield (the limit of proportionality) the restoring force increment will be reduced and instability will occur. The response is called whirling and the speed at which instability occurs is known as the whirling speed, given by

$$n_w = 0.5\, \pi\, (E\, I/(\mu L^4))^{0.5} \tag{15.125}$$

where n_w is the whirling speed in cycles per second, E the modulus of elasticity for the shaft material, I the moment of inertia of the shaft cross-section in bending $I_{x,y} = (r^4 - r_i^4)\, \pi/4$, μ the density of the shaft per unit length and L the shaft length between supports. The whirling speed is independent of eccentricity of the shaft and is inversely proportional to the distance between supports squared. Long transmission shafts therefore need intermediate supports to keep the design speed below whirling speed. Since the phenomenon is one of instability, it is normally recommended to stay at least 20% below n_w.

Shafts having very stiff bearings may behave more like a beam on fixed end supports, which would increase the whirling speed somewhat. SES and ACV design generally results in flexible rather than stiff structures, so it is more logical to employ self-aligning bearings to design the shafting runs so as to be well below whirling speed assuming pin-jointed supports at the bearings. For shafts with one or more intermediate bearings, it is preferable to have differing shaft lengths, so that vibration due to other dynamic forces will not affect all sections of a shaft at the same time.

Once acceptable shaft lengths between bearings have been determined, based on shaft dimensions derived from the torque requirements, an optimization might be carried out to find the lowest weight combination of shaft diameter, wall thickness, material and bearing distances.

A shaft should itself be balanced so that any exciting forces on the bearings are minimized, since the bearing life will be significantly reduced due to the unsteady loading of the rollers or balls on the bearing tracks. There will be unsteady dynamic loadings from both static imbalance and aerodynamic or hydrodynamic force variations at harmonics of the propeller blade frequency ($f = n\, n_b$, $2f$, $3f$,$4f$,$5f$, etc.). These excitations will be the main source of fatigue in the shaft.

A propeller or fan mounted on the end of a shaft will generate a vibration with a fundamental natural frequency as follows [87]:

$$n_1 = \frac{\pi}{2}\left[\frac{EI}{I_D\,(b + L/3) + (W_p b^2/g)(b/2 + L/3) + \mu(b^4/8 + Lb^3/9 + 7L^4/360)}\right]^{0.5} \quad (15.126)$$

where n_1 is the natural frequency in cycles per second, I_D the moment of inertia of propeller about its diameter (= half polar moment of inertia) (Note: add approx 60% for entrained water for marine propellers), W_p the propeller weight (Note: add approx 25% for entrained water for marine propellers), L the length between bearings and b the length of overhang.

This shaft section should be designed so that this frequency is higher than the design operating speed, again by a factor of 20%.

Fatigue endurance

Design for fatigue requires the dynamic fluctuations in stress in a shaft at nominally constant power to be determined. These are primarily at shaft rotation frequency and caused by out of balance causing shaft whirling and bending moments caused by masses attached to the shaft such as fans and propellers, including out of balance and dynamic vibration forces. The stress fluctuations are greatest for propellers or fans mounted on overhung shafting.

The operational profile for the craft has first to be determined, relative to the projected service hours, including cruise, slow-speed manœuvring etc., which define the engine speed and torque applied to the transmission. The shear stress in the shaft due to the torque is first calculated, i.e. the mean loading, and then the alternating stress due to the static bending moment from the principal masses, plus any dynamic bending moments due to fan/propeller out of balance.

The number of cycles to failure at a given stress amplitude can be determined from a standard S–N curve, for example Fig. 15.48. The degradation as a portion of the

total fatigue life of the shaft material is determined for that stress amplitude and number of cycles experienced by the craft. The total degradation is then calculated by summing the components of the craft operational profile, the Miner sum. The fatigue service life can then be estimated by the reciprocal of the degradation, assuming that the operational profile does not change. If N_i is the total number of cycles at σ_i for fatigue failure and n_i the number of cycles experienced by craft over operational period (days, months or years) then

$$D_i = n_i/N_i \tag{15.127}$$

$$\mathrm{D} = \sum_{i=1}^{n} n_i/N_i \quad \text{referred to as the Miner sum} \tag{15.128}$$

$$L = 1/D \quad \text{endurance in days, years or operational cycles} \tag{15.129}$$

The accepted factors between calculated fatigue endurance and design fatigue life are 3 for components which can be regularly inspected and replaced and 10 for components which cannot be inspected. The reason for this is that crack initiation is rather uncertain in metallic materials. It is sensitive to microscopic inclusions, surface finish and surface corrosion, especially pitting.

ACVs and SES operate in an environment where corrosion is an important issue. The design factor of 3 represents the average uncertainty for the data in *S–N* curves such as Fig. 15.48 and so if shafts are likely to be subject to surface corrosion in

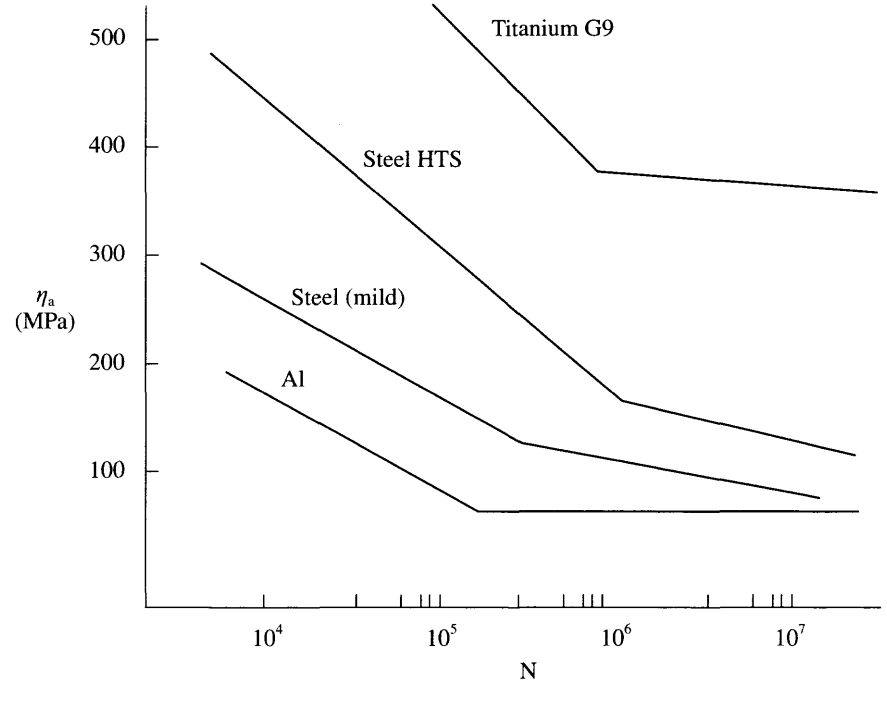

Fig. 15.48 *S-N* curves for fatigue analysis of transmission shafts.

service, a 'corrosion allowance' should be added, in the same way as structural member scantlings are increased. Corrosion protection coatings can be an effective alternative, so long as regular inspection allows coating damage to be repaired. A combination of corrosion allowance and coating can be used to increase the inspection intervals by allowing some degradation before repair. Shafts which are not inspectable need to incorporate a corrosion allowance consistent with the craft design life and operational environment.

Craft design life is a key issue for designers, as it can add significant cost. An operator would typically expect that an ACV or SES would have a useful operating life before replacement of at least 20 years and perhaps in excess of 30 years with some repair work to the main structure. It is suggested therefore that transmission shafts should have a design fatigue life exceeding 75 years from analysis.

Couplings, bearings and supports

There are a wide variety of design options available to the ACV and SES designer for shaft bearings and couplings. Smaller craft can use systems adapted from automobile practice, while larger craft, particularly SES, use lightweight marine transmission components.

To reduce vibration, main engines are often flexibly mounted, so that a flexible coupling is also needed between it and the reduction or vee drive gearbox. Such couplings are often also used between sections of shafting to accommodate flexure of the craft structure in operation. Axial movement can be accommodated using splined shaft couplings.

Shaft sections may have bolted flanges for connection, or if the shaft end is solid, mechanical tapered locking sleeves or hydraulic locking can be employed for connecting devices, gearbelt pulley mounting, or direct mounting of propellers or impellers.

Shaft connections have to comply with the same design requirements as the shafts themselves. Having determined the design torque and fatigue loadings for a shaft these data can be used to select a suitable coupling based on performance data given by the manufacturer. Where bolting is used to secure couplings, vibration resistant locking devices will need to be installed. Flail guards are also necessary to protect against failure of universal joints on smaller craft.

Shaft bearings may be of ball or roller type. Roller bearings are more suitable for higher torque loadings as the surface pressure is lower on the race, leading to longer service life. A roller bearing, particularly the taper roller type, provides bending moment capacity and so is suited to support cantilevered propeller or water-jet pump shafts. Taper roller bearings are also able to resist the thrust loading from a propeller.

Selection of bearings is carried out initially from manufacturers' standard data, followed by direct advice. The service life rating of most bearings is based upon industrial or automotive applications and may not be conservative compared with ACV or SES use which involves frequent power level changes and start/stop cycles. The operational life of bearings in SES and ACVs before replacement is likely to be 5–10 years rather than the full craft life. Unplanned removal and replacement would cause unnecessary downtime for a craft, so such components are best selected with care.

Reduction drives and gearboxes

Utility ACVs driven by diesel engines in the power range to around 600 kW are able to use toothed non-metallic belt drive rather than gearboxes. Toothed belt drives generate very little noise and require no lubrication. Protection from foreign objects and airborne sand/grit is advisable to prevent unnecessary wear of the belt and toothed pulley surfaces. Pulleys are fabricated in aluminium alloy for minimum weight and coupled to the transmission shafts by bolted flange or taper locking interference friction couplings. Selection of pulley diameters and belt width is based on power to be transmitted, the design torque and the reduction ratio.

The principal market for this type of drive is industrial machinery such as heating and ventilating fans. Suppliers (Goodyear, Uniroyal and Fenner are examples in UK/Europe) are therefore familiar with power transmission from electrical motors, but less so for diesel engine transmission applications. The recommendations for selection are likely to be conservative and need some discussion and interpretation by the ACV designer. Larger craft such as the BHC SR.N series in the 1970s have used gearboxes specially designed and built for the application. More recently, standard lightweight industrial gearboxes have been used on some utility ACVs as an alternative to toothed belts.

SES use lightweight marine gearboxes which are manufactured in standard ranges by a number of suppliers. Manufacturers of marine gearboxes now supply ranges which allow matching of propellers, water jets and other equipment such as lift fans to the main engine types available.

A gearbox consists of a cast steel or aluminium housing containing a series of gearwheels which change the direction (parallel, right angle, vee or U drive) and/or speed of the output shaft relative to the engine input. The gearwheel shafts rotate on bearings locked into the housing. Shaft direction of rotation is reversed (e.g. clockwise to anticlockwise) unless an intermediate gearwheel is included. Support on both sides of gearwheels reduces moments applied to the bearings reducing loading and wear. References 115, 116 and 117 give guidance on gearbox design.

Bearings have to absorb any axial forces developed by gearwheels, which can be significant in the case of bevel gears and spiral cut parallel gears. In addition the gearbox may be designed to react to the propeller thrust rather than have a separate thrust bearing. This favours the use of taper roller bearings.

Gearwheels transmit torque across a line contact between the intermeshing tooth profiles. The geometry is designed to give rolling contact on the pitch line at which maximum load is transmitted, and sliding on entry and exit which is limited so as to minimize surface wear. Gearwheel service life is therefore dependent on efficient lubrication.

In a similar way to shafting, gearbox design varies according to the type of driver. Reference 116 suggests application factors for gear teeth as follows:

Driver	Coupling	Application factor K_A
Gas turbine		1.15
Diesel engine	Hydraulic	1.10
	Elastic (flexible)	1.30
	Other (e.g. bolted flange)	1.50

Higher factors apply where increased unsteady loadings will occur at the gearwheels. Further design issues for gears are provision of sufficient line contact to transmit the torque, which controls diameter and gearbox width. The tooth profile has then to withstand the bending moment generated at the contact line and transmit this back into the body of the wheel. Since teeth are cyclically loaded each revolution, the highest stresses in the tooth must be kept below the endurance limit of the material for fatigue based on normal service conditions. Craft operations above normal service limits which are infrequent must be checked to ensure fatigue degradation is acceptable and that surface contact pressures are still within the required limits.

The torque which can be transmitted and the rate of wear is also a function of the material surface hardness. The higher the strength/hardness, the more compact a gearbox can be for a given power rating. Gearwheels are surface hardened by carburizing. The wheel is heated to 900–950 °C in a furnace in the presence of hydrocarbon gasses so that carbon is absorbed into the steel. The depth of the hard case formed, normally between 0.5 (light) and 1.5 mm (heavy), is dependent on the exposure temperature and time. Gearwheels are normally hardened to a heavy specification for maximum resistance to wear.

Gearwheels are first machined to design geometry and either ground or honed to final surface finish after case hardening. Manufacturers of standard-range gearboxes design according to rules such as [116] and provide certification to that effect on request by a client. Gearboxes which are designed as one-off special units may also be designed to Classification Society rules, though costs would be higher due to the verification analysis for the unit.

Larger gearwheels are manufactured in the form of a ring carrying the teeth which is bolted to a separate boss/shaft. Heat treatment of the ring is then easier, with less tendency to distortion during treatment and quenching.

Typical power losses in a gearbox are 0.5–1.0% of transmitted power (for SES and ACV applications). This is transformed into heat at the gear teeth. Lubricating oil is usually transferred through holes in the casing walls from a suction at the bottom of the gearbox so as to spray the gear teeth on entry and exit from meshing. This assists heat dispersion and also minimizes noise generated. Spur or straight cut gear teeth produce greater noise than spiral cut teeth. High-speed marine gearboxes are therefore spiral cut. Many gearboxes include integral power offtake and hydraulic pump for circulation of lubricating oil and clutch operation if this is needed.

Monitoring of gearbox condition is normally by continuous measurement of lubricating oil temperature and pressure and inspection of lubricating oil filters or gearbox magnetic plugs at preset intervals for metallic particles which are evidence of wear. Oil temperature is a key variable since it represents the heat being dissipated. If the gears are badly worn this will increase.

Figure 15.49 shows a sample gearbox power flow diagram for a permanently meshed reversing marine box with integral hydraulic clutches. The unit itself is depicted in Fig. 15.50.

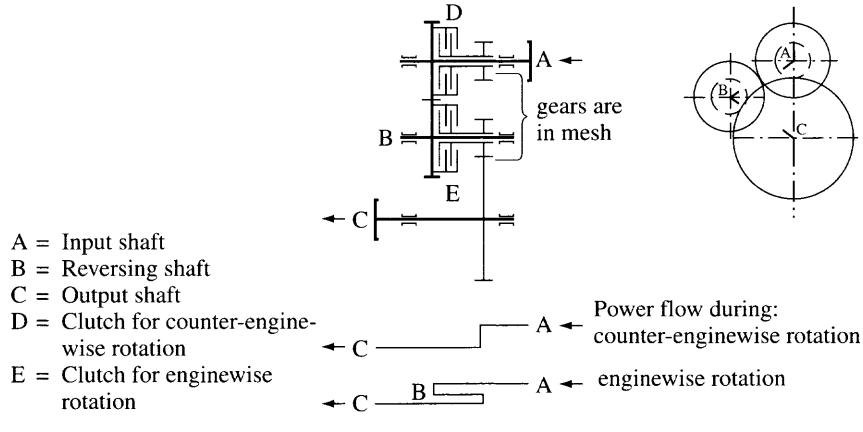

Fig. 15.49 Gearbox power flow diagram.

15.7 Surface contact propulsion

Design considerations

The use of surface contact propulsion is normally to push or tow an air cushion platform across sensitive terrain to deliver heavy or bulky equipment to a remote site. Examples are hoverplatforms which are towed across ice from supply ships to deliver provisions along the north coast of Russia, platforms used to deliver contruction equipment across tundra in the north of Canada and north-east China, and platforms used as river ferries across rivers which ice over in the winter. Fig. 15.4 illustrates some of these.

The platform speed is governed by the chosen propulsion means, either towage by tractor, winching for river ferries, or hydraulically driven balloon wheels from power on board. In special cases Schottel units have been used to propel platforms over water and air jets have been used for propulsion or control assistance.

Brief guidelines

The main design considerations are the craft drag, mainly skirt contact drag over the appropriate terrain (see Chapter 3), which determines the pulling force, wind forces on the platform and gravitational forces when climbing or traversing slopes over land.

Towing a platform into wind on flat terrain or pulling directly up a slope is straightforward to analyse. If a platform meets a side wind, or cross slope, the situation becomes more complex. If the propulsion system is to be directly mounted on the platform and slopes to be traversed are significant, then contact wheels at both ends will help control the unit. The ground contact force of the propulsion unit should be sufficient to resist side wind forces and gravity forces on a side slope. A starting assumption may be a slope of 1 : 10 or approximately 6°.

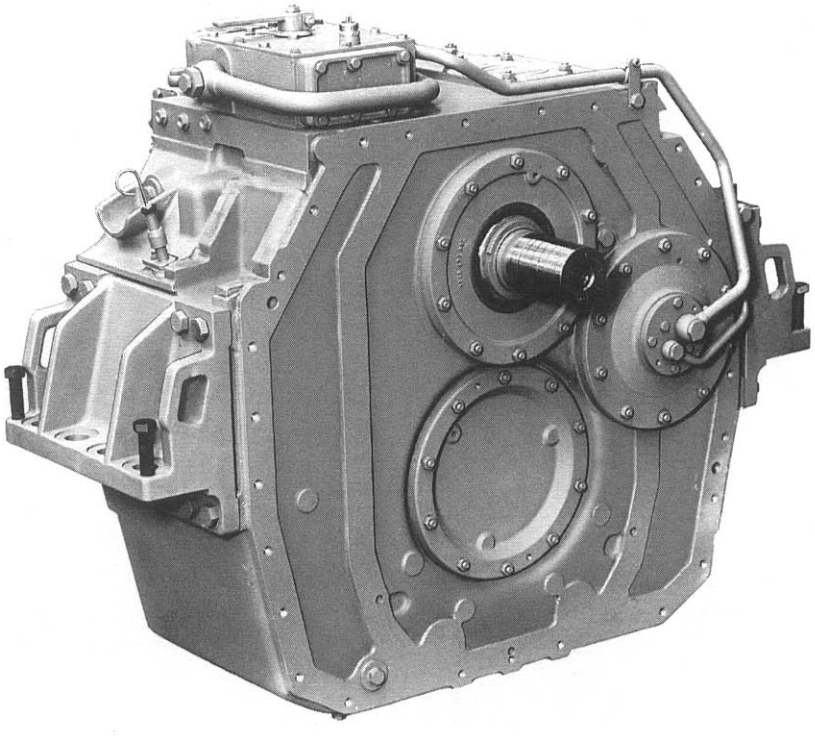

(a)

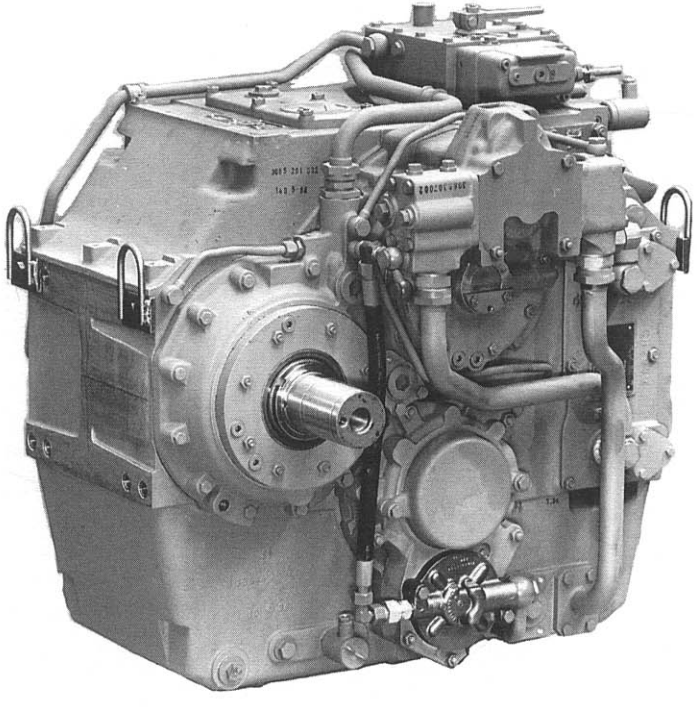

(b)

Fig. 15.50 ZF gearbox type BW 450.

If the platform is to be towed, if the terrain is very open, for example over an ice field, then it may be acceptable for the platform to be towed skewed downwind, though the addition of a smaller vehicle with a control line at the stern will improve manœuvrability significantly.

16

Power unit selection

16.1 Introduction

An ACV or SES requires power for propulsion, air cushion and for electrical and other systems on board. Depending on the craft size, all the needs may be supplied by one motor, or one or more units may be installed for each individual function.

The first step towards power unit selection is to identify the power requirements for each of these functions. A methodology for this is given in section 16.2. Selection of the optimum power unit for a particular SES or ACV also needs consideration of a number of parameters, as discussed below.

Consistent with the approach throughout this book, we approach power unit selection from a 'user' point of view, with a summary of aspects relating to use for fast marine craft. Detailed background on marine diesel and gas turbine engines can be found in textbooks such as ref. 117.

Power units for ACV and SES should be selected and rated with care. A touch of conservatism is advised! Optimism has in the past resulted in craft with limited power margins, and operation at or above MCR (Maximum Continuous power Rating) leading to much reduced MTBO (Mean Time Between Overhaul). Negative consequences include higher noise, vibration and fuel consumption. Care should also be exercised in interpreting engine manufacturers power ratings to ensure that the appropriate duty cycle is being used for reference. In order to obtain a reasonable time between overhauls, it is important for the ACV or SES designer to clearly identify the average cycle time between starts, and the times at service speed, idle, etc., based on the craft intended service.

Total system weight

The ACV/SES designer's primary target is minimum total installed weight for the power unit system. This includes the engine itself, the transmission system of gearbox and shafting, auxiliary systems, enclosures and skid mountings, and the fuel payload required for the craft mission. By achieving this, the useful payload can be maximized. Including the fuel takes account of the craft range necessary for its service

requirement and the engine fuel efficiency. Initial weight estimates have been outlined in Chapter 11.

Fast marine craft have been designed and built with steam turbines, nuclear power plant, electric motors, gas turbines and reciprocating engines fuelled by gasoline and diesel fuel. Steam and nuclear power plant can be designed for very high power ratings, but are not suitable for small craft. The same applies to electric drive, which is normally powered by a steam generator system. While project proposals have been made for large ACV and SES with nuclear power plant for example, so far, the engines which have been successfully applied are gas turbines and diesel engines, and gasoline engines on light ACVs

In most countries regulations for passenger-carrying vehicles prevent the use of fuel with a flashpoint of lower than 35°C, consistent with paragraph 7.5.8 of the IMO High Speed Code [118]. Diesel fuels normally have flashpoints between 65 and 120°C, kerosene and gasoline 33–50°C. For fuels with flashpoint below 43°C fuel tanks have to be physically separated from machinery spaces and inboard of shell plate and bulkheads which might be damaged in a collision.

Gasoline engines (referred to as petrol engines in Europe) are suitable for small recreational and utility craft, but due to the volatile nature of gasoline, are not generally suitable for commercial vehicles. This leaves gas turbines and diesel engines as the primary candidates for SES and ACVs. Marine gas turbines are lower in weight than diesel engines, but in general have higher specific fuel consumption. For endurances longer than about 12 hours the total installed weight for a high speed diesel system is least, as shown in Fig. 16.1.

Where the total installed power required is very high, for example for large SES, the only practical option is a gas turbine system. While multiple high-speed diesels could be linked to the same output shaft, this would add to the weight with additional

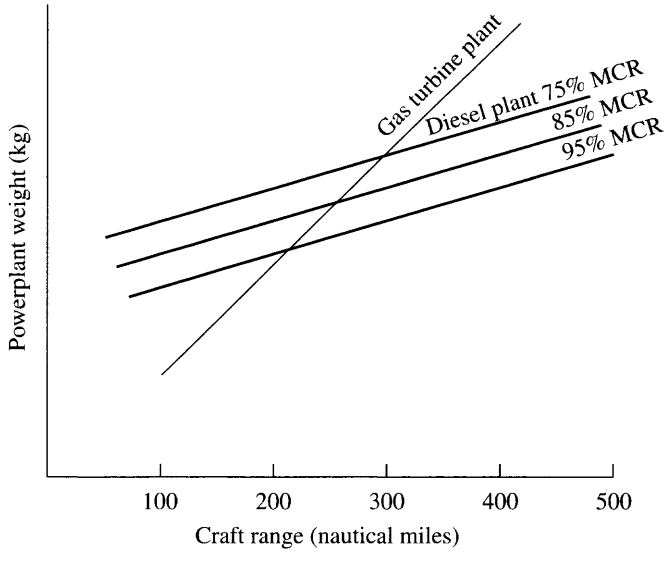

Fig. 16.1 Total installed weight vs craft range for different power settings.

gearboxes and shafting. Craft range for large SES is therefore limited by the fuel load which can be carried without reducing the payload for goods or passengers below the designer's target.

Engine power ranges

Engines are available in a limited range of power ratings and so the designer often has to adjust craft sizing or mission parameters to optimise around the chosen motor(s). Figures 16.2 and 16.3 show examples of diesel and gas turbine engines which have been used for ACV and SES to date.

Engine suppliers are constantly improving their products, mainly in response to demands from the industrial and marine markets which procure many thousands of units each year. ACVs and SES are too small a market to justify more than minor adjustments to the base product.

Multiple engines

Except for craft smaller than 1000 kg payload it is generally convenient to install multiple engines. This has an additional safety advantage of redundancy in the case of failure, so long as the craft design takes this into account by ensuring an acceptable emergency performance with one engine only.

It is normal on medium-size craft to install dedicated diesel motor/generator sets for auxiliary power. Dependent on the range of services required, these motors may be duplicated. Starting power is by battery, which is also used to supply the emergency power system on board an SES or ACV. Generator sets on an ACV need to be air cooled, or liquid cooled by a closed circuit system. The latter type is much quieter, but has a weight penalty. SES can use open circuit cooled units, saving the weight of the

Fig. 16.2(a) Aircooled Deutz diesel installed in Griffon 1500 ACV.

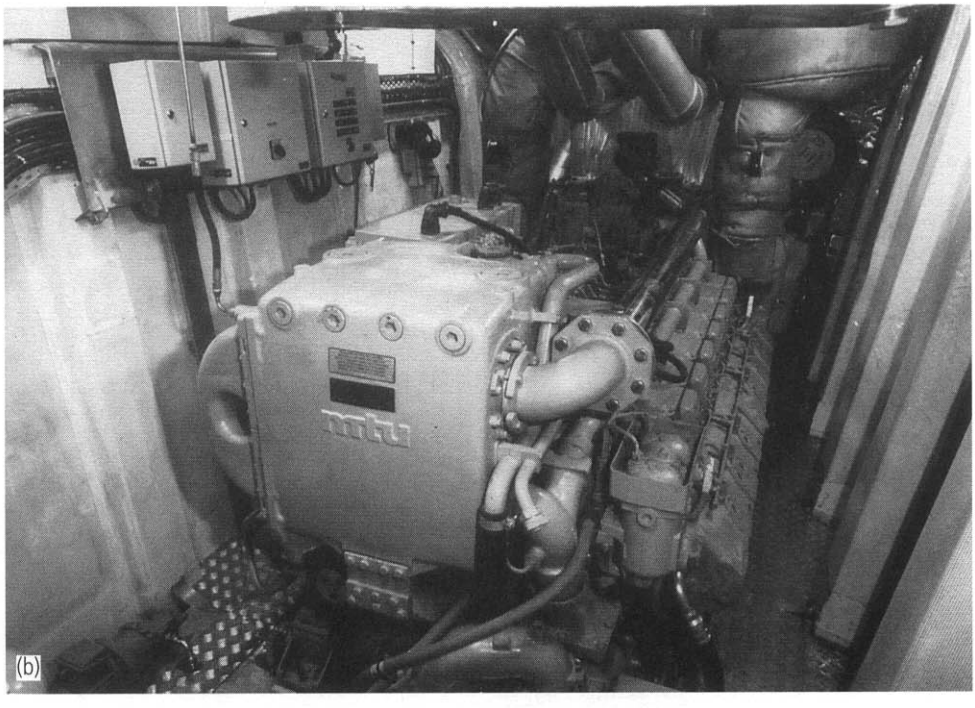

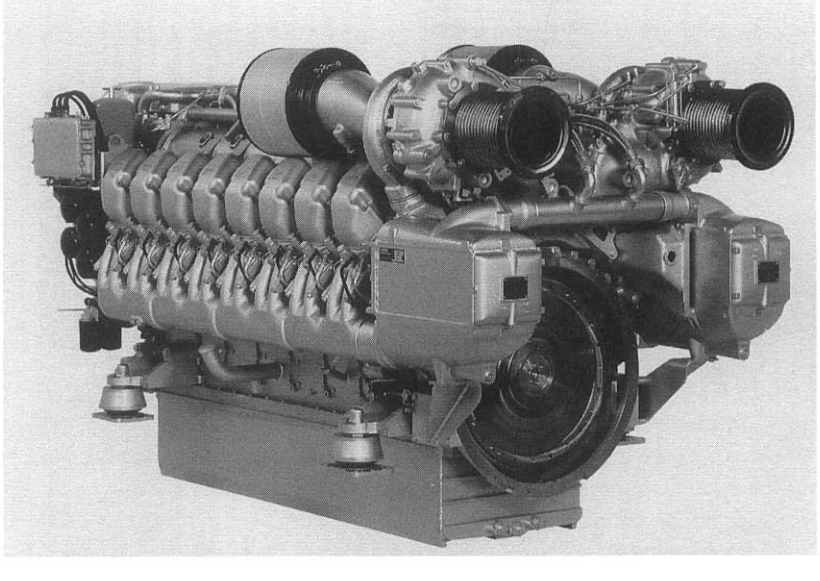

Fig 16.2 (b) MTU TB 396 installed in an SES side hull; (c) MTU 4000 V16 diesel engine.

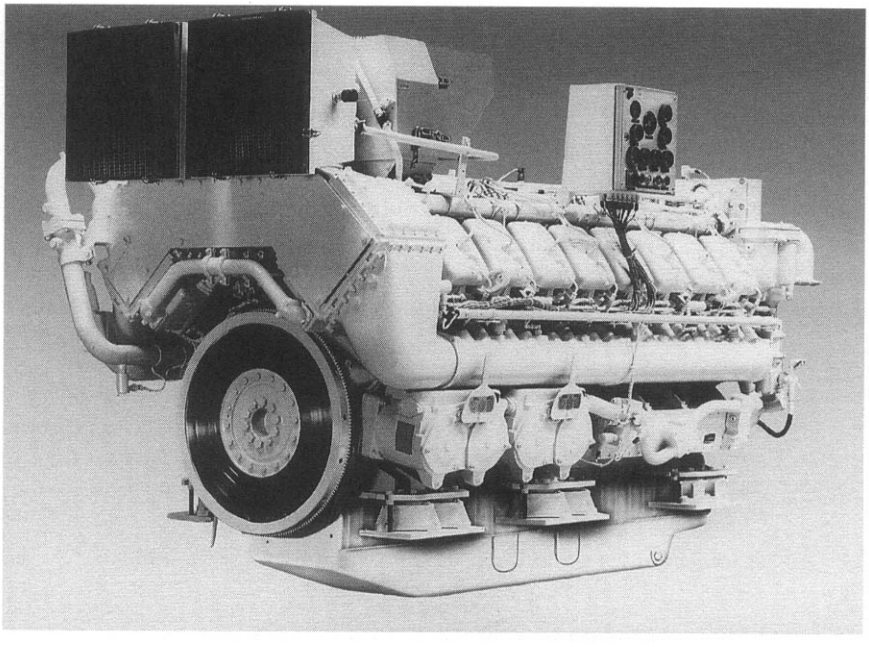

Fig. 16.2(d) Deutz MWM TB 32 V16 water cooled diesel.

heat exchanger, at a penalty of introducing a small drag component from the cooling water intake, and the need to use specifications for the cooling system and generator which are corrosion resistant to sea water.

Above the powering range where a single engine can supply the power for propulsion, it is convenient to install twin propulsion systems. Large SES, similar to fast catamarans, sometimes use two engines per shaft for large water jets, or four engines each driving a separate water-jet system.

Until recently suitable lightweight diesel engines were not available for power ratings above about 3 000 kW; this ceiling is now closer to 6 000 kW, so the break point above which gas turbines are the only option is being raised. For large SES, where power installations of 50 000–100 000 kW are necessary, gas turbines are the only realistic option for the foreseeable future and so interest continues to focus on improving fuel efficiency.

Engine operating characteristics

Diesel engines suitable for primary power use on an ACV have been adapted from industrial plant power units, such as the Deutz air-cooled diesel range, or from truck or heavy vehicle power units which have a closed circuit cooling system, for example Caterpillar diesels. Such engines are not normally run at maximum power and so a designer has to be careful to specify the craft operating characteristics at a power rating consistent with the mission. Most diesels will safely run for long periods (more than 3 hours per day) at 85% maximum continuous rated power (MCR), so this is a safe specification. Above 90% should only be considered for 'burst' operations of 30

minutes or less, or emergency conditions. Diesels are flexible in operation from idle at 15–20% maximum rpm up to cruise rating, and so control of lift and propulsion can be by throttle.

Gas turbines are not flexible in their operating speed. They are specified with a continuous power output, which may be varied in a range +10% and −20% approximately. This does not need to be derated for continuous use in ACVs or SES. Outside this range the available torque drops off rapidly. Gas turbine installations therefore need an independent means of thrust variation. ACVs with gas turbine powering generally have variable pitch propellers or fans. SES installed with gas turbines have thrust control systems fitted to their water jets, or variable pitch propellers.

Transmission configuration

A gas turbine has a very low specific mass (mass/kW), but due to the very high rotational speed of the compressor and power turbine wheels (15 000–30 000 rpm), a reduction gearbox is necessary to reduce this to a suitable speed for a propeller, fan, or water jet (500–3000 rpm).

High-speed diesel engines normally operate in the range 1500–3500 rpm. A gearbox is also often required, but with a reduction of 1.5–2.5. This reduction can also be

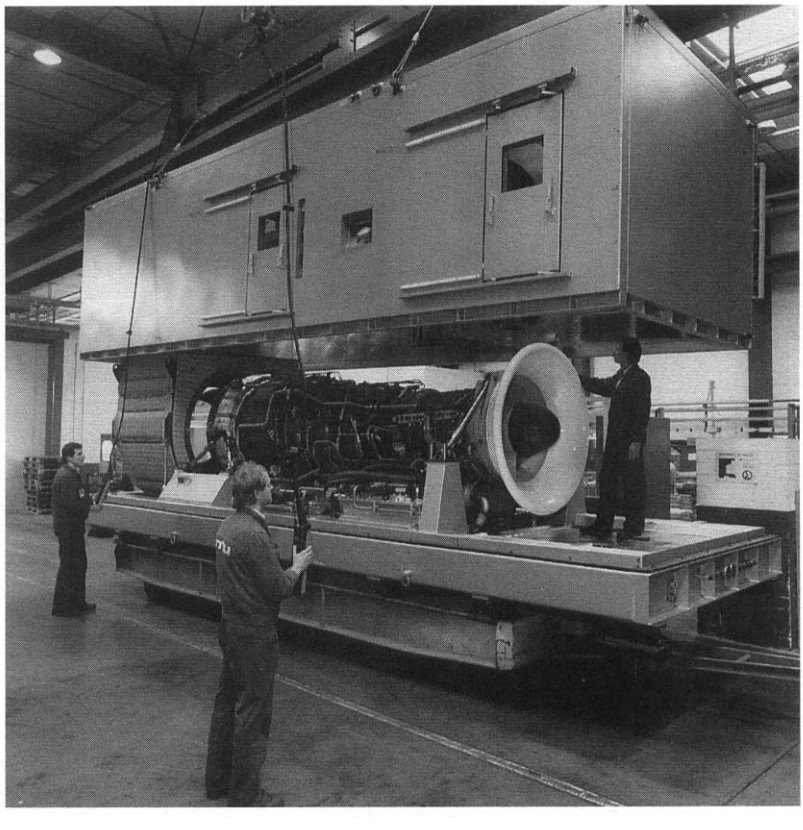

Fig 16.3(a) Kvaemer/GE LM 2500 gas turbine propulsion package.

(b)

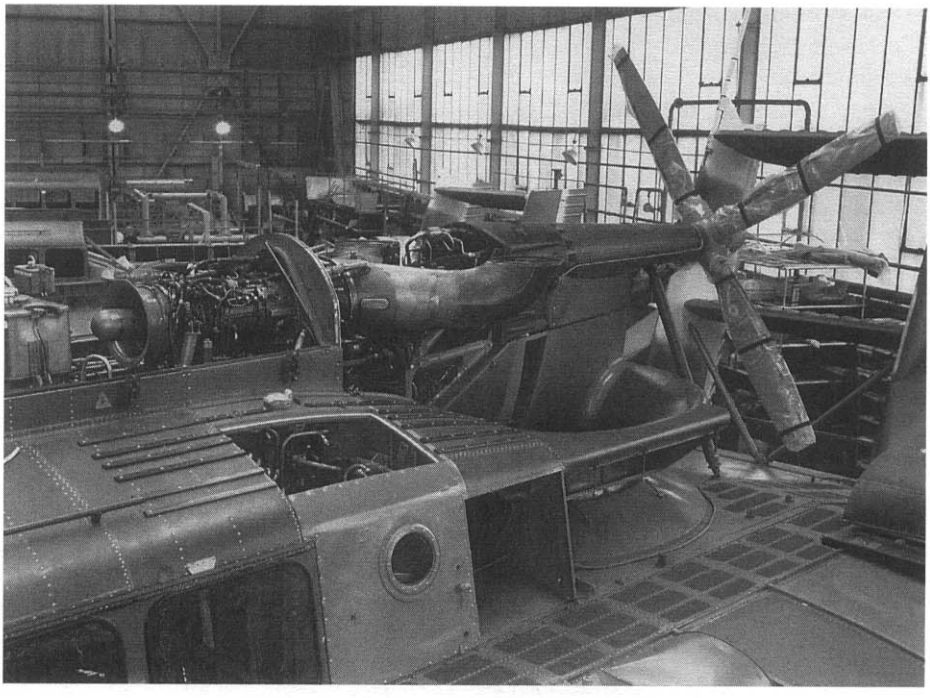

(c)

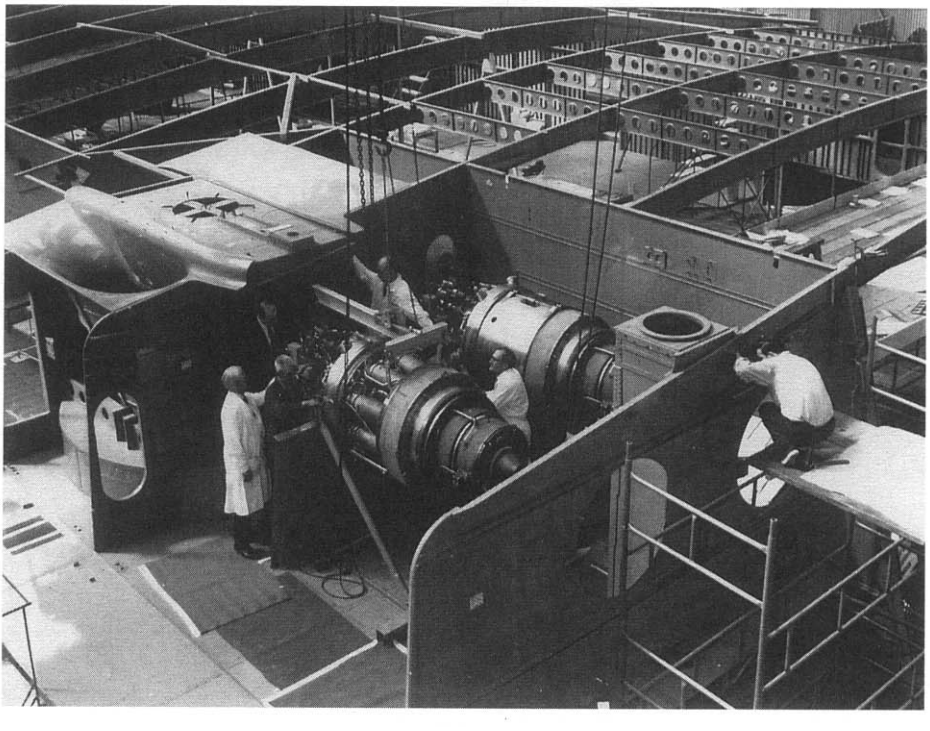

Fig. 16.3 (b) Rolls Royce Gnome gas turbine installation in SR.N6; (c) Rolls Royce Proteus gas turbine installation in SR.N4.

achieved by using a reduction belt drive for power ratings up to about 600 kW, which is often convenient for lift fans or propellers. Medium speed diesels run at 750–1500 rpm and so for propulsors such as water jets generally no gearbox is needed at all. This is now changing for the largest water jet systems, where a gearbox with a ratio of 1.5:1 is needed.

Each engine may be coupled to both a propulsion device and a lift fan (e.g. the SR.N4 or LCAC), or may be dedicated to a lift or propulsion system (e.g. the AP1.88 or Cirrus SES). Where an integrated system is used, such as on the SR.N4, (see Fig. 6.7), the gearbox and transmission system can be quite complex and has to be designed and constructed specially for the craft. BHC's parent company Westland build helicopters which have similar power trains and so they have the experience and capacity to design and build these. Implementation of bespoke transmission designs of this kind has become very expensive since the mid 1980s and requires a craft build of many units to justify the initial development cost. The trend has therefore been towards using simpler transmission systems based on use of standard marine units.

Gearboxes and transmission systems for diesels are generally also selected from standardized marine or industrial units. The propeller(s) or lift fan(s) therefore have to be designed to fit the available shaft speed and power profile. The advantage is much lower cost, at a penalty of higher weight, as ships are not so sensitive to power train mass.

Some craft have also used hydraulic power transmission on lift systems, where the engine drives a hydraulic pump and the fan is rotated by a hydraulic motor. The Hovermarine HM.2 bow lift fan is one example. This can be useful where, as on the HM.2, the engines are installed at the stern and a lift fan is needed at the bow to optimize cushion flow while minimizing air ducting.

Power loss with increased temperature and engine heating for sub-zero temperatures

Both gas turbines and diesels give reduced power at increased temperature. Typically a gas turbine will give 7% less power for each 10°C temperature increase, while a diesel will reduce by about 2%, compared with the normal standard temperature for measuring power of 20°C. Where a craft is to operate in a hot climate, it is therefore important to specify the engine power rating at the normal operating temperature, rather than standard conditions.

Diesel engines depend on the cooling system, whether forced air, or water, to maintain operating temperature. It is important in this case to specify the engine cooling system based on the maximum expected operating temperature and to obtain guidance from the manufacturer on continuous operating envelope when outside this range. Coolant flow will then be controlled by thermostat for lower temperatures.

At the opposite end of the spectrum, in very cold climates, fuel and engine heaters may be required at least for cold starts. Below about −20°C, special lubricating oils must be used (modern synthetic oils are ideal for this), while below −40°C, in high Arctic or Antarctic, diesel fuel begins to solidify and so must be warmed. Engine powering must be considered for above zero conditions, since for most Arctic logistics applications, summer temperatures will be well above zero.

Costs

Diesel engines are much cheaper to procure than gas turbines – of order 900–1700$/kW compared with 1200–2250$/kW at 1996 prices. In addition, so long as a diesel is run within specification (at or below the agreed %MCR), mean time between overhauls (MTBO) can be between 5000 and 20 000 hours for medium- and high-speed diesels in the 500–3000 kW range and up to 60 000 hours for larger engines which operate at constant power for long periods.

Diesels also use fuel which is considerably cheaper than that suitable for gas turbines. Medium- and high-speed diesels use light to medium distillate gas oil with cetane number between 50 and 60. Typically diesel fuel may cost around 70% of the equivalent fuel oil suitable for gas turbine use (approx. $130 per tonne at 1996 European prices). Gas turbines are currently being developed for heavier fuels, but cleanliness of the fuel will remain an issue for gas turbine power turbines (see below).

It can be seen that diesels lend themselves to utility applications where resilience and maintainability in the field are more important than maximized payload. Gas turbines can be efficient on a regular service for passengers or freight where overhauls can be planned ahead. A craft in regular passenger service can benefit from the additional productivity offered by the increased payload, while a utility craft will benefit most by reduction in capital costs so long as the design mission can be fulfilled.

16.2 Powering estimation

The first stage in sizing a craft is to make an overall weight estimate, as described in Chapter 11. Initial estimates for the known components (payload for example) are grossed up by use of relations for the unknown components based on previous experience. It is also necessary to investigate the craft overall dimensions and cushion parameters (P_c, Q_c) at least in a preliminary way before trying to estimate powering.

A choice between diesel or gas turbine power may be left open at the initial stage, unless the craft mission demands a specific type of power unit, based on the discussion above. The weight data and cushion parameters may then be used to estimate installed power, which in turn can be used to re-estimate total craft weight. If very few parameters are fixed initially, it may be necessary to make several projections before the weight and power estimates converge. The relation used to predict power is typically:

$$P_t = K_t W^{0.825} \tag{16.1}$$

where power is measured in shp and W is measured in tonnes. (N.B. shp = kW × 1.34).

Based on statistical analysis of craft from the 1960s and 1970s K_t was found to be close to 165. This has reduced to closer to 125 in recent years for ACVs and to about 100 for SES. The original analysis [4] showed most craft to cluster around the above relationship regardless of design speed, though at this time design speeds were usually in the region of 40–50 knots in calm water. These global coefficients may nevertheless be used as a starting point for craft aimed at typical coastal ferry roles, or equivalent.

Figures 16.4 and 16.5 plot the installed lift and propulsion power as a function of

total craft weight × speed (shp/tonne.knot) for a number of existing craft. These may be used for reference where the craft mission is outside 'normal' specifications. These data may be reduced to the relations.

$$P_l = P_c\, Q_c/550\ \eta \text{ where } \eta \text{ is normally in the range 0.6–0.8 . . .} \qquad (16.2)$$

for lift systems. η is the total efficiency of the lift system including losses in the fans, ducting and cushion; and

$$P_p = K_p W^{0.825} \qquad (16.3)$$

for propulsion systems, where K_p varies dependent on the propulsor type (see Chapter 15).

To use these relations to check the initial estimates, the craft cushion system initial design needs to have been carried out (see Chapters 10, 3 and 12, in turn). Further, the craft propulsion estimates need to have been made (see Chapters 4 and 15, in turn). Once the power estimate has been made, an estimate of the engine weight is possible,

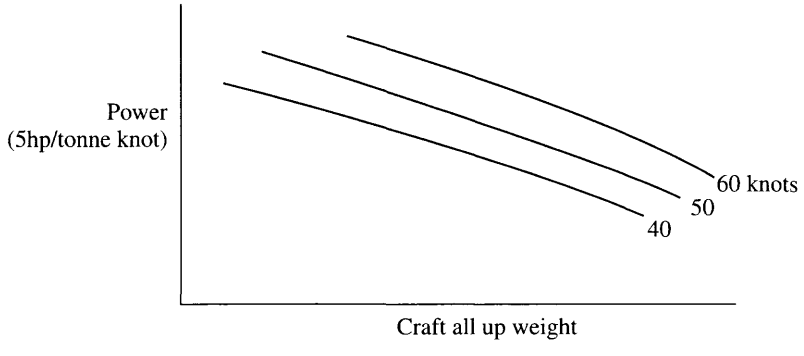

Fig. 16.4 Shp/tonne.knot lift.

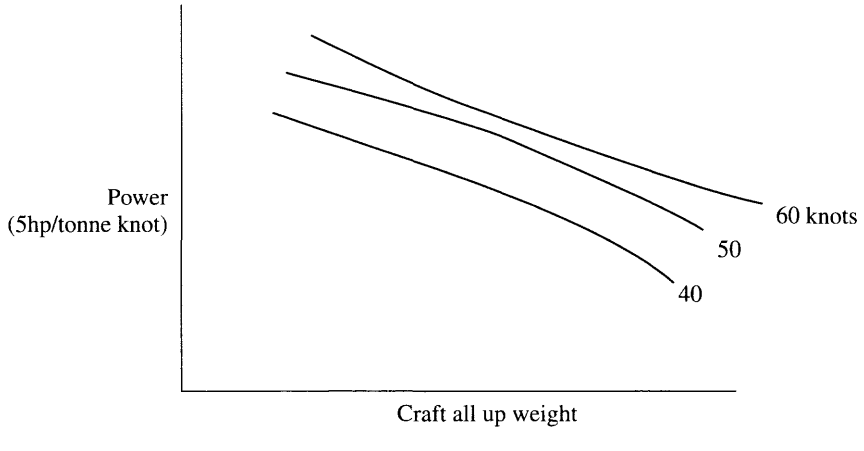

Fig. 16.5 Shp/tonne.knot thrust, and total.

allowing a second cycle of estimation. Initial guidance is given in the table below, based on some data extracted from ref. 119.

Engine Type	Specific Weight (lb/shp)	Gearbox Weight (lb/shp)
Medium speed diesel	$580/P^{0.5}$	0 – assumed direct (750 with aux)
High speed diesel	$250/P^{0.5}$	$100/P^{0.5}$
Air cooled high speed diesel	$200/P^{0.5}$	$100/P^{0.5}$ or $30/P^{0.5}$ if belt drive
Marine gas turbine	$65/P^{0.5}$	$55/P^{0.5}$
Aerospace gas turbine	$14/P^{0.5}$	$55/P^{0.5}$

The next step is an estimate of fuel weight. First we need to assess the fuel consumption depending on the choice of engine type and the installed power. For guidance the following relations may be used:

Engine type	RPM range	Fuel consumption C_f (lb/shp.hr)	Consumption (kg/kWhr)
Medium speed diesel	750–1500	0.34	0.21
High speed diesel	1500–4000	0.35	0.22
Air cooled high speed diesel	1500–4000	0.38	0.23
Aerospace gas turbine	10 000–30 000	0.6–0.25	0.36–0.15
Marine gas turbine	10 000–30 000	0.5–0.2	0.3–0.15
Industrial gas turbine	10 000–30 000	0.5–0.3	0.3–0.18

Diesel engine fuel consumption changes slightly with power output, small/medium diesels consuming 0.2–0.25 kg/kWhr while very large diesels consume 0.18–0.23 kg/kWhr. There is no clear relationship, so it is necessary to seek data from the manufacturers of candidate engines to complete an evaluation. Large gas turbines are significantly more fuel efficient than smaller units, approaching the efficiency of diesels.

The fuel weight can now be estimated, assuming a mission duration T_m and a reserve time T_r in hours. The mission duration in turn can be determined from the craft fixed route, or longest distance between refuelling points:

$$W_f = [C_{f1} P_l + C_{f2} P_p] [T_m + T_r] \tag{16.4}$$

A typical reserve may be 20–100% of the normal mission duration. If fuel is used as ballast for trimming, the higher value may be used as a starting value and optimized later in the design process. Craft operating short ferry crossings where refuelling will be once every 2 to 4 trips might use a 25% reserve, or one leg, while craft for coastal patrol may have a reserve determined in hours of operation, dependent on the greatest distance from a temporary or permanent base.

Once estimates of engine and fuel weight from this procedure have been compared with the craft initial weight estimate, the procedure will need to be repeated by adjusting earlier weight component assumptions and recalculating until convergence is reached. At this point, sufficient data should be available to begin detailed studies of the cushion system and craft drag components based upon the earlier estimates referred to above, so as to obtain a detailed estimate of craft powering, using the methodology in Chapters 2–6.

16.3 Diesel engines

A diesel engine works on the compression ignition principle. The lowest piston position in the cylinder is referred to as bottom dead centre (BDC) and the highest as top dead centre (TDC). The distance BDC to TDC is the stroke. While the piston travels from BDC to TDC the trapped air is compressed by the ratio of the cylinder volume at BDC to that at TDC. This is the compression ratio.

There are two diesel engine types, the 2-stroke cycle and the 4-stroke cycle. The 2-stroke engine completes all four processes of compression–power–exhaust–scavenge for each 360 degree rotation of the crank, while the 4-stroke engine uses a second rotation for exhaust and scavenge. The 4-stroke process allows much closer control of the compression and exhaust processes and so is more fuel efficient, while it requires a larger cylinder swept volume to achieve the same power rating.

Marine diesels have fuel injectors at the cylinder top which inject fuel as the piston reaches TDC. The compression raises the air temperature sufficiently for fuel to burn spontaneously. Injection is continued into the power stroke just far enough to maximize the power generated without leaving unburned fuel in exhaust gases.

A 2-stroke engine relies on the remaining overpressure for exhaust gas to be scavenged. This is assisted marginally by an overpressured air supply system refilling the cylinder with fresh air through valved ports which open when the piston is close to BDC. Cams are positioned so as to open cylinder head valves for the correct period during the piston stroke for exhaust and inlet. A cam shaft is positioned at the side of the cylinder, rotated by gears, chains, or a belt drive from the main crankshaft. The cam shaft rotates at half crank speed on 4-stroke engines.

SES and ACV craft require high speed (for small motors) and medium speed (for higher power ranges) diesels, in order that engine weight is acceptable Medium speed engines are approximately 500–1200 rpm, while high speed diesels are anything higher. Both classes of engine are generally 4-stroke motors having trunk type piston/crank arrangements and a short stroke (stroke to bore 1.0 to 1.5:1). Up to 10 cylinders in line and 24 in vee formation are common.

Most engines are turbocharged and aftercooled. Turbocharging is compression of the inlet air before it is released into the cylinder, increasing the density. The unit is usually a rotary compressor driven by a turbine powered by engine exhaust gas. The higher pressure inlet gas allows greater power to be extracted, while at the same time improving fuel burn and so reducing specific fuel consumption.

Once the power rating is known from the procedure in section 16.2, the designer can consider his design options and check whether his preferences increase or decrease the weight estimate so far.

Number of engines and layout

ACV small craft selection starts on the basis of a single air cooled engine with power outputs for an integrated lift/propulsion ducted fan (Fig. 16.6), or separate propulsor and lift fan (Fig. 16.7 (a), (b)). Larger craft may simply duplicate this arrangement. Utility and small ferry craft begin to employ separate power units for lift and thrust (Fig. 16.8). This has the advantage that the lift motor(s) can be sized to supply

Fig. 16.6 Small craft integrated lift/propulsion from single ducted fan with horizontal splitter plate.

additional air to bow thrusters (see Figs 6.3 and 6.9), as an alternative to variable pitch propellers or fans.

Due to the limited available power range of air cooled diesels, for higher ratings liquid cooled diesels need to be considered. These have been installed in variants of the AP1-88 (Fig. 16.9) and the PUC-22 built by Wartsila in the 1980s (Fig. 16.10). Until recently the high installed weight of liquid cooled engines has meant that payload was significantly reduced, making this choice an inefficient one. This is now changing due to market demands from other industrial users.

Use of multiple engines minimizes transmission requirements, while creating a need for several engine compartments, each with stiff structural support, air intake filtering, maintenance access panels, sound attenuation and fire protection. In general, the optimum selection is that where the minimum possible number of engines is used. Care should also be taken with the craft CG for lightweight operating conditions. If engines are placed too far to the stern, this can increase the requirement for static trimming ballast, which then needs to be accounted for in the craft weight estimates.

The most common diesel engine arrangement for SES consists of two engines each for lift and propulsion (Fig. 16.11). Propulsion engines are best mounted towards midships to minimize VCG and static trimming ballast. The sidewall geometry can be adjusted to accommodate them on smaller craft, so also reducing the shaft inclination, whether for water jets or free propellers.

Lift engines are relatively small for SES compared to craft size and so can be mounted in the same area as the lift fan units, normally somewhere just forward of amidships, with ducting to the bow and stern seals. Care should be taken to effectively sound insulate the lift system compartments.

(a)

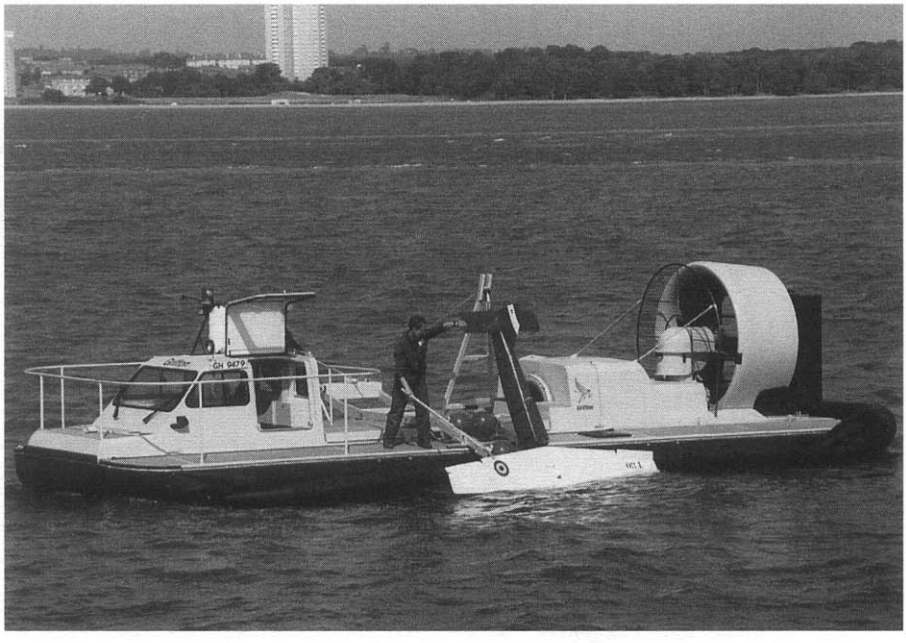

(b)

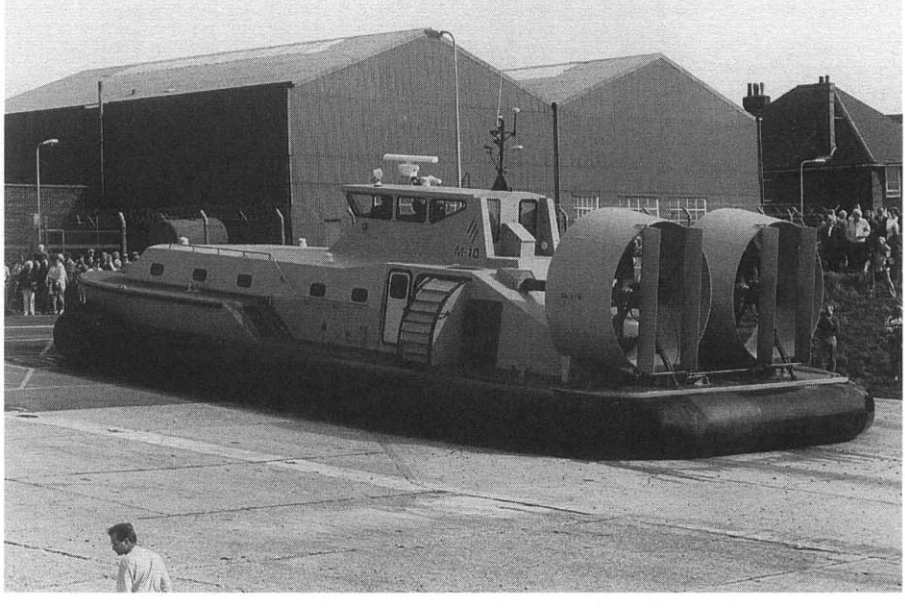

Fig. 16.7 (a) Utility craft integrated lift and propulsion (Griffon 2000); (b) Utility craft integrated lift/propulsion, the ABS M10 (see also Fig. 15.47(c)).

Cooling

ACVs have a choice between air cooled and closed circuit liquid cooled engines. The simplicity of air-cooled engines and their light weight has made them a popular

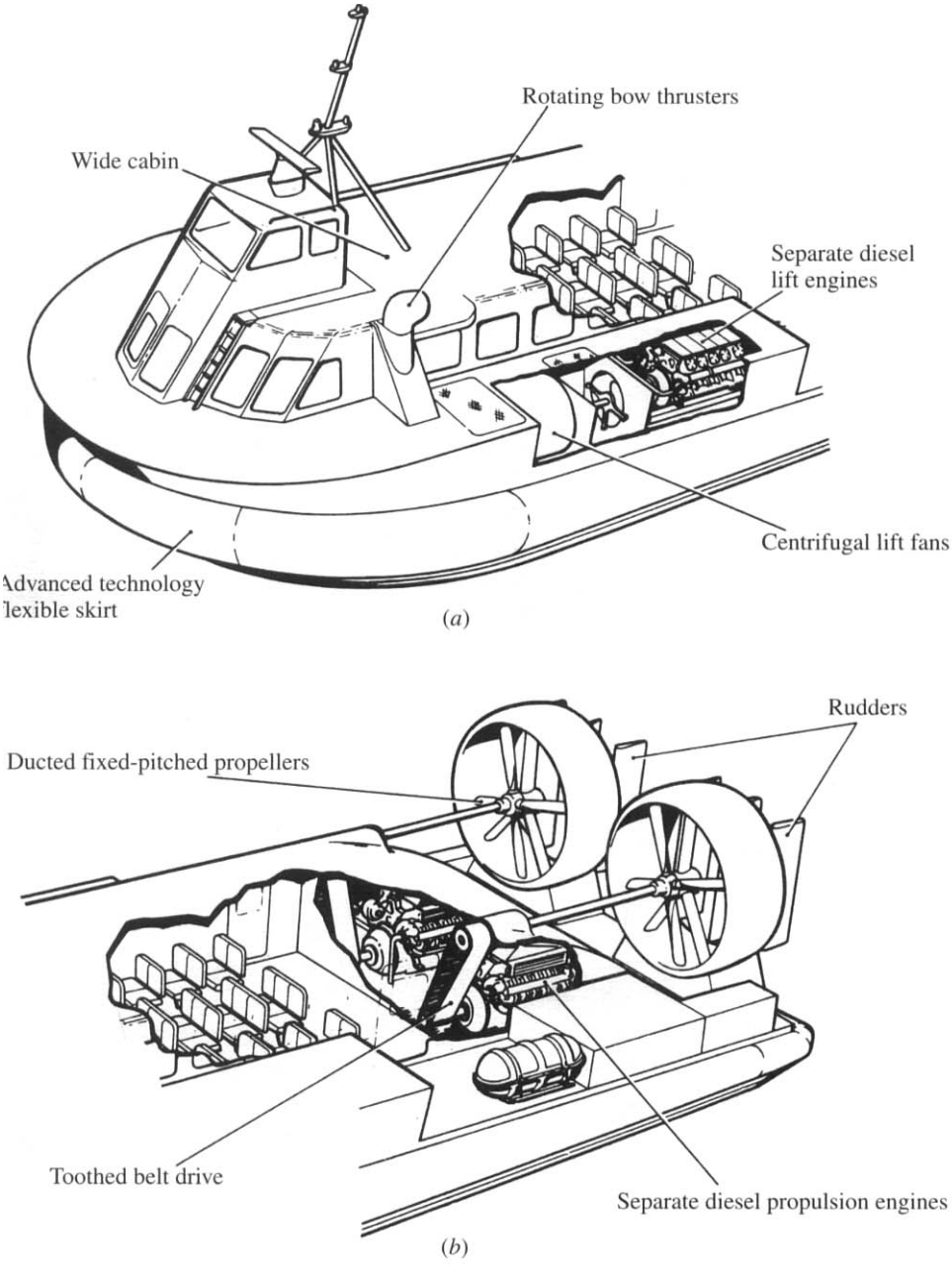

Fig. 16.8 Larger ACV separate power units, the API-88 power system.

choice during the 1980s and 90s. Liquid cooled diesels are becoming available which will extend the power range above that offered by air cooled motors. This should allow designers to develop ACV designs which are larger than the current limit typified by the AP1-88.400 (Fig. 16.12).

Fig. 16.9 AP1.88 Cominco craft.

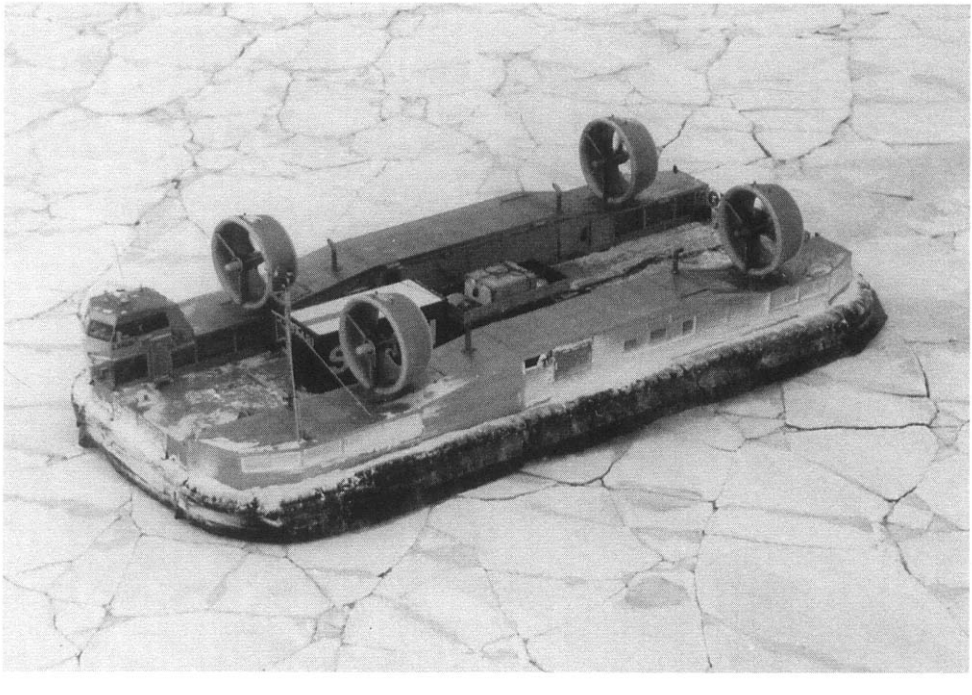

Fig. 16.10 Wartsila PUC-22, with water cooled diesels driving rotating ducted propellers.

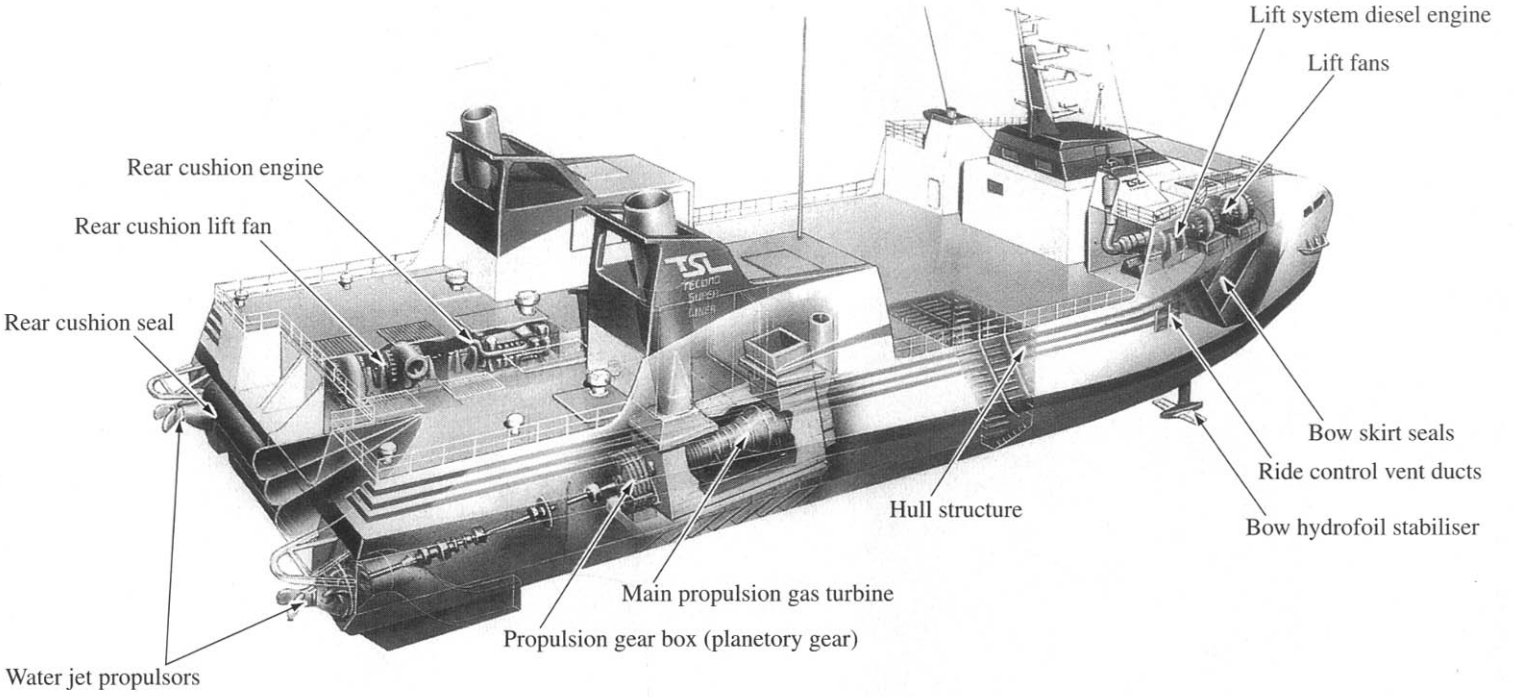

Fig. 16.11 SES power system layout. The TSL-A.

Fig. 16.12 AP1.88 400 design.

SES choice is between closed circuit cooling and open circuit sea-water cooling. Since there is very little drag penalty from a well designed cooling water intake, this is the system of choice. Closed circuit cooling might be chosen for a lift engine on the basis of market availability and cost.

Specific design issues which should then be taken into account during ACV and SES design include:

Vibration characteristics and damping

A diesel main engine is the largest individual mass installed in an SES or ACV. In larger craft it can weigh as much as 30 to 40 t. While larger modern engines with 12–20 cylinders are well balanced, the vibration energy is still significant. Diesel engines are stiff structures, due to the high internal forces developed. Mounting direct to the structure of an ACV or SES will require careful analysis of the local supporting structure to determine its natural frequency and harmonics and response to the engine vibration energy spectrum (see Chapter 14). A resilient mounted engine will also require this type of analysis, with the additional parameter of the resilient mount damping response applied to the engine excitation. Resilient mounts assist to isolate noise transmission from diesel (or gasoline) engines in a metal hull structure. GRP does not transmit noise so efficiently, while foam sandwich panels act as noise attenuators.

In addition to considering engine vibration and noise transmission through the craft structure, it is important to determine the transmission axial and whirling

natural vibration frequencies. If there is significant response to any of the main engine vibration frequencies, then stiffness of the transmission shafts or bearing spacing may have to be changed. On small- to medium-sized craft, the damping properties of toothed rubber belt transmission can be used to provide isolation between an engine and a transmission train.

Water-cooled diesel engines generally emit less noise than air cooled diesels, due to the damping of the water jacket. The engine space for an air-cooled diesel may therefore need additional noise absorbing cladding. Forced draft air cooling will also need to be exhausted from the engine compartment in such a way as to ensure it does not recirculate, or become ingested into the cushion air system.

Engine lubrication system

Effective lubrication is particularly important for diesel engines, to ensure rated power is developed and engine life maintained. Most diesel engines operate a duty cycle which includes a significant period at part power or idling conditions. In these conditions, usually slow speed manoeuvring, the lubrication system should be fully effective. It is best to take advice from the selected engine supplier regarding the lubrication system specification for the required craft mission profile.

Exhausts

Engine exhausts should be designed so as to prevent recirculation into machinery space ventilation, or air cushion system intakes. Cooling and exhaust ejection at or under the water-line on an SES can be a convenient way to minimize the in-air noise signature, though non-return flaps are needed to prevent flooding and undesirable backpressure in the exhaust system during start-up. Some military missions such as mine countermeasures may demand exhaust above the water line to minimize the underwater signature.

Relief valves

Diesel engines with bores larger than about 200 mm need to have relief valves installed for relief of excess pressure both in the cylinder head and in the crankcase spaces. Guidance is available from rules such as ref. 116. In this case release into the engine room by opening vent valves needs to be accounted for in designing the ventilation system. This issue should only be significant for large SES craft. Advice can be sought from the engine supplier.

Generators

Generator motors should be rated so as to be able to continuously drive the generators at their full rated output. In addition it is normal to design the system to give an overload power of not less than 110% for 15 minutes or so.

16.4 Gas turbines

A gas turbine is a rotary engine comprising an air compressor, a combustor and a power turbine. The compressor turbine and power turbine can be mounted on the same shaft, or two separate shafts (referred to a spools) may be used, one for the compressor and a power turbine to drive it and one for the main power output. The advantage of this two-shaft arrangement is that it allows the turbine wheels to be separately optimized for maximum efficiency. Some aerospace derivative engines also have low- and high-pressure compressor turbines running on separate concentric shafts to increase compression ratio and further improve efficiency.

The simple gas turbine with free power turbine (Fig. 16.13(a)) can achieve specific fuel consumption as low as 0.25 kg/kWhr for steady operation at design power rating if a compression ratio of 16:1 were used. Marine turbines do not generally operate in this region, 9–12: 1 being more common and with fuel consumption between 0.3 and 0.5 kg/kWhr.

To improve performance a number of measures are possible. The most interesting for fast marine craft is recuperative heating of the compressed air inlet to the combustors by using air from the engine exhaust. This can increase the thermal efficiency by 20–30% so long as the engine is optimized for it.

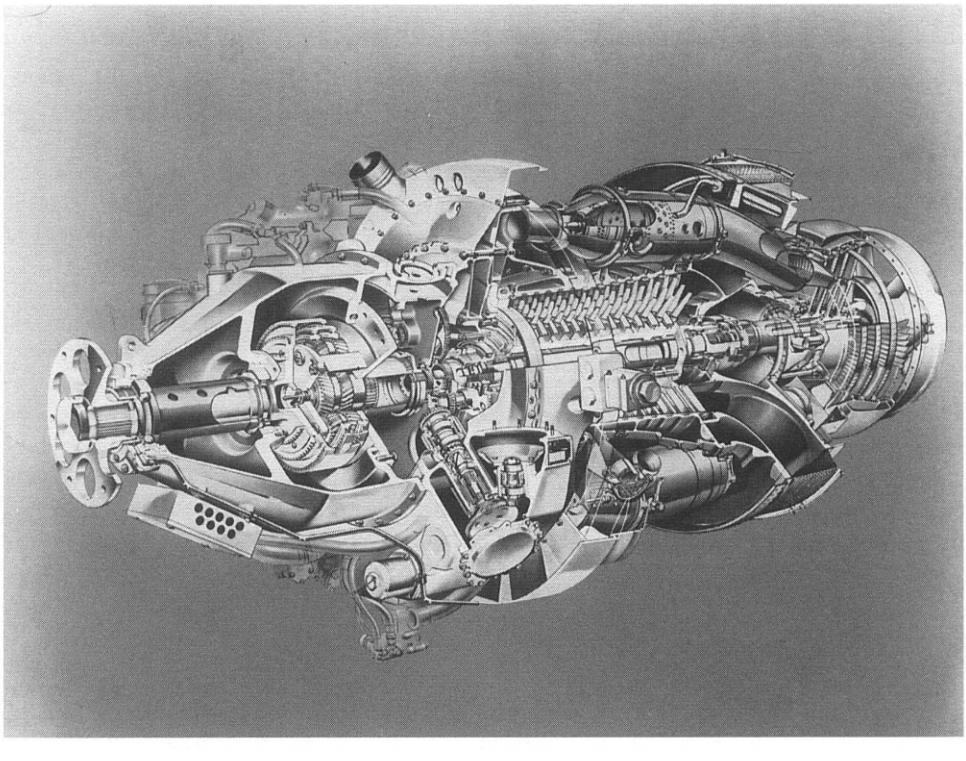

Fig. 16.13 Gas turbine diagrammatic sketches: (a) Rolls Royce Proteus.

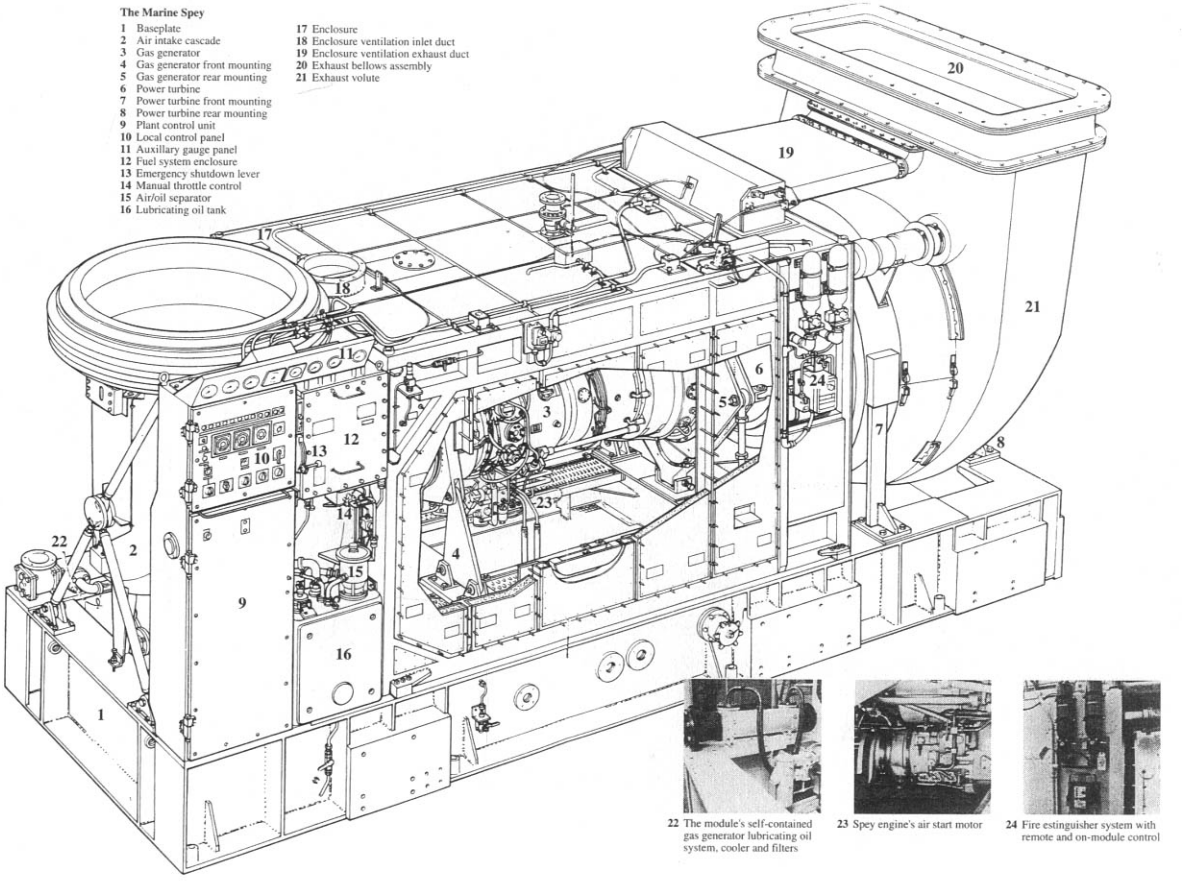

Fig. 16.13(b) Rolls Royce Marine Spey propulsion package.

Gas turbines have a relatively high air volume flow and so pressure losses at the intake and exhaust will significantly affect power generated. A pressure drop of 1% at the inlet will reduce power output by 1.5–2%, while a similar pressure rise at the exhaust due to diffusion will reduce power by 0.5–0.75%. In addition the required thermal energy and so fuel consumption, is increased by around 0.5% in each case. When designing an SES or ACV gas turbine installation, the intake plenum chamber characteristics and exhaust ducting need careful attention. Consultation with the gas turbine manufacturer is recommended!

Axial compressors derived from aerospace machines have limited pressure ratio per disc, resulting in several discs with static straightener vanes for each compressor or turbine stage. This makes for a complex engine and costly major overhauls. In an attempt to simplify engine design a number of manufacturers have produced industrial engines with centrifugal flow compressor stages. At present the power rating available from such machines is limited, but can be expected to improve in the near future.

A gas turbine has to be mounted on a stiff structural skid assembly (see Fig. 16.13(b)) to maintain shaft alignment. In the past this, combined with a need to provide protection against flying debris in the case of rotating disc failure, fire protection and noise suppression, led to development of packaged units. These were fine for displacement ships, but give a weight penalty for fast craft such as ACVs and SES. Consequently gas turbines installed in ACV/SES are normally bare engine/gearbox units, with support frame or skid. The machinery compartment is then designed to fulfil the other functions.

The development of industrial gas turbines has encouraged the design of power units which are modularized, allowing the compressor, combustor or power turbine sections to be removed separately. This is particularly important for larger engines in the 10 000–30 000 kW range, as it also implies exchangeability of modules between engines, leading to reduced spares holding.

There are several design issues which need to be considered when using gas turbines in ACV or SES, as follows:

Layout and engine selection issues

Many of the earliest ACVs used aerospace derivative gas turbines. The SR.N series built at Saunders Roe/BHC developed a design based around an assembly of an engine driving a vertical shaft through a gearbox, which transmitted power to a vertical axis centrifugal lift fan and upwards inside a rotating pylon to a further gearbox and a propeller (Fig. 6.3). This arrangement was light, efficient and scalable but proved expensive to construct.

Bell Textron developed a somewhat simpler power train assembly for the LCAC in the early 1980s, (Fig. 16.14). This is based on a fixed ducted propeller system and separately powered centrifugal lift fans. The LCAC arrangement has similarities to that of the diesel powered AP1.88, except that due to the compactness of the gas turbines, all the machinery is contained in the side structures. Moving the machinery to the sides of the craft allows considerable flexibility for design of the payload area, including the possibility for driving vehicles on and off, as was put to good effect also on the SR.N4. If this is not an issue then the propulsion machinery may be moved into stern

Fig. 16.14 Bell Textron Jeff (B) Showing two sets of 3 TF40 gas turbines driving lift fans and bow thrusters forward, and ducted propellers at the stern. Aerojet General Jeff (A) is in the background.

compartments. An advantage with this arrangement is a lower noise signature in passenger areas. Where fixed ducted propulsion is installed, it is preferable to have a separately powered lift system, with rotatable bow thrusters to give good slow-speed manœuvring.

Until recently only military SES have used gas turbine powering, notably the experimental US Navy SES-100A and 100B in the 1970s. In the 1990s the first major project for a large cargo-carrying SES was started by a consortium in Japan – the Techno Superliner. The half-scale prototype (70m waterline length) for this craft completed trials in 1996. Figure 16.15 shows an artist's impression of the full scale craft while Fig. 16.16 shows the prototype. Machinery installation comprises four gas turbines driving water jets at the stern and four smaller units driving lift fans, two at the stern and two at the bow. In a craft this size the designer is not faced with particular space problems to install machinery. The majority of the outfit may be optimized in stern located areas. The main consideration for an SES is to have 50 to 60% of the lift power located at the bow to feed the bow seal. Machinery should all fit into the sidehull areas, so leaving the centre area free for the mission-oriented layout.

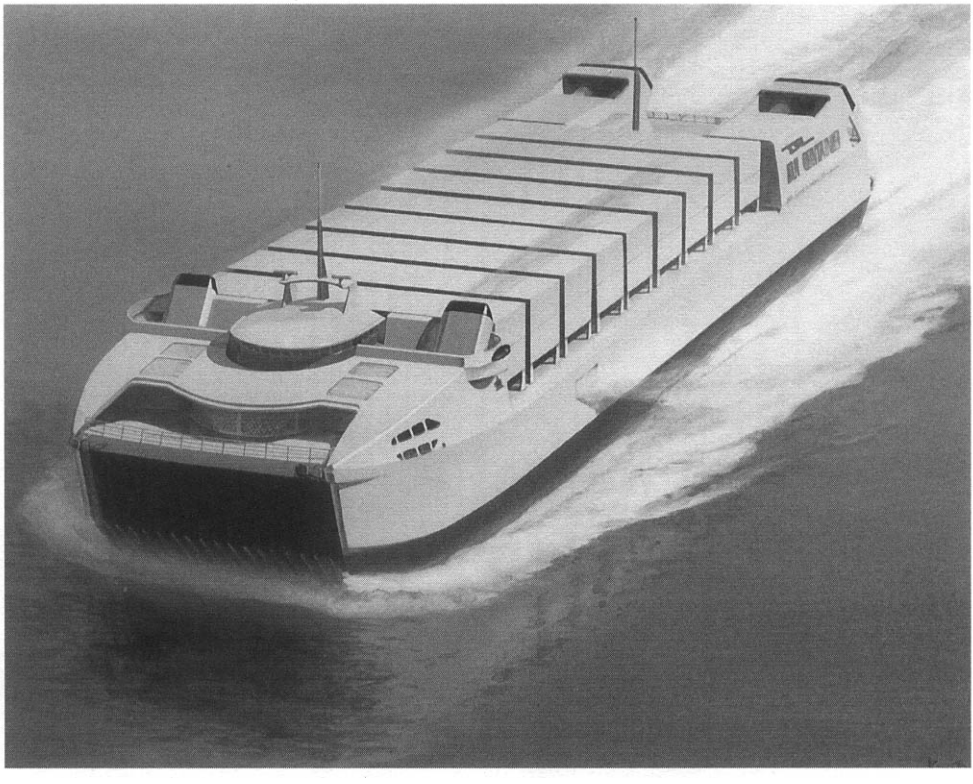

Fig. 16.15 TSL-A full scale short sea cargo SES design.

Air intake flow requirements and inflow distortions

Gas turbines have a high air volume flow requiring careful design of the intake and exhaust systems (see Fig. 16.17(a)). On the intake side there should be sufficient plenum volume so that the air can settle and not cause rapid changes in dynamic head or turbulence, otherwise the engine compressor blade fatigue may be accelerated and in the worst case lead to failure. Current practice is to design an inlet which does not face the craft bow, so as to avoid ram effects, and to aim at 3–5 m/s velocity into the engine intake itself. Engine exhausts are generally a simple stack, see for example Fig. 16.16, if noise is not an issue. The stack should be on an ACV or directed away from propulsors, or comprise a diffuser volute to reduce the exhaust velocity.

Gas turbine power generators are very small, between 0.001 and 0.008 m^3/shp and so the main design issues for this type of power unit are arranging the intake and exhaust, while providing personnel access to the turbine itself for maintenance.

Protection from foreign object damage

ACVs and SES are surface vehicles which often operate in conditions which cause water or sand spray. The air cushion can also throw up other small objects. Spray sup-

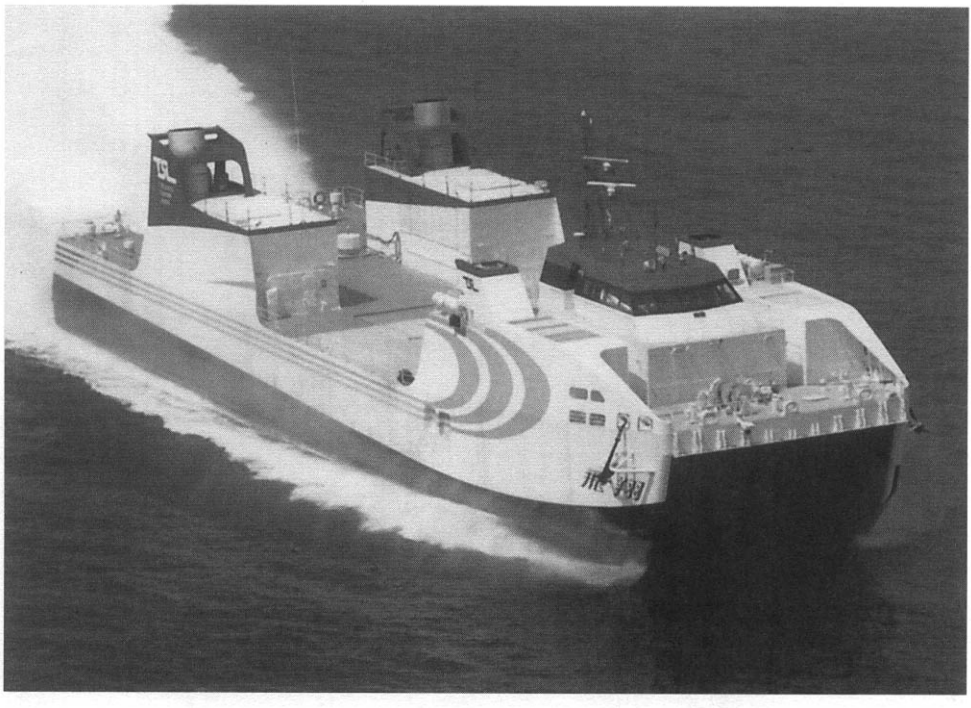

Fig. 16.16 TSL-A prototype SES Nissho.

pression skirts can be fitted, but these cannot remove the problem totally. In addition, any debris left in the intake volute after maintenance can be sucked into compressor blading. Such incidents are rare, but have occurred in the past. This problem can be minimized by using ship practice for engine space design, see Fig. 16.17(a), making the intake volute space easy for personnel entry or access and providing effective air intake filtration.

Air intake filtration – protection from salt, sand and snow

Removal of water droplets, sand particles and debris from the intake air stream demands the use of mesh type filters. Multi-layer nylon or polypropylene knitted mesh, mounted in a configuration so that the entering air flows up through it, has been found effective (see Fig. 16.18). The filter trays can be removed for cleaning out salt or trapped particles on a regular basis. An alternative 3 stage air drying system is shown in Fig. 16.17(b). Systems of this type are installed on military ship gas turbine intakes.

Gas turbine blades are sensitive to the presence of salt, which increases the corrosion rate and fatigue degradation. Reduction to levels as low as 0.01 ppm of salt are needed before engine life is not affected.

Mesh filters will remove droplets, but will not dry the intake air: it is still at 100% humidity and will have some fine water droplets present. Further reduction requires secondary filtration with a finer mesh filter similar to systems used in industrial HVAC systems and possibly also adoption of the strategy used on the BHC craft whereby the

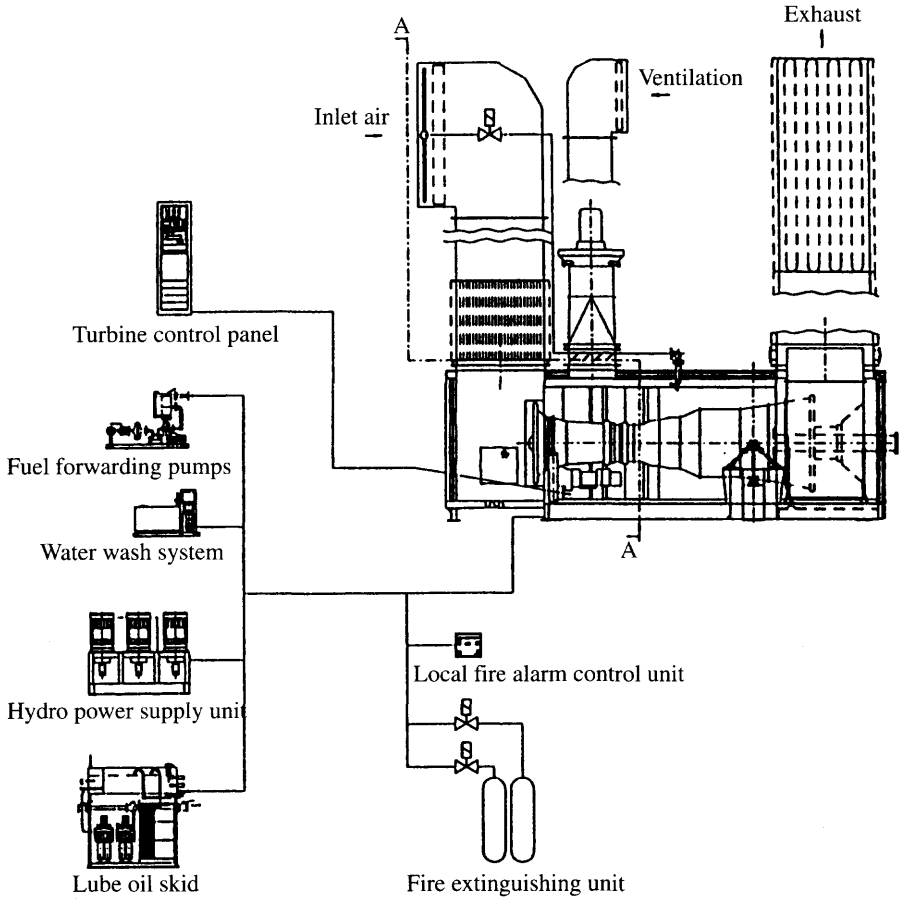

(*a*)

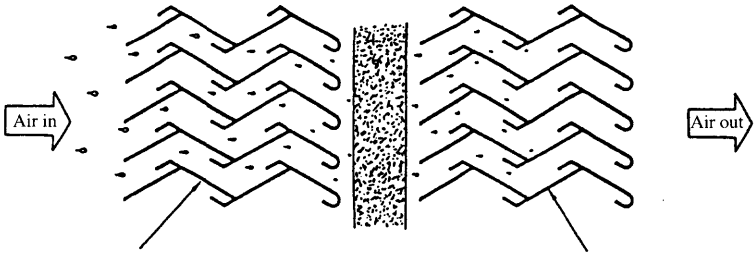

First stage
For the removal from the airstream of: wave tops, heavy sprays, light sprays, larger aerosol drop–lets down to 13 microns dia

Second stage
The aerosols below 13 microns dia which pass through the first stage are coalesced by the second stage into a smaller number of larger droplets. These droplets are detached from the rear face of the coalescer and carried by the air stream to the third stage

Third stage
For the removal of the droplets detaching from the second stage

(*b*)

Fig. 16.17 Gas turbine inlet and exhaust system.

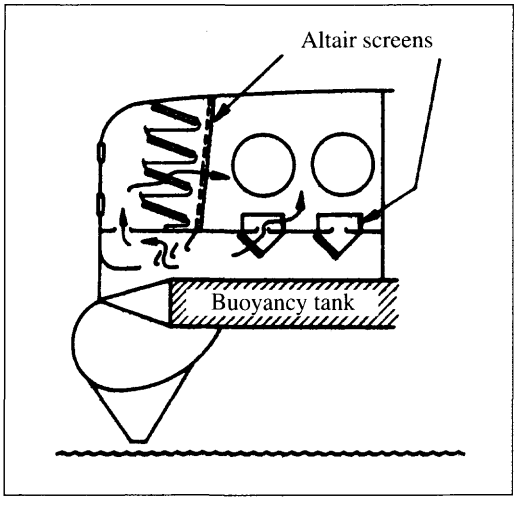

Fig. 16.18 Knitmesh filter diagram.

engine air is supplied from the cushion, as well as having both knitmesh and fine filter screens. Filter systems such as the Primaberg filter are able to meet this requirement (Fig. 16.17(b)).

Eventual salt build-up on gas turbine compressors is inevitable for ACVs and so an effective engine wash or soft blast grit cleaning system is also essential to maximize MTBO, which for the SR.N4 Rolls-Royce Proteus engines is between 2000 and 3000 hours.

Attenuation of engine noise

Gas turbine noise, if not attenuated by muffler systems of some kind, can cause problems in populated areas. Based on sample measurements, Hamilton Standard in the USA proposed a relation as follows:

$$\text{Noise level} = 72 + 8.2 \log P \text{ dBA at 30m}$$

where P is the engine power rating in shp. The noise level is variable ± 5 dBA between noisy and quiet engines. This suggests a range between 91 and 105 dBA for 1000 shp class engines without silencing.

From an environmental point of view and to compete with other vehicles such as fast catamarans, external noise levels above 80 dBA close by the vessel would be considered noisy and so would require attenuation. Gas turbine exhaust silencing therefore typically needs to cope with noise power reductions of order 80–90% (approximately 20 dBA). This can be achieved by enclosing the engine itself in an acoustic enclosure (this may be the machinery space itself, suitably clad) and using attenuating cladding at the exhaust ducting.

16.5 General design requirements

When designing machinery systems and spaces on board an ACV or SES the following design requirements need to be taken into account, based on IMO and classification society typical requirements.

Vessel trim and dynamic motions

Machinery and associated systems should be designed so as to continue functioning safely while the craft is rolled and pitched to its design maximum angles for normal operation. Designers should also consider if there is a need for a craft to be able to continue emergency operation if collision damage is sustained. Auxiliary machinery should at least be able to continue operation so as to provide power and pumping capacity. For guidance, Lloyds Register Special Service Craft rules [116] part 9, section 4.2 specifies the following inclinations:

Inclination angle (Degrees)	Transverse inclination		Longitudinal inclination	
	Static	Dynamic	Static	Dynamic
Main and auxiliary machinery	15	22.5	5 or 500/L for craft above 100m long	7.5
Emergency machinery and equipment	22.5	22.5	10	10

Machinery control and remote monitoring

Machinery controls should be from the wheelhouse or control cabin. Larger craft (Category B or cargo vessels in IMO) should have duplicates of the main machinery controls close by the engine room(s). A typical monitoring/alarm scheme may include the following (extracted from Lloyds Register Special Craft Rules). These are the key parameters for engine health monitoring.

Item		Alarm	Notes
Lub oil inlet*	Pressure	Low	Automatic shutdown, medium/high speed engines
	Temp	High	Alarm monitor
Exhaust gas*	Temp	High	Alarm monitor
Overspeed*	rpm	High	Above 20% for main engines, 15% for auxiliary, independent of governor controls if fitted
Piston coolant outlet	Flow	Low	Alarm monitor
	Temp	High	Alarm monitor
Cylinder coolant inlet	Flow	Low	Alarm monitor
Cylinder coolant outlet	Temp	High	Automatic shutdown, medium/high speed engines
Thrust bearing	Temp	High	Alarm monitor
Oil fuel	Temp	High	Alarm monitor
		Low	Alarm monitor
Turbocharger exhaust gas	Temp	High	Alarm monitor
Above 1500 kW:			
Lub oil sump	Level	Low	Alarm monitor

Item		Alarm	Notes
Lub oil filters	Diff. pressure	High	Alarm monitor
Cylinder lubricator	Flow	Low	Alarm monitor
Piston coolant inlet	Pressure	Low	If a separate system
Seawater cooling	Pressure	Low	Alarm monitor
Fuel valve coolant	Pressure	Low	If a separate system
	Temp	High	If a separate system
Oil fuel booster pump	Pressure	Low	Alarm monitor
Charge air cooler outlet	Temp	High	4 stroke medium and high speed engines
		Low	4 stroke medium and high speed engines
Scavenge air	Temp	High	Alarm monitor
Turbocharger lub oil inlet	Pressure	Low	If system not integral with turbocharger
	Temp	High	If system not integral with turbocharger
Automatic engine start	Failure		Lloyds allow 3 attempts at start based on start system design

Gas turbines should have alarms fitted for items marked* and in addition a vibration monitor should be fitted and flame and ingition failure should be monitored. Automatic shutdown should be linked to each of these events, as manual control is unlikely to be quick enough to avoid major machinery damage.

ACV and SES machinery rooms should be designed for unmanned operation. While for smaller craft this may be self evident, for larger vessels this may require a significant outfit of remotely operable machinery and supervisory instrumentation. Outfit will include automatic fire detection and protection and a bilge alarm system in addition to the remote machinery operation systems.

Engines should be protected against overspeed, high temperature, loss of coolant or lubricating oil pressure and overload by safety devices which can be tested. The safety protection devices should not cause complete shutdown without prior warning, except where there is a risk of explosion or major damage. There should be at least two independent means of shutting down machinery at the engine room or space, in addition to the wheelhouse controls.

Starting

It should be borne in mind that ACVs and SES may need to black start while at sea or at an unsupported overnight stop. Equipment for starting the auxiliary and in turn the main machinery, should therefore be self contained and suitable to the craft mission – take care to account for extremes of cold or heat. An FMEA (Failure Modes and Effects Analysis) should be carried out to identify the need for duplicated systems, such as batteries, see below.

Fuel system

In all cases it is important that fuel supply lines are protected from heat from engine cylinders or hot parts. Modern diesel engine fuel injection systems run at relatively high pressures and so these lines are best designed as metallic pipework, shielded by a secondary barrier against heat and to prevent leakage of fuel to engine hot parts in the case of rupture.

Fuel filtering

To minimize wear on diesel fuel injection systems, fuels need to be filtered to remove fine grit which is often present. High-speed engines normally require a fabric or felt filter rather than gauze. If the engine is to run on heavier quality fuel, it is possible that wax may solidify in cold weather and so a fuel pre-heater before filtering may be required.

Gas turbines can also be engineered to run on diesel fuel rather than kerosene, as used in the aerospace industry, where the operating conditions are not as demanding. In this case attention must be given to grit filtering and to both salt water content and sulphur content, which can lead to accelerated corrosion. High speed diesel fuel may have 1.5% sulphur compared with 0.1–0.3% in kerosene fuel.

Failure modes and effects

Both the IMO and other regulatory bodies now require Failure Modes and Effects Analyses (FMEA) to be carried out. This has been encouraged by analysis of a number of high speed ferry accidents in recent years. The *IMO High Speed Code* [118] gives a useful guide to this technique. FMEA of machinery and their control systems is an important task for a designer once the main craft design is complete. This analysis will highlight any weaknesses in the choice of engine type and number, and the control system and its redundancy.

16.6 Machinery space layout

There should be sufficent access space around each engine, gearbox and transmission coupling to allow for the regular inspection and maintenance operations which need to be carried out in place and for removal of items for workshop or remote maintenance. In the case of diesel engines this implies stripping the engine and removal of components, while gas turbines will generally be removed complete, or in modules (LP and HP gas compressors, combustor, power turbine, etc.).

Engine removal normally requires a hatch vertically above the engine itself to allow access for craneage. Gas turbines will need removable hatches, while larger diesel installations may only be removed complete in the case of a major failure. In this case it may be acceptable to design the deck(s) above the engine room in such a way that panels can be cut away for access and re-welded back in place after the engine has been replaced.

Small craft machinery spaces are normally designed for access while standing or kneeling on hull hard structure outside the space after removal of protective panels or access hatches. Daily maintenance operations can be carried out this way, while external cranage or lifting gantry frames are used to remove the main machinery items for major overhaul in a workshop.

Design of machinery spaces should cater for the need to be able to drain engine fuel and lubricating oil lines to a safe place. As a minimum for small craft, drip trays should be installed under items such as fuel and lubricating oil filters, and sump drainage points.

Machinery compartments should be naturally or force ventilated sufficient to maintain a safe environment in normal operation. Air for ventilation will need to be filtered to remove sand, dust, water particles and salt. The filter system will require cleaning

by removal and backwashing or replacement. External surfaces of machinery compartments should be suitable for hose cleaning. ACVs in particular operate in conditions where mud and salt can build up.

16.7 Systems and controls

Monitoring and control of engine functions for high speed marine diesels or gas turbines is carried out through a computer system which addresses a series of sensors. Groups of sensors may be linked together into a module via a data bus, and then each module linked to the computer processing unit by a data netword.

The modularization of such a system will allow for simple change out of the components, or uprating of specifications as this technology advances. Redundant systems can also be simply arranged with such a design, which may be important for military craft to allow for some level of damage to a craft in battle. Data from the sensors are processed by the main processor, and then fed out to additional computers which further process the data and present information in a series of screen displays designed to inform the engineer, or the craft driver. A block diagram of this type of system as implemented by MTU is shown in Fig. 16.19. Figure 16.20 shows a drawing of a typical peripheral interface module, comprising a microprocessor motherboard and sockets to receive printed circuit boards containing the logic for a particular sensor group. Each sensor group may include the functions for a particular machine.

The same approach may be adopted by the SES or ACV designer to monitor and control other primary systems on board the craft, such as water jets, cabin heating and ventilation, and safety instrument systems. Adoption of a consistent modularized approach for all such systems will then give minimized maintenance for the craft.

Design and supply of these systems is carried out by the main engine supplier, based on functional requirements provided by the ACV or SES designer. Care should be taken to ensure close liaison between the engine supplier's specialist and the electrical/instrument engineer designing the ACV or SES total craft system.

16.8 Operation and maintenance

Operation

A diesel engine is a relatively dense metallic structure – primarily cast and forged steel and aluminium components. Start-up from cold involves considerable internal heat transfer, and higher wear between moving parts until heated to design operating temperature so that clearances are optimal.

Through the operating period between maintenance activities, gradual degradation of lubrication oils occurs, as abrasion and combustion products from the upper cylinder are absorbed. Abrasion also occurs from particles taken in with the air mixture. Gradual degradation of bearings occurs, leading to increased tolerances and vibration. Fatigue of components due to vibration within the engine gradually increases. Fuel economy will gradually worsen as these effects build up, together with coking of the piston crown and combustion chamber.

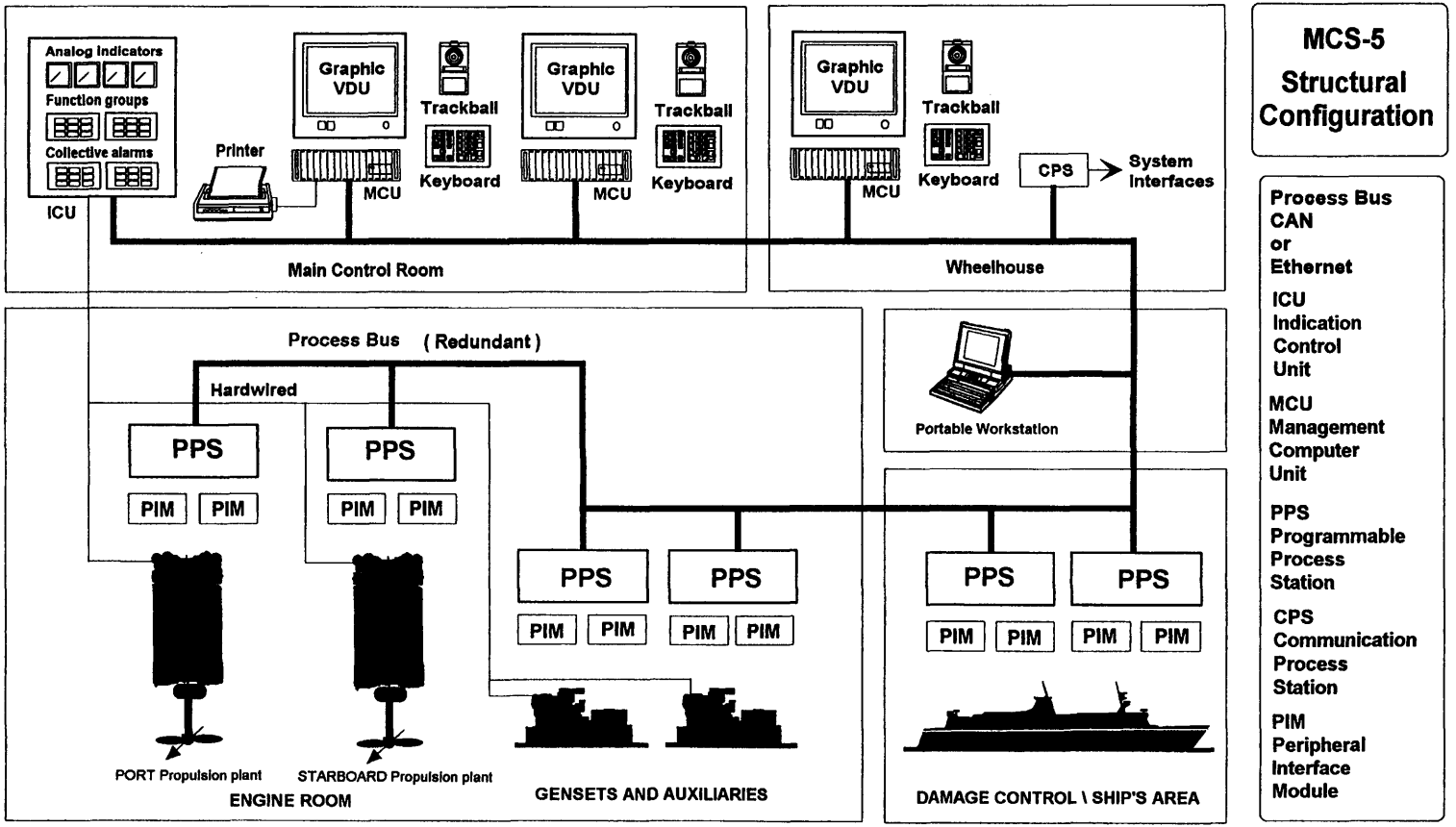

Fig. 16.19 MTU Engine Monitoring and control system example block diagram.

The PIM is available in two versions:

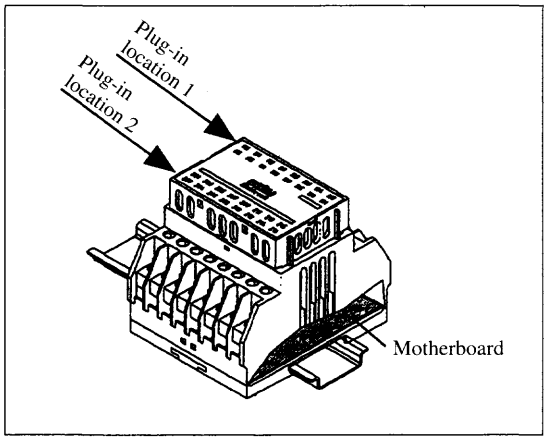

Type: **PIM 1**

The PIM 1 comprise:

- the modular cassette with printed circuit board COB (motherboard)
- plug-in location 1: printed circuit board MPU 23 (microprocessor)
- plug-in location 2: free plug-in location for selected printed circuit board

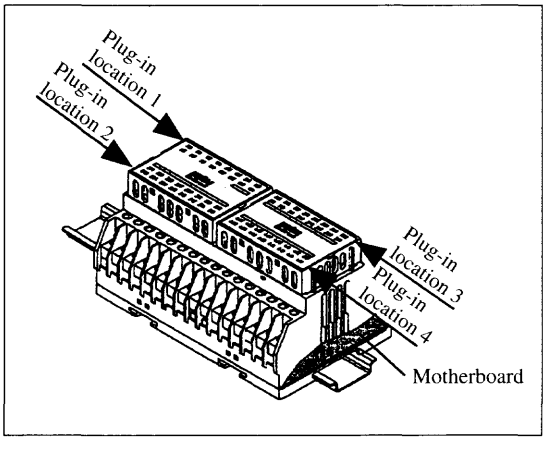

Type: **PIM 2**

The PIM 2 comprise:

- the modular cassette with printed circuit board COB (motherboard)
- plug-in loaction 1: printed circuit board MPU 23 (microprocessor)
- plug-in location 2, 3 and 4 free plug-in location for selected printed circuit board

Fig. 16.20 MTU Peripheral Interface Module (PIM).

Monitoring of engine vibration, fuel consumption and lubrication oil condition can provide a useful health check, and assist to predict when an overhaul will be required. Operation at above 85% MCR (Maximum Continuous Rating) can lead to very much increased rates of wear and degradation and so craft which require operations above this rating – for example military craft for sprint performance – should be subject to reduced periods between major engine inspections. Manufacturers will give advice on the appropriate procedures.

Engine auxiliaries can be prone to failures when operating in extreme environmental conditions, for example starter motors in low temperatures. Specification of auxiliaries should take this into account where possible. In low temperatures it is also necessary to provide for lubricating oil and fuel heating for start up.

Diesel engines have a wide useable range of rpm, so it is possible to use engine speed to regulate fan or propeller speed, rather than specifying variable pitch rotors for

propulsion. The use of rotating bow thrusters can provide adequate slow speed manœuvring. Engines may be left running at idle on bus stop type passenger services to avoid the stress cycle of a shutdown. It is preferable that diesel engines be specified by the ACV or SES designer for normal service speed at 85% MCR or less. This will then ensure that the period between major overhauls is in the range between 5000 and 10 000 hours.

Gas turbines have fewer moving parts than diesels, but operate at much higher rotative speeds – a factor of 5 to 10 higher. Main shaft bearings are sensitive to efficient lubrication and accuracy of rotor balance. Degradation will lead to vibration. Dust particles and salt in intake air will abrade the rotor blades, leading to reduced efficiency and thus increased fuel consumption and additional increased vibration. Operation at reduced power ratings can cause increased deposition of combustion products. Rotors should therefore be cleaned regularly to remove salt and combustion products. Typically a gas turbine is washed weekly or daily, depending on the intensity of operations. Monitoring of engine fuel consumption and vibration is useful as a health monitor, similar to diesels.

Gas turbines operate efficiently over a much smaller rotative speed range than diesels, and so propulsion fans, propellers or water jets will normally be specified with variable pitch, or some other means of varying the thrust independent of engine speed. Greatest efficiency will normally be obtained if a gas turbine installation is designed for normal service speed at about 95% maximum power rating. This will give a suitable power margin for extreme weather conditions, while allowing the turbine to operate close to its optimum for most of the time. This should also maximize the time between major overhauls. Typically a major gas turbine overhaul will be required every 2000 to 5000 operating hours for aero derivative units, depending on the number of starts. Industrial gas turbines generally have MTBO times between 5000 to 20 000 hours where operation is continuous for very long periods. When used in ACV or SES, these periods will be reduced by at least half, due to the number of start cycles.

Maintenance

Diesel engine MTBO is controlled by hours of operation, number of starts, and the operating cycle. The definition will be guided by power loss due to steady build up of coke – ash products from burnt fuel which fuse to the piston and cylinder surfaces. Heavily coked engines tend to smoke, particularly on start-up. Typical regular maintenance operations may be as follows, all based on monitoring performance of the engine during service:

Operating hours	Maintenance
500–1000	Sample lubricating oil and renew if required Check cooling water in closed circuits and treat or renew
1000–2000	Check exhaust valve seal, remove and clean, reseat, or replace Remove test and recondition fuel injectors
2000–5000	Check cam surfaces, clearances, and reset as necessary Check all major nut and bolt security
5000 and upwards	Major overhaul to manufacturer specification Main engine bearings and thrust bearing inspection
10 000–25 000	Overhaul of turbocharger, governer (if fitted), engine ancillaries

A major overhaul will usually be done in situ and consists of stripping the cylinder heads, removing and replacing worn parts, particularly valves and sleeve bearings, and de-coking the cylinder head and pistons. To achieve this efficiently, the engine room should have personnel access space around the engines and lifting arrangements/hatches to remove the heavier items to the workshop.

Gas turbine in service maintenance will follow the pattern below.

Operating hours	Maintenance
Each day, or each shutdown between voyages	Engine wash or cleanliness check Backwash air intake coarse filters
500–1000	Sample lubricating oil and renew if required Check cooling water in closed circuits and treat or renew
1000 and upwards	Major overhaul to manufacturer specification
10 000–25 000	Overhaul of governer (if fitted), engine ancillaries

Marine gas turbines in the power range 500 to 5000 kW normally have a maintenance schedule which requires regular attention from mechanics (regular engine and air intake washing to remove salt, etc.) and MTBO in the 2000–5000 hour range. The MTBO will depend on a combination of the number of hours operation and the number of cold starts. Typically, each cold start counts as one hour operation.

Development of marinized versions of high power industrial gas turbines, in the range 10 000–30 000 kW for large fast ferries is leading to much higher MTBO, in the same range as large diesel engines. For these applications the duty cycle includes fewer starts and a higher proportion of constant power output. A gas turbine overhaul consists of a complete strip and clean, rebuilding of main rotors replacing damaged blades, re-balancing and rebuilding. This is a specialist operation which is not normally done outside the suppliers' workshops. Intensive operation of a gas turbine craft will therefore require a spare turbine unit, or an exchange agreement with the supplier. Where an ACV or SES operator has several craft, it may be economically viable to set up an inhouse maintenance organization with mechanics trained by the engine supplier. Engine rooms for gas turbines need to include lifting gear and a removal route for the complete turbine unit.

References

1. Hayward L. *The History of Air Cushion Vehicles*. Kalerghi–McLeavy Publications, 1963.
2. King HF. *Aeromarine Origins*. Putnam & Co. Ltd, 1966.
3. Wheeler RL. *From River to Sea – the Marine Heritage of Sam Saunders*. Cross Publishing, Newport, Isle of Wight, 1993, ISBN 1 873295 05 7 (contains extensive summary of SRN and BHC series ACV design development).
4. Mantle PJ. *A Technical Summary of Air Cushion Craft Development*, David W. Taylor Naval Ship Research and Development Center, Report 80/012, January 1980.
5. Colotkin CA. *Damage to ACV and HFC*. Shipbuilding Press of former USSR, 1981 (in Russian).
6. Russell BJ. *The Interservice Hovercraft (Trials) Unit*. Hover Publications, Gosport Hampshire, England, April 1979.
7. Yun L, Gu X, Zhu JZ. *The Technical Evaluation of a 65 tonne Amphibious Hovercraft*. CACTS 1989.
8. Lamb H. *Hydrodynamics*, sixth edition. Cambridge University Press (Dover Publications in USA), 1932, Library of Congress Card 46–1891.
9. Benya YY, D'Yachenko VK. *Basic Theories of Air Cushion Vehicles*, AD742425.
10. West AA. On the performance of the hovercraft single wall skirt. *Aeronautical Quarterly (UK)*, November 1967.
11. Kaplan P, Schneider J, Goodman TH. *Motions of Air Cushion Vehicles in Waves*. Symposium on the Dynamics of Marine Vehicles and Structures in Waves, U.S.A., 1974.
12. Yun L, Ju ZX, Huang WJ. *Hovering Characteristics and Experimental Investigation of Two Dimensional Bag-Finger Type Skirt*. MARIC report, 1975 (in Chinese).
13. Yun L, Lee CL. On the hydrodynamic problem in hovercraft research and design. *Annual Meeting Proceedings of CSNAME*, 1982 (in Chinese).
14. Ju ZX, Hua Y. *Experimental Investigation of Scale Effect and Vertical Stability for Static Hovering of Two Dimensional Skirt with Bag Finger Type*. MARIC report, 1997 (in Chinese).
15. Barratt MJ, Everest JT, Hogben N, Shipway JC, Wheatley JHW. *Estimation of Power and Drag for Marine Hovercraft*. NPL Hovercraft Unit Report No.11, 1969.
16. Beardsley MW. *Wave Pumping and its Effect on the Design and Operation of Air Cushion Ships*. ADA-022583, 1975.
17. Newman JN. *Marine Hydrodynamics*. MIT Press, 1977, ISBN 0 262 14026 8.
18. Newman JN, Poole FAP. Wave resistance of a moving pressure distribution in a canal. *Schiffs-technik*, **9**, January 1962.
19. Colezaev BA *et al. Handbook of the Design of Ships with Hydrodynamic Support Principle*. Shipbuilding Press of the former USSR, 1980 (in Russian).

20. Everest JJ, Hogben NA. Theoretical and experimental study of the wavemaking of hovercraft of arbitrary plan form and angle of yaw. *Transactions of the RINA*, **111**, 1969.
21. Doctors JJ, Sharma SD. The wave resistance of air cushion vehicle in accelerated motion. *JSR*, **16**, 1972, published by SNAME.
22. Tatinclaux JC. On the wave resistance of surface effect ships. *SNAME Transactions*, **83**, 1975.
23. Hoerner SF. *Fluid Dynamic Drag*. Published by the Author, Hoerner Fluid Dynamics, P.O. Box 342, Brick Town, New Jersey, USA 08723, 1965.
24. Plackett M. *Design Aspect of Seal System for Air Cushion Vehicles*. AIAA paper 78–755, 1978.
25. Plackett MJ. *Design Aspects of Seal Systems for Air Cushion Vehicles*. AIAA/SNAME Advanced Marine Vehicles Conference, San Diego, California, U.S.A, 1978.
26 Chaplin JB. *Amphibious Surface Effect Vehicle Technology – Past, Present and Future*. AIAA paper no. 74–318, 1974.
27. Hua Y, Dang FS, Lee GL, Yun L. *The Method for Predicting Drag of Hovercraft on Calm Water*. MARIC report, 1989 (in Chinese).
28. Murao R. On the propulsion performance of SES on water surface (second part). *Journal of the Japan Society for Aeronautical and Space Science*, **24**, No. 26, 1979 (in Japanese).
29. Lee GL. The influence of changing the geometric parameters of sidewalls on the drag of SES. *Jiang Su Ship*, 1987 (in Chinese).
30. Yim B. On the wave resistance of surface effect ships. *JSR*, **15**, 1971.
31. Ozawa H, Tanaka H. The drag characteristics of catamaran type air cushion vehicles. *Journal of the Japan Society for Aeronautics and Space Sciences*, February 1979.
32. Rong HZ. *Calculation of Wave Profile Induced by Moving SES*. Master Thesis at MARIC, 1982.
33. Chaplin HR, Ford AG. *Some Design Principles of Ground Machines, Section D – Drag*. Report AD636277.
34. Blount DL, Fox DL. Small craft power prediction. *Marine Technology*, January 1976 (SNAME).
35. Hardler IB. The prediction of performance on planing craft. *SNAME Transactions*, 1966.
36. Fowler HS. *On the Lift Air Requirement of Air Cushion Vehicles, and its Relation to the Terrain and Operational Mode*. National Research Council of Canada (NRC) report, 1979.
37. Fowler HS. *Overland and Amphibious ACV Design : Data Relating to Performance*. NRC Report No. 17423, 1979.
38. Wilson RA, Wells SM, Heber CE. *Powering Prediction for Surface Effect Ships Based on Model Results*. AIAA paper 78–741, 1978.
39. Wilson RA. Status of hydrodynamics technology related to model tests of high speed marine vehicles. *Proceedings of 16th ITTC (International Towing Tank Conference)*.
40. Yen TK. *Isolation Technology for Mechanical Vibration*. Shanghai Scientific and Technology Press, 1985.
41. Yun E, Xu YC, Lin XC. *On the Transverse Stability of SES on Cushion (part 1)*. Second International Conference on Stability of Ships and Ocean Vehicles, Tokyo, October 1982.
42. Blyth AG. The roll stability of surface effect ships. *Transactions of the Royal Institution of Naval Architects (RINA)*, pp 271–285 (ex 138), 1993.
43. Chekhof CA. *Sidewall Hovercraft*. Translated and published by Research Institute of Water Transportation of Heilong-Jiang Province of China, 1983 (in Russian).
44. Bogdanov AY *et al. Experimental Investigation of the effect of speed on the stability of SES During Ultimate Rolling Angle*. Sea Fleet Literature No 246 (in Russian).
45. Zhou WL, Hua Y, Clao X. Analysis of the Stability of ACV. *Proceedings of Second National Conference on High Performance Vehicles*, China, 1984.
46. Hua Y, Zhou WL, Dang FS. *The Influence of Geometic Parameters of ACV on Transverse Stability*. MARIC Report, 1982 (in Chinese).

47. Coles AV. *Demonstrated Performance of the Amphibious Assault Landing Craft JEFF(B)*. The Third International Conference on Air Cushion Technology; Brighton, UK, 1976 (Ref FFI).
48. *Marine Technology Requirements Board. Stability and Control of Hovercraft, Notes for Commanders*. Published by Department of Industry, HM Stationary Office, London, 1980 (BHC Technical Report SP 4432).
49. Cook CC, Duffy RE. *Forward Speed Effects on Peripheral Jet Air Support Systems*. AIAA paper No.71–908.
50. Crago WA. Problems associated with the use of skirts on Hovercraft. *Hovering Craft and Hydrofoil*, April 1966 (Ref. Fast Ferry International which succeeded H&HI).
51. Lavis DR. *The Development of Stability Standards for Dynamically Supported Craft, A Progress Report*. The Third International Conference on Air Cushion Technology, Brighton, UK, 1976.
52. Kozalev BA. *Handbook on Hydrofoil and Hovercraft*. Translated and published by National Defence Press of China, 1985 (in Russian).
53. Huang TT, Wong KK. Disturbance induced by a pressure distribution moving over a free surface. *Journal of Ship Research, SNAME*, (JSR), **14**, 1970.
54. Standing RG. *Experience in Computing the Wavemaking of Hovercraft*. NPL report, *Ship 191*, September 1975.
55. Fein JA, Magnuson AH, Moran DD. *Dynamic Performance of Air Cushion Vehicles in a Marine Environment*. AIAA Paper 74–323.
56. Svensson R. *Experience with the KaMeWa Waterjet Propulsion System*. AIAA Paper No 89–1440–CP, 1989.
57. Zheng XJ. *On the Manoeuvrability of ACV*. First National Conference on High Speed Craft, China, 1979.
58. Murao R and Nojiri T. *On the Manoeuvring Simulation of an Antarctic Hovercraft*. Joint International Conference on Air Cushion Technology, Canadian Air Cushion Technology Society, 1985.
59. Wheeler RL. Control of single propeller hovercraft with particular reference to BH-7. *Canadian Aeronautics and Space Institute Journal*, May 1971.
60. Zeitfuss W Jr, Brooks EN Jr. *An Analysis of Desired Maneuvering Characteristics of Large Arctic SEV's*. AIAA paper No.72–600.
61. Waldo RD. Some speed problems in SES. *Journal of Hydronautics*, **2**, No 3, July 1968.
62. Xic YN, Hua YT. *Static Calculation of Forces Acting on Bag-finger Type Skirt*. Joint International Conference on Air Cushion Technology, 1985 (in Chinese).
63. Hua Y, Zheng N. *Analysis of Forces Acting on Three Dimensional Skirt of Bag-finger Type*. MARIC Report, 1986 (in Chinese).
64. Zheng N, Wu TF. Approach to the influence of bottom pressure under the stern seal on the formation of skirts. *Ship Engineering*, No 5, 1984 (in Chinese).
65. Boland JA. *Lift and Drag Measurement and Analysis of the Stern Seal of the Captured Air Bubble Testcraft XR-3*. ADA 039149.
66. Zhou WL, Ma T. *The Experimental Investigation of Bounce Characteristics of ACV Responsive Skirt*. CACTS International Conference on Air Cushion Technology, 1986.
67. Reynolds AJ, West RP, Brook BE. Heaving and pitching response of a hovercraft moving over regular waves. *Journal of Mechanical Engineering Science*, **14**, October 1972.
68. Doctors LJ. Nonlinear motion of an air cushion vehicle over waves. *Journal of Hydronautics*, April 1975.
69. Zhou WL, Hua Y, Yun L. *Nonlinear Equations for Coupled Heave and Pitch Motions of Surface Effect Ships in Regular Waves*. CACTS International Conference, Ottawa, Canada, 1980.
70. Zhou WL, Hua Y. *Seakeeping Quality of ACV, and the Influence of Compressibility of Cushion Air on Seakeeping*. MARIC Report, 1984 (in Chinese).

71. Lavis DR. *On the Prediction of Acceleration Response of Air Cushion Vehicles to Random Seaways, and the Distortion Effect of the Cushion Inherent in Scale Models.* AIAA paper 72–598.
72. Magnuson AH. *Seakeeping Trials of the BH-7 Hovercraft.* Report ADA 016340.
73. Moran DD, Fein JA, Ricci JJ. Seakeeping characteristics of a high length-to-beam ratio surface effect ship. *Journal of Hydronautics*, **17**, No.3, July 1977.
74. Xin SD. *Experimental Report on the Seakeeping Quality of Craft Model 711CM11.* CSSRC report, 1982 (in Chinese).
75. Yu ZD. Experimental investigation of SES with bow fin. *Shipbuilding in China* No.2, 1981 (in Chinese).
76. Gersten A. *A Synthesis of AALC Program ACV Seakeeping Data.* ADA 040122, April 1977.
77. Yun L, Wu TF, Cheng YN. *Coupled Roll and Heave Motions of Surface Effect Ships in Beam Seas.* The Hovercraft Society (THS) International Conference on Hovercraft Technology, Southampton, England, May 1987.
78. Arfiliev MY *et al. Inland River Transport Catamarans.* 1980 (in Russian).
79. Barr R. Supercavitating and superventilated propellers. *Transactions SNAME*, **76**, 1970.
80. Bhattacharyya R. *Dynamics of Marine Vehicles* (US Naval Academy, Anapolis Maryland, USA). Published by J Wiley & Sons, 1978.
81. Hua Y, Cheng YN. *Tensile Tests for Skirt Materials.* MARIC Report, 1980 (in Chinese).
82. Castor EB. *TMB 2, 3, and 4 Bladed Supercavitating Propeller Series.* DTMB (NSRDC) Report 1637, January 1963.
83. Cox JN. The evolution of safety requirements for dynamically supported craft. *Hovercraft and Hydrofoil*, November 1977.
84. *Current Status of U.S. Navy Stability and Buoyancy Criteria for Advanced Marine Vehicles.* AIAA paper 74–332, 1974.
85. Tachmindji AJ, Morgan WB. *The Design and Estimated Performance of a Series of Supercavitating Propellers.* Second Symposium on Naval Hydrodynamics, Office of Naval Research, US Navy, 1958.
86. *Rules and Regulations for Classification and Construction of Inland River Vessels (3).* Inland River Ship Register of Russia, 1979.
87. Du Cane R. *High Speed Small Craft*, revised third edition. David & Charles, 1974, ISBN 0 7153 5926 6.
88. Allison JL. Propellers for high performance craft. *SNAME Marine Technology*, **15**, pp335–380, Oct. 1978.
89. *The Fundamentals of ACV Habitability and Ride Characteristics.* SAE paper No.710534, 1971.
90. Troost L. Open water test series with modern propeller forms. *Transactions of the North East Coast Institution of Engineers and Shipbuilders*, Part 1, **54**, 1937–38, Part 2, **56**, 1939–40, Part 3, **67**, 1950–51.
91. van Lammeren WP, van Manen JD, Oosterveld MWC. The Wageningen B-screw Series. *Transactions SNAME*, **77**, 1969.
92. Elsley GH. *Hovercraft Towards the Second Quarter Century.* 3rd International Hovercraft Conference, The Hovercraft Society, UK, November 1981.
93. Vaganov AM. *Design of High Speed Vessels.* Shipbuilding Press of the former USSR, 1978 (in Russian).
94. Tremills JA, Band EGU, St Laurent R. A Design Synthesis Model for ACV/SES Lift Systems. *Proceedings of Canadian Symposium on Air Cushion Technology*, pp 143–180, 1981.
95. *Development of ACV's in BHC.* General information leaflet issued by the Company, 1980.
96. Ram recovery of a flush intake for air cushion vehicles. *Hovering Craft & Hydrofoil*, September 1968.

97. Tang ZF. Selection and design of lift fans on hovercraft. *MARIC Hovercraft Bulletin*, November 1981 (in Chinese).
98. *Introduction to the Design of Power Plant of Hovercraft*. Published by MARIC, December 1971 (in Chinese).
99. Wheeler RL. *Hovercraft Skirts*. International Hovercraft, Hydrofoil, and Advanced Transit System Conference, U.K., 1979.
100. Zhou J. Design of ACV 7202. *MARIC Hovercraft Bulletin*, November 1981 (in Chinese).
101. Wheeler RL. An appraisal of present and future large commercial hovercraft. *Proceedings of the Royal Institution of Naval Architects*, July 1976.
102. Men ZX, Yu YF. *Approach for Design Criteria of ACV/SES Structures*. First National Conference on High Speed Craft, 1979 (in Chinese).
103. Yen ZL, Wong F, Zhao WS. Calculation of overall longitudinal strength and external loads of/on the hull structure of an ACV. *Proceedings of Annual Meeting of Structural Mechanics Committee of CSNAME*, 1991 (in Chinese).
104. Elsley GH, Devereux AT. *Hovercraft Design and Construction*. David & Charles, UK, 1968.
105. *Hull Structure of Hovercraft – Construction Rules for River Hovercraft of USSR*. Translated from Russian and published by MARIC, 1983 (in Chinese).
106. Bureau Veritas. *Building and Operations of Vibration Free Propulsion Plants in Ships*, Chapter C: responses of propulsion apparatus and auxiliary engines.
107. *Classification of Seagoing Ships and Rules for Construction of USSR – Technical Standards for Vibration*. Translated and published by MARIC, 1974 (in Chinese).
108. Mitchell JS. *An Introduction to Machinery Analysis and Monitoring* (second edition). Penn Well, 1993.
109. Newton RN, Rader HP. Performance data of propellers for high speed craft. *RINA Transactions*, pp 93–118, 1961.
110. Osborne WC. *Fans*. Pergamon Press, 1967, Library of Congress Card 66–18408.
111. Abbott IH, von Doenhoff AE. *Theory of Wing Sections*. Dover Publications, 1959.
112. Gawn RWL, Burrill LC. Effect of cavitation on the performance of a series of 16-inch model propellers. *Transactions of RINA*, 1957.
113. Allison JL. Marine waterjet propulsion. *SNAME Transactions*, **101**, pp 275–335, 1993.
114. Lewis RI. *Turbomachinery Performance Analysis*. Arnold, 1996, ISBN 0 340 63191 0, and Wiley 1996, ISBN 0 470 23596 9.
115. Civil Aviation Authority. *British Hovercraft Safety Requirements*. ISBN 0 86039 128 0.
116. Lloyds Register of Shipping. *Rules and Regulations for the Classification of Special Service Craft*, 1996.
117. Harrington RL. *Marine Engineering*. The Society of Naval Architects and Marine Engineers, 1992 edition, ISBN 0 939773 10 4.
118. *IMO High Speed Craft Code*. Document IMO-187–E (English), 1996, ISBN 92 801 1326 7.
119. Trillo RL. *Jane's High Speed Marine Craft and Air Cushion Vehicles*. UK, 1986.

Sources

Given below are contact details for the main sources of technical papers given as references above.

Chinese Society of Naval Architects & Marine Engineers (CSNAME)
Ship Design Committee, CSNAME, c/o Marine Design and Research Institute of China,
1340 Xin Zhao Zhou Road, Shanghai 200011, China
Tel. +86 216 377 0171, Fax +86 216 377 9744

Royal Institution of Naval Architects
10 Upper Belgrave Street, London, SW1X 8BQ, UK
Tel. +44 171 235 4622, Fax +44 171 245 6959

Society of Naval Architects and Marine Engineers (SNAME)
601 Pavonia Avenue, Jersey City, New Jersey 07306, USA
Tel. +1 201 798 4800, Fax +1 201 798 4975, Internet http://www.sname.org

Canadian Air Cushion Technology Society (CACTS), which is a constituent Society of :
Canadian Aeronautics and Space Institute,
130 Slater Street, Suite 818, Ottowa, Ontario K1P 6E2, Canada
Tel. +1 613 234 0191, Fax +1 613 234 9039, E-mail: casi@casi.ca

The Hovercraft Society (THS)
24 Jellicoe Avenue, Alverstoke, Gosport, Hampshire, PO12 2PE, UK

The Civil Aviation Authority (CAA)
Printing and Publication Services, Greville House, 37 Gratton Road, Cheltenham, Gloucestershire, GL50 2BN, UK
Tel. +44 1242 485 151, Fax +44 1242 485 139

Intergovernmental Marine Organisation (IMO)
4 Albert Embankment, London SE1 7SR, UK
Tel. +44 171 735 7611, Fax +44 171 587 3241
Refer to Publications section for High Speed Craft Code, Document IMO-187–E (English).

Lloyds Register (LR)
100 Leadenhall Street, London EC3A 3BP, UK
Tel. +44 171 709 9166, Fax +44 171 488 4796
Refer to the Special Service Craft Approval Group, Construction Services Department for advice on Lloyds Special Service Craft Rules, which include SES and ACV.

The American Society of Naval Engineers (ASNE)
1452 Duke Street, Alexandria, Virginia, VA 22314–3458, USA
Tel. +1 703 836 6727, Fax +1 703 836 7491

Fast Ferry International (previously High Speed Surface Craft, earlier Hovering Craft and Hydrofoil)
Milroy House, Sayers Lane, Tenderden, Kent TN30 6BW, UK
Tel. +44 1580 766960, Fax +44 1580 766961, Internet http://www.fastferry.co.uk

American Institute of Aeronautics and Astronautics (AIAA)
1290 Avenue of the Americas, New York, NY 10019, USA

Det Norske Veritas (DnV)
Veritasveien 1, N-1322 Høvik, Norway
Tel. +47 67 57 99 00, Fax +47 67 57 91 60
Reference for Rules for Classification of High Speed Light Craft, 1985

Jane's Information Group (Jane's)
Sentinel House, 163 Brighton Road, Coulsdon, Surrey CR5 2NH, UK
Tel. +44 181 763 1030, Fax +44 181 763 1006

Index